frontiers | Research Topics

Mechanisms of biofilm development and antibiofilm strategies

Edited by
Huancai Lin, Dongmei Deng and Fang Yang

Published in
Frontiers in Microbiology

ISSN 1664-8714
ISBN 978-2-8325-2205-9
DOI 10.3389/978-2-8325-2205-9

About Frontiers

Frontiers is more than just an open access publisher of scholarly articles: it is a pioneering approach to the world of academia, radically improving the way scholarly research is managed. The grand vision of Frontiers is a world where all people have an equal opportunity to seek, share and generate knowledge. Frontiers provides immediate and permanent online open access to all its publications, but this alone is not enough to realize our grand goals.

Frontiers journal series

The Frontiers journal series is a multi-tier and interdisciplinary set of open-access, online journals, promising a paradigm shift from the current review, selection and dissemination processes in academic publishing. All Frontiers journals are driven by researchers for researchers; therefore, they constitute a service to the scholarly community. At the same time, the *Frontiers journal series* operates on a revolutionary invention, the tiered publishing system, initially addressing specific communities of scholars, and gradually climbing up to broader public understanding, thus serving the interests of the lay society, too.

Dedication to quality

Each Frontiers article is a landmark of the highest quality, thanks to genuinely collaborative interactions between authors and review editors, who include some of the world's best academicians. Research must be certified by peers before entering a stream of knowledge that may eventually reach the public - and shape society; therefore, Frontiers only applies the most rigorous and unbiased reviews. Frontiers revolutionizes research publishing by freely delivering the most outstanding research, evaluated with no bias from both the academic and social point of view. By applying the most advanced information technologies, Frontiers is catapulting scholarly publishing into a new generation.

What are Frontiers Research Topics?

Frontiers Research Topics are very popular trademarks of the *Frontiers journals series*: they are collections of at least ten articles, all centered on a particular subject. With their unique mix of varied contributions from Original Research to Review Articles, Frontiers Research Topics unify the most influential researchers, the latest key findings and historical advances in a hot research area.

Find out more on how to host your own Frontiers Research Topic or contribute to one as an author by contacting the Frontiers editorial office: frontiersin.org/about/contact

Mechanisms of biofilm development and antibiofilm strategies

Topic editors
Huancai Lin — Sun Yat-sen University, China
Dongmei Deng — Academic Centre for Dentistry Amsterdam, VU Amsterdam, Netherlands
Fang Yang — Qingdao Municipal Hospital, China

Topic coordinator
Liangyue Pang — Sun Yat-sen University, China

Citation
Lin, H., Deng, D., Yang, F., eds. (2023). *Mechanisms of biofilm development and antibiofilm strategies*. Lausanne: Frontiers Media SA.
doi: 10.3389/978-2-8325-2205-9

The authors declare that the research was conducted in the absence of any commercial or financial relationships that could be construed as a potential conflict of interest.

Table of contents

frontiers | Frontiers in Microbiology

TYPE Editorial
PUBLISHED 04 April 2023
DOI 10.3389/fmicb.2023.1190611

OPEN ACCESS

EDITED AND REVIEWED BY
Rustam Aminov,
University of Aberdeen, United Kingdom

*CORRESPONDENCE
Huancai Lin
✉ linhc@mail.sysu.edu.cn

SPECIALTY SECTION
This article was submitted to Antimicrobials, Resistance and Chemotherapy, a section of the journal Frontiers in Microbiology

RECEIVED 21 March 2023
ACCEPTED 23 March 2023
PUBLISHED 04 April 2023

CITATION
Pang L, Lin H, Yang F and Deng D (2023) Editorial: Mechanisms of biofilm development and antibiofilm strategies.
Front. Microbiol. 14:1190611.
doi: 10.3389/fmicb.2023.1190611

Editorial: Mechanisms of biofilm development and antibiofilm strategies

Liangyue Pang[1,2], Huancai Lin[1,2]*, Fang Yang[3] and Dongmei Deng[4]

[1]Hospital of Stomatology, Sun Yat-sen University, Guangzhou, Guangdong, China, [2]Guangdong Provincial Key Laboratory of Stomatology, Sun Yat-sen University, Guangzhou, Guangdong, China, [3]Qingdao Hospital, University of Health and Rehabilitation Sciences, Qingdao, Shandong, China, [4]Department of Preventive Dentistry, Academic Center for Dentistry Amsterdam (ACTA), University of Amsterdam and VU University Amsterdam, Amsterdam, Netherlands

KEYWORDS

biofilm, mechanism, antibiofilm, antimicrobial agents, antibiofilm strategies

Editorial on the Research Topic
Mechanisms of biofilm development and antibiofilm strategies

Biofilms refer to the surface-attached groups of microbial cells embedded in an extracellular matrix. Biofilms' development is a complex dynamic process, including five stages: initial attachment, EPS production leading to "irreversible" attachment, early development of biofilm architecture, maturation of biofilm architecture and dispersion of single cells (Tim, 2015). It is estimated that biofilms are related to 65–80% of infectious diseases. Understanding the biological mechanisms associated with the biofilm development process is of great significance for the development of novel antibiofilm agents. It has been known that microbes in biofilms are less susceptible to antimicrobial agents than their planktonic counterparts, and as a result, biofilm-related diseases are extremely difficult to prevent and cure (Wang et al., 2022). Most antibiofilm agents available till date have been antimicrobial agents with bactericidal effects, which are ineffective for treating biofilm-related infections and can lead to microbial resistance when used for a long time (Sun et al., 2013). Hence, it is critically important to design or screen novel antibiofilm agents that can effectively prevent biofilm formation or eradicate existing biofilm. We are honored to serve as Guest Editors, aiming to gather contributions to the Frontiers Research Topic on "Mechanisms of Biofilm Development and Antibiofilm Strategies". We have compiled 15 papers which present state-of-the-art knowledge on the Research Topic, covering various bacterial species, namely *Pseudomonas aeruginosa*, *Acinetobacter baumannii*, *Corynebacterium matruchotii*, *Staphylococcus aureus*, *Streptococcus mutans*, and *Candida albicans*. The studies published in this Research Topic can be categorized into two groups: (1) the mechanisms underlying biofilms' development stages and (2) novel strategies to prevent biofilm formation or eradicate existing biofilm.

Extracellular DNA (eDNA) is a critical component in the extracellular matrix (ECM) of bacterial biofilms (Devaraj et al., 2019). Wang Y. et al. used the *Myxococcus xanthus* biofilm model to investigate the mechanisms underlying how eDNA integrated into the ECM through potential macromolecular interactions. Their results showed that eDNA was able to combine with *M. xanthus* EPS to form a macromolecular conjugate. During the biofilm formation process, the eDNA-EPS complex not only facilitated the initial cell adhesion and subsequent establishment of ECM architecture, but also renderd cells within biofilms stress resistances that are relevant to the survival of *M. xanthus* in hostile environments.

Furthermore, the EPS protected the conjugated DNA from degradation by nucleic acid hydrolases, which led to the continuous and stable existence of eDNA in the native ECM of *M. xanthus* biofilms.

Biofilm formation has been found to be closely related to the drug resistance of *Acinetobacter baumannii*. Yang et al. focus on a new gene labeled with a locus tag of BIT33_RS14560 in the NCBI database. This new gene belongs to the Major Facilitator superfamily, some of which have been confirmed to be closely related to biofilm formation and drug resistance. They demonstrated that when BIT33_RS14560 was overexpressed in *A. baumannii*, the biofilm formation capacity and virulence were both enhanced, and they also presented RNA sequencing evidence to elucidate possible mechanisms for these changes.

Quorum sensing (QS), as the main signaling mechanism bacteria use for cell-to-cell communication, plays a key role in biofilm formation (Zhou et al., 2020). Wang N. et al. demonstrated that the QS regulatory protein PdeR promoted biofilm formation in *P. denitrificans*. They also revealed the underlying regulatory mechanism of PdeR during biofilm development: PdeR mainly promoted the intracellular degradation of amino acids and fatty acids, as well as siderophore biosynthesis and transportation, thus providing cells with enough energy and iron to form a thicker biofilm. This finding contributes to our understanding of QS regulation in biofilm development. A new antibacterial strategy based on inhibiting bacterial quorum sensing has emerged as a promising method of attenuating bacterial pathogenicity and preventing bacterial resistance to antibiotics. Bai et al. examined Echinatin (Ech) with high-efficiency anti-QS and verified the significantly synergistically increased antibacterial activity in overcoming the antibiotic resistance of *E. coli*, suggesting the potent anti-QS and novel antibacterial synergist candidate of Ech for treating *E. coli* infections.

Corynebacterium matruchotii is a gram-positive calcifying bacterium which presents in dental plaque on the tooth surface and serves as one of the most predominant bacterial species at the site. Li et al. reviewed the role of *C. matruchotii* in supragingival plaque based on biofilm structure, microbial interactions, and potential connections with oral diseases. The coexistence of *S. mutans* and *C. albicans* is closely related to the progression of early childhood caries, and exopolysaccharides play important roles in the cross-kingdom interaction between *S. mutans* and *C. albicans*. Lu et al. constructed the *C. albicans DCR1* low-expressing and over-expressing strains and co-cultured them with *S. mutans* wild type or *rnc*-mutant strains to explore the roles of *rnc* and *DCR1* in the modulation of dual-species biofilms of *S. mutans* and *C. albicans*. Their result indicating that the *DCR1* gene in *C. albicans* regulated the fungal yeast-to-hyphae transition, spatial structure, acid production and EPS/microorganism volume ratio of biofilms. While *rnc* gene in *S. mutans* prominently contributed to biofilm formation by increasing biofilm extracellular polysaccharide synthesis and *C. albicans* virulence, resulting in increased biomass, biofilm roughness, and acid production of the dual-species biofilms, which facilitated the assembly of a cariogenic cross-kingdom biofilm and the generation of an intensive acidic milieu.

Bacteria in the biofilm state are more tolerant to various antibiotics and, thus, are more difficult to control than bacteria in the planktonic state, and this sharply limits the application of existing antimicrobial therapies. Dispersion of biofilms is a promising avenue for the treatment of biofilm-associated diseases. To some extent, dispersion and eradication of mature biofilms are very important for biofilm control. Inducing dispersion would be a gentle and specific approach that would not influence the development of dysbiosis or the balance of the oral microbiome (Lin et al., 2022). Furthermore, the bacteria become much more sensitive to antimicrobial agents as they separate from the biofilm. Chen Y. et al. summarized strategies for the dispersion of cariogenic biofilms, including biofilm environment, signaling pathways, biological therapies, and nanovehicle-based adjuvant strategies. These strategies may provide great opportunities for the clinical treatment of dental diseases in the future.

Pseudomonas aeruginosa is one of the top three major pathogens implicated in human opportunistic infections and a common cause of clinically persistent infections. *P. aeruginosa* biofilm formation results in multiple antibiotic resistance, posing a significant challenge to conventional antibiotic therapeutic approaches. Yin et al. briefly introduced the process and regulation of *P. aeruginosa* biofilm formation and reviewed several traditional methods for biofilm treatment as well as current innovative treatment technologies with significant curative effects, providing new directions for the treatment of *P. aeruginosa* biofilm infection. Wang M. et al. investigated the antibiofilm property and antibiofilm pathway of a new antimicrobial peptide, named PEW300, against *P. aeruginosa*. Their results showed that PEW300 exhibited strong antibiofilm activity against *P. aeruginosa*. PEW300 dispersed biofilm preferentially by degrading extracellular DNA and adopted multiple action modes to cause cell death. In addition, PEW300 could dramatically reduce the virulence of *P. aeruginosa* by down-regulating the expression of virulence genes. Their results suggested that PEW300 has good potential to be an efficient antibacterial agent to combat *P. aeruginosa* biofilm.

Bacterial biofilm is an important mechanism mediating the antibiotic resistance of methicillin-resistant *S. aureus* (MRSA) as well. Using small molecules to enhance the efficacy of existing antibiotics is an economical and practical strategy to cope with biofilm-induced resistance. Chen R. et al. investigated the synergies of two small molecules, isobavachalcone and curcumin, both with anti-osteoporosis, anti-inflammation, and anti-bacteria characteristics, and demonstrated that the combination of these two molecules could enhance the susceptibility of MRSA to gentamicin, thus promoting the eradication of MRSA biofilm. When administered as a cocktail *in vivo*, they could significantly modify local inflammation in orthopedic implant-related infection and protect bone microstructure. Biofilms are recalcitrant to antibiotic treatment due to multiple tolerance mechanisms (phenotypic resistance) (Ciofu et al., 2017). Therefore, effective biofilm-targeting compounds are currently highly sought after. Long et al. found Elasnin as a potent and safe biofilm eradicator against MRSA which destroyed their biofilm matrix, reduced virulence, and increased their sensitivity to β-lactam antibiotics. Elasnin's mode of action was also elucidated, which highlighted the key genes that govern this process and the crucial role of

sarZ during elasnin-induced biofilm eradication, pointing out the potential role of *sarZ* in regulating staphylococcal biofilm development. This study provides new strategies against the eradication of MRSA biofilms and new insights into the molecular targets for biofilm eradication in MRSA.

Now, more and more documents have focused on antimicrobial peptides (AMPs) as a substitute candidate for conventional antimicrobial agents against Multidrug-resistant (MDR) and biofilm-associated infections. Mirzaei et al. evaluated melittin's antibacterial and antibiofilm activity alone and/or in combination with gentamicin, ciprofloxacin, rifampin, and vancomycin on biofilm-forming MDR-*P. aeruginosa* and MDR-MRSA strains. Their results showed that melittin alone was effective against the strong biofilm of MDR pathogens and also offered sound synergistic effects with antibiotics without cytotoxicity, suggesting combining melittin and antibiotics can be a potential candidate for further evaluation of *in vivo* infections by MDR pathogens. Villanueva et al. attempted optimizing the antibiofilm potency of different commercially available tannins against bacteria by modifying their chemical structure with different derivatizations. Their results showed distinct correlations between certain chemical qualities of the tannins and their antibiofilm activity and spectrum. The authors suggested that the spectrum and the antibiofilm potency of the tannins could be modulated by the applied chemical modifications.

Natural products are promising medicines against the overgrowth of oral pathogens in biofilms due to their excellent antibiofilm effects, abundant sources, relatively low cost, and safety. Chi et al. summarized the antibiofilm effects and mechanisms of natural products against mono- or multi-species biofilms, targeting the different stages of biofilm development, including adhesion, cell proliferation, maturation, and dispersion, as well as the combinational advantages with other strategies to enhance the antibiofilm properties of natural products, providing a new direction for antibiofilm agents. EPS plays a role in altering microbial behavior and virulence and can also enhance bacterial drug resistance (Gupta et al., 2016; Liu et al., 2016); targeting EPS may be an effective breakthrough point for removing or controlling biofilms. established a periodontitis-related microbial multi-species biofilm containing the EPS encapsulating bacterial group and demonstrated that bovine trypsin could destroy the biofilm structure, dispersed the biofilm and bacteria, and significantly reduced the amount of EPS and biomass.

Altogether, this Research Topic outlines the mechanisms underlying biofilms' development stages and the novel strategies to prevent biofilm formation or eradicate existing biofilm. The information availed in the articles will advance our understanding of the mechanisms of biofilm development and antibiofilm strategies. The data presented in these articles will contribute to providing new directions for antibiofilm agents.

Author contributions

All authors listed have made a substantial, direct, and intellectual contribution to the work and approved it for publication.

Acknowledgments

We highly acknowledge the contributions of every author and reviewers that made their contribution to this Research Topic.

Conflict of interest

The authors declare that the research was conducted in the absence of any commercial or financial relationships that could be construed as a potential conflict of interest.

Publisher's note

References

Ciofu, O., Rojo-Molinero, E., Macià, M. D., and Oliver, A. (2017). Antibiotic treatment of biofilm infections. *APMIS*. 125, 304–319. doi: 10.1111/apm.12673

Devaraj, A., Buzzo, J. R., Mashburn-Warren, L., Gloag, E. S., Novotny, L. A., Stoodley, P., et al. (2019). The extracellular DNA lattice of bacterial biofilms is structurally related to Holliday junction recombination intermediates. *Proc. Natl. Acad. Sci. U S A.* 116, 25068–25077. doi: 10.1073/pnas.1909017116

Gupta, P., Sarkar, S., Das, B., Bhattacharjee, S., and Tribedi, P. (2016). Biofilm, pathogenesis and prevention—a journey to break the wall: a review. *Arch. Microbiol.* 198 1–15. doi: 10.1007/s00203-015-1148-6

Lin, Y., and Zhou, X., and Li, Y. (2022). Strategies for streptococcus mutans biofilm dispersal through extracellular polymeric substances disruption. *Mol. Oral. Microbiol.* 37, 1–8. doi: 10.1111/omi.12355

Liu, Y., Kamesh, A. C., Xiao, Y., Sun, V., Hayes, M., Daniell, H., et al. (2016). Topical delivery of low-cost protein drug candidates made in chloroplasts for biofilm disruption and uptake by oral epithelial cells. *Biomaterials* 105, 156–166. doi: 10.1016/j.biomaterials.2016.07.042

Sun, F., Qu, F., Ling, Y., Mao, P., Xia, P., Chen, H., et al. (2013). Biofilm-associated infections: antibiotic resistance and novel therapeutic strategies. *Future Microbiol.* 8, 877–886. doi: 10.2217/fmb.13.58

Tim, T. N. (2015). Biofilm development. *Microbiol Spectr*. 3:MB-0001–2014. doi: 10.1128/microbiolspec.MB-0001-2014

Wang, K., Dou, Z., Gong, G., Li, H., Jiang, B., Xu, Y., et al. (2022). Anti-larval and anti-algal natural products from marine microorganisms as sources of anti-biofilm agents. *Mar Drugs*. 20, 90. doi: 10.3390/md20020090

Zhou, L., Zhang, Y., Ge, Y., Zhu, X., and Pan, J. (2020). Regulatory mechanisms and promising applications of quorum sensing-inhibiting agents in control of bacterial biofilm formation. *Front Microbiol.* 11, 589640. doi: 10.3389/fmicb.2020.589640

frontiers | Frontiers in Microbiology

ORIGINAL RESEARCH
published: 22 April 2022
doi: 10.3389/fmicb.2022.861865

Physicochemical and Biological Insights Into the Molecular Interactions Between Extracellular DNA and Exopolysaccharides in *Myxococcus xanthus* Biofilms

Yan Wang[1], Tingyi Li[1], Weiwei Xue[1], Yue Zheng[1], Yipeng Wang[1], Ning Zhang[1], Yue Zhao[2], Jing Wang[2], Yuezhong Li[1], Chuandong Wang[1] and Wei Hu[1]**

[1]State Key Laboratory of Microbial Technology, Microbial Technology Institute, Shandong University, Qingdao, China, [2]College of Pharmaceutical Science, Shandong University of Traditional Chinese Medicine, Jinan, China

OPEN ACCESS

Edited by:
Fang Yang,
Qingdao Municipal Hospital, China

Reviewed by:
Jin He,
Huazhong Agricultural University, China
Xuesong He,
The Forsyth Institute, United States

***Correspondence:**
Chuandong Wang
wangchuandong@sdu.edu.cn
Wei Hu
hw_1@sdu.edu.cn

Specialty section:
This article was submitted to Antimicrobials, Resistance and Chemotherapy, a section of the journal Frontiers in Microbiology

Received: 25 January 2022
Accepted: 06 April 2022
Published: 22 April 2022

Citation:
Wang Y, Li T, Xue W, Zheng Y, Wang Y, Zhang N, Zhao Y, Wang J, Li Y, Wang C and Hu W (2022) Physicochemical and Biological Insights Into the Molecular Interactions Between Extracellular DNA and Exopolysaccharides in Myxococcus xanthus Biofilms. Front. Microbiol. 13:861865. doi: 10.3389/fmicb.2022.861865

Extracellular DNA (eDNA) is a critical component in the extracellular matrix (ECM) of bacterial biofilms, while little is known about the mechanisms underlying how eDNA integrates into the ECM through potential macromolecular interactions. *Myxococcus xanthus* biofilm was employed as a suitable model for the investigation due to the co-distribution of eDNA and exopolysaccharides (EPS) owing to their direct interactions in the ECM. DNA is able to combine with *M. xanthus* EPS to form a macromolecular conjugate, which is dominated by the electrostatic forces participating in the polymer-polymer interactions. Without intercalation binding, DNA-EPS interactions exhibit a certain degree of reversibility. Acting as a strong extracellular framework during biofilm formation process, the eDNA-EPS complex not only facilitates the initial cell adhesion and subsequent establishment of ECM architecture, but also renders cells within biofilms stress resistances that are relevant to the survival of *M. xanthus* in some hostile environments. Furthermore, the EPS protects the conjugated DNA from the degradation by nucleic acid hydrolases, which leads to the continuous and stable existence of eDNA in the native ECM of *M. xanthus* biofilms. These results will shed light on developing prevention and treatment strategies against biofilm-related risks.

Keywords: extracellular DNA, exopolysaccharides, extracellular matrix, biofilm, macromolecular interactions, *Myxococcus xanthus*, antimicrobial resistance

INTRODUCTION

In both natural and artificial ecosystems, bacterial cells can aggregate and embed in a self-produced macromolecular extracellular matrix (ECM) to form highly organized and structured biofilms, which adhere to the biotic and abiotic surfaces or suspend in the fluid as flocs (Flemming et al., 2016; van Wolferen et al., 2018). The lifestyle of bacterial biofilms differs remarkably from their free-living style represented by the planktonic growth cells, in terms of the population characteristics of internal cells, physical and chemical properties of ECM,

and the intercellular interactions (Penesyan et al., 2021). As a self-protective survival strategy developed by prokaryotes in responding to environmental stresses (i.e., predator attack, chemical treatment, nutrient limitation, oxidative stress, hypoxia and drought, etc.; de la Fuente-Nunez et al., 2013; Gambino and Cappitelli, 2016; Gupta et al., 2016), biofilm is not only essential for the survival of bacteria under hostile conditions but also has a wide range of impacts on human life. Medical device-associated infections (Arciola et al., 2018), bacterial contaminations during food processing and storage (Galie et al., 2018), and biofouling in industrial production (Davidson et al., 2016) mainly originate from the failure of bacterial biofilm eradication. Although our increasing understanding of biofilms is rapidly changing the strategies, the control of biofilm formation and the treatment of existing biofilm are still tenuous with few options (Koo et al., 2017), and the ECM is always considered one of the most promising targets to tackle the challenges (Karygianni et al., 2020).

As a physical framework to maintain the biofilm architecture, ECM is normally a mixture of exopolysaccharides (EPS), proteins, nucleic acids, and other components, which provides diverse benefits to the cells within the biofilm, e.g., acting as a molecular glue to facilitate cell adhesion, conferring protections from different stresses, maintaining biofilm structural integrity, and allowing the establishment of nutrient and waste product gradients (Limoli et al., 2015; Karygianni et al., 2020). Moreover, there is some evidence to indicate that ECM also participates in cell-cell communications, cell migration, and genetic exchange either being freely shared with other species or being exclusive to the siblings (Dragos and Kovacs, 2017). In many bacterial biofilms, EPS and proteins are demonstrated as the key components for ECM to fulfill the functions, while extracellular DNA (eDNA) has attracted more attention owing to its biological importance (Montanaro et al., 2011; Panlilio and Rice, 2021). After the exposure to DNase I, the dissipation of *Pseudomonas aeruginosa* young biofilms suggests that eDNA acts as a structural building block in the early events of its biofilm formation (Whitchurch et al., 2002). Ever since then, the eDNA has been elucidated to be crucial in maintaining the structural integrity of ECM and in promoting bacterial biofilm development (Okshevsky et al., 2015; Panlilio and Rice, 2021). While intensive research has focused on defining the functions of eDNA (Das et al., 2013), the mechanisms underlying that eDNA integrates into the ECM network through potential macromolecular interactions remain elusive, which is critical not only to deeply understand the bacterial biofilm establishments but also to prevent and eliminate biofilm-related risks.

Myxococcus xanthus is one of the fascinating Gram-negative bacterial groups that have made the successful transition from unicellular to multicellular life (Cao et al., 2015). It has emerged as a versatile model organism in biofilm research due to its complicated lifestyles, including a nondevelopmental biofilm and a highly organized developmental biofilm (*a.k.a.* fruiting body; Jelsbak and Sogaard-Andersen, 2000; Bretl and Kirby, 2016). Within the ECM of *M. xanthus* biofilms, EPS are found to form a dense reticular network surrounding cells, connect neighboring cells to each other as well as to the surface, and constitute the basic skeleton structure of the ECM (Merroun et al., 2003; Hu et al., 2013). It has been suggested that the isolated *M. xanthus* EPS are composed of at least nine different monosaccharides, including galactose, glucosamine, glucose, rhamnose, xylose, arabinose, mannose, N-acetylglucosamine, and N-acetylmannosamine (Behmlander and Dworkin, 1994; Gibiansky et al., 2013), while the exact structure of its EPS is still unknown (Whitfield et al., 2015). According to our previous studies, both nondevelopmental and developmental biofilms formed by *M. xanthus* have been found to contain an extensive amount of eDNA (Wang et al., 2011; Hu et al., 2012a). Most intriguingly, the eDNA is shown to be closely intertwined with the EPS network and followed the same structural pattern with the EPS, which led to the obviously colocalized distributions of eDNA and EPS in *M. xanthus* biofilm ECM (Hu et al., 2012a). These findings strongly indicate the existence of macromolecular interactions between eDNA and *M. xanthus* EPS, which may drive the formation of integrated and organized ECM structures. In this study, we sought to investigate the physicochemical mechanisms and biological functions of eDNA-EPS interactions in *M. xanthus* biofilms.

MATERIALS AND METHODS

Bacterial Strains and Cultural Conditions

Myxococcus xanthus DK1622 (wild type; Kaiser, 1979), DK10547 (Welch and Kaiser, 2001), and SW504 (Δ*difA*; Yang et al., 1998) cells were routinely cultured on CTT agar (Hodgkin and Kaiser, 1977) at 30°C. The nondevelopmental and developmental biofilms were prepared as previously described (Hu et al., 2012a). Briefly, the exponential cells were collected, washed three times with MOPS buffer (10 mM Mops, 4 mM $MgSO_4$, pH 7.6), and resuspended in MOPS buffer to a final concentration of 5×10^8 cells/ml. After the incubation in eight-well chambered coverslips (Lab-Tek II Chamber Slide System, Nalge Nunc, United States) for 24 h, the nondevelopmental biofilm was observed on the bottom of the well. To grow the developmental biofilm, *M. xanthus* cells were diluted to 2.5×10^7 cells/ml in CTT medium and incubated at 30°C for 24 h. Subsequently, the medium was removed and the well was replenished with the same volume of MMC buffer (10 mM MOPS, 4 mM $MgSO_4$, 2 mM $CaCl_2$, pH 7.6). After the incubation at 30°C for 24 h, the initial developmental biofilm was obtained, and the mature developmental biofilm was observed after 48 h of incubation. If needed, a total of 200 μg/ml DNase I (Sangon Biotech, China) was added to the inoculum of *M. xanthus* and the medium to remove any eDNA during the growth of biofilms.

Confocal Laser Scanning Microscopy

The presence of EPS, eDNA/dead cells, viable cells, and cellular membrane was labeled by Alexa 350-conjugated Wheat Germ Agglutinin (WGA, excitation/emission 346 nm/442 nm), SYTOX orange (excitation/emission 547 nm/570 nm), STYO 9 (excitation/emission 480 nm/500 nm), and FM 4–64 (excitation/emission 515 nm/640 nm), respectively. All the fluorescent dyes were

purchased from Thermo Fisher Scientific (United States). The images of *M. xanthus* biofilms were acquired on an LSM 700 confocal laser scanning microscopy (CLSM; Zeiss, Germany) using a 60× oil immersion objective or a 40× objective lens. The CLSM images were captured by ZEN software (Zeiss, Germany) and exported using the ImageJ software (Rasband, 1997–2018). The statistical analysis was performed using the colocalization colormap (Jaskolski et al., 2005) and JACoP (Bolte and Cordelieres, 2006) plugins of ImageJ. The Pearson's correlation coefficient (PCC), overlap coefficients M1 and M2, and an intensity correlation quotient (ICQ) were calculated as previously described (Li et al., 2004).

Isolation of *Myxococcus xanthus* Chromosomal DNA and EPS

The chromosomal DNA of *M. xanthus* DK1622 was extracted as previously described (Avery and Kaiser, 1983). The protein and nucleic acid-free insoluble EPS (i-EPS) of DK1622 cells were isolated following the standard procedure (Chang and Dworkin, 1994; Hu et al., 2012a), and the soluble EPS (s-EPS) was purified as previously described (Gibiansky et al., 2013) with minor modifications. The sample incubation at 37°C with 200 μg/ml DNase I and RNase (Sangon Biotech, China) were carried out for 24 h to remove the DNA and RNA contaminations from EPS. The Sevag assay (Pan et al., 2019) was employed to remove the remaining proteins. The Bradford Protein Quantification Kit (Vazyme Biotech Co., ltd, China) was used to detect residual protein. The carbohydrate content of purified EPS was determined by the anthrone assay (Roe and Dailey, 1966).

DNA Precipitation by i-EPS and *Myxococcus xanthus* Cells

The chromosomal DNA was dissolved to a final concentration of 200 μg/ml in 50 mM Tris-HCl buffer (pH 7.5) containing 2 μg/ml propidium iodide (PI). After the addition of 1 mg/ml i-EPS or *M. xanthus* SW504 cells (1×10^8 cells/ml), the mixtures were extensively vortexed, stationarily incubated at 30°C for 120 min, and centrifugated at 12,000 × *g* for 10 min. The fluorescence intensity of the supernatant was measured at an excitation wavelength of 518 nm and an emission wavelength of 620 nm. Triplicate experiments were conducted.

Isothermal Titration Calorimetry

The calorimetric data of the chromosomal DNA binding to s-EPS were measured at 25°C on a MicroCal PEAQ-ITC system (Malvern Instruments, United Kingdom). The DNA and s-EPS were dissolved in the binding buffer (50 mM Tris-HCl, pH 7.5), respectively. A 300 μl aliquot of DNA solution was placed in the sample cell followed by 19 sequential titrations in 2 μl aliquot injections of s-EPS from a syringe stock solution into the sample cell. The injection interval was 150 s, and the agitation speed was set as 750 rpm. The control titration of s-EPS into the binding buffer without DNA was performed to measure the heat of mixings and dilutions, which was subtracted from the titration results with the presence of DNA. The raw data was analyzed using MicroCal PEAQ-ITC Analysis Software (Ver 1.1.01262). The data were corrected by deducting the equivalent dilution heats of control titration. The integration of the area under each peak and the deduction of the heat of dilution give the thermogram of the molecular interaction between s-EPS and DNA.

Transmission Electron Microscopy and Scanning Electron Microscopy

Chromosomal DNA solution (10 mg/L) and EPS suspension (10 mg/L) were prepared in Tris-HCl buffer (50 mM) at pH 7.6, and DNA-EPS suspension was prepared by mixing EPS and DNA solutions at a ratio of 1:1. For the transmission electron microscopy (TEM) observation, 2 μl of sample suspension was dripped onto a carbon-coated 400-mesh Ni grid (EMS, United States). After deposition for 1 min, excess water was removed by touching the edge of the grid with a filter paper, followed by adding a drop of 0.7% *w*/*v* uranyl acetate onto the grid. After washing with water three times, the grid was evaporated to dryness at room temperature. The TEM images were taken using a FEI Tecnai G2 F20 microscope (Thermo Fisher Scientific, United States) operated at 80 kV electron beam accelerating voltage in the brightfield mode. For the scanning electron microscopy (SEM) observation, the nondevelopmental biofilms were cultured on the glass coverslips (18 × 18 mm, Sangon Biotech, China). The sterilized glass coverslip was placed into the 12-well cell culture plate (NEST Biotechnology, China) and submerged in a growth medium inoculated with *M. xanthus* DK1622 cells, and DNase I was added if needed. After 24 h incubation, the biofilm samples were washed three times with PBS buffer (137 mM NaCl, 2.7 mM KCl, 10 mM Na_2HPO_4, 2 mM KH_2PO_4, pH 7.2) and subsequently fixed in 2.5% glutaraldehyde solution overnight at 4°C. The samples were prepared using a standard method for electron microscopy examination (Velicer and Yu, 2003), and observed under a QUANTA FEG250 scanning electron microscope (Thermo Fisher Scientific, United States).

Atomic Force Microscopy

Chromosomal DNA solution (10 mg/L) and EPS suspension (10 mg/L) were prepared in Tris-HCl buffer at pH 7.6, and DNA-EPS suspension was prepared by mixing EPS and DNA solutions at a ratio of 1:1. For the atomic force microscopy (AFM) observation, 10 μl aliquot of chromosomal DNA, EPS, or DNA-EPS mixture was, respectively, deposited on the surface of a clean and freshly cleaved mica disk, and air-dried at room temperature. AFM imaging was performed on the acoustic mode at 1 Hz scanning speed using a Multimode Nanoscope VIII AFM (Bruker AXS, Germany) equipped with an 80 kHz frequency silicon cantilever (NanoAndMore Corp, United States). The particle diameter and porosity were determined by using ImageJ. Briefly, an image was chosen, the threshold was adjusted to select the pore, and the pore turned red while the background remained black. Once the appropriate threshold was set, the program determined the percentage region covered by the pore to calculate the porosity. The particle diameters were measured manually. Approximately 10 microscopic fields of view were

taken from each sample, and the widths of 50 individuals were measured to calculate the mean value.

The force–separation curves were used to determine the nano-characteristics of *M. xanthus* biofilms with or without DNase I treatment. Briefly, the force–separation curves were measured using an Si3N2 MSNL cantilever (Veeco Digital Instruments, United States) with experimentally measured spring constants of 0.03 N/m and a 10 nm tip radius. The AFM tip was pressed against the surface of biofilm at room temperature with a force of less than 2 nN and subsequently retracted to determine the force–separation curves. All the force measurements were recorded at a pulling rate of 1 Hz on the contact mode.

Resonance Light Scattering Spectroscopy

The resonance light scattering (RLS) spectra of the EPS-DNA conjugates were obtained as previously described (Chen et al., 2013) with some modifications. In order to measure the spectra, the i-EPS sample was sonicated at 50 Hz for 1 h or homogenized through 20,000 rpm/min grinding to increase its solubility. The mixture of 100 μg EPS and 10 μg chromosomal DNA was suspended in 1 ml Tris-HCl buffer (pH 7.5). The solution was vortexed thoroughly and kept at room temperature for 10 min. One milliliter of the sample was added into a standard 1 cm path-length fluorescence microcuvette. The RLS spectra were recorded on a F-4600 fluorescence spectrometer (Hitachi Corp., Japan). The excitation and emission spectra were recorded in the range of 200–550 nm with synchronous scanning ($\lambda_{Ex} = \lambda_{Em}$, $\Delta\lambda = 0$ nm). Both the excitation and emission slit widths were kept at 5.0 nm. The chitosan-DNA complex was prepared according to the method from literature (Liu et al., 2005b) and used as a positive control. The pH values of suspension were adjusted from 5.5 to 7 with HCl solution or from 8 to 12.5 with NaOH solution. Different amounts of NaCl were added to the solutions to change the ionic strength for the RLS spectrum measurements.

Competitive Displacement Assay

The competitive displacement of polysaccharides for the DNA polyelectrolyte complex was conducted as previously described (Liu et al., 2005b) with minor modifications. Briefly, the chromosomal DNA and ethidium bromide (EB) were dissolved in 50 mM Tris-HCl buffer (pH 7.5) at a final concentration of 10 and 1.6 μg/ml, respectively. An aliquot chitosan (a positive control) or EPS solution was titrated into the DNA-EB solution at various concentrations and incubated at room temperature for 30 min. The fluorescence intensity of mixtures was measured on a Hitachi F-4600 fluorescence spectrometer with an excitation wavelength of 510 nm and an emission wavelength of 600 nm (Tripathy et al., 2013).

Differential Scanning Calorimetry

The differential scanning calorimetry (DSC) experiments were carried out on a VP-Capillary DSC system (GE Healthcare, United States). The chromosomal DNA was dissolved in 50 mM Tris-HCl buffer (pH 7.5) at a final concentration of 300 μg/ml supplemented with 700 μg/ml EPS or 70 μg/ml chitosan, respectively. Samples were degassed and pre-equilibrated at 4°C using a ThermoVac degassing station (GE Healthcare, United States) to minimize the formation of bubbles before loading into the syringe, sample cell, and reference cell. All samples were equilibrated at 20°C for 15 min, followed by heating from 40°C to 100°C at the scan rate of 1°C/min. The DSC thermograms of excess heat capacity versus temperature were analyzed using the Microcal, LLC ITC package for Origin version 7.0 (Origin Lab Corporation, MA).

Fourier Transform Infrared Spectroscopy

Chromosomal DNA (100 μg) was mixed with 100 μg s-EPS or i-EPS in 1 ml Tris-HCl buffer (50 mM, pH 7.5) and incubated at room temperature for 30 min. For the DNA-i-EPS complex, the pellet was collected by centrifugation at 10,000 rpm for 10 min, followed by triple washing with double distilled water to remove unbound DNA. The s-EPS-DNA and i-EPS-DNA samples were dried to form films in a vacuum at 50°C overnight. The Fourier transform infrared (FTIR) spectra were measured over 2,000–600 cm^{-1} on a Nicolet iS50 spectrophotometer (Thermo Fisher Scientific, United States).

Circular Dichroism Spectroscopy

The circular dichroism (CD) detections of chromosomal DNA (50 μg/ml) in combination with s-EPS or i-EPS at different concentrations in 50 mM Tris-HCl buffer (pH 7.5) were conducted on a Chirascan V100 spectropolarimeter (Applied Photophysics Ltd., United Kingdom) equipped with a 150 W air-cooled Xe arc lamp as the light source. The CD spectra were collected in a 10 mm length quartz cuvette within a range of 320–200 nm at 25°C. Three scans were averaged per spectrum, and the spectra were corrected by subtracting the background spectrum of buffer solution.

DNA Degradation by DNases

To investigate the protective effects of EPS on DNA, the free or i-EPS bounded chromosomal DNA was treated with 50 μg/ml of DNase I or DNase II (Sangon Biotech, China) in the reaction buffer (50 mM Tris-HCl, 10 mM $MgCl_2$, pH 7.5) at 37°C for 10 min. The residual DNA was extracted from the samples by phenol/chloroform and electrophoresed on 1.0% agarose gel at 120 V for 40 min. The gels were visualized by EB staining.

Measurement of Specific Viscosity

The intrinsic viscosity of chromosomal DNA, i-EPS, and DNA-i-EPS complex was measured using an Ubbelohde viscometer in a water bath at 25°C. The specific viscosity η_{sp} was calculated by the reported equations: $\eta_{sp} = (\eta/\eta_0) - 1 = (T/T_0) - 1$, where T_0 is the flow time of solvent and T is the flow time of tested solution (Song et al., 2009).

Susceptibility of *Myxococcus xanthus* Biofilms to the Surfactants and Antibiotics

Myxococcus xanthus DK1622 nondevelopmental biofilm was cultured in 24-well flat-bottom cell culture plates (NEST

Biotechnology, China) for 24 h as described above, and 200 μg/ml DNase I was supplemented if needed. After exposure to 2 ml MOPS buffer containing 0.1% sodium dodecyl sulfate (SDS) or 0.1% cetylpyridinium chloride (CPC) for 4 h, the suspensions were removed and the residual biofilm was rinsed twice with water by pipetting up and down. The remained biofilms were stained with 1 ml of 0.1% crystal violet solution at room temperature for 5 min. After staining, the plates were washed in slowly running tap water and dried. The bound crystal violet of each well was dissolved in 1 ml 30% acetic acid solution, and the optical density was measured at 590 nm using a microplate reader (Infinite M200 PRO, Tecan, Switzerland). The 24-h nondevelopmental biofilms of DK1622 were prepared as described above. Spectinomycin or streptomycin was added to the medium at a final concentration of 256 mg/L for 24 h, and the survived cells within the biofilms were determined by counting the colony forming unit (CFU) on CTT medium (Hu et al., 2012b). All experiments were performed in triplicate.

Susceptibility of *Myxococcus xanthus* Cells to the Extrinsically Supplied DNA

Myxococcus xanthus DK1622 or SW504 cells were inoculated in CTT medium and incubated with 200 rpm shaking at 30°C for 24 h. The cells were collected by centrifugation and were adjusted to the concentration of 5×10^8 cells/ml using CTT medium. Two milliliters of cell suspension were transferred into a 10 ml centrifuge tube containing 2 ml CTT medium supplemented with 0.5% (*w*/*v*) calf thymus DNA (Sigma-Aldrich, United States), followed by shaking at 200 rpm and 30°C for 36 h. At different time points, the cell density was measured by detecting the optical density at 600 nm. The number of living cells was determined by CFU counting.

Statistical Analysis

Unless indicated otherwise, SPSS 23.0 software (SPSS Inc., United States) was used for statistical analysis in the current study. All experiments were conducted at least in triplicate. Quantitative data were expressed as mean ± standard deviation. The Student's *t*-test was utilized for statistical contrast.

RESULTS

The Colocalization of eDNA and EPS Reveals Their Close Interactions in the ECM of Both Nondevelopmental and Developmental *Myxococcus xanthus* Biofilms

A nondevelopmental and two developmental (24-h and 48-h) DK1622 biofilms were systematically investigated *in situ* using specific indicator dyes combined with confocal laser scanning microscopy. The viable DK1622 cells with intact membranes were visualized by STYO 9 in green, eDNA and dead cells were stained as red by SYTOX orange, and EPS was revealed in blue using Alexa 350-conjugated WGA. Consistent with the previous observations (Hu et al., 2012a), the red fluorescence presents both dot-like and smeared patterns in nondevelopmental and 24 h-developmental biofilms, while relatively well-organized red structures are revealed in the 48 h-developmental biofilms (**Supplementary Figure S1**). In the merged panels of **Supplementary Figure S1**, purple signals are observed as a result of the overlay of blue and red fluorescence. To gain further insight into the colocalization between red and blue signals, a superior visual representation of the spatial description of pixel overlaps and relative intensity was performed by a colormap. As shown in **Figure 1A** (upper panel), the hot colors represent a positive correlation, while the cold colors represent a negative correlation. By calculating the M1, M2, PCC, and ICQ values, the observed colocalization was further quantified (**Figure 1A**, lower panel). The M1 coefficient represents the fraction of the red signal colocalized with the blue, and the M2 reflects the fraction of the blue that colocalized with the red. In all native structures (without DNase I), a high level of M1 indicates that a large proportion of the red signals coincides with the blue, while the smaller M2 coefficient suggests a wider distribution of the blue signals compared to that of the red. The PCC and ICQ values describe the correlation of the intensity distribution between the blue and red. The former ranges from −1 (perfect negative correlation) to +1 (perfect positive correlation), and zero means no significant correlation (Dunn et al., 2011). The latter ranges from −0.5 (complete segregation) to 0.5 (complete colocalization), and zero means randomness (Bolte and Cordelieres, 2006). The results show that the red (eDNA) and blue (EPS) signals exhibit a positive colocalization, and most of eDNA coexist with EPS in *M. xanthus* biofilms.

After exposure to DNase I, the red signal in DK1622 biofilms decreases due to the degradation of eDNA, while the green and blue signals that represent live cells and EPS are not affected (**Supplementary Figure S1**). Statistical analysis confirms a significant reduction of the fluorescence pixel ratio of red versus blue (red/blue) after the addition of DNase I (**Figure 1B**). It is also observed in **Supplementary Figure S1** that only the smeared red signals are disappeared, while most of the dot-like signals remain intact after DNase I treatment. The nucleic acid molecules located in dead cells might be stained as red dots and not susceptible to DNase I digestion. To prove this, the nondevelopmental biofilms formed by *M. xanthus* DK10547 (a *gfp*-expressing derivative of DK1622) were stained with SYTOX orange and membrane-specific dye FM 4-64 (**Figure 1C**). After DNase I treatments, the detected SYTOX orange signals (red) only exhibit in dotted form encircled by FM 4-64 (blue) labeled membrane, indicating that the smeared red signals came from the eDNA rather than chromosomal DNA in dead or membrane-damaged cells. Furthermore, DNase I remarkably reduces the M2 ($p < 0.001$) but not M1 values in the tested biofilms (**Figure 1A**), which also supports that most SYTOX orange-stained structures are eDNA. As shown above, eDNA follows a similar pattern of spatial distribution with EPS to participate in the building of *M. xanthus* biofilms, which indicates the potential chemical interactions between these two

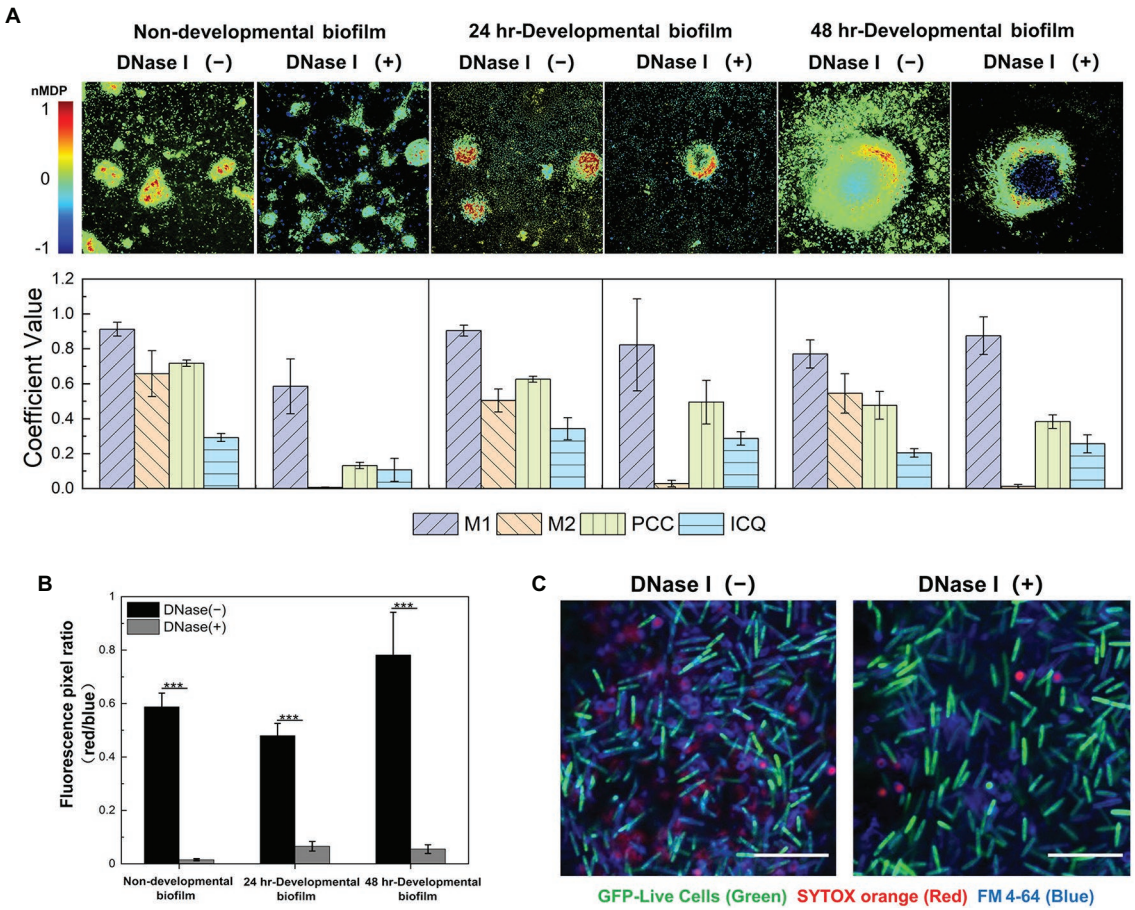

FIGURE 1 | eDNA colocalizes with exopolysaccharides (EPS) in the extracellular matrix (ECM) of both non-developmental and developmental *Myxococcus xanthus* biofilms. **(A)** Quantitative colocalization analysis of the STYOX orange and Alexa 350-conjugated WGA fluorescent signals. The colocalization colormap is shown in the upper panel. The hot color represents a positive correlation, and the cold color represents a negative correlation. Further color divisions within groups are indicated by the color scale bar. In the lower panel, the histogram was generated from the calculated colocalization coefficient (M1 and M2), Pearson's correlation coefficient (PCC), and an intensity correlation quotient (ICQ; $n = 5$). **(B)** The fluorescence pixel ratio (red/blue) of the samples with/without DNase I treatment. The significance was determined by Student's *t*-test ($n = 5$; $^{***}p < 0.001$). **(C)** The non-developmental biofilm (24 h) formed by *Myxococcus xanthus* DK10547 (live cells, GFP-green) was stained with SYTOX orange (eDNA and dead cells, red) and FM 4-64 (cell membrane, blue). Scale bars represent 20 μm.

macromolecules mediate and dominate the construction of a complex ECM network.

Myxococcus xanthus EPS and DNA Interact With Each Other to Form a Macromolecular Conjugate *in vitro*

The purified DNA and EPS from *M. xanthus* DK1622 were employed to investigate the potential DNA-EPS interactions. Due to the interference by EPS, the isolation of a large amount of eDNA from DK1622 biofilms was unsuccessful (data not shown). Considering the possible origin of eDNA and our previous results (Hu et al., 2012a), DK1622 chromosomal DNA was prepared to conduct the subsequent experiments. Both the insoluble EPS (i-EPS) and soluble EPS (s-EPS) were purified from DK1622 cells, and the potential nucleic acid contamination was eliminated by an excessive treatment using nucleic acid hydrolases.

According to the different solubility of i-EPS and s-EPS, a precipitation assay and an isothermal titration calorimetry (ITC) analysis were, respectively, employed to investigate their binding abilities with the chromosomal DNA. In the precipitation assay, a red fluorescent dye PI was used to bind and track the DNA molecules. In order to increase the precipitation of i-EPS, the EPS deficient mutant SW504 cells were added into the solution, which was capable of binding with i-EPS (Hu et al., 2011). As shown in **Figure 2A**, after centrifugation, SW504 cells are not able to pull down DNA from the solution, while they are co-precipitated with i-EPS and DNA, which results in a dramatic decrease of fluorescence signal in the supernatant ($p < 0.001$). The affinity of s-EPS for DNA was determined by an ITC assay, and a representative result is shown in **Figure 2B**. The observed enthalpy change of DNA and s-EPS interaction is in the range of −0.95 to −0.35 kcal/mol and free energy change (ΔG) is −5.43 kcal/mol, which indicates a binding of s-EPS to DNA. The raw corresponding heat evolution curves are

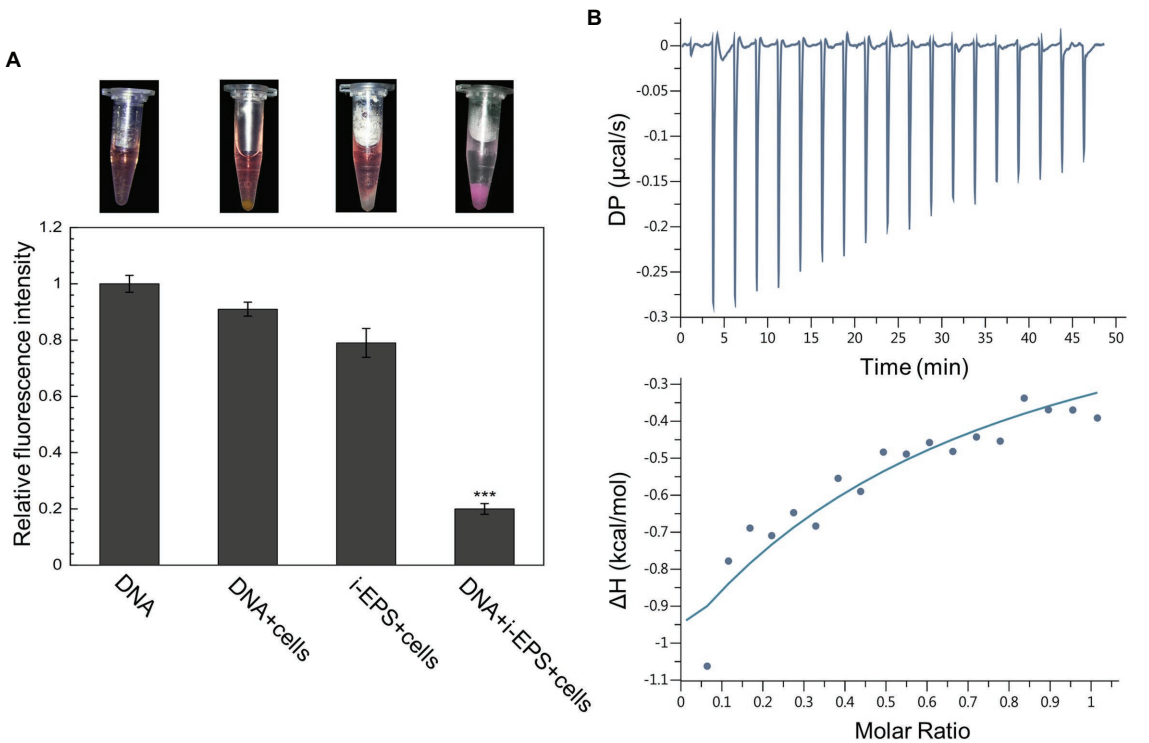

FIGURE 2 | DNA interacts with both i- and s-EPS of *Myxococcus xanthus in vitro*. **(A)** Result of the precipitation assay. The representative photograph of the sample after centrifugation is shown in the upper panel. The fluorescence intensity of the supernatant was measured at an excitation wavelength of 518 nm and an emission wavelength of 620 nm (lower panel; $n = 3$; $^{***}p < 0.001$). **(B)** Isothermal titration calorimetry (ITC) profile for the titration of s-EPS with DNA. The upper panel represents the raw data for the sequential injections of s-EPS into DNA solution, and the lower panel shows the integrated and dilution-corrected data peak area plotting of the titration data.

caused by the thermal changes during the combination of DNA and s-EPS. The sharp negative peak produced after each individual injection indicates that the process is an obvious exothermic interaction. With the increasing concentration of s-EPS, the amount of released heat decreases gradually, which indicates that the binding sites on DNA are progressively saturated by s-EPS.

Ultrastructure of EPS-DNA conjugates was revealed by transmission electron microscopy (**Figure 3A**). s-EPS forms spherical nano-aggregates with an average radius of 16.80 ± 4.32 nm ($n = 50$), and i-EPS forms both spherical and short rope-shaped aggregates. The rope structures are fairly homogeneous in diameter from 11.03 to 39.16 nm, while variates in length from 85.33 to 1,067.21 nm ($n = 50$). In the DNA + s-EPS sample, smeared patch-shaped aggregates are observed, which is apparently different from the observation on DNA or s-EPS sample. In the DNA + i-EPS sample, strand-like structures are observed, which is different from the i-EPS sample while similar to the shape of DNA. However, the diameter of the DNA + i-EPS strand (20 ± 9.71 nm, $n = 50$) is significantly larger than that of the DNA strand (9.88 ± 3.86 nm, $n = 50$; $p < 0.001$). Interestingly, the DNA + i-EPS structures observed in our study partially resembles the ultrastructure of *M. xanthus* ECM (named as fibrils at that time) previously revealed using scanning electron microscopy (Behmlander and Dworkin, 1994), which suggests that the self-building of ECM network by *M. xanthus* cells follows the similar construction rules of DNA-EPS conjugation *in vitro*.

Due to the fixation process of sample preparation, one question that emerged from the electron microscopy of the conjugates was whether the structures observed by TEM accurately reflected the nature of the DNA-EPS complex. Therefore, the samples were further visualized using atomic force microscopy. As shown in **Figure 3B**, the individual DNA fragment is filamented, and the individual i-EPS or s-EPS appear as reticular structures. These observations are consistent with the previous findings that many polysaccharides exist as a network structure in an aqueous environment while as a clump or patch-like structure after dehydration (Reese and Guggenheim, 2007; Robic et al., 2009). In the DNA + s-EPS sample, not only the strands become much thicker than those of the DNA or s-EPS sample (**Figure 3C**), but also some clump-shaped aggregates are observed (**Figure 3B**). In the DNA + i-EPS sample, more dense reticular structures (**Figure 3B**) formed by thicker strands (**Figure 3C**) are revealed. The porosity of the AFM ultrastructure was quantified using the contrast analysis of ImageJ software. The compactness of the DNA-EPS complex structures is significantly higher than that of DNA or EPS samples (**Figure 3D**), indicating that the conjugation of DNA and EPS results in the formation of larger aggregates. These results demonstrate that *M. xanthus* EPS and

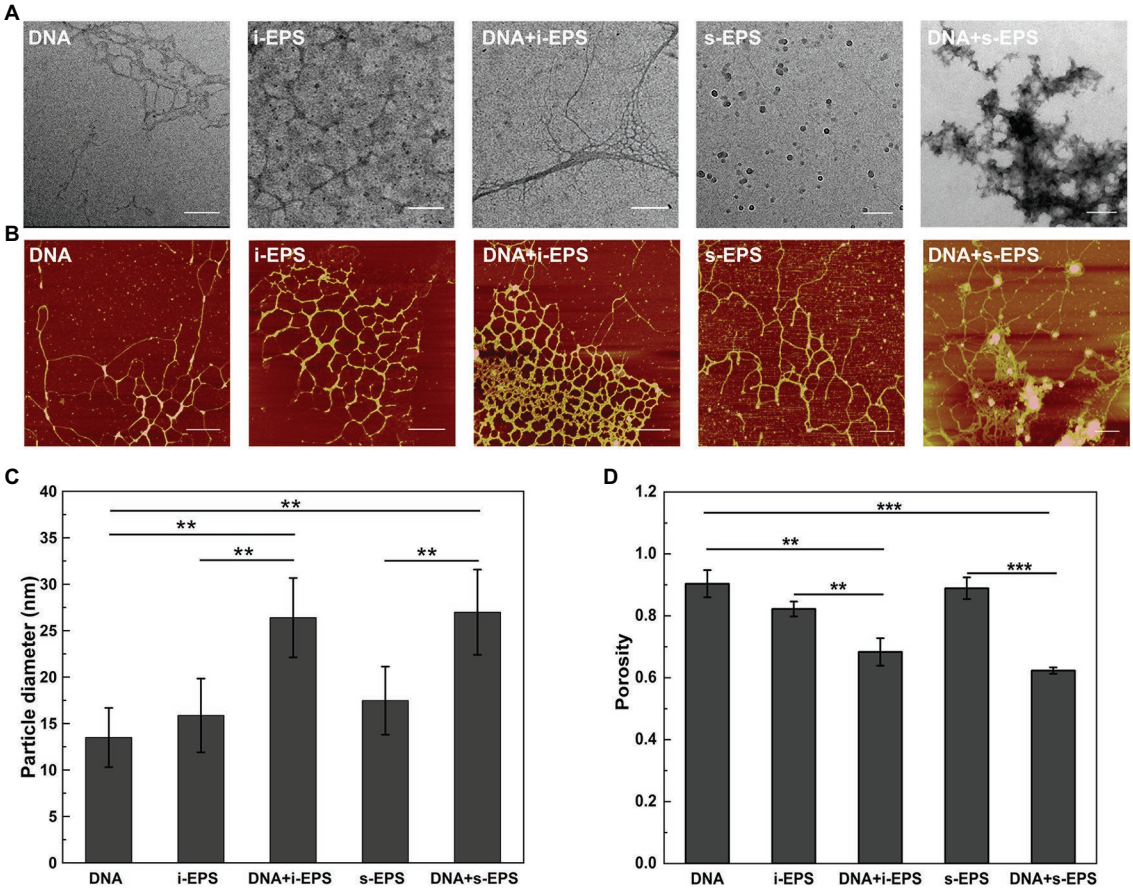

FIGURE 3 | Visualization of the DNA, exopolysaccharides (EPS), and DNA-EPS complex. Representative TEM **(A)** and atomic force microscopy (AFM; **B**) observations of *Myxococcus xanthus* chromosomal DNA (DNA), insoluble EPS (i-EPS), DNA-insoluble EPS complex (DNA + i-EPS), soluble EPS (s-EPS), and DNA-soluble EPS complex (DNA + s-EPS). Scale bars represent 200 nm in **(A)** and 500 nm in **(B)**. The particle diameter of the aggregates **(C)** and the porosity of the molecules **(D)** observed by atomic force microscopy (AFM) were measured by ImageJ software ($n = 20$; $^{**}p < 0.01$; $^{***}p < 0.001$).

DNA interact with each other to form a macromolecular conjugate *in vitro*.

Electrostatic Force Plays an Essential Role in the DNA-EPS Interactions

To reveal the chemical nature of DNA-EPS interactions, the resonance light scattering spectra of chromosomal DNA, EPS, and DNA-EPS conjugates were measured. As previously reported (Murphy, 1997; Liu et al., 2005a), when two macromolecules bind as a complex, the light scattering intensity of the formed larger particles or aggregates will theoretically increase and positively correlate with the particle size. Chitosan was used as a positive control in the experiment due to its great ability to form conjugates with DNA molecules (Liu et al., 2005b; Bravo-Anaya et al., 2016). As expected, the light scattering intensity of the DNA-chitosan complex is remarkably higher than that of DNA or chitosan (**Figure 4A**). Similarly, all EPS samples show weak light scattering signals over the wavelength range of 200–550 nm. When DNA is mixed with s-EPS or the pre-treated i-EPS, the light scattering intensity is enhanced, indicating the interaction between DNA and EPS molecules (**Figures 4B–D**). There are three types of weak forces involved in the interactions among macromolecules within bacterial ECM, i.e., dispersion forces, electrostatic interactions, and hydrogen bonds (Mayer et al., 1999). A variety of studies have well demonstrated that the DNA is a polyanion and forms complex with positively charged chitosan through electrostatic interactions in the natural environment (Agudelo et al., 2016; Bravo-Anaya et al., 2016). Similar to the N-acetyl-glucosamine and glucosamine monomer units composed in the chitosan (Cao et al., 2006), the glucosamine identified in the *M. xanthus* EPS (Behmlander and Dworkin, 1994) probably contributes the cationic moieties of EPS to interact with the negatively charged DNA. To test this hypothesis, the difference between the light scattering intensity at 398 nm (ΔI_{LS}) of homogenized i-EPS sample and DNA + homogenized i-EPS complex was measured in the solutions with different pH or ionic strength. As shown in **Figure 4E**, the light scattering intensity of the DNA-EPS complex is changed according to the pH of the solution and reaches the maximum pH of 7.5. Under extremely high or low pH, the decreased ΔI_{LS} value possibly results from the disturbance of the DNA-EPS combination. The influence of ionic strength on the formation of the DNA-EPS complex was further

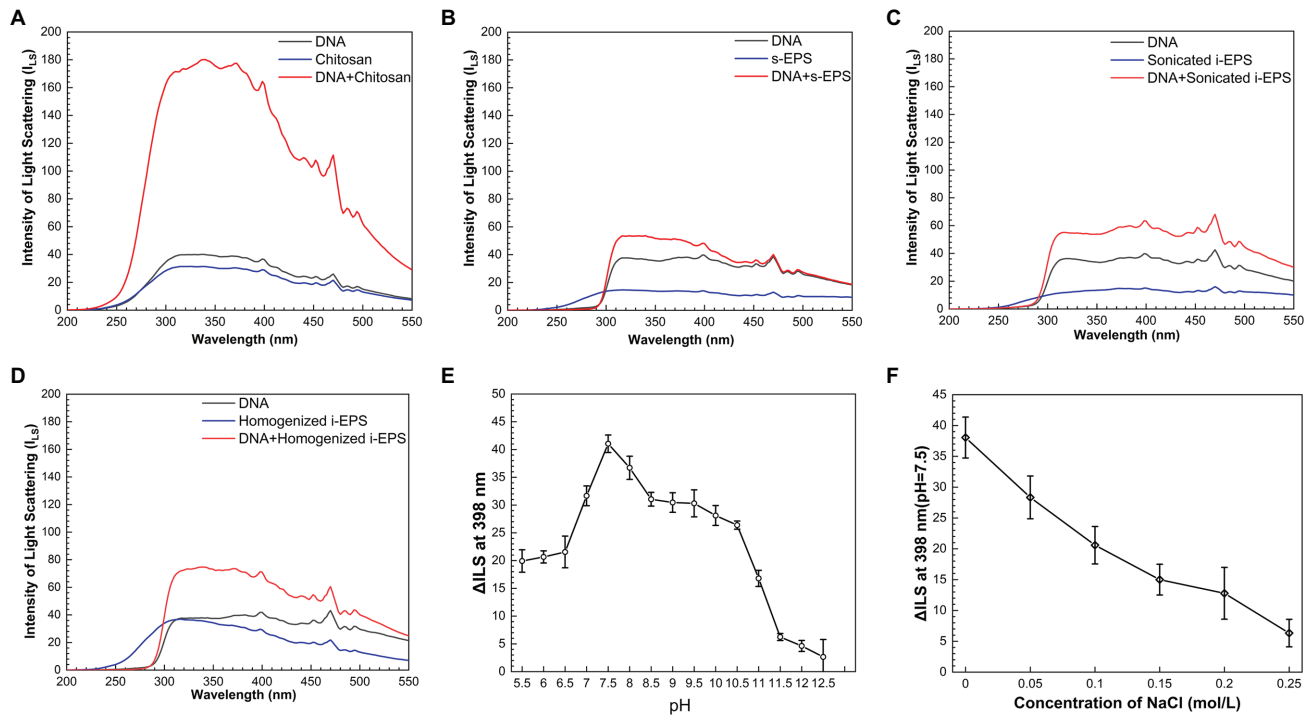

FIGURE 4 | Resonance light-scattering analysis of the interaction between DNA and exopolysaccharides (EPS). The light scattering spectra of chitosan **(A)**, s-EPS **(B)**, sonicated i-EPS **(C)**, homogenized i-EPS **(D)**, and their complex with DNA were detected by fluorescence spectrometer with synchronous scanning in the range of 200–550 nm. The effects of different pH **(E)** and NaCl concentrations **(F)** on the changed value of light scattering spectra intensity (ΔI_{LS}) of DNA-homogenized i-EPS complex were measured at 398 nm ($n = 3$). I_{LS}, the intensity of light scattering.

studied by observing the change of ΔI_{LS} through the addition of NaCl into the solution. With the increased concentration of NaCl, ΔI_{LS} value decreases linearly (**Figure 4F**), which is likely due to the addition of sodium ions attenuating the electrostatic interaction between DNA and EPS by competition for phosphate groups on the DNA molecules. These observations correspond to the previous reports that the stability of the chitosan-DNA complex depends on the degree of protonation of chitosan (relating to pH) and the external salt concentration (Bravo-Anaya et al., 2019).

As a fluorescent probe, EB remarkably increases its fluorescent intensity after inserting into DNA molecule (Kabir and Kumar, 2014), which is used in the competitive displacement assay to determine the binding affinity of the biomolecules to DNA (Liu et al., 2005b). Consistent with the previous finding (Liu et al., 2005b), the fluorescence intensity of the EB-DNA complex significantly decreases after the addition of chitosan (**Figure 5Aa**). Similarly, when i-EPS or s-EPS is added, the fluorescence intensity decreases gradually according to the EPS concentration (**Figures 5Ab,c**), indicating that *M. xanthus* EPS is able to compete for the DNA-binding sites and replace EB from the EB-DNA complex. Moreover, the observed efficiency of EPS (at 30 μg/ml) displacement for EB is only 20–30%, while that of chitosan at 30 μg/ml reaches approximately 70%, suggesting the potential differences between the binding of chitosan-DNA and EPS-DNA. It has been demonstrated that there are two binding modes between EB and DNA, i.e., intercalation binding and electrostatic binding (Vardevanyan et al., 2016). Intercalation occurs due to stacking contact with base pairs, which stabilizes the DNA double helix structure and causes its melting temperature (Tm) to increase by about 5–8°C. Meanwhile, the electrostatic interaction with negatively charged phosphates of DNA will not cause an obvious increase of the Tm (Sun et al., 2008). Therefore, the differential scanning calorimetry assay was used to determine Tm values of DNA-chitosan and DNA-EPS conjugates. The Tm of DNA increases from 77.87°C to 85.71°C with the presence of 70 μg/ml chitosan (**Figure 5Ba**), while the Tm value remains at approximately 78°C after the addition of 700 μg/ml i-EPS or s-EPS, respectively (**Figures 5Bb,c**). To further verify this observation, the conformation of DNA molecules in the DNA-EPS conjugate was determined.

DNA Remains B-Type Conformation in the DNA-EPS Complex

The Fourier transform infrared spectra of chromosomal DNA, i-EPS, s-EPS, and DNA-EPS complexes were determined (**Figure 6**). In the spectra, the vibrational bands of DNA at 1,604, 1,644, 1,689, and 1,485 cm^{-1} are assigned to adenine (A), thymine (T), guanine (G), and cytosine (C) nitrogenous bases, respectively. The DNA adopts B-type conformation suggested by the phosphoryl ester bond at 1,232 cm^{-1} and the 2′-deoxyribose at 961 cm^{-1}. The band observed at 1,631 cm^{-1} (s-EPS) or 1,640 cm^{-1} (i-EPS) is assigned to the NH_2 scissoring vibration, and the characteristic band of carbonyl asymmetric stretching vibration exhibits at 1,549 cm^{-1} (s-EPS) or 1,550 cm^{-1} (i-EPS). The pyranose ring

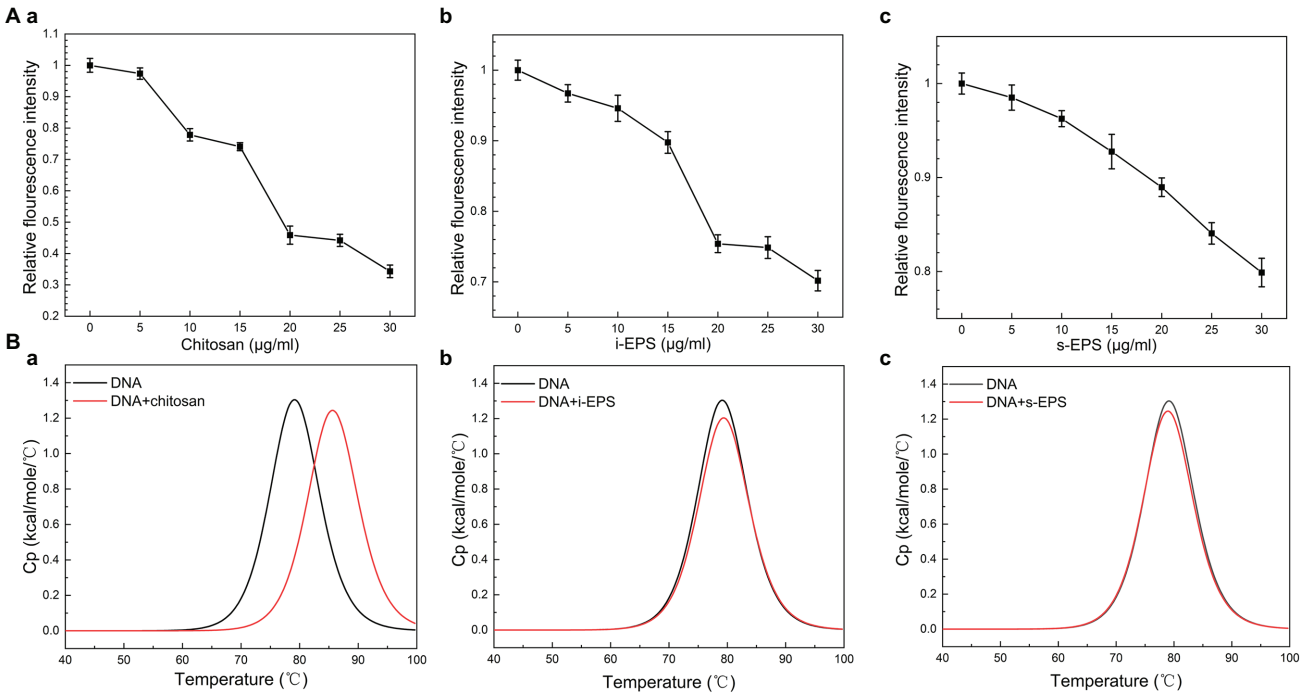

FIGURE 5 | The role of electrostatic force in the DNA-EPS interactions. **(A)** Competitive displacement of EB bond to DNA by chitosan (a), i-EPS (b), and s-EPS (c) at pH 7.5. The fluorescence intensity was monitored using an excitation and emission wavelength of 510 and 600 nm. **(B)** Differential scanning calorimetry (DSC) curves for thermal melting of DNA in the presence of chitosan (a), i-EPS (b), and s-EPS (c). The DSC melting data was generated by subtracting the buffer response and normalized to the concentration of DNA.

(890 cm^{-1}) of s-EPS or i-EPS is still discernable in the presence of DNA, revealing the formation of the complexes. Compared with the spectrum of DNA, the vibration bands of both DNA + s-EPS and DNA + i-EPS conjugates remain nearly unchanged, suggesting that the B-type conformation of DNA is maintained in the complexes. This conclusion is also supported by the measurement of circular dichroism (CD) spectra (**Supplementary Figure S2**). DNA appears in a typical B conformation with the base pair perpendicular to the double helix axis. The positive band at ~277 nm is due to base stacking, while the negative band at ~243 nm is due to helicity (Agarwal et al., 2013; Rehman et al., 2015), which are sensitive to the interactions between ligand and DNA (Zhao et al., 2014). As the ratio of EPS to DNA increased, no significant changes are observed both in the positive and negative bands of DNA. Based on these findings, it is concluded that *M. xanthus* EPS binds with DNA to form a complex without changing DNA's B-type conformation.

Myxococcus xanthus EPS Protects the DNA in the EPS-DNA Complex From the Digestion by DNA Hydrolases

As shown above, there is a considerable amount of eDNA stably presented in *M. xanthus* biofilms, while *M. xanthus*, as a predatory bacterium, secrets a large number of DNA hydrolases extracellularly (Evans et al., 2012). In order to understand this paradox, the DNA degradations by DNases with or without *M. xanthus* i-EPS were determined. After the treatment with DNase I or DNase II, residual DNA was extracted from the i-EPS-DNA complex using phenol/chloroform and detected by gel electrophoresis. As shown in **Figure 7A**, the chromosomal DNA without i-EPS is completely digested by DNase I (Lane 2 and 4). In the presence of a sufficient amount of i-EPS, the undegraded chromosomal DNA is detected (Lane 6), which is not due to any eDNA contamination in the isolated i-EPS sample (Lane 7), indicating that i-EPS is able to prevent DNA digestion by DNase I in a concentration-dependent manner. Similar results were obtained from the DNase II degradation experiment (**Figure 7B**). Small DNA fragments resulting from DNase II digestion of chromosomal DNA are revealed in the absence (lane 5) or in the presence of low concentrations of i-EPS (Lanes 1–3). Despite slight degradation, a high concentration (1,000 μg/ml) of i-EPS prevents DNA degradation by DNase II (Lane 4). These results suggest that, in *M. xanthus* EPS-DNA complexes, the protection by EPS confers DNA resistance to the self-produced nucleic acid hydrolases by cells, which leads to the continuous and stable existence of eDNA in the *M. xanthus* biofilm ECM.

DNA-EPS Complex Increases the Nanomechanical Strength of *Myxococcus xanthus* ECM

It is necessary for ECM to reach a certain viscosity and cohesiveness during the initial process of biofilm formation, which is essential to fulfilling its functions in cell adhesion and matrix formation (Verstraeten et al., 2008). The specific viscosity of chromosomal

DNA, i-EPS, and DNA-i-EPS complex was measured, respectively. As shown in **Figure 8A**, *M. xanthus* i-EPS produces a relatively high-viscosity aqueous suspension at the tested concentration,

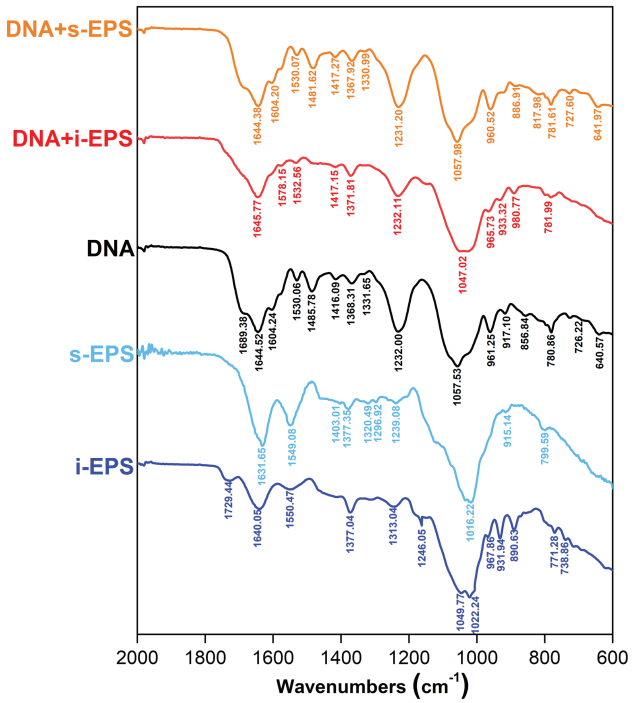

FIGURE 6 | Fourier transform infrared (FTIR) spectra of DNA, exopolysaccharides (EPS), and DNA-EPS complex. The spectrum was collected in the range of 2,000–600 cm^{-1}. i-EPS, insoluble EPS; s-EPS, soluble EPS; DNA + i-EPS, complex of DNA and insoluble EPS; DNA + s-EPS, complex of DNA and soluble EPS.

and DNA-i-EPS conjugate exhibits significantly higher specific viscosity ($p < 0.001$), which might be due to the complex molecular interactions between DNA and i-EPS. Under scanning electron microscopy (SEM; **Figure 8B**), DK1622 cells in the native nondevelopmental biofilm are surrounded by the dense ECM. After the removal of eDNA by DNase I, no significant changes in the morphology of DK1622 cells are revealed, while more cells are exposed out of a slightly damaged ECM. This observation is confirmed by the AFM images (**Figure 8C**, right panels). Therefore, the nanomechanical properties of the two biofilms ECM were further investigated by determination of force–separation curves using the AFM. As shown in **Figure 8C** (left panels), compared with the DNase I-treated ECM, more adhesion events arising from the breakage are observed between the tip of cantilever and native ECM. The adhesive events of the native sample usually stop when the tip retraction length reaches approximately 1 μm, while the DNase I-treated sample shows an extended retraction length of approximately 2–4 μm (**Figure 8C**). Meanwhile, the average adhesion force between the native biofilm and the tip is significantly higher than that of the DNase I-treated biofilm (**Figure 8D**).

The eDNA in ECM Is Critical for the Stress Resistance of *Myxococcus xanthus* Cells

Chemical disruptions are practical approaches to remove and prevent bacterial biofilms attaching to solid surfaces, where the surfactants are commonly employed (Simoes et al., 2005). As shown in **Figure 9A**, the cationic surfactant cetylpyridinium chloride (CPC) exhibits a higher efficiency (~60%) in the removal of DK1622 nondevelopmental biofilm than the anionic surfactant sodium dodecyl sulfate (SDS, ~5%). Compared with the native biofilm, the CPC and SDS treatments exhibit a more significant removal efficiency in the biofilm without eDNA in the ECM,

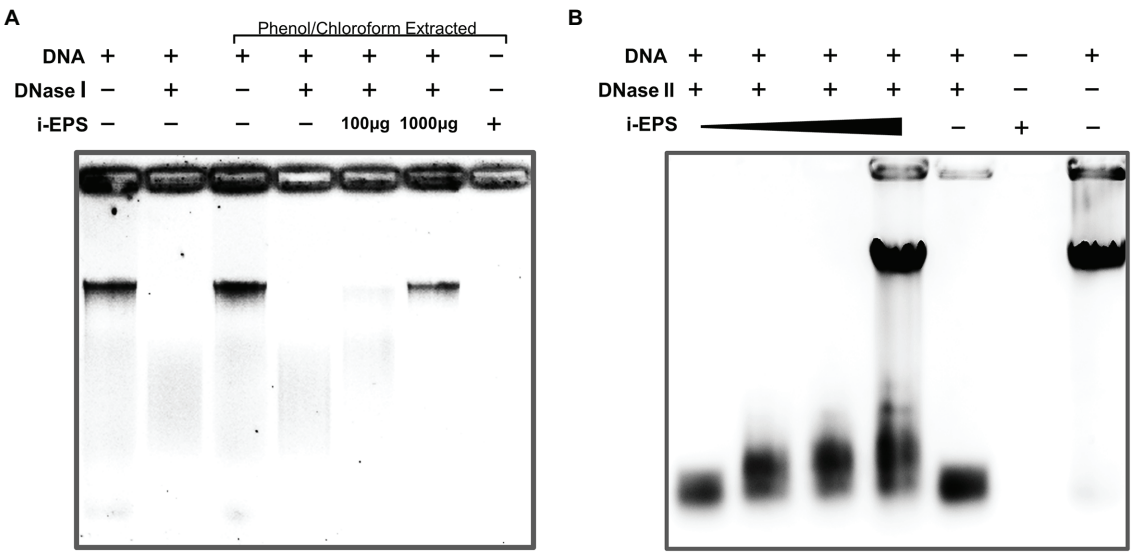

FIGURE 7 | Electrophoretic profile of digested DNA by DNase I **(A)** and DNase II **(B)** in the presence (+) and absence (–) of i-EPS. The DNA was electrophoresed on a 1.0% agarose gel. The gels were stained with EB and photographed under UV light with a gel documentation system. Images of stained DNA fragments were black/white inverted for a better observation.

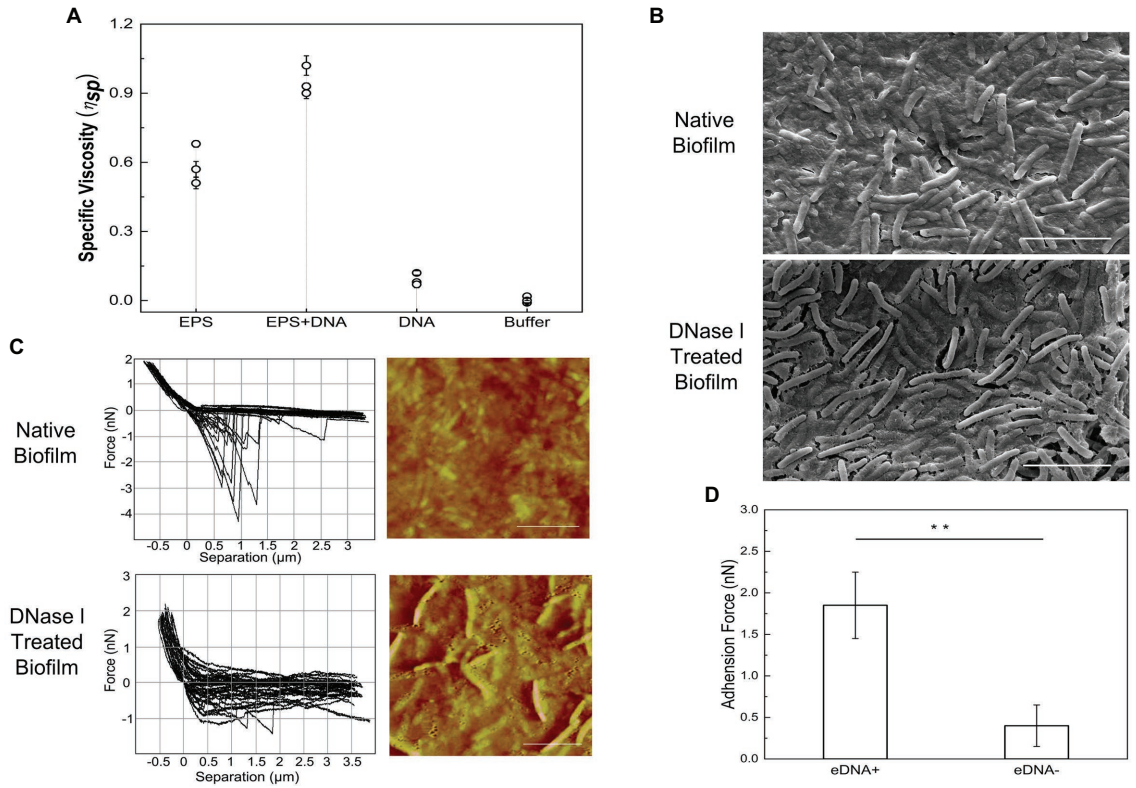

FIGURE 8 | Nanomechanical strength of DNA-EPS complex. **(A)** Specific viscosity of DNA, exopolysaccharides (EPS) and DNA-EPS complex. **(B)** SEM images of native (upper panel) or DNase I treated (lower panel) *Myxococcus xanthus* DK1622 biofilms. Scale bars represent 5 μm. **(C)** Representative force curves and atomic force microscopy (AFM) images of native (upper panel) or DNase I treated (lower panel) *Myxococcus xanthus* DK1622 biofilms. Scale bars represent 5 μm. **(D)** The average adhesion force between extracellular matrix (ECM) with (+) or without (–) eDNA and the tip of AFM cantilever. $^{**}p < 0.01$.

ranging to 77 and 8%, respectively. This result suggested that the polyanion DNA molecules trapped in the ECM by interaction with EPS play important roles in resisting the treatment of surfactants, especially for cationic chemicals. Furthermore, the susceptibilities of *M. xanthus* biofilms to cationic antibiotics in the presence or absence of DNA were determined. Streptomycin and spectinomycin are cationic aminoglycosides capable of killing planktonic *M. xanthus* DK1622 cells (Magrini et al., 1998) at the concentrations used in the experiment. As shown in **Figure 9B**, the killing percentage of DK1622 cells in the native biofilm is approximate 42% for spectinomycin and 55% for streptomycin, which becomes more evident in the presence of DNase I, especially for the streptomycin treatment (~80%).

Moreover, it has been shown that eDNA at a final concentration of 0.5% (*w*/*v*) definitely inhibits the growth of *P. aeruginosa* planktonic cells (Mulcahy et al., 2008). When 0.5% calf thymus DNA was supplied in the CTT medium, the growth of wild-type *M. xanthus* DK1622 cells is not affected compared with the cells in the medium without DNA supplement (**Supplementary Figure S3**). This observation can be explained by the fact that EPS on the cell surface conjugates with DNA and prevents its further bactericidal effect. To test the hypothesis, the EPS deficient mutant SW504 cells were cultured in the medium with or without supplied DNA. Unexpectedly, both the cell concentration and live cell number of SW504 slightly increased after incubation for 12 h in the medium with 0.5% DNA (**Figure 10**). Furthermore, compared to cells in the DNA-free medium, SW504 is able to grow and reach a significantly higher cell concentration in the CTT medium with DNA, which has been observed in some other bacterial species (Mulcahy et al., 2010; Chimileski et al., 2014; Gumpenberger et al., 2016; McDonough et al., 2016). Similar results were obtained when DNA was added in the medium to a higher concentration than 0.5% (data not shown). These results suggest that the EPS deficient *M. xanthus* cells are not only insusceptible to extrinsic DNA but also capable of utilizing the DNA as a nutrient to support their growth.

DISCUSSION

The focus on the investigation of some model bacteria has revealed that the formation of biofilm is a complex process with multiple factors, and the interactions among ECM components are essential for the adaptive structures in the process of adhesion, maturation and dispersion (Hobley et al., 2015; Payne and Boles, 2016). It is necessary to understand the complexity of macromolecular interactions within biofilms, which will provide a rationale for multi-targeted treatments to either prevent the initiation of biofilms or disrupt mature biofilms (Koo et al., 2017).

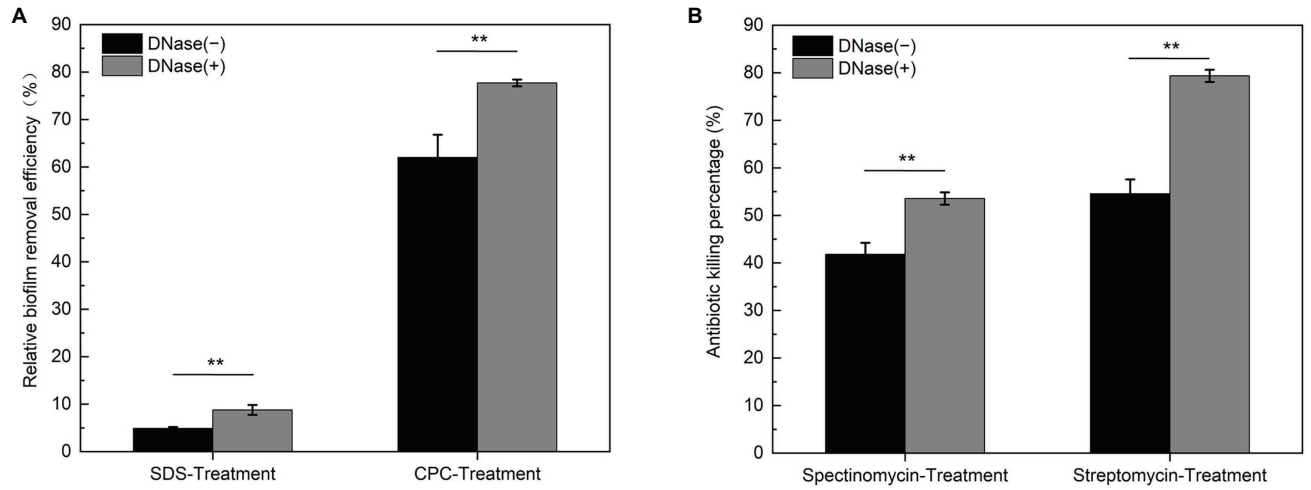

FIGURE 9 | Susceptibility of native and DNase I treated *Myxococcus xanthus* biofilms to the surfactants and antibiotics. The native (DNase I–) and DNase I treated (DNase I+) DK1622 non-developmental biofilms were prepared. **(A)** The relative biofilm removal efficiency was quantified by crystal violet stain after SDS or CPC treatment, respectively. **(B)** The killing percentage by streptomycin and spectinomycin to the cells within biofilms was determined by colony forming unit (CFU) counting, respectively. $^{**}p < 0.01$.

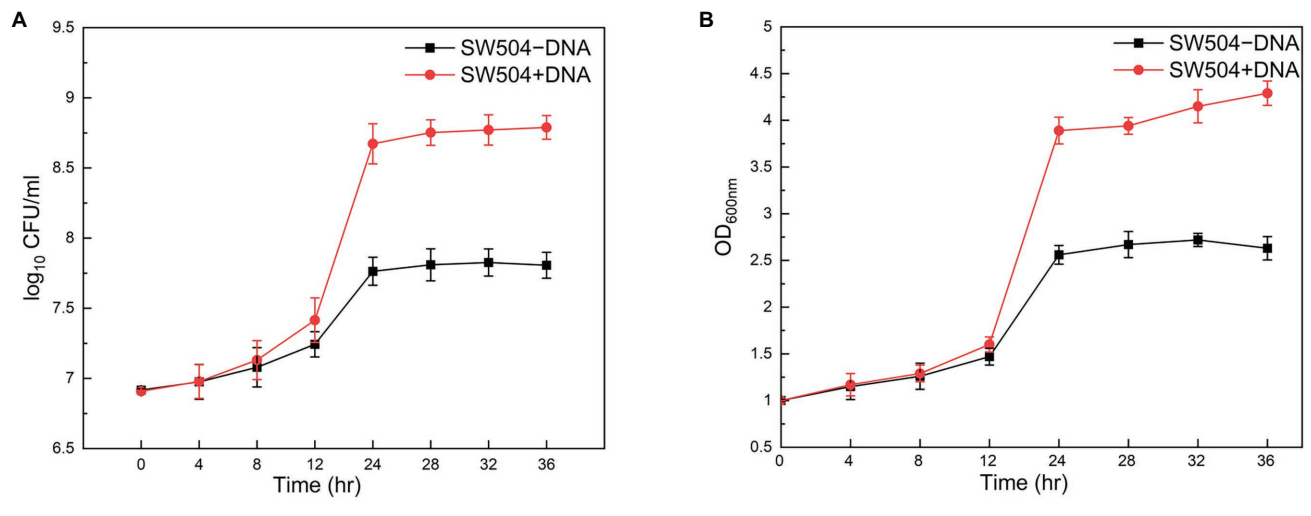

FIGURE 10 | Susceptibility of *Myxococcus xanthus* SW504 cells to the extrinsically supplied DNA. Growth curves of *Myxococcus xanthus* SW504 cells in the CTT medium supplemented with (+) or without (–) 0.5% (*w*/*v*) calf thymus DNA were plotted by measuring the optical density at 600 nm **(A)** and colony forming unit (CFU) counting **(B)**.

Bacteria are able to produce eDNA through different specific mechanisms, e.g., cell autolysis, active secretion, and association with the membrane vesicles (de Aldecoa et al., 2017). Prolific outer-membrane vesicles have been observed in the *M. xanthus* biofilms (Evans et al., 2012), which contain a complex mixture of lipids, carbohydrates, secondary metabolites, and proteins, but not nucleic acids (Berleman et al., 2014; Remis et al., 2014). The coexistence of dead cells and eDNA in the same *M. xanthus* biofilm structure suggests that cell lysis is at least one of the major sources for eDNA production, which is supported by the previous findings that extensive programmed cell death events occur during the starvation-induced *M. xanthus* developmental process (Sogaard-Andersen and Yang, 2008). While abundant eDNA is found to present a well-organized structure similar in appearance to *M. xanthus* EPS organization, the potential molecular interactions between eDNA and EPS are still unknown (Hu et al., 2012a). In this study, the co-distribution of eDNA and EPS in the ECM of *M. xanthus* nondevelopmental and developmental biofilms was proved to be attributed to their direct interactions, which allows eDNA to combine with EPS to form a macromolecular conjugate. Complexing with DNA, *M. xanthus* EPS forms a cohesive, dense, and mechanically strong framework to facilitate the initial cell

adhesion and subsequent ECM architecture construction during the biofilm formation process. Due to technical problems in isolation of enough amount of eDNA from *M. xanthus* biofilms, it is reasonable to use DK1622 chromosomal DNA as a substitute for eDNA to conduct the *in vitro* experiments considering the most possible origin of its eDNA. Moreover, small sized commercial salmon sperm DNA has been shown to bind with *M. xanthus* EPS *in vitro* (Hu et al., 2012a), which resembles the observations in current study. It is suggested that the interactions between eDNA and *M. xanthus* EPS are independent of the size and source of DNA. In a multispecies microbial community, this nonspecific EPS-DNA binding facilitates *M. xanthus* cells to absorb the eDNA from other bacteria and environment to grow its own biofilm, which may be one of the reasons that myxobacteria are a ubiquitous group of microorganisms living in very diverse habitats.

Our results demonstrate that, as a potential analogue of chitosan, *M. xanthus* EPS binds to DNA through electrostatic interactions, and the stability of the EPS-DNA complex is significantly influenced by environmental pH and ion concentration. The smaller light scattering intensity of the EPS-DNA conjugate compared with that of the chitosan-DNA complex implies the relatively lower affinity between EPS and DNA, which is supported by the results of EB competitive displacement assay. Consistently, the intercalated interaction is not detected between DNA and EPS by the measurement of Tm values using DSC, while it plays an important role in the combination of chitosan with DNA (Liu et al., 2005b). The unchanged Tm value and B-type conformation of DNA after complexing with EPS demonstrate the lack of insertion mode within their interactions, which is also due to the weaker binding between DNA-EPS. Among the polymer-polymer interactions, the electrostatic forces dominate DNA-EPS complex formation in *M. xanthus* ECM, and the relatively weaker interactions exhibit a certain degree of reversibility. It has been reported that EPS blocks the plasmid transformation in *M. xanthus* (Wang et al., 2011), and the sufficient EPS produced by wild-type cells reduces the local concentration of plasmid DNA to access the cell surface. Our findings explain that *M. xanthus* becomes naturally transformable when the EPS production is dramatically down-regulated or the cells are grown under specific conditions (Wang et al., 2011).

Several studies have shown that DNA could be a nutrition source for bacterial cells (Mulcahy et al., 2010; Chimileski et al., 2014; Gumpenberger et al., 2016; McDonough et al., 2016). As we have shown above, EPS deficient *M. xanthus* cells (like SW504) are capable of utilizing the DNA to support their growth, while the same phenomenon has not been observed in the wild type strain DK1622. As a predatory bacterium, *M. xanthus* can produce a large number of nucleases to hydrolyze the DNA released from the prey for self-growth (Evans et al., 2012), which is contradictory to the fact that abundant eDNA exists in the *M. xanthus* ECM. After elucidating the interactions between EPS and eDNA, it is proposed that *M. xanthus* cells with sufficient EPS are covered by EPS-eDNA complexed ECM, and EPS not only protects eDNA from the nuclease degradation but also prevents the utilizing of eDNA by the cells. Under the conditions of poor nutrition, *M. xanthus* lacks enough energy and materials to synthesize large amounts of EPS, which provides the possibility for wild-type strain to use DNA as nutrition. Indeed, within the starvation induced nondevelopmental biofilm, *M. xanthus* cells with less EPS occasionally disperse from the top of the structure and colonize to a new surface, in that case, eDNA is able to support their subsequent activities. In the developmental biofilms, myxospores are released from the mature fruiting bodies and germinate to produce EPS-free vegetative cells in a favorable environment, where the eDNA is also used as a source to provide nutrition. These results imply that the precisely regulated EPS production is important for *M. xanthus* cells to use eDNA either as a structural component for biofilm establishment or as a nutrient for cell growth.

In *M. xanthus* biofilms, the integrated DNA-EPS matrix confers cells stress resistances against certain surfactant and antibiotic treatments, suggesting that the presence of eDNA and its interaction with EPS is highly relevant to the survival of *M. xanthus* in hostile environments. Consistent with the findings in some pathogenic bacteria, eDNA enhances the resistance of their biofilms to aminoglycoside (Wilton et al., 2016) and glycopeptide antibiotics (Doroshenko et al., 2014). For many established cases, DNase treatment serves important functions in dispersing biofilm and increasing cell susceptibility to biocides and antibiotics by removal of eDNA. Therefore, eDNA is regarded as an promising target for biofilm control through the combination of DNase and drugs therapy, and a better understanding of molecular mechanisms involving eDNA interactions with EPS will help to treat and prevent hospital-derived microbial biofilm infections.

CONCLUSION

This study elucidates the physicochemical mechanism and biological functions of the eDNA-EPS interactions in *M. xanthus* biofilms. Under CLSM, abundant eDNA possibly released from the lysed dead cells exhibits a spatial structure similar to the *M. xanthus* EPS organization in the biofilms. This co-distribution of eDNA and EPS is on account of their direct interactions, which allows EPS to combine with eDNA to form a macromolecular conjugate. It is also demonstrated that the electrostatic forces participating in the polymer-polymer interactions dominate the DNA-EPS complex formation in *M. xanthus* ECM. Due to the lack of intercalation by EPS, the binding ability of DNA-EPS is relatively weaker than that of DNA-chitosan, and DNA remains its B-type conformation in DNA-EPS conjugate, which endows a certain degree of reversibility for the complex. Acting as a cohesive, dense, and mechanically strong network, the eDNA-EPS complex facilitates the initial cell adhesion and subsequent ECM architecture establishment, and renders cells within biofilms stress resistances relevant to the survival of *M. xanthus* in some hostile environments, e.g., the presence of surfactants and cationic

antibiotics, and nutrient limitation. Furthermore, in the DNA-EPS complex, the protection by EPS confers DNA resistance to the degradations by self-produced nucleic acid hydrolases, which leads to the continuous and stable existence of eDNA in *M. xanthus* ECM. As a potential target for microbial biofilm control, a better understanding of interactions between eDNA and other ECM components will shed light on developing novel prevention and treatment strategies against biofilm-associated risks.

DATA AVAILABILITY STATEMENT

The original contributions presented in the study are included in the article/**Supplementary Material**, further inquiries can be directed to the corresponding authors.

AUTHOR CONTRIBUTIONS

YaW, TL, WX, and YZe performed the experiments. YiW, NZ, and YZa analyzed the experimental results. JW and YL provided resources. YaW and CW wrote the manuscript. CW and WH revised the manuscript. JW, CW, and WH provided financial support. All authors contributed to the article and approved the submitted version.

FUNDING

This research was funded by National Key R&D Program of China (2021YFC2101000, to WH), National Natural Science Foundation of China (32070100, to WH), Taishan Industry Leading Talent Program (Tscy20200334, to WH), China Postdoctoral Science Foundation (2020M672048, to CW), Shandong Provincial Natural Science Foundation (ZR2021MC082, to JW, ZR2021QC087, to CW), and Science and Technology Planning Project of Traditional Chinese Medicine of Shandong Province (2019-0027, to JW).

ACKNOWLEDGMENTS

The authors would like to thank Xiaoju Li and Zhifeng Li from State Key Laboratory of Microbial Technology (Shandong University) for the technical assistance in electron microscopy, isothermal titration calorimetry, and differential scanning calorimetry experiments.

SUPPLEMENTARY MATERIAL

The Supplementary Material for this article can be found online at: https://www.frontiersin.org/articles/10.3389/fmicb.2022.861865/full#supplementary-material

REFERENCES

Agarwal, S., Jangir, D. K., and Mehrotra, R. (2013). Spectroscopic studies of the effects of anticancer drug mitoxantrone interaction with calf-thymus DNA. *J. Photochem. Photobiol. B* 120, 177–182. doi: 10.1016/j.jphotobiol.2012.11.001

Agudelo, D., Kreplak, L., and Tajmir-Riahi, H. A. (2016). Microscopic and spectroscopic analysis of chitosan-DNA conjugates. *Carbohydr. Polym.* 137, 207–213. doi: 10.1016/j.carbpol.2015.09.080

Arciola, C. R., Campoccia, D., and Montanaro, L. (2018). Implant infections: adhesion, biofilm formation and immune evasion. *Nat. Rev. Microbiol.* 16, 397–409. doi: 10.1038/s41579-018-0019-y

Avery, L., and Kaiser, D. (1983). Construction of tandem genetic duplications with defined endpoints in *Myxococcus xanthus*. *Mol. Gen. Genet.* 191, 110–117. doi: 10.1007/BF00330897

Behmlander, R. M., and Dworkin, M. (1994). Biochemical and structural-analyses of the extracellular-matrix fibrils of *Myxococcus xanthus*. *J. Bacteriol.* 176, 6295–6303. doi: 10.1128/jb.176.20.6295-6303.1994

Berleman, J. E., Allen, S., Danielewicz, M. A., Remis, J. P., Gorur, A., Cunha, J., et al. (2014). The lethal cargo of *Myxococcus xanthus* outer membrane vesicles. *Front. Microbiol.* 5:474. doi: 10.3389/fmicb.2014.00474

Bolte, S., and Cordelieres, F. P. (2006). A guided tour into subcellular colocalization analysis in light microscopy. *J. Microsc.* 224, 213–232. doi: 10.1111/j.1365-2818.2006.01706.x

Bravo-Anaya, L. M., Fernandez-Solis, K. G., Rosselgong, J., Nano-Rodriguez, J. L. E., Carvajal, F., and Rinaudo, M. (2019). Chitosan-DNA polyelectrolyte complex: influence of chitosan characteristics and mechanism of complex formation. *Int. J. Biol. Macromol.* 126, 1037–1049. doi: 10.1016/j.ijbiomac.2019.01.008

Bravo-Anaya, L. M., Soltero, J. F., and Rinaudo, M. (2016). DNA/chitosan electrostatic complex. *Int. J. Biol. Macromol.* 88, 345–353. doi: 10.1016/j.ijbiomac.2016.03.035

Bretl, D. J., and Kirby, J. R. (2016). Molecular mechanisms of signaling in *Myxococcus xanthus* development. *J. Mol. Biol.* 428, 3805–3830. doi: 10.1016/j.jmb.2016.07.008

Cao, P. B., Dey, A., Vassallo, C. N., and Wall, D. (2015). How Myxobacteria cooperate. *J. Mol. Biol.* 427, 3709–3721. doi: 10.1016/j.jmb.2015.07.022

Cao, W. D., Easley, C. J., Ferrance, J. P., and Landers, J. P. (2006). Chitosan as a polymer for pH-induced DNA capture in a totally aqueous system. *Anal. Chem.* 78, 7222–7228. doi: 10.1021/ac060391l

Chang, B. Y., and Dworkin, M. (1994). Isolated fibrils rescue cohesion and development in the dsp mutant of *Myxococcus xanthus*. *J. Bacteriol.* 176, 7190–7196. doi: 10.1128/jb.176.23.7190-7196.1994

Chen, Z. G., Wang, Z., Chen, X., Xu, H. X., and Liu, J. B. (2013). Chitosan-capped gold nanoparticles for selective and colorimetric sensing of heparin. *J. Nanopart. Res.* 15:1930. doi: 10.1007/s11051-013-1930-9

Chimileski, S., Dolas, K., Naor, A., Gophna, U., and Papke, R. T. (2014). Extracellular DNA metabolism in *Haloferax volcanii*. *Front. Microbiol.* 5:57. doi: 10.3389/fmicb.2014.00057

Das, T., Sehar, S., and Manefield, M. (2013). The roles of extracellular DNA in the structural integrity of extracellular polymeric substance and bacterial biofilm development. *Environ. Microbiol. Rep.* 5, 778–786. doi: 10.1111/1758-2229.12085

Davidson, I., Scianni, C., Hewitt, C., Everett, R., Holm, E., Tamburri, M., et al. (2016). Mini-review: assessing the drivers of ship biofouling management – aligning industry and biosecurity goals. *Biofouling* 32, 411–428. doi: 10.1080/08927014.2016.1149572

de Aldecoa, A. L. I., Zafra, O., and Gonzalez-Pastor, J. E. (2017). Mechanisms and regulation of extracellular dna release and its biological roles in microbial communities. *Front. Microbiol.* 8:1390. doi: 10.3389/fmicb.2017.01390

de la Fuente-Nunez, C., Reffuveille, F., Fernandez, L., and Hancock, R. E. W. (2013). Bacterial biofilm development as a multicellular adaptation: antibiotic resistance and new therapeutic strategies. *Curr. Opin. Microbiol.* 16, 580–589. doi: 10.1016/j.mib.2013.06.013

Doroshenko, N., Tseng, B. S., Howlin, R. P., Deacon, J., Wharton, J. A., Thurner, P. J., et al. (2014). Extracellular DNA impedes the transport of vancomycin in *Staphylococcus epidermidis* biofilms preexposed to subinhibitory concentrations of vancomycin. *Antimicrob. Agents Chemother.* 58, 7273–7282. doi: 10.1128/AAC.03132-14

Dragos, A., and Kovacs, A. T. (2017). The peculiar functions of the bacterial extracellular matrix. *Trends Microbiol.* 25, 257–266. doi: 10.1016/j.tim.2016.12.010

Dunn, K. W., Kamocka, M. M., and McDonald, J. H. (2011). A practical guide to evaluating colocalization in biological microscopy. *Am. J. Physiol. Cell Physiol.* 300, C723–C742. doi: 10.1152/ajpcell.00462.2010

Evans, A. G. L., Davey, H. M., Cookson, A., Currinn, H., Cooke-Fox, G., Stanczyk, P. J., et al. (2012). Predatory activity of *Myxococcus xanthus* outer-membrane vesicles and properties of their hydrolase cargo. *Microbiology* 158, 2742–2752. doi: 10.1099/mic.0.060343-0

Flemming, H. C., Wingender, J., Szewzyk, U., Steinberg, P., Rice, S. A., and Kjelleberg, S. (2016). Biofilms: an emergent form of bacterial life. *Nat. Rev. Microbiol.* 14, 563–575. doi: 10.1038/nrmicro.2016.94

Galie, S., Garcia-Gutierrez, C., Miguelez, E. M., Villar, C. J., and Lombo, F. (2018). Biofilms in the food industry: health aspects and control methods. *Front. Microbiol.* 9:898. doi: 10.3389/fmicb.2018.00898

Gambino, M., and Cappitelli, F. (2016). Mini-review: biofilm responses to oxidative stress. *Biofouling* 32, 167–178. doi: 10.1080/08927014.2015.1134515

Gibiansky, M. L., Hu, W., Dahmen, K. A., Shi, W. Y., and Wong, G. C. L. (2013). Earthquake-like dynamics in *Myxococcus xanthus* social motility. *Proc. Natl. Acad. Sci. U. S. A.* 110, 2330–2335. doi: 10.1073/pnas.1215089110

Gumpenberger, T., Vorkapic, D., Zingl, F. G., Pressler, K., Lackner, S., Seper, A., et al. (2016). Nucleoside uptake in *Vibrio cholerae* and its role in the transition fitness from host to environment. *Mol. Microbiol.* 99, 470–483. doi: 10.1111/mmi.13143

Gupta, P., Sarkar, S., Das, B., Bhattacharjee, S., and Tribedi, P. (2016). Biofilm, pathogenesis and prevention-a journey to break the wall: a review. *Arch. Microbiol.* 198, 1–15. doi: 10.1007/s00203-015-1148-6

Hobley, L., Harkins, C., MacPhee, C. E., and Stanley-Wall, N. R. (2015). Giving structure to the biofilm matrix: an overview of individual strategies and emerging common themes. *FEMS Microbiol. Rev.* 39, 649–669. doi: 10.1093/femsre/fuv015

Hodgkin, J., and Kaiser, D. (1977). Cell-to-cell stimulation of movement in nonmotile mutants of *Myxococcus*. *Proc. Natl. Acad. Sci. U. S. A.* 74, 2938–2942. doi: 10.1073/pnas.74.7.2938

Hu, W., Hossain, M., Lux, R., Wang, J., Yang, Z., Li, Y., et al. (2011). Exopolysaccharide-independent social motility of *Myxococcus xanthus*. *PLoS One* 6:e16102. doi: 10.1371/journal.pone.0016102

Hu, W., Li, L. N., Sharma, S., Wang, J., McHardy, I., Lux, R., et al. (2012a). DNA builds and strengthens the extracellular matrix in *Myxococcus xanthus* biofilms by interacting with exopolysaccharides. *PLoS One* 7:e51905. doi: 10.1371/journal.pone.0051905

Hu, W., Lux, R., and Shi, W. (2013). Analysis of exopolysaccharides in *Myxococcus xanthus* using confocal laser scanning microscopy. *Methods Mol. Biol.* 966, 121–131. doi: 10.1007/978-1-62703-245-2_8

Hu, W., Wang, J., McHardy, I., Lux, R., Yang, Z., Li, Y. Z., et al. (2012b). Effects of exopolysaccharide production on liquid vegetative growth, stress survival, and stationary phase recovery in *Myxococcus xanthus*. *J. Microbiol.* 50, 241–248. doi: 10.1007/s12275-012-1349-5

Jaskolski, F., Mulle, C., and Manzoni, O. J. (2005). An automated method to quantify and visualize colocalized fluorescent signals. *J. Neurosci. Methods* 146, 42–49. doi: 10.1016/j.jneumeth.2005.01.012

Jelsbak, L., and Sogaard-Andersen, L. (2000). Pattern formation: fruiting body morphogenesis in *Myxococcus xanthus*. *Curr. Opin. Microbiol.* 3, 637–642. doi: 10.1016/S1369-5274(00)00153-3

Kabir, A., and Kumar, G. S. (2014). Probing the interaction of spermine and 1-naphthyl acetyl spermine with DNA polynucleotides: a comparative biophysical and thermodynamic investigation. *Mol. BioSyst.* 10, 1172–1183. doi: 10.1039/C3MB70616H

Kaiser, D. (1979). Social gliding is correlated with the presence of pili in *Myxococcus xanthus*. *Proc. Natl. Acad. Sci. U. S. A.* 76, 5952–5956. doi: 10.1073/pnas.76.11.5952

Karygianni, L., Ren, Z., Koo, H., and Thurnheer, T. (2020). Biofilm matrixome: extracellular components in structured microbial communities. *Trends Microbiol.* 28, 668–681. doi: 10.1016/j.tim.2020.03.016

Koo, H., Allan, R. N., Howlin, R. P., Stoodley, P., and Hall-Stoodley, L. (2017). Targeting microbial biofilms: current and prospective therapeutic strategies. *Nat. Rev. Microbiol.* 15, 740–755. doi: 10.1038/nrmicro.2017.99

Li, Q., Lau, A., Morris, T. J., Guo, L., Fordyce, C. B., and Stanley, E. F. (2004). A syntaxin 1, G alpha(o), and N-type calcium channel complex at a presynaptic nerve terminal: analysis by quantitative immunocolocalization. *J. Neurosci.* 24, 4070–4081. doi: 10.1523/JNEUROSCI.0346-04.2004

Limoli, D. H., Jones, C. J., and Wozniak, D. J. (2015). Bacterial extracellular polysaccharides in biofilm formation and function. *Microbiol. Spectr.* 3:MB-0011-2014. doi: 10.1128/microbiolspec.MB-0011-2014

Liu, W., Cellmer, T., Keerl, D., Prausnitz, J. M., and Blanch, H. W. (2005a). Interactions of lysozyme in guanidinium chloride solutions from static and dynamic light-scattering measurements. *Biotechnol. Bioeng.* 90, 482–490. doi: 10.1002/bit.20442

Liu, W. G., Sun, S. J., Cao, Z. Q., Xin, Z., Yao, K. D., Lu, W. W., et al. (2005b). An investigation on the physicochemical properties of chitosan/DNA polyelectrolyte complexes. *Biomaterials* 26, 2705–2711. doi: 10.1016/j.biomaterials.2004.07.038

Magrini, V., Creighton, C., White, D., Hartzell, P. L., and Youderian, P. (1998). The *aadA* gene of plasmid R100 confers resistance to spectinomycin and streptomycin in *Myxococcus xanthus*. *J. Bacteriol.* 180, 6757–6760. doi: 10.1128/JB.180.24.6757-6760.1998

Mayer, C., Moritz, R., Kirschner, C., Borchard, W., Maibaum, R., Wingender, J., et al. (1999). The role of intermolecular interactions: studies on model systems for bacterial biofilms. *Int. J. Biol. Macromol.* 26, 3–16. doi: 10.1016/S0141-8130(99)00057-4

McDonough, E., Kamp, H., and Camilli, A. (2016). *Vibrio cholerae* phosphatases required for the utilization of nucleotides and extracellular DNA as phosphate sources. *Mol. Microbiol.* 99, 453–469. doi: 10.1111/mmi.13128

Merroun, M. L., Ben Chekroun, K., Arias, J. M., and Gonzalez-Munoz, M. T. (2003). Lanthanum fixation by *Myxococcus xanthus*: cellular location and extracellular polysaccharide observation. *Chemosphere* 52, 113–120. doi: 10.1016/S0045-6535(03)00220-0

Montanaro, L., Poggi, A., Visai, L., Ravaioli, S., Campoccia, D., Speziale, P., et al. (2011). Extracellular DNA in biofilms. *Int. J. Artif. Organs* 34, 824–831. doi: 10.5301/ijao.5000051

Mulcahy, H., Charron-Mazenod, L., and Lewenza, S. (2008). Extracellular dna chelates cations and induces antibiotic resistance in *Pseudomonas aeruginosa* biofilms. *PLoS Pathog.* 4:e1000213. doi: 10.1371/journal.ppat.1000213

Mulcahy, H., Charron-Mazenod, L., and Lewenza, S. (2010). *Pseudomonas aeruginosa* produces an extracellular deoxyribonuclease that is required for utilization of DNA as a nutrient source. *Environ. Microbiol.* 12, 1621–1629. doi: 10.1111/j.1462-2920.2010.02208.x

Murphy, R. M. (1997). Static and dynamic light scattering of biological macromolecules: what can we learn? *Curr. Opin. Biotechnol.* 8, 25–30. doi: 10.1016/S0958-1669(97)80153-X

Okshevsky, M., Regina, V. R., and Meyer, R. L. (2015). Extracellular DNA as a target for biofilm control. *Curr. Opin. Biotechnol.* 33, 73–80. doi: 10.1016/j.copbio.2014.12.002

Pan, F., Hou, K., Li, D. D., Su, T. J., and Wu, W. (2019). Exopolysaccharides from the fungal endophytic *Fusarium* sp. A14 isolated from *Fritillaria unibracteata* Hsiao et KC Hsia and their antioxidant and antiproliferation effects. *J. Biosci. Bioeng.* 127, 231–240. doi: 10.1016/j.jbiosc.2018.07.023

Panlilio, H., and Rice, C. V. (2021). The role of extracellular DNA in the formation, architecture, stability, and treatment of bacterial biofilms. *Biotechnol. Bioeng.* 118, 2129–2141. doi: 10.1002/bit.27760

Payne, D. E., and Boles, B. R. (2016). Emerging interactions between matrix components during biofilm development. *Curr. Genet.* 62, 137–141. doi: 10.1007/s00294-015-0527-5

Penesyan, A., Paulsen, I. T., Kjelleberg, S., and Gillings, M. R. (2021). Three faces of biofilms: a microbial lifestyle, a nascent multicellular organism, and an incubator for diversity. *NPJ Biofilms Microbiomes* 7:80. doi: 10.1038/s41522-021-00251-2

Rasband, W. S. (1997–2018). *ImageJ [Online]*. Bethesda, Maryland, USA: U. S. National Institutes of Health. Available at: https://imagej.nih.gov/ij/ (Accessed September 28, 2021).

Reese, S., and Guggenheim, B. (2007). A novel TEM contrasting technique for extracellular polysaccharides in in vitro biofilms. *Microsc. Res. Tech.* 70, 816–822. doi: 10.1002/jemt.20471

Rehman, S. U., Sarwar, T., Husain, M. A., Ishqi, H. M., and Tabish, M. (2015). Studying non-covalent drug-DNA interactions. *Arch. Biochem. Biophys.* 576, 49–60. doi: 10.1016/j.abb.2015.03.024

Remis, J. P., Wei, D. G., Gorur, A., Zemla, M., Haraga, J., Allen, S., et al. (2014). Bacterial social networks: structure and composition of *Myxococcus xanthus* outer membrane vesicle chains. *Environ. Microbiol.* 16, 598–610. doi: 10.1111/1462-2920.12187

Robic, A., Gaillard, C., Sassi, J. F., Lerat, Y., and Lahaye, M. (2009). Ultrastructure of ulvan: a polysaccharide from green seaweeds. *Biopolymers* 91, 652–664. doi: 10.1002/bip.21195

Roe, J. H., and Dailey, R. E. (1966). Determination of glycogen with the anthrone reagent. *Anal. Biochem.* 15, 245–250. doi: 10.1016/0003-2697(66)90028-5

Simoes, M., Pereira, M. O., and Vieira, M. J. (2005). Effect of mechanical stress on biofilms challenged by different chemicals. *Water Res.* 39, 5142–5152. doi: 10.1016/j.watres.2005.09.028

Sogaard-Andersen, L., and Yang, Z. M. (2008). Programmed cell death: role for MazF and MrpC in *Myxococcus* multicellular development. *Curr. Biol.* 18, R337–R339. doi: 10.1016/j.cub.2008.02.060

Song, B. F., Zhang, W., Peng, R., Huang, J., Me, T., Li, Y., et al. (2009). Synthesis and cell activity of novel galactosylated chitosan as a gene carrier. *Colloid Surf. B Biointerfaces* 70, 181–186. doi: 10.1016/j.colsurfb.2008.12.018

Sun, Y. T., Bi, S. Y., Song, D. Q., Qiao, C. Y., Mu, D., and Zhang, H. Q. (2008). Study on the interaction mechanism between DNA and the main active components in *Scutellaria baicalensis* Georgi. *Sens. Actuator B Chem.* 129, 799–810. doi: 10.1016/j.snb.2007.09.082

Tripathy, D. R., Dinda, A. K., and Dasgupta, S. (2013). A simple assay for the ribonuclease activity of ribonucleases in the presence of ethidium bromide. *Anal. Biochem.* 437, 126–129. doi: 10.1016/j.ab.2013.03.005

van Wolferen, M., Orell, A., and Albers, S. V. (2018). Archaeal biofilm formation. *Nat. Rev. Microbiol.* 16, 699–713. doi: 10.1038/s41579-018-0058-4

Vardevanyan, P. O., Antonyan, A. P., Parsadanyan, M. A., Torosyan, M. A., and Karapetian, A. T. (2016). Joint interaction of ethidium bromide and methylene blue with DNA. The effect of ionic strength on binding thermodynamic parameters. *J. Biomol. Struct. Dyn.* 34, 1377–1382. doi: 10.1080/07391102.2015.1079557

Velicer, G. J., and Yu, Y. T. (2003). Evolution of novel cooperative swarming in the bacterium *Myxococcus xanthus*. *Nature* 425, 75–78. doi: 10.1038/nature01908

Verstraeten, N., Braeken, K., Debkumari, B., Fauvart, M., Fransaer, J., Vermant, J., et al. (2008). Living on a surface: swarming and biofilm formation. *Trends Microbiol.* 16, 496–506. doi: 10.1016/j.tim.2008.07.004

Wang, J., Hu, W., Lux, R., He, X. S., Li, Y. Z., and Shi, W. Y. (2011). Natural transformation of *Myxococcus xanthus*. *J. Bacteriol.* 193, 2122–2132. doi: 10.1128/JB.00041-11

Welch, R., and Kaiser, D. (2001). Cell behavior in traveling wave patterns of myxobacteria. *Proc. Natl. Acad. Sci. U. S. A.* 98, 14907–14912. doi: 10.1073/pnas.261574598

Whitchurch, C. B., Tolker-Nielsen, T., Ragas, P. C., and Mattick, J. S. (2002). Extracellular DNA required for bacterial biofilm formation. *Science* 295:1487. doi: 10.1126/science.295.5559.1487

Whitfield, G. B., Marmont, L. S., and Howell, P. L. (2015). Enzymatic modifications of exopolysaccharides enhance bacterial persistence. *Front. Microbiol.* 6:471. doi: 10.3389/fmicb.2015.00471

Wilton, M., Charron-Mazenod, L., Moore, R., and Lewenza, S. (2016). Extracellular DNA acidifies biofilms and induces aminoglycoside resistance in *Pseudomonas aeruginosa*. *Antimicrob. Agents Chemother.* 60, 544–553. doi: 10.1128/AAC.01650-15

Yang, Z. M., Geng, Y. Z., Xu, D., Kaplan, H. B., and Shi, W. Y. (1998). A new set of chemotaxis homologues is essential for *Myxococcus xanthus* social motility. *Mol. Microbiol.* 30, 1123–1130. doi: 10.1046/j.1365-2958.1998.01160.x

Zhao, T., Bi, S., Wang, Y., Wang, T., Pang, B., and Gu, T. (2014). In vitro studies on the behavior of salmeterol xinafoate and its interaction with calf thymus DNA by multi-spectroscopic techniques. *Spectrochim. Acta A Mol. Biomol. Spectrosc.* 132, 198–204. doi: 10.1016/j.saa.2014.04.158

Conflict of Interest: The authors declare that the research was conducted in the absence of any commercial or financial relationships that could be construed as a potential conflict of interest.

Publisher's Note: All claims expressed in this article are solely those of the authors and do not necessarily represent those of their affiliated organizations, or those of the publisher, the editors and the reviewers. Any product that may be evaluated in this article, or claim that may be made by its manufacturer, is not guaranteed or endorsed by the publisher.

frontiers | Frontiers in Microbiology

ORIGINAL RESEARCH
published: 25 April 2022
doi: 10.3389/fmicb.2022.867770

Overexpression of *BIT33_RS14560* Enhances the Biofilm Formation and Virulence of *Acinetobacter baumannii*

Ruifu Yang[1†], Bipeng Lai[1†], Kang Liao[2], Baomo Liu[1], Lixia Huang[1], Shaoli Li[1], Jincui Gu[1], Ziying Lin[1], Yili Chen[2], Shuaishuai Wang[1], Yanli Qiu[1], Jiating Deng[1], Simin Chen[1], Chao Zhuo[3]* and Yanbin Zhou[1]*

[1]Department of Pulmonary and Critical Care Medicine, The First Affiliated Hospital of Sun Yat-sen University, Guangzhou, China, [2]Department of Clinical Laboratory, The First Affiliated Hospital of Sun Yat-sen University, Guangzhou, China, [3]State Key Laboratory of Respiratory Disease, The First Affiliated Hospital of Guangzhou Medical University, Guangzhou, China

OPEN ACCESS

Edited by:
Huancai Lin,
Sun Yat-sen University, China

Reviewed by:
Juan Carlos Vázquez Ucha,
Institute of Biomedical Research of A Coruña (INIBIC), Spain
Israa M. S. Al-Kadmy,
Al-Mustansiriya University, Iraq

***Correspondence:**
Yanbin Zhou
zhouyb@mail.sysu.edu.cn
Chao Zhuo
chaosheep@sina.com

[†]These authors have contributed equally to this work

Specialty section:
This article was submitted to Antimicrobials, Resistance and Chemotherapy, a section of the journal Frontiers in Microbiology

Received: 01 February 2022
Accepted: 22 March 2022
Published: 25 April 2022

Citation:
Yang R, Lai B, Liao K, Liu B, Huang L, Li S, Gu J, Lin Z, Chen Y, Wang S, Qiu Y, Deng J, Chen S, Zhuo C and Zhou Y (2022) Overexpression of BIT33_RS14560 Enhances the Biofilm Formation and Virulence of Acinetobacter baumannii. Front. Microbiol. 13:867770. doi: 10.3389/fmicb.2022.867770

Acinetobacter baumannii, a strictly aerobic, non-lactose fermented Gram-negative bacteria, is one of the important pathogens of nosocomial infection. Major facilitator superfamily (MFS) transporter membrane proteins are a class of proteins that widely exists in microbial genomes and have been revealed to be related to biofilm formation in a variety of microorganisms. However, as one of the MFS transporter membrane proteins, little is known about the role of BIT33_RS14560 in *A. baumannii*. To explore the effects of BIT33_RS14560 on biofilm formation of *A. baumannii*, the biofilm formation abilities of 62 isolates were firstly investigated and compared with their transcript levels of *BIT33_RS14560*. Then, this specific gene was over-expressed in a standard *A. baumannii* strain (ATCC 19606) and two isolates of extensively drug-resistant *A. baumannii* (XDR-Ab). Bacterial virulence was observed using a *Galleria mellonella* infection model. High-throughput transcriptome sequencing (RNA seq) was performed on ATCC 19606 over-expressed strain and its corresponding empty plasmid control strain. *Spearman's* correlation analysis indicated a significant negative correlation ($R = -0.569$, $p = 0.000$) between the $\triangle$CT levels of BIT33_RS1456 and biofilm grading of *A. baumannii* isolates. The amount of *A. baumannii* biofilm was relatively high within 12–48 h. Regardless of standard or clinical strains; the biofilm biomass in the *BIT33_RS14560* overexpression group was significantly higher than that in the control group ($p < 0.0001$). Kaplan–Meier survival curve analysis showed that the mortality of *G. mellonella* was significantly higher when infected with the *BIT33_RS14560* overexpression strain ($\chi^2 = 8.462$, $p = 0.004$). RNA-Seq showed that the mRNA expression levels of three genes annotated as OprD family outer membrane porin, glycosyltransferase family 39 protein, and glycosyltransferase family 2 protein, which were related to bacterial adhesion, biofilm formation, and virulence, were significantly upregulated when *BIT33_RS14560* was over-expressed. Our findings provided new insights in identifying potential drug targets for the inhibition of biofilm formation. We also developed a practical method to construct an over-expressed vector that can stably replicate in XDR-Ab isolates.

Keywords: *Acinetobacter baumannii*, *BIT33_RS14560*, biofilm, overexpression, RNA sequencing, extensively drug-resistant

INTRODUCTION

Acinetobacter baumannii, a Gram-negative bacterium that exists widely in nature, is one of the most important opportunistic pathogens responsible for nosocomial infection. Immunocompromised or severe patients in the intensive care unit are more vulnerable to this pathogen, causing a wide range of infectious diseases, including pneumonia, meningitis, peritonitis, infections of the urinary tract and skin, and posing a great threat to severe patients (Ayoub Moubareck and Hammoudi Halat, 2020). The treatment of *A. baumannii* infection has always been a challenging problem in clinical practice due to its increased resistance to commonly-used antibacterial drugs, leading to a global epidemic of multidrug-resistant *A. baumannii* (MDR-Ab; Ibrahim et al., 2021) and extensively drug-resistant *A. baumannii* (XDR-Ab; Kengkla et al., 2018).

In addition to β-lactamase and aminoglycoside modification enzymes production, active efflux, modification of target sites, and changes in outer membrane permeability (Lee et al., 2017), the drug resistance mechanism of *A. baumannii* was also found to be closely related to the formation of biofilms (Yang et al., 2019; Saipriya et al., 2020). Biofilm refers to the complex, sessile communities of microbes found either attached to a surface or buried firmly in an extracellular matrix as aggregates (Roy et al., 2018). The biofilm formation of *A. baumannii* is a complex process regulated by many factors, including the pili assembly system (Tomaras et al., 2003), BfmRS two-component regulatory systems (Gaddy and Actis, 2009), bacterial quorum-sensing system (Zhang et al., 2020), biofilm-related proteins (Bap; Fattahian et al., 2011) and outer membrane protein A (OmpA; Gaddy et al., 2009), and so on. Most clinically isolated *A. baumannii* strains have been observed to have a strong ability to form biofilms, which results in significantly low sensitivity to antimicrobial agents.

Major facilitator superfamily (MFS), a class of transporter membrane proteins, belongs to the efflux pump families and has a strong substrate specificity, which is reflected in the transportation of secondary metabolites by an ion concentration gradient. Some MFS superfamily members have been confirmed to be closely related to biofilm formation and drug resistance. For example, in a pathogenic strain *A. baumannii* AIIMS 7, *pmt*, a putative MFS transporter-like ORF of 453 bp, was identified and found to be associated with adherence, biofilm formation, and probable extracellular DNA release (Sahu et al., 2012). The efflux gene *A1S_1117*, an MFS superfamily vanillate transporter, was reported to be expressed only in biofilm cells but inhibited in planktonic cells (Rumbo-Feal et al., 2013). AbaF, another member of the MFS superfamily, was proved to mediate the efflux of intracellular fosfomycin and promote the ability to form biofilms in *A. baumannii* (Sharma et al., 2017). Therefore, the in-depth study of MFS family members is of great significance to elucidate the mechanisms of biofilm formation in *A. baumannii* and control chronic infections.

Here, we focus on a new gene, which is labeled with a locus tag of *BIT33_RS14560* in National Center of Biotechnology Information (NCBI) and presumed as a member of the MFS family. In this work, we successfully constructed two recombinant plasmids of *BIT33_RS14560* over-expression, with one aimed at the standard *A. baumannii* strain (ATCC 19606) and the other on account of two XDR-Ab isolates. We transformed them into the target strains and managed to overexpress this target gene. We found that when *BIT33_RS14560* was over-expressed, the abilities to form biofilm were significantly promoted in both standard and clinical strains of *A. baumannii*, which was also confirmed by quantitative real-time PCR (qRT-PCR) assays of 62 clinical isolates. Compared with wild-type ATCC 19606 strain, *BIT33_RS14560* overexpression strain displayed higher mortality of *Galleria mellonella* ($\chi^2 = 8.462$, $p = 0.004$). We also presented RNA sequencing evidence to elucidate possible mechanisms for these phenotypic changes.

MATERIALS AND METHODS

Construction of Phylogenetic Trees

DNA or amino acid sequences of *BIT33_RS14560* gene or protein (corresponding Accession Number: CP058289.1 or WP_002047564.1) and its homologs were searched using BLAST at the (NCBI) website[1] and downloaded in a separate FASTA format. These sequences were analyzed to construct phylogenetic trees to determine the phylogenetic relationships between the selected strains (**Supplementary Tables S1**, **S2**). The best DNA or protein model (GTR + G + I) with the highest parameter was determined and chosen before the construction of phylogenetic trees. Dendrograms were generated by Maximum Likelihood (ML) with bootstrap values corresponding to 1,000 replications using the (MEGA) 11.0 software (Tamura et al., 2021).

Strains, Plasmids, Reagents, and Culture Media

Bacterial strains and plasmids used in this study are listed in **Table 1**. Of 62 *A. baumannii* isolates, 43 strains (69.4%) including two XDR-Ab isolates, XAb53 (Strain No. A53; Stored on June 2, 2021) and XAb50 (Strain No. A50; Stored on May 19th, 2020), were isolated from the First Affiliated Hospital of Sun Yat-sen University, the other 19 strains (30.6%) were obtained from the Microbiology Laboratory of State Key Laboratory of Respiratory Diseases, Guangzhou Medical University. Sources and proportion of 62 *A. baumanii* isolates used in this study were presented in **Supplementary Table S3**. *Escherichia coli* DH5α competent cells (Cat. No. 9057; TaKaRa) were purchased from Guangzhou Ruizhen Biotechnology Co., Ltd. The suicide plasmid pMo130-telR (Cat. No. P4951-ea; Wonder Biotech) was purchased from Guangzhou Qunlan Biotechnology Co., Ltd. Bacterial culturing was performed using Luria-Bertani (LB) agar medium (Cat. No. CM0337B; OXOID) or LB broth medium (Cat. No. CM0405; OXOID).

Reverse Transcription PCR and qRT-PCR

Overnight culture of *A. baumannii* strain was inoculated into fresh LB broth until the mid-log phase (OD = 0.6–0.8) was

[1]http://www.ncbi.nlm.nih.gov/BLAST/

TABLE 1 | Strains and plasmids used in this study.

Strain/Plasmid	Description	Source or Reference
Strain		
DH5α competent cell	A strain for screening or storing (recombinant) plasmids	Purchased from TAKARA
DH5α/pWH1266	A strain with a pWH1266 plasmid	Lab stock
ATCC 19606	A standard *A. baumannii* strain, wild-type	Lab stock
19,606/p-RS	An overexpressed strain of *BIT33_RS14560*, containing a pWH1266 plasmid whose TetR was deleted and replaced by *BIT33_RS14560*	This study
19,606/p	A control strain, containing a pWH1266△(TetR) plasmid but without the insertion by *BIT33_RS14560*	This study
XAb53	An XDR-Ab isolate, wild-type	This study
XAb53/p-telRs-RS	An overexpressed XDR-Ab strain of *BIT33_RS14560*, containing a pWH1266△(TetR) plasmid inserted by *BIT33_RS14560* and its AmpR was replaced by TelR	This study
XAb53/p-telRs	A control strain, containing a pWH1266△(TetR) plasmid without the insertion by *BIT33_RS14560*, but its AmpR was also replaced by TelR	This study
XAb50	An XDR-Ab isolate, wild-type	This study
XAb50/p-telRs-RS	An overexpressed XDR-Ab strain of *BIT33_RS14560*, containing a pWH1266△(TetR) plasmid inserted by *BIT33_RS14560* and its AmpR was replaced by TelR	This study
XAb50/p-telRs	A control strain, containing a pWH1266△(TetR) plasmid without the insertion by *BIT33_RS14560*, but its AmpR was also replaced by TelR	This study
Plasmid		
pWH1266	A shuttle plasmid with AmpR and TetR	Extracted from DH5α/pWH1266 strain
pMo130-telR	A suiside plasmid with TelR, NeoR, and/or KanR	Purchased from Wonder Biotech

XDR-Ab isolates refer to clinic isolates with resistance to at least one agent in all but two or fewer antimicrobial categories (Magiorakos et al., 2012). The two XDR-Ab isolates were identified by antibiotic susceptibility testing. TetR, tetracycline resistance; XDR-Ab, extensively drug-resistant A. baumannii; AmpR, ampicillin resistance; TelR, tellurite resistance; NeoR, neomycin resistance; and KanR, kanamycin resistance.

TABLE 2 | Primers used in this study.

Primer	Sequences (5′–3′)	Usage
RS14560-EcoRI-F	CGC**GAATTC**GGAAATCCTTTGATTTGTGC	The amplification of *BIT33_RS14560*
RS14560-6his-BamHI-R	CGC**GGATCC**CTAATGGTGATGGTGATGAT GAGGTGCTGTTTTAAGTGAGA	
Pwh1266-F	GCCCTTTCGTCTTCAAGA	Verification of recombinant vector
Pwh1266-R	GTGATGTCGGCGATATAGG	
telR-PstI-F	TAT**CTGCAG**TTGACTTAGTTGGTATT	The amplification of the TelR cassette
telR-PvuI-R	CGC**CGATCG**TTTGAAGCTGATGTGCT	
telR-F	ACTTTATCCGCCTCCAT	Verification of the TelR cassette replacement
telR-R	GCCTTCCTGTTTTTGCT	
rpoB-F	GTGCTGACTTGACGCGTGAT	Amplification of the reference gene *rpoB* by fluorescence quantitative PCR
rpoB-R	AGCGTTCAGAAGAGAAGAACAAGTT	
RS14560-F	GTCTACAGGTTATGGCATTGG	Amplification of the target gene *BIT33_RS14560* by fluorescence quantitative PCR
RS14560-R	GCACTAATCAGCAACATCACT	

The restriction enzyme sites are highlighted using bold fonts and the His(6)-Tag is underlined in the primer sequences.

reached. Total RNA was extracted using the E.Z.N.A.® Bacterial RNA Kit (Cat. No. R6950-01; Omega). The quality and concentration of RNA were determined *via* spectrophotometry (NanoDrop 2000c; Fisher Scientific, United States). For reverse transcription PCR (RT-PCR), reverse transcription was performed using ProFlex PCR System cycler (Applied Biosystems, United States). The purified RNA (1 μg/ml) was reverse-transcribed into cDNA by the Evo M-MLV RT Premix for qPCR kit (Cat. No. AG11706; Accurate Biology), in a 20 μl reaction mixture containing 4 μl of Evo M-MLVRT Master Mix and 15 μl of RNAase free water, which was incubated for 15 min at 37°C and 5 s at 85°C. Then, the qRT-PCR assay was performed on a Roche LightCycler® 960 real-time PCR system. Here, SYBR Green Premix Pro Taq HS qPCR kit (Cat. No. 78 AG11702; Accurate Biology) was employed. Around 2 μl of the resulting cDNA products were put into a 20 μl reaction mixture containing 10 μl of SYBR® Green Pro Taq HS Premix II, 0.8 μl (or 10 μM) of each primer and 6.4 μl RNase free water. The parameters of PCR were set as followed: initial heat activation at 95°C for 30 s, followed by 35 cycles of the two-step cycling condition of denaturation at 95°C for 10 s and then annealing at 60°C for 30 s. The melting data of PCR products were measured and collected following the completion of PCR cycling. The *rpoB* gene was used as an internal reference for normalization. △CT value, defined as the CT value of the target gene minus that of the reference *rpoB*, was used to calculate the *BIT33_RS14560* mRNA levels of *A. baumannii*. For each sample, three technical replicates were performed and the gene transcript levels were determined using the $2^{-\triangle\triangle Ct}$ method. Primers used in this part are listed in **Table 2**.

Construction of Gene Overexpression Strains

All primers used in this study are listed in **Table 2**. PCR amplification was achieved using DNA polymerase (Cat. No. AG12202; Accurate 79 Biology). A plasmid DNA extraction kit (Cat. No. D2156-01; Omega), a DNA fragment purification kit (Cat. No. 9761; 77 TaKaRa), and a DNA Ligation kit (Cat. No. 6023; Accurate Biology) were also employed. The novel *BIT33_RS14560* gene was PCR-amplified from the genomes of *A. baumannii* ATCC 19606 using specific primers RS14560-EcoRI-F and RS14560-6his-BamHI-R with the following conditions—initial hold at 94°C for 4 min, followed by 32 cycles of 98°C for 10 s, 55°C for 5 s, 72°C for 8 s, and final extension at 72°C for 7 min. Purified PCR products and pWH1266 plasmid were digested with BamHI and EcoRI, then, according to the manufacturer's instructions, ligated to make a recombinant plasmid of overexpression, named as p-RS14560. After digesting with EcoRI and BamHI, blunt ends to the large fragments of pWH1266 plasmid were created with high-fidelity DNA polymerase and then self-ligated to make into an empty plasmid, known as p. Each plasmid was transformed into *E. coli* DH5α competent cells and then introduced into the *A. baumannii* ATCC 19606 by electroporation (1.75 kV). After overnight culture (16–18 h) at 37°C, monoclonal colony PCR was performed with Pwh1266-F and Pwh1266-R primers to select positive transformants on LB agar supplemented with 50 μg/ml Carbenicillin.

For the overexpression of XDR-Ab, based on the above work, we reconstructed a specific recombinant plasmid by replacing the Ampicillin resistance (AmpR) cassette in the p-RS plasmid with the Tellurite resistance (TelR) cassette. Briefly, the TelR cassette was amplified from the plasmid pMo130-telR using telR-PstI-F/telR-PvuI-R primers. After purification, these PCR products and p-RS plasmid were digested with PstI and PvuI then ligated to make a new plasmid p-telR-RS14560. Similarly, a corresponding empty plasmid p-telR was constructed according to the above-mentioned method. Each plasmid was transformed into *E. coli* DH5α competent cells and then electroporated into *A. baumannii* XAb53 and XAb50 isolates at the same voltage of 1.75 kV. Of particular note, when selecting positive transformants with telR-F/telR-R primers, the concentration of tellurite added into the LB agar should not be completely fixed and rigid, that is, 25 μg/ml for *E. coli* DH5α and 80 μg/ml for XAb53 or XAb50 isolates. Of note, these two XDRAB clinical isolates were randomly selected according to their results of multilocus sequence typing, that was, XAb50 was assigned to ST1145 (*gltA*-1, *gyrB*-3, *gdhB*-3, *recA*-102, *cpn60*-2, *gpi*-97, and *rpoD*-3), an ST recently prevalent at the First Affiliated Hospital of Sun Yat-sen University, while XAb53 was considered a new ST (*gltA*-1, *gyrB*-3, *gdhB*-3, *recA*-102, *cpn60*-1, *gpi*-103, and *rpoD*-26). The media should be cultured overnight for 24–30 h at 37°C.

Microtiter-Plate Test

We performed a microtiter-plate test to evaluate the biofilm formation ability of *A. baumannii* according to the method described previously (Rodríguez-Baño et al., 2008), but with certain modifications. Prior to inoculation, all strains were transferred from the stock cultures onto LB agar plates and incubated aerobically at 37°C for 18 h. Colonies from these plates were suspended in phosphate-buffered saline (PBS). After a 0.5 McFarland turbidity standard suspension (corresponding to 1.5×10^8 CFU/ml) of each isolate was determined, a 100-fold dilution with sterile LB broth was prepared. Then, 200 μl of each bacterial suspension were filled into no less than six wells of a sterile 96-well flat-bottomed plastic tissue culture plate with a lid. Negative and positive control wells contained sterile LB broth and standardized suspension of *P. aeruginosa* strain ATCC 27853, respectively. The plates were covered and incubated aerobically at 37°C for 0, 6, 12, 18, 24, 30, 36, 42, 48, 60, and 72 h, respectively. Then, the content of each well was gently aspirated, and each well was washed three times with 250 ml of ultrapure deionized water and left to dry. Each well was stained for 20 min at room temperature with 200 μl of 10 g/L crystal violet. Excess stain was rinsed off by sterile water. After the plates were air-dried, each well was added with 200 μl of 33.3% glacial acetic acid and resolubilized for 20 min. Absorbance at 570 nm (OD570) of each well was measured by Epoch 2 microplate reader (BioTek). A cut-off OD (ODc) was defined as three standard deviations (SDs) above the mean OD of the negative control. All strains were classified into the following categories (Stepanović et al., 2007): non-adherent ($OD \leq ODc$, 0), weakly adherent ($ODc < OD \leq 2 \times ODc$, +), moderately adherent ($2 \times ODc < OD \leq 4 \times ODc$, ++), or strongly adherent ($4 \times ODc < OD$, +++). The results were averaged after all tests were carried out three times.

G. mellonella Infection Experiment

Bacterial cell suspensions at a concentration equivalent to a 0.5 McFarland Standard were prepared and followed by a 100-fold dilution with sterile LB broth. To make an infection model, the last instar healthy larvae with 2–3 cm long and 180–250 mg in weight were selected and randomly divided into groups with 10 individuals in each group. Each insect was carefully given an injection with 20 μl of bacterial solution (1.5×10^6 CFU/ml) and put in a Petri dish of 8 cm in diameter. Infect at least 30 larvae for each strain. Then place the dishes at 37°C in an incubator and check larval mortality regularly over a 6 h period for 3 days. *A. baumannii* 5075, a strain with high virulence, was served as the positive control while PBS served as the negative. Mortality data were analyzed using the Kaplan–Meier method.

Transcriptome Sequencing

Four single colonies, two derived from the overexpressed strain constructed by ATCC 19606, and two from the corresponding empty plasmid strain, were picked into 3 ml LB medium supplemented with 50 μg/ml Carbenicillin and inoculated, respectively. These cultures were grown for 18 h at 37°C and cells were then collected by centrifugation at 6,000 rpm for 10 min and washed three times with RNase free water. Total

RNA extraction and the subsequent transcriptome sequencing were performed by Shanghai Majorbio Bio-pharm Technology Co., Ltd. After the quality analysis, clean data were obtained and analyzed on the online platform of Majorbio Cloud Platform.[2] Basic functional annotation analysis was performed on the provided reference genome (Organism: *A. baumannii*; Genome ID: GCF_008632635.1). The sequences were then annotated with the following databases including NCBI Nr, NCBI Nt, Pfam,[3] eggNOG[4], SwissProt[5], GO[6], and KEGG.[7] Differentially expressed genes (DEGs) were identified by DESeq2 software, Version 1.24.0.[8] Those mRNAs with absolute value log2[Fold Change (FC)] ≥ 1 and *p-adjust* < *0.05* were considered as significant.

Statistical Analysis

The IBM SPSS 26.0 statistical software was used for statistical analysis. The *t* test was applied to compare the difference of measurement data, which were presented as mean ± SD. *Spearman's* rank correlation was conducted to analyze the correlations between biofilm formation and gene expression levels. The Kaplan–Meier method was used to construct a survival curve, with a calculation of *p* value by the log-rank test. $p < 0.05$ was considered to be statistically significant.

RESULTS

Phylogenetic Analysis

In the case of the DNA sequences, *BIT33_RS14560* gene widely existed in all 14 *A. baumannii* strains with different identities and two clades were identified in the phylogenetic tree (**Supplementary Figure S1**). In the monophyletic clade I, the *BIT33_RS14560* gene was found to most closely related to *A. baumannii* ATCC 17961 and they both clustered into a subgroup with other five *A. baumannii* isolates. Interestingly, the pattern strain *A. baumannii* ATCC 17978 was subgrouped with another six isolates into clade II, indicating a distant relationship with *A. baumannii* ATCC 19606.

When it came to the amino acid sequences, the phylogenetic tree showed that the BIT33_RS14560 membrane transporter was most closely related to *A. baumannii* WP_0657191181 (**Supplementary Figure S2**). In addition, this protein of interest was clustered into a subgroup with its homologous proteins *A. baumannii* HAV5588984.1, *A. baumannii* HAV6132876.1, *A. baumannii* HAV4460275.1, and *Klebsiella pneumoniae* SSW87290.1. What is more, the target protein was constituted into an evolutionary clade together with *Acinetobacter nosocomialis* WP_004709884.1, *A. nosocomialis* HAB71326.1, *A. nosocomialis* WP_207694075.1 as well as *A. baumannii* HAV5002142.1.

[2]www.majorbio.com
[3]http://pfam.xfam.org/
[4]http://eggnogdb.embl.de/
[5]http://uniprot.org
[6]http://www.geneontology.org/
[7]http://www.genome.jp/kegg/
[8]http://bioconductor.org/packages/stats/bioc/DESeq2/

Investigation on the Relationship Between Biofilm-Forming Capability and *BIT33_RS14560* mRNA Levels of *A. baumannii* Isolates

In this study, when biofilm biomass was measured at 72 h by crystal violet staining, 62 *A. baumannii* isolates showed a various range of OD570 from 0.09 to 2.29 nm, indicating varying abilities of biofilm formation. Among all the isolates, 9 (14.5%), 28 (45.2%), and 17 (27.4%) were strong, moderate, and weak biofilm producers, respectively, while no biofilm was observed in eight (12.9%) isolates. Interestingly, we found that these *A. baumannii* isolates also differed considerably in their mRNA levels of *BIT33_RS14560*, with the △CT ranging from 0.47 to 19.51 (**Table 3**). *Spearman*'s rank correlation analysis indicated that the △CT value of *BIT33_RS14560* was negatively correlated with the biofilm rank of those *A. baumannii* isolates ($R = -0.569$, $p = 0.000$), which suggested that a stronger biofilm-forming ability could be followed by a relative higher the expression level of *BIT33_RS14560* (**Supplementary Table S4**).

Construction of Overexpression Vectors

Fragment of *BIT33_RS14560* coding sequence (CDS) plus its preceding promoter was cloned from the ATCC 19606 genome and 1% agarose gel electrophoresis of the PCR products yielded an expected band, 1,632 bp in size. The purified PCR products were inserted into pWH1266 to construct a vector p-RS14560 for the overexpression of *BIT33_RS14560* in ATCC 19606. PCR analysis of the cloned plasmid followed by gene sequencing showed that the target fragment was successfully and correctly cloned into pWH1266 plasmid and the cloned gene was the same as *BIT33_RS14560* (NCBI Reference Sequence: NZ_MJHA01000008.1) in the GenBank. These findings indicated that the expression vector p-RS14560 was successfully constructed (**Supplementary Figures S3**, **S4**). A 3,075 bp TelR cassette was successfully cloned from the suicide vector pMo130telR and inserted into the p-RS14560 plasmid to construct a new vector p-telR-RS14560. These were confirmed by obtaining two expected bands, 3,075 and 3,526 bp in size, respectively (**Figure 1**). Surprisingly, we managed to overexpress the target gene *BIT33_RS14560* in two XDR-Ab isolates with this recombinant plasmid (see this article below).

Validation of the Effect of *BIT33_RS14560* Overexpression on the Biofilm Formation in *A. baumannii* Strains

As mentioned above, those clinical *A. baumannii* isolates with higher *BIT33_RS14560* mRNA levels tended to possess a stronger capacity of biofilm formation. To further investigate this relationship, a standard *A. baumannii* strain ATCC 19606, together with two XDR-Ab isolates, were transformed with the overexpression plasmids, p-RS14560 and p-telR-RS14560, respectively. To confirm if over-expression of *BIT33_RS14560* occurred in the ATCC 19606 and these two XDR-Ab isolates, relative quantification of the *BIT33_RS14560* transcript levels were determined by qRT-PCR with the corresponding strains transformed with empty plasmids as the control. In ATCC 19606, there was no significant difference between empty plasmid

TABLE 3 | The correlation between the biofilm biomass of 62 *A. baumannii* and their mRNA levels of *BIT33_RS14560*.

Strain designation	OD570 (nm)	Biofilm rank	△CT
7646	2.29	+++	13.05
3416	1.65	+++	11.12
3358	0.89	++	14.29
2599_2	2.75	+++	11.44
8017	0.57	++	17.68
7334	0.51	+	17.22
4695	0.24	–	17.15
1937	0.74	++	18.35
1421	0.44	+	19.06
4530	1.02	++	18.29
8578	0.52	+	19.33
1313	0.61	++	15.73
2499	0.43	+	19.40
8679	0.67	++	18.22
9436	0.32	+	18.55
2844	0.40	+	17.50
3679	0.77	++	17.64
8076	0.33	+	18.04
4108	0.32	+	17.17
6860	0.93	++	15.71
8036	0.28	+	18.18
5629	0.27	+	17.30
2194	0.87	++	17.14
2410	0.34	+	17.65
2241	0.93	++	17.05
1916	0.41	+	17.55
3542	0.71	++	18.66
3328	0.81	++	16.41
3508	0.42	+	19.51
3475	0.91	++	17.02
1705	0.68	++	18.48
1594	1.25	+++	17.05
1583	0.62	++	18.36
1076	1.59	+++	8.53
8124	1.42	+++	16.41
2326	1.33	+++	1.13
9252	2.16	+++	0.47
1666	0.71	++	18.90
1883	0.48	+	19.39
2346	1.05	+++	16.52
2281	0.88	++	18.47
2579	0.87	++	18.37
3388	0.83	++	18.05
1725	0.51	+	18.08
1983	0.63	++	17.31
2140	0.85	++	13.85
27	0.85	++	16.34
22	0.58	++	16.66
50	0.74	++	18.62
1	0.29	+	17.46
33	0.49	+	17.84
32	1.02	++	17.79
36	0.77	++	17.40
41	0.52	++	17.04
A67	0.13	–	18.11
A59	0.22	–	18.50
A50▲	0.14	–	18.01
A53▲	0.61	++	16.78
A143	0.09	–	18.12
A132	0.13	–	18.09
A116	0.10	–	18.34
A48	0.09	–	19.29

(Continued)

TABLE 3 | Continued

Different abilities of biofilm formation are presented as the categories: –, non-adherent; +, weakly adherent; ++, moderately adherent; +++, strongly adherent. △CT is defined as the CT value of the target gene minus that of the reference rpoB gene. ▲A50 referred to XAb50 while A53 referred to XAb53.

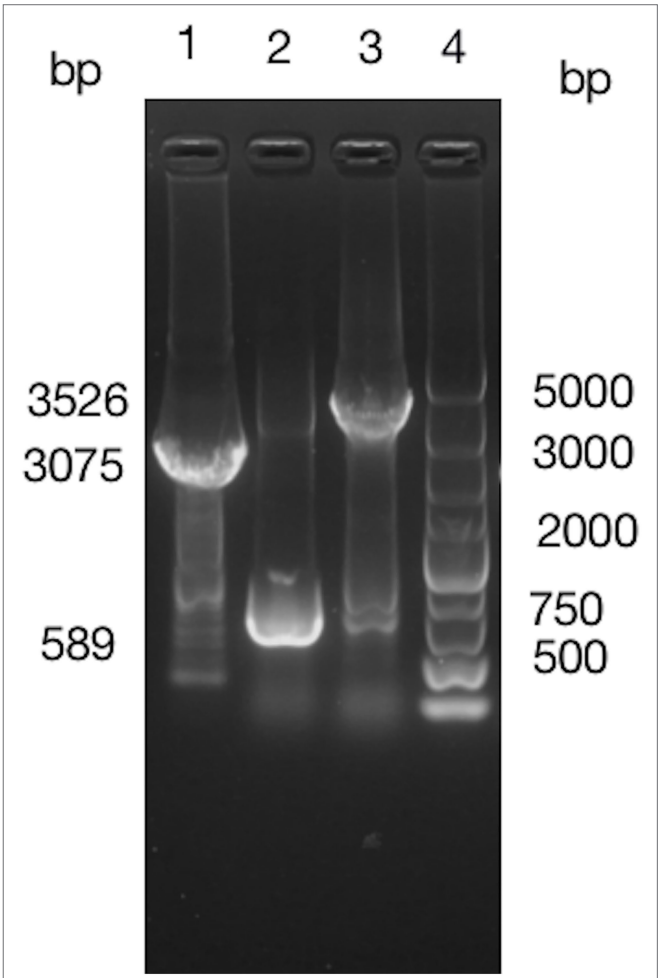

FIGURE 1 | Around 1% agarose gel electrophoresis of PCR products indicates a successful construction of p-telR-RS14560 vector. The AmpR fragment in the p-RS14560 plasmid is replaced by telR cassette amplified from the pMo130telR vector. Lane 1: PCR products of telR cassette; lane 2: PCR products of p-RS14560 plasmid as negative control, lane 3: PCR products of positive clone, and lane 4: DNA marker 5,000 bp.

group and wild-type group, indicating that the transformation of two recombinant plasmids had little effect on the expression of *BIT33_RS14560* gene ($p > 0.05$). For ATCC 19606 strain with the plasmid overexpressing the gene of interest, when compared with its control group, the expression level of the *BIT33_RS14560* was significantly increased at 311.5 folds ($p < 0.0001$). For XAb53 strain, the relative expression levels of *BIT33_RS14560* in the overexpression group was surprisingly higher at about 586

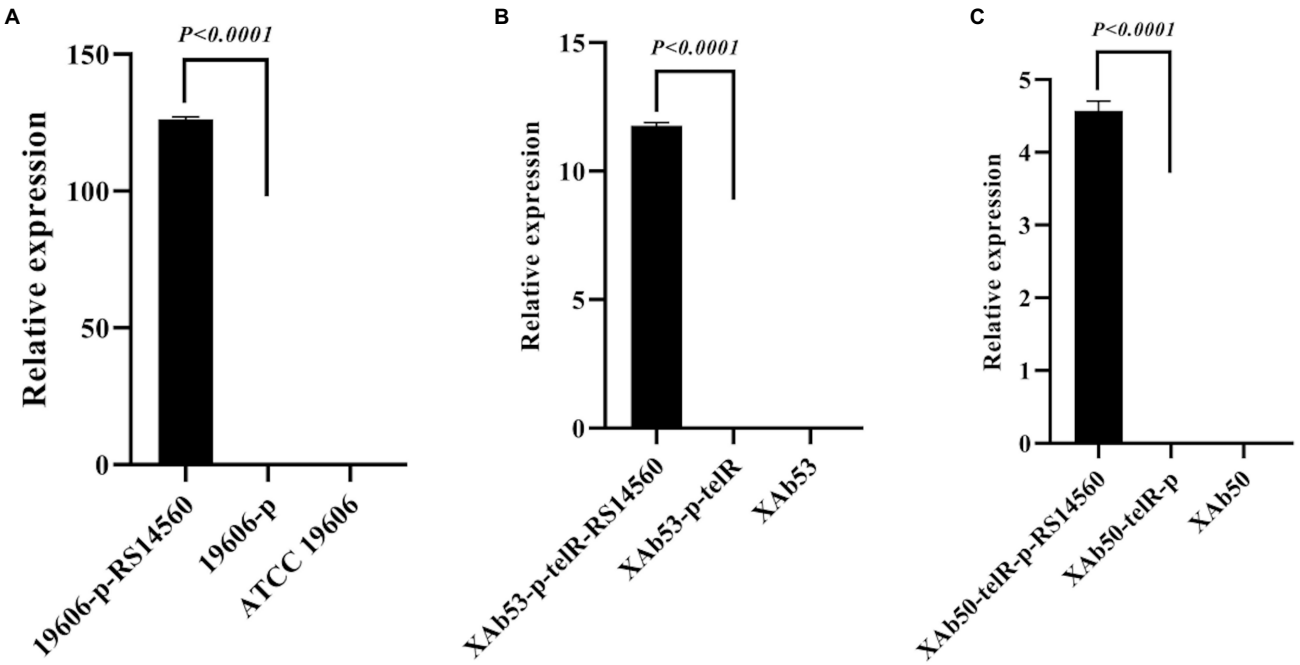

FIGURE 2 | Relative expression of *BIT33_RS14560* by qRT-PCR. The *x*-axis represents the *A. baumannii* strains, and the *y*-axis represents the relative mRNA levels of *BIT33_RS14560* ($2^{-\triangle CT}$). $p < 0.05$ indicates a statistical significance. **(A)** Overexpression of ATCC 19606 strain; **(B)** Overexpression of XAb53 isolate; and **(C)** Overexpression of XAb50 isolate.

1000-fold than that of its control group ($p < 0.0001$). Similarly, for the other XDR-Ab strain, XAb50, the overexpression group significantly displayed approximately 619 1000-fold higher *BIT33_RS14560* mRNA levels in comparison with its empty plasmid group ($p < 0.0001$). These results indicated the success of overexpression of *BIT33_RS14560* in the three *A. baumannii* strains (**Figure 2**). The breathtaking multiples of overexpression in two XDR-Ab isolates may probably come from their very low transcript levels (or relative high $\triangle$CT values) of this target gene, as shown in **Table 3**.

To verify the effect of *BIT33_RS14560* overexpression on the biofilm formation of three *A. baumannii* strains, we evaluated the biofilm biomass with the microtiter-plate test at different points of time. We found that these three wild-type *A. baumannii* strains, including ATCC 19606 and other two XDR-Ab isolates, differed in their peak time of biofilm formation, but normally displayed relatively high levels of production within 12–48 h. When compared with each control group transformed with empty plasmids, we observed significantly higher biofilm biomass in the experimental groups of *BIT33_RS14560*-overexpression, whether in the standard strain ATCC 19606 or the two isolates XAb53 and XAb50 (**Figure 3**).

G. mellonella Survival Influenced by *BIT33_RS14560* Overexpression

We used the *G. mellonella* infection model to investigate the effect on the virulence of the standard strain ATCC 19606 when *BIT33_RS14560* was overexpressed. None of the *G. mellonella* died within 72 h when given with the equivalent PBS. By contrast, all *G. mellonella* died within 12 h following infection with the high-virulent strain *A. baumannii* 5075, which served as the positive control. When infected with the ATCC 19606 wild-type strain, *G. mellonella* mortality was 40.0% within 12 h and then rose to 70.0% at 24 h. In contrast, *G. mellonella* mortality following infection with the *BIT33_RS14560* overexpression strain was 60.0% at 12 h and reached 90% within 24 h. No significant difference was observed in the survival rates between the wild-type strain ATCC 19606 and its empty plasmid strain 19,606-p ($p > 0.05$). As shown in **Figure 4**, Kaplan–Meier survival curve analysis showed that the survival rate of *G. mellonella* was significantly lower when infected with the *BIT33_RS14560* overexpression strain ($\chi^2 = 8.462$, $p = 0.004$).

Screening of the Candidate Genes Related to *A. baumannii* Biofilm Formation Influenced by Overexpressed *BIT33_RS14560* Based on RNA-Seq

To better understand the mechanisms of the relationship between *BIT33_RS14560* overexpression and *A. baumannii* biofilm formation, in the current study, we conducted a comparative transcriptomic analysis of four samples, including the treated group (two samples derived from ATCC 19606 with target gene overexpression) and the control group (two samples derived from ATCC 19606 with empty plasmid). A total of over 7.0 Gigabyte raw data were obtained, and the

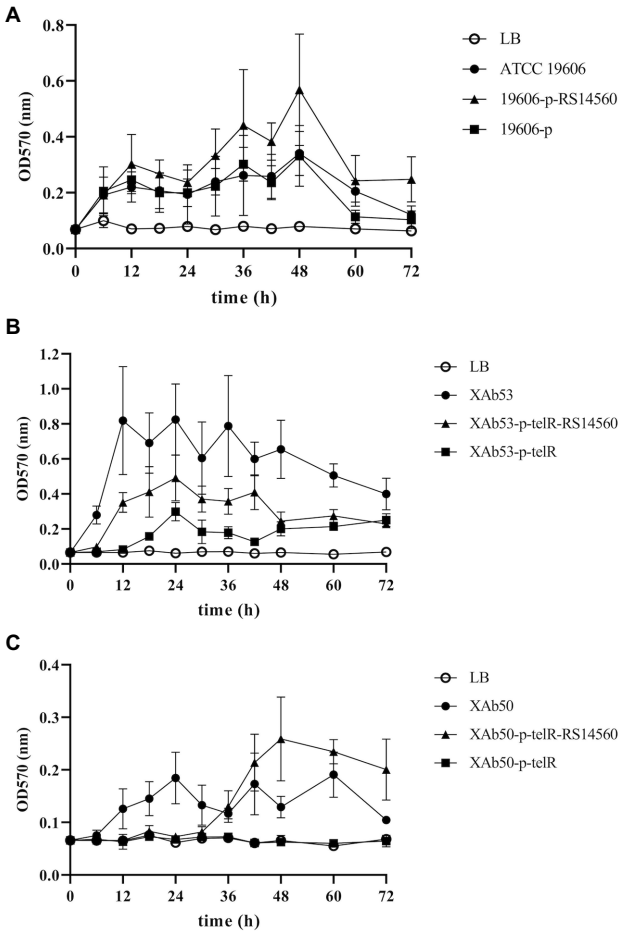

FIGURE 3 | The dynamic changes of biofilm biomass produced by the nine *A. baumannii* strains at different time points. ATCC 19606, XAb53, and XAb50 are wild-type strains. 19,606-p-RS14560, XAb53-p-telR-RS14560, and XAb50-p-telR-RS14560 are *BIT33_RS14560*-overexpressed strains. 19,606-p, XAb53-p-telR, and XAb50-p-telR are empty plasmid control strains. The overexpression of *BIT33_RS14560* exhibits enhancing effects, but with various time patterns, on the biofilm formation of strains in the experimental groups. Values are means ± SD of over three independent experiments. **(A)** Wild-type and recombinant strains of ATCC 19606; **(B)** Wild-type and recombinant strains of XAb53; and **(C)** Wild-type and recombinant strains of XAb50.

percentage of Q30 (an important index for the assessment of RNA-Seq quality, a higher value usually indicates a lower probability of base error) reached above 94.65%. Totally, 3,232 expressed genes were detected in this analysis, including 3,208 mRNAs and 24 small RNAs (sRNAs). Under the threshold of $|\log2(FC)| \geq 1$ and *p-adjust* < *0.05*, a total of 12 DEGs (seven upregulated and five downregulated) were screened for subsequent analysis. The volcano plot and heatmap of these DEGs were drawn in **Figures 5, 6**, respectively. To further explore the biological functions of these DEGs, we performed GO and KEGG enrichment analysis. As presented in **Figure 7**, none of these DEGs were involved in GO biological process or cellular component category. However, in molecular function(MF)category, they significantly enriched in "magnesium transmembrane transporter activity, phosphorylative mechanism" (GO:0015444), "3-oxoacid CoA-transferase activity" (GO:0008260), "acetate CoA-transferase activity" (GO:0008775), "ATPase-coupled cation transmembrane transporter activity" (GO:0019829), and "transferase activity, transferring glycosyl groups" (GO:0016757; all *FDR*<*0.05*). In terms of the KEGG pathway, "aminobenzoate degradation" (map00627) and "valine, leucine, and isoleucine degradation" (map00280) were involved (*FDR* < *0.05*; **Figure 8**).

DISCUSSION

Phylogenetic Analysis

To investigate the distribution of the *BIT33_RS134560* gene and its encoding protein in *A. baumannii* strains as well as their relationship, we conducted phylogenetic tree analysis. Our results showed that this gene existed in all the 14 *A. baumannii* strains of different genomic homology (**Supplementary Figure S1**). Similarly, the BIT33_RS14560 protein and its homologous ones could be found in many other strains of *A. baumannii*, even in other *Acinetobacter* spp. and *K. pneumoniae* (**Supplementary Figure S2**). These results indicated a wide distribution of the *BIT33_RS134560* gene and its protein in *A. baumannii* strains. It was interesting to note that this target gene in ATCC19606 was very closely related to ATCC17961, but not to ATCC17978, although they were all pattern strains of *A. baumannii*. We have not figured out why and how this gene evolved the way it did. Further study of the difference in the expression of the *BIT33_RS14560* gene between these two clades may shed light on the causes of this phenomenon.

In addition, that the BIT33_RS14560 protein was closely related to the MFS homologs of *A. nosocomiae* and *K. pneumoniae* indicated potential pathogenicity of this protein due to the fact that the latter two bacteria were also important pathogens of nosocomial infections (Nho et al., 2015; Wang et al., 2020). Therefore, we believed this gene of interest needed to be noticed.

Construction of Overexpression Vector in XDR-Ab Isolates

The *E. coli*/*Acinetobacter* shuttle vector pWH1266 containing AmpR and TetR was initially generated for the cloning experiments of *Acinetobacter calcoaceticus* and *E. coli* (Hunger et al., 1990) and has been successfully applied in the overexpression construction of *A. baumannii* (Zander et al., 2013; Liou et al., 2014). However, for XDR-Ab, it should be mentioned that due to its extreme drug resistance, the number of antibiotic selection markers for transformants was greatly limited. One solution to this problem was that the antibiotic concentration should be increased as much as possible within the tolerant range of the vector's resistance. In this case, we made our attempt to transform the recombinant plasmid p-RS14560, which contained only AmpR, into an XDR-Ab isolate by increasing the concentration of Carbenicillin

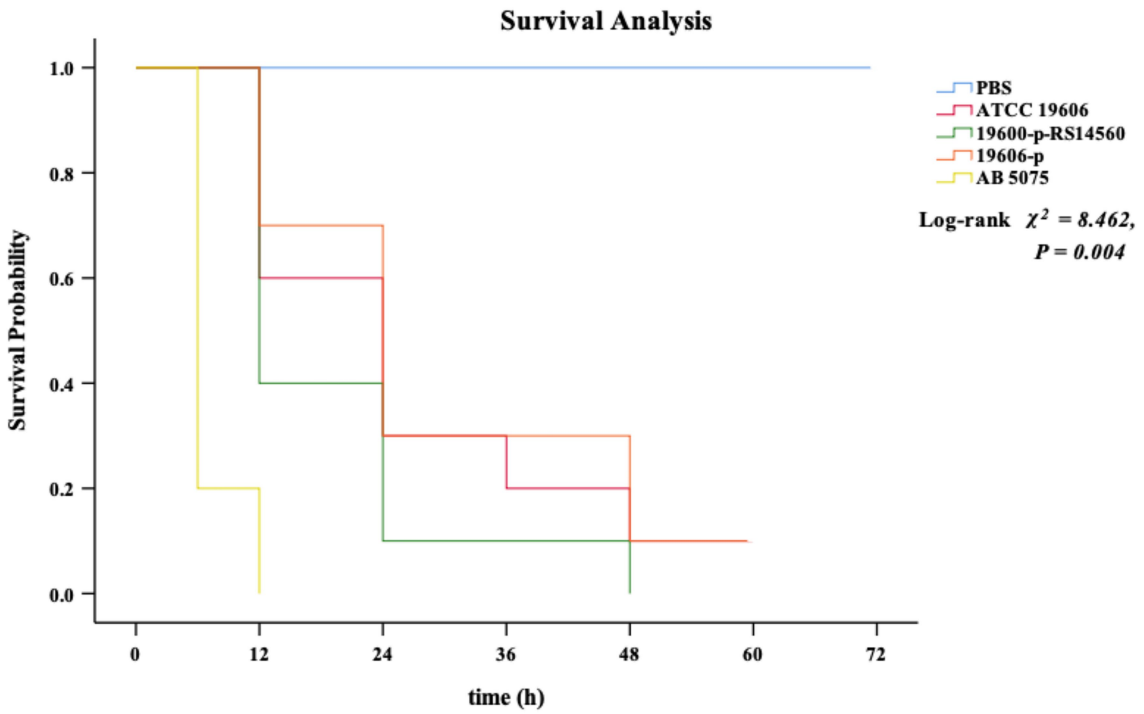

FIGURE 4 | Kaplan–Meier curve analysis of the survival of *G. mellonella* after infection. PBS is the negative control group, ATCC 19606 is the wild-type strain, 19,606-p-RS14560 is the overexpression strain, 19,606-p is the empty plasmid control group, and *A. baumannii* 5075 is the positive control group. PBS, phosphate buffered saline. $p < 0.05$ indicates a statistical significance.

from 50 to 1,700 μg/ml. However, we failed because the XDR-Ab was still able to grow at such a high concentration of Carbenicillin. To achieve this goal of overexpression in XDR-Ab, a replacement of AmpR by other resistant genes was the key to the deal.

When we made our attempts to knock out this target gene using a marker-less method (Amin et al., 2013), the TelR cassette of pMo130telR vector caught our attention. This suicide vector was derived from the modification of the pMo130 vector (Hamad et al., 2009) by carrying a TelR cassette (Sanchez-Romero et al., 1998). Researchers had tested *A. baumannii* isolates, including MDR-Ab isolates, and found that they were susceptible to tellurite (Amin et al., 2013). We also tested several XDR-Ab isolates to confirm their susceptibilities to tellurite and found that they could be counter-selected in LB agar containing tellurite of 30–100 μg/ml (data not shown). Fortunately, we managed to overexpress the target gene *BIT33_RS14560* in two XDR-Ab isolates by replacing the AmpR with the TelR. The transformation of two recombinant vectors, p-telR and p-telR-RS14560, might to some extent make an impact on the transcript expression of *BIT33_RS14560*. This could be explained by the fitness cost of bacteria (San Millan and MacLean, 2017; Nang et al., 2018). Large plasmids could impose a metabolic burden for host bacterial strains (Ma et al., 2018). However, to our knowledge, this was the first time to achieve stable gene overexpression in XDR-Ab by the replacement of AmpR with telR, which would provide guidance for further investigations on XDR-Ab strains.

Biofilm-Forming Capabilities and *BIT33_RS14560* mRNA Levels of *A. baumannii* Isolates

Like many other bacteria, *A. baumannii* displays a robust biofilm formation on many abiotic surfaces in hospital environments, raising the risk of chronic infections. Previous studies have shown that the degree of biofilm formation varied considerably depending on the *A. baumannii* isolates (Rodríguez-Baño et al., 2008). Our study also showed different abilities of biofilm formation among 62 *A. baumannii* isolates when measured at 72 h. Those with robust abilities of biofilm formation were more likely to survive under desiccation and nutrition-limiting conditions, which explained why some clinical isolates possessed more tenacious vitality in hospitals than others. As shown in **Supplementary Table S4**, *Spearman's* rank correlation analysis suggested that a stronger biofilm-forming ability could be followed by a relatively higher expression level of *BIT33_RS14560* (the $\triangle$CT value vs. biofilm rank, $R = -0.569$, $p = 0.000$). This was validated by overexpression of the *BIT33_RS14560* gene in the standard strain ATCC 19606 and the two isolates XAb53 and XAb50 (**Figure 3**).

Here, three wild-type *A. baumannii* strains used for the construction of *BIT33-RS14560* overexpression normally

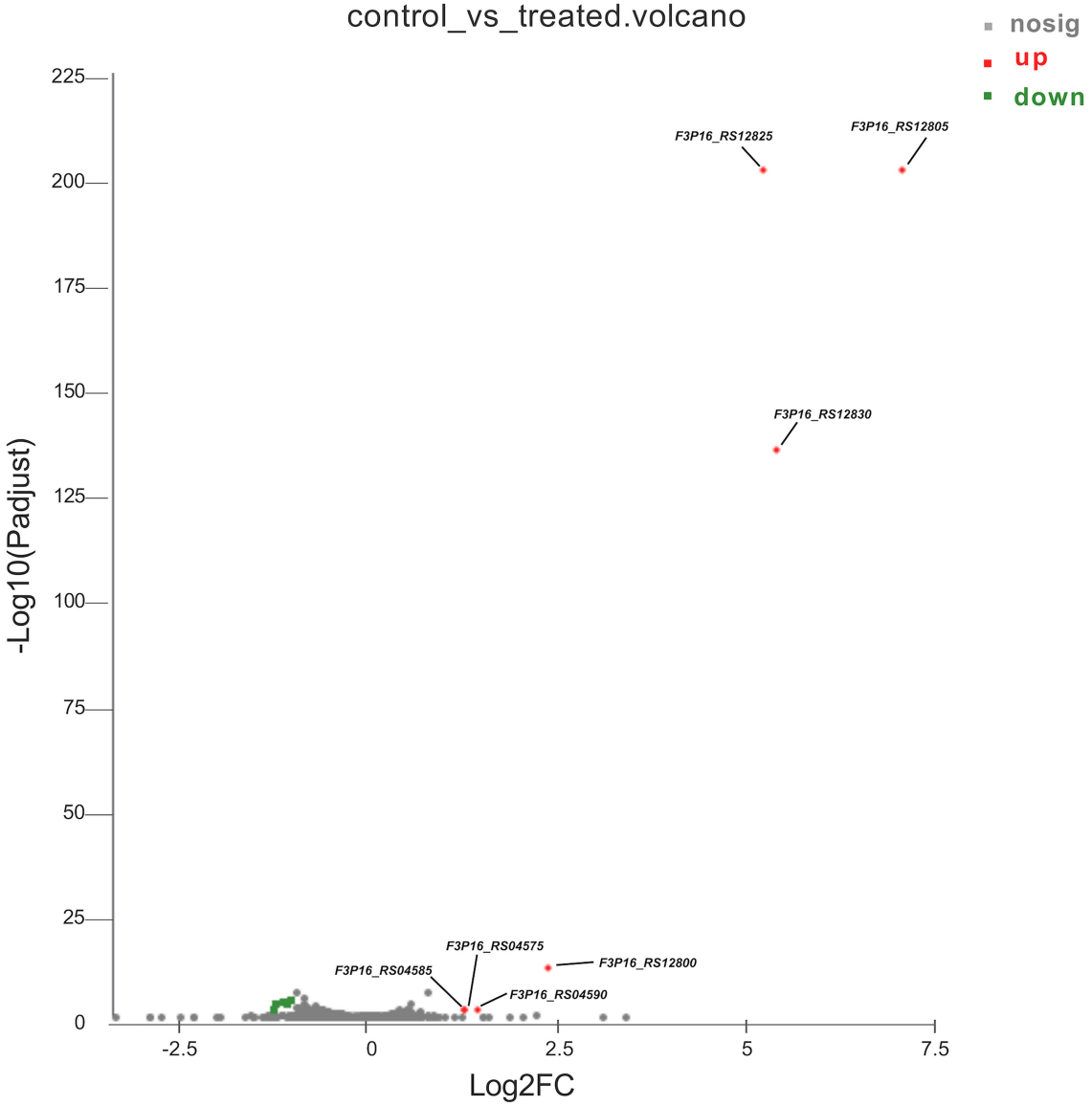

FIGURE 5 | The volcano plot of differentially expressed genes identified by RNA-Seq. The *x*-axis represents the $\log_2$(FC), and the *y*-axis represents $-\log_{10}$ (*p-adjust*) calculated by the Student's *t*-test. The red dots represent the upregulated genes with statistical significance (*p-adjust* < *0.05* and $|\log_2(FC)| \geq 1$). The green dots represent genes with down-regulated expression, while the gray ones represent genes with no statistical significance. Those upregulated DEGs are indicated. FC, fold change.

displayed relatively high levels of production within 12–48 h, which was in accordance with the previous study (Rodríguez-Baño et al., 2008). However, the enhancing effects of *BIT33_RS14560* on biofilm formation appeared to be variable in these three *A. baumannii* strains (**Figure 3**). Within 48 h, for the ATCC 19606 strain, overexpression of *BIT33_RS14560* exhibited a gradual upward trend of facilitating biofilm formation, while in the XAb53 isolate; this effect seemed to be more stable, keeping it in fairly high levels of biofilm biomass. However, when it came to XAb50 isolate, the amount of biofilm remained relatively unchanged over the past 30 h, then, rose sharply into about 3.24-fold (data not shown) at 48 h. Further investigation is warranted to elucidate the mechanisms for this phenomenon.

RNA-Seq Reveals Possible Mechanisms by Which *BIT33_RS14560* Affects Biofilm Formation and Virulence of *A. baumannii*

Currently, *A. baumannii* biofilm formation, of which the mechanisms are still not fully elucidated, is still a tough issue in the treatment of refractory and chronic infections. As one of the largest superfamily of secondary carriers known to date, MFS family membrane transporters exist widely in

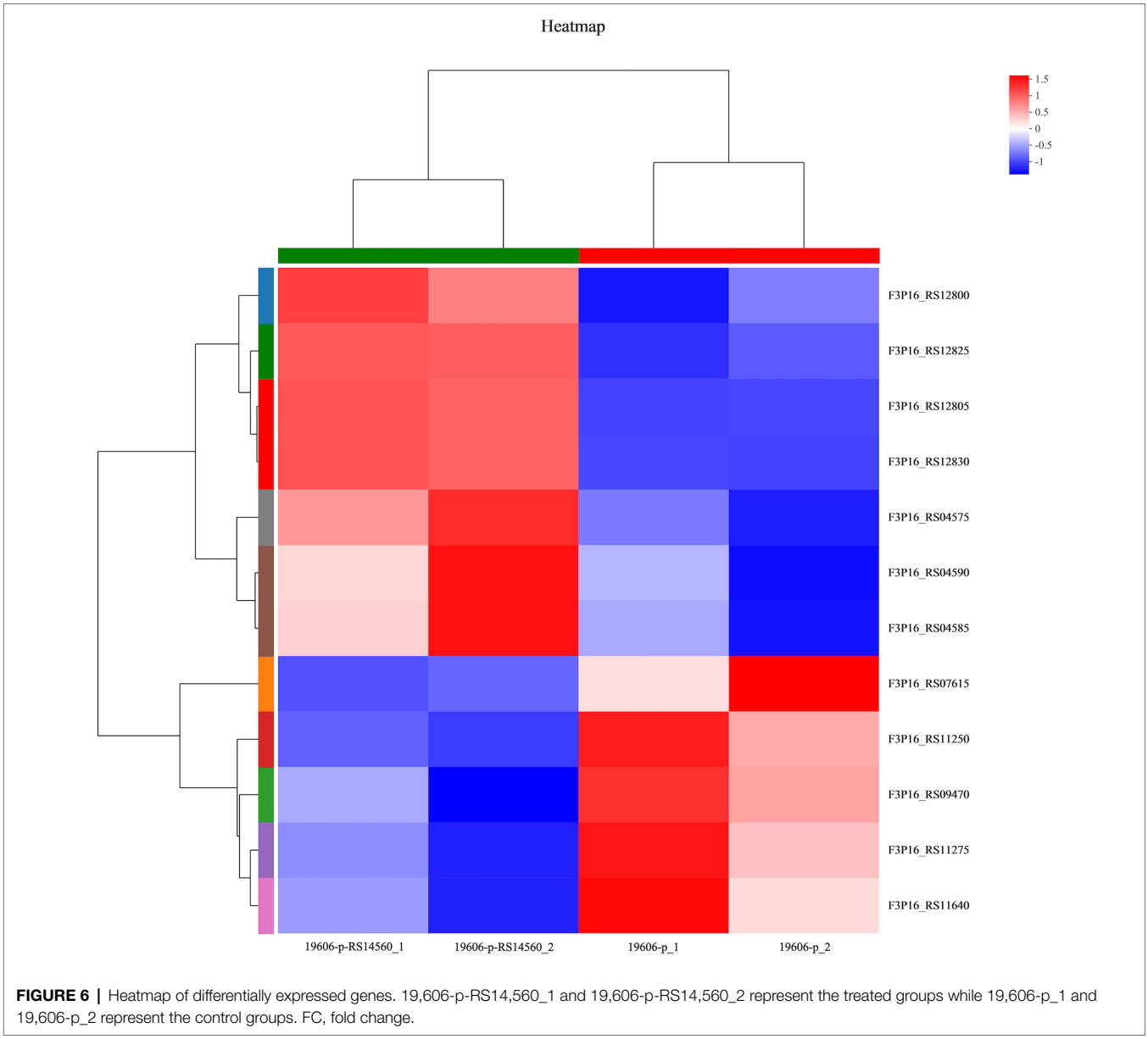

FIGURE 6 | Heatmap of differentially expressed genes. 19,606-p-RS14,560_1 and 19,606-p-RS14,560_2 represent the treated groups while 19,606-p_1 and 19,606-p_2 represent the control groups. FC, fold change.

the whole biological world (Reddy et al., 2012) and they are considered to be closely related to a wide variety of life phenomena due to a basic function of assisting in transmembrane transport of certain substances, including monosaccharides, oligosaccharides, amino acids, enzyme cofactors, drugs, and so on (Lorca et al., 2007; Chen et al., 2008; Yen et al., 2010). In bacteria, MFS superfamily proteins have been found not only to play an important role in the transport of many substances but also to be a member of the efflux pumps large families (Pasqua et al., 2019), which are involved in biofilm formation and drug resistance (Bay et al., 2017; Saranathan et al., 2017; Poudyal and Sauer, 2018; Tang et al., 2020).

BIT33_RS14560, although considered to be categorized into the MFS family, is still lacking reports about its effects on the biofilm formation of *A. baumannii*. In this study, we conducted a comparative transcriptomic analysis to investigate the possible mechanisms by which *BIT33_RS14560* overexpression had an impact on the biofilm formation and virulence of *A. baumannii* ATCC19606. As shown in **Table 4**, we found that three DEGs, including *F3P16_RS12800*, *F3P16_RS04575*, and *F3P16_RS04585*, although displayed different up or down multiples, were hypothesized to be related more or less to bacterial biofilm formation or virulence.

F3P16_RS12800 was annotated as an OprD family outer membrane porin. The OprD family was described first for *P. aeruginosa*, but ever since that time, it has been found in many metabolically versatile soil bacteria and comprises over 100 members (Tamber et al., 2006). In the current study, we found that the overexpression of *BIT33_RS14560* led to a

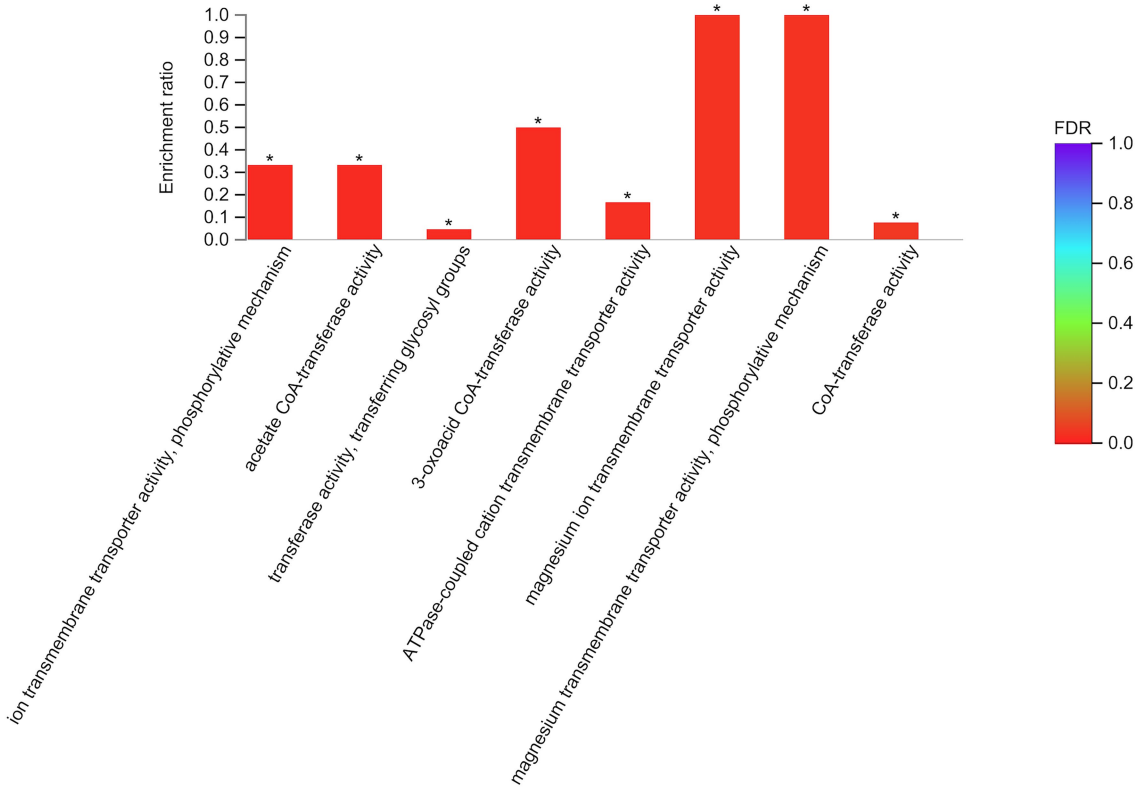

FIGURE 7 | GO enrichment analysis of differentially expressed genes. The *x*-axis represents GO terms, and the *y*-axis represents the enrichment ratio. A higher ratio means a greater degree of enrichment. GO, Gene Ontology; *FDR*, false discovery rate. *$FDR < 0.05$.

significant upregulation of *F3P16_RS12800*, suggesting that in *A. baumannii*, *BIT33_RS14560* may enhance biofilm formation by upregulating the expression of this outer membrane porin. This was supported by a previous comparative proteomics study (Cabral et al., 2011) revealing that some membrane proteins including OprD-like protein were involved in the adhesion and biofilm formation of *A. baumannii*.

Most importantly, we got *F3P16_RS04575* and *F3P16_RS04585*, both encoded proteins belonging to the glycosyltransferase (GT) family and were upregulated when *BIT33_RS14560* was overexpressed. GTs mainly participate in the transfer process of glycosyl from an activated donor to a receptor, such as sugar, lipid, protein, and nucleic acid and play an important role in pathogenic adhesion, biofilm formation, and virulence (Breton et al., 2006; Ribet and Cossart, 2010a). Structural analysis of three-dimensional (3D) protein fold has shown that the catalytic domains of GTs are categorized into GT-A, GT-B, and GT-C three types, the most common of which are GT-A and GT-B (Moremen and Haltiwanger, 2019). GT-B or GT-C is believed to play a role in adhesion, biofilm formation, and virulence of pathogenic bacteria while GT-A enters the host cell and interferes it with post-translational modifications thus affecting its signal transduction, protein translation, and immune response. It was also important to note that the protein glycosylation of GT was closely related to the virulence of pathogenic bacteria (Ribet and Cossart, 2010b; Yakovlieva and Walvoort, 2020). Many bacterial pathogens were found to bear toxic GTs that interfere with host post-translational modifications to promote their own survival and replication (Lu et al., 2015). Interestingly, when we further analyzed with the Carbohydrate-Active Enzymes (CAZy) database,[9] we found that the proteins encoded by *F3P16_RS04575* and *F3P16_RS04585* belonged to GT-C and GT-A, respectively. This might explain why ATCC 19606 became more virulent when *BIT33_RS14560* was overexpressed (**Figure 4**).

It was reported that proteins and carbohydrates were the main components of biofilm formation (Costerton et al., 1995). Amino acid metabolism, glycerolipid, and tricarboxylic acid cycle were also observed to be mostly affected during bacterial biofilm formation (Lu et al., 2019). Our results of GO and KEGG analysis (**Figures 7, 8**) also indicated that most DEGs

[9]http://www.cazy.org

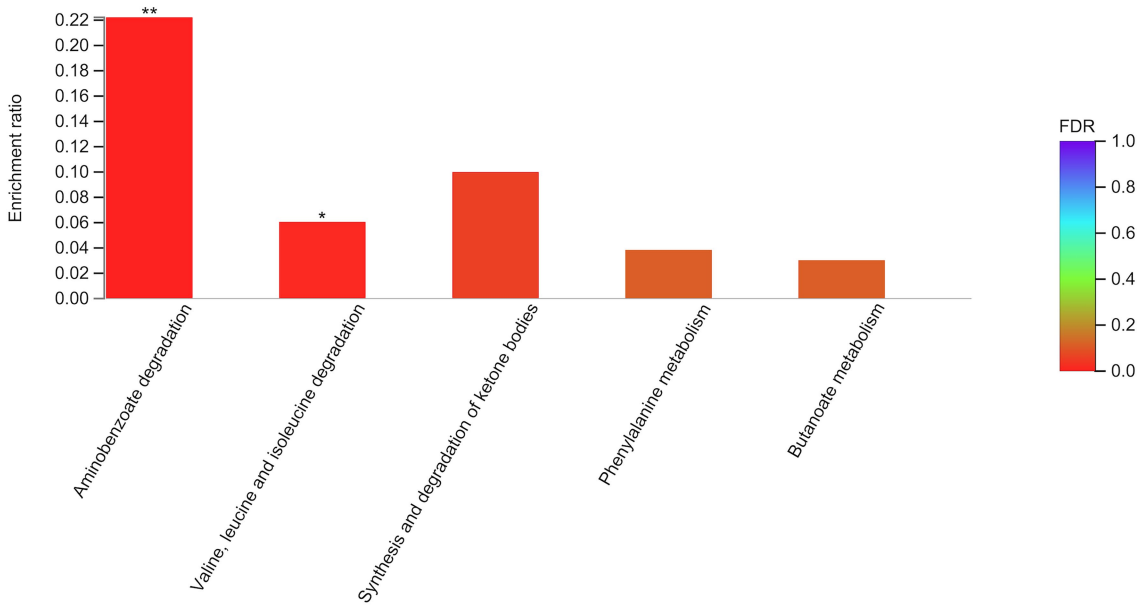

FIGURE 8 | KEGG enrichment analysis of differentially expressed genes. The *x*-axis represents KEGG terms, and the *y*-axis represents the enrichment ratio. A higher ratio means a greater degree of enrichment. KEGG, Kyoto Encyclopedia of Genes and Genome. *FDR*, false discovery rate. *$FDR < 0.05$, **$FDR < 0.01$.

TABLE 4 | Differentially expressed genes identified by RNA-Seq.

Gene identity	Description	log_2(FC)	*P*	*P-adjust*	Regulation
F3P16_RS12805	MFS transporter	7.100932775	0	0	up
F3P16_RS12825	Aromatic ring-hydroxylating dioxygenase subunit alpha	5.270041648	7.88E-206	1.26E-202	up
F3P16_RS12830	PDR/VanB family oxidoreductase	5.447523987	5.15E-139	5.51E-136	up
F3P16_RS12800	OprD family outer membrane porin	2.405050832	1.88E-15	1.50E-12	up
F3P16_RS04590	ChbG/HpnK family deacetylase	1.473469534	5.46E-05	0.009736754	up
F3P16_RS04575	Glycosyltransferase family 39 protein	1.29285042	0.000175063	0.02065165	up
F3P16_RS04585	Glycosyltransferase family 2 protein	1.280990985	0.000240526	0.024890574	up
F3P16_RS07615	Magnesium-translocating P-type ATPase	−1.011635328	2.24E-07	8.99E-05	down
F3P16_RS09470	CoA transferase subunit A	−1.098553066	8.82E-07	0.000314477	down
F3P16_RS11250	DcaP-like protein	−1.209536537	1.62E-06	0.000518977	down
F3P16_RS11275	Methylcrotonoyl-CoA carboxylase	−1.052143105	1.93E-06	0.000541303	down
F3P16_RS11640	Phenylacetate-CoA oxygenase subunit PaaJ	−1.227463257	9.57E-05	0.013948752	down

Differentially expressed genes were screened by DESeq2 software, under a threshold of $|log_2(FC)| \geq 1$ and p-adjust < 0.05. Of note, the F3P16_RS12805 gene refers to the target gene BIT33_RS14560. FC, fold change.

participated in complicated metabolic processes including amino acid, carbohydrate metabolism, which also suggested the complexity of bacterial biofilm formation. However, the specific effects of these DEGs on *A. baumannii* biofilm formation and what metabolic pathways these DEGs may be involved in remained further investigations.

CONCLUSION

In this study, we demonstrated that when *BIT33_RS14560*, a member of the MFS family, was over-expressed, the abilities to form biofilm and the virulence of *A. baumannii* were significantly enhanced, no matter in standard or clinically isolated strains. This gene of interest existed widely in *A. baumannii* strains and its protein was closely related to the MFS homologs of *A. nosocomiae* and *K. pneumoniae*. Three DEGs including *F3P16_RS12800*, *F3P16_RS04575*, and *F3P16_RS04585*, annotated as OprD family outer membrane porin, glycosyltransferase family 39 protein and glycosyltransferase family 2 protein, respectively, were identified by RNA-Seq and speculated to be related to the biofilm formation and virulence of *A. baumannii*, which

needs further studies. These findings provided new insights in identifying potential drug targets for the inhibition of biofilm formation. Besides, we developed a method for the construction of XDR-Ab overexpression, which may promote further microbiological research on their genotypes and phenotypes.

DATA AVAILABILITY STATEMENT

The data presented in the study are deposited in the Sequence Read Archive (SRA) repository, accession number at: https://www.ncbi.nlm.nih.gov/sra/PRJNA821219.

AUTHOR CONTRIBUTIONS

RY and BLa contributed to the conception and design of this study. RY, BLa, and BLi performed the experiments. KL, YC, and CZ provided the study materials. RY, LH, SL, JG, ZL, and SW analyzed and interpreted the data. YZ, CZ, and KL gave administrative supports. All authors contributed to the article and approved the submitted version.

FUNDING

This work is supported by grants from the National Natural Science Foundation of China (81570008, YZ) and the Natural Science Foundation of Guangdong Province of China (2021A1515010480, YZ).

ACKNOWLEDGMENTS

We thank the Microbiology Laboratory of State Key Laboratory of Respiratory Diseases, Guangzhou Medical University for scientific research. We are grateful to Shanghai Majorbio Bio-pharm Technology Co., Ltd. for the analysis of RNA-Seq data.

SUPPLEMENTARY MATERIAL

The Supplementary Material for this article can be found online at: https://www.frontiersin.org/articles/10.3389/fmicb.2022.867770/full#supplementary-material

Supplementary Figure S1 | Phylogenetic analysis of *BIT33_RS14560* gene. Bootstrap values >50 are displayed on the branches. A higher bootstrap value indicates a better reliability.

Supplementary Figure S2 | Phylogenetic analysis of BIT33_RS14560 protein. Bootstrap values >50 are displayed on the branches. A higher bootstrap value indicates a better reliability.

Supplementary Figure S3 | The construction of p-RS14560 overexpressed vector. **(A)** The amplification of *BIT33_RS14560* fragment. Lane 1: DNA marker 2,000 bp, lane 2: sample; **(B)** PCR products of pWH1266 plasmid as negative control. Lane 1: DNA marker 2,000 bp, lane 2: PCR products of pWH1266 plasmid as negative control **(C)** Recombinant plasmid is successively transformed into competent *E. coli* DH5α and ATCC 19606 strains, with the Pwh1266-F/Pwh1266-R primers being used to ensure the success of directional linkage. Lane 1: DNA marker 2,000 bp, lane 2: PCR products of p-RS14560 plasmid as positive control, lane 3: PCR products of positive clone.

Supplementary Figure S4 | A representative part of the sequence alignment between the target gene in the p-RS14560 vector and the comparative analysis to the *BIT33_RS14560* gene.

REFERENCES

Amin, I. M., Richmond, G. E., Sen, P., Koh, T. H., Piddock, L. J., and Chua, K. L. (2013). A method for generating marker-less gene deletions in multidrug-resistant *Acinetobacter baumannii*. *BMC Microbiol.* 13:158. doi: 10.1186/1471-2180-13-158

Ayoub Moubareck, C., and Hammoudi Halat, D. (2020). Insights into *Acinetobacter baumannii*: a review of microbiological, virulence, and resistance traits in a threatening nosocomial pathogen. *Antibiotics* 9:119. doi: 10.3390/antibiotics9030119

Bay, D. C., Stremick, C. A., Slipski, C. J., and Turner, R. J. (2017). Secondary multidrug efflux pump mutants alter *Escherichia coli* biofilm growth in the presence of cationic antimicrobial compounds. *Res. Microbiol.* 168, 208–221. doi: 10.1016/j.resmic.2016.11.003

Breton, C., Snajdrová, L., Jeanneau, C., Koca, J., and Imberty, A. (2006). Structures and mechanisms of glycosyltransferases. *Glycobiology* 16, 29R–37R. doi: 10.1093/glycob/cwj016

Cabral, M. P., Soares, N. C., Aranda, J., Parreira, J. R., Rumbo, C., Poza, M., et al. (2011). Proteomic and functional analyses reveal a unique lifestyle for *Acinetobacter baumannii* biofilms and a key role for histidine metabolism. *J. Proteome Res.* 10, 3399–3417. doi: 10.1021/pr101299j

Chen, D. E., Podell, S., Sauer, J. D., Swanson, M. S., and Saier, M. H. Jr. (2008). The phagosomal nutrient transporter (Pht) family. *Microbiology* 154, 42–53. doi: 10.1099/mic.0.2007/010611-0

Costerton, J. W., Lewandowski, Z., Caldwell, D. E., Korber, D. R., and Lappin-Scott, H. M. (1995). Microbial biofilms. *Annu. Rev. Microbiol.* 49, 711–745. doi: 10.1146/annurev.mi.49.100195.003431

Fattahian, Y., Rasooli, I., Mousavi Gargari, S. L., Rahbar, M. R., Darvish Alipour Astaneh, S., and Amani, J. (2011). Protection against *Acinetobacter baumannii* infection via its functional deprivation of biofilm associated protein (bap). *Microb. Pathog.* 51, 402–406. doi: 10.1016/j.micpath.2011.09.004

Gaddy, J. A., and Actis, L. A. (2009). Regulation of *Acinetobacter baumannii* biofilm formation. *Future Microbiol.* 4, 273–278. doi: 10.2217/fmb.09.5

Gaddy, J. A., Tomaras, A. P., and Actis, L. A. (2009). The *Acinetobacter baumannii* 19606 OmpA protein plays a role in biofilm formation on abiotic surfaces and in the interaction of this pathogen with eukaryotic cells. *Infect. Immun.* 77, 3150–3160. doi: 10.1128/IAI.00096-09

Hamad, M. A., Zajdowicz, S. L., Holmes, R. K., and Voskuil, M. I. (2009). An allelic exchange system for compliant genetic manipulation of the select agents *Burkholderia pseudomallei* and *Burkholderia mallei*. *Gene* 430, 123–131. doi: 10.1016/j.gene.2008.10.011

Hunger, M., Schmucker, R., Kishan, V., and Hillen, W. (1990). Analysis and nucleotide sequence of an origin of DNA replication in *Acinetobacter calcoaceticus* and its use for *Escherichia coli* shuttle plasmids. *Gene* 87, 45–51. doi: 10.1016/0378-1119(90)90494-c

Ibrahim, S., Al-Saryi, N., Al-Kadmy, I. M. S., and Aziz, S. N. (2021). Multidrug-resistant *Acinetobacter baumannii* as an emerging concern in hospitals. *Mol. Biol. Rep.* 48, 6987–6998. doi: 10.1007/s11033-021-06690-6

Kengkla, K., Kongpakwattana, K., Saokaew, S., Apisarnthanarak, A., and Chaiyakunapruk, N. (2018). Comparative efficacy and safety of treatment options for MDR and XDR *Acinetobacter baumannii* infections: a systematic review and network meta-analysis. *J. Antimicrob. Chemother.* 73, 22–32. doi: 10.1093/jac/dkx368

Lee, C. R., Lee, J. H., Park, M., Park, K. S., Bae, I. K., Kim, Y. B., et al. (2017). Biology of *Acinetobacter baumannii*: pathogenesis, antibiotic resistance mechanisms, and prospective treatment options. *Front. Cell. Infect. Microbiol.* 7:55. doi: 10.3389/fcimb.2017.00055

Liou, M. L., Soo, P. C., Ling, S. R., Kuo, H. Y., Tang, C. Y., and Chang, K. C. (2014). The sensor kinase BfmS mediates virulence in *Acinetobacter baumannii*. *Microbiol. Immunol. Infect.* 47, 275–281. doi: 10.1016/j.jmii.2012.12.004

Lorca, G. L., Barabote, R. D., Zlotopolski, V., Tran, C., Winnen, B., Hvorup, R. N., et al. (2007). Transport capabilities of eleven gram-positive bacteria: comparative genomic analyses. *Biochim. Biophys. Acta* 1768, 1342–1366. doi: 10.1016/j.bbamem.2007.02.007

Lu, Q., Li, S., and Shao, F. (2015). Sweet talk: protein glycosylation in bacterial interaction with the host. *Trends Microbiol.* 23, 630–641. doi: 10.1016/j.tim.2015.07.003

Lu, H., Que, Y., Wu, X., Guan, T., and Guo, H. (2019). Metabolomics deciphered metabolic reprogramming required for biofilm formation. *Sci. Rep.* 9:13160. doi: 10.1038/s41598-019-49603-1

Ma, K., Feng, Y., and Zong, Z. (2018). Fitness cost of a mcr-1-carrying IncHI2 plasmid. *PLoS One* 13:e0209706. doi: 10.1371/journal.pone.0209706

Magiorakos, A. P., Srinivasan, A., Carey, R. B., Carmeli, Y., Falagas, M. E., Giske, C. G., et al. (2012). Multidrug resistant, extensively drug resistant and pan drug resistant bacteria: an international expert proposal for interim standard definitions for acquired resistance. *Clin. Microbiol. Infect.* 18, 268–281. doi: 10.1111/j.1469-0691.2011.03570.x

Moremen, K. W., and Haltiwanger, R. S. (2019). Emerging structural insights into glycosyltransferase-mediated synthesis of glycans. *Nat. Chem. Biol.* 15, 853–864. doi: 10.1038/s41589-019-0350-2

Nang, S. C., Morris, F. C., McDonald, M. J., Han, M. L., Wang, J., Strugnell, R. A., et al. (2018). Fitness cost of mcr-1-mediated polymyxin resistance in *Klebsiella pneumoniae*. *J. Antimicrob. Chemother.* 73, 1604–1610. doi: 10.1093/jac/dky061

Nho, J. S., Jun, S. H., Oh, M. H., Park, T. I., Choi, C. W., Kim, S. I., et al. (2015). *Acinetobacter nosocomialis* secretes outer membrane vesicles that induce epithelial cell death and host inflammatory responses. *Microb. Pathog.* 81, 39–45. doi: 10.1016/j.micpath.2015.03.012

Pasqua, M., Grossi, M., Zennaro, A., Fanelli, G., Micheli, G., Barras, F., et al. (2019). The varied role of efflux pumps of the MFS family in the interplay of bacteria with animal and plant cells. *Microorganisms* 7:285. doi: 10.3390/microorganisms7090285

Poudyal, B., and Sauer, K. (2018). The ABC of biofilm drug tolerance: the MerR-like regulator BrlR is an activator of ABC transport systems, with PA1874-77 contributing to the tolerance of *Pseudomonas aeruginosa* biofilms to tobramycin. *Antimicrob. Agents Chemother.* 62, e01981–e01917. doi: 10.1128/AAC.01981-17

Reddy, V. S., Shlykov, M. A., Castillo, R., Sun, E. I., and Saier, M. H. Jr. (2012). The major facilitator superfamily (MFS) revisited. *FEBS J.* 279, 2022–2035. doi: 10.1111/j.1742-4658.2012.08588.x

Ribet, D., and Cossart, P. (2010a). Pathogen-mediated posttranslational modifications: a re-emerging field. *Cell* 143, 694–702. doi: 10.1016/j.cell.2010.11.019

Ribet, D., and Cossart, P. (2010b). Post-translational modifications in host cells during bacterial infection. *FEBS Lett.* 584, 2748–2758. doi: 10.1016/j.febslet.2010.05.012

Rodríguez-Baño, J., Martí, S., Soto, S., Fernández-Cuenca, F., Cisneros, J. M., Pachón, J., et al. (2008). Biofilm formation in *Acinetobacter baumannii*: associated features and clinical implications. *Clin. Microbiol. Infect.* 14, 276–278. doi: 10.1111/j.1469-0691.2007.01916.x

Roy, R., Tiwari, M., Donelli, G., and Tiwari, V. (2018). Strategies for combating bacterial biofilms: a focus on anti-biofilm agents and their mechanisms of action. *Virulence* 9, 522–554. doi: 10.1080/21505594.2017.1313372

Rumbo-Feal, S., Gómez, M. J., Gayoso, C., Álvarez-Fraga, L., Cabral, M. P., Aransay, A. M., et al. (2013). Whole transcriptome analysis of *Acinetobacter baumannii* assessed by RNA-Sequencing reveals different mRNA expression profiles in biofilm compared to planktonic cells. *PLoS One* 8:e72968. doi: 10.1371/journal.pone.0072968

Sahu, P. K., Iyer, P. S., Gaikwad, M. B., Talreja, S. C., Pardesi, K. R., and Chopade, B. A. (2012). An MFS transporter-like ORF from MDR *Acinetobacter baumannii* AIIMS 7 is associated with adherence and biofilm formation on biotic/abiotic surface. *Int. J. Microbiol.* 2012:490647. doi: 10.1155/2012/490647

Saipriya, K., Swathi, C. H., Ratnakar, K. S., and Sritharan, V. (2020). Quorum-sensing system in *Acinetobacter baumannii*: a potential target for new drug development. *J. Appl. Microbiol.* 128, 15–27. doi: 10.1111/jam.14330

San Millan, A., and MacLean, R. C. (2017). Fitness costs of plasmids: a limit to plasmid transmission. *Microbiol. Spectr.* 5, 1–12. doi: 10.1128/microbiolspec.MTBP-0016-2017

Sanchez-Romero, J. M., Diaz-Orejas, R., and De Lorenzo, V. (1998). Resistance to tellurite as a selection marker for genetic manipulations of *pseudomonas* strains. *Appl. Environ. Microbiol.* 64, 4040–4046. doi: 10.1128/AEM.64.10.4040-4046.1998

Saranathan, R., Pagal, S., Sawant, A. R., Tomar, A., Madhangi, M., Sah, S., et al. (2017). Disruption of tetR type regulator adeN by mobile genetic element confers elevated virulence in *Acinetobacter baumannii*. *Virulence* 8, 1316–1334. doi: 10.1080/21505594.2017.1322240

Sharma, A., Sharma, R., Bhattacharyya, T., Bhando, T., and Pathania, R. (2017). Fosfomycin resistance in *Acinetobacter baumannii* is mediated by efflux through a major facilitator superfamily (MFS) transporter-AbaF. *J. Antimicrob. Chemother.* 72, 68–74. doi: 10.1093/jac/dkw382

Stepanović, S., Vuković, D., Hola, V., Di Bonaventura, G., Djukić, S., Cirković, I., et al. (2007). Quantification of biofilm in microtiter plates: overview of testing conditions and practical recommendations for assessment of biofilm production by staphylococci. *APMIS* 115, 891–899. doi: 10.1111/j.1600-0463.2007.apm_630.x

Tamber, S., Ochs, M. M., and Hancock, R. E. (2006). Role of the novel OprD family of porins in nutrient uptake in *Pseudomonas aeruginosa*. *J. Bacteriol.* 188, 45–54. doi: 10.1128/JB.188.1.45-54.2006

Tamura, K., Stecher, G., and Kumar, S. (2021). MEGA11: molecular evolutionary genetics analysis version 11. *Mol. Biol. Evol.* 38, 3022–3027. doi: 10.1093/molbev/msab120

Tang, M., Wei, X., Wan, X., Ding, Z., Ding, Y., and Liu, J. (2020). The role and relationship with efflux pump of biofilm formation in *Klebsiella pneumoniae*. *Microb. Pathog.* 147:104244. doi: 10.1016/j.micpath.2020.104244

Tomaras, A. P., Dorsey, C. W., Edelmann, R. E., and Actis, L. A. (2003). Attachment to and biofilm formation on abiotic surfaces by *Acinetobacter baumannii*: involvement of a novel chaperone-usher pili assembly system. *Microbiology* 149, 3473–3484. doi: 10.1099/mic.0.26541-0

Wang, G., Zhao, G., Chao, X., Xie, L., and Wang, H. (2020). The characteristic of virulence, biofilm and antibiotic resistance of *Klebsiella pneumoniae*. *Int. J. Environ. Res. Public Health* 17:6278. doi: 10.3390/ijerph17176278

Yakovlieva, L., and Walvoort, M. T. C. (2020). Processivity in bacterial Glycosyltrans-ferases. *ACS Chem. Biol.* 15, 3–16. doi: 10.1021/acschembio.9b00619

Yang, C. H., Su, P. W., Moi, S. H., and Chuang, L. Y. (2019). Biofilm formation in *Acinetobacter baumannii*: genotype-phenotype correlation. *Molecules* 24:1849. doi: 10.3390/molecules24101849

Yen, M. R., Chen, J. S., Marquez, J. L., Sun, E. I., and Saier, M. H. (2010). Multidrug resistance: phylogenetic characterization of superfamilies of secondary carriers that include drug exporters. *Methods Mol. Biol.* 637, 47–64. doi: 10.1007/978-1-60761-700-6_3

Zander, E., Chmielarczyk, A., Heczko, P., Seifert, H., and Higgins, P. G. (2013). Conversion of OXA-66 into OXA-82 in clinical *Acinetobacter baumannii* isolates and association with altered carbapenem susceptibility. *J. Antimicrob. Chemother.* 68, 308–311. doi: 10.1093/jac/dks382

Zhang, K., Yang, X., Yang, J., Qiao, X., Li, F., Liu, X., et al. (2020). Alcohol dehydrogenase modulates quorum sensing in biofilm formations of *Acinetobacter baumannii*. *Microb. Pathog.* 148:104451. doi: 10.1016/j.micpath.2020.104451

Conflict of Interest: The authors declare that the research was conducted in the absence of any commercial or financial relationships that could be construed as a potential conflict of interest.

Publisher's Note: All claims expressed in this article are solely those of the authors and do not necessarily represent those of their affiliated organizations, or those of the publisher, the editors and the reviewers. Any product that may

be evaluated in this article, or claim that may be made by its manufacturer, is not guaranteed or endorsed by the publisher.

frontiers | Frontiers in Microbiology

MINI REVIEW
published: 06 July 2022
doi: 10.3389/fmicb.2022.940643

Corynebacterium matruchotii: A Confirmed Calcifying Bacterium With a Potentially Important Role in the Supragingival Plaque

Qinyang Li[1,2†], *Fangjie Zhou*[1,2†], *Zhifei Su*[1,2], *Yuqing Li*[1*] and *Jiyao Li*[1,2*]

[1] State Key Laboratory of Oral Diseases, National Clinical Research Center for Oral Diseases, West China Hospital of Stomatology, Sichuan University, Chengdu, China, [2] Department of Cariology and Endodontics, West China Hospital of Stomatology, Sichuan University, Chengdu, China

Corynebacterium matruchotii is a reported calcifying bacterium that can usually be isolated from dental calculus and induce mineralization *in vitro*. In recent years, based on *in situ* hybridization probe and sequencing technology, researchers have discovered the central "pillar" role of *C. matruchotii* in supragingival plaque, and many studies focused on bacterial interactions in the biofilm structure dominated by *C. matruchotii* have been conducted. Besides, *C. matruchotii* seems to be an indicator of "caries-free" oral status according to imaging and sequencing studies. Therefore, in this review, we summarize *C. matruchotii* 's role in supragingival plaque based on the structure, interactions, and potential connections with oral diseases.

Keywords: ***Corynebacterium matruchotii*, supragingival plaque, biofilm structure, bacterial interaction, oral diseases**

OPEN ACCESS

Edited by:
Huancai Lin,
Sun Yat-sen University, China

Reviewed by:
Feng Chen,
Peking University, China

***Correspondence:**
Yuqing Li
liyuqing@scu.edu.cn
Jiyao Li
jiyaoliscu@163.com

†These authors have contributed equally to this work

Specialty section:
This article was submitted to Antimicrobials, Resistance and Chemotherapy, a section of the journal Frontiers in Microbiology

Received: *10 May 2022*
Accepted: *30 May 2022*
Published: *06 July 2022*

Citation:
Li Q, Zhou F, Su Z, Li Y and Li J (2022) Corynebacterium matruchotii: A Confirmed Calcifying Bacterium With a Potentially Important Role in the Supragingival Plaque. Front. Microbiol. 13:940643. doi: 10.3389/fmicb.2022.940643

INTRODUCTION

Corynebacterium matruchotii (previously known as *Leptothrix buccalis* and *Bacterionema matruchotii*) is a gram-positive aerobic bacterium that was first discovered in 1925 (Ennever and Creamer, 1967). Of all the anatomical sites in the oral cavity, it occurs most in dental plaque on the tooth surface and serves as one of the most predominant bacteria at the site (Mark Welch et al., 2016; Eriksson et al., 2017; Esberg et al., 2020). During the 1960's−2000's, the bacterium was verified to precipitate calcium phosphate on the intracytoplasmic membranes and share a similar calcified nucleator with dental calculus (Vogel and Smith, 1976; Boyan-Salyers et al., 1978; Ennever et al., 1978, 1979; Sidaway, 1978a). However, after these investigations reported this calcifying ability, studies on *C. matruchotii* in the oral ecosystem were strikingly absent from the literature for the next decade or so.

In the past few years, with the development of laboratory techniques such as fluorescence *in situ* hybridization with probes and high-throughput sequencing, the taxonomy of bacteria in highly structured dental plaque has been clearly depicted, and *C. matruchotii* has once again become a focus of research. As reported recently, *C. matruchotii* is in the center of supragingival plaque and interacts with a variety of bacteria around it *via* its special morphology, which may indicate a new sight for plaque development and maturation. In addition, several studies on oral diseases associated with supragingival plaque have pointed out *C. matruchotii* as a potential indicator of healthy status since there is an increase in the relative abundance of *C. matruchotii* compared with the morbid state, implying *C. matruchotii* might play more hidden roles in the development of different oral status.

This review is aimed at summarizing the latest findings of *C. matruchotii* in supragingival plaque, including its bio-geographic position in the organized oral biofilm, interactions with other bacteria, and possible effects in oral diseases, attempting to better understand the characteristics of dental plaque in various conditions to explore ways to maintain oral health from a microbial perspective.

C. MATRUCHOTII IN THE STRUCTURE OF SUPRAGINGIVAL PLAQUE

C. matruchotii was discovered in much higher abundance and prevalence in the supragingival plaque and subgingival plaque than in saliva or other oral surfaces such as the tongue, buccal mucosa, and keratinized gingivae (Mark Welch et al., 2016). Therefore, the potential big role for it in oral biofilms came to attention. In 2016, Borisy et al. used a fluorescence *in situ* hybridization probe to determine the bio-geographic location of each bacterium and first clearly showed the central position of *C. matruchotii* in the hedgehog structures in healthy people's supragingival plaque (Mark Welch et al., 2016; Borisy and Valm, 2021). The "hedgehog" structure is a special consortium of various bacteria named by its morphology seen under electron microscopy as spiny, radially oriented filaments, and within the structure, *C. matruchotii* stood in the center of the field of vision with a variety of bacteria surrounding it. Combined with a recent metaproteome study claiming that *C. matruchotii* represented a large proportion of the protein activity in supragingival dental plaque, which suggested its strong biological activity and metabolic capacity (Belda-Ferre et al., 2015), a hypothesis can be drawn that it undertakes numerous information exchanges among bacteria and performs important functions in healthy oral status. Additionally, based on the recent research conducted on the metabolic current production by *C. matruchotii*, the radial "hedgehog" structure may support electrically coupled organics oxidation and oxygen reduction in dental biofilm as in the cases of long-range extracellular electron transport which could facilitate colonization of various bacteria in the anaerobic environment (Naradasu et al., 2020). From the basal layer closest to the tooth surface outward, *Corynebacterium* traversed through the whole distance; from the staining, an ordered arrangement could be seen in the form of a small amount of *Actinomyces* located near the tooth base, *Capnocytophaga/ Fusobacterium/ Leptotrichia* forming a ring between the periphery and the base, *Neisseriaceae* clustering in and near the periphery, and *Streptococcus/ Haemophilus/ Porphyromonas* being located at the periphery encircling *Corynebacterium* as the "corncob structure." The organized "hedgehog" structure was determined by the metabolism and biochemicals of different bacteria according to the group supposed, and *Streptococcus* seemed to be the major driver of this organized structure which used external oxygen to produce hydrogen peroxide, carbon dioxide, and a series of metabolites to impact growth and survival adaption of other bacteria.

THE INTERACTIONS BETWEEN *C. MATRUCHOTII* AND OTHER COMMENSAL BACTERIA CLOSE IN BIO-GEOGRAPHY TO SUPRAGINGIVAL PLAQUE

The development and maturation of oral biofilm were determined by the relationship between participating bacteria, which presented as bacterial co-aggregation and co-adhesion (Kolenbrander et al., 2010). Recently, to further explore a vital part of *C. matruchotii* in biofilm, Anders Esberg et al. systematically performed an *in vivo* and *in vitro* study to seek bacterial interactions in coaggregation and co-adhesion assays (Esberg et al., 2020). Consistent with the fact that *C. matruchotii* were in close proximity with *Actinomyces spp* reported by Borisy, Esberg et al. demonstrated an indispensable role of *Actinomyces spp* for *C. matruchotii* binding on the tooth surface. The group hypothesized that *Actinomyces naeslundii* could be an initial tooth colonizer binding to the saliva pellicle and providing attachment sites for *C. matruchotii* since *in vivo* the abundance of *A. naeslundii* was similar to *C. matruchotii* at all ages, and *in vitro*, *A.naeslundii* bound *C.matruchotii* both in the state of plankton and biofilm and had the ability to recruit *C. matruchotii* to the tooth surface.

In the "hedgehog" consortium of supragingival plaque, a unique structure named "corncob" could be seen at the periphery of supragingival plaque away from the enamel surface (Mark Welch et al., 2016), which was formed at the very beginning of the acquired pellicle and closest to the outside air, which determined a different metabolism to the inside bacteria (Rickard et al., 2003). This local, specific structure was made of the central filament *C. matruchotii* encased by cocci *Streptococcus*, which could not be formed around other filamentous bacteria nearby such as *Fusobacterium*, *Leptotrichia*, or *Capnocytophaga*, revealing a particularly close relationship between *C. matruchotii* and *Streptococcus*. Previous studies showed that the species belonging to *Streptococcus* involved in corncob structure included *Streptococcus sanguis* and *Streptococcus cristatus* (Listgarten et al., 1973; Takazoe et al., 1978). However, the results claimed by Anders Esberg et al. only verified the co-aggregation and co-adhesion between *C. matruchotii* and *Streptococcus cristatus*, which may imply a connection that did not result from directly binding specific components to the respective cell surfaces. Puthayalai Treerat et al. co-cultured *Corynebacterium* and *S. sanguinis* in transwell culture plates that prevented direct contact between bacteria and found out free fatty acid transported by membrane vesicles of *Corynebacterium* could elongate chains and promote fitness of *S. sanguinis* (Treerat et al., 2020). The free fatty acids mediated by membrane vesicles as potential signaling molecules to impact *Streptococcus* and participate in biological activity without direct contact were also reported in other *Corynebacterium* (Boyan et al., 1984; Bomar et al., 2016), which implied a specific role of membrane vesicles enveloping fatty acids.

Besides, around the "corncob" region, an interesting manifestation could be observed: only when *Streptococcus* bound to *Corynebacterium* did *Haemophilus/Aggregatibacter* appear

next to *Corynebacterium* (Mark Welch et al., 2016). Recently, a group verified the co-occurrence between *Haemophilus parainfluenzae* and *Streptococcus mitis* and assumed their proximity may be attributed to *H.parainfluenzae*'s dependence on NAD produced by *S. mitis* (Perera et al., 2022). Though many *streptococci* shared the common ability to generate hydrogen peroxide (H_2O_2), which inhibited other bacteria's growth, *H.parainfluenzae* seemed to evolve a hydrogen peroxide redundant system on account of frequent co-occurrence with *Streptococcus* (Kreth et al., 2009; Perera et al., 2022). Thus, from the local "corncob" region, it can be confirmed that behind the organized architecture of supragingival plaque, bacteria do have functional connections that match spatial structures, and there may be a strict temporal order for them to be involved. Additionally, *C. matruchotii*, as the predominant bacteria of *Corynebacterium* in the supragingival plaque, probably plays a big part in the beginning in shaping the biofilm structure.

C. MATRUCHOTII IN ORAL DISEASES ASSOCIATED WITH SUPRAGINGIVAL PLAQUE

C. matruchotii and Caries

Dental caries remains one of the most prevalent chronic diseases in both children and adults, and it is shown to be a result of the demineralization of tooth enamel by acid corrosion (Heng, 2016). *Streptococcus mutans* is the primary pathogen of dental caries, and based on its strong ability of acid production and acid resistance, along with its possession of glycotransferase, it can use dietary sugar to produce insoluble glucans to form oral biofilm and generate acid to decalcify dental enamel and cause caries (Johansson et al., 2016). Recently, with the popularity of sequencing technology in clinical practice, the role of *C. matruchotii* seems to act as an opposite to *S. mutans* and tends to be considered as a marker of a caries-free state, which is depicted in **Figure 1**.

Muawia A Qudeimat et al. collected supragingival plaque samples from 64 caries-active and 64 caries-free middle eastern children and performed 16S rRNA sequencing (Qudeimat et al., 2021), and their results showed that *C. matruchotii* was relatively more abundant in the caries-free group. This result was consistent with the research conducted by Nezar Noor Al-Hebshi et al. using metagenome sequencing (Al-Hebshi et al., 2019). Based on the abundance alteration in different situations, these findings implied that *C. matruchotii* may own protective property and could be a representative species for caries-free status. At the same time, in all these studies, *S. mutans* showed a predominant abundance in the caries group and with the progression of caries, the abundance of *S.mutans* became higher, while the abundance of *C. matruchotii* decreased gradually (Gross et al., 2010). The consequence seemed to show a reciprocal relationship between *S. mutans* and *C. matruchotii* in microecology of supragingival plaque and dental caries was the outcome of transferred superiority from *C. matruchotii* to *S.mutans*.

In 2020, Dongyeop Kim et al. discovered a 3D corona-like structure with a high frequency of detection in people with caries by fluorescence *in situ* hybridization in intact biofilms formed on carious teeth of toddlers; this was constructed with an inner core of *S. mutans* surrounded by outer layers of other bacteria linked via extracellular polysaccharide (Kim et al., 2020). The highly organized rotund-shaped architecture, on the one hand, created localized regions of acidic pH and caused acute enamel demineralization, on the other hand, built a protective barrier against antimicrobials while increasing bacterial acid fitness. Compared with the *in situ* biofilm imaging study in healthy people by Gary G. Borisy et.al, the detection rate of "hedgehog" centered on *C. matruchotii* was cut in half, however, at the same time, the dominant "rotund-shaped" *S. mutans* became the most commonly detected architecture in people with caries (Mark Welch et al., 2016). Thus, combined with the "pillar" role of *C. matruchotii* in the structure of dental plaque in healthy people, it could be inferred that *C. matruchotii* might perform a key part in the formation and stabilization of healthy dental plaque. In contrast, the reduction of *C. matruchotii* may directly lead to the break of biofilm homostasis. Meanwhile, the decreased abundance of *C. matruchotii,* based on the close relationship shown in corncob structure of supragingival biofilm, might also be part of the reduction of commensal *streptococci,* such as *Streptococcus gordonii* and *S. sanguinis* (Agnello et al., 2017; Richards et al., 2017), reported before, which showed an antagonistic effect against *S. mutans via* their capability of producing hydrogen peroxide (Kreth et al., 2008). The alteration could finally contribute to a replacement of dominant species in the oral ecosystem and induce the formation of diseased-adapted supragingival plaque determined by *S. mutans* that lead to disorders in acid-base metabolism and eventually cause the demineralization of tooth enamel. In general, *C. matruchotii* is a potential indicator of a caries-free state, and the reduction of its abundance may indicate the evolution from healthy plaque to caries biofilm.

C. matruchotii and Supragingival Calculus Associated With Periodontal Diseases

Supragingival calculus is the plaque and sediment that has calcified or is calcifying on the tooth surface touching or above the gingival margin, which can cause gingival inflammation and contribute to periodontal diseases. As reported before, *C. matruchotii* was a calcified bacterium that had the strong ability to deposit calcium and induce mineralization *in vitro* and may participate in the formation of supragingival calculus (Sidaway, 1978a; Takazoe and Itoyama, 1980; van Dijk et al., 1998) (**Figure 2**). With the superior ability to accumulate and mineralize calcium (Sidaway, 1978b), together with the fact that salivary levels of calcium increased in higher calculus formers and in periodontal diseases (Mandel, 1972; Sutej et al., 2012), *C. matruchotii* seemed to be an "organ" responsible for calcium metabolism in oral ecosystems analogous to *Entotheonella sp* in marine ecosystems in that they may prompt a similar absorption, accumulation, and mineralization process of ions (Keren et al., 2017).

The reason for supragingival calculus to promote periodontal diseases, as past scholars have highlighted, is attributed to

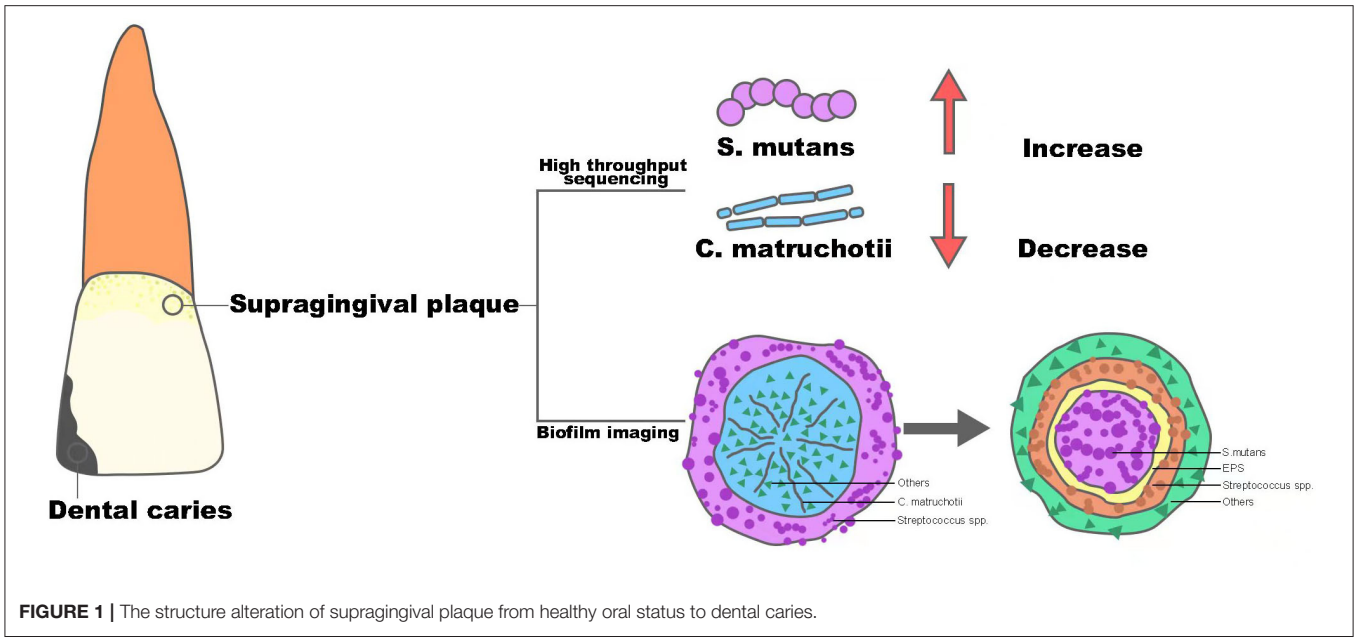

FIGURE 1 | The structure alteration of supragingival plaque from healthy oral status to dental caries.

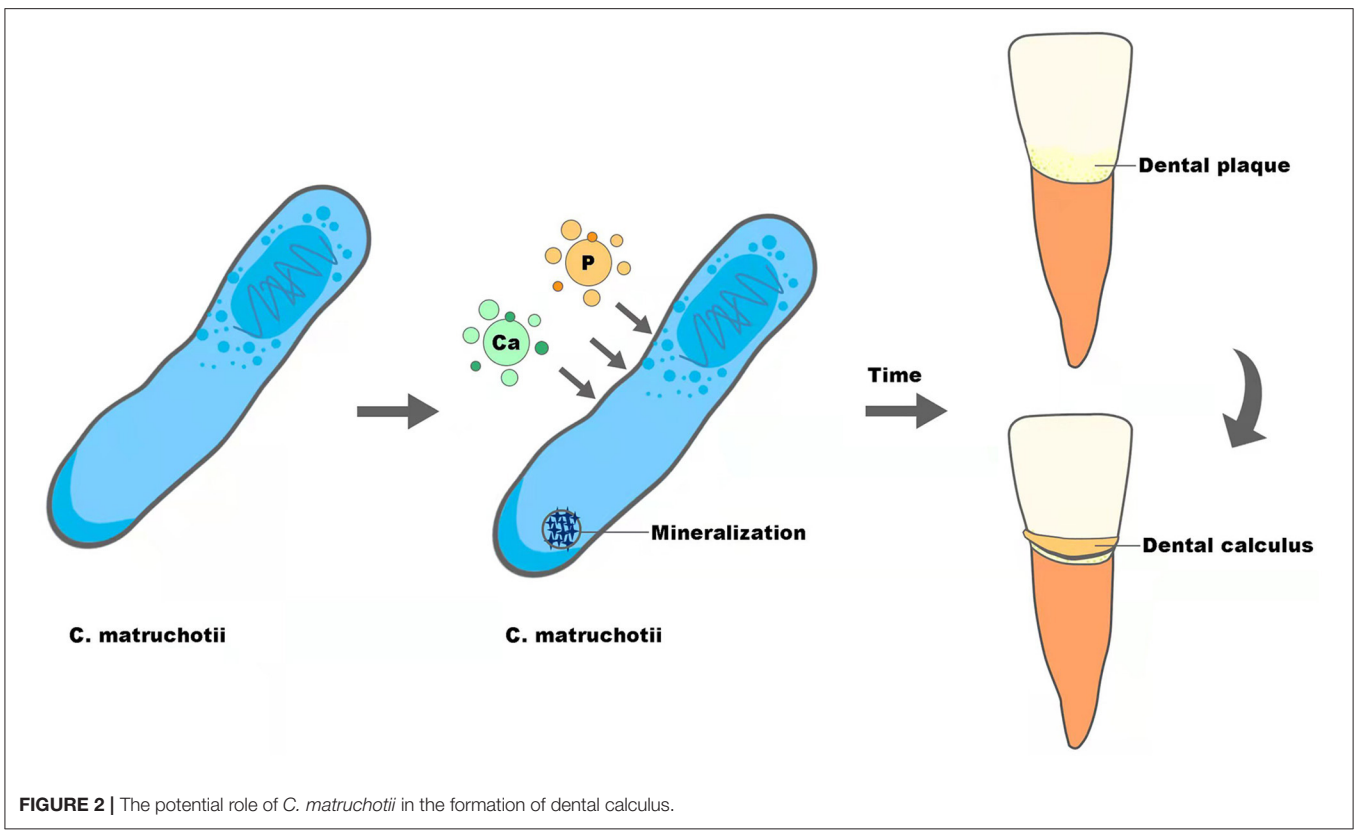

FIGURE 2 | The potential role of *C. matruchotii* in the formation of dental calculus.

the porous structure derived from dental calculus, which accommodated a large number of periodontitis-related pathogenic bacteria such as *Porphyromonas gingivalis* and their virulence factors (Socransky, 1970; Velsko et al., 2019). Recently, in addition to bacterial factors, studies showed that crystal properties or small calcium phosphate particles contained in dental calculus could directly cause periodontal inflammation as well. Experiments by Jorge Luis Montenegro Raudales et al. demonstrated that after heating dental calculus at 250°C for 1 h to eliminate residual bacteria, the treated calculus still activated

NLRP3 inflammasome and promoted IL-1β secretion, which was involved in bone resorption and could also be induced by *P. gingivalis* (Ziauddin et al., 2018). In another study, Yu Sakai et al. found that tiny calcium phosphate particles stimulated gingival epithelial cells through the NF-kB pathway leading to a significant increase in the expression of interleukin-8 at the gene and protein levels, which could attract more neutrophils to participate in the development of periodontitis (Sakai et al., 2014). Thus, whether supragingival calculus is a deposit of pathogenic bacteria or an independent physical stimulus factor, the potentially important calculus former, *C. matruchotii,* seems to indirectly influence the progression of periodontal diseases.

The formation of dental calculus can be separated into three steps, formation of the acquired pellicle, plaque maturation, and plaque mineralization, and the first two are similar to the formation of dental biofilm. Inspired by recent research displaying dental calculus as the revelator of information about plenty of biological information (Weyrich et al., 2017; Jersie-Christensen et al., 2018; Willmann et al., 2018), we speculate that calculus could also be able to mirror the characteristics of dental plaque that forms it. The ability of calcification, along with the relatively high abundance and biogeography in the center of supragingival plaque, may give *C. matruchotii* a necessary role in calculus formation, though the transformation from dental plaque to calculus indicates alteration of plaque composition and structure (Velsko et al., 2019). Therefore, to give a more convincing conclusion about the role of *C. matruchotii* in supragingival calculus, studies with more samples are needed.

CONCLUSION AND FUTURE PERSPECTIVES

After a long period of silence, *C. matruchotii* has once again appeared in research as a "pillar-like" structure in supragingival plaque, studies declaring its important role in oral biofilm and close interaction with numerous resident oral bacteria. Thus, it is promising to explore cooperative or competitive relationships between *C. matruchotii* and other commensals for a better understanding of the mechanisms behind the unique structure. Moreover, since interactions among bacteria determine the order for different bacteria joining in the formation of plaque, dynamics studies on a timeline can help us have a greater knowledge of the formation process of supragingival plaque and discover the "keystone" to stabilize or facilitate healthy plaque. The distinctive supragingival architecture along with microbial high-throughput sequencing results between caries-active and caries-free people shows the potential of *C. matruchotii* as an indicator of a healthy state, so it's worthy to investigate the function of the structure dominated by *C. matruchotii*. Additionally, it is also intriguing to see how carious "corona" replaces the healthy "hedgehog" to seek essential external or internal factors that cause a change in the nature of plaque; this can provide more insights into the development of strategies to prevent caries, precisely targeting on specific biofilm architecture.

Dental calculus in contact with gingival epithelial can induce inflammation to some extent and be an important contributing factor to periodontal diseases. The hidden reasons for its pathogenicity lie in the pathogens stuck in it as previously demonstrated and crystalline substances as recently claimed. *C. matruchotii* is confirmed to have a calcified ability, and it serves a central role in supragingival plaque establishing close associations with plenty of bacteria, which endow it with a non-negligible effect in the formation of biofilm and calculus. Moreover, in subgingival plaque of patients with periodontitis, *C. matruchotii* was reported to over-express a large number of putative virulence factors that could have importance in the evolution of the disease (Duran-Pinedo et al., 2014). Therefore, it is interesting to conduct studies on the relationship between *C. matruchotii*, calculus, and periodontal diseases, which may help us better understand the role *C. matruchotii* plays in plaque-related gingival diseases. Moreover, combined with the latest hot reports pointing out dental calculus as a potential repository of bio-information, we make an assumption that it can also reflect the bacterial composition of dental plaque in different calculus states, which may provide some clues on whether there are certain bacteria such as *C. matruchotii* that determine an individual's heterogeneity in the number and rate of calculus formation.

Apart from dental caries and periodontal diseases, there has been a study conducted on the bacteria isolated from patients with apical periodontitis demonstrating that *C. matruchotii* was present significantly more frequently in the root canal of patients with chronic periapical periodontitis compared with patients with endo-perio lesions or pulp necrosis without obvious changes in the periapical tissue X-ray image (Korona-Glowniak et al., 2021). Apical periodontitis is a result of pulpitis, and the bacteria probably contributing to apical inflammation came from the carious lesion, which went through the apical openings of the root canals, the lateral or chamber-periodontium canals, and the pathological gingival pocket. *C. matruchotii* has hardly been investigated in this apical niche, and the abnormal enrichment in this place may make its role distinct from that in dental biofilm. Besides, *C. matruchotii* was also found a higher prevalence and a dominant part in saliva and buccal mucosa of patients with oral lichen planus, a common chronic mucocutaneous inflammatory disease (Zhong et al., 2020). To sum up, *C. matruchotii* may perform multiple roles in different areas of the oral cavity and thus deserves more studies in the future.

AUTHOR CONTRIBUTIONS

QL, FZ, YL, and JL: conceptualization, methodology, and writing-original draft preparation. QL, FZ, ZS, YL, and JL: writing-review and editing. YL and JL: supervision and project administration. All authors contributed to the article and approved the submitted version.

FUNDING

This study was supported by the National Natural Science Foundation of China (81991500, 81991501).

REFERENCES

Agnello, M., Marques, J., Cen, L., Mittermuller, B., Huang, A., Chaichanasakul Tran, N., et al. (2017). Microbiome associated with severe caries in canadian first nations children. *J. Dent. Res.* 96, 1378–1385. doi: 10.1177/0022034517718819

Al-Hebshi, N. N., Baraniya, D., Chen, T., Hill, J., Puri, S., Tellez, M., et al. (2019). Metagenome sequencing-based strain-level and functional characterization of supragingival microbiome associated with dental caries in children. *J. Oral Microbiol.* 11, 1557986. doi: 10.1080/20002297.2018.1557986

Belda-Ferre, P., Williamson, J., Simón-Soro, Á., Artacho, A., Jensen, O. N., and Mira, A. (2015). The human oral metaproteome reveals potential biomarkers for caries disease. *Proteomics* 15, 3497–3507. doi: 10.1002/pmic.201400600

Bomar, L., Brugger, S. D., Yost, B. H., Davies, S. S., and Lemon, K. P. (2016). Corynebacterium accolens releases antipneumococcal free fatty acids from human nostril and skin surface triacylglycerols. *mBio* 7, e01725–e01715. doi: 10.1128/mBio.01725-15

Borisy, G. G., and Valm, A. M. (2021). Spatial scale in analysis of the dental plaque microbiome. *Periodontol 2000*. 86, 97–112. doi: 10.1111/prd.12364

Boyan, B. D., Landis, W. J., Knight, J., Dereszewski, G., and Zeagler, J. (1984). Microbial hydroxyapatite formation as a model of proteolipid-dependent membrane-mediated calcification. *Scan Electron Microsc.* 1793–800.

Boyan-Salyers, B. D., Vogel, J. J., and Ennever, J. (1978). Pre-apatitic mineral deposition in Bacterionema matruchotii. *J. Dent. Res.* 57, 291–295. doi: 10.1177/00220345780570022501

Duran-Pinedo, A. E., Chen, T., Teles, R., Starr, J. R., Wang, X., Krishnan, K., et al. (2014). Community-wide transcriptome of the oral microbiome in subjects with and without periodontitis. *ISME J.* 8, 1659–1672. doi: 10.1038/ismej.2014.23

Ennever, J., and Creamer, H. (1967). Microbiologic calcification: bone mineral and bacteria. *Calcif Tissue Res.* 1, 87–93. doi: 10.1007/BF02008078

Ennever, J., Riggan, L. J., Vogel, J. J., and Boyan-Salyers, B. (1978). Characterization of Bacterionema matruchotii calcification nucleator. *J. Dent. Res.* 57, 637–642. doi: 10.1177/00220345780570041901

Ennever, J., Vogel, J. J., Boyan-Salyers, B., and Riggan, L. J. (1979). Characterization of calculus matrix calcification nucleator. *J. Dent. Res.* 58, 619–623. doi: 10.1177/00220345790580021401

Eriksson, L., Lif Holgerson, P., and Johansson, I. (2017). Saliva and tooth biofilm bacterial microbiota in adolescents in a low caries community. *Sci. Rep.* 7, 5861. doi: 10.1038/s41598-017-06221-z

Esberg, A., Barone, A., Eriksson, L., Lif Holgerson, P., Teneberg, S., and Johansson, I. (2020). *Corynebacterium matruchotii* demography and adhesion determinants in the oral cavity of healthy individuals. *Microorganisms* 8, 1780. doi: 10.3390/microorganisms8111780

Gross, E. L., Leys, E. J., Gasparovich, S. R., Firestone, N. D., Schwartzbaum, J. A., Janies, D. A., et al. (2010). Bacterial 16S sequence analysis of severe caries in young permanent teeth. *J. Clin. Microbiol.* 48, 4121–4128. doi: 10.1128/JCM.01232-10

Heng, C. (2016). Tooth decay is the most prevalent disease. *Fed. Pract.* 33, 31–33.

Jersie-Christensen, R. R., Lanigan, L. T., Lyon, D., Mackie, M., Belstrøm, D., Kelstrup, C. D., et al. (2018). Quantitative metaproteomics of medieval dental calculus reveals individual oral health status. *Nat. Commun.* 9, 4744. doi: 10.1038/s41467-018-07148-3

Johansson, I., Witkowska, E., Kaveh, B., Lif Holgerson, P., and Tanner, A. C. (2016). The Microbiome in Populations with a low and high prevalence of caries. *J. Dent. Res.* 95, 80–86. doi: 10.1177/0022034515609554

Keren, R., Mayzel, B., Lavy, A., Polishchuk, I., Levy, D., Fakra, S. C., et al. (2017). Sponge-associated bacteria mineralize arsenic and barium on intracellular vesicles. *Nat. Commun.* 8, 14393. doi: 10.1038/ncomms14393

Kim, D., Barraza, J. P., Arthur, R. A., Hara, A., Lewis, K., Liu, Y., et al. (2020). Spatial mapping of polymicrobial communities reveals a precise biogeography associated with human dental caries. *Proc. Natl. Acad. Sci. U. S. A.* 117, 12375–12386. doi: 10.1073/pnas.1919099117

Kolenbrander, P. E., Palmer, R. J. Jr., Periasamy, S., and Jakubovics, N. S. (2010). Oral multispecies biofilm development and the key role of cell-cell distance. *Nat. Rev. Microbiol.* 8, 471–480. doi: 10.1038/nrmicro2381

Korona-Glowniak, I., Piatek, D., Fornal, E., Lukowiak, A., Gerasymchuk, Y., Kedziora, A., et al. (2021). Patterns of oral microbiota in patients with apical periodontitis. *J. Clin. Med.* 10, 2707. doi: 10.3390/jcm10122707

Kreth, J., Merritt, J., and Qi, F. (2009). Bacterial and host interactions of oral streptococci. *DNA Cell Biol.* 28, 397–403. doi: 10.1089/dna.2009.0868

Kreth, J., Zhang, Y., and Herzberg, M. C. (2008). *Streptococcal antagonism* in oral biofilms: *Streptococcus sanguinis* and *Streptococcus gordonii* interference with *Streptococcus mutans. J. Bacteriol.* 190, 4632–4640. doi: 10.1128/JB.00276-08

Listgarten, M. A., Mayo, H., and Amsterdam, M. (1973). Ultrastructure of the attachment device between coccal and filamentous microorganisms in "corn cob" formations of dental plaque. *Arch. Oral Biol.* 18, 651–656. doi: 10.1016/0003-9969(73)90105-2

Mandel, D. (1972). Biochemical aspects of calculus formation. *J. Periodontal Res.* 7–8.

Mark Welch, J. L., Rossetti, B. J., Rieken, C. W., Dewhirst, F. E., and Borisy, G. G. (2016). Biogeography of a human oral microbiome at the micron scale. *Proc. Natl. Acad. Sci. U. S. A.* 113, E791–800. doi: 10.1073/pnas.1522149113

Naradasu, D., Miran, W., and Okamoto, A. (2020). Metabolic current production by an oral biofilm pathogen *Corynebacterium matruchotii*. *Molecules*. 25, 3141. doi: 10.3390/molecules25143141

Perera, D., McLean, A., Morillo-López, V., Cloutier-Leblanc, K., Almeida, E., Cabana, K., et al. (2022). Mechanisms underlying interactions between two abundant oral commensal bacteria. *ISME J.* 16, 948–957. doi: 10.1038/s41396-021-01141-3

Qudeimat, M. A., Alyahya, A., Karched, M., Behbehani, J., and Salako, N. O. (2021). Dental plaque microbiota profiles of children with caries-free and caries-active dentition. *J. Dent.* 104, 103539. doi: 10.1016/j.jdent.2020.103539

Richards, V. P., Alvarez, A. J., Luce, A. R., Bedenbaugh, M., Mitchell, M. L., Burne, R. A., et al. (2017). Microbiomes of site-specific dental plaques from children with different caries status. *Infect. Immun.* 85:e00106–17. doi: 10.1128/IAI.00106-17

Rickard, A. H., Gilbert, P., High, N. J., Kolenbrander, P. E., and Handley, P. S. (2003). Bacterial coaggregation: an integral process in the development of multi-species biofilms. *Trends Microbiol.* 11, 94–100. doi: 10.1016/S0966-842X(02)00034-3

Sakai, Y., Nemoto, E., Kanaya, S., Shimonishi, M., and Shimauchi, H. (2014). Calcium phosphate particles induce interleukin-8 expression in a human gingival epithelial cell line via the nuclear factor-κB signaling pathway. *J. Periodontol.* 85, 1464–1473. doi: 10.1902/jop.2014.130709

Sidaway, D. A. (1978a). A microbiological study of dental calculus. I. The microbial flora of mature calculus. *J. Periodontal Res.* 13, 349–359. doi: 10.1111/j.1600-0765.1978.tb00189.x

Sidaway, D. A. (1978b). A microbiological study of dental calculus. II. The *in vitro* calcification of microorganisms from dental calculus. *J. Periodontal Res.* 13, 360–366. doi: 10.1111/j.1600-0765.1978.tb00190.x

Socransky, S. S. (1970). Relationship of bacteria to the etiology of periodontal disease. *J. Dent. Res.* 49, 203–222. doi: 10.1177/00220345700490020401

Sutej, I., Peros, K., Benutic, A., Capak, K., Basic, K., and Rosin-Grget, K. (2012). Salivary calcium concentration and periodontal health of young adults in relation to tobacco smoking. *Oral Health Prev. Dent.* 10, 397–403. doi: 10.3290/j.ohpd.a28911

Takazoe, I., and Itoyama, T. (1980). Analytical electron microscopy of *Bacterionema matruchotii* calcification. *J. Dent. Res.* 59, 1090–1094. doi: 10.1177/00220345800590062101

Takazoe, I., Matsukubo, T., and Katow, T. (1978). Experimental formation of "corn cob" *in vitro. J. Dent. Res.* 57, 384–387. doi: 10.1177/00220345780570024101

Treerat, P., Redanz, U., Redanz, S., Giacaman, R. A., Merritt, J., and Kreth, J. (2020). Synergism between Corynebacterium and *Streptococcus sanguinis* reveals new interactions between oral commensals. *ISME J.* 14, 1154–1169. doi: 10.1038/s41396-020-0598-2

van Dijk, S., Dean, D. D., Liu, Y., Zhao, Y., Chirgwin, J. M., Schwartz, Z., et al. (1998). Purification, amino acid sequence, and cDNA sequence of a novel calcium-precipitating proteolipid involved in calcification of corynebacterium matruchotii. *Calcif. Tissue Int.* 62, 350–358. doi: 10.1007/s002239900443

Velsko, I. M., Fellows Yates, J. A., Aron, F., Hagan, R. W., Frantz, L. A. F., Loe, L., et al. (2019). Microbial differences between dental plaque and historic dental calculus are related to oral biofilm maturation stage. *Microbiome* 7, 102. doi: 10.1186/s40168-019-0717-3

Vogel, J. J., and Smith, W. N. (1976). Calcification of membranes isolated from *Bacterionema matruchotii*. *J. Dent. Res*. 55, 1080–1083. doi: 10.1177/00220345760550061201

Weyrich, L. S., Duchene, S., Soubrier, J., Arriola, L., Llamas, B., Breen, J., et al. (2017). Neanderthal behaviour, diet, and disease inferred from ancient DNA in dental calculus. *Nature* 544, 357–361. doi: 10.1038/nature21674

Willmann, C., Mata, X., Hanghoej, K., Tonasso, L., Tisseyre, L., Jeziorski, C., et al. (2018). Oral health status in historic population: Macroscopic and metagenomic evidence. *PLoS ONE*. 13, e0196482. doi: 10.1371/journal.pone.0196482

Zhong, E. F., Chang, A., Stucky, A., Chen, X., Mundluru, T., Khalifeh, M., et al. (2020). Genomic analysis of oral lichen planus and related oral microbiome pathogens. *Pathogens* 9, 952. doi: 10.3390/pathogens9110952

Ziauddin, S. M., Yoshimura, A., Montenegro Raudales, J. L., Ozaki, Y., Higuchi, K., Ukai, T., et al. (2018). Crystalline structure of pulverized dental calculus induces cell death in oral epithelial cells. *J. Periodontal. Res*. 53, 353–361. doi: 10.1111/jre.12520

Conflict of Interest: The authors declare that the research was conducted in the absence of any commercial or financial relationships that could be construed as a potential conflict of interest.

frontiers | Frontiers in Microbiology

TYPE Original Research
PUBLISHED 29 July 2022
DOI 10.3389/fmicb.2022.963292

OPEN ACCESS

EDITED BY
Huancai Lin,
Sun Yat-sen University, China

REVIEWED BY
Kaiqi Lian,
Anyang Institute of Technology, China
Manash C. Das,
Government of Tripura,
India

*CORRESPONDENCE
Jufang Wang
jufwang@scut.edu.cn

SPECIALTY SECTION
This article was submitted to Antimicrobials, Resistance and Chemotherapy, a section of the journal Frontiers in Microbiology

RECEIVED 07 June 2022
ACCEPTED 12 July 2022
PUBLISHED 29 July 2022

CITATION
Wang M, Deng Z, Li Y, Xu K, Ma Y, Yang S-T and Wang J (2022) Antibiofilm property and multiple action of peptide PEW300 against *Pseudomonas aeruginosa*. *Front. Microbiol.* 13:963292. doi: 10.3389/fmicb.2022.963292

Antibiofilm property and multiple action of peptide PEW300 against *Pseudomonas aeruginosa*

Meng Wang[1], Zifeng Deng[1], Yanmei Li[1], Keyong Xu[2], Yi Ma[1,3], Shang-Tian Yang[4] and Jufang Wang[1,3]*

[1]School of Biology and Biological Engineering, South China University of Technology, Guangzhou, China, [2]Kaiping Healthwise Health Food Co., Ltd, Kaiping, China, [3]Guangdong Provincial Key Laboratory of Fermentation and Enzyme Engineering, South China University of Technology, Guangzhou, China, [4]Department of Chemical and Biomolecular Engineering, The Ohio State University, Columbus, OH, United States

Pseudomonas aeruginosa (*P. aeruginosa*), an opportunistic pathogen, is often associated with difficulties in treating hospital-acquired infections. Biofilms formed by *P. aeruginosa* significantly improve its resistance to antimicrobial agents, thereby, posing a great challenge to the combat of *P. aeruginosa* infection. Antimicrobial peptides (AMPs) have recently emerged as promising antibiofilm agents and increasingly attracting the attention of scientists worldwide. However, current knowledge of their antibiofilm behavior is limited and their underlying mechanism remains unclear. In this study, a novel AMP, named PEW300, with three-point mutations (E9H, D17K, and T33A) from Cecropin A was used to investigate its antibiofilm property and antibiofilm pathway against *P. aeruginosa*. PEW300 displayed strong antibacterial and antibiofilm activity against *P. aeruginosa* with no significant hemolysis or cytotoxicity to mouse erythrocyte and human embryonic kidney 293 cells. Besides, the antibiofilm pathway results showed that PEW300 preferentially dispersed the mature biofilm, leading to the biofilm-encapsulated bacteria exposure and death. Meanwhile, we also found that the extracellular DNA was a critical target of PEW300 against the mature biofilm of *P. aeruginosa*. In addition, multiple actions of PEW300 including destroying the cell membrane integrity, inducing high levels of intracellular reactive oxygen species, and interacting with genomic DNA were adopted to exert its antibacterial activity. Moreover, PEW300 could dramatically reduce the virulence of *P. aeruginosa*. Taken together, PEW300 might be served as a promising antibiofilm candidate to combat *P. aeruginosa* biofilms.

KEYWORDS

antimicrobial peptides, *Pseudomonas aeruginosa*, antibiofilm, Cecropin A, mode of action

Introduction

Pathogens including *Pseudomonas aeruginosa* (*P. aeruginosa*), *Staphylococcus aureus*, *Enterococcus faecium*, *Acinetobacter baumannii*, *Klebsiella pneumonia*, and *Enterobacter* species (called "ESKAPE") infections have already been a significant problem of hospital infections and seriously threaten public health owing to their inherent antibiotic

resistance (Zhen et al., 2019b; De Oliveira et al., 2020). Biofilms are surface-associated microbial communities embedded in self-produced extracellular polymeric substances (EPSs; Lee and Zhang, 2015). Biofilm formation is beneficial for bacteria survival under adverse environmental conditions and is implicated in the majority of bacterial infections (Thi et al., 2020). With the powerful protection of biofilms, these pathogens can attach to inert surfaces of medical devices, living tissues, and implanted prostheses, and successfully "escape" the damage of antibacterial agents (Ciofu and Tolker-Nielsen, 2019; Tagliaferri et al., 2019; Thi et al., 2020). The severity of pathogen infections and the invalidation of antibiotics have resulted in high morbidity and mortality (Founou et al., 2017; Zhen et al., 2019a; Manandhar et al., 2020; Yungyuen et al., 2021).

Pseudomonas aeruginosa, a Gram-negative (G^-) bacterium, is an opportunistic human pathogen associated with clinical and chronic infections such as urinary tract infections, chronic wound infections, ventilator-associated pneumonia, and biofilm-related systemic infections (Serra et al., 2015; Shortridge et al., 2019; Abbott et al., 2020; Garcia-Clemente et al., 2020). Epidemiological surveillance reports from the European Centre for Disease Prevention and Control (ECDC) and the International Nosocomial Infection Control Consortium (INIC) revealed that *P. aeruginosa* was the most prevalent bacteria isolated from clinical samples in ICU-acquired pneumonia episodes and ICU-acquired bloodstream infections (Pang et al., 2019). As a member of the "ESKAPE" pathogens, *P. aeruginosa* has already been stipulated as a "critical" pathogen among the bacterial pathogens list of the World Health Organization (WHO), emphasizing the urgent need for the exploration and development of novel antibacterial agents to combat *P. aeruginosa* biofilms (Tacconelli et al., 2018).

In recent decades, antimicrobial peptides (AMPs) have been regarded as promising therapeutics against biofilm-forming pathogens due to their broad-spectrum antibacterial activity and inability to induce resistance (Cardoso et al., 2019; Di Somma et al., 2020; Hancock et al., 2021). Several studies on bacteria in the planktonic state have shown that AMPs adopt a unique membrane-targeting mechanism of action, unlike conventional antibiotics with specific targets, which disturb bacterial membranes mainly by interaction with negatively charged phospholipids and cause cell death (Chen et al., 2020; Li et al., 2020a; Luna et al., 2021). Significantly different from bacteria in the planktonic state, the control of biofilm-encapsulated bacteria is very difficult because of their extremely low permeability to antimicrobial agents (Gilbert et al., 2002; Hall and Mah, 2017). Previous studies have shown that biofilms could increase antibiotic resistance by up to 1,000-fold compared with planktonic bacteria (Kouidhi et al., 2015). However, these studies have mostly focused on the development of AMPs on bacteria biofilms, study on antibiofilm mechanism is still in its infancy. Hence, thorough and systematic studies on the antibiofilm mechanisms of AMPs are urgent priorities to accelerate the clinical development of AMPs as antibiofilm agents.

In our previous research, a novel AMP named PEW300 was designed by three mutations (E9H, D17K, and T33A) from Cecropin A (an natural AMP that is possible to use in medical and agricultural fields as a new and safe biocontrol agent), which had shown strong antimicrobial activity against several Gram-positive (G^+) and G-bacteria (Wang et al., 2019; Hashemi et al., 2021). In this study, PEW300 was utilized to explore the antimicrobial and antibiofilm effect on *P. aeruginosa* and reveal its mechanism of action. Initially, the physicochemical properties, hemolysis, and cytotoxicity of PEW300 were assessed. Then, we studied the antimicrobial and antibiofilm ability of PEW300 on *P. aeruginosa* and determined its antibiofilm pathway. To explore the potential targets of PEW300, the mature biofilm components, cell membrane integrity, intracellular disturbance effected by PEW300 were then investigated. Considering that virulence factors are the main culprits of bacterial infections, we also explored the impact of PEW300 on *P. aeruginosa* virulence production. This study may provide a new reference for the research on the antibiofilm mechanisms of AMPs and demonstrate that PEW300 have good potential to be a safe and efficient antibacterial agent to combat *P. aeruginosa* biofilms.

Materials and methods

Strains, chemicals, and peptide preparation

Pseudomonas aeruginosa JCM5962 was preserved in our laboratory; *E. coli* DH5α and BL21(DE3) competent cells were purchased from Tiangen Biotech (China). Dulbecco's-modified eagle medium (DMEM) and Fetal bovine serum (FBS) were purchased from Gibco (United States). The crystal violet, kanamycin, and gentamicin were obtained from Sangon Biotech Co. (China). Fluorescein isothiocyanate-labeled concanavalin A (FITC-ConA), 4′,6-diamidino-2-phenylindole (DAPI), Nile red, and SYPRO red were purchased from Sigma-Aldrich Co. (USA). The N-Phenyl-1-naphthylamine (NPN) and 3,3′-Dipropylthiadicarbocyanine iodide ($DiSC_3$-5) were purchased from Aladdin (China). All other chemicals and reagents used in this study were of reagent grade.

PEW300 peptide was produced by our previous established protein expression and purification system (Wang et al., 2018). In this system, a high yield of AMPs can be acquired by simple centrifugation, with no expensive steps like NTA affinity chromatography and high-performance liquid phase separation. Purified PEW300 was dialyzed to PBS buffer and stored at-80°C for further experiment.

Antibacterial and antibiofilm assays

The minimum inhibitory concentration (MIC) was assessed by the previously described method (Wiegand et al., 2008). Antibiofilm

assays contain inhibition of biofilm formation assay and dispersion of preformed biofilm assay. The biomass of biofilm was quantified by the crystal violet stain method (Qi et al., 2020). In inhibition of biofilm formation assay, bacteria mixed with different concentrations (0, 5, 10, 20, 50, and 100 μg/ml) of PEW300 were loaded into a sterile 96-well plate and incubated at 37°C for biofilm formation (without shaking). Twenty four hours later, the supernatant was discarded and residual planktonic cells were washed with PBS twice. The biomass of biofilm was quantified by the crystal violet stain method. In dispersion of preformed biofilm assay, the preformed biofilms were incubated with different concentrations of PEW300 peptide (0, 5, 10, 20, 50, 100 μg/ml) at 37°C and the crystal violet stain method was performed to quantify the remaining biofilm. For cell viability detection, the mature biofilms were scraped with the pipette and sonicated for 10 min under low power condition (60 W) to release the viable bacteria. The sonicated suspensions were diluted and 50 μl was coated on a Mueller-Hinton agar plate. After incubation at 37°C for 16 ~ 18 h, the CFUs were counted.

Hemolytic test, cytotoxicity, and drug resistance assays

For hemolytic test, the erythrocytes separated from mice blood were washed twice with 0.9% saline solution and then treated with 100 μl serial dilutions of PEW300 for 1 h. The hemolysis activity was determined by the hemoglobin content obtained from the absorbance of the supernatant at 570 nm after centrifugation. PBS and 0.1% Triton X-100 treatment were served as negative (0 hemolysis) and positive (100% hemolysis) controls. Human embryonic kidney 293 (HEK293) cells were adjusted to 1×10^5 cells/ml with DMEM and dispensed into 96-well plates per 100 μl. Subsequently, increased concentrations of PEW300 (8 ~ 276 μg/ml) were added into 96-well plates separately and incubated with 5% CO_2 for 48 h at 37°C. Cell viability was examined by cell counting kit-8 (CCK-8) assay (Beyotime, China). The drug resistance of *P. aeruginosa* to PEW300 and gentamicin were evaluated by the sequential passaging method according to the previous description (Huang et al., 2020). Briefly, *P. aeruginosa* cells were cultured to log phase and diluted to 2×10^5 CFU/ml. Then, sub-MIC concentrations (1/2 MIC) of PEW300 and gentamicin, respectively, were incubated with the above bacterial suspension for 24 h at 37°C (*P. aeruginosa* grows for approximately 12 generations). These steps were repeated until 300 generations of growth were obtained. The number of generations was calculated from the value of $\log_2$ (bacterial concentration/2×10^5). After every 24 h, the MIC values of PEW300 and gentamicin against *P. aeruginosa* were determined as described above.

Circular dichroism measurement

The Circular dichroism (CD) spectra of PEW300 were measured on a Chirascan qCD Spectrometer (Applied Photophysics, United Kingdom) with wavelengths ranging from 190 to 260 nm using a 1 mm path length cuvette in 30 mM SDS and double-distilled water, respectively. Spectra were recorded with a band-width of 1 nm, a duration time of 1 s, and a scan speed of 100 nm/min. Each measurement was repeated three times to calculate the mean value. The spectra from the solvent were subtracted as background in data analysis.

EPS analysis

After biofilm formation in 96-well flat-bottomed plate, the wells were washed with PBS twice and 100 μl of PEW300 at a concentration of 60 μg/ml were added into the wells and incubation for 24 h at 37°C. After incubation, the treated biofilms were washed with PBS and subsequently stained with 100 μl of the following fluorescent dyes (1:500 diluent of SYPRO red for proteins, 50 μg/ml FITC-ConA for carbohydrates, 0.5 μg/ml DAPI for extracellular DNA (eDNA), and 20 μM Nile red for lipids) at room temperature in the dark. The stained biofilms were visualized under a Leica DMI 6000 microscope (Germany).

Mature biofilms treated with increased concentrations (0, 10, 20, 40, 60 μg/ml) of PEW300 were incubated at 37°C for 24 h. Subsequently, EPS was extracted using a previous reported sonication method (Li et al., 2020c), and the amounts of carbohydrates, eDNA, and proteins were then analyzed. Quantitation of carbohydrates was applied by the phenol-sulfuric acid method as previously reported (Kim and Park, 2013). The amount of eDNA was determined using a Quant-iTTM PicoGreen R dsDNA Assay Kit (Invitrogen, United Kingdom). The protein content in EPS was quantified by the Lowry method using a Stable Lowry Protein Assay Kit (Sangon Biotech, China).

Lipopolysaccharides binding assay, outer membrane permeability assay, and inner membrane depolarization test

The Lipopolysaccharides (LPS) (from *E. coli* O111:B4, Sigma-Aldrich, United States) binding affinity of PEW300 was assessed by monitoring the bacteria growth (OD_{600}) inhibition with PEW300 pretreated with different concentrations (0, 5, 10, 20, 40, 80, and 160 μg/ml) of LPS; Permeabilization of *P. aeruginosa* outer membrane (OM) was evaluated by detecting the changes in fluorescence emission intensity of NPN with increased concentrations (0, 20, 40, and 80 μg/ml) of PEW300 according to the previous reported method (Wang et al., 2020); The IM depolarizing ability of PEW300 (8.25, 17.5, 35, and 70 μg/ml) was detected by monitoring the changes in fluorescence emission intensity of the $DiSC_3$-5 dye at excitation and emission wavelengths of 622 and 670 nm, respectively (Li et al., 2020b).

Transmission electron microscopy and scanning electron microscopy analyses

For transmission electron microscopy (TEM) observation, log-phase *P. aeruginosa* were treated with 20 μg/ml PEW300 and incubated at 37°C for 0, 10, 30, and 120 min. Then, a drop of bacteria suspension was placed on the prepared carbon film copper mesh for 5 min, cells were negatively stained with 3% phosphotungstic acid (Aladdin, China) for 3 min and blotted dry. Unbound phosphotungstic acid was washed with deionized water twice. Then cells were viewed on a Talos L120C TEM (Thermo Fisher Scientific, United States). For scanning electron microscopy (SEM) analysis, 1 ml of the diluted *P. aeruginosa* suspension ($OD_{600} \approx 0.1$) in cation-adjusted Mueller-Hinton broth (CAMHB) was cultured in a 24-well plate with round glass bottom at 37°C for 24 h. Later, the supernatant was discarded and the plate was washed by PBS three times, then the preformed biofilms were incubated with 50 μg/ml PEW300 at 37°C for 2, 4, 6, 8, and 10 h. Untreated biofilm served as the control. After incubation, biofilms were fixed in 2.5% glutaraldehyde (Aladdin, China) at 4°C overnight and dehydrated with a graded series (70%, 85%, 95%) of ethanol for 10 min and soaked in 100% ethanol for 20 min. Dehydrated biofilms were dried with liquid CO_2 at the critical point using an Autosamdri-815 (Tousimis, United States). Eventually the biofilms were coated by a gold sputter coater and examined using a HitachiS-500 SEM (Hitachi, Japan).

Flow cytometric assay

Pseudomonas aeruginosa cultured in Mueller-Hinton broth (MHB) were harvested and washed with PBS three times, followed by resuspended in PBS. 10 μg/ml of Propidium Iodide (PI) was added to the suspension and incubated at room temperature for 10 min. Afterward, 20 μg/ml of PEW300 peptides were added to the suspensions and incubated at 37°C for 10, 20, 30, 60, and 120 min, separately. After incubation, the unbound PI was removed by centrifugation at 5,000×*g* for 5 min and the samples were analyzed using a CytoFLEX flow cytometer (Beckman Coulter, United States).

DNA binding assay and intracellular reactive oxygen species assay

About 200 ng of purified *P. aeruginosa* genome DNA was mixed with different amounts (0, 4, 8, and 16, 32 μg/ml) of PEW300 and incubated at room temperature for 10 min. The mixtures were electrophoresed in 1% agarose gels containing 0.5 μg/ml ethidium bromide and the DNA bands were visualized using a gel documentation and image analysis system (BLT, China). The intracellular reactive oxygen species (ROS) level in *P. aeruginosa* was performed as described previously (Xiao et al., 2020). Briefly, *P. aeruginosa* cells at log-phase were mixed with 40 mM of 2,7-Dichlorodihydrofluorescein diacetate (DCF-DA) and incubated at 37°C for 30 min. After incubation, the cells were washed with PBS twice and an aliquot of 90 μl of diluted cells (1×10^8 CFU/ml) was mixed with 10 μl of different concentrations (5, 10, 20, and 40 μg/ml) of PEW300 in a 96-well plate. PBS and 1% Triton X-100 were used as negative and positive controls. Then, the DCF fluorescence intensity was recorded on a SpectraMax M2 plate reader using an excitation wavelength of 488 nm and an emission wavelength of 530 nm.

Real-time quantitative PCR and evaluation of *Pseudomonas aeruginosa* virulence

Pseudomonas aeruginosa cells were diluted to 10^8 CFU/ml with MHB, then incubated with 10 μg/ml of PEW300 at 37°C for 8 h, cells with no PEW300 treatment as control. Total RNA was extracted from 5 ml cultures. The RNA extraction was assessed using RNAprep Pure Cell/Bacteria Kit (TIANGEN, China) according to the manufacturer's instructions. Real-time quantitative PCR (qPCR) was carried out using LightCycler®96 (Roche, Switzerland) with SYBR Premix Ex Taq II (Tli RNaseH Plus) according to the manufacturer's instructions. The expression level of 16S rRNA was used to normalize that of other genes. All experiments were repeated at least three times, and the primer sequences used in this experiment are publicly available (Supplementary Table S1).

A549 cells were adjusted to 1×10^4 cells/mL and 100 μl of cells were seeded into a 96-well plate and incubated at 37°C with 5% CO_2 for 48 h. Cells containing different concentrations (0, 5, 10, and 20 μg/ml) of PEW300 were infected with *P. aeruginosa* at a multiplicity of infection (MOI) of 10 for 6 h and the cell viability was assessed by CCK-8 assay. Besides, 4 μM calcein-AM (Santa Cruz, United States) was incubated with A549 cells at a density of 1×10^5 cells/dish for 20 min in D-Hanks buffer and observed using a Leica DMI 6000 microscope. For comparative analysis of virulence production (pyocyanin, elastase, and alginate) with or without PEW300 treatment, *P. aeruginosa* cells were adjusted to an initial OD_{600} at 0.1 and incubated with increasing concentrations (0, 10, and 20 μg/ml) of PEW300 at 37°C for 8 h. Elastolytic activity was assessed using a 1% skimmed milk plate as previously reported (Cowell et al., 2003); Pyocyanin content was determined by chloroform-hydrochloric acid extraction method as previously described (Xu et al., 2016); The amount of alginate was quantified using the borate-carbazole method with sodium alginate (Sigma, United States) as a standard (Knutson and Jeanes, 1968).

Statistical analysis

Each experiment was performed in triplicate and the data were analyzed by SPSS 16.0 software (SPAA Inc., Chicago, IL, United States). The data were presented as the means ± standard deviation and the statistical significance was defined as $p < 0.05$.

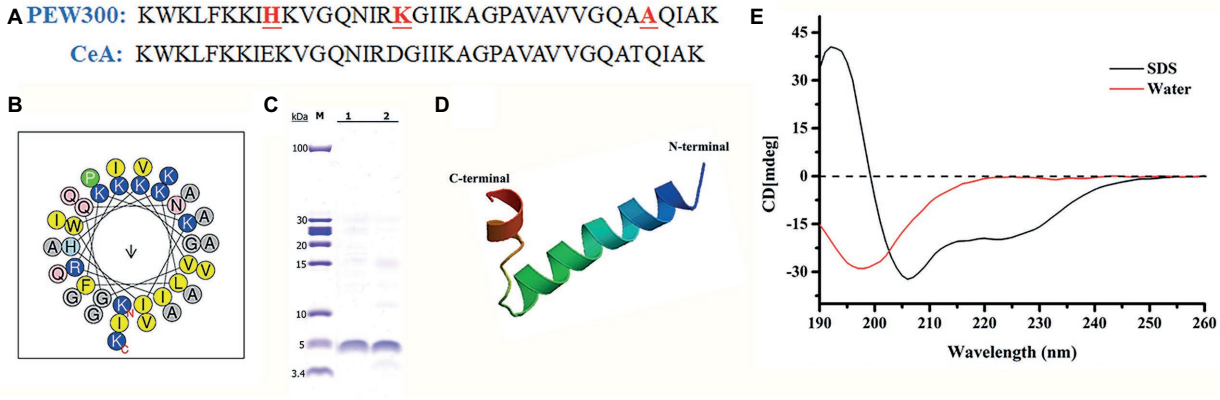

FIGURE 1
Physicochemical properties of the PEW300 peptide. **(A)** The sequences of PEW300 and Cecropin A (CeA). The red font and underline sites indicate mutation sites of the PEW300 peptide. **(B)** Predicted alpha-helical wheel of PEW300 peptide (https://heliquest.ipmc.cnrs.fr/cgi-bin/ComputParams.py). The hydrophobic residues are yellow, positively charged hydrophilic residues are blue, and non-charged polar residues are gray. **(C)** Purification of PEW300 peptide. Line 1 and line 2 are purified PEW300 peptides. **(D)** The secondary structure of PEW300 predicted by SWISS-MODEL (https://swissmodel.expasy.org/interactive). **(E)** CD spectra of the PEW300 peptide.

Results and discussion

Characterization of PEW300 peptide

Compared with Cecropin A peptide, PEW300 owns three mutations in residues 9 (Glu to His), 17 (Asp to Lys), and 33 (Thr to Ala; Figure 1A). As predicted by Helical-wheel projection, PEW300 exhibited no negatively charged residues and was mainly composed of hydrophobic residues, non-polar residues, and positively charged residues, which is consistent with the general sequence properties of AMPs (Figure 1B). In addition, we analyzed the hydrophobicity and electrostatic potential of PEW300 surface, which showed its good amphipathic property and the strong positive charge at its N-terminus, indicating that PEW300 might possess higher antibacterial activity (Supplementary Figure S1). In this study, high purity of PEW300 peptide was acquired by our previously established peptide expression system (Figure 1C; Wang et al., 2018). The secondary structure of PEW300 as predicted by SWISS-MODEL showed it belongs to α-helical AMPs (Figure 1D). To investigate the structure of PEW300 in aqueous and mimic hydrophobic membrane environments, CD spectroscopy was performed. As shown in Figure 1E, PEW300 displayed a disordered structure in double-distilled water. In 30 mM sodium dodecyl sulfate (SDS), PEW300 exhibited two negative peaks at about 208 and 225 nm and a positive peak at about 192 nm, demonstrating a typical α-helical structure predisposition which is consistent with the predicted result (Figure 1D).

Hemolytic activity, cytotoxicity, and drug resistance of PEW300

As high hemolysis and cytotoxicity of AMPs are two critical factors that considerably hinder their further application (Zhu et al., 2020), we assessed the hemolytic activity and cytotoxicity of PEW300. As shown in Figure 2A, PEW300 showed negligible hemolytic activity at concentrations ranging from 50 to 250 μg/ml. The cell toxicity of PEW300 was determined using HEK293 cells by CCK-8 assay and the result showed that PEW300 had no cytotoxicity to HEK293 cells when ~276 μg/ml of PEW300 was used (Figure 2B). These results implied that PEW300 had good biosafety and might have good potential for further application. Although many studies had demonstrated that *P. aeruginosa* hardly developed drug resistance toward AMPs (Mahlapuu et al., 2016; de Breij et al., 2018), it is still necessary to assess the tendency of drug resistance of *P. aeruginosa* against PEW300. In the presence of sub-MIC levels of PEW300, we performed serial passage of nearly 300 generations of *P. aeruginosa* with no resistance as PEW300 continued to inhibit the growth of *P. aeruginosa* at MIC level (Figure 2C). However, the drug resistance of *P. aeruginosa* toward gentamicin appeared as early as the 36th generation and the MIC value increased approximately three times after 300 generations (Figure 2C). Taken together, these results indicated that PEW300 were less likely to cause *P. aeruginosa* resistance.

Antibiofilm pathway of PEW300 against *Pseudomonas aeruginosa*

In our previous study, PEW300 showed a broad-spectrum antibacterial activity and inhibited most pathogenic bacteria including *Klebsiella pneumoniae*, *S. aureus*, *Staphylococcus epidermidis*, and *Bacillus cereus* among others with MICs between 4.93 to 28.35 μg/ml (Wang et al., 2019). Consistent with our expectations, PEW300 showed strong antimicrobial activity against *P. aeruginosa* with a MIC of 12.5 μg/ml (Figure 3A). Commonly used antibiotics in hospital such as gentamicin and kanamycin were

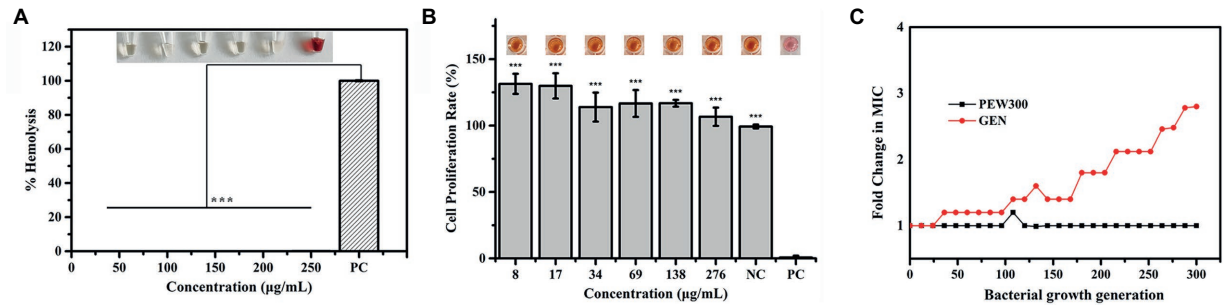

FIGURE 2
Hemolytic activity, cytotoxicity, and drug resistance of PEW300. **(A)** Hemolytic activity of PEW300 in mouse red blood cells. 0.1% Triton X-100 was used as the positive control (PC); ***p<0.005 compared with PC group. **(B)** Cytotoxicity of PEW300 in HEK293 cells was determined by a CCK-8 assay. 0.1% Triton-X 100 and PBS were used as positive control (PC) and negative control (NC), respectively. Error bars represent the standard error from mean cell viabilities from three replicates, *** indicates p<0.005 compared with PC group. **(C)** Drug resistance of the PEW300 and gentamicin. GEN, gentamicin.

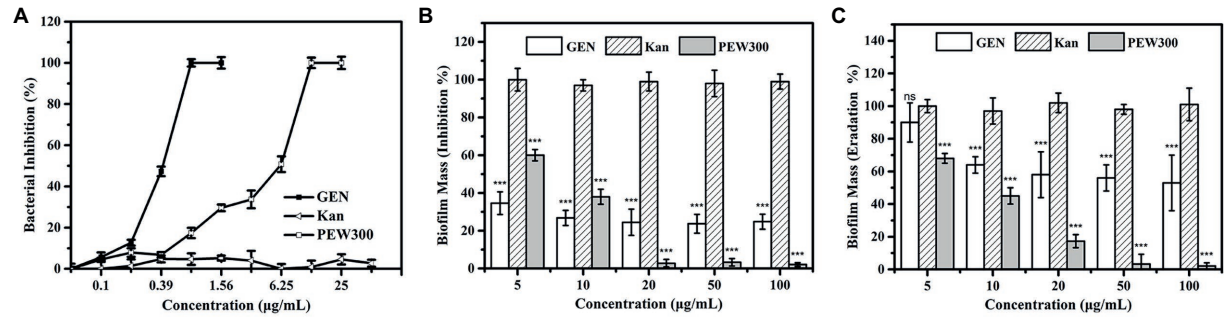

FIGURE 3
Antibacterial and antibiofilm properties of PEW300. **(A)** Antibacterial activity of PEW300, kanamycin (Kan), and gentamicin (GEN) against *Pseudomonas aeruginosa* JCM5962. **(B)** Inhibition and **(C)** dispersion activity of PEW300 against *P. aeruginosa* JCM5962 biofilms. Error bars represent standard error from mean values as determined by three repeated experiments, *** indicates p<0.005 and ns means no significant difference compared with Kan-treated groups.

selected as controls. As depicted in Figure 3A, compared with PEW300, gentamicin exhibited the strongest antimicrobial activity against *P. aeruginosa* (MIC value was 0.78 μg/ml), while kanamycin was ineffective with a MIC value greater than 100 μg/ml. In determination of antibiofilm ability, PEW300 showed a dose-dependent manner and approximately 98% of biofilm formation was inhibited when treated with 20 μg/ml of PEW300 (Figure 3B). Adopted the same manner, a dose-dependent dispersion activity of PEW300 on mature biofilm was observed and nearly 95% of mature biofilms were eradicated with 50 μg/ml of PEW300 treatment (Figure 3C). However, gentamicin was ineffective in both inhibition of biofilm formation and mature biofilm dispersion, especially as only 50% of mature biofilms were eradicated when treated with gentamicin at concentrations up to 100 μg/ml (Figures 3B, C). Previous studies demonstrated that the main cause of this failure of antibiotics against biofilms was the incomplete penetration of antibiotics into biofilm and thus caused the inability to interact with them (Roy et al., 2018; Sharma et al., 2019). Instead, AMPs could freely penetrate into biofilm because of their amphipathic properties and flexible structures, this might confer their antibiofilm ability. These results demonstrated that PEW300 exhibited excellent antibiofilm activity on *P. aeruginosa* biofilms.

To investigate whether PEW300 act preferentially on the biofilm or the bacteria encased by biofilm, preformed biofilms were incubated with 50 μg/ml of PEW300 for 0, 2, 4, 8, 12, and 24 h. Cell viability and biofilm mass were analyzed at the same time. As depicted in Figure 4A, interestingly, we discovered PEW300 preferentially acted on the preformed biofilms, and nearly 60% of biofilms were eradicated within the first 2 h of incubation. Afterward, cell viability significantly decreased during 4 to 8 h of incubation and ~100% of cells were dead after 8 h of PEW300 treatment. To further understand the antibiofilm property of PEW300 on *P. aeruginosa*, a time-killing kinetic assay was also performed. As indicated in Figure 4B, PEW300 exhibited a dose-dependent dispersion of established biofilms and approximately 65% of the preformed biofilms were eradicated within 30 min, indicating that PEW300 has a rapid and efficient effect on the preformed biofilms. Similarly, PEW300 interacted with bacteria in a dose-dependent fashion and nearly 100% of bacteria were killed within 30 min (Figure 4C). Based on these

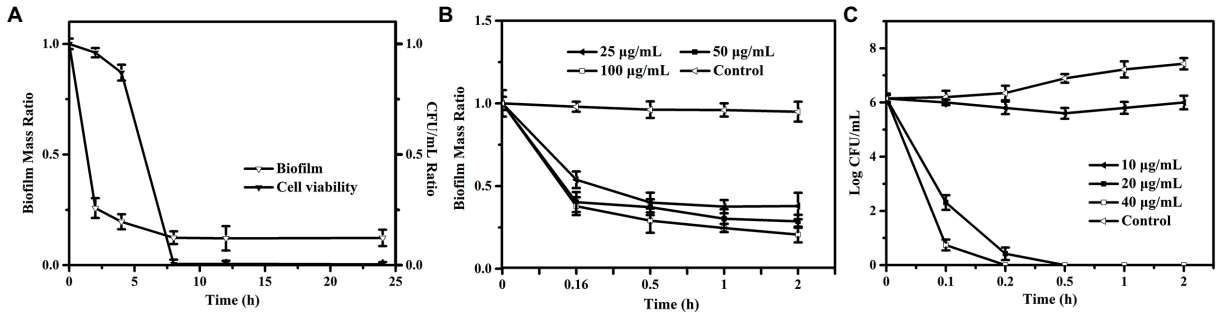

FIGURE 4
Antibiofilm pathway and time-killing kinetic analysis of PEW300 against *Pseudomonas aeruginosa*. **(A)** Antibiofilm pathway of PEW300 against *P. aeruginosa*. Reductive effect of PEW300 against *P. aeruginosa* biofilm **(B)** and planktonic cells **(C)**.

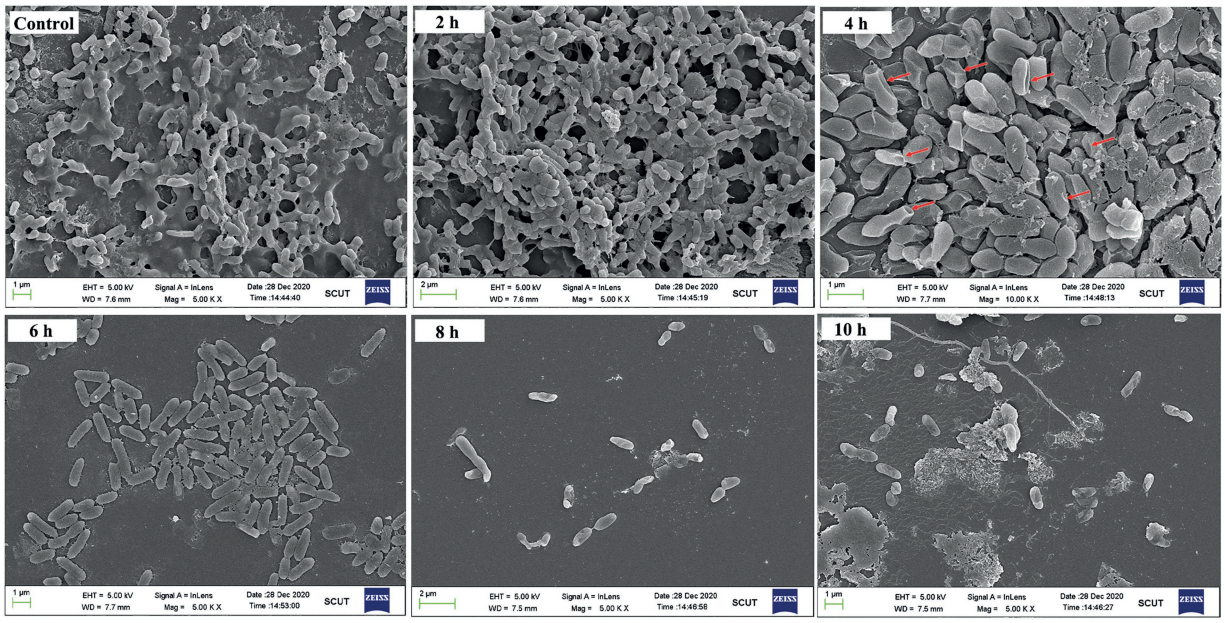

FIGURE 5
SEM observation of preformed biofilm of *Pseudomonas aeruginosa* JCM5962 affected by PEW300. The red arrow indicates the damaged JCM5962 cells.

findings, we speculate that PEW300 may preferentially act on the preformed biofilm and result in its degradation, the removal of biofilm led to the bacteria exposure that was then killed by PEW300 in a further incubation time.

To confirm this conclusion, an SEM observation was performed. As shown in Figure 5, in the absence of PEW300 treatment, massive biofilms enveloping *P. aeruginosa* cells were observed. After 2 ~ 4 h of PEW300 treatment, most biofilms disappeared and the encased *P. aeruginosa* cells were exposed. It is worth noting that the majority of bacteria were intact and no morphological abnormalities had been found within 2 h of PEW300 treatment. However, after 4 h of treatment, the cell morphology showed obvious wrinkles, fractures, and fragments, indicating that PEW300 destroyed the integrity of cell membrane. A significant reduction of *P. aeruginosa* cells was noticed with the prolongation of the incubation time (6 ~ 10 h; Figure 5). These results are consistent with the results of Figure 4A and confirm our speculations.

Impact of PEW300 on the components of *Pseudomonas aeruginosa* biofilm

Based on the above observations, we then investigated how PEW300 eradicated the preformed biofilms of *P. aeruginosa*. Four specific fluorescent dyes (FITC-ConA, Nile red, DAPI, and SYPRO red, which are separately able to bind to carbohydrates, lipids, eDNA, and proteins in biofilm) were utilized in this experiment. As shown in Figure 6A, PEW300 had a negligible

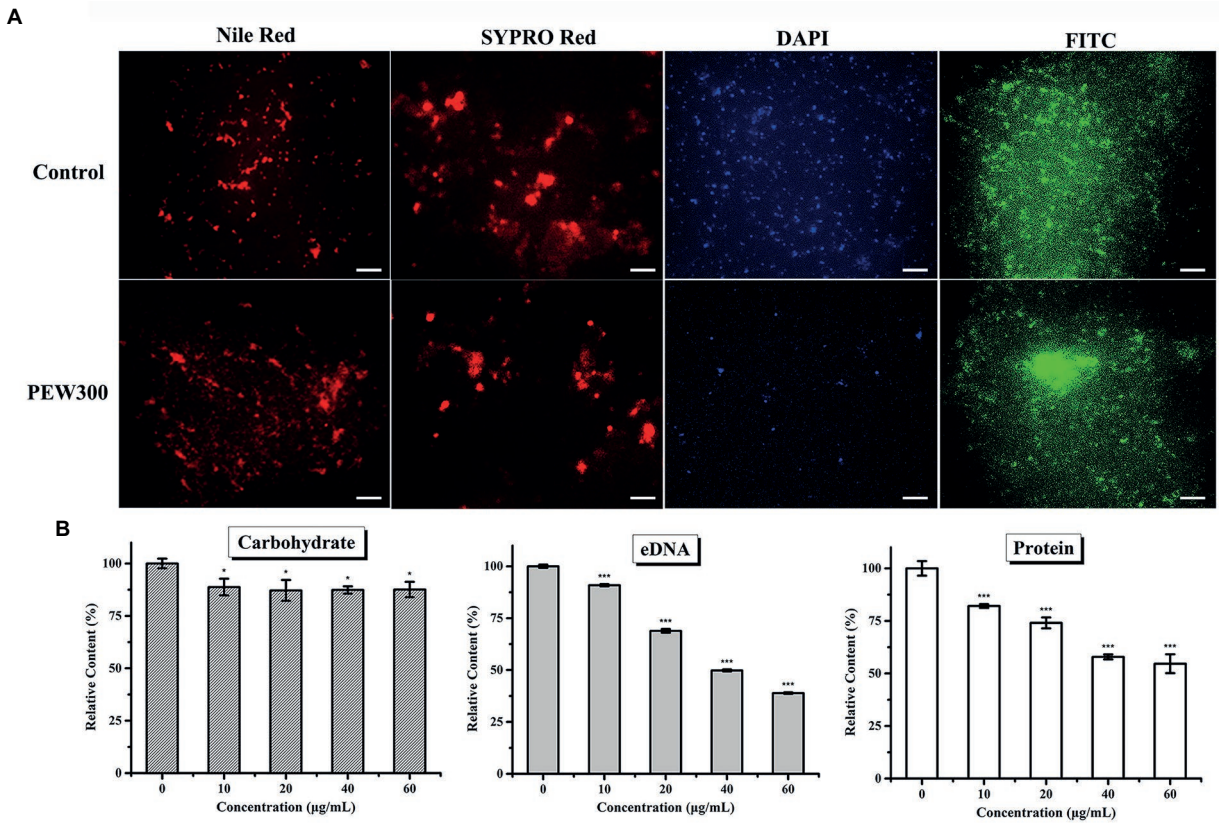

FIGURE 6
Eliminative action of PEW300 on *Pseudomonas aeruginosa* mature biofilm. **(A)** Fluorescence analysis of PEW300 on *P. aeruginosa* mature biofilm components. The scale bar is 200μm. **(B)** Quantification analysis of mature biofilms components of *P. aeruginosa* JCM5962 affected by PEW300. * Indicates statistical significance compared to the control groups (*p<0.05; ***p<0.005).

impact on lipids and carbohydrates but showed degradation activity on eDNA and proteins, especially on eDNA component. To further confirm this observation, we also carried out quantitative analyses of the carbohydrate, eDNA, and protein components with or without PEW300 treatment. Consistent with fluorescence observation, the degradation activity of PEW300 on eDNA and protein components in mature biofilm was in a dose-dependent manner, ~75% and 45% of eDNA and proteins were separately eradicated when treated with 60 μg/ml of PEW300 (Figure 6B). Previous studies reported the AMPs could interact with eDNA and also could cleave eDNA *via* a nuclease-like activity (Zhang et al., 2020; Portelinha and Angeles-Boza, 2021). We speculate that PEW300 probably mainly degraded the eDNA *via* its amphipathic structure and cationicity and caused the collapse of the 3D architecture of biofilm, which eventually led to the significant destruction of the matured biofilm.

Membrane disruption and the intracellular disturbance induced by PEW300

Previous studies have reported that most AMPs could induce cell membrane disruption (Domingues et al., 2020; Liu et al., 2020; Wang et al., 2020). To explore whether PEW300 adopt the same manner, TEM observation was applied to directly observe the effect of PEW300 on the ultrastructure of *P. aeruginosa*. As shown in Figure 7A, the surface morphology of cells treated with PEW300 exhibited shrink, perforation, and mesosome-like structures while untreated cells were intact and smooth, indicating that PEW300 could destroy the cell membrane integrity, resulting in the extravasation of cytoplasmic content and enlargement of the extracellular matrix. To confirm the disruption effect of PEW300 on a membrane, a nuclear fluorescent probe PI which can traverse impaired cell membrane, combined with flow cytometry was applied. As shown in Figure 7B, untreated cells had almost no PI fluorescence signal (0.049%), indicating the intact bacterial membranes. While, the signals of cells treated with PEW300 (20 μg/ml) for 10 min was 28.7%, 20 min was 89.8%, and 30 min was 97.2%, indicating that the percentage of membrane rupture was in a time-dependent manner. As anticipated, nearly all *P. aeruginosa* cell membranes (99.7%) were ruptured when incubated with PEW300 for 2 h (consistent with the result of Figure 4C). These results demonstrated that PEW300 could destroy the integrity of *P. aeruginosa* cell membrane.

As we all know, the OM of G-bacteria is a robust permeability barrier to harsh environments (Domingues et al., 2020). β-lactam

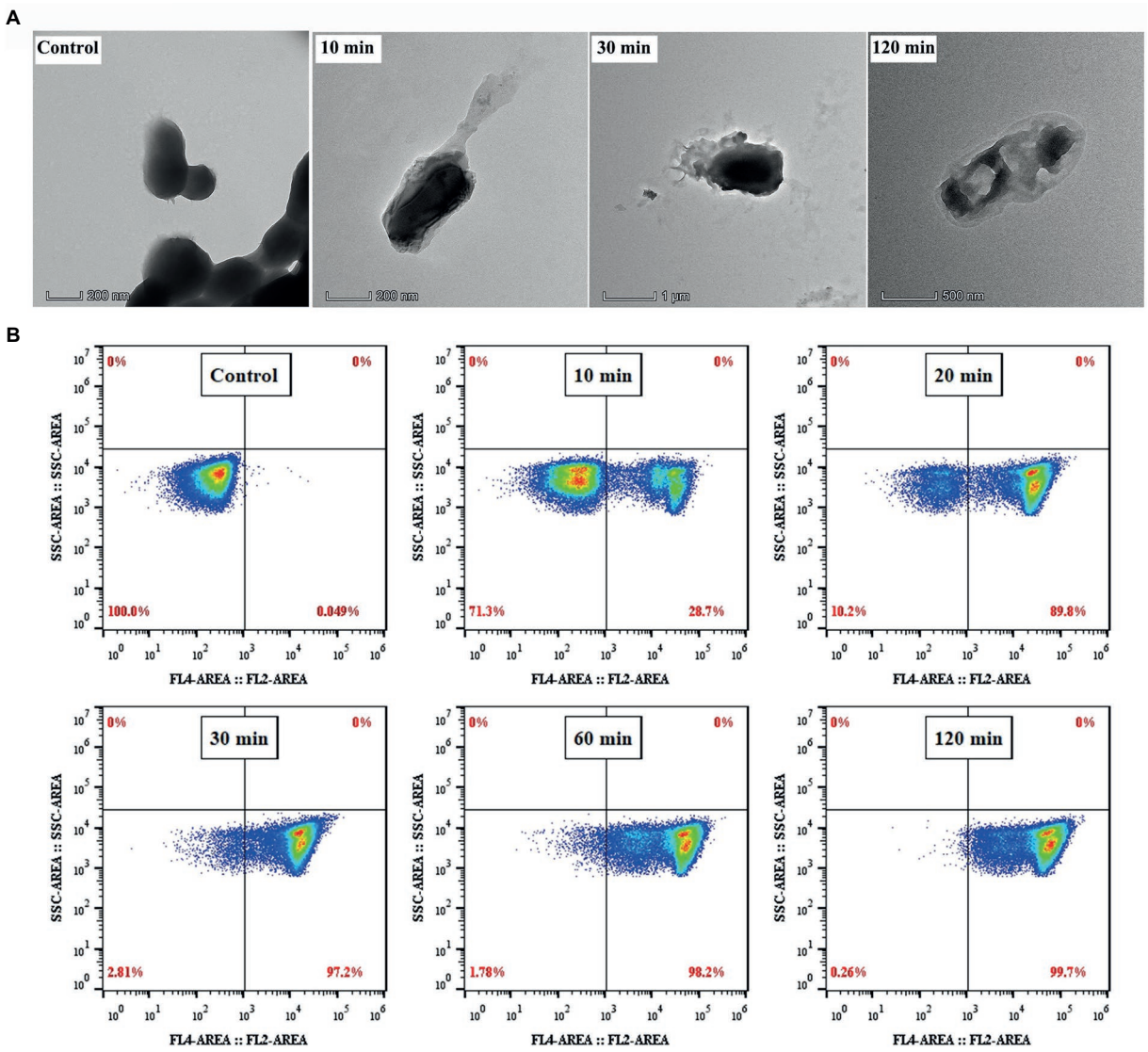

FIGURE 7
Disruption effect of PEW300 on *Pseudomonas aeruginosa* membrane. **(A)** TEM micrographs of *P. aeruginosa* JCM5962 treated with or without PEW300 (Control). **(B)** Flow cytometry analysis of the disruption ability of PEW300 on *P. aeruginosa* membrane.

and quinolone antibiotics have no antibacterial activity against *P. aeruginosa* due to they cannot pass through the OM layer to reach their intracellular targets (Bruchmann et al., 2013; Torres et al., 2019; Hirsch et al., 2020). Thus, to study the permeabilization effect of PEW300, an environment-sensitive hydrophobic fluorescent probe NPN, which emits strong fluorescence in a hydrophobic environment and weak fluorescence in an aqueous environment, was used (Soh et al., 2020). As depicted in Figure 8A, the relative fluorescence units (RFU) of cells treated with PEW300 exhibited a sharp increase and reached a maximum within 1 min, showing that the OM permeabilization of *P. aeruginosa* caused by PEW300 was fast, and in dose-and time-dependent manner. LPS are the main components of the OM of G-bacteria (Chou et al., 2019) and we further explored the interaction between PEW300 and LPS. As shown in Figure 8B, the antibacterial activity of PEW300 was unaffected when treated with 0 ~ 20 μg/ml of LPS. However, when treated with 40 μg/ml of LPS, nearly 50% of the antimicrobial activity was lost, and the antimicrobial activity of PEW300 was completely disabled with 160 μg/ml of LPS treatment. The result suggested that PEW300 combined with LPS to exert the OM permeabilization. Unlike OM, the IM served as a barrier to protect the interior environment and played a key role in the transportation of nutrients and metabolites (Xie et al., 2018). Depolarization of IM will cause the release of $DiSC_3$-5 and result in enhanced fluorescence (Zhu et al., 2020). As shown in Figure 8C, the IM depolarization of *P. aeruginosa* cells treated with PEW300 appeared in a dose-and time-dependent manner. The interaction between the negatively charged LPS and PEW300 led to an increase in OM permeability, which accelerated the permeation of PEW300 from the OM layer to the IM layer.

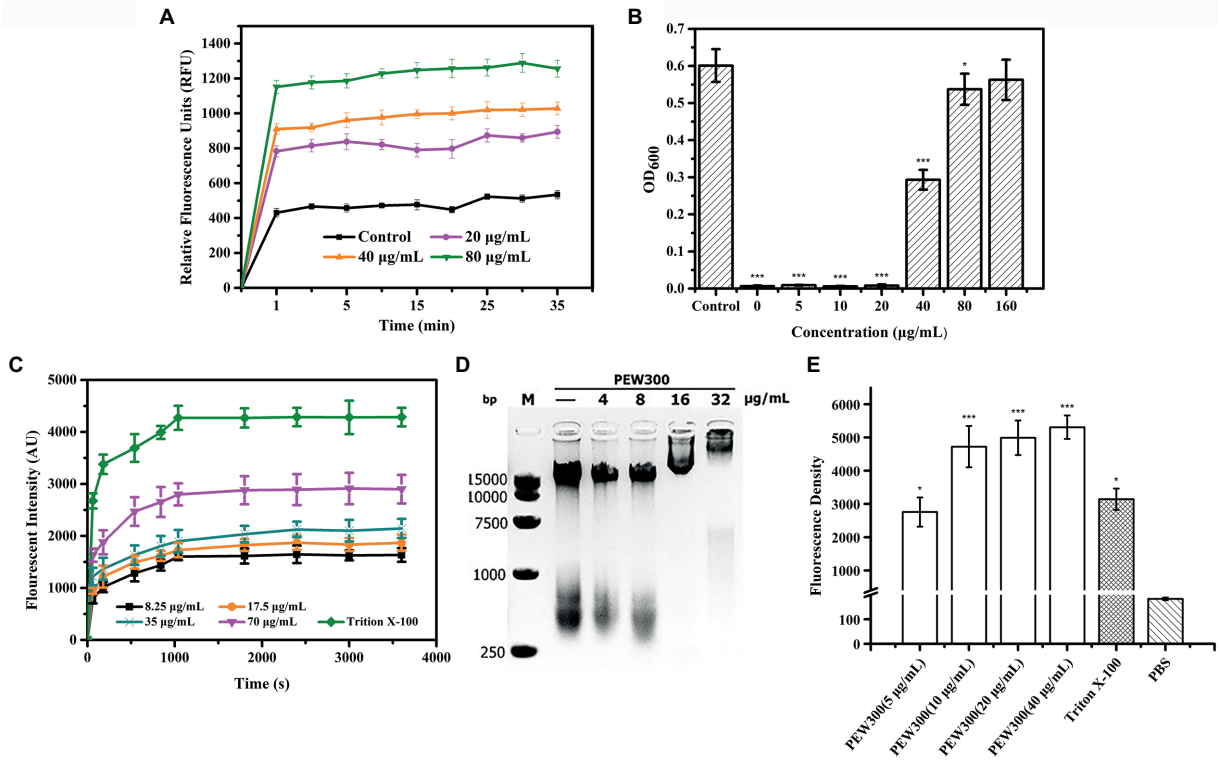

FIGURE 8
Membrane analysis and intracellular disturbance induced by PEW300. **(A)** Effects of PEW300 on OM permeabilization of *Pseudomonas aeruginosa* JCM5962. Control represents cells with no PEW300 treatment. **(B)** LPS-binding affinities of PEW300. Control means the growth of *P. aeruginosa* JCM5962 with no PEW300 and LPS incubation. *p<0.05, ***p<0.005 compared with control. **(C)** The IM depolarization induced by PEW300. **(D)** The electrophoretic mobility shift analysis of the interaction between *P. aeruginosa* JCM5962 genomic DNA (200ng) and PEW300 peptide. **(E)** Intracellular ROS intensity produced by *P. aeruginosa* JCM5962 in the presence of PBS, 1% Triton X-100, and series concentrations of PEW300 peptide. *p<0.05, ***p<0.005 compared with PBS-treated group.

Disruption of the IM induced by PEW300 led to the imbalance of electrical potential inside and outside the IM and eventually depolarization of the IM (Shao et al., 2018). These results confirmed that PEW300 could permeabilize the OM, depolarize the IM, and destroy the integrality of the cell membrane and then cause cell death.

Besides, we also tested the impact of PEW300 on *P. aeruginosa* genomic DNA. According to our assumption, if PEW300 is combined with genomic DNA, the migration of genomic DNA would be hindered in the agarose gel. As expected, the migration of genomic DNA appeared to be concentration-dependent and completely stayed in the gel pores when treated with 32 μg/ml of PEW300 (Figure 8D). These results suggested that PEW300 could not only act on the *P. aeruginosa* membrane but also on genomic DNA. Moreover, the intracellular ROS levels were also studied. As depicted in Figure 8E, there was a substantial increase in intracellular ROS in *P. aeruginosa* after incubation with different concentrations of PEW300 when compared with negative control (PBS treated cells), implying that PEW300 could cause the intracellular disturbance and result in the elevated ROS level. Consistent with the previous study (Xiao et al., 2020), this fairly high level of ROS within *P. aeruginosa* might be due to the disruption of the cell membrane (permeabilization of OM and depolarization of IM) or the interaction with genomic DNA by PEW300. All these results suggested that PEW300 exerted antimicrobial activity might through a multiple-action mechanism.

PEW300 reduced the production of virulence factors of *Pseudomonas aeruginosa*

As the virulence factors play a key role during the infection process of *P. aeruginosa*, we also investigated whether PEW300 could reduce the virulence of *P. aeruginosa*. Initially, a cytotoxicity experiment was performed. A549 cells were infected with *P. aeruginosa* mixture (containing increased concentrations of PEW300), and the cell viability was assessed by CCK-8 assay and calcein-AM staining. As shown in Figures 9A,B, the co-incubation of A549 with PEW300 (up to 126 μg/ml) had no impact on cell proliferation and viability while the co-incubation A549 with *P. aeruginosa* had resulted

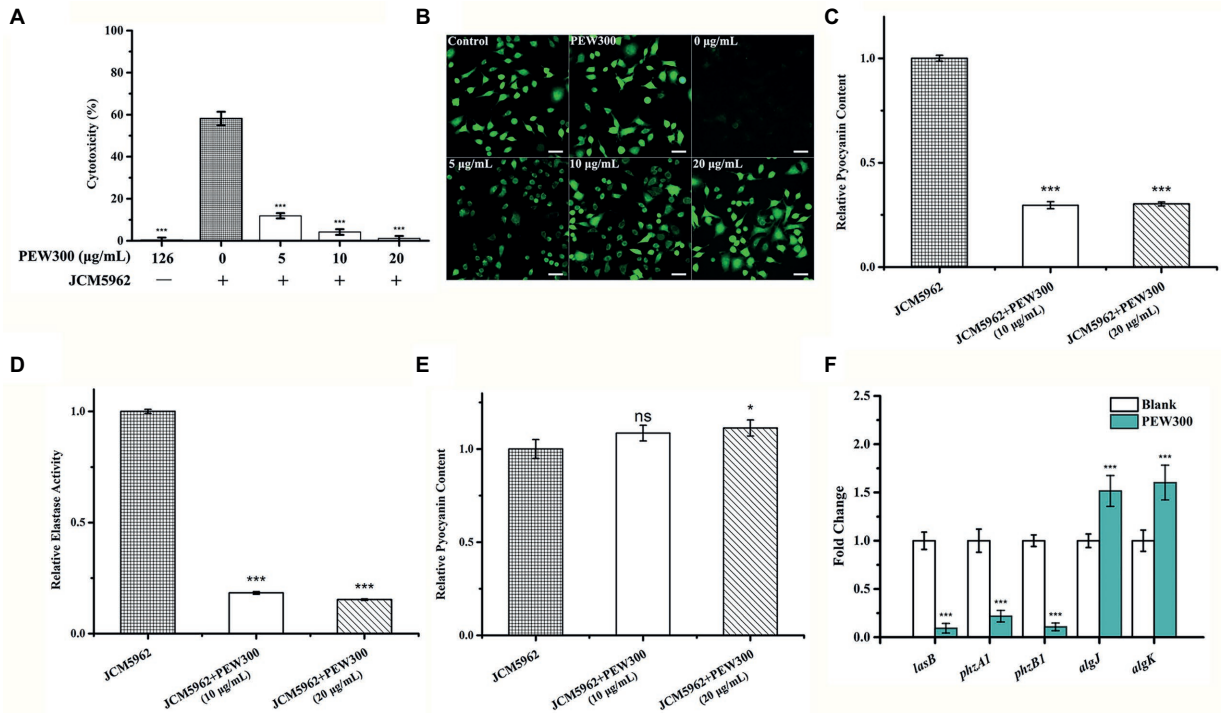

FIGURE 9
Analysis of *Pseudomonas aeruginosa* virulence factors affected by PEW300. PEW300 results in decreased virulence of *P. aeruginosa* JCM5962 in A549 cells characterized by **(A)** CCK-8 assay and **(B)** calcein-AM staining. ***$p<0.005$ compared with *P. aeruginosa* JCM5962-treated group. Scale bar is 100μm. Comparative analysis of **(C)** pyocyanin content, **(D)** elastase activity and **(E)** alginates content in *P. aeruginosa* JCM5962 treated with or without PEW300 peptide. **(F)** qPCR analysis of virulence-related gene expression. Data represent the mean±SD from three independent experiments performed in triplicate. * indicates $p<0.05$, *** indicates $p<0.005$; ns means no significant difference compared with control.

in nearly 60% of cells death. In addition, compared with the blank control group, the cytotoxicity of *P. aeruginosa* incubated with 5 and 10 μg/ml of PEW300 was dramatically decreased (5% ~ 10%) and was in a dose-dependent manner. Notably, the cell viability of *P. aeruginosa*-infected cells was high with almost complete survival of the cells (97.77%) when treated with 20 μg/ml of PEW300, implying that PEW300 could decrease the cytotoxicity of *P. aeruginosa*.

A previous study showed that elastase, pyocyanin, pyoverdine, and alginate are key virulence factors of *P. aeruginosa* for promoting its host pathogenicity (Xu et al., 2016). To further explore the effect of PEW300 on these virulence factors, we quantified the production of these virulence factors in *P. aeruginosa* cells with or without PEW300 treatment. As shown in Figures 9C–E, cells treated with 10 and 20 μg/ml of PEW300 both significantly decreased elastase and pyocyanin production, while the production of alginate was slightly increased. These results suggested that the reduced production of virulence factors caused by PEW300 might result in the decreased cytotoxicity of *P. aeruginosa*. In addition, we also evaluated the transcription levels of genes involving virulence factors expression by qPCR. As shown in Figure 9F, the elastase LasB encoding gene (*lasB*) and phenazine (intermediate metabolic product of pyocyanin) synthesis-related genes (*phzA1* and *phzB1*) were significantly downregulated in *P. aeruginosa* treated with PEW300; Besides, the expression levels of genes encoding alginate (*algK* and *algJ*) were upregulated in the PEW300-treated group. These results are consistent with virulence factors quantitation, demonstrating that PEW300 reduced the production of virulence factors of *P. aeruginosa* through downregulating the virulence-related gene expression.

As an important immunodominant molecule, LPS is involved in host cell attachment at the onset of infection and is essential for the virulence of many bacteria such as *P. aeruginosa* and *E. coli* (Jann and Jann, 1987; Pier, 2007), bacteria lacking LPS can diminish their virulence (Gupta et al., 1997; Davis and Goldberg, 2012). In addition, previous studies have reported that host innate immunity produces ROS during bacterial infection (Ramond et al., 2021). ROS include superoxide anions ($O_2^{\bullet-}$), hydrogen peroxide (H_2O_2), and hydroxyl radicals ($OH^{\bullet}$), which damage bacterial cellular components, including DNA, membrane lipids and proteins, leading to cell death (Ezraty et al., 2017; Ramond et al., 2021). In the present study, the high intracellular ROS levels induced by PEW300 and the strong binding activity of PEW300 with *P. aeruginosa* LPS suggested two additional ways in which PEW300 reduces the virulence of *P. aeruginosa*.

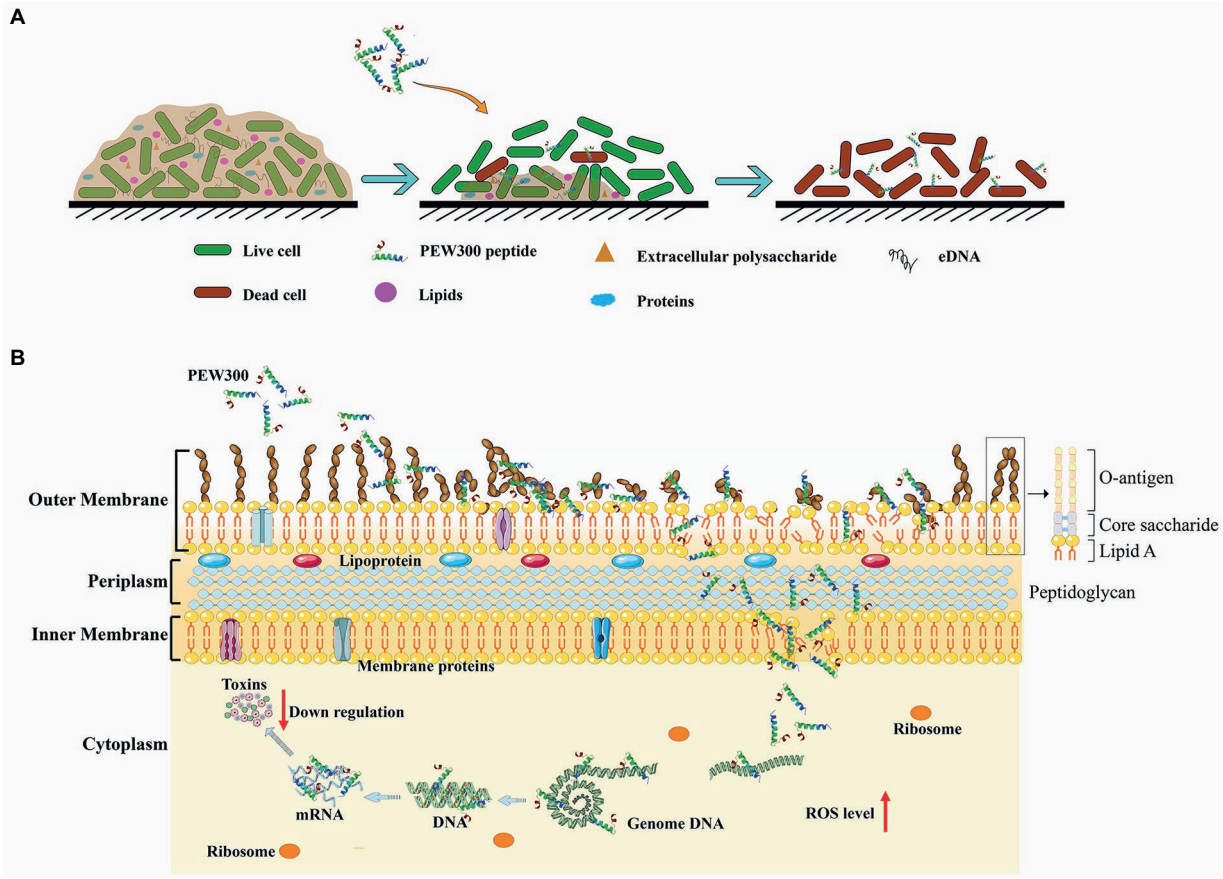

FIGURE 10
Schematic illustration of the **(A)** antibiofilm pathway and **(B)** the multiple actions of PEW300 against *Pseudomonas aeruginosa*.

To sum all, PEW300 adopted a unique mode of action to exert its antibiofilm activity, in which PEW300 preferentially eliminated the matured biofilm mainly by degradation of eDNA component and led to the wrapped bacteria exposure; then, the interactions between PEW300 and *P. aeruginosa* eventually resulted in the cell death (Figure 10A). In the process of interactions with *P. aeruginosa*, multiple actions of PEW300 were adopted to cause cell death, like increased the OM permeability, interacted with LPS, destroyed the integrity of cell membrane, and depolarization of IM; interacted with genome DNA, and caused high level of intracellular ROS. Besides, PEW300 also reduced the production of virulence factors (elastase, pyocyanin, pyoverdine, and alginate) by downregulating the virulence-related gene expression (Figure 10B).

Conclusion

In the present study, we show that PEW300 has strong antibiofilm activity against *P. aeruginosa*. The excellent performance of PEW300 toward *P. aeruginosa* confers it as a potential alternative antimicrobial agent. Besides, our findings establish the antibiofilm mechanism of PEW300 against *P. aeruginosa* and provide a reference for the study of antibiofilm mechanism of other AMPs.

Data availability statement

The datasets presented in this study can be found in online repositories. The names of the repository/repositories and accession number(s) can be found in the article/Supplementary material.

Author contributions

JW conceived the project and designed the experiment. MW performed the experimental work and wrote the first draft of the manuscript. ZD and YL performed the hemolytic assay and the cytotoxicity assay. KX analyzed the data. YM and S-TY reviewed and edited the manuscript. All authors contributed to the article and approved the submitted version.

Funding

This work was supported by the Guangdong Major Project of Basic and Applied Basic Research (2020B0301030005).

Conflict of interest

KX was employed by Kaiping Healthwise Health Food Co., Ltd.

The remaining authors declare that the research was conducted in the absence of any commercial or financial relationships that could be construed as a potential conflict of interest.

Publisher's note

Supplementary material

The Supplementary material for this article can be found online at: https://www.frontiersin.org/articles/10.3389/fmicb.2022.963292/full#supplementary-material

References

Abbott, I. J., van Gorp, E., Wijma, R. A., Dekker, J., Croughs, P. D., Meletiadis, J., et al. (2020). Efficacy of single and multiple oral doses of fosfomycin against *Pseudomonas aeruginosa* urinary tract infections in a dynamic in vitro bladder infection model. *J. Antimicrob. Chemother.* 75, 1879–1888. doi: 10.1093/jac/dkaa127

Bruchmann, S., Dötsch, A., Nouri, B., Chaberny, I. F., and Häussler, S. (2013). Quantitative contributions of target alteration and decreased drug accumulation to *Pseudomonas aeruginosa* fluoroquinolone resistance. *Antimicrob. Agents Chemother.* 57, 1361–1368. doi: 10.1128/AAC.01581-12

Cardoso, M. H., Orozco, R. Q., Rezende, S. B., Rodrigues, G., Oshiro, K. G. N., Cândido, E. S., et al. (2019). Computer-aided Design of Antimicrobial Peptides: are we generating effective drug candidates? *Front. Microbiol.* 10:3097. doi: 10.3389/fmicb.2019.03097

Chen, C., Li, G., Cui, X., Chen, J., Yu, Q., Zong, C., et al. (2020). Mechanistic investigation of a self-assembling peptide against. *Langmuir* 36, 9800–9809. doi: 10.1021/acs.langmuir.0c01311

Chou, S., Wang, J., Shang, L., Akhtar, M. U., Wang, Z., Shi, B., et al. (2019). Short, symmetric-helical peptides have narrow-spectrum activity with low resistance potential and high selectivity. *Biomater. Sci.* 7, 2394–2409. doi: 10.1039/c9bm00044e

Ciofu, O., and Tolker-Nielsen, T. (2019). Tolerance and resistance of biofilms to antimicrobial agents-how can escape antibiotics. *Front. Microbiol.* 10:913. doi: 10.3389/fmicb.2019.00913

Cowell, B. A., Twining, S. S., Hobden, J. A., Kwong, M. S. F., and Fleiszig, S. M. J. (2003). Mutation of lasA and lasB reduces *Pseudomonas aeruginosa* invasion of epithelial cells. *Microbiology* 149, 2291–2299. doi: 10.1099/mic.0.26280-0

Davis, M. R., and Goldberg, J. B. (2012). Purification and visualization of lipopolysaccharide from gram-negative bacteria by hot aqueous-phenol extraction. *J. Vis. Exp.* 63:3196. doi: 10.3791/3916

de Breij, A., Riool, M., Cordfunke, R. A., Malanovic, N., de Boer, L., Koning, R. I., et al. (2018). The antimicrobial peptide SAAP-148 combats drug-resistant bacteria and biofilms. *Sci. Transl. Med.* 10:eaan4044. doi: 10.1126/scitranslmed.aan4044

De Oliveira, D. M. P., Forde, B. M., Kidd, T. J., Harris, P. N. A., Schembri, M. A., Beatson, S. A., et al. (2020). Antimicrobial resistance in ESKAPE pathogens. *Clin. Microbiol. Rev.* 33:e00181-19. doi: 10.1128/CMR.00181-19

Di Somma, A., Moretta, A., Canè, C., Cirillo, A., and Duilio, A. (2020). Antimicrobial and Antibiofilm peptides. *Biomol. Ther.* 10:652. doi: 10.3390/biom10040652

Domingues, T. M., Perez, K. R., and Riske, K. A. (2020). Revealing the mode of action of Halictine antimicrobial peptides: a comprehensive study with model membranes. *Langmuir* 36, 5145–5155. doi: 10.1021/acs.langmuir.0c00282

Ezraty, B., Gennaris, A., Barras, F., and Collet, J.-F. (2017). Oxidative stress, protein damage and repair in bacteria. *Nat. Rev. Microbiol.* 15, 385–396. doi: 10.1038/nrmicro.2017.26

Founou, R. C., Founou, L. L., and Essack, S. Y. (2017). Clinical and economic impact of antibiotic resistance in developing countries: a systematic review and meta-analysis. *PLoS One* 12:e0189621. doi: 10.1371/journal.pone.0189621

Garcia-Clemente, M., de la Rosa, D., Máiz, L., Girón, R., Blanco, M., Olveira, C., et al. (2020). Impact of infection on patients with chronic inflammatory airway diseases. *J. Clin. Med.* 9:3800. doi: 10.3390/jcm9123800

Gilbert, P., Maira-Litran, T., McBain, A. J., Rickard, A. H., and Whyte, F. W. (2002). The physiology and collective recalcitrance of microbial biofilm communities. *Adv. Microb. Physiol.* 46, 202–256. doi: 10.1016/S0065-2911(02)46005-5

Gupta, S. K., Masinick, S., Garrett, M., and Hazlett, L. D. (1997). *Pseudomonas aeruginosa* lipopolysaccharide binds galectin-3 and other human corneal epithelial proteins. *Infect. Immun.* 65, 2747–2753. doi: 10.1128/iai.65.7.2747-2753.1997

Hall, C. W., and Mah, T.-F. (2017). Molecular mechanisms of biofilm-based antibiotic resistance and tolerance in pathogenic bacteria. *FEMS Microbiol. Rev.* 41, 276–301. doi: 10.1093/femsre/fux010

Hancock, R. E. W., Alford, M. A., and Haney, E. F. (2021). Antibiofilm activity of host defence peptides: complexity provides opportunities. *Nat. Rev. Microbiol.* 19, 786–797. doi: 10.1038/s41579-021-00585-w

Hashemi, S., Niazi, A., Baghizadeh, A., and Taghizadeh, M. S. (2021). Successful use of *Nicotiana tabacum* hairy roots for the recombinant production of Cecropin A peptide. *Biotechnol. Appl. Biochem.* 69, 876–886. doi: 10.1002/bab.2158

Hirsch, E. B., Brigman, H. V., Zucchi, P. C., Chen, A., Anderson, J. C., Eliopoulos, G. M., et al. (2020). Ceftolozane-tazobactam and ceftazidime-avibactam activity against β-lactam-resistant *Pseudomonas aeruginosa* and extended-spectrum β-lactamase-producing Enterobacterales clinical isolates from U.S. medical centres. *J. Glob. Antimicrob. Resist.* 22, 689–694. doi: 10.1016/j.jgar.2020.04.017

Huang, T., Holden, J. A., Reynolds, E. C., Heath, D. E., O'Brien-Simpson, N. M., and O'Connor, A. J. (2020). Multifunctional Antimicrobial Polypeptide-Selenium Nanoparticles Combat Drug-Resistant Bacteria. *ACS Appl. Mater. Interfaces* 12, 55696–55709. doi: 10.1021/acsami.0c17550

Jann, K., and Jann, B. (1987). Polysaccharide antigens of *Escherichia coli*. *Rev. Infect. Dis.* 9, S517–S526. doi: 10.1093/clinids/9.Supplement_5.S517

Kim, H.-S., and Park, H.-D. (2013). Ginger extract inhibits biofilm formation by *Pseudomonas aeruginosa* PA14. *PLoS One* 8:e76106. doi: 10.1371/journal.pone.0076106

Knutson, C. A., and Jeanes, A. (1968). A new modification of the carbazole analysis: application to heteropolysaccharides. *Anal. Biochem.* 24, 470–481. doi: 10.1016/0003-2697(68)90154-1

Kouidhi, B., Al Qurashi, Y. M. A., and Chaieb, K. (2015). Drug resistance of bacterial dental biofilm and the potential use of natural compounds as alternative for prevention and treatment. *Microb. Pathog.* 80, 39–49. doi: 10.1016/j.micpath.2015.02.007

Lee, J., and Zhang, L. (2015). The hierarchy quorum sensing network in *Pseudomonas aeruginosa*. *Protein Cell* 6, 26–41. doi: 10.1007/s13238-014-0100-x

Li, J., Shang, L., Lan, J., Chou, S., Feng, X., Shi, B., et al. (2020b). Targeted and intracellular antibacterial activity against of the chimeric peptides based on pheromone and cell-penetrating peptides. *ACS Appl. Mater. Interfaces* 12, 44459–44474. doi: 10.1021/acsami.0c12226

Li, W., Wang, J. J., Qian, H., Tan, L., Zhang, Z., Liu, H., et al. (2020c). Insights Into the role of extracellular DNA and extracellular proteins in biofilm formation of. *Front. Microbiol.* 11:813. doi: 10.3389/fmicb.2020.00813

Li, J.-F., Zhang, J.-X., Li, G., Xu, Y.-Y., Lu, K., Wang, Z.-G., et al. (2020a). Antimicrobial activity and mechanism of peptide CM4 against *Pseudomonas aeruginosa*. *Food Funct.* 11, 7245–7254. doi: 10.1039/d0fo01031f

Liu, Y., Ma, A., Han, P., Chen, Z., and Jia, Y. (2020). Antibacterial mechanism of brevilaterin B: an amphiphilic lipopeptide targeting the membrane of *Listeria monocytogenes*. *Appl. Microbiol. Biotechnol.* 104, 10531–10539. doi: 10.1007/s00253-020-10993-2

Luna, E., Kim, S., Gao, Y., Widmalm, G., and Im, W. (2021). Influences of lipid A types on LPS bilayer properties. *J. Phys. Chem. B* 125, 2105–2112. doi: 10.1021/acs.jpcb.0c09144

Mahlapuu, M., Håkansson, J., Ringstad, L., and Björn, C. (2016). Antimicrobial peptides: An emerging category of therapeutic agents. *Front. Cell. Infect. Microbiol.* 6:194. doi: 10.3389/fcimb.2016.00194

Manandhar, S., Zellweger, R. M., Maharjan, N., Dongol, S., Prajapati, K. G., Thwaites, G., et al. (2020). A high prevalence of multi-drug resistant gram-negative bacilli in a Nepali tertiary care hospital and associated widespread distribution of extended-Spectrum Beta-lactamase (ESBL) and carbapenemase-encoding genes. *Ann. Clin. Microbiol. Antimicrob.* 19:48. doi: 10.1186/s12941-020-00390-y

Pang, Z., Raudonis, R., Glick, B. R., Lin, T.-J., and Cheng, Z. (2019). Antibiotic resistance in *Pseudomonas aeruginosa*: mechanisms and alternative therapeutic strategies. *Biotechnol. Adv.* 37, 177–192. doi: 10.1016/j.biotechadv.2018.11.013

Pier, G. B. (2007). *Pseudomonas aeruginosa* lipopolysaccharide: a major virulence factor, initiator of inflammation and target for effective immunity. *Int. J. Med. Microbiol.* 297, 277–295. doi: 10.1016/j.ijmm.2007.03.012

Portelinha, J., and Angeles-Boza, A. M. (2021). The antimicrobial peptide Gad-1 clears *Pseudomonas aeruginosa* biofilms under cystic fibrosis conditions. *ChemBioChem* 22, 1646–1655. doi: 10.1002/cbic.202000816

Qi, R., Zhang, N., Zhang, P., Zhao, H., Liu, J., Cui, J., et al. (2020). Gemini peptide Amphiphiles with broad-Spectrum antimicrobial activity and potent Antibiofilm capacity. *ACS Appl. Mater. Interfaces* 12, 17220–17229. doi: 10.1021/acsami.0c01167

Ramond, E., Jamet, A., Ding, X., Euphrasie, D., Bouvier, C., Lallemant, L., et al. (2021). Reactive oxygen species-dependent innate immune mechanisms control methicillin-resistant *Staphylococcus aureus* virulence in the larval model. *MBio* 12:e0027621. doi: 10.1128/mBio.00276-21

Roy, R., Tiwari, M., Donelli, G., and Tiwari, V. (2018). Strategies for combating bacterial biofilms: A focus on anti-biofilm agents and their mechanisms of action. *Virulence* 9, 522–554. doi: 10.1080/21505594.2017.1313372

Serra, R., Grande, R., Butrico, L., Rossi, A., Settimio, U. F., Caroleo, B., et al. (2015). Chronic wound infections: the role of *Pseudomonas aeruginosa* and *Staphylococcus aureus*. *Expert Rev. Anti Infect. Ther.* 13, 605–613. doi: 10.1586/14787210.2015.1023291

Shao, C., Tian, H., Wang, T., Wang, Z., Chou, S., Shan, A., et al. (2018). Central β-turn increases the cell selectivity of imperfectly amphipathic α-helical peptides. *Acta Biomater.* 69, 243–255. doi: 10.1016/j.actbio.2018.01.009

Sharma, D., Misba, L., and Khan, A. U. (2019). Antibiotics versus biofilm: an emerging battleground in microbial communities. *Antimicrob. Resist. Infect. Control* 8:76. doi: 10.1186/s13756-019-0533-3

Shortridge, D., Gales, A. C., Streit, J. M., Huband, M. D., Tsakris, A., and Jones, R. N. (2019). Geographic and temporal patterns of antimicrobial resistance in Over 20 years From the SENTRY antimicrobial surveillance program, 1997-2016. *Open Forum Infect. Dis.* 6, S63–S68. doi: 10.1093/ofid/ofy343

Soh, S. M., Jang, H., and Mitchell, R. J. (2020). Loss of the lipopolysaccharide (LPS) inner core increases the electrocompetence of *Escherichia coli*. *Appl. Microbiol. Biotechnol.* 104, 7427–7435. doi: 10.1007/s00253-020-10779-6

Tacconelli, E., Carrara, E., Savoldi, A., Harbarth, S., Mendelson, M., Monnet, D. L., et al. (2018). Discovery, research, and development of new antibiotics: the WHO priority list of antibiotic-resistant bacteria and tuberculosis. *Lancet Infect. Dis.* 18, 318–327. doi: 10.1016/S1473-3099(17)30753-3

Tagliaferri, T. L., Jansen, M., and Horz, H.-P. (2019). Fighting pathogenic Bacteria on two fronts: phages and antibiotics as combined strategy. *Front. Cell. Infect. Microbiol.* 9:22. doi: 10.3389/fcimb.2019.00022

Thi, M. T. T., Wibowo, D., and Rehm, B. H. A. (2020). *Pseudomonas aeruginosa* Biofilms. *Int. J. Mol. Sci.* 21:8671. doi: 10.3390/ijms21228671

Torres, A., Chalmers, J. D., Dela Cruz, C. S., Dominedò, C., Kollef, M., Martin-Loeches, I., et al. (2019). Challenges in severe community-acquired pneumonia: a point-of-view review. *Intensive Care Med.* 45, 159–171. doi: 10.1007/s00134-019-05519-y

Wang, M., Lin, J., Sun, Q., Zheng, K., Ma, Y., and Wang, J. (2019). Design, expression, and characterization of a novel cecropin A-derived peptide with high antibacterial activity. *Appl. Microbiol. Biotechnol.* 103, 1765–1775. doi: 10.1007/s00253-018-09592-z

Wang, Q., Miao, J., Feng, K., Liu, J., Li, W., Li, J., et al. (2020). Antibacterial action of peptide F1 against colistin resistance *E. coli* SHP45 (mcr-1). *Food Funct.* 11, 10231–10241. doi: 10.1039/d0fo01923b

Wang, M., Zheng, K., Lin, J., Huang, M., Ma, Y., Li, S., et al. (2018). Rapid and efficient production of cecropin A antibacterial peptide in *Escherichia coli* by fusion with a self-aggregating protein. *BMC Biotechnol.* 18:62. doi: 10.1186/s12896-018-0473-7

Wiegand, I., Hilpert, K., and Hancock, R. E. W. (2008). Agar and broth dilution methods to determine the minimal inhibitory concentration (MIC) of antimicrobial substances. *Nat. Protoc.* 3, 163–175. doi: 10.1038/nprot.2007.521

Xiao, X., Zhang, S., Chen, S., Qian, Y., Xie, J., Cong, Z., et al. (2020). An alpha/beta chimeric peptide molecular brush for eradicating MRSA biofilms and persister cells to mitigate antimicrobial resistance. *Biomater. Sci.* 8, 6883–6889. doi: 10.1039/d0bm01211d

Xie, R., Taylor, R. J., and Kahne, D. (2018). Outer membrane Translocon communicates with inner membrane ATPase to stop lipopolysaccharide transport. *J. Am. Chem. Soc.* 140, 12691–12694. doi: 10.1021/jacs.8b07656

Xu, X., Yu, H., Zhang, D., Xiong, J., Qiu, J., Xin, R., et al. (2016). Role of ppGpp in *Pseudomonas aeruginosa* acute pulmonary infection and virulence regulation. *Microbiol. Res.* 192, 84–95. doi: 10.1016/j.micres.2016.06.005

Yungyuen, T., Chatsuwan, T., Plongla, R., Kanthawong, S., Yordpratum, U., Voravuthikunchai, S. P., et al. (2021). Nationwide surveillance and molecular characterization of critically drug-resistant gram-negative Bacteria: results of the research university network Thailand study. *Antimicrob. Agents Chemother.* 65:e0067521. doi: 10.1128/AAC.00675-21

Zhang, J., Chen, C., Chen, J., Zhou, S., Zhao, Y., Xu, M., et al. (2020). Dual mode of anti-biofilm action of G3 against *Streptococcus mutans*. *ACS Appl. Mater. Interfaces* 12, 27866–27875. doi: 10.1021/acsami.0c00771

Zhen, X., Lundborg, C. S., Sun, X., Hu, X., and Dong, H. (2019a). The clinical and economic impact of antibiotic resistance in China: a systematic review and Meta-analysis. *Antibiotics.* 8:115. doi: 10.3390/antibiotics8030115

Zhen, X., Lundborg, C. S., Sun, X., Hu, X., and Dong, H. (2019b). Economic burden of antibiotic resistance in ESKAPE organisms: A systematic review. *Antimicrob. Resist. Infect. Control* 8:137. doi: 10.1186/s13756-019-0590-7

Zhu, Y., Shao, C., Li, G., Lai, Z., Tan, P., Jian, Q., et al. (2020). Rational avoidance of protease cleavage sites and symmetrical end-tagging significantly enhances the stability and therapeutic potential of antimicrobial peptides. *J. Med. Chem.* 63, 9421–9435. doi: 10.1021/acs.jmedchem.0c00583

frontiers | Frontiers in Microbiology

TYPE Original Research
PUBLISHED 04 August 2022
DOI 10.3389/fmicb.2022.951291

OPEN ACCESS

EDITED BY
Fang Yang,
Qingdao Municipal Hospital, China

REVIEWED BY
Jinghua Li,
Henan University of Science and Technology, China
Amit Kumar,
Laboratory Corporation of America Holdings (LabCorp), United States

*CORRESPONDENCE
Lijun Huo
danling430@126.com

SPECIALTY SECTION
This article was submitted to Antimicrobials, Resistance and Chemotherapy, a section of the journal Frontiers in Microbiology

RECEIVED 23 May 2022
ACCEPTED 11 July 2022
PUBLISHED 04 August 2022

CITATION
Zhou J, Meng XH, Han QC, Huang YX, Huo LJ and Lei YY (2022) An *in vitro* study on the degradation of multispecies biofilm of periodontitis-related microorganisms by bovine trypsin. *Front. Microbiol.* 13:951291. doi: 10.3389/fmicb.2022.951291

An *in vitro* study on the degradation of multispecies biofilm of periodontitis-related microorganisms by bovine trypsin

Jing Zhou[1,2], Xinhui Meng[1,2], Qunchao Han[1,2], Yinxue Huang[1,2], Lijun Huo[1,2]* and Yayan Lei[1,2]

[1]Department of Operative Dentistry, Preventive Dentistry and Endodontics, School of Stomatology, The Affiliated Stomatology Hospital, Kunming Medical University, Kunming, China, [2]Yunnan Key Laboratory of Stomatology, Kunming, China

To investigate the degradation effect of bovine trypsin on multispecies biofilm of periodontitis-related bacteria and to provide an experimental reference for exploring new methods for controlling biofilms of periodontitis-related microorganisms, the multispecies biofilm of periodontitis-related microorganisms was established. Standard strains of *Porphyromonas gingivalis, Fusobacterium nucleatum* subsp. *polymorpha*, *Actinomyces viscosus*, and *Aggregatibacter actinomycetemcomitans* were co-cultured to form the biofilm. The experimental groups were treated with bovine trypsin, distilled water was applied as the blank control group, and phosphate saline buffer (pH = 7.4) as the negative control group. Morphological observation and quantitative analysis of extracellular polymeric substances (EPS), live bacteria, and dead bacteria were conducted using a laser confocal microscope. The morphological changes of EPS and bacteria were also observed using a scanning electron microscope. The results of morphological observations of modeling were as follows. EPS aggregated as agglomerates, and bacteria flora were wrapped by them, showing a three-dimensional network structure, and channel-like structures were inside the biofilm. Live bacteria were distributed on the surface of the EPS or embedded in them, dead bacteria aggregated between live flora and the bottom layer of biofilms. After being treated with bovine trypsin, the three-dimensional network structure and the channel-like structure disappeared, and the EPS and live and dead bacteria decreased. Quantitative analysis results are as follows. When biofilm was treated for 30 s, 1 min, and 3 min, the minimum effective concentrations of bovine trypsin to reduce EPS were 2 mg/ml ($P < 0.05$), 0.5 mg/ml ($P < 0.05$), and 0.25 mg/ml ($P < 0.05$), respectively. The minimum effective concentrations of bovine trypsin to reduce the live or dead bacteria were 2 mg/ml ($P < 0.05$), 0.5 mg/ml ($P < 0.05$), and 0.5 mg/ml ($P < 0.05$), respectively. There was no significant difference in the ratio of live/dead bacteria after the biofilm was treated for 30 s with bovine trypsin at the concentration of 0.25, 0.5, 1, and 2 mg/ml

($P > 0.05$), and the minimum effective concentration to reduce the ratio of live bacteria/dead bacteria was 0.25 mg/ml ($P < 0.05$) after treatment for 1 min and 3 min. Therefore, bovine trypsin can destroy biofilm structure, disperse biofilm and bacteria flora, and reduce the EPS and bacterial biomass, which are positively correlated with the application time and concentration.

KEYWORDS

bovine trypsin, periodontitis, multispecies biofilm, extracellular polymeric substances, biofilm degradation

Introduction

Dental plaque biofilm is the initiating factor of periodontitis. Periodontitis is not only a local disease of the oral cavity, but it is also closely related to diseases such as diabetes and coronary atherosclerosis, which pose a serious threat to human health (Mealey and Oates, 2006; Zijnge et al., 2010; Pérez-Losada et al., 2016; Peng et al., 2017). Biofilms, composed of microbial flora and extracellular polymeric substances (EPS), are highly ordered microbial combinations embedded in EPS (Valm, 2019), which play an important role in mediating the transition of periodontal tissues from healthy to diseased states. EPS are mainly composed of water, extracellular polysaccharides, extracellular proteins, extracellular deoxyribonucleotides (eDNA), and lipids (Yan et al., 2016). The "multi-functional network framework" formed by EPS is the basis for the expression of the biological properties of biofilms and directly determines the living environment of cells (Koo et al., 2013; Flemming et al., 2016). EPS play a role in altering microbial behavior and virulence in biofilms and can also enhance bacterial drug resistance (Gupta et al., 2016; Liu et al., 2016).

The current treatment for periodontitis mainly involves mechanically removing or controlling the biofilm on the root surface and periodontal pocket. However, due to the viscoelasticity of the biofilm, it only partially deforms rather than falls off when subjected to shear stress (Bowen et al., 2018). Mature biofilms are mechanically difficult to remove from the tooth surface, especially in hidden parts such as the adjacent root surfaces, root depressions, and root bifurcations. Antibacterial drugs such as chlorhexidine (CHX) are also used in clinical practice as a supplement to mechanical treatment methods. However, it has certain side effects, such as cytotoxicity, teeth, and fillings discoloration (Karpiński and Szkaradkiewicz, 2015), and even oral flora imbalance. Antibacterial drugs have limited lethality to bacteria in biofilms (Banar et al., 2016; Wang et al., 2020) and cannot degrade EPS (Payne et al., 2008). The presence of EPS and continued antibiotic exposure can lead to the development of genetic resistance in bacteria, resulting in the persistence of biofilm infections (Ciofu et al., 2017). Therefore, targeting EPS may be an effective breakthrough point for removing or controlling biofilms.

Biofilm inhibitors have gradually become a research hotspot. The reported biofilm inhibitors include fibrinolytics (Hogan et al., 2018), metalloproteinases (Saggu et al., 2019), antimicrobial peptides (Zhang et al., 2019), and other eradication agent (Verderosa et al., 2019). Antibiofilm formulations targeting EPS have also been reported (Singh et al., 2002). Trypsin is a serine proteolytic enzyme that affects the formation of the intercellular skeleton to disperse cells (Niazi et al., 2014) and can significantly reduce the biofilm of oral actinomycetes and inhibit the formation of biofilms (Mugita et al., 2017). Studies by Niazi et al. (2015) have shown that the simultaneous action of trypsin with 2% chlorhexidine and ultrasound can effectively reduce the total bacterial survival in a single root canal and destroy the biofilm. However, the role and influence of trypsin on periodontitis-related biofilms are still unknown.

Therefore, in this experiment, a multispecies biofilm model of periodontitis-related microorganisms was established *in vitro*. After the action of bovine trypsin, the changes in biofilm EPS, live bacteria, dead bacteria, and the live bacteria/dead bacteria ratio were detected. The influence of the bovine trypsin on periodontitis-related microbial multispecies biofilm are expected to provide an experimental reference for the new way of the removal of periodontitis-related microbial multispecies biofilm.

Materials and methods

Materials and equipment

Actinomyces viscous (ATCC19246, China Industrial Microbial Culture Collection and Management Center); *Fusobacterium nucleatum* subsp. *polymorpha* (CGMCC1.2528, China General Microorganism Culture Collection and Management Center); *Aggregatibacter actinomycetemcomitans* (NCTC9710, China Common Microbial Bacteria Species Collection Management Center); *Porphyromonas gingivalis* (ATCC33277, China Industrial Microorganism Culture Collection Management Center); Bovine trypsin (Sigma-Aldrich, MO, United States); PBS buffer (pH 7.4) (Beyotime,

Shanghai, China); Dextran, Alexa Fluor^{TM} 647 (Thermo Fisher Scientific, Waltham, MA, United States); LIVE/DEAD BacLight Bacterial Viability Kit (Thermo Fisher Scientific, Waltham, MA, United States); BacLight^{TM} mounting oil (Thermo Fisher Scientific, Waltham, MA, United States); 6-well plate (Corning, NY, United States); Coverslip (24 mm × 24 mm) (HaiLun, Nantong, China); Brain heart leachate broth (HuanKai Microbial, Guangzhou, China); Tri-Gas INCUBATOR (Heal Force, Hong Kong, China); Confocal laser scanning electron microscope (Nikon, Tokyo, Japan); and Scanning Electron Microscope (FEI, Eindhoven, Netherlands).

Preparation of bovine trypsin solution

100 mg Bovine trypsin was dissolved in 10 ml of PBS buffer (pH = 7.4) to form 10 mg/ml of trypsin solution, which was diluted to the required concentration according to the experimental needs, and preheated in a constant temperature water bath at 37°C for 30 min.

Establishment of multispecies biofilms of periodontitis-related microorganisms

The bacteria were recovered in the logarithmic phase according to the growth curve of each species, the concentration of each bacteria solution was adjusted to 1×10^8 CFU/ml, and the bacteria solutions were mixed in equal proportions. The pretreated coverslips (4% HF treatment for 3 min, then sterilized and dried) were put into a sterile 6-well plate. Then, 200 μl of mixed bacterial solution and 1.8 ml of fresh sterile BHI liquid medium were added (1% sucrose by mass, 1% hemin-vitamin K_1 solution by volume, 10% fetal bovine serum by volume) and incubated aerobically at 37°C (80% N_2, 10% CO_2, 10% H_2) for 2 weeks, and the medium was replaced every 2 days.

Experimental groups

The treatment times of bovine trypsin were 30 s (group A), 1 min (group B), and 3 min (group C). The bovine trypsin concentration of each group was as follows. Group A_1 was 0.25 mg/ml, A_2 0.5 mg/ml, A_3 1 mg/ml, and A_4 2 mg/ml. Group B_1 was 0.25 mg/ml, B_2 0.5 mg/ml, and B_3 1 mg/ml. Group C_1 was 0.125 mg/ml, C_2 0.25 mg/ml, C_3 0.5 mg/ml, and C_4 1 mg/ml. The blank control group was treated with distilled water, and the negative control group was treated with PBS buffer.

Scanning electron microscope observation of periodontitis-related microbial multispecies biofilm

The slides with biofilms were placed in 2.5% glutaraldehyde solution, fixed at 4°C for 2 h, washed three times with sterile distilled water, dehydrated with alcohol gradient, dried, and sprayed with gold.

Confocal laser scanning microscopy observation of periodontitis-related microbial multispecies biofilm

Observation of live and dead bacteria

In the dark, the coverslips were washed three times with sterile distilled water. Then, 200 μl of SYTO 9/PI mixed fluorescent dye solution was added to each slide, allowed to stand for 15 min under anaerobic conditions in a 37°C incubator, and washed again three times with sterile distilled water. The slides were air dried naturally, 200 μl of anti-fluorescence quencher was applied and sealed for inspection. Three areas were randomly observed on each slide. SYTO 9 excitation/emission wavelengths were 480/500 nm and PI excitation/emission wavelengths were 490/635 nm. Images were generated by 3D reconstruction of biofilms using NIS-Elements AR Analysis software. The experiment was repeated three times.

Observation of extracellular polymeric substances

Alexa Fluor^{TM} 647 fluorescent dye was added during the biofilm incubation. Coverslips were washed three times with sterile distilled water in the dark. Then, 200 μl of SYTO 9 fluorescent dye was added to each slide, left for 15 min under anaerobic conditions in a 37°C incubator, and washed three times with sterile distilled water. The slides were air dried naturally, 200 μl of anti-fluorescence quencher was applied and sealed for inspection. Three areas were randomly observed on each slide. The excitation/emission wavelengths were 650/668 nm for Alexa Fluor^{TM} 647 and 480/500 nm for SYTO 9. The biofilms were reconstructed in 3D by NIS-Elements AR Analysis software and images were generated. The experiment was repeated three times.

Statistical analysis

Statistical analysis was performed using SPSS software version 23.0. Two independent samples *T*-test was used for comparisons between groups, while one-way ANOVA was used for comparisons within groups, measurement data were presented as mean ± SD.

Results

Modeling results of periodontitis-related microbial multispecies biofilm

The morphology of EPS observed by confocal laser scanning microscopy (CLSM) is shown in **Figure 1A**. The EPS was revealed in orange using Alexa Fluor^{TM} 647 fluorescent dye, live bacteria were stained as green by SYTO 9. The orange aggregates are connected in the form of clumps, showing a three-dimensional network structure with micro-voids in it; the green colonies are aggregated on the surface of the orange clumps or embedded in them. The communities of live and dead bacteria are shown in **Figure 1B**. Dead bacteria were visualized by PI in red, live bacteria were stained as green by SYTO 9. Live bacteria gather in groups, and dead bacteria are scattered among the live bacteria groups and at the bottom of the biofilm.

The morphology of the biofilm observed by scanning electron microscope (SEM) is shown in **Figure 1C**. The biofilm has a three-dimensional network structure with channel-like structures of varying sizes. The biofilm contains four types of bacteria, namely short rods, pairs or clusters of rods, small globules, and short chains. The bacteria aggregate, make contact with each other, and are wrapped by EPS.

The effect of bovine trypsin on extracellular polymeric substances in periodontitis-related microbial multispecies biofilms

Biofilm morphological changes after bovine trypsin treatment observed by scanning electron microscope

The SEM observation results of biofilm morphology after treatment with 2 mg/ml bovine trypsin for 30 s, 1 mg/ml bovine trypsin for 1 min, and 1 mg/ml bovine trypsin for 3 min, respectively, are shown in **Figure 2**. The biofilm morphology of the blank control group was similar to that of the negative control group. After bovine trypsin treatment, the biofilm became thinner, the three-dimensional network and channel-like structures disappeared, only a layer of scattered bacteria remained, and EPS were significantly

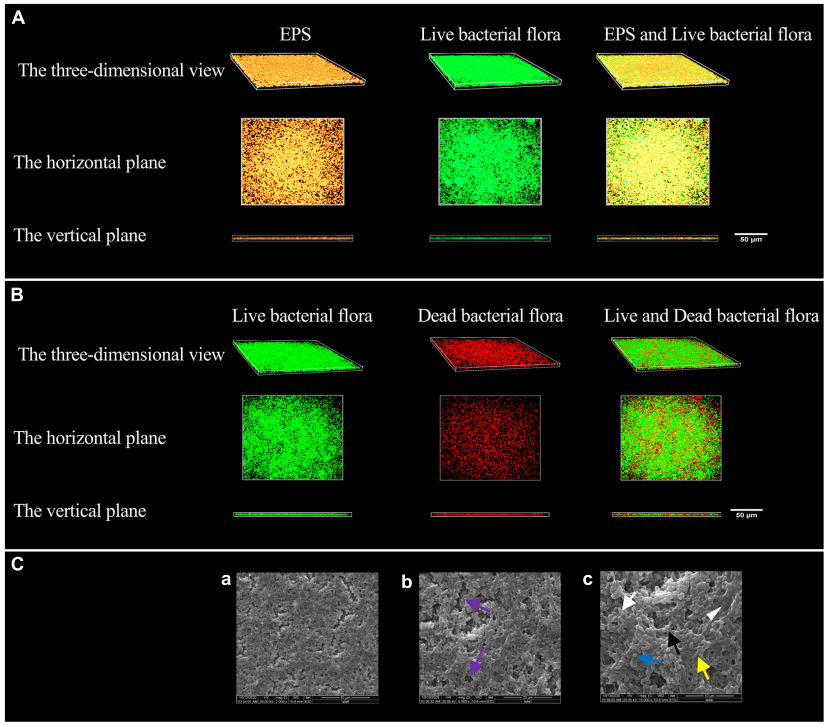

FIGURE 1
Modeling results of periodontitis-related microbial multispecies biofilm. **(A)** The three-dimensional morphology of EPS and live bacterial flora observed by CLSM. **(B)** The three-dimensional shape of the live and dead bacteria groups observed by CLSM. **(C)** The SEM observation of the biofilm morphology. **(a)** ×2000, **(b)** ×5000, and **(c)** ×10000. Channel-like structures (purple arrows) are shown in **(b)**, EPS (white triangle) in **(c)**, the short rod-shaped bacteria (white arrows) (*Actinomyces viscosus*), the paired ball-shaped bacteria (black arrows) (*Aggregatibacter actinomycetemcomitans*), the small spherical bacteria (blue arrow) (*Porphyromonas gingivalis*), and the bacteria arranged in short chains (yellow arrow) (*F. nucleatum* subsp. *polymorpha*) are shown in **(c)**.

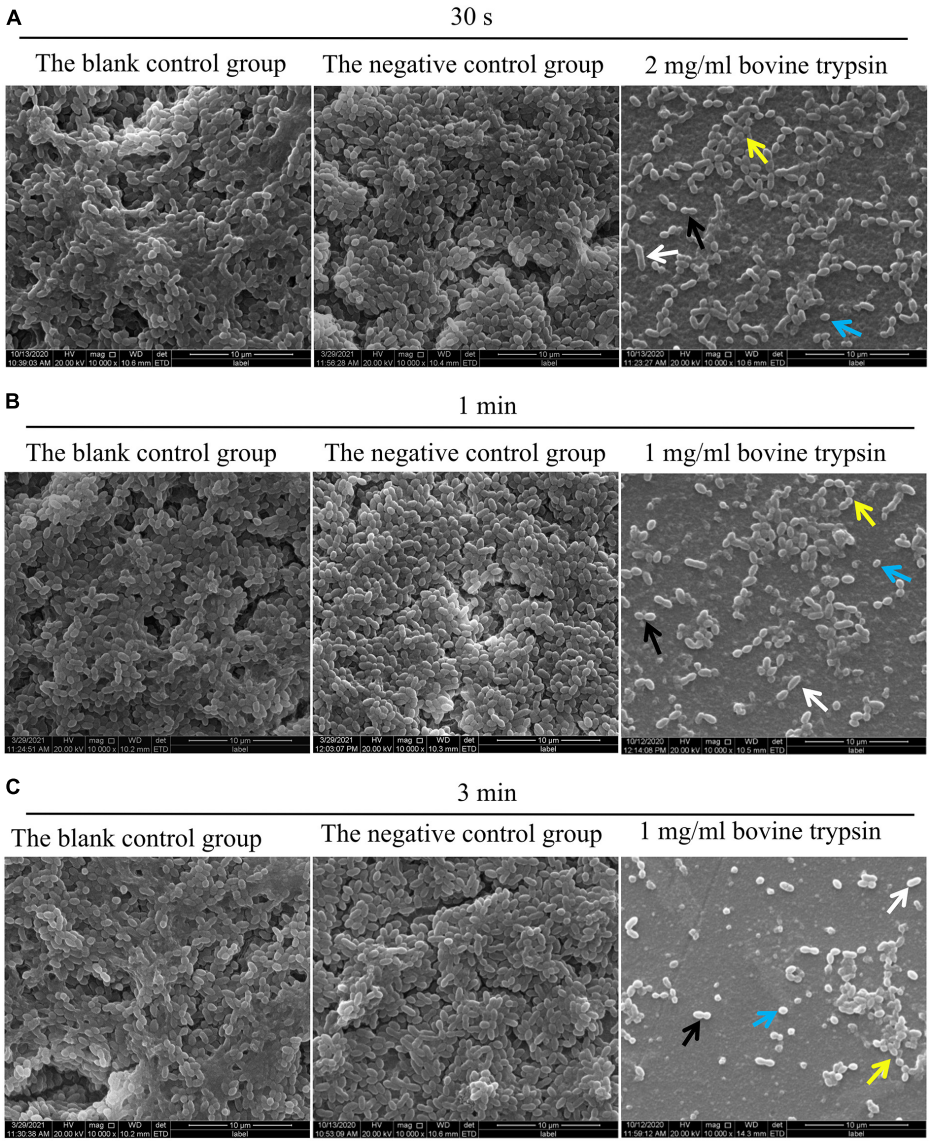

FIGURE 2
SEM observation of biofilm morphology after bovine trypsin action. **(A)** The morphology of the biofilm after 2 mg/ml bovine trypsin treatment for 30 s (×1000). **(B)** The morphology of the biofilm after 1 mg/ml bovine trypsin treatment for 1 min (×1000). **(C)** The morphology of the biofilm after 1 mg/ml bovine trypsin treatment for 3 min (×1000). The short rod-shaped bacteria (white arrows), the paired ball-shaped bacteria (black arrows), the small spherical bacteria (blue arrows), and the bacteria arranged in short chains (yellow arrows).

reduced. However, four types of bacteria were still visible in the residual biofilm, and the bacterial morphology did not change significantly.

Morphological changes and quantitative analysis of extracellular polymeric substances after bovine trypsin treatment according to confocal laser scanning microscopy observation

Figure 3 shows the morphology of EPS after the biofilm was treated with bovine trypsin for 30 s, 1 min, and 3 min, respectively. With the prolongation of the action time and the increase of the action concentration, the orange fluorescence of EPS weakened and became sparse, the voids increased, and the cross-linking decreased.

The results of the quantitative analysis of biofilm EPS after bovine trypsin treatment for 30 s, 1 min, and 3 min are shown in Figure 4. In Figure 4A, the difference between the negative control group and group A_4 was statistically significant ($P < 0.05$); in Figure 4B, the negative control group was significantly different from groups B_2 and B_3, respectively ($P < 0.05$); in Figure 4C, there were significant

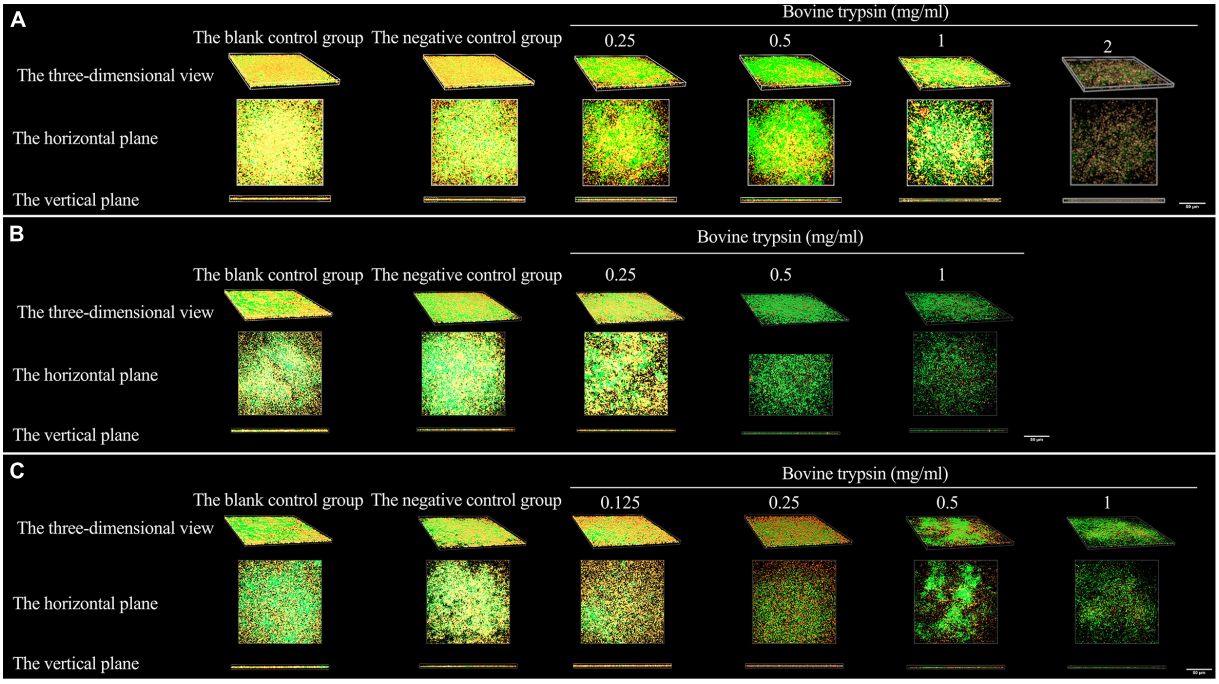

FIGURE 3
The three-dimensional morphology observation of biofilm EPS after 30 s, 1 min, and 3 min of bovine trypsin treatment by CLSM. **(A)** The morphology of EPS after 30 s of action by bovine trypsin. **(B)** The morphology of EPS after 1 min of action by bovine trypsin. **(C)** The morphology of EPS after 3 min of action by bovine trypsin.

differences between the negative control group and groups C_2, C_3, and C_4, respectively ($P < 0.05$). The results showed that when bovine trypsin acted for 30 s, 1 min, and 3 min, the minimum effective concentrations of EPS were 2, 0.5, and 0.25 mg/ml, respectively.

Morphological changes and quantitative analysis of live and dead bacteria after bovine trypsin treatment according to confocal laser scanning microscopy observation

Figure 5 shows the morphology of live and dead bacteria after the action of bovine trypsin on the biofilm for 30 s, 1 min, and 3 min. The live bacteria show green fluorescence, and the dead bacteria show red fluorescence. After the action of bovine trypsin, as the concentration increased, the action time increased, the biofilm structure became dispersed, and the green and red fluorescence decreased.

Quantitative analysis of live bacteria after 30 s, 1 min, and 3 min of bovine trypsin action on the biofilms are shown in Figure 6. In Figure 6A, the difference between the negative control group and group A_4 was statistically significant ($P < 0.05$); in Figure 6B, the negative control group was compared with groups B_2 and B_3, and the difference was statistically significant ($P < 0.05$); in Figure 6C, the negative control group was compared with groups C_3 and C_4, and the difference was statistically significant ($P < 0.05$). The results suggested that when bovine trypsin acted for 30 s, 1 min, and 3 min, the lowest effective concentrations for reducing live bacteria in the biofilm were 2, 0.5, and 0.5 mg/ml, respectively.

Quantitative analysis of dead bacteria after 30 s, 1 min, and 3 min of bovine trypsin acting on biofilms are shown in Figure 7. In Figure 7A, the negative control group was compared with group A4, and the difference was statistically significant ($P < 0.05$); in Figure 7B, the negative control group was compared with groups B_2 and B_3, and the difference was statistically significant ($P < 0.05$); in Figure 7C, the negative control group was compared with groups C_3 and C_4, and the difference was statistically significant ($P < 0.05$). The results suggested that when bovine trypsin acted for 30 s, 1 min, and 3 min, the lowest effective concentrations for reducing dead bacteria in the biofilm were 2, 0.5, and 0.5 mg/ml, respectively.

The analysis of changes in the ratio of live bacteria to dead bacteria after 30 s, 1 min, and 3 min of bovine trypsin action on the biofilm are shown in Figure 8, respectively. In Figure 8A, there was no significant difference between

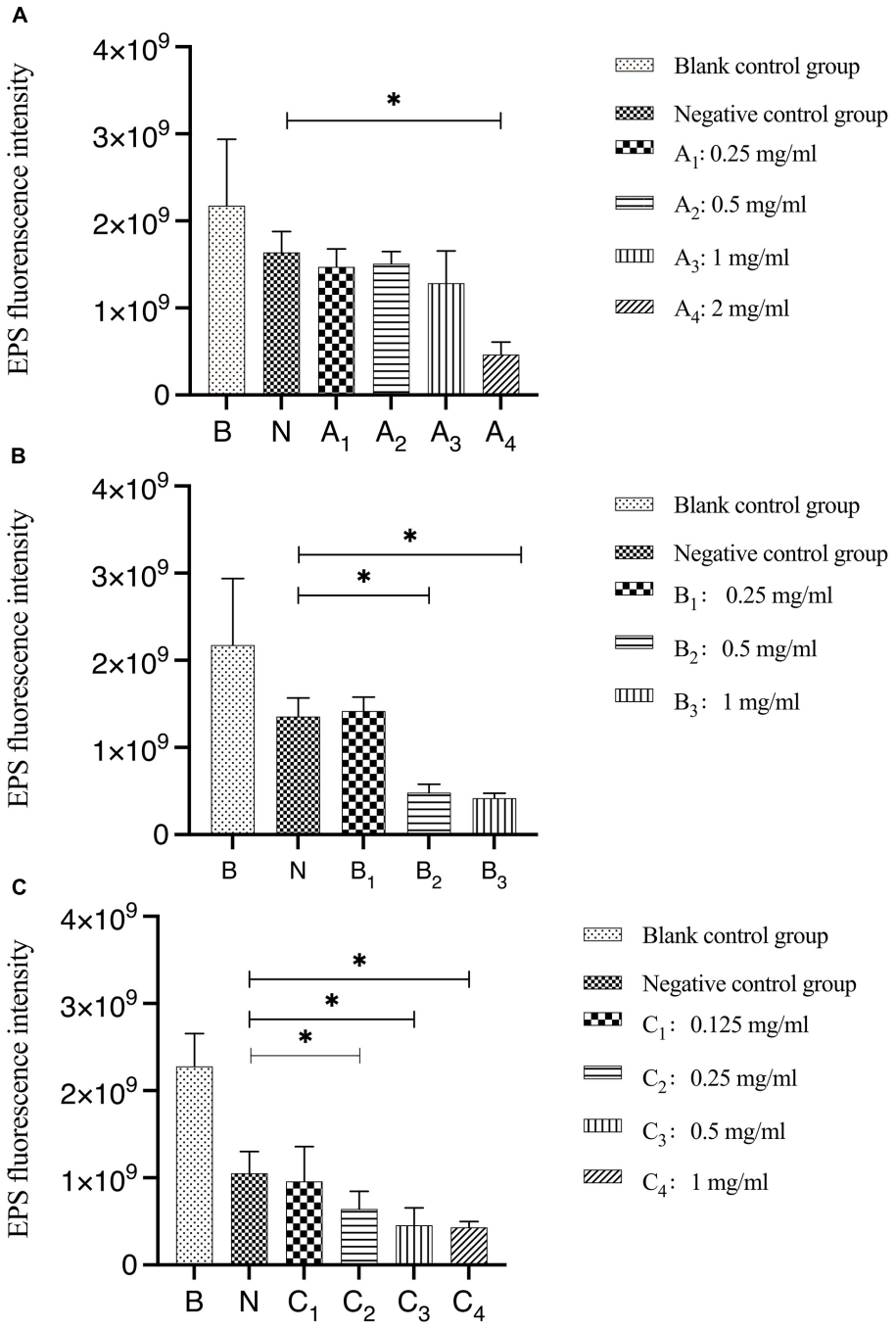

FIGURE 4
Quantitative analysis of the total amount of EPS in biofilms after bovine trypsin treatment for 30 s, 1 min, and 3 min. **(A–C)** Are the quantitative analysis of the total amount of EPS in the biofilms after bovine trypsin treatment for 30 s, 1 min, and 3 min, respectively. *Indicates that there is a statistically significant difference compared with the negative control group ($P < 0.05$).

the negative control group and the bovine trypsin treatment groups ($P > 0.05$); in Figure 8B, the negative control group was compared with groups B_1, B_2, and B_3, and the difference was statistically significant ($P < 0.05$); in Figure 8C, the negative control group was compared with groups C_2, C_3, and C_4, and the difference was statistically significant ($P < 0.05$). The results showed that when bovine trypsin acted for 30 s, all concentrations of bovine trypsin did not significantly change the ratio of live/dead bacteria. Moreover, when bovine trypsin acted for 1 min and 3 min, the lowest

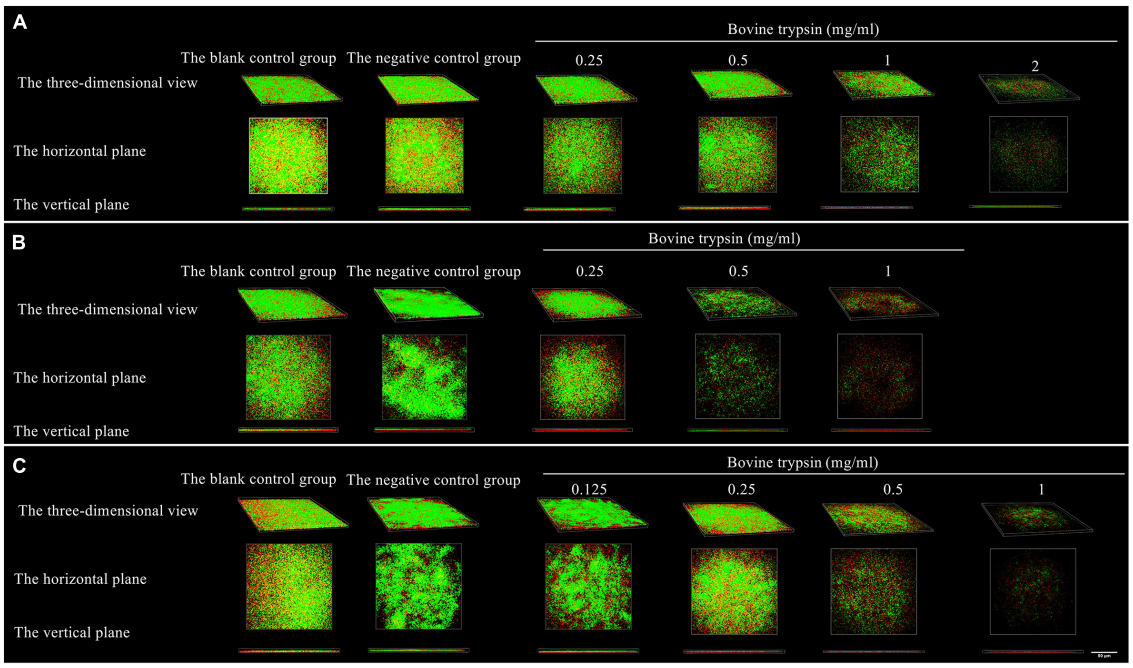

FIGURE 5
The three-dimensional morphology observation of live and dead bacteria after 30 s, 1 min, and 3 min of bovine trypsin treatment by CLSM. **(A–C)** Are the form of live and dead bacteria in the biofilm after 30 s, 1 min, and 3 min of ovine trypsin treatment, respectively.

effective concentration for reducing the ratio of live/dead bacteria was 0.25 mg/ml.

Discussion

The main purpose of periodontal therapy is to eliminate infection, which can be achieved with mechanical debridement and antimicrobial agents. However, bacteria in periodontal pockets often exist in the form of biofilms, which can make them more resistant to antimicrobials. In addition, the complex anatomical structure of the root and periodontal system provides a hiding place for the biofilm, which makes it difficult to remove the biofilm in these parts with traditional mechanical debridement. Moreover, due to the protection offered by EPS, the effect of antibacterial drugs on the biofilm is not strong enough. Therefore, the chemical drugs used to remove the biofilm in the periodontal pocket should also possess the ability to destroy the biofilm EPS. EPS can be used as a target to destroy the structure and stability of the biofilm, promote the degradation of the biofilm and cause the separation of bacteria in it, and sensitize the bacteria in the biofilm. Meanwhile, it can be combined with antibacterial drugs to enhance the effect of antibacterial drugs (Wolfmeier et al., 2018; Zhao et al., 2018). However, the specific target proteins of bovine trypsin to degrade periodontitis-related microbial multispecies biofilms have not been fully studied. The mechanism by which bovine trypsin degrades biofilms has been somewhat understood in recent years, but many details remain unclear, and more studies are needed to fill in the gaps.

The results of this study showed that after the action of bovine trypsin, the biofilm degraded, EPS dispersed and the total amount decreased; thus, bovine trypsin could degrade EPS. The reduction of EPS by bovine trypsin was positively correlated with the duration of action and the concentration of bovine trypsin. With the prolongation of bovine trypsin action time, EPS decreased more obviously, and the minimum effective concentration decreased. When the minimum effective concentration was reached, the total amount of EPS decreased significantly. According to previous researches, the main reports on the biofilm degradation mechanism mainly include the degradation of EPS, which is related to the hydrolysis of composition-related proteins of EPS. It is speculated that the mechanism of reduction of EPS is related to the composition-related proteins of EPS that can be hydrolyzed by bovine trypsin: (1) Bovine trypsin hydrolyzes bacterial cell surface proteins. The EPS protein components of the biofilms of bacteria such as *Staphylococcus aureus* include cell surface proteins, mainly composed of fibronectin binding protein A (FnBPA), fibronectin binding protein B (FnBPB), Biofilm associated protein (Bap), Clustering factor B (ClfB) (Lister and Horswill, 2014). The extracellular serine protease (Esp) secreted by *Staphylococcus epidermidis* hydrolyzes Bap associated with the formation of *Staphylococcus*

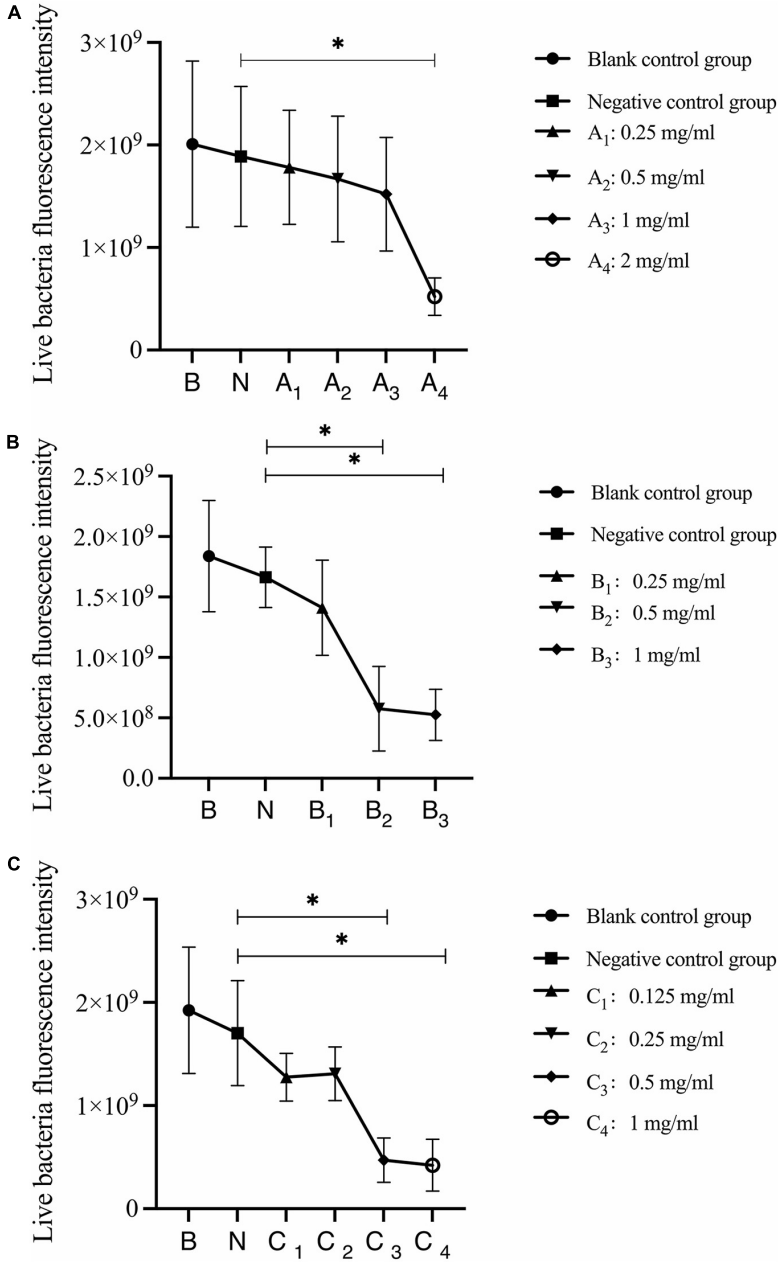

FIGURE 6
Quantitative analysis of live bacteria in biofilms after bovine trypsin treatment for 30 s, 1 min, and 3 min. **(A–C)** Show the quantitative analysis of biofilm live bacteria after 30 s, 1 min, and 3 min of bovine trypsin treatment, respectively. *Indicates that there is a statistically significant difference compared with the negative control group ($P < 0.05$).

aureus biofilms (Sugimoto et al., 2013). Bovine trypsin also acts as a serine protease; thus, it is speculated that the reduction of EPS in the biofilm of periodontitis-related microorganisms established in this experiment may be related to the hydrolysis of cell surface proteins; (2) Bovine trypsin can hydrolyze bacterial extracellular proteins, which are an important part of EPS. Protease can lead to the hydrolysis of proteins in EPS and reduce the stability of biofilm and is the most potent biofilm-degrading enzyme (Lister and Horswill, 2014). Proteinase K, trypsin, and dispase B can all hydrolyze protein components in the EPS of *staphylococcal* biofilms, degrade biofilms, and promote the dispersion of established biofilm colonies (Chaignon et al., 2007). It is speculated that trypsin acts on the biofilm in this experiment, which may be related to the hydrolysis of extracellular proteins.

10.3389/fmicb.2022.951291

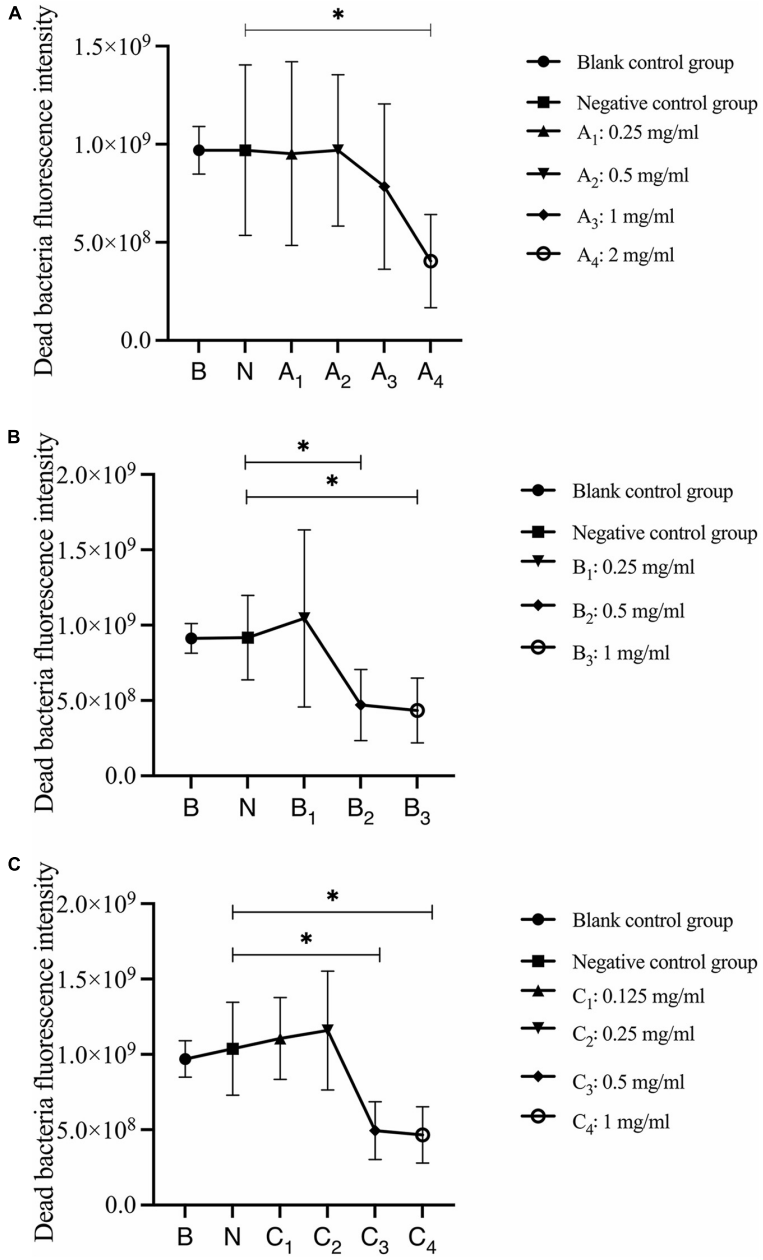

FIGURE 7
Quantitative analysis of dead bacteria in biofilm after bovine trypsin treatment for 30 s, 1 min, and 3 min. **(A–C)** Show the quantitative analysis of biofilm dead bacteria after 30 s, 1 min, and 3 min of bovine trypsin treatment, respectively. *Indicates that there is a statistically significant difference compared with the negative control group ($P < 0.05$).

Bacterial biomasses are reduced by the action of bovine trypsin, and the ratio of live/dead bacteria is negatively correlated with the action time and concentration of bovine trypsin. When the action time is short, after the bovine trypsin concentration reaches the minimum effective concentration, the biofilm structure is effectively destroyed, the biofilm is dispersed, and the live and dead bacteria are reduced. It is speculated that the reasons are as follows: (1) EPS is hydrolyzed, causing the bacteria embedded in the biofilm EPS to detach from the biofilm; (2) Bovine trypsin destroys the adhesion of the bacteria, and the bacteria detach from the biofilm. When the action time is prolonged, before the bovine trypsin concentration reaches the minimum effective concentration that reduces the total amount of live and dead bacteria, the EPS on the surface of the biofilm is hydrolyzed, the bacteria of

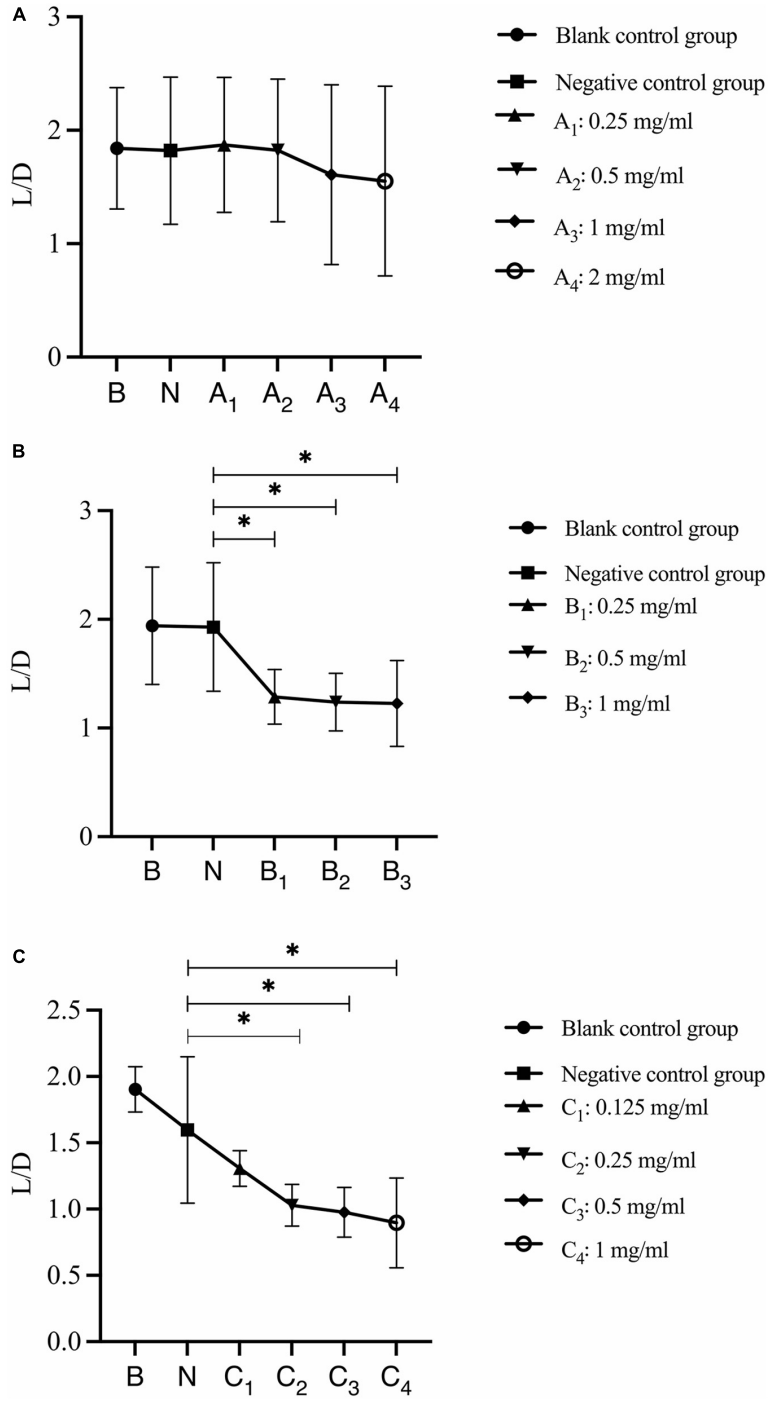

FIGURE 8
Changes in the ratio of live/dead bacteria after bovine trypsin treatment for 30 s, 1 min, and 3 min. **(A–C)** Show the quantitative analysis of the ratio of live bacteria/dead bacteria in the biofilms after 30 s, 1 min, and 3 min of bovine trypsin treatment, respectively. *Indicates that there is a statistically significant difference compared with the negative control group ($P < 0.05$).

the biofilm is separated from the biofilm partially, and there are more live bacteria at this site, resulting in a decrease in live bacteria. After the EPS surface part was hydrolyzed, the bacteria without EPS protection that contacted bovine trypsin died, and the dead bacteria in the middle and lower layers of the biofilm remained in the biofilm; therefore, the amount of dead bacteria increased, which led to a decrease in the ratio of live bacteria/dead bacteria.

After the bovine trypsin concentration reaches the minimum effective concentration to reduce the total amount of live and dead bacteria, the biofilm structure is destroyed completely, the biofilm is dispersed, and the bacteria are separated from the biofilm; therefore, the total amount of bacteria reduces. After the biofilm is dispersed, the bottom layer persists, the bacteria partially adheres to the surface of the glass slide, and the number of dead bacteria in the biofilm gradually increases from the surface layer to the bottom layer; therefore, the ratio of live bacteria/dead bacteria decreases.

After the action of bovine trypsin, the bacteria in the biofilm became dispersed and the bacteria died, but the bacterial morphology did not change significantly. Bacterial death can be achieved in two way: (1) destruction of the cell membrane, resulting in cell death and deformation of the bacteria; and (2) targeted binding to the DNA gyrase/topoisomerase IV-DNA complex, preventing DNA replication and breaking it, which results in bacterial death and may not affect the bacterial morphology in a short time (Hooper and Jacoby, 2016). There was no obvious change in bacterial morphology in this experiment, and the specific mechanism needs to be further studied.

Further research on this topic will lead to the development of new therapeutic options for biofilm-mediated periodontitis.

Conclusion

Periodontitis-related microbial multispecies biofilm established in this study is formed by the EPS encapsulating the bacterial group and has a three-dimensional network structure, which is in line with the characteristics of biofilms. Bovine trypsin can destroy the biofilm structure, disperse the biofilm and bacteria, and significantly reduce the EPS and bacterial biomass. The effect of bovine trypsin on degrading periodontitis-related microbial multi-species biofilm was positively correlated with the action time and concentration.

Data availability statement

The raw data supporting the conclusions of this article will be made available by the authors, without undue reservation.

Author contributions

JZ contributed to data acquisition, data analysis, and manuscript preparation. XM, QH, YH, and YL contributed to data acquisition and data analysis. LH contributed to the design of the study and professionally revised the manuscript. All authors read and approved the final manuscript.

Funding

This research was funded by the Kunming Medical University Postgraduate Innovation Fund (2020S115).

Acknowledgments

We wish to thank LH for her valuable contributions to the research.

Conflict of interest

The authors declare that the research was conducted in the absence of any commercial or financial relationships that could be construed as a potential conflict of interest.

Publisher's note

References

Banar, M., Emaneini, M., Satarzadeh, M., Abdellahi, N., Beigverdi, R., Van Leeuwen, W. B., et al. (2016). Evaluation of mannosidase and trypsin enzymes effects on biofilm production of *Pseudomonas aeruginosa* isolated from burn wound infections. *PLoS One* 11:e0164622. doi: 10.1371/journal.pone.0164622

Bowen, W. H., Burne, R. A., Wu, H., and Koo, H. (2018). Oral Biofilms: Pathogens, Matrix, and Polymicrobial Interactions in Microenvironments. *Trends Microbiol.* 26, 229–242. doi: 10.1016/j.tim.2017.09.008

Chaignon, P., Sadovskaya, I., Ragunah, C., Ramasubbu, N., Kaplan, J. B., and Jabbouri, S. (2007). Susceptibility of staphylococcal biofilms to enzymatic treatments depends on their chemical composition. *Appl. Microbiol. Biotechnol.* 75, 125–132. doi: 10.1007/s00253-006-0790-y

Ciofu, O., Rojo-Molinero, E., Macià, M. D., and Oliver, A. (2017). Antibiotic treatment of biofilm infections. *Apmis* 125, 304–319. doi: 10.1111/apm.12673

Flemming, H. C., Wingender, J., Szewzyk, U., Steinberg, P., Rice, S. A., and Kjelleberg, S. (2016). Biofilms: an emergent form of bacterial life. *Nat. Rev. Microbiol.* 14, 563–575. doi: 10.1038/nrmicro.2016.94

Gupta, P., Sarkar, S., Das, B., Bhattacharjee, S., and Tribedi, P. (2016). Biofilm, pathogenesis and prevention—a journey to break the wall: a review. *Arch. Microbiol.* 198, 1–15. doi: 10.1007/s00203-015-1148-6

Hogan, S., O'Gara, J. P., and O'Neill, E. (2018). Novel treatment of staphylococcus aureus device-related infections using fibrinolytic agents. *Antimicrob. Agents Chemother.* 62:e2008–e2017. doi: 10.1128/AAC.02008-17

Hooper, D. C., and Jacoby, G. A. (2016). Topoisomerase inhibitors: fluoroquinolone mechanisms of action and resistance. *Cold Spring Harb. Perspect. Med.* 6:a025320. doi: 10.1101/cshperspect.a025320

Karpiński, T. M., and Szkaradkiewicz, A. K. (2015). Chlorhexidine - Pharmaco-biological activity and application. *Eur. Rev. Med. Pharmacol. Sci.* 19, 1321–1326.

Koo, H., Falsetta, M. L., and Klein, M. I. (2013). The Exopolysaccharide Matrix: A Virulence Determinant of Cariogenic Biofilm. *J. Dent. Res.* 92, 1065–1073. doi: 10.1177/0022034513504218

Lister, J. L., and Horswill, A. R. (2014). Staphylococcus aureus biofilms: recent developments in biofilm dispersal. *Front. Cell. Infect. Microbiol.* 4:178. doi: 10.3389/fcimb.2014.00178

Liu, Y., Kamesh, A. C., Xiao, Y., Sun, V., Hayes, M., Daniell, H., et al. (2016). Topical delivery of low-cost protein drug candidates made in chloroplasts for biofilm disruption and uptake by oral epithelial cells. *Biomaterials* 105, 156–166. doi: 10.1016/j.biomaterials.2016.07.042

Mealey, B. L., and Oates, T. W. (2006). Diabetes Mellitus and Periodontal Diseases. *J. Periodontol.* 77, 1289–1303. doi: 10.1902/jop.2006.050459

Mugita, N., Nambu, T., Takahashi, K., Wang, P. L., and Komasa, Y. (2017). Proteases, actinidin, papain and trypsin reduce oral biofilm on the tongue in elderly subjects and in vitro. *Arch. Oral Biol.* 82, 233–240. doi: 10.1016/j.archoralbio.2017.04.035

Niazi, S. A., Al-Ali, W. M., Patel, S., Foschi, F., and Mannocci, F. (2015). Synergistic effect of 2% chlorhexidine combined with proteolytic enzymes on biofilm disruption and killing. *Int. Endod. J.* 48, 1157–1167. doi: 10.1111/iej.12420

Niazi, S. A., Clark, D., Do, T., Gilbert, S. C., Foschi, F., Mannocci, F., et al. (2014). The effectiveness of enzymic irrigation in removing a nutrient-stressed endodontic multispecies biofilm. *Int. Endod. J.* 47, 756–768. doi: 10.1111/iej.12214

Payne, W. G., Salas, R. E., Ko, F., Naidu, D. K., Donate, G., Wright, T. E., et al. (2008). Enzymatic debriding agents are safe in wounds with high bacterial bioburdens and stimulate healing. *Eplasty* 8:e17.

Peng, C. H., Yang, Y. S., Chan, K. C., Kornelius, E., Chiou, J. Y., and Huang, C. N. (2017). Periodontal treatment and the risks of cardiovascular disease in patients with type 2 diabetes: a retrospective cohort study. *Intern. Med.* 56, 1015–1021. doi: 10.2169/internalmedicine.56.7322

Pérez-Losada, F., de, L., Jané-Salas, E., Sabater-Recolons, M., del, M., Estrugo-Devesa, A., et al. (2016). Correlation between periodontal disease management and metabolic control of type 2 diabetes mellitus. A systematic literature review. *Med. Oral Patol. Oral Cir. Bucal* 21:e440–e446. doi: 10.4317/medoral.21048

Saggu, S. K., Jha, G., and Mishra, P. C. (2019). Enzymatic degradation of biofilm by metalloprotease from microbacterium sp. Sks10. *Front. Bioeng. Biotechnol.* 7:192. doi: 10.3389/fbioe.2019.00192

Singh, P. K., Parsek, M. R., Greenberg, E. P., and Welsh, M. J. (2002). A component of innate immunity prevents bacterial biofilm development. *Nature* 417, 552–555. doi: 10.1038/417552a

Sugimoto, S., Iwamoto, T., Takada, K., Okuda, K. I., Tajima, A., Iwase, T., et al. (2013). Staphylococcus epidermidis Esp degrades specific proteins associatedwith staphylococcus aureus biofilm formation and host-pathogen interaction. *J. Bacteriol.* 195, 1645–1655. doi: 10.1128/JB.01672-12

Valm, A. M. (2019). The Structure of Dental Plaque Microbial Communities in the Transition from Health to Dental Caries and Periodontal Disease. *J. Mol. Biol.* 431, 2957–2969. doi: 10.1016/j.jmb.2019.05.016

Verderosa, A. D., Totsika, M., and Fairfull-smith, K. E. (2019). *Bacterial Biofilm* Eradication Agents?: A Current Review. *Front. Chem.* 7:824. doi: 10.3389/fchem.2019.00824

Wang, Z., Shen, Y., and Haapasalo, M. (2020). Dynamics of Dissolution, Killing, and Inhibition of Dental Plaque Biofilm. *Front. Microbiol.* 11:964. doi: 10.3389/fmicb.2020.00964

Wolfmeier, H., Pletzer, D., Mansour, S. C., and Hancock, R. E. W. (2018). New Perspectives in Biofilm Eradication. *ACS Infect. Dis.* 4, 93–106. doi: 10.1021/acsinfecdis.7b00170

Yan, L., Zhang, X., Hao, G., Guo, Y., Ren, Y., Yu, L., et al. (2016). Insight into the roles of tightly and loosely bound extracellular polymeric substances on a granular sludge in ammonium nitrogen removal. *Bioresour. Technol.* 222, 408–412. doi: 10.1016/j.biortech.2016.10.011

Zhang, L. Y., Fang, Z. H., Li, Q. L., and Cao, C. Y. (2019). A tooth-binding antimicrobial peptide to prevent the formation of dental biofilm. *J. Mater. Sci.* 30:45. doi: 10.1007/s10856-019-6246-6

Zhao, T., Zhang, Y., Wu, H., Wang, D., Chen, Y., Zhu, M. J., et al. (2018). Extracellular aminopeptidase modulates biofilm development of *Pseudomonas aeruginosa* by affecting matrix exopolysaccharide and bacterial cell death. *Environ. Microbiol. Rep.* 10, 583–593. doi: 10.1111/1758-2229.12682

Zijnge, V., Van Leeuwen, M. B. M., Degener, J. E., Abbas, F., Thurnheer, T., Gmür, R., et al. (2010). Oral biofilm architecture on natural teeth. *PLoS One* 5:9321. doi: 10.1371/journal.pone.0009321

frontiers | Frontiers in Microbiology

TYPE Original Research
PUBLISHED 08 August 2022
DOI 10.3389/fmicb.2022.967845

OPEN ACCESS

EDITED BY
Huancai Lin,
Sun Yat-sen University, China

REVIEWED BY
Dariusz Nowicki,
University of Gdansk,
Poland
Appadurai Muthamil Iniyan,
Manonmaniam Sundaranar University,
India
Vijayakumar Sekar,
Shandong University, China
Atte Von Wright,
University of Eastern Finland, Finland

*CORRESPONDENCE
Pei-Yuan Qian
boqianpy@ust.hk
Henry Lam
kehlam@ust.hk

SPECIALTY SECTION
This article was submitted to Antimicrobials, Resistance and Chemotherapy, a section of the journal Frontiers in Microbiology

RECEIVED 13 June 2022
ACCEPTED 20 July 2022
PUBLISHED 08 August 2022

CITATION
Long L, Sulaiman JE, Xiao Y, Cheng A, Wang R, Malit JJ, Wong WC, Liu W, Li Y-X, Chen F, Lam H and Qian P-Y (2022) Mode of action of elasnin as biofilm formation eradicator of methicillin-resistant *Staphylococcus aureus*. *Front. Microbiol.* 13:967845. doi: 10.3389/fmicb.2022.967845

Mode of action of elasnin as biofilm formation eradicator of methicillin-resistant *Staphylococcus aureus*

Lexin Long[1,2,3], Jordy Evan Sulaiman[4], Yao Xiao[1,3], Aifang Cheng[1,3], Ruojun Wang[1,3], Jessie James Malit[1,3], Wai Chuen Wong[1,3], Wenchao Liu[1,3], Yong-Xin Li[5,6], Feng Chen[7], Henry Lam[4]* and Pei-Yuan Qian[1,3]*

[1]Department of Ocean Science, The Hong Kong University of Science and Technology, Kowloon, Hong Kong, China, [2]SZU-HKUST Joint PhD Program in Marine Environmental Science, Shenzhen University, Shenzhen, China, [3]Southern Marine Science and Engineering Guangdong Laboratory (Guangzhou), Guangzhou, China, [4]Department of Chemical and Biological Engineering, The Hong Kong University of Science and Technology, Kowloon, Hong Kong SAR, China, [5]Department of Chemistry, The University of Hong Kong, Pokfulam, Hong Kong SAR, China, [6]The Swire Institute of Marine Science and Hong Kong Branch of Southern Marine Science and Engineering Guangdong Laboratory (Guangzhou), The University of Hong Kong, Pokfulam, Hong Kong SAR, China, [7]Institute for Advanced Study, Shenzhen University, Shenzhen, China

Biofilm is made up of microbes and their extracellular matrix, making microorganisms highly tolerant, resistant, and resilient to a wide range of antimicrobials. Biofilm treatment with conventional antimicrobial agents can accelerate the evolution and spread of resistance due to the reduced efficacy and increased gene transfer and differentiation within biofilms. Therefore, effective biofilm-targeting compounds are currently highly sought after. In the present study, we identified elasnin as a potent biofilm-targeting compound against methicillin-resistant *Staphylococcus aureus* (MRSA). Elasnin effectively inhibited biofilm formation and especially eradicated the pre-formed biofilms of MRSA with low cytotoxicity and low risk of resistance development and retains its activity in a chronic wound biofilms model. A comprehensive mechanistic study using multi-omics and confocal and scanning electron microscopy revealed that elasnin induced the biofilm matrix destruction in a time-dependent manner and interfered with the cell division during the exponential phase, primarily by repressing the expression of virulence factors. Cells released from the elasnin-treated biofilms exhibited a defective appearance and became more sensitive to beta-lactam antibiotic penicillin G. Through gene overexpression and deletion assay, we discovered the key role of *sarZ* during elasnin-induced biofilm eradication. Overall, the present study identified elasnin as a potent biofilm eradicator against MRSA that harbors potential to be developed for biofilm removal and chronic wound treatment, and provided new insights into the molecular targets for biofilm eradication in MRSA.

KEYWORDS

elasnin, biofilms, MRSA, resistance, antimicrobials, eradication, antibiofilm

Introduction

Biofilms consist of microorganisms that grow on various surfaces. Microbial cells in biofilms are organised and embedded in a matrix that contains diverse self-produced extracellular polymeric substances (EPSs) including polysaccharides, proteins, nucleic acids and lipids (Flemming and Wingender, 2010; Flemming et al., 2016). Cells in biofilms are usually more tolerant, resistant, and resilient to external threats than their planktonic cells (Mah and O'Toole, 2001; Stewart and William Costerton, 2001; Hall and Mah, 2017). Consequently, conventional antimicrobial agents gradually lose their efficacies against biofilms, and extremely high concentrations are often required to eradicate the pre-formed biofilms (Hengzhuang et al., 2012; Wu et al., 2015).

Biofilm-associated infection is currently a major problem in clinics and the healthcare industry, accounting for about 80% of bacterial infections and 65% of nosocomial infections (Jamal et al., 2018). Biofilm formation is crucial for bacterial pathogenesis and is the leading cause of chronic and device-related infections (Madalina Mihai et al., 2015). Bacteria in the genus of Staphylococci are the most frequently reported source of biofilm-related infections. Among the reported cases of infections, one of the most dangerous pathogens in clinics to date is Staphylococcus aureus, whose resistance is related to biofilm formation (Lister and Horswill, 2014; Moormeier and Bayles, 2017). The typical process of Staphylococcus biofilm development requires the participation of many virulence factors and secreted substances such as adhesive surface proteins, degradative enzymes, EPSs and toxins (Antunes and Ferreira, 2011; Otto, 2019). These substances facilitate the adhesion and colonisation of bacteria and assist biofilm maturation and rapid cell proliferation. However, the dependence of matrix components on biofilm development for different *S. aureus* strains varies. For instance, PIA production encoded by ica operon is essential for methicillin-sensitive *S. aureus* (MSSA; O'Neill et al., 2007), whereas biofilms of methicillin-resistant *S. aureus* (MRSA) commonly form in an ica-independent manner and require adhesive surface proteins such as FnBPA and FnBPB (O'Neill et al., 2008), SasG (Corrigan et al., 2007), and Atl and extracellular DNA (eDNA; Houston et al., 2011; Bose et al., 2012). Apart from shaping the biofilm structure, degradative enzymes induce biofilm detachment and then facilitate the systemic dissemination of bacterial infection (Otto, 2019).

Biofilm formation is tightly controlled by the coordination of multiple signalling pathways, in which the quorum-sensing system Agr and the global regulators *SarA* protein family play the central roles (Jenul and Horswill, 2019; Otto, 2019). The Agr system encodes two different transcripts, namely, RNAII and RNAIII, in which RNAIII functions as an intracellular effector that directly or indirectly controls the expression of numerous virulence factors (e.g., proteases and surface adhesins), which are involved in biofilm formation, and cell wall hydrolases with roles in cell cycle and pathogenesis (Boisset et al., 2007; Monteiro et al., 2015). The *SarA* protein family consists of many members, such as *SarZ*, *SarX*, and *SarR*, most of which control the expression of virulence factors. Among all the proteins in this family, *SarA* is the most extensively studied. *SarA* is a global regulator that positively controls PIA synthesis, agr system, adhesins and toxins, and it represses its own expression and the production of proteases (Beenken et al., 2003; Cheung et al., 2008). Notably, many studies have revealed the interconnected roles of *sarA* and agr in the switching between the formation and detachment of *S. aureus* biofilm. The upregulation of adhesins, PIA, and protease inhibitors by *sarA* induces early biofilm adherence, and the activation of peptides and nucleases by agr assist biofilm dispersion (Beenken et al., 2010; Vasudevan, 2019).

Biofilm-related infections have significantly threatened human health. However, current biofilm control strategies are limited, and long-term and high-dose combinational treatments are general therapeutic strategies for biofilm infections (Wu et al., 2015). Previous drug discoveries mostly focused on treating planktonic cells and thus, cells in biofilms that had already been exposed to conventional antimicrobials are easier to develop resistance due to the limited penetration, enzyme degradation, increased gene transfer, and differentiation within biofilms (Mah and O'Toole, 2001). Recently, there are efforts in discovering new antibiofilm agents, such as those that target the EPS by inhibiting EPS production, binding to EPS adhesins or degrading the EPSs (dispersin B and DNase I). Other strategies such as inducing biofilm dispersal and metabolic interference are also potential directions for future drug discoveries and developments (Koo et al., 2017; Li and Lee, 2017).

In the present study, we showed that elasnin serves as a potent biofilm-targeting compound against MRSA which effectively inhibited and especially eradicated their pre-formed biofilms. Elasnin is a small molecule containing a 2-pyrone (α-pyrone) structure and was discovered to be effective in inhibiting marine biofilms in our previous study (Long et al., 2021). To elucidate elasnin's mode of action, the combination of multi-omics analyses, microscopy imaging, gene manipulation, and other bioassays were performed. The results provided the detailed process of elasnin-induced biofilm eradication and highlighted the key genes that govern this process, including the transcriptional regulator gene *sarZ*.

Abbreviations: MRSA: Methicillin-resistant *Staphylococcus aureus*; MSSA: Methicillin-sensitive *S. aureus*; EPS: Extracellular polymeric substances; eDNA: Extracellular DNA; MIC: Minimum inhibitory concentration; MBC: minimum bactericidal concentration; MBIC: Minimum biofilm inhibitory concentration; MBEC: Minimal biofilm eradication concentration; LCMB model: Lubbock chronic wound biofilm model; TSBG: TSB complemented with 0.5% glucose; DEGs/DEPs: Differentially expressed genes/proteins; CLSM: Confocal laser scanning microscopy; SEM: Scanning electron microscope; GO: Gene ontology; KEGG: Kyoto Encyclopaedia of Genes and Genomes.

Materials and methods

Strains, media and chemicals

Twelve actinobacterial strains (Supplementary Table S1) were obtained from the German Collection of Microorganisms and Cell Cultures (Braunschweig, Germany). The MRSA ATCC 43300,

Escherichia coli ATCC 25922 and *S. aureus* ATCC 25923 strains were obtained from American Type Culture Collection. Soybean powder was obtained from Wugumf, Shenzhen, China. Soluble starch was obtained from Affymetrix, Santa Clara, CA, United States. Magnesium sulphate hydrate was obtained from Riedel-de-Haën, Seelze, Germany. Bacteriological peptone and tryptone soya broth (TSB) were obtained from Oxoid, Milan, Italy. Mueller-Hinton broth (MHB) was obtained from Fluka Chemie AG, Buchs, Switzerland. Proteinase K was obtained from Qiagen NV, Venlo, Netherlands. Phosphate-buffered saline (PBS) and DNase I were obtained from Thermo Fisher Scientific Inc., San Jose, CA, United States. Lysogeny broth (LB), glucose, 3-(4,5-dimethylthiazol-2-yl)-2,5-diphenyltetrazolium bromide (MTT) and 1-butanol were obtained from VWR International Ltd., Leicestershire, United Kingdom. Antibiotics, stains and all other chemicals were supplied by Sigma-Aldrich Corporation, Saint Louis, MO, United States.

Antibacterial assay

Minimum inhibitory concentration (MIC) and minimum bactericidal concentration (MBC) were determined using MRSA ATCC 43300 and *E. coli* ATCC 25922 according to the Clinical and Laboratory Standards Institute guideline CLSI M100 (2018). In a typical procedure, a 10^5 CFU/ml overnight culture of test strains was inoculated into MHB and treated with testing compounds in a series of concentrations. After incubation for 24 h, the minimum concentrations at which no bacterial growth was visible were recorded as the MICs. MBCs were measured following MIC assay by plating 1 ml of suitably diluted culture broth from each well on Mueller-Hinton agar (MHA) plate. MBC was defined as the lowest concentration at which an antimicrobial agent caused >99.9% reduction in cells. Each assay was performed in duplicate and repeated thrice.

MRSA ATCC 43300 was used for the concentration–response curve study. A culture of 4×10^5 CFU/ml MRSA in the exponential phase was inoculated into MHB with various concentrations of elasnin and vancomycin in 15 ml falcon tubes. Tubes were incubated at 37°C on a rotary shaker for 24 h. Then, 1 ml of culture broth in each tube was diluted with MHB, and 1 ml of diluted bacteria was plated on MHA plates for CFU counting. Culture broth from each well was inoculated on two plates, and the experiments were repeated thrice.

Antibiofilm assay

Minimum biofilm inhibitory concentration (MBIC) and minimal biofilm eradication concentration (MBEC) were determined as previously described (Nair et al., 2016; Yin et al., 2019; Long et al., 2021). The time-course biofilm formation on MRSA cells is shown in Supplementary Figure S1A. An overnight culture of test strains was diluted into approximately 10^7 CFU/ml with LB and 0.5% glucose and treated with various concentrations of testing compounds in 96-well cell culture plates. These plates were then incubated at 37°C for 24 h and rinsed twice with 1 × PBS to remove non-adhering and planktonic cells. After rinsing, MTT staining assay was conducted to measure viable cells in the biofilms, because MTT can react with dehydrogenase enzymes in viable cells to form blue-violet formazan, which can be detected at 570 nm after dissolving in DMSO. $MBIC_{50}$ and $MBIC_{90}$ were defined as the lowest concentrations required to inhibit 50 and 90% of biofilm formation, respectively.

For MBEC assay, an overnight culture of test strains was incubated for 24 h in 96-well cell culture plates to form mature biofilm before rinsing twice with 1 × PBS and compound treatment. After 24 h of incubation at 37°C, each well was rinsed twice with 1 × PBS, and OD_{570nm} was recorded after MTT assay as described above. The lowest concentration of a compound resulting in 50% decrease in $OD_{570\,nm}$ were recorded as $MBEC_{50}$. Biofilm inhibition/eradication efficiency was calculated using the following equation: Biofilm inhibition/eradication (%) = [1 − (OD_{570nm} of test compound) / (OD_{570nm} of control)] × 100%. Experiments were performed in triplicate and repeated thrice.

Antibiofilm assays in modified Lubbock chronic wound biofilm model

The antibiofilm activity of elasnin was assessed using a modified LCWB model that simulates the conditions in chronic wounds (Sun et al., 2008; Brackman et al., 2011). Briefly, an overnight culture of MRSA was diluted into approximately 10^6 CFU/ml with Bolton broth supplemented with 50% plasma (Sigma-Aldrich) and 5% freeze–thaw laked horse blood (Thermo Fisher Scientific). Then, the sample was treated with (MBIC) or without (MBEC) various concentrations of elasnin/vancomycin in 96-well cell culture plates. The plate was then incubated for 24 h at 37°C followed by medium removal and rinse with physiological saline (PS, Sigma-Aldrich). Afterwards, MTT staining was conducted to measure viable cells for MBIC assay. For MBEC assay, grown biofilm cells were treated with elasnin/vancomycin and incubated for another 24 h before MTT staining assay. Experiments were performed in triplicate and repeated twice, and MBIC and MBEC were calculated as described above.

Monitoring of biofilm eradication and change in cell susceptibility

Mature biofilms of MRSA ATCC 43300 were first grown in 96-well cell culture plates and treated with various concentrations of elasnin as described above. Plates were then collected after 0, 3, 6, 12, 18, and 24 h of treatment, and $OD570_{nm}$ values were recorded after rinsing and MTT assay. To assess the resistance development risks of elasnin, we conducted a susceptibility change study as previously described (Li et al., 2018). In a typical procedure, MRSA ATCC

43300 cells were grown in the presence of antibiotics (e.g., elasnin, vancomycin and ciprofloxacin) at final concentrations of 0.5×, 1×, 2×, 4×, and 8× of the MICs of the antibiotics. The cells were incubated at 37°C for 24 h, and we recorded the new MIC, which was the lowest concentration of antibiotic without no visible bacterial growth. Then, aliquots from the culture in which the second-highest antibiotic concentration (0.5 × of new MICs) showed visible growth were diluted for 1,000 times in MHB for the subsequent assay. The diluted culture was again grown in the presence of antibiotics at final concentrations of 0.5×, 1×, 2×, 4× and 8× of the previously measured MICs for 24 h, and the new MIC values were recorded. This process was repeated for 45 days. The experiment was performed in triplicate, and the fold change was calculated as the ratio between the measured MICs compared with the MIC on the first day.

Cytotoxicity test

HT22 and Neuro2a (N2a) cells from ATCC were used in the MTT assay to test the cytotoxicity of the compounds. Cells were grown in DMEM with 10% FBS and 1% penicillin–streptomycin at 37°C with 5% CO_2. Then, 5×10^3 cells were seeded in each well of 96-well plates and cultured for 24 h. After cell treatment with different concentrations of the compounds dissolved in DMSO for another 24 h, 20 µl of MTT (5 mg/ml) was added to each well, followed by incubation for 4 h at 37°C before adding 100 µl of DMSO to dissolve formazan. The absorbance was measured using the Multiskan™ FC microplate photometer at 570 nm. IC_{50} data were analysed using the GraphPad Prism software.

Confocal laser scanning microscopy observation with biofilm staining

Biofilms were grown on glass cover slides as described for the MBIC and MBEC assay. Treated biofilms were then rinsed twice with 1 × PBS and stained with FilmTracer™ FM® 1–43 green biofilm cell stain and FilmTracer™ SYPRO® Ruby Biofilm Matrix Stain at room temperature for 30 min in the dark. Leica Sp8 confocal microscope was used to observe the cells and the matrix in the biofilm at 488 nm.

To visualise the changes in biofilm matrix components after elasnin treatment, we prepared the biofilms as described above in the MBEC assays and stained them with TOTO™-1 Iodide and Concanavalin A to observe eDNA and polysaccharides within the biofilm matrix according to the manufacturer's instruction. A Zeiss LSM 710 confocal microscope was used for observation, and ImageJ was used for quantification.

Total RNA extraction and transcriptomic analysis

Overnight cultures of 10^7 CFU/ml MRSA cells were inoculated into TSB complemented with 0.5% glucose (TSBG) at 37°C to obtain mature biofilms. After 24 h of incubation, mature biofilms were rinsed twice with 1 × PBS and treated with 5 µg/ml elasnin or media. Biofilm and released cells were collected at 6 and 12 h, and RNA was immediately stabilised with RNAprotect bacterial Reagent (Qiagen, Hilden, German) according to the manufacturer's protocol. Total RNA was then extracted using the RNeasy PowerBiofilm Kit (Qiagen, Hilden, German) and sequenced using Illumina Novaseq platform with 150 bp short-insert library to generate 2 Gb paired-end reads for each sample. The raw reads were trimmed with Trimmomatic v0.36 (Bolger et al., 2014) to remove adapters and low-quality bases with the setting ILLUMINACLIP: TruSeq3-PE.fa:2:30:10 and then mapped to the S. aureus ATCC 43300 genome by using Bowtie2 v2.3.5 (Langmead and Salzberg, 2012).[1] Salmon v.0.13.1 (Patro et al., 2017) was used to quantify the abundance of successfully mapped transcripts, and differential expression analysis was conducted using Perl scripts align_and_estimate_abundance.pl. and run_DE_analysis.pl. by using the edgeR (Robinson et al., 2010)[73] method in Trinity v2.8.5 (Grabherr et al., 2011; Haas et al., 2013) toolkits. Transcripts with false discovery rates <0.05 and an absolute fold-change value >2 were defined as differentially expressed genes (DEGs).

Sample preparation for proteomics analysis

Preformed biofilms were prepared using the same method as those described for transcriptome analysis, treated with 5 µg/ml elasnin (or media for control) for 2, 6 and 12 h, and then rinsed twice. Biofilm matrix and total proteins were extracted as previously described (Sugimoto et al., 2013) with slight modification. In a typical procedure, biofilms were collected from the bottom of the dish, washed with washing buffer consisting of 10 mM Tris–HCl (pH 8.0) and protease inhibitor cocktail (Sigma-Aldrich), and centrifuged at 5,000 × *g* for 10 min. The pellet was dissolved in a matrix-extraction buffer comprising 10 mM Tris–HCl (pH 8.0), 1 M NaCl and protease-inhibitor cocktail followed by incubation at 25°C for 30 min with gentle rotation. The mixture was centrifuged at 5,000 × *g* for 10 min after incubation, and the supernatant was collected as the biofilm-matrix protein. To extract the total protein, we lysed the pellet with B-PER™ bacterial protein extraction reagent (Thermo Scientific) according to the manufacturer's instructions and sonicated it using a Q125 Sonicator (Qsonica) set at 65% amplitude (five blasts each lasting 15 s with 30 s pauses). The supernatant was collected as the total protein after centrifugation. For all proteomics experiments, three biological replicates were performed for each sample, including the control sample.

1 https://genomes.atcc.org/genomes/79691302ed634fef?_ga=2.259377226.1584810311.1616483300-1172888945.1616483300

The Collected proteins were desalted with Thermo Pierce C18 spin tips and digested with trypsin (Pierce™ Trypsin Protease, MS Grade) before injecting into the Bruker TimsTOF Pro Massspectrometer (Bruker Headquarters Billerica, MA, United States) with captive spray ion source. Approximately 200 ng of the digested protein was injected into the Bruker nanoElute system and separated on a C18 column (ionoptiks Aurora UPLC column, Part no. AUR2-25075C18A-CSI), and the sample was eluted with a 30 min gradient of 2–95% aqueous acetonitrile containing 0.1% formic acid at a flow rate of 0.3 µl/min. The m/z range recorded in the MS full scan was 100–1,700 Da.

Sequence database searching and label-free quantification of proteomics data

The data analysis workflow followed a previously described protocol (Sulaiman et al., 2021). The generated raw data were converted to mgf files by Bruker Compass DataAnalysis and subsequently converted to mzML files by msconvert of the ProteoWizard (Kessner et al., 2008). The mzML files were searched using Comet (version 2016.01 rev.2; Eng et al., 2013) with a custom database. In a typical procedure, the genome sequence of MRSA ATCC 43300 was converted into a protein database by using the GeneMark (Lukashin and Borodovsky, 1998) gene prediction tool. Proteins were then annotated using BLASTp from NCBI by using MRSA NCTC 8325 as the protein database. The sequences of common contaminants such as trypsin and human keratins and the decoy sequences generated by shuffling amino acid sequences between tryptic cleavage sites were added to the database. The decoy sequences in the database were used for the false FDR estimation of identified peptides. The search parameters criteria were set as follows: 15 ppm peptide mass tolerance, monoisotopic mass type, fully digested enzyme termini, 0.05 amu fragment bin tolerance, 0 amu fragment bin offset, carbamidomethylated cysteine and oxidated methionine as the fixed and variable modifications. The Search results from Comet were processed using PeptideProphet (Keller et al., 2002), iProphet and ProteinProphet of the Proteomics Pipeline (Deutsch et al., 2010) in the decoy-assisted non-parametric mode. Every mzML run was analysed independently. Protein identifications were filtered at FDR of 0.01 as predicted by ProteinProphet.

Label-free quantification of proteomics data was accomplished by spectral counting by using the parameters in our previous study (Sulaiman and Lam, 2020). Briefly, proteins that were identified in at least two out of three biological replicates were used for label-free quantification by spectral counting. Proteins were quantified using the normalised spectral-abundance factor (NSAF; Paoletti et al., 2006) where the number of peptide-spectrum matches (PSMs) for each protein divided by the length of the corresponding protein was normalized to the total number of PSMs divided by the lengths of protein for all identified proteins. The DEPs were filtered using the following cutoff: average spectral counts of at least three, p value for Student's t-test on the NSAF values of less than 0.05 and fold changes of ±1.5-fold. Moreover, unique proteins that were only detected in the treatment or control samples were retained for analysis, because they are likely to be upregulated or downregulated after elasnin treatment. To minimize false positives, we only focused on uniquely detected proteins with spectral counts greater than 4. Here, we assume that these unique proteins with sufficiently high spectral counts were also induced/upregulated (if detected only in treatment samples and not in control samples) or repressed/downregulated (if detected only in control samples and not in treatment samples).

Scanning electron microscope analysis of biofilms treated with elasnin

Samples for SEM analysis were prepared as previously described with slight modification (Kong et al., 2018; Boudjemaa et al., 2019). Preformed biofilms on a copper strip surface were treated with elasnin (5 µg/ml) or TSBG for 6 h followed by overnight fixation with 4% (v/v) glutaraldehyde under 4°C. Thereafter, biofilms were dehydrated in a graded ethanol series (30, 50, 70 and 90% v/v with distilled water and thrice with 100% ethanol for 10 min each step), followed by air drying. Samples were then gold-coated using a gold coater Scancoat Six (Edwards, Irvine, CA, United States) and observed using SEM (JSM-6390, JEOL, Akishima, Tokyo, Japan).

Bioinformatics analysis

PCA was performed to determine the correlation between individuals and the expression level of transcripts on R by using DESeq2 (Love et al., 2014). Functional annotation and enrichment analysis of DEGs/DEPs was performed using The Database for Annotation, Visualization and Integrated Discovery v6.8 (Huang et al., 2009; Sherman and Lempicki, 2009; ease = 0.01). Cluster analysis was constructed to reveal the similarity of gene expression between the control and elasnin-treated groups based on Bray–Curtis distance matrix by using PAST (version 2.0; Hammer et al., 2001). To construct the interaction network between the DEGs/DEPs, we used STRING v11 (Szklarczyk et al., 2019) to predict the protein–protein interactions.

Gene deletion, transcription inhibition and overexpression of DEGs

The expression of upregulated DEGs was inhibited, and *icaADBC* was deleted using CRISPR/Cas9 system pCasiSA and pCasSA as described previously (Chen et al., 2017). The genes downregulated by elasnin were overexpressed using the tetracycline-inducible expression vector pRMC2 in the relevant *S. aureus* strains. All plasmids, bacterial strains and primers used

in this study are listed in Supplementary Tables S2, S3. pRMC2 was obtained from Tim Foster (Corrigan and Foster, 2009; Addgene plasmid #68940; RRID: Addgene 68,940).[2] pCasiSA was constructed by mutating pCasSA plasmid, and pCasSA was obtained from Quanjiang Ji (Addgene plasmid #98211; RRID: Addgene_98,211).[3]

Constructed plasmid was transported into the wild-type MRSA ATCC43300 by electroporation. Competent cells were prepared as previously described (Chen et al., 2017) and stored at −80°C. For electroporation, 50 µl of competent cells was thawed on ice for 10 min, mixed with 1–2 µg of plasmid and transferred into a 1 mm electroporation cuvette (Bio-Rad, Hercules, CA, United States). Cells were then pulsed at 2.5 kV, 100 Ω and 25 µF and incubated in 1 ml of TSB at 30°C for 1 h, followed by plating on a TSB agar plate containing 7.5 µg/ml chloramphenicol. The plates containing pRMC2 plasmid were incubated at 37°C, whereas plates with pCasiSA, pCasSA and their derivatives were incubated at 30°C. Mutant strains were then used in the relevant MBIC and MBEC assays as described above. All strains containing pCasiSA, pCasSA and their derivatives were incubated at 30°C throughout the entire assay. The PCR confirmation of ica-deleted mutants is shown in Supplementary Figure S2.

Biochemical-composition study of biofilms

To determine the biochemical composition of the biofilms, we conducted MBIC and MBEC assays as described above with the addition of DNase I (100 U/ml) and proteinase K (100 µg/ml) for eDNA and protein degradation, respectively. We used two *S. aureus* strains, namely, MRSA ATCC 43300 and MSSA ATCC 25923. The ica-deleted mutants were constructed with MRSA and MSSA, and their biofilm formation was tested as described in the MBIC assay without the addition of antibiotics.

Quantitative real-time PCR

A 3 ml overnight culture of mutant MRSA strains, in which 0.2 µg/ml anhydrotetracycline was added in overexpressed strains, was harvested and stabilised, and the total RNA was extracted as described above. cDNA was then synthesised with RevertAid H Minus First-Strand cDNA Synthesis Kit after removing genomic DNA by using DNase I (Thermo Fisher Scientific Inc., Waltham, MA, United States) followed by quantification on a Roche Diagnostics GmbH LightCycler 480 Instrument II Realtime PCR System using the SYBR Green RT-PCR Reagents Kit (Applied Biosystems). In this process, polymerase activation was carried out at 95°C for 10 min, followed by annealing and extension at 55°C for 1 min for 40 cycles. The specificity of primer pairs for PCR amplification was checked using the melting-curve method. Two biological and three technical replicates were employed for each sample, and the relative gene expression level was calculated based on the 2ΔΔCt using *gyrB* as the internal-reference gene.

Statistical analyses

Statistical analyses for all data were performed using GraphPad Prism 8.0.2 software and Microsoft Excel 2012 Edition (Microsoft, Redmond, WA, United States).

Results

Bioassay-guided isolation of compounds that target biofilm

Secondary metabolites produced by 12 actinobacterial strains under different culture conditions were assessed for bioactivities against Gram-positive bacteria (MRSA) and Gram-negative bacteria (*E. coli*, E. coli). This was followed by bioassay-guided fractionation which led to the isolation of three antimicrobial compounds (e.g., xanthone, hitachimycin, and resistomycin) and the antibiofilm compound - elasnin, which was isolated from Streptomyces mobaraensis DSM 40847 and showed potent activity against MRSA (Supplementary Table S1). To assess elasnin's activity, we compared purified elasnin with vancomycin in terms of MIC, MBC, MBIC, and MBEC against MRSA. The MIC values reflect the antibiotics' antimicrobial activities against planktonic cells. Results show that MRSA was susceptible to vancomycin (MIC of 0.63–1.25 µg/ml) and elasnin (MIC of 1.25–2.5 µg/ml, Figure 1A). The MBC values measure the compounds' killing effect on cells. Vancomycin exhibited strong bactericidal activities in a concentration-dependent manner and had MBC values ranging from 10 to 50 µg/ml, whereas elasnin showed bacteriostatic activity, had a higher MBC value than vancomycin, and did not cause significant changes in cell density in the concentration of more than 100 µg/ml (Figures 1A,B). The MBIC values represent the ability of the compounds to inhibit biofilm formation, whereas the MBEC values indicate the ability to eradicate pre-formed mature biofilms. Elasnin and vancomycin showed strong biofilm-inhibiting activities against MRSA with $MBIC_{90}$ values of 1.25–2.5 µg/ml (Figure 1C). The pre-formed biofilms showed strong resistance to vancomycin with $MBEC_{50}$ of 10–20 µg/ml. However, they can still be eradicated with elasnin at a much lower $MBEC_{50}$ between 0.63–1.25 µg/ml (Figure 1D). When being tested in a LCWB model that mimics chronic wound biofilms, both elasnin and vancomycin showed an increase in the effective concentrations with $MBIC_{90}$ of 250–500 and 20–100 µg/ml, respectively, and with the same $MBEC_{50}$ of 100–500 µg/ml (Supplementary Figure S3). Overall, elasnin exhibited higher effectiveness in biofilm inhibition and especially in biofilm

2 http://n2t.net/addgene:68940
3 http://n2t.net/addgene:98211

A

Bioactivities	Van		Elasnin	
	μg/mL	μM	μg/mL	μM
MIC	0.63-1.25	0.43 – 0.86	1.25-2.50	3.18 – 6.37
MBC	10-50	6.90 – 34.50	>100	> 254.71
$MBIC_{90}$	1.25-2.5	0.86 – 1.72	1.25-2.5	3.18 – 6.37
$MBEC_{50}$	10-20	6.9 – 13.80	0.63-1.25	1.59 – 3.18

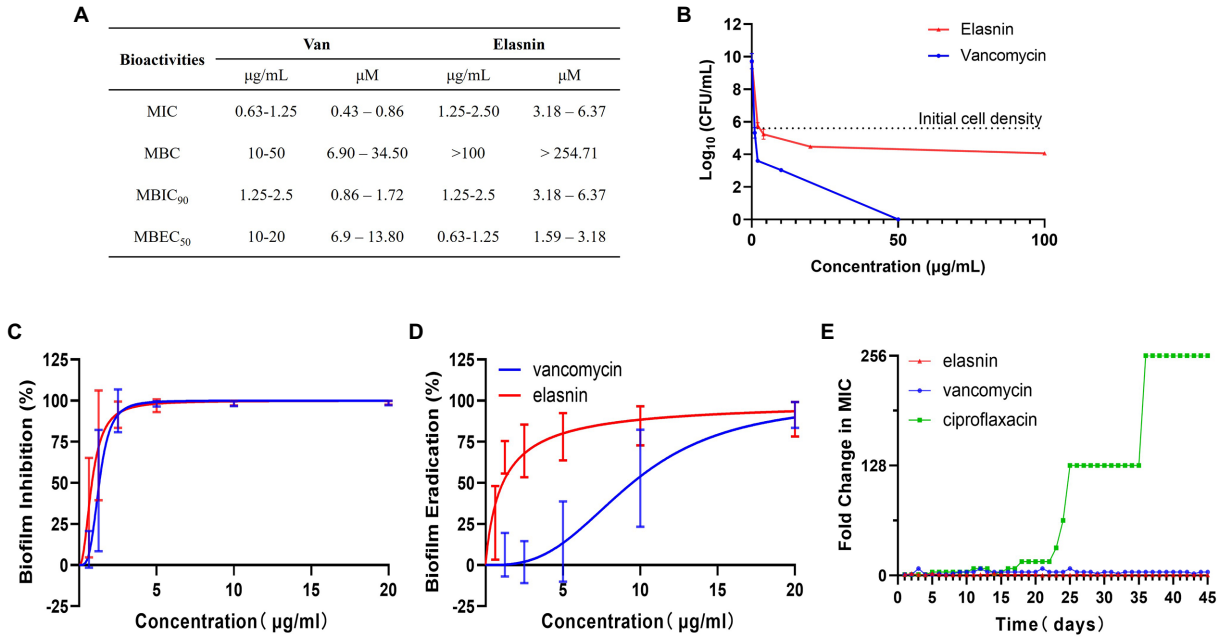

FIGURE 1
Bioactivities and resistance-development study of elasnin against MRSA. **(A)** Summary of MICs, MBCs, MBICs and MBECs of MRSA towards vancomycin and elasnin. **(B)** Cell viability of MRSA after 24h of treatment with various concentrations of elasnin and vancomycin (n=3). **(C)** Minimum concentration needed to inhibit 90% of biofilm formation (n=12, average±standard deviation). **(D)** Minimum concentration needed to eradicate 50% of pre-formed biofilms (n=12, average±standard deviation). **(E)** Fold change in MICs towards elasnin, vancomycin and ciprofloxacin after 45-days of exposure under sub-inhibitory concentrations (0.5×MIC) of the respective antimicrobials (n=3).

eradication, relative to its activities against planktonic cells. Cells can still proliferate after being exposed to elasnin, suggesting that elasnin could be used as a biofilm-targeting compound that interferes with biofilm formation and maintenance rather than killing the planktonic cells.

In addition, in the test for the potential development of resistance, the MIC of MRSA treated with elasnin did not change over a period of 45-days (Figure 1E; Supplementary Table S4), suggesting that the cell susceptibility to elasnin treatment did not change. Elasnin also did not show any cytotoxicity against Neuro2 cell lines at a concentration of 10 μg/ml (Supplementary Figure S4A) or HT22 cells at concentrations of up to 25 μg/ml, which is 10 times its $MBIC_{90}$ and $MBEC_{50}$ (Supplementary Figure S4A). Elasnin's effect on cell viability was only observed at concentrations higher than 25 μg/ml (Supplementary Figure S4B).

Elasnin destroyed the biofilm matrix

CLSM was used to observe the effect of elasnin on biofilm structures. Biofilm-inhibition assay showed that untreated biofilms had distinct shapes with a high density of organised cells and matrix (Figure 2A), whereas the elasnin-treated biofilms exhibited a significant decrease in cell density and matrix and both biofilms were randomly distributed (Figure 2B). Biofilm-eradication assay revealed that the pre-formed biofilms were eradicated by elasnin because most of the biofilm cells were released into the medium (Figure 2D). CLSM images demonstrated that the distribution patterns of the cells changed after elasnin treatment, in which the untreated biofilm cells were distributed as clumps with rough edges (Figure 2C), whereas elasnin-treated biofilm cells were distributed as narrow strips with smooth edges (Figure 2D). Similarly, the high density of organised biofilm matrix became sparse and scattered after elasnin treatment. Quantitative analysis showed that the biofilm cells and matrix were significantly reduced after treatment. In comparison with untreated biofilms, elasnin-treated ones exhibited ~80 and 35% decrease in cell density and matrix in the biofilm-inhibition assay (Figure 2E). In the biofilm-eradication assay, cells and matrix densities decreased by over 50 and 70% (Figure 2F).

Gene expression of virulence factors and products in the extracellular region were downregulated following elasnin treatment

Among the 2,791 detected gene transcripts, 1,010 were differentially expressed (≥2.0-fold change in gene expression) on MRSA biofilm cells treated with elasnin for 6 h compared with untreated biofilm cells (control). The percentage of eradicated cells after 6 h of treatment is shown in Supplementary Figure S1B. The number of differentially expressed genes (DEGs) decreased to 668 when the treatment time was extended to 12 h. For cells released

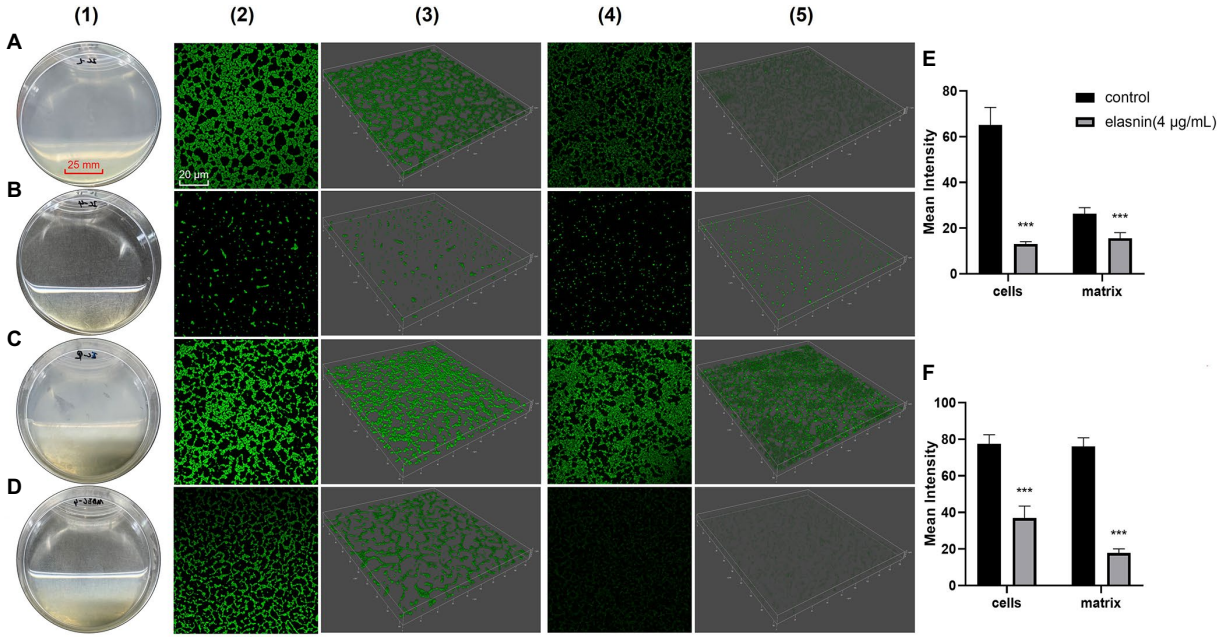

FIGURE 2
Comparison between the effect of elasnin on MRSA biofilm cells and matrix. **(A)** Image of the biofilms after incubation for 24 h (control). **(B)** Image of the biofilms after incubation for 24h with 4μg/ml elasnin. **(C)** Image of the pre-formed biofilms after another incubation for 18 h (control). **(D)** Image of the pre-formed biofilms after another incubation for 18 h with 4 μg/ml elasnin. **(E)** Quantitative analysis of confocal images acquired in biofilm-inhibition assay and **(F)** biofilm-eradication assay. Differences between different groups were calculated by Student's *t*-test and are indicated by asterisks as follows: ***for $p<0.001$. Series 1 show the images of biofilms under direct observation. Series 2 and 3 are the two-and three-dimensional confocal images of biofilm cells stained with FilmTracer™ FM® 1–43 green biofilm cell stain, respectively. Series 4 and 5 are the 2D and 3D images of biofilm matrix stained by FilmTracer™ SYPRO® Ruby Biofilm Matrix Stain, respectively. Confocal images were acquired under the same conditions, and quantitative analysis was conducted using Leica Application Suite X based on the relative fluorescence of 3D confocal images.

from the biofilms, 720 and 609 genes were differentially expressed between the treatment and control groups at 6 and 12 h, respectively (Figure 3A). Principal component analysis showed a clear separation between the clusters of elasnin-treated and untreated samples along the PC1 axis, indicating that elasnin treatment mainly accounts for the differences in gene expression (Figure 3B).

DEGs were then processed using gene ontology (GO) enrichment analysis in terms of their molecular function, cellular component, and biological process (Figure 3C). In the samples treated for 6 h, amongst the enriched GO terms of downregulated genes, the cellular component of the extracellular region was observed only for biofilm samples, whereas the biological process of pathogenesis was shown only in released cells samples. Additionally, the GO terms of translation, transmembrane transport and integral component of the membrane were downregulated in biofilm and released cells. In the 12 h treated samples, downregulated genes were enriched in the extracellular region and pathogenesis in the biofilm and released cells, whereas membrane components were observed only in the released cells.

Figure 4A shows the gene expression in selected pathways of DEGs that were analysed using the Kyoto Encyclopaedia of Genes and Genomes (KEGG) pathway assessment. Signal transduction-related genes (two-component system and HIF-1 signalling pathway) were overexpressed in the elasnin treatment group, whereas many genes related to membrane transport (ABC transporters, phosphotransferase system, and bacterial secretion system), quorum sensing, and especially Staphylococcus infection and β-lactam resistance were downregulated. The results of hierarchical clustering of gene expression data (Figure 4B) revealed that biofilm cells exhibited the most unique gene-expression pattern after 6 h of elasnin treatment. Subsequently, the biofilm samples treated for 6 h were used to build the gene interaction network (Figure 4C) which shows that elasnin-treated biofilm cells exhibited low expression levels of genes involved in pathogenesis, including global regulon (*sarA* and RNAIII), EPS production (*icaA, icaB, and icaC*), murein hydrolases and autolysins (*atl, lytR, and cidA*), serine protease (*sspA, sspB, sspC, sspP, and splB*), toxin (*hld, hlgC, and hly*), and adhesins (*fnbA, clfB, sdrD, and emp*). Interestingly, genes related to cell wall organisation and cell division, that is, *murB, murC, murD, mraY, diviB, and ftsZ*, were upregulated after 6 h of elasnin treatment.

Effects of elasnin on the cell cycle and EPS production of MRSA and cell resistance to penicillin G

To further investigate the mode of action of elasnin in the growth inhibition and biofilm eradication of MRSA, we used

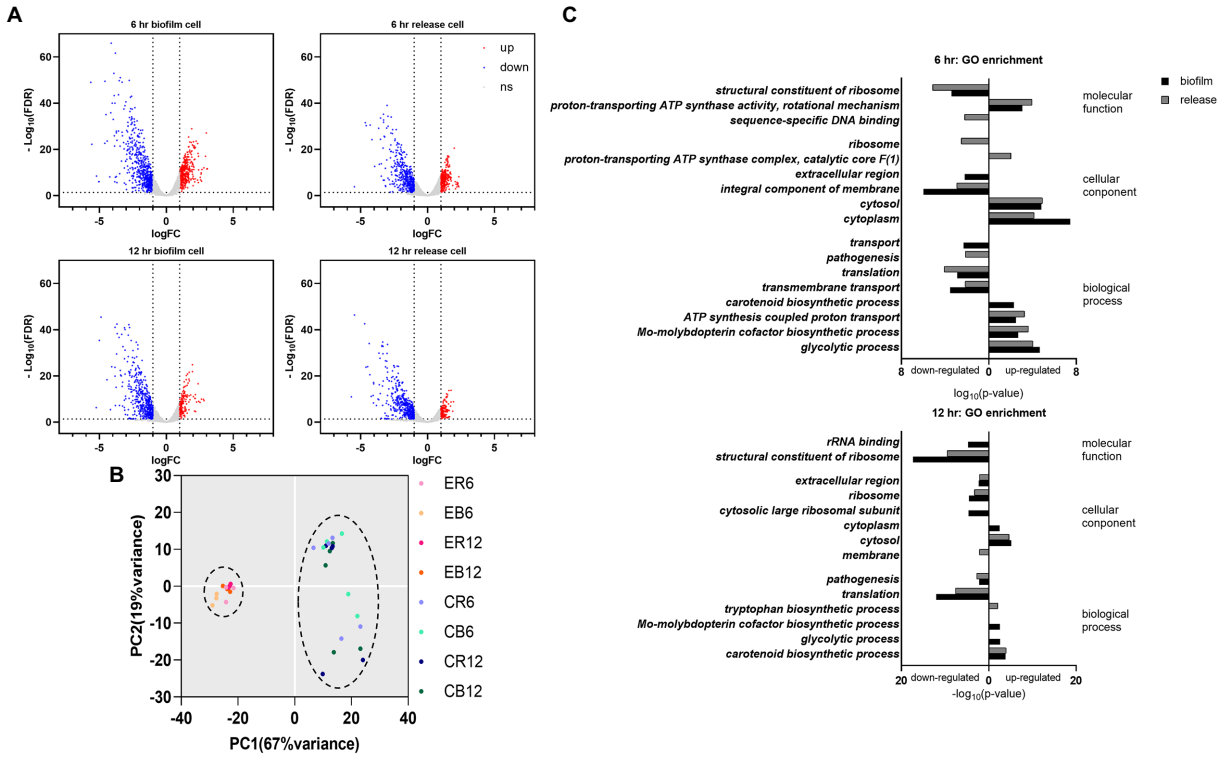

FIGURE 3
Changes in the gene expression of MRSA cells after elasnin treatment. **(A)** Volcano plot of RNA-seq profiles of MRSA cells showing the altered gene expression pattern of collected samples (up: upregulated, corresponding to the red dots; down: downregulated, corresponding to the blue dots; ns: not significantly changed, corresponding to the gray dots). **(B)** Principal component analysis of RNA-seq samples (treated with elasnin and untreated), in which elasnin treatment mainly caused the altered gene expression. ER: cells released from elasnin-treated biofilms; CR: cells naturally released from the biofilms; EB: elasnin-treated biofilms cells; CB: biofilm cells. The numbers following the letters indicate the duration of elasnin treatment (in hour). **(C)** Gene ontology enrichment analysis of differentially expressed genes (in biofilm and released cells, marked by black and gray bars, respectively), highlighting the alterations in genes for pathogenesis and those located in the extracellular region and the integral component of the membrane.

label-free quantitative proteomics analysis to study the protein expression dynamics of MRSA biofilm cells during biofilm eradication after elasnin treatment (Figure 5A). The analysis revealed that 105 proteins were differentially expressed in the MRSA biofilm cells treated with elasnin for 2 h compared with untreated samples. The proteins involved in DNA repair and replication, cell division and cell wall organisation, pathogenesis (e.g., virulence regulator *SarX* and SaeR), and secreted virulence factors (EsxA) were down-regulated and repressed. Alternately, amidohydrolase (AID39263.1) and secreted lipase, and dipeptidyl-peptidase (AID41306.1) were upregulated. After 6 h of treatment, the number of DEPs reached 250, which was the highest among all time points (2 and 12 h). At 6 h, elasnin downregulated or repressed numerous proteins involved in DNA repair and replication, cell division, cell wall organisation, and the production of virulence factors (e.g., adhesin SdrD, toxin HlgB and HlgC and autolysin LytM). On the other hand, the expression levels of secreted peptidase (Staphylococcal superantigen-like 1 [Ssl1]) and amidase (AID41356.1) were upregulated. When the treatment duration was prolonged to 12 h, the number of DEPs decreased to 154, and most DEPs were primarily related to translation and pathogenesis, with a few involved in cell division and cell wall organisation. Except for LytM and lipase, no other hydrolases, lyases, and proteins involved in DNA replication and repair were differentially expressed.

Changes in the expression levels of several hydrolases and proteins related to cell division and cell-wall organisation in the control samples showed the abundance of hydrolases encoded by IsaA, LytM, and Atl reached the highest at 6 h, and the abundance of Ssl1 should be reduced during this period (Figure 5B). However, elasnin treatment reduced the abundance of IsaA and LytM, repressed the expression of autolysin (Atl), and stopped the changes in Ssl1. In the control samples, the abundance of SepF exhibited a continued increase from 2 h to 12 h, and the abundance of proteins involved in cell wall biogenesis (Mur family proteins) remained stable. However, elasnin-treated biofilm cells exhibited decreased abundance in Mur family proteins after 6 h of treatment, and SepF was repressed throughout the entire process.

The effect of elasnin treatment on biofilm matrix composition was shown in Figure 5C and Supplementary Figure S5. The number of polysaccharides and eDNA in the biofilm matrix was remarkably reduced after elasnin treatment. Cells released from

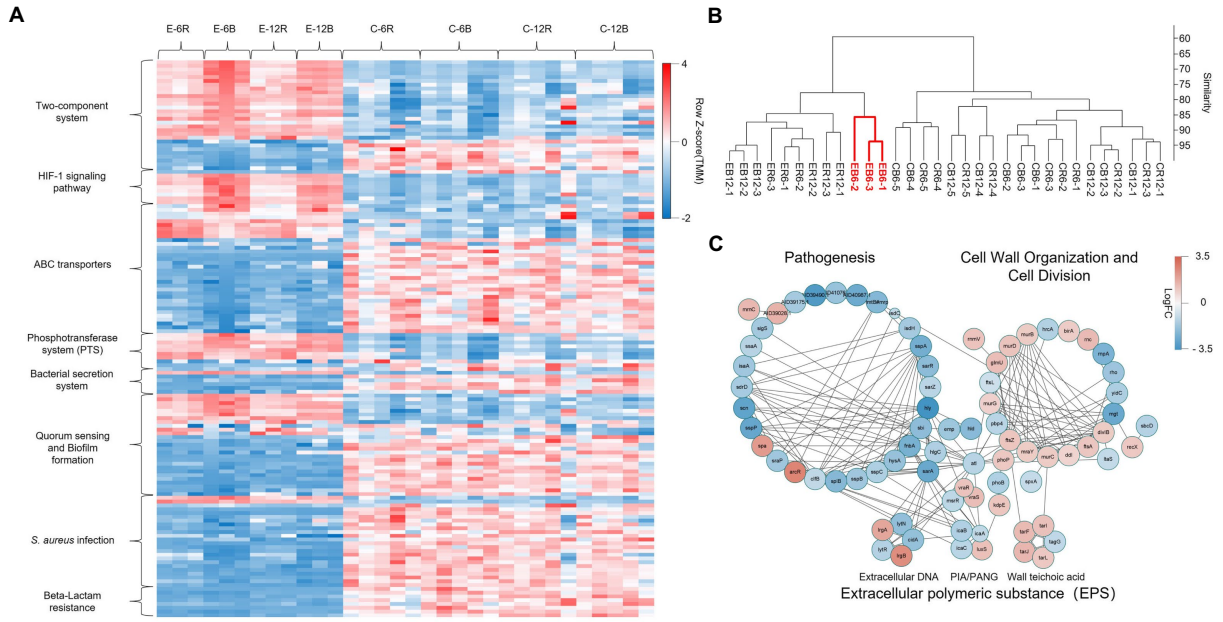

FIGURE 4
Gene expression of the MRSA biofilm cells treated for 6 h having the most distinct one among all groups. **(A)** Heatmap of the expression level of DEGs for selected KEGG pathways, revealing the increased signal transduction, reduced membrane transport, quorum sensing, *Staphylococcus* infection and β-lactam resistance in elasnin-treated samples. **(B)** Hierarchical clustering of the RNA-seq data by using the normalised reads count, revealing that biofilm cells exhibited the most unique gene expression pattern after 6 h of elasnin treatment. **(C)** Networks of DEGs of biofilm cells after 6 h of elasnin treatment and their functional associations. The nodes represent the differentially expressed genes between the control and treatment groups after 6 h of treatment, and the edges indicate their associations as predicted by STRING. Red colour indicates upregulated gene expression, whereas blue colour indicates downregulated gene expression following elasnin treatment. The size is inversely proportional to the *p* value, as described in the Material and Method section (a larger node corresponds to a smaller *p* value).

the biofilms were collected for MIC and MBC assay by using a β-lactam antibiotic, penicillin G. Consistent with the transcriptomic analysis results, the released cells treated by elasnin (ER, Figure 5D) exhibited lower resistance to penicillin G in which the MIC (0.8–4 μg/ml) and MBC (4–20 μg/ml) decreased by approximately five times compared to the MIC (4–20 μg/ml) and MBC (>100 μg/ml) of naturally released cells (CR; Figure 5D).

Effects of elasnin on the cell wall of MRSA cells, and role of *sarZ* on elasnin-induced biofilm eradication

Transcriptomics and proteomics analysis revealed that combined with the increased sensitivity of elasnin-treated cells towards penicillin G, elasnin may also interfere with the proper cell division and cell wall organisation process during the exponential phase when numerous cells are undergoing cell division (Figure 6). To validate our hypothesis that elasnin causes cell wall defects in biofilm cells, the morphological changes in MRSA cells after 6 h of exposure were examined under SEM (Figure 7A). Consistent with our hypothesis, untreated biofilms showed a dense layer of normal grape-like cell clusters, whereas elasnin-treated biofilms were scattered, in which a majority of cells exhibited a defective appearance with clear collapses around the centre of the cell. Interestingly, defective cells were observed in the untreated biofilms, but they accounted only for less than 1% (2 of ~200) of the total cells, whereas the proportion of defective cells was more than 70% (25 of 34) in elasnin-treated biofilm.

Considering the complex regulatory network of virulence factors, we determined the main determinant by comparing the biofilm-eradication activity of transcription-inhibited mutants and overexpressed strains (Figure 7B). The regulators (e.g., *rot and sarX*) induced following elasnin treatment were transcriptionally inhibited by CRISPR/Cas9 transcription inhibition system pCasiSA, whereas the downregulated genes (e.g., *sarA, sarZ, sarR*, and RNAIII) were overexpressed with the expression vector pRMC2 (see RT-qPCR results in Supplementary Figure S6). In comparison with the control strains (strains with empty plasmids), the mutants of *sarA, sarR*, and RNAIII showed an increased MBECs of 1.25–2.5 μg/ml, and a decreased eradication rates varied from 50.1 to 77.8%. $MBEC_{50}$ did not increase in mutants of *rot* and *sarX*, but the eradication efficiency (5 μg/ml) of elasnin was reduced to 69.4 and 59.6%, respectively. Among all the mutants, the *sarZ*-overexpressed mutant showed the highest resistance to elasnin with an MBEC of above 10 μg/ml and an eradication rate of almost 0%, and the ability of elasnin to inhibit the biofilm formation of the *sarZ*-overexpressed mutant was largely reduced at an $MBIC_{90}$ above 10 μg/ml (Supplementary Table S5). Simultaneously, the

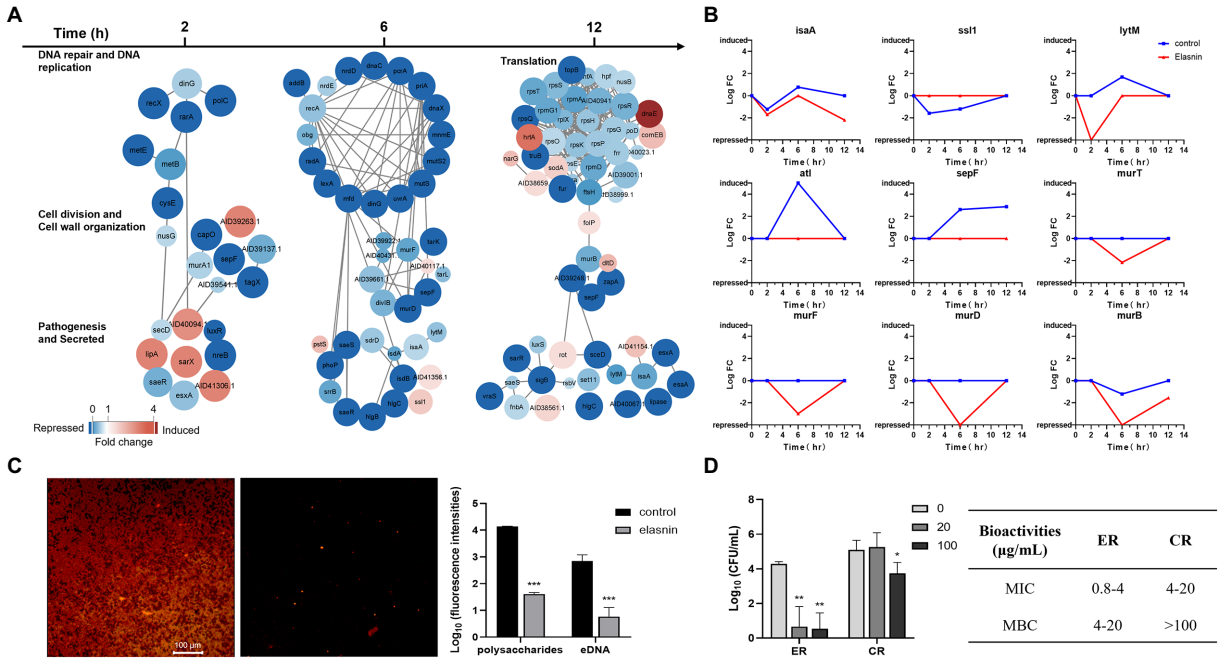

FIGURE 5
Elasnin interfered with cell cycle and EPS production and reduced the antibiotic resistance of MRSA. **(A)** Differentially expressed proteins in selected functional subsets after 2, 6 and 12h of elasnin treatment. **(B)** Changes in the expression level of selected DEPs during the biofilm eradication with elasnin. **(C)** Effect of elasnin on the production of polysaccharides (red, stained with Concanavalin A) and eDNA (green, stained with TOTO-1) of MRSA biofilm, as visualised by confocal microscopy. Fluorescence intensities were calculated based on acquired 3D confocal images (n=3). Here, the polysaccharides and the eDNA were stained simultaneously. A separate staining image of polysaccharides alone and eDNA alone is shown in Supplementary Figure S4D. **(D)** Antibiotic susceptibility of MRSA cells against Penicillin G after being released from the biofilms (n=3). ER are the cells released from the biofilms after elasnin treatment, and CR are the cells released naturally (without any treatment). Differences between different groups were calculated by Student's t-test and are indicated by asterisks as follows: *for p<0.05, **for p<0.01 and ***for p<0.001.

sarZ-deleted MRSA mutant NE567 exhibited increased sensitivity to elasnin treatment with reduced values in $MBIC_{90}$ and $MBEC_{50}$, respectively, (Supplementary Figure S7). All other mutants showed resistance to elasnin in the biofilm-formation inhibition assay with $MBIC_{90}$ of 5–10 μg/ml for the mutants of *sarA, rot*, and *sarX*, and $MBIC_{90}$ higher than 10 μg/ml for the mutants of *sarR* and RNAIII. Interestingly, the overexpressed mutants of *sarR*, RNAIII, and especially *sarZ* showed a remarkable reduction in terms of biofilm formation compared to the control strains and the wild-type strain. To conclude, the effect of elasnin on virulence regulons affected biofilm formation, and the repression of *sarZ* was responsible for the biofilm eradication (Figure 7C).

Discussion

The selective pressure exerted by antimicrobials enriches the naturally existing antibiotic-resistant bacteria in the environment, thereby accelerating the development of resistance (Martinez, 2009; Holmes et al., 2016). Considering the protection provided by the biofilm matrix and the intense gene transfer and differentiation within the biofilm, compounds that simply kill cells but leave the biofilm matrix intact for microbial utilisation are likely to boost resistance development. With the inevitable increase in antibiotic resistance and the considerable challenges in biofilm-associated antimicrobial therapy, effective antibiofilm agents, particularly those that can effectively eradicate established biofilms, are urgently needed. In the present work, we conducted bioassay-guided compound isolation to identify the biofilm-targeting compounds that can effectively inhibit and eradicate the biofilms without killing the cells. Elasnin was identified as a potent biofilm-eradicating drug candidate against MRSA. It eradicates biofilms by destroying the biofilm matrix and does not remarkably affect the viability of the released cells. Therefore, theoretically, the risk of cells developing reduced susceptibility towards elasnin is low, as confirmed by the non-observable increase in MIC upon subjecting MRSA cells to continuous serial passaging in the presence of sub-inhibitory concentrations of elasnin. The cells released following elasnin treatment were also more susceptible to the β-lactam antibiotic penicillin G. Elasnin further exhibited low cytotoxicity towards different cell lines, which is consistent with a previous study (Ohno et al., 1978). Elasnin was effective in a chronic wound biofilm model with the presence of blood and plasma, indicating the therapeutic potential of elasnin as a safe and potent biofilm-eradicating agent against MRSA biofilm.

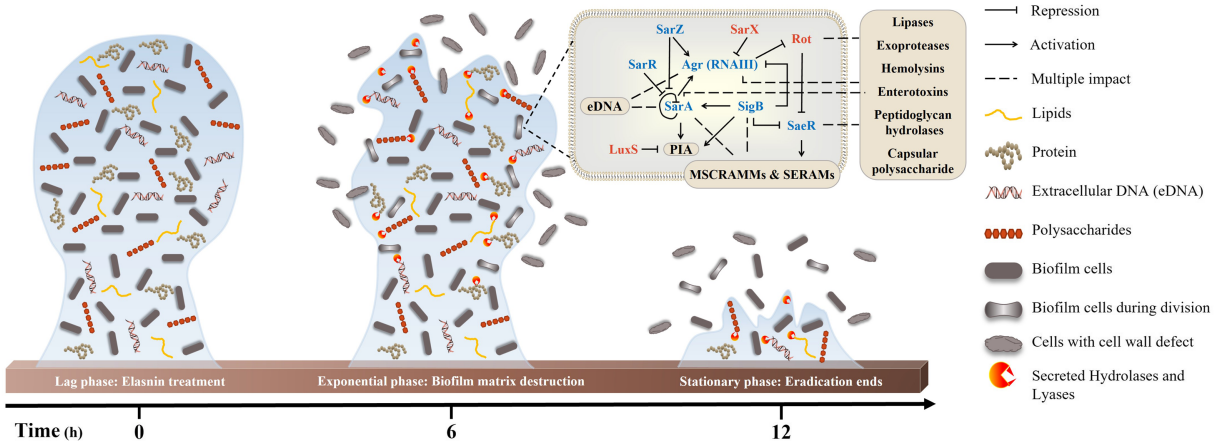

MSCRAMMs: Microbial surface components recognizing adhesive matrix molecules, including clumping factors A and B (ClfA, ClfB), the serine/aspartate-rich protein (Sdr) and fibronectin-binding protein A and B (FnBPA, FnBPB).

SERAMs: Secretable expanded repertoire adhesive molecules, including extracellular adherence protein Eap, extracellular matrix and plasma binding protein Emp (Extracellular matrix binding protein homologues Ebh is also included in here).

FIGURE 6
Proposed model of MRSA-biofilm eradication by elasnin. The peak of eradication occurred in the exponential phase, when a large amount of biofilm cells was undergoing cell division. Elasnin inhibited the expression of virulence regulons that controls virulence factors, such as adhesive proteins, cell-wall hydrolases and EPS, thereby interfering with cell division and generating cell-wall-defective cells. Moreover, the increased production of hydrolases and lyases degraded the old EPSs and subsequently released the biofilm cells from the biofilms.

Therefore, elasnin harbors great potential to be developed as a disinfectant for biofilm removal and to be used for treating chronic wounds.

The mechanism in which elasnin eradicates the established MRSA biofilm was then elucidated through a series of analyses (Figure 6). As a part of pathogenesis, the production of adhesive proteins and PIA or poly-β(1–6)-N-acetylglucosamine encoded by ica operon was essential for the biofilm formation of MRSA ATCC 43300 (Supplementary Figure S8B). Moreover, the maintenance of the established biofilms required the participation of adhesive proteins and eDNA (Supplementary Figures S8A,C) and the cell cycle and cell wall hydrolases (LytM and autolysin) that are essential for cell separation, which are all regulated by the virulence regulons. Therefore, many proteases and cell wall hydrolases are expressed during the exponential phase when biofilms undergo proliferation and maturation. However, since elasnin represses the virulence regulons, the production of some cell wall hydrolases, adhesins and EPSs was inhibited during treatment. Consequently, cells could not properly divide, and thus, very limited EPSs were synthesised. Meanwhile, some lipase and proteases were largely secreted, causing the degradation of the existing EPSs and the destruction of the biofilm matrix. The biofilm cells were released back to the media, and most of them had defective cell wall structures caused by the inhibition of the cell division process and the down-regulation of the expression of cell wall-related proteins. Consequently, cells released from the elasnin-treated biofilms showed increased susceptibility to the β-lactam antibiotic penicillin G, highlighting the possible application of elasnin in combinatorial treatment for rescuing old drugs that had become ineffective due to resistance.

Staphylococcus aureu has a very complex regulatory network of biofilm formation and virulence expression, in which many important regulators are affected by elasnin. Accordingly, multiple mutants were generated to reveal the key determinants by comparing elasnin's activities against the mutants. All mutants showed increased ability in resisting elasnin in the biofilm inhibition assay. The overexpression of *sarA* can increase the production of EPSs and adhesins assisting with biofilm maturation, whereas the overexpression of *sarR* and RNAIII and the repression of *sarX* can increase the production of proteases and cell wall-related proteins for cell division. *sarZ* activates the expression of RNAIII, represses *sarA*, and regulates the production of proteases independently (Ballal et al., 2009; Tamber and Cheung, 2009). The overexpression of *sarZ* restored the cell's ability to divide to some extent (Supplementary Table S5; Figure S7E) possibly by repressing *sarA* and increasing the production of proteases and cell wall-related proteins through or independent from *sarA* and RNAIII (Figure 7C). Consequently, these mutants exhibited increased resistance to the biofilm inhibition caused by elasnin. Some of these mutants (e.g., RNAIII, *sarR*, and *sarZ* overexpressed mutant) showed reduced ability to form biofilms, perhaps due to the increased production of proteases and hydrolases (Figure 7C; Supplementary Table S5).

Elasnin lost its efficacy only in eradicating the established biofilm of mutants overexpressed with *sarZ* and exhibited increased activity against the *sarZ*-deleted mutant (Supplementary Figures S7A,B), suggesting the crucial role of *sarZ* during the elasnin-induced biofilm eradication. Based on our results, deletion of *sarZ* does not influence elasnin's efficiency in cell growth inhibition (Supplementary Figures S7D,E), suggesting

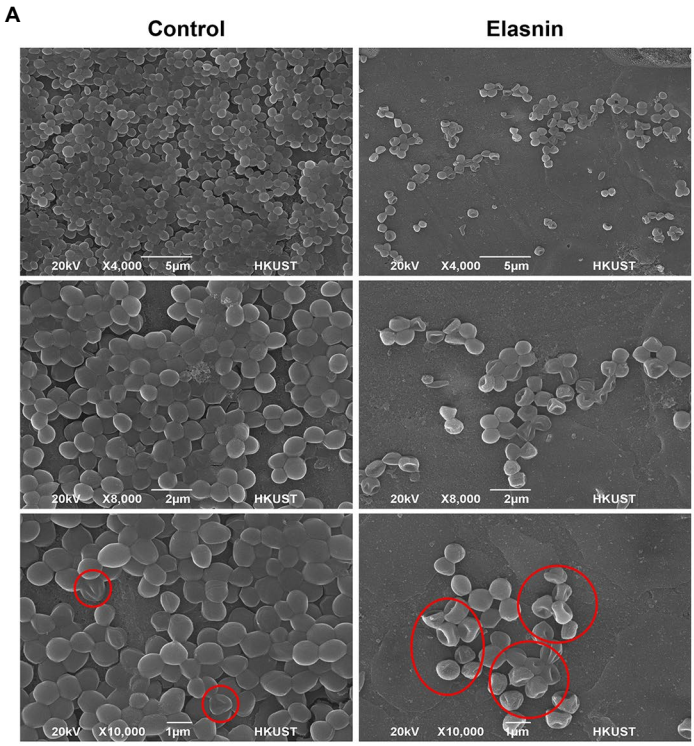

B

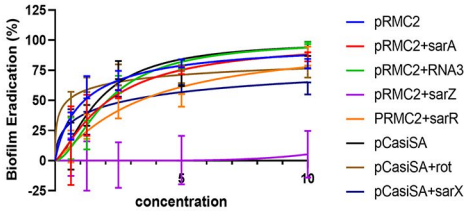

	$MBEC_{50}$	Biofilm Eradication (5 μg/mL, %)
Wild Type	0.625-1.25	81.41±7.45
pRMC2	0.625-1.25	80.66±3.22
pRMC2+RNAIII	1.25-2.50	77.75±1.60
pRMC2+*sarA*	1.25-2.50	75.16±3.20
pRMC2+*sarR*	1.25-2.50	50.08±4.95
pRMC2+*sarZ*	>10	0.38±19.09
pCasiSA	1.25-2.50	82.13±5.34
pCasiSA+*rot*	0.625-1.25	69.40±4.74
pCasiSA+*sarX*	1.25-2.50	59.61±3.94

C

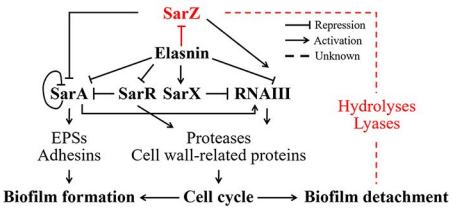

FIGURE 7
Validation of the proposed mode of action of elasnin. **(A)** Scanning electron microscopy observation of untreated and elasnin-treated (5 μg/ml) biofilm cells, illustrating the large amount of defective cells within elasnin-treated biofilms. Regions marked with red outlines indicate cells with cell wall defect. **(B)** MBEC and biofilm-eradication efficacy of elasnin (5 μg/ml) against transcription-inhibited and overexpressed strains (n=9, average±standard deviation). The expression of overexpressed genes was induced by 0.2 μg/ml anhydrotetracycline. **(C)** Schematic of the regulatory network affected by elasnin during MRSA biofilm formation and biofilm detachment. This figure highlights the important role of *SarZ* in regulating degradative enzymes during elasnin-induced biofilm eradication.

increased antibiofilm activity is not related to elasnin's inhibition of cell division. Moreover, we found that MRSA had higher dependence on adhesive proteins for biofilm formation and maintenance than MSSA (Supplementary Figure S8C; Table S6), and elasnin exhibited higher antibiofilm activities against MRSA than MSSA (Supplementary Table S7). Therefore, elasnin-induced degradation of existing adhesive proteins is crucial for eradicating the established biofilms, and stopping biofilm eradication (as shown in the *sarZ*-overexpressed mutant; Figure 7B) required the inhibition of the matrix destruction caused by the increase in degrading exoproteins. However, the role of *sarZ* in this process has not been reported. Therefore, we proposed that (i) *sarZ* may be a repressor of the production of the degrading exoproteins, or (ii) the proteases upregulated by *sarZ* inactivate the corresponding exoproteins, and this regulatory pathway was independent of the above-mentioned regulons.

Biofilm development and its regulation has been extensively studied, but gaping holes remain to be filled. Previous studies have reported that increased SarA level and/or reduced protease production in a *sarZ*-deleted MRSA mutant resulted in increased biofilm formation (Tamber and Cheung, 2009), which is consistent with our observation of reduced biofilm formation in the *sarZ*-overexpressed mutant. Meanwhile, the increased expression of degradative enzymes like lipases and putative hemolysin reported in the *sarZ*-deleted Staphylococcus epidermidis (Wang et al., 2008) was also observed in the elasnin-treated biofilm cells when *sarZ* was repressed, which is believed to be responsible for the elasnin-induced biofilm eradication. Staphylococci produce different factors for different stages of infection (colonization, invasion, proliferation, dissemination, etc.), and biofilm development assist in these different stages (biofilm formation assist in colonization, whereas biofilm dispersion/detachment assist in dissemination). Considering the regulatory effect of *sarZ* on biofilm development in *S. aureus* and *S. epidermidis*, *sarZ* might be an important regulator that controls the transition among different stages, especially that *sarZ* exerts a regulatory effect on several traits and is expressed differentially at different growth phases (Kaito et al., 2006; Ballal et al., 2009; Chen et al., 2009). Yet, the exact regulations on how *sarZ* governs biofilm development are still unclear, and therefore, detailed studies on the regulations of *sarZ* during staphylococcal biofilm development should be further investigated. Besides, the roles of elasnin in intra-and intercell communications are also worth exploring, because elasnin is produced by multiple Streptomyces species and has a similar chemical structure to photopyrones, the novel quorum-sensing signals in Photorhabdus.

To conclude, the present study discovered elasnin as a potent biofilm-eradicating compound and elucidated its mode of action. Elasnin destroyed the biofilm matrix of MRSA and reduced cells' resistance to penicillin G, exhibiting low cytotoxicity and a low risk of resistance development. Mechanistic study revealed that elasnin repressed the expression of virulence factors and increased the secretion of degradative exoproteins, thus inhibiting cell division and leading to the degradation of the biofilm matrix. Through genetic manipulation assay, we determined the role of affected regulons during the elasnin-induced biofilm eradication and discovered that *sarZ* is an attractive target for Staphylococcal biofilm eradication. Overall, our study identified elasnin as a potent anti-virulence and biofilm-eradicating compound that harbors great potential in controlling MRSA biofilms with reduced risks in resistance development and provided new insights into the molecular targets for the discovery of MRSA biofilm eradicator.

Data availability statement

The datasets presented in this study can be found in online repositories. The names of the repository/repositories and accession number(s) can be found at: https://www.ncbi.nlm.nih.gov/genbank/, PRJNA740277 and http://www.proteomexchange.org/, PXD026836.

Author contributions

LL designed and carried out the experiments, did transcriptomic and related bioinformatics analysis, interpreted the data, and prepared the manuscript. JS did the proteomic analysis, wrote related methods, and did revision of the manuscript. YX did the PCA and bioinformatics analysis and wrote related methods. AC did the cytotoxicity test, interpreted the data, and wrote related methods. RW did the cluster analysis and wrote related methods. JM, WW, and WL helped in the experiments and data interpretation. Y-XL helped in experiment design. FC gave technical support. HL and P-YQ supervised this study, gave technical support and conceptual advice, and did the major edition of the manuscript. All authors reviewed and edited the manuscript, contributed to the article, and approved the submitted version.

Funding

This work was financially supported by the National Key R&D Program of China (2018YFA0903200), the Key Special Project for Introduced Talents Team of Southern Marine Science and Engineering Guangdong Laboratory (Guangzhou, GML2019ZD0409), the China Ocean Mineral Resources Research and Development Association (COMRRDA17SC01), the Hong Kong Branch of Southern Marine Science and Engineering Guangdong Laboratory (Guangzhou, SMSEGL20SC01), a CRF grant from the HKSAR government (C6026-19G-A), and the Research Grant Council of the Hong Kong Special Administrative Region, and China (grant no. 16102821).

Acknowledgments

The following reagent was provided by the Network on Antimicrobial Resistance in *S. aureus* (NARSA) for distribution through BEI Resources, NIAID, NIH: *S. aureus subsp. aureus*, Strain JE2, NR-46543 and *S. aureus subsp. aureus*, Strain JE2, Transposon Mutant NE567 (SAUSA300_2331), NR-47110.

Conflict of interest

The authors declare that the research was conducted in the absence of any commercial or financial relationships that could be construed as a potential conflict of interest.

Publisher's note

Supplementary material

The Supplementary material for this article can be found online at: https://www.frontiersin.org/articles/10.3389/fmicb.2022.967845/full#supplementary-material

References

Antunes, L. C. M., and Ferreira, R. B. R. (2011). Biofilms and bacterial virulence. *Rev. Medical Microbio.* 22, 12–16. doi: 10.1097/MRM.0b013e3283410d22

Ballal, A., Ray, B., and Manna, A. C. (2009). sarZ, a Sar A family gene, is transcriptionally activated by MgrA and is involved in the regulation of genes encoding exoproteins in *Staphylococcus aureus*. *J. Bacteriol.* 191, 1656–1665. doi: 10.1128/JB.01555-08

Beenken, K. E., Blevins, J. S., and Smeltzer, M. S. (2003). Mutation of sarA in *Staphylococcus aureus* limits biofilm formation. *Infect. Immun.* 71, 4206–4211. doi: 10.1128/IAI.71.7.4206-4211.2003

Beenken, K. E., Mrak, L. N., Griffin, L. M., Zielinska, A. K., Shaw, L. N., Rice, K. C., et al. (2010). Epistatic relationships between sarA and agr in *Staphylococcus aureus* biofilm formation. *PLoS One* 5:e10790. doi: 10.1371/journal.pone.0010790

Boisset, S., Geissmann, T., Huntzinger, E., Fechter, P., Bendridi, N., Possedko, M., et al. (2007). *Staphylococcus aureus* RNAIII coordinately represses the synthesis of virulence factors and the transcription regulator rot by an antisense mechanism. *Genes Dev.* 21, 1353–1366. doi: 10.1101/gad.423507

Bolger, A. M., Lohse, M., and Usadel, B. (2014). Trimmomatic: a flexible trimmer for Illumina sequence data. *Bioinformatics* 30, 2114–2120. doi: 10.1093/bioinformatics/btu170

Bose, J. L., Lehman, M. K., Fey, P. D., and Bayles, K. W. (2012). Contribution of the *Staphylococcus aureus* Atl AM and GL murein hydrolase activities in cell division, autolysis, and biofilm formation. *PLoS One* 7:e42244. doi: 10.1371/journal.pone.0042244

Boudjemaa, R., Steenkeste, K., Canette, A., Briandet, R., Fontaine-Aupart, M.-P., and Marlière, C. (2019). Direct observation of the cell-wall remodeling in adhering Staphylococcus aureus 27217: An AFM study supported by SEM and TEM. *The Cell Surface* 5:100018. doi: 10.1016/j.tcsw.2019.100018

Brackman, G., Cos, P., Maes, L., Nelis, H. J., and Coenye, T. (2011). Quorum sensing inhibitors increase the susceptibility of bacterial biofilms to antibiotics In vitro and In vivo. *Antimicrob. Agents Chemother.* 55, 2655–2661. doi: 10.1128/AAC.00045-11

Chen, P. R., Nishida, S., Poor, C. B., Cheng, A., Bae, T., Kuechenmeister, L., et al. (2009). A new oxidative sensing and regulation pathway mediated by the MgrA homologue SarZ in *Staphylococcus aureus*. *Mol. Microbiol.* 71, 198–211. doi: 10.1111/j.1365-2958.2008.06518.x

Chen, W., Zhang, Y., Yeo, W.-S., Bae, T., and Ji, Q. (2017). Rapid and efficient genome editing in *Staphylococcus aureus* by using an engineered CRISPR/Cas9 system. *J. Am. Chem. Soc.* 139, 3790–3795. doi: 10.1021/jacs.6b13317

Cheung, A. L., Nishina, K., and Manna, A. C. (2008). SarA of *Staphylococcus aureus* binds to the sarA promoter to regulate gene expression. *J. Bacteriol.* 190, 2239–2243. doi: 10.1128/JB.01826-07

Corrigan, R. M., and Foster, T. J. (2009). An improved tetracycline-inducible expression vector for *Staphylococcus aureus*. *Plasmid* 61, 126–129. doi: 10.1016/j.plasmid.2008.10.001

Corrigan, R. M., Rigby, D., Handley, P., and Foster, T. J. (2007). The role of *Staphylococcus aureus* surface protein SasG in adherence and biofilm formation. *Microbiology* 153, 2435–2446. doi: 10.1099/mic.0.2007/006676-0

Deutsch, E. W., Mendoza, L., Shteynberg, D., Farrah, T., Lam, H., Tasman, N., et al. (2010). A guided tour of the trans-proteomic pipeline. *Proteomics* 10, 1150–1159. doi: 10.1002/pmic.200900375

Eng, J. K., Jahan, T. A., and Hoopmann, M. R. (2013). Comet: an open-source MS/MS sequence database search tool. *Proteomics* 13, 22–24. doi: 10.1002/pmic.201200439

Flemming, H. C., and Wingender, J. (2010). The biofilm matrix. *Nat. Rev. Microbiol.* 8, 623–633. doi: 10.1038/nrmicro2415

Flemming, H. C., Wingender, J., Szewzyk, U., Steinberg, P., Rice, S. A., and Kjelleberg, S. (2016). Biofilms: an emergent form of bacterial life. *Nat. Rev. Microbiol.* 14, 563–575. doi: 10.1038/nrmicro.2016.94

Grabherr, M. G., Haas, B. J., Yassour, M., Levin, J. Z., Thompson, D. A., Amit, I., et al. (2011). Trinity: reconstructing a full-length transcriptome without a genome from RNA-Seq data. *Nat. Biotechnol.* 29, 644–652. doi: 10.1038/nbt.1883

Haas, B. J., Papanicolaou, A., Yassour, M., Grabherr, M., Blood, P. D., Bowden, J., et al. (2013). De novo transcript sequence reconstruction from RNA-seq using the trinity platform for reference generation and analysis. *Nat. Protoc.* 8, 1494–1512. doi: 10.1038/nprot.2013.084

Hall, C. W., and Mah, T. F. (2017). Molecular mechanisms of biofilm-based antibiotic resistance and tolerance in pathogenic bacteria. *FEMS Microbiol. Rev.* 41, 276–301. doi: 10.1093/femsre/fux010

Hammer, Ø., Harper, D. A., and Ryan, P. D. (2001). PAST: paleontological statistics software package for education and data analysis. *Palaeontol. Electron.* 4, 9.

Hengzhuang, W., Wu, H., Ciofu, O., Song, Z., and Høiby, N. (2012). In vivo pharmacokinetics/pharmacodynamics of colistin and imipenem in *Pseudomonas aeruginosa* biofilm infection. *Antimicrob. Agents Chemother.* 56, 2683–2690. doi: 10.1128/AAC.06486-11

Holmes, A. H., Moore, L. S. P., Sundsfjord, A., Steinbakk, M., Regmi, S., Karkey, A., et al. (2016). Understanding the mechanisms and drivers of antimicrobial resistance. *Lancet* 387, 176–187. doi: 10.1016/S0140-6736(15)00473-0

Houston, P., Rowe, S. E., Pozzi, C., Waters, E. M., and O'Gara, J. P. (2011). Essential role for the major autolysin in the fibronectin-binding protein-mediated *Staphylococcus aureus* biofilm phenotype. *Infect. Immun.* 79, 1153–1165. doi: 10.1128/IAI.00364-10

Huang, D. W., Sherman, B. T., and Lempicki, R. A. (2009). Bioinformatics enrichment tools: paths toward the comprehensive functional analysis of large gene lists. *Nucleic Acids Res.* 37, 1–13. doi: 10.1093/nar/gkn923

Jamal, M., Ahmad, W., Andleeb, S., Jalil, F., Imran, M., Nawaz, M. A., et al. (2018). Bacterial biofilm and associated infections. *J. Chin. Med. Assoc.* 81, 7–11. doi: 10.1016/j.jcma.2017.07.012

Jenul, C., and Horswill, A. R. (2019). Regulation of *Staphylococcus aureus* virulence. *Microbiol Spectr* 7, 7–2. doi: 10.1128/microbiolspec.GPP3-0031-2018

Kaito, C., Morishita, D., Matsumoto, Y., Kurokawa, K., and Sekimizu, K. (2006). Novel DNA binding protein SarZ contributes to virulence in *Staphylococcus aureus*. *Mol. Microbiol.* 62, 1601–1617. doi: 10.1111/j.1365-2958.2006.05480.x

Keller, A., Nesvizhskii, A. I., Kolker, E., and Aebersold, R. (2002). Empirical statistical model to estimate the accuracy of peptide identifications made by MS/MS and database search. *Anal. Chem.* 74, 5383–5392. doi: 10.1021/ac025747h

Kessner, D., Chambers, M., Burke, R., Agus, D., and Mallick, P. (2008). ProteoWizard: open source software for rapid proteomics tools development. *Bioinformatics* 24, 2534–2536. doi: 10.1093/bioinformatics/btn323

Kong, C., Chee, C.-F., Richter, K., Thomas, N., Rahman, N. A., and Nathan, S. (2018). Suppression of *Staphylococcus aureus* biofilm formation and virulence by a benzimidazole derivative, UM-C162. *Sci. Rep.* 8, 1–16. doi: 10.1038/s41598-018-21141-2

Koo, H., Allan, R. N., Howlin, R. P., Stoodley, P., and Hall-Stoodley, L. (2017). Targeting microbial biofilms: current and prospective therapeutic strategies. *Nat. Rev. Microbiol.* 15, 740–755. doi: 10.1038/nrmicro.2017.99

Langmead, B., and Salzberg, S. L. (2012). Fast gapped-read alignment with bowtie 2. *Nat. Methods* 9, 357–359. doi: 10.1038/nmeth.1923

Li, X. H., and Lee, J. H. (2017). Antibiofilm agents: A new perspective for antimicrobial strategy. *J. Microbiol.* 55, 753–766. doi: 10.1007/s12275-017-7274-x

Li, Y.-X., Zhong, Z., Zhang, W.-P., and Qian, P.-Y. (2018). Discovery of cationic nonribosomal peptides as gram-negative antibiotics through global genome mining. *Nat. Commun.* 9, 1–9. doi: 10.1038/s41467-018-05781-6

Lister, J. L., and Horswill, A. R. (2014). *Staphylococcus aureus* biofilms: recent developments in biofilm dispersal. *Front. Cell. Infect. Microbiol.* 4:178. doi: 10.3389/fcimb.2014.00178

Long, L., Wang, R., Chiang, H. Y., Ding, W., Li, Y.-X., Chen, F., et al. (2021). Discovery of Antibiofilm activity of Elasnin against marine biofilms and its application in the marine antifouling coatings. *Mar. Drugs* 19, 19. doi: 10.3390/md19010019

Love, M., Anders, S., and Huber, W. (2014). Differential analysis of count data–the DESeq2 package. *Genome Biol.* 15, 10–1186. doi: 10.1186/s13059-014-0550-8

Lukashin, A. V., and Borodovsky, M. (1998). GeneMark. Hmm: new solutions for gene finding. *Nucleic Acids Res.* 26, 1107–1115. doi: 10.1093/nar/26.4.1107

Madalina Mihai, M., Maria Holban, A., Giurcaneanu, C., Gabriela Popa, L., Mihaela Oanea, R., Lazar, V., et al. (2015). Microbial biofilms: impact on the pathogenesis of periodontitis, cystic fibrosis, chronic wounds and medical device-related infections. *Curr. Top. Med. Chem.* 15, 1552–1576. doi: 10.2174/1568026615666150414123800

Mah, T. F., and O'Toole, G. A. (2001). Mechanisms of biofilm resistance to antimicrobial agents. *Trends Microbiol.* 9, 34–39. doi: 10.1016/S0966-842X(00)01913-2

Martinez, J. L. (2009). Environmental pollution by antibiotics and by antibiotic resistance determinants. *Environ. Pollut.* 157, 2893–2902. doi: 10.1016/j.envpol.2009.05.051

Monteiro, J. M., Fernandes, P. B., Vaz, F., Pereira, A. R., Tavares, A. C., Ferreira, M. T., et al. (2015). Cell shape dynamics during the staphylococcal cell cycle. *Nat. Commun.* 6, 1–12. doi: 10.1038/ncomms9055

Moormeier, D. E., and Bayles, K. W. (2017). *Staphylococcus aureus* biofilm: a complex developmental organism. *Mol. Microbiol.* 104, 365–376. doi: 10.1111/mmi.13634

Nair, S., Desai, S., Poonacha, N., Vipra, A., and Sharma, U. (2016). Antibiofilm activity and synergistic inhibition of *Staphylococcus aureus* biofilms by bactericidal protein P128 in combination with antibiotics. *Antimicrob. Agents Chemother.* 60, 7280–7289. doi: 10.1128/AAC.01118-16

Ohno, H., Saheki, T., Awaya, J., Nakagawa, A., and Omura, S. (1978). Isolation and characterization of elasnin, a new human granulocyte elastase inhibitor produced by a strain of Streptomyces. *J. Antibiot. (Tokyo)* 31, 1116–1123. doi: 10.7164/antibiotics.31.1116

O'Neill, E., Pozzi, C., Houston, P., Humphreys, H., Robinson, D. A., Loughman, A., et al. (2008). A novel *Staphylococcus aureus* biofilm phenotype mediated by the fibronectin-binding proteins, FnBPA and FnBPB. *J. Bacteriol.* 190, 3835–3850. doi: 10.1128/JB.00167-08

O'Neill, E., Pozzi, C., Houston, P., Smyth, D., Humphreys, H., Robinson, D. A., et al. (2007). Association between methicillin susceptibility and biofilm regulation in *Staphylococcus aureus* isolates from device-related infections. *J. Clin. Microbiol.* 45, 1379–1388. doi: 10.1128/JCM.02280-06

Otto, M. (2019). Staphylococcal biofilms. *J. Clin. Microbiol.* 8, 699–711. doi: 10.1128/9781683670131.ch43

Paoletti, A. C., Parmely, T. J., Tomomori-Sato, C., Sato, S., Zhu, D., Conaway, R. C., et al. (2006). Quantitative proteomic analysis of distinct mammalian mediator complexes using normalized spectral abundance factors. *Proc. Natl. Acad. Sci.* 103, 18928–18933. doi: 10.1073/pnas.0606379103

Patro, R., Duggal, G., Love, M. I., Irizarry, R. A., and Kingsford, C. (2017). Salmon provides fast and bias-aware quantification of transcript expression. *Nat. Methods* 14, 417–419. doi: 10.1038/nmeth.4197

Robinson, M. D., McCarthy, D. J., and Smyth, G. K. (2010). edgeR: a bioconductor package for differential expression analysis of digital gene expression data. *Bioinformatics* 26, 139–140. doi: 10.1093/bioinformatics/btp616

Sherman, B. T., and Lempicki, R. A. (2009). Systematic and integrative analysis of large gene lists using DAVID bioinformatics resources. *Nat. Protoc.* 4, 44–57. doi: 10.1038/nprot.2008.211

Stewart, P. S., and William Costerton, J. (2001). Antibiotic resistance of bacteria in biofilms. *Lancet* 358, 135–138. doi: 10.1016/S0140-6736(01)05321-1

Sugimoto, S., Iwamoto, T., Takada, K., Okuda, K.-I., Tajima, A., Iwase, T., et al. (2013). *Staphylococcus epidermidis* Esp degrades specific proteins associated with *Staphylococcus aureus* biofilm formation and host-pathogen interaction. *J. Bacteriol.* 195, 1645–1655. doi: 10.1128/JB.01672-12

Sulaiman, J. E., and Lam, H. (2020). Proteomic study of the survival and resuscitation mechanisms of filamentous Persisters in an evolved *Escherichia coli* population from cyclic ampicillin treatment. *Msystems* 5, e00462–e00420. doi: 10.1128/mSystems.00462-20

Sulaiman, J. E., Long, L., Wu, L., Qian, P.-Y., and Lam, H. (2021). Comparative proteomic investigation of multiple methicillin-resistant *Staphylococcus aureus* strains generated through adaptive laboratory evolution. *Iscience* 24:102950. doi: 10.1016/j.isci.2021.102950

Sun, Y., Dowd, S. E., Smith, E., Rhoads, D. D., and Wolcott, R. D. (2008). In vitro multispecies Lubbock chronic wound biofilm model. *Wound Repair Regen.* 16, 805–813. doi: 10.1111/j.1524-475X.2008.00434.x

Szklarczyk, D., Gable, A. L., Lyon, D., Junge, A., Wyder, S., Huerta-Cepas, J., et al. (2019). STRING v11: protein–protein association networks with increased coverage, supporting functional discovery in genome-wide experimental datasets. *Nucleic Acids Res.* 47, D607–D613. doi: 10.1093/nar/gky1131

Tamber, S., and Cheung, A. L. (2009). SarZ promotes the expression of virulence factors and represses biofilm formation by modulating SarA and agr in *Staphylococcus aureus*. *Infect. Immun.* 77, 419–428. doi: 10.1128/IAI.00859-08

Vasudevan, R. (2019). Agr/sarA: molecular switches of biofilm regulation in *Staphylococcus aureus*. *J. Microbiol. Exp* 7, 17–18. doi: 10.15406/jmen.2019.07.00233

Wang, L., Li, M., Dong, D., Bach, T.-H. L., Sturdevant, D. E., Vuong, C., et al. (2008). SarZ is a key regulator of biofilm formation and virulence in *Staphylococcus epidermidis*. *J. Infect. Dis.* 197, 1254–1262. doi: 10.1086/586714

Wu, H., Moser, C., Wang, H.-Z., Høiby, N., and Song, Z.-J. (2015). Strategies for combating bacterial biofilm infections. *Int. J. Oral Sci.* 7, 1–7. doi: 10.1038/ijos.2014.65

Yin, Q., Liang, J., Zhang, W., Zhang, L., Hu, Z. L., Zhang, Y., et al. (2019). Butenolide, a marine-derived broad-Spectrum Antibiofilm agent Against Both gram-positive and gram-negative pathogenic Bacteria. *Mar. Biotechnol. (N.Y.)* 21, 88–98. doi: 10.1007/s10126-018-9861-1

frontiers | Frontiers in Microbiology

TYPE Original Research
PUBLISHED 10 August 2022
DOI 10.3389/fmicb.2022.966976

OPEN ACCESS

EDITED BY
Huancai Lin,
Guanghua School of Stomatology,
Sun Yat-sen University, China

REVIEWED BY
Lin Zhong,
Shandong University,
China
Karishma Bisht,
Princeton University,
United States

*CORRESPONDENCE
Jie Gao
jiegao@rcees.ac.cn
Guoqiang Zhuang
gqzhuang@rcees.ac.cn

SPECIALTY SECTION
This article was submitted to Antimicrobials, Resistance and Chemotherapy, a section of the journal Frontiers in Microbiology

RECEIVED 12 June 2022
ACCEPTED 21 July 2022
PUBLISHED 10 August 2022

CITATION
Wang N, Gao J, Xiao S and Zhuang G (2022) Overexpression of *pdeR* promotes biofilm formation of *Paracoccus denitrificans* by promoting ATP production and iron acquisition. *Front. Microbiol.* 13:966976. doi: 10.3389/fmicb.2022.966976

Overexpression of *pdeR* promotes biofilm formation of *Paracoccus denitrificans* by promoting ATP production and iron acquisition

Na Wang[1,2], Jie Gao[1,3]*, Shujie Xiao[1,3] and Guoqiang Zhuang[1,3]*

[1]CAS Key Laboratory of Environmental Biotechnology, Research Center for Eco-Environmental Sciences, Chinese Academy of Sciences, Beijing, China, [2]Jinan Microecological Biomedicine Shandong Laboratory, Jinan, China, [3]College of Resources and Environment, University of Chinese Academy of Sciences, Beijing, China

Bacterial biofilms are ubiquitous in natural environments and play an essential role in bacteria's environmental adaptability. Quorum sensing (QS), as the main signaling mechanism bacteria used for cell-to-cell communication, plays a key role in bacterial biofilm formation. However, little is known about the role of QS circuit in the N-transformation type strain, *Paracoccus denitrificans*, especially for the regulatory protein PdeR. In this study, we found the overexpression of *pdeR* promoted bacterial aggregation and biofilm formation. Through RNA-seq analysis, we demonstrated that PdeR is a global regulator which could regulate 656 genes expression, involved in multiple metabolic pathways. Combined with transcriptome as well as biochemical experiments, we found the overexpressed *pdeR* mainly promoted the intracellular degradation of amino acids and fatty acids, as well as siderophore biosynthesis and transportation, thus providing cells enough energy and iron for biofilm development. These results revealed the underlying mechanism for PdeR in biofilm formation of *P. denitrificans*, adding to our understanding of QS regulation in biofilm development.

KEYWORDS

biofilm, quorum sensing, PdeR, RNA-seq, *Paracoccus denitrificans*

Introduction

Biofilms are one of the most prevalent and important forms of life for bacteria, in which cells are encased in the extracellular matrix that can serve as a barrier to multiple adverse environmental factors (Steenackers et al., 2016; Jo et al., 2022). Previous studies showed that the environmental stresses that microbes would face can be highly variable and complex, including mechanical damage, antibiotics pressures, oxidative stresses, etc.

(Starosta et al., 2014). Thus, over 80% of bacteria would form a biofilm to resist environmental stresses and to make sure the whole community survives better (Mohammad Reza, 2018). For example, under extreme conditions such as the deep sea, microorganisms would form microbial mats and produce more extracellular polymeric substances (EPS) to resist mechanical stress (Bolhuis et al., 2014). Moreover, EPS could work as a protective barrier, which contributes to the lower sensitivity and higher resistance of biofilms to antibiotics (Hoiby et al., 2010; Yan and Bassler, 2019), and biofilm also promotes the efficiency of resistance genes horizontal transfer (Orazi and O'Toole, 2019). Typically, biofilm formation and maturation are regulated by various factors, including cell-to-cell communication and environmental factors.

Quorum sensing (QS) is a widely used bacterial communication mechanism, by which bacteria could secret and sense signaling molecules called autoinducers to coordinate gene expression according to the population density (Papenfort and Bassler, 2016; Mukherjee and Bassler, 2019). Bacteria use QS to precisely coordinate various of group behaviors, including biofilm formation, carbon metabolism, EPS production, virulence factors production, luminescence, etc. (Davies et al., 1998; Hense and Schuster, 2015). Previous studies have shown that the mutation of QS system severely damaged the ability of biofilm formation, such as in *Pseudomonas aeruginosa*, *Burkholderia cepacia*, *Streptococcus mutans*, etc. (Lewenza et al., 1999; Parsek and Greenberg, 2005). QS coordinates the initiation and maturation of biofilm by regulating the expression of a series of functional genes, including EPS production related genes, cell motility genes, and so on. Gilbert et al. demonstrated that the QS regulation protein LasR in *P. aeruginosa* could directly regulate the expressional level of the extracellular polysaccharide (Psl) biosynthetic genes (Gilbert et al., 2009). Moreover, when the second QS circuit *rhl* was mutant, the production of another kind of polysaccharide Pel significantly decreased in *P. aeruginosa* (Sakuragi and Kolter, 2007). In addition, QS could coordinate the expression of cell motility genes, such as IV pilus gene clusters which are associated with cell attachment during the early stage of biofilm formation, as well as the genes for flagella synthesis which are essential for biofilm matures as a mushroom-like structure (Yu and Ma, 2017; Yan and Bassler, 2019). However, research on the mechanism of QS regulating biofilm formation is mostly concentrated in pathogenic microorganisms, such as *P. aeruginosa*, *Staphylococcus aureus*, etc., while studies on environmental bacteria are relatively rare.

Paracoccus denitrificans is widely distributed in soil and water, possessing the ability of heterotrophic nitrification-aerobic denitrification (HNAD), and thus is taken as the model strain for nitrogen transformation research (Ji et al., 2015). We have demonstrated that *P. denitrificans* harbored a LuxI/R-type QS circuit, PdeI/R (Zhang et al., 2018). The AHL synthetase PdeI could catalyze the biosynthesis of *N*-hexadecanoyl-L-Homoserine lactone (C16-HSL), and PdeR protein is the corresponding regulatory protein which could bind with C16-HSL and regulate genes expression. It has been shown that *P. denitrificans* forms a peculiarly thin biofilm at the gas–liquid interface, which consisted of almost a monolayer of cells (Yoshida et al., 2017). Biofilms for *Paracoccus* species have many important applications, especially in wastewater nitrogen removal bioreactors, while the detailed mechanism of biofilm formation in this genus is largely unknown (Morinaga et al., 2020). Previous studies showed that in the *pdeI* mutant strain, cell aggregation was more obvious and bacteria formed thicker biofilm, while exogenous C16-HSL addition inhibited cell aggregation (Morinaga et al., 2018). Nevertheless, the underlying mechanism of QS regulating biofilm formation in *P. denitrificans* still remains unclear, especially for the role of PdeR protein.

In this study, we constructed the *pdeR* overexpression strain to explore the role of PdeR on biofilm formation of *P. denitrificans* PD1222 at the initiation stage. The results of physiological tests indicated overexpressed *pdeR* promoted cell aggregation and EPS production, and thus the *pdeR* overexpression strain formed thicker biofilm. Furthermore, through transcriptomic analysis as well as biochemical experiments, we demonstrated that PdeR promotes adenosine triphosphate (ATP) production and iron absorption during the initial stage of biofilm formation to provide sufficient energy and iron for biofilm development. The results of this study deepened our understanding of the QS regulation mechanism for biofilm formation of *P. denitrificans*, providing some useful references for the optimization of *P. denitrificans* in applications.

Materials and methods

Bacterial strains, plasmids, and growth conditions

Bacterial strains and plasmids used in this study are listed in Table 1. *P. denitrificans* and its derived strains were cultivated at 30°C, 180 rpm. *Escherichia coli* and its derived strains were cultivated at 37°C, 180 rpm. All strains were grown in Luria-Bertani (LB) medium, if necessary, supplied with rifampicin 50 μg/ml, kanamycin 100 μg/ml, ampicillin 100 μg/ml, or chloramphenicol 34 μg/ml to maintain plasmids and select for recombinants.

Construction of a *pdeR* overexpression strain

The fragment of *pdeR* gene (Pden_0786) was amplified *via* PCR from the genome of *P. denitrificans* PD1222 with the addition of a 6× His tag and then fused with a *tac* promoter (5′-GTGTGGAATTGTGTTGACAATTAATCATCGGCTCGTATAATGTGTGGAATTGTG-3′). Primers used in this study are listed in Table 2. The obtained *tac-pdeR*-His fragment and the broad-host-range plasmid pBBR1MCS-2 were all double

TABLE 1 Strains and plasmids used in this study.

Strain or plasmid	Relevant characteristic (s)[a]	Source or references
Strains		
Paracoccus denitrificans		
PD1222	Wild type, G^-, Rif^r	Zhang et al., 2018
PD-pdeR	PdeR overexpression strain, Rif^r, Kan^r	This study
PD-pBBR	PD1222 containing empty pBBR1MCS, Rif^r, Kan^r	This study
Escherichia coli		
DH5α	Host strain for pBBR-pdeR, pBBR1MCS-2; used as donor in triparental conjugation	Takara
Plasmids		
pBBR1MCS-2	Broad-host-range cloning vector, Kan^r	Kovach et al., 1995
pRK600	Helper plasmid, mob^+ tra^+, Cm^r	Lab stock
pBBR-*pdeR*	Constructed overexpression vector, Kan^r	This study
pKK223-3	Used to amplify the Tac promoter, Amp^r	Lab stock

[a]G^-, Gram negative; Rif^r, rifampin resistant; Kan^r, kanamycin resistant; Cm^r, chloramphenicol resistant; mob^+, plasmid mobility; tra^+, plasmid transferability; Amp^r, ampicillin resistant.

TABLE 2 Primers used for plasmid construction.

Primer name	Primer sequence (5′–3′)
pKK-1	GCTCTAGACAAGGCGCACTCCCGTTCTGGATAATG
pKK-RH-2	CTTGGCGAGTGCTGCATTGATTTCCGCGCGAGACGACATTTCTGTTTCCTGTGTGAAATTGT
pKK-RH-3	GTGTGGAATTGTGAGCGGATAACAATTTCACACAGGAAACAGAAATGTCGTCTCGCGCGGAAATCAAT
R-His	GCACCGGTTTAATGATGATGATGATGATGCAGCAAGCGGTAATCCTTGGC
pden-NC-F	TCGGAATTACTGGGCGTAAAG
pden-NC-R	TCGAACTCCAGACCGATAGT
P0786-11	ATCACGGCCTGCACTATG
P0786-12	CGATCTCGTCATCCGTGAAT

digested by AgeI (NEB, United States) and XbaI (NEB) in 37°C, 2 h. Ligations were performed overnight at 16°C, using T4 DNA ligase (NEB). The constructed plasmid pBBR-*pdeR* was then introduced into PD1222 by triparental conjugation. Briefly, PD1222 was used as the recipient, *E. coli* DH5α harboring pBBR-*pdeR* was used as a donor, *E. coli* DH5α harboring pRK600 was used as a helper, and strains were mixed with the ratio of 3:1:1. After being cultivated in a fresh LB agar plate for 24 h, the mixture was spread on the plate supplemented with rifampin (100 μg/ml) and kanamycin (50 μg/ml) to select *pdeR* overexpression strain PD-pdeR. And the control strain PD-pBBR that harbors the empty plasmid pBBR1MCS-2 was constructed in the same way.

Biofilm and EPS characterization

Crystal violet staining was performed as previously described to characterize the difference in biofilm formation between PD-pdeR and PD-pBBR with some modifications (Wang et al., 2019). Cultures of PD-pdeR and PD-pBBR were incubated in polystyrene 12-well microtiter plates at 30°C, 180 rpm. Cells were collected after 12, 24, and 36 h incubation, respectively. The cell suspensions were decanted and the remained cells were softly washed by PBS buffer three times and then fixed at 60°C for 10 min. The attached cells were quantified by staining with 0.1% (*w*/*v*) crystal violet solution for 15 min, and then washed three times with PBS and air dried. The bound crystal violet was extracted using 95% ethanol. A spectrophotometer (PerkinElmer, EnSpire2300) was used to detect the absorbance at 595 nm. Three parallel experiments were carried out.

The cationic exchange resin method was used to extract EPS as previously described (Wang et al., 2022). Briefly, cells after 36 h incubation were collected by centrifuging at 8,000 *g* for 10 min, and resuspended again in sterile water. Cationic exchange resin (0.25 g/ml) was added to the suspension and transferred to a conical flask to extract EPS. The conical flasks were put in a shaking incubator at 200 rpm overnight at room temperature. Then the suspension was centrifuged at 10,000 *g* for 10 min at 4°C and the supernatant was filtered through 0.45 μm filter. The content of exopolysaccharides was determined by the phenol sulfuric acid method (Dubois et al., 1956), and glucose solutions were used for the standard curve. The content of extracellular protein was measured using the Pierce™ Coomassie Assay Kit (Thermo Fisher Scientific, United states), using bovine serum protein as the calibration curve standard.

Scanning electron microscope observation

PD-pBBR and PD-PdeR have incubated in polystyrene 48-well microtiter plates in which cover glasses were pre-placed in each well. After 36 h, cell suspensions were carefully removed and the remaining cells adhered to the slides were fixed with 2.5% glutaraldehyde overnight at 4°C. The fixed slides were washed three times in PBS buffer and dehydrated using 50, 70, 80, 90, and 100% ethanol solutions (15 min at each gradient). After lyophilized for 2 h using a freeze–drying device, the slides were sprayed with gold and observed by a scanning electron microscope.

Real-time quantitative PCR

Cells of PD1222, PD-pBBR and PD-pdeR were harvested when OD_{600} was about 1.5. Total RNAs were isolated and purified with an RNeasy mini system (Qiagen, Germany) and then reverse transcribed by PrimeScript™RT Master Mix (Takara, Japan) according to manufacturer's instructions. Quantitative PCR reactions were performed using the SYBR® Premix Ex Taq Kit (Takara, Japan) and a 7,500 real-time PCR system (Bio-Rad, United States). The primers used in Real-time Quantitative PCR (RT-qPCR) analyses were designed by Primer premier 5 and are listed in Table 2. The relative expression of *pdeR* was calculated by the $2^{-\Delta\Delta CT}$ method (Livak and Schmittgen, 2001) with 16 s rRNA of *P. denitrificans* used as an internal control. All reactions were carried out in triplicate.

Transcriptome analysis

Triplicate cultures of PD-pBBR vector and PD-pdeR were grown in LB medium at 30°C, 180 rpm. When the OD_{600} reached ~1.5, cells were harvested, and total RNAs were extracted. The total RNA extraction of PD-pBBR and PD-pdeR was performed by using the RNeasy Mini kit (Qiagen, Germany), treated with DNase I (Qiagen, Germany). The quality of isolated RNAs was analyzed by electrophoresis and quantified by a NanoDrop 2000 spectrophotometer (NanoDrop Technologies). And then the RNAs were subjected to Solexa/Illumina sequencing at Beijing Auwigene Tech.

The clean data were obtained by removing reads that contained possible sequencing errors and were mapped to the downloaded reference genome sequences of *P. denitrificans* PD1222 using Bowtie2. The relative transcript abundance was measured by FPKM (Fragments per kilobase of exon model per million mapped reads). The criteria for differentially expressed genes screening was p. adjust value of less than 0.05. Furthermore, the functional enrichment analyses including gene ontology (GO) and Kyoto Encyclopaedia of Genes and Genomes (KEGG), were performed to dig out the biological function of differentially expressed genes (DEGs).

Acetyl-CoA and ATP quantitation

Cells of PD-pBBR and PD-pdeR were harvested when OD_{600} was about 1.5 by centrifugation at 4°C, 10,000 *g* for 5 min, and then resuspended in extraction buffer (methanol: acetonitrile: water = 45:45:10, *v:v:v*). Cells were then broken by ultrasonication (power 40%, 2 s-working, 1 s-pause, total time 10 min). The lysates were centrifuged at 14,000 *g*, 4°C for 10 min to remove the cell debris.

For acetyl-CoA extraction, add ice-cold perchloric acid (final concentration, 1 M) into the supernatant, and incubated on ice for 5 min. Then centrifuged at 4°C, 13,000 *g* for 2 min, transfer the supernatant to a new EP tube, adding ice-cold KOH solution to make sure its final concentration is 34%, then vortexed to mix the contents. Then adjust the pH value to 6.5–8 using 0.1 M KOH, 4°C, 13,000 *g*, centrifuged for 15 min, and transfer the supernatant to a new tube. The quantitation of acetyl-CoA was performed using PicoProbe Acetyl CoA Assay Kit (Abcam, United Kingdom), according to the manufacturer's instructions. And the fluorescent intensity was measured using a SpectraMax i3× microplate reader (Ex/Em = 535/587 nm).

For ATP detection, adding 500 µl chloroform to per mL cell lysates, mixed well then centrifuged at 4°C, 10,000 *g* for 3 min, and collected the supernatant. The quantitation of ATP was performed using ATP Detection Kit (Solarbio, China). The operation was done according to the kit instructions. And samples were detected by absorbance at 340 nm.

Siderophore detection

Arnow test was used to quantify the catechol siderophore followed the previous method with minor changes (Arnow, 1937). Briefly, bacterial cultures were collected after 12, 24, 36 and 48 h incubation by centrifugation at 10,000 *g* for 5 min. 1 ml of bacterial culture supernatant was mixed with 1 ml of 0.5 M HCl solution, 1 ml of nitrite-molybdate reagent, and 1 ml of 1 M NaOH solution in order. Mix thoroughly and add water to make 5 ml, incubated at room temperature for 10 min. The mixture solution was measured using a spectrophotometer (PerkinElmer, EnSpire2300) at 510 nm. All detective assays were carried out in triplicate.

2,3-Dihydroxybenzoic acid addition experiment

The 2,3-dihydroxybenzoic acid (DHBA) was purchased from Sigma-Aldrich. DHBA was first formulated into a mother liquor of 1 mg/ml and 10 mg/ml, then filter sterilized. The DHBA solutions were added into LB medium to make sure the final-concentrations were 1 µg/ml and 10 µg/ml, respectively. Same volume of sterile water was added as control. PD-pBBR and PD-pdeR were seeded in the medium with different concentrations

of DHBA, and incubated for 36 h and then the biofilm formation was detected.

Statistical analysis

All tests in this study were carried out in triplicate, and the results are presented as means ± SD (standard deviation of means). The significance among groups was analyzed by one-way ANOVA test ($p < 0.05$ were considered as significant) using the SPSS Statistics 24.0 software.

Results

Bacterial growth and morphological characteristics

Recombinant strains PD-pBBR and PD-pdeR were constructed from parent strain *P. denitrificans* PD1222. To validate the overexpression of *pdeR* gene, RT-qPCR was performed to examine the expressional level of pdeR in PD-pBBR, PD-pdeR and PD1222 cells. As shown in Supplementary Figure S1, *pdeR* was up-regulated about 38-fold in PD-pdeR strain comparing with PD1222 cells, while *pdeR* transcription in PD-pBBR strain was comparable to wild type cells. To determine the effect of PdeR protein on *P. denitrificans* growth, PD1222, PD-pBBR and PD-pdeR were seeded into the same medium and incubated for 48 h. The growth curves suggested *pdeR* overexpression slightly inhibited bacterial growth rate and led to a longer lag phase (Figure 1). While the empty plasmid did not show any significant effect on bacterial growth.

However, the *pdeR* overexpressed strains produced a distinctive colony morphology on the LB agar plate (Figure 2A). The colony of PD-pdeR showed a wrinkled appearance, while the colony surface of PD-pBBR was smoother. In bacteria, wrinkled or rugose colonies are assumed to be a consequence of the formation of biofilms on the colony surface (Mandel and Dunn, 2016), thus we further detected the biofilm formation and EPS production of PD-pBBR and PD-pdeR, respectively. As the results showed, bacteria started to form detectable biofilm after 12 h cultivation, in which enhanced biofilm formation of

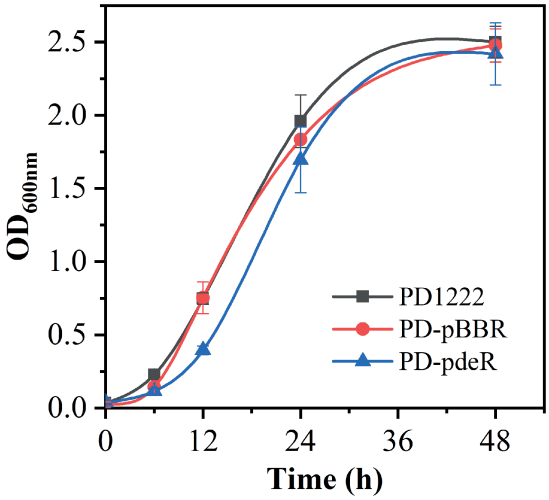

FIGURE 1
The growth curve of PD1222, PD-pdeR and PD-pBBR. Black, PD122; red, PD-pBBR; blue, PD-pdeR. Data are presented as mean±SD, *n*=3.

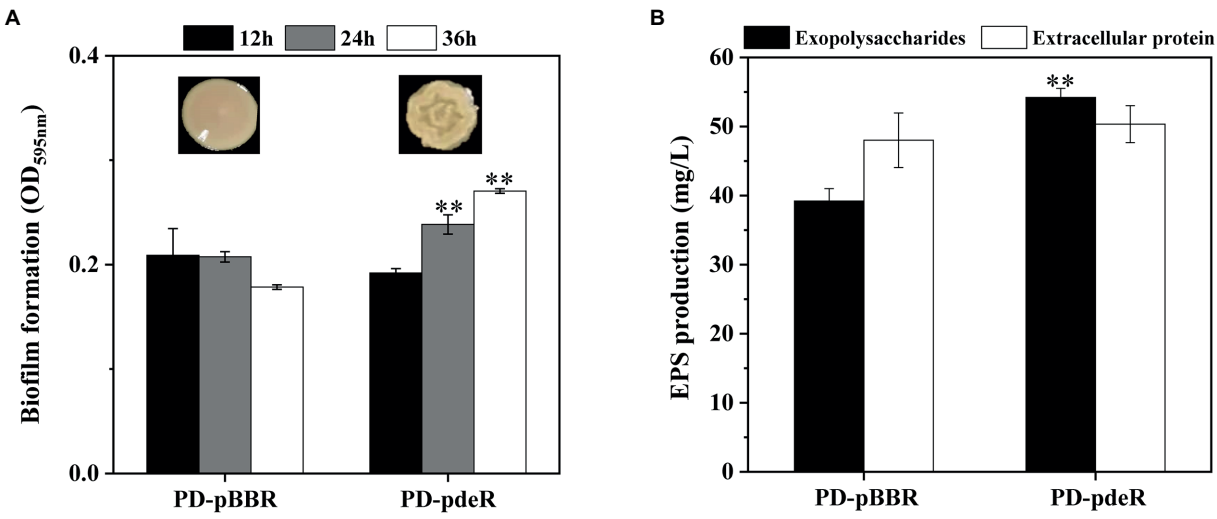

FIGURE 2
(A) The colony morphology and the biofilm formation of PD-pBBR (left) and PD-pdeR (right) strains after 12, 24 and 36h incubation, respectively. **(B)** The exopolysaccharides and extracellular protein production of PD-pBBR and PD-pdeR after 36h incubation. Data are presented as mean±SD, *n*=3. ***p*<0.01 compared with the control strain PD-pBBR.

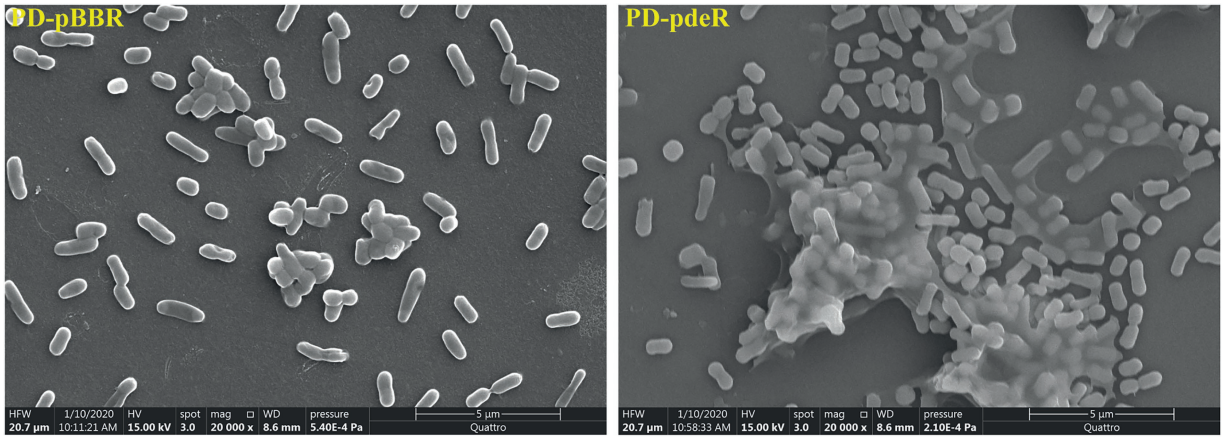

FIGURE 3
The morphology of PD-pBBR and PD-pdeR using SEM (scale bar=5μm). Cells were incubated in LB medium for 36h, the glass slides that were pre-placed in 24-well plates were directly processed for Scanning Electron Microscope (SEM) observation.

PD-pdeR strains was observed, especially in 24 and 36 h (Figure 2A). Accordingly, PD-pdeR strains produced more EPS especially exopolysaccharides than PD-pBBR strains after 36 h incubation (Figure 2B). Moreover, as observed by SEM, cells of PD-pdeR had conspicuous aggregation and were covered by extracellular matrix (Figure 3). The results above clearly indicated the role of PdeR protein in the biofilm formation of *P. denitrificans*; however, the molecular mechanisms of PdeR protein involved in biofilm formation remain to be further investigated.

pdeR overexpression altered gene transcription profiles in *Paracoccus denitrificans* PD1222

To determine which genes are regulated by PdeR, we performed RNA-seq analysis to collect the DEGs after *pdeR* overexpressed in *P. denitrificans*. As shown in Figure 4, around 656 genes were under the regulation of PdeR, of which 333 genes were downregulated and 323 genes were up-regulated. We further analyzed the enrichment of the KEGG pathways through the KEGG database.[1] The top 20 KEGG pathways are presented, in which DEGs involved in ribosome and biosynthesis of siderophore group nonribosomal peptides pathway were significantly enriched (Figure 5). Besides, various carbon metabolism pathways such as glycolysis, pyruvate metabolism, tricarboxylic acid cycle (TCA cycle), pentose phosphate pathway, starch and sucrose metabolism were also included. Amino acid metabolism including valine, leucine, isoleucine degradation and tryptophan, glycine, serine, threonine, cysteine and methionine metabolism were enriched. Moreover, the enriched KEGG

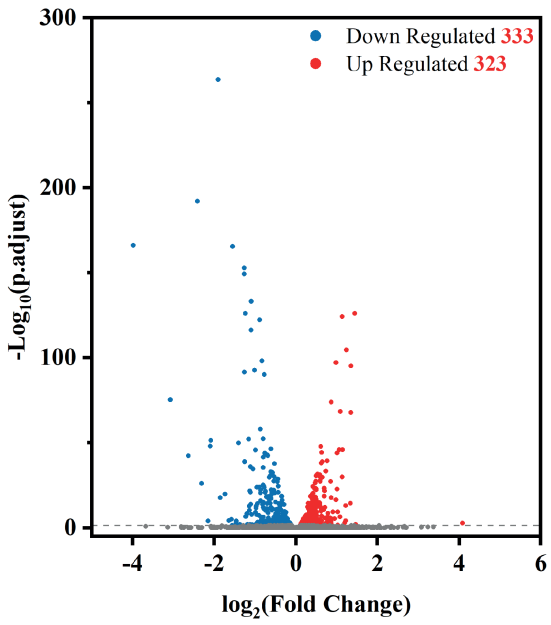

FIGURE 4
Volcano plot of differentially expressed genes between PD-pdeR and PD-pBBR (red, up-regulated genes; blue, downregulated genes; gray, non-differentially expressed genes).

pathways also included fatty acid metabolism and antibiotics resistance-related pathways (Figure 5). In addition, three genes participating in O-Antigen nucleotide sugar biosynthesis pathway were also significantly up-regulated in PD-pdeR (Supplementary Table S1). Previous studies have demonstrated that nucleotide sugars are the precursors for exopolysaccharide biosynthesis (Padmanabhan et al., 2018). These results suggested that PdeR regulates multiple genes and metabolic pathways, functioning as a global regulator in *P. denitrificans*.

1 https://www.genome.jp/kegg

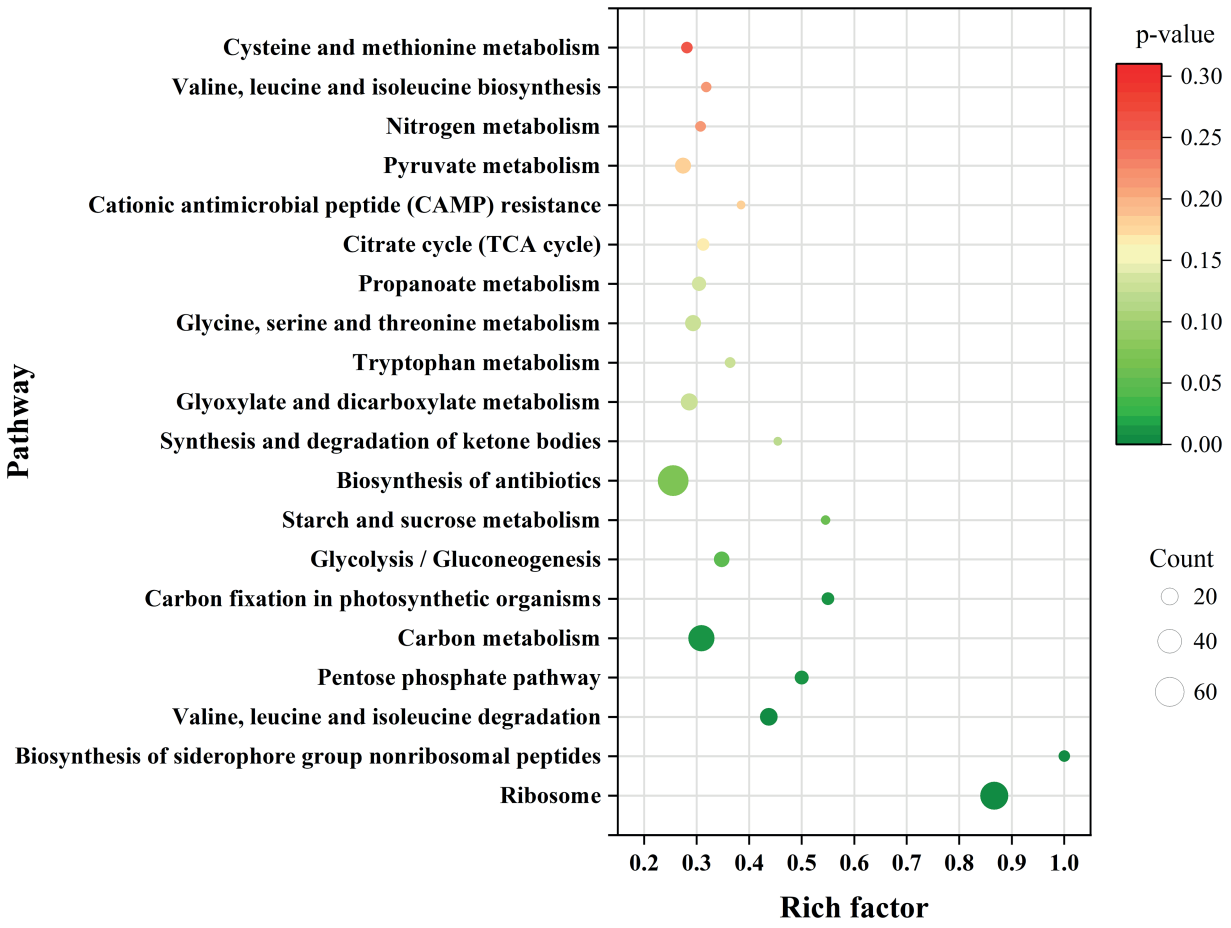

FIGURE 5
Scatterplot of top 20 KEGG pathway enrichment for differentially expressed genes (DEGs) in PD-pdeR. Data was displayed with the parameters of gene count, gene ratio and value of *p*.

pdeR overexpression promoted ATP synthesis in *Paracoccus denitrificans* PD1222

In order to explore the underlying mechanism of PdeR promoting biofilm formation, we performed further in-depth data mining on transcription analysis results, mainly focused on the energy production related pathways, including amino acid degradation, carbon metabolic pathways, fatty acid degradation and oxidative phosphorylation. As shown in Figure 6, taking leucine degradation as an example, leucine is catabolized to acetyl-CoA catalyzing by a series of enzymes, and genes encoding these enzymes were all up-regulated in PD-pdeR (detailed different expression values are listed in Supplementary Table S1), suggesting PdeR promoted amino acids degradation. Meanwhile, fatty acid degradation was promoted as well. The transcriptome analysis indicated the expressional level of key enzymes involved in β-oxidation was up-regulated, including 3-hydroxyacyl-CoA dehydrogenase (EC: 4.2.1.17) and 3-hydroxyacyl-CoA dehydrogenase (EC: 1.1.1.35). The up-regulated amino acids and fatty acids degradation yielded more NADH, $FADH_2$ and acetyl-CoA which could enter the TCA cycle and oxidative phosphorylation to produce ATP.

Besides, the central carbon metabolism was also affected by PdeR. First, part of the key enzymes that participated in glycolysis was downregulated, such as glucokinase (EC: 2.7.1.2), pyruvate kinase (EC: 2.7.1.40), and pyruvate dehydrogenase (EC: 1.2.4.1 and EC: 2.3.1.12), and thus, the production of acetyl-CoA deriving from glycolysis was decreased (Figure 6). Besides, enzymes catalyzing critical steps of the pentose phosphate pathway that related to NADPH generation including EC: 1.1.1.49, EC: 3.1.1.31and EC: 1.1.1.44, were all inhibited in PD-pdeR (Figure 6). Nevertheless, the expressional level of genes related to three-, four-, five-, six-and seven-carbon compounds transformation was promoted, such as EC: 2.2.1.1 and EC: 5.1.3.1.

Moreover, enzymes involved in the oxidative phosphorylation pathway were also up-regulated in PD-pdeR, including the NAD-dependent dehydratase (also known as complex I, EC: 7.1.1.2 and EC: 1.6.99.3), the cytochrome c oxidase (also known as complex IV, EC: 1.9.3.1) and ATP synthase (also known as complex V, EC: 7.1.2.2), suggesting the ATP production in PD-pdeR was accelerated (Figure 6).

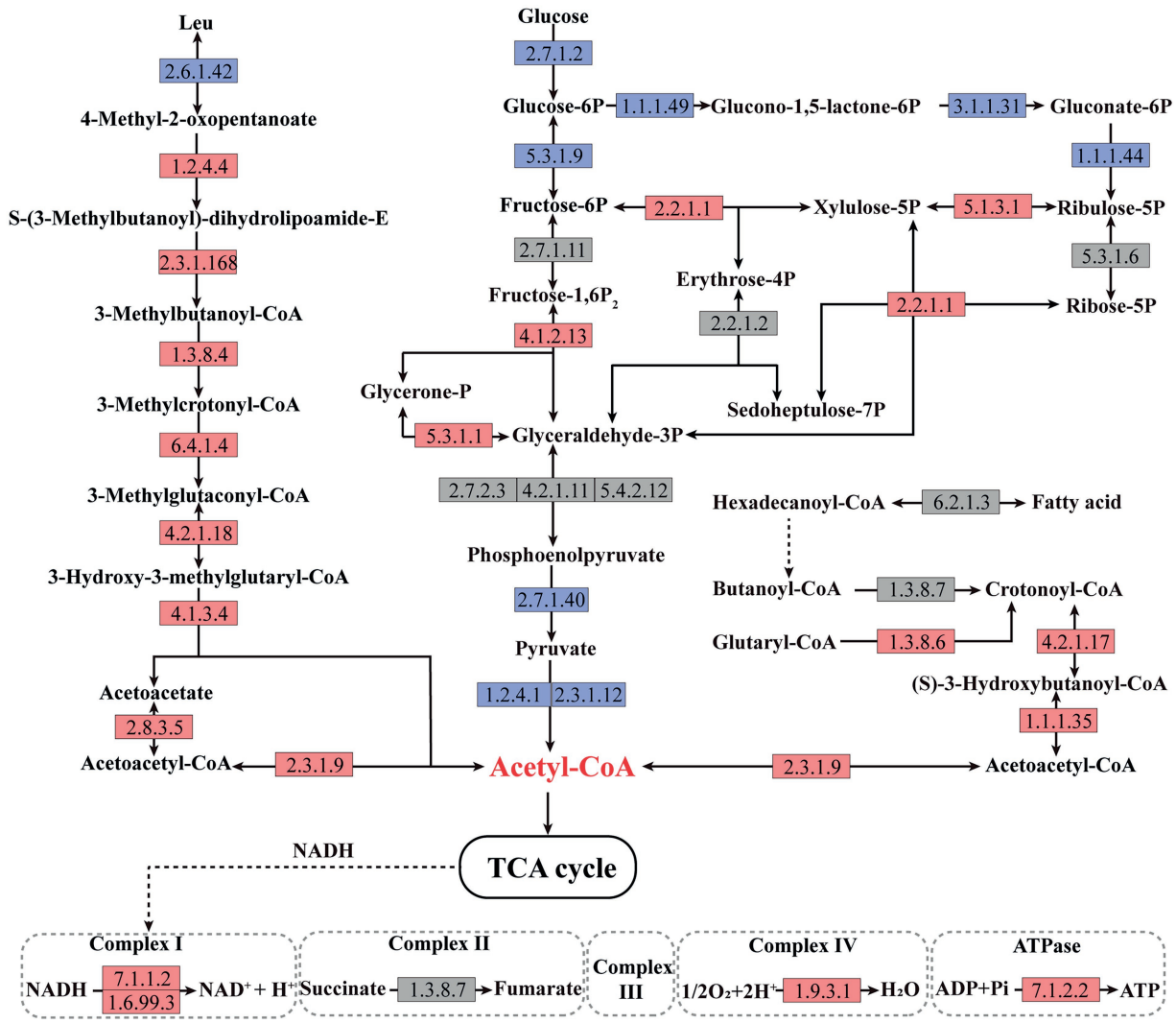

FIGURE 6
Schematic metabolic pathways of amino acid degradation, fatty acid degradation, central carbon metabolic and oxidative phosphorylation in *Paracoccus denitrificans* per the KEGG pathway database (https://www.genome.jp/kegg/pathway.html). The up-regulated, downregulated, and non-differentially expressed genes of the catalytic enzymes are marked with red, blue, and gray colors, respectively. The detailed different expression values could be found in Supplementary Table S1.

Subsequently, we detected the amount of acetyl-CoA and ATP in PD-pdeR as well as PD-pBBR, respectively. As shown in Figure 7A, neither PD-pdeR nor PD-pBBR had detected significant acetyl-CoA accumulation (all values were less than 1 nM/10^8 cells). We speculate that this may be because acetyl-CoA would be rapidly consumed after generating (Kremer et al., 2019). In contrast, compared with PD-pBBR, the cells of PD-pdeR contained more ATP (about 41.5 nM/10^8 cells), suggesting the overexpressed PdeR protein promoted ATP production (Figure 7B).

pdeR overexpression promoted iron absorption in *Paracoccus denitrificans* PD1222

Previous studies showed iron is essential for bacteria growth as well as biofilm formation (Banin et al., 2005; Kang and Kirienko, 2018). To obtain necessary iron, most bacteria secrete various iron-chelators, called siderophores, to efficiently chelate environmental iron (usually Fe^{3+}; Andrews et al., 2003). It has been shown *P. denitrificans* could produce a catechol siderophore, called parabactin, and its derivatives to seize iron from the environment (Tait, 1975). In *P. denitrificans*, parabactin is synthesized from chorismate catalyzed by a series of enzymes, including isochorismate synthase (EC: 5.4.4.2), isochorismatase (EC: 3.3.2.1), 2,3-dihydro-2,3-dihydroxybenzoate dehydrogenase (EC: 1.3.1.28) and nonribosomal peptide synthetase (EC: 6.3.2.14), which were all up-regulated in PD-pdeR strain as shown in Figure 8 (detailed values are displayed in Supplementary Table S1). Moreover, we also found several genes encoding iron transporters were all up-regulated in PD-pdeR, including the TonB-dependent iron transporters, ABC-type iron transporters, and heme transporters (Supplementary Table S2).

10.3389/fmicb.2022.966976

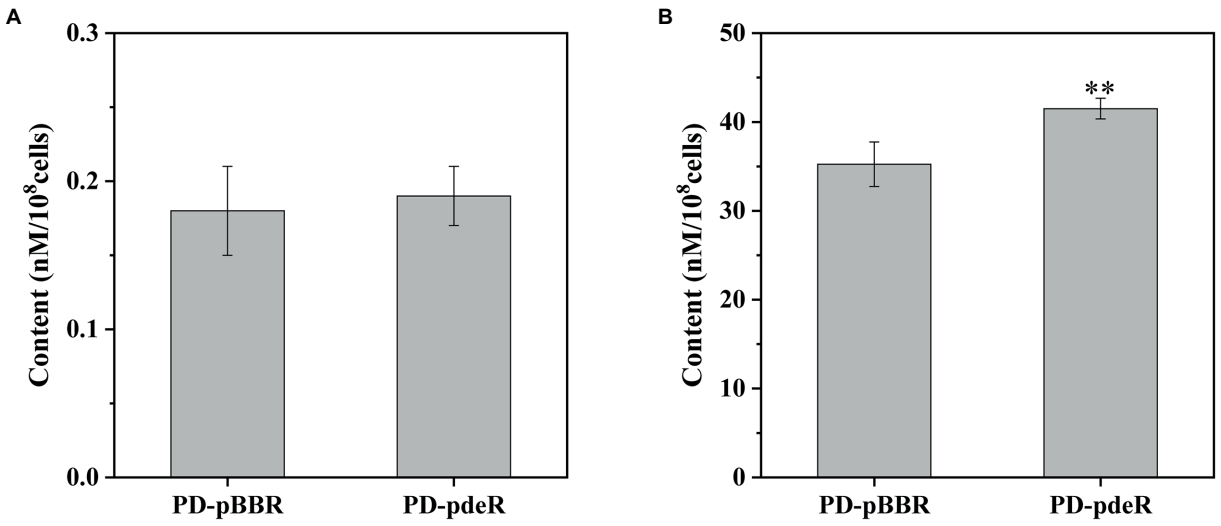

FIGURE 7
The content of acetyl-CoA **(A)** and ATP **(B)** in PD-pBBR and PD-pdeR. Cells were cultivated in LB medium and collected when OD_{600} was about 1.5. Data are presented as mean±SD, n=3. $^{**}p<0.01$ compared with the control strain PD-pBBR.

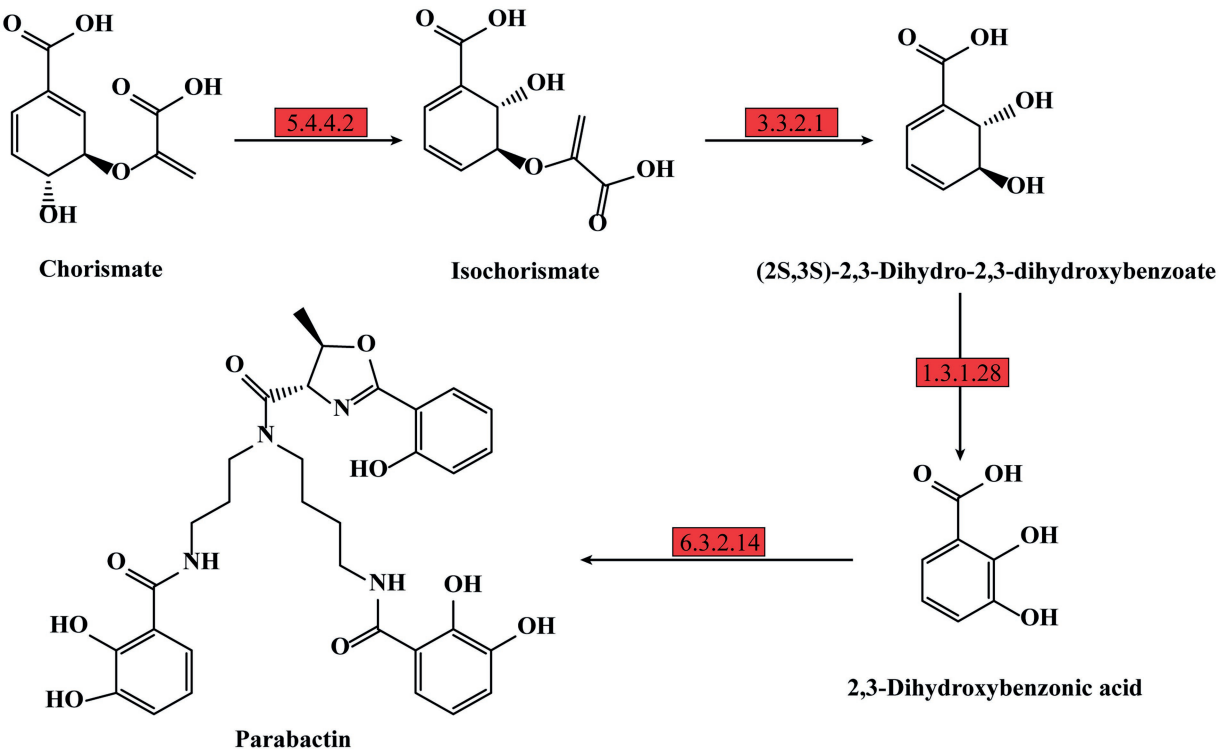

FIGURE 8
Schematic metabolic pathway of parabactin biosynthesis in *P. denitrificans* per the KEGG pathway database (https://www.genome.jp/kegg/pathway.html). The up-regulated expressed genes of the enzymes are marked with red, and the detailed different expression values could be found in Supplementary Table S2.

Next, we quantified the siderophore production of PD-pBBR and PD-pdeR at different growth stages using the Arnow test. Consistent with transcriptomic analysis, during growth, PD-pdeR did yield more siderophore (Figure 9A). Besides, we also examined the effect of 2,3-dihydroxybenzoic acid (DHBA) on bacterial biofilm formation. As the important product of siderophore

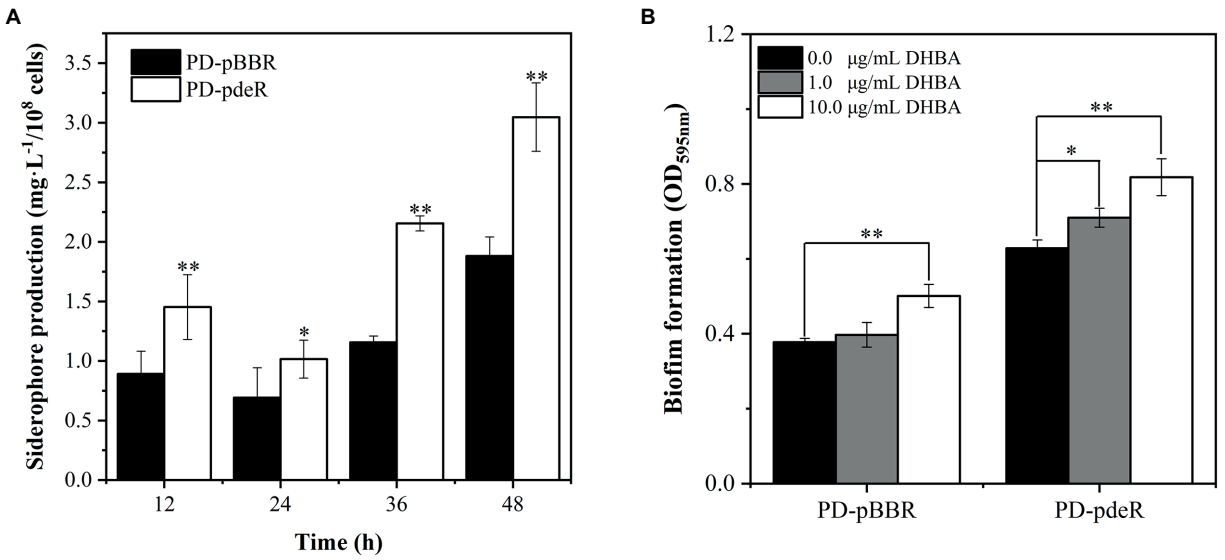

FIGURE 9
(A) Detection of siderophore production of PD-pBBR (black bar) and PD-pdeR (white bar) using Arnow test after 12, 24, 36 and 48h incubation, respectively. **(B)** The effect of DHBA addition on biofilm formation. The addition concentrations of DHBA were 0, 1 and 10μg/ml, and biofilm was detected after 36h incubation. Data are presented as mean±SD, n=3. *p<0.05, **p<0.01 compared with the negative control group.

biosynthesis pathway as well as a powerful iron-chelating molecule, addition of DHBA significantly promoted biofilm formation (Figure 9B). These results showed that *pdeR* overexpression promoted siderophore production and transportation, thus promoted iron absorption to form thicker biofilm.

Discussion

Paracoccus denitrificans is widely spread in either natural or artificial environments, functioning as a driver of the nitrogen cycle (Wang et al., 2021). To survive better, environmental bacteria usually exist in the form of biofilms. And it is well known that biofilm requires QS system regulation for its initiation and maturation (P. Stoodley et al., 2002). Previous studies showed *P. denitrificans* harbors a LuxI/R-type QS circuit, PdeI/R (Zhang et al., 2018). However, little is known about the role and regulation mechanism of QS on biofilm formation of *P. denitrificans* PD1222. In this study, we constructed the *pdeR* overexpression strain and performed phenotypic as well as global transcriptomic studies to provide information on the function of PdeR in *P. denitrificans* PD1222.

Results showed the *pdeR* overexpression strain PD-pdeR produced more EPS and formed thicker biofilm compared with the control strain PD-pBBR (Figures 2, 3). These results are in keeping with previous observational studies, for examples, the *lasI* mutant cells of *P. aeruginosa* could only form flat and undifferentiated biofilms (Davies et al., 1998); and in *Vibrio parahaemolyticus*, the lack of QS regulator protein AphA reduced the EPS production and thus hampered cells' ability of biofilm formation (Wang et al., 2013). To explore the molecular mechanism of PdeR promoting biofilm formation, we performed transcriptome sequencing analysis. As the results showed, PdeR is a global regulation factor, it could directly or indirectly control the expression of multiple genes which are involved in various metabolic pathways (Figures 4, 5). However, exactly which genes are the key contributing to biofilm initiation needs to be further explored.

In *P. denitrificans*, several molecules have been demonstrated with the ability to affect biofilm formation: that is, the adhesion protein BapA that initiates biofilm formation, the intracellular second messenger cyclic diguanosine monophosphate (Cyclic-di-GMP) and nitric oxide (Kumar and Spiro, 2017; Yoshida et al., 2017). However, these related genes' expressional levels were not affected by the overexpressed PdeR. Moreover, although three genes participating in O-Antigen nucleotide sugar biosynthesis pathway were up-regulated in PD-pdeR, the expressional level of other genes related to polysaccharide synthesis and flagella or pili assembly was not affected by PdeR much. Remarkably, we found that PdeR promoted a series of metabolic pathways participating in ATP production, including amino acids degradation pathway, fatty acid degradation pathway and oxidative phosphorylation pathway (Figure 6). Similarly to our findings, Pisithkul et al. had also reported during biofilm development in *Bacillus subtilis*, several metabolic alterations which were hitherto unrecognized as biofilm-associated had been detected, such as the tricarboxylic acid (TCA) cycle, fatty acid biosynthesis and degradation, etc. (Pisithkul et al., 2019). These results suggested bacteria tend to promote the degradation of organic substances and accelerate the production of energy during biofilm formation. This is understandable given the fact

that biofilm formation needs a large number of extracellular polysaccharides, proteins and a wide variety of secondary metabolites (Payne and Boles, 2016). The biosynthesis and transportation of these molecules are both energy-consuming, thus cells need to generate enough energy to support the synthesis and secretion of these essential substances (Sutherland, 2001). Consistently, we indeed detected higher ATP concentration in PD-pdeR strain cells, indicating PdeR promoted ATP production and thus benefit bacterial biofilm formation.

In addition to energy, siderophore, as the main tool bacteria used to obtain iron is also essential for bacterial growth as well as biofilm formation. Previous studies showed the growth rate of *B. subtilis* mutant strains that lack the function of siderophore biosynthesis was significantly inhibited (Rizzi et al., 2019). Qin et al. demonstrated that the siderophore biosynthetic genes mutant cells of *B. subtilis* showed reduced biofilm formation, while the addition of exogenous iron chelator DHBA could restore mutant strains' biofilm formation (Qin et al., 2019). And in *B. cepacia*, the production of siderophore ornibactin was affected by the *luxR* homolog *cepR* (Lewenza et al., 1999). Our results in this work are in accord with these previous studies indicating that the increased siderophore production and iron transportation is another key point of PdeR promoting bacterial biofilm formation.

In conclusion, PdeR plays a key role in promoting *P. denitrificans* biofilm formation, mainly through accelerating ATP production and increasing iron transportation at the initiation period. These data brought information about detailed mechanisms that may at least in part explain how QS regulates biofilm formation of *P. denitrificans*, adding to our understanding of QS regulation in biofilm development.

Data availability statement

The datasets presented in this study can be found in online repositories. The names of the repository/repositories and accession number(s) can be found at: https://www.ncbi.nlm.nih.gov/, bioproject: PRJNA847411.

Author contributions

NW and JG conceived and designed the experiments. NW and SX performed the experiments and carried out the analysis. NW drafted the manuscript. JG and GZ revised the manuscript. All authors were involved in the discussion of the results and in writing the manuscript. All authors contributed to the article and approved the submitted version.

Funding

This work was supported by the Beijing Natural Science Foundation (no. 5222025), the National Key Research and Development Program of China (no. 2018YFA090024-04) and the National Natural Science Foundation of China (no. 41501250).

Conflict of interest

The authors declare that the research was conducted in the absence of any commercial or financial relationships that could be construed as a potential conflict of interest.

Publisher's note

All claims expressed in this article are solely those of the authors and do not necessarily represent those of their affiliated organizations, or those of the publisher, the editors and the reviewers. Any product that may be evaluated in this article, or claim that may be made by its manufacturer, is not guaranteed or endorsed by the publisher.

Supplementary material

The supplementary material for this article can be found online at: https://www.frontiersin.org/articles/10.3389/fmicb.2022.966976/full#supplementary-material

References

Andrews, S. C., Robinson, A. K., and Rodríguez-Quiñones, F. (2003). Bacterial iron homeostasis. *FEMS Microbiol. Rev.* 27, 215–237. doi: 10.1016/s0168-6445(03)00055-x

Arnow, L. E. (1937). Colorimetric determination of the components of 3, 4-dihydroxyphenylalanine-tyrosine mixtures. *J. Biol. Chem.* 118, 531–537. doi: 10.1016/S0021-9258(18)74509-2

Banin, E., Vasil, M. L., and Greenberg, E. P. (2005). Iron and *Pseudomonas aeruginosa* biofilm formation. *Proc. Natl. Acad. Sci. U. S. A.* 102, 11076–11081. doi: 10.1073/pnas.0504266102

Bolhuis, H., Cretoiu, M. S., and Stal, L. J. (2014). Molecular ecology of microbial mats. *FEMS Microbiol. Ecol.* 90, 335–350. doi: 10.1111/1574-6941.12408

Davies, D. G., Parsek, M. R., Pearson, J. P., Iglewski, B. H., Costerton, J. W., and Greenberg, E. P. (1998). The involvement of cell-to-cell signals in the development of a bacterial biofilm. *Science* 280, 295–298. doi: 10.1126/science.280.5361.295

Dubois, M., Gilles, K. A., Hamilton, J. K., Rebers, P. A., and Smith, F. (1956). Colorimetric method for determination of sugars and related substances. *Anal. Chem.* 28, 350–356. doi: 10.1021/ac60111a017

Gilbert, K. B., Kim, T. H., Gupta, R., Greenberg, E. P., and Schuster, M. (2009). Global position analysis of the *Pseudomonas aeruginosa* quorum-sensing transcription factor LasR. *Mol. Microbiol.* 73, 1072–1085. doi: 10.1111/j.1365-2958.2009.06832.x

Hense, B. A., and Schuster, M. (2015). Core principles of bacterial autoinducer systems. *Microbiol. Mol. Biol. Rev.* 79, 153–169. doi: 10.1128/MMBR.00024-14

Hoiby, N., Bjarnsholt, T., Givskov, M., Molin, S., and Ciofu, O. (2010). Antibiotic resistance of bacterial biofilms. *Int. J. Antimicrob. Agents* 35, 322–332. doi: 10.1016/j.ijantimicag.2009.12.011

Ji, B., Yang, K., Zhu, L., Jiang, Y., Wang, H., Zhou, J., et al. (2015). Aerobic denitrification: A review of important advances of the last 30 years. *Biotechnol. Bioprocess Eng.* 20, 643–651. doi: 10.1007/s12257-015-0009-0

Jo, J., Price-Whelan, A., and Dietrich, L. E. P. (2022). Gradients and consequences of heterogeneity in biofilms. *Nat. Rev. Microbiol.* 21, 1–15. doi: 10.1038/s41579-022-00692-2

Kang, D., and Kirienko, N. V. (2018). Interdependence between iron acquisition and biofilm formation in *Pseudomonas aeruginosa*. *J. Microbiol.* 56, 449–457. doi: 10.1007/s12275-018-8114-3

Kovach, M. E., Elzer, P. H., Hill, D. S., Robertson, G. T., Farris, M. A., II, R. M. R., et al. (1995). Four new derivatives of the broad-host-range cloning vector pBBR1MCS, carrying different antibiotic-resistance cassettes. *Gene* 166, 175–176. doi: 10.1016/0378-1119(95)00584-1

Kremer, K., van Teeseling, M. C. F., Schada von Borzyskowski, L., Bernhardsgrutter, I., van Spanning, R. J. M., Gates, A. J., et al. (2019). Dynamic metabolic rewiring enables efficient acetyl coenzyme A assimilation in *Paracoccus denitrificans*. *mBio* 10, e00805–e00819. doi: 10.1128/mBio.00805-19

Kumar, S., and Spiro, S. (2017). Environmental and genetic determinants of biofilm formation in *Paracoccus denitrificans*. *mSphere* 2, e00350–e00317. doi: 10.1128/mSphereDirect.00350-17

Lewenza, S., Conway, B., Greenberg, E. P., and Sokol, P. A. (1999). Quorum sensing in *Burkholderia cepacia* identification of the LuxRI homologs CepRI. *J. Bacteriol.* 181, 748–756. doi: 10.1128/JB.181.3.748-756.1999

Livak, K. J., and Schmittgen, T. D. (2001). Analysis of relative gene expression data using real-time quantitative PCR and the 2−ΔΔCT method. *Methods* 25, 402–408. doi: 10.1006/meth.2001.1262

Mandel, M. J., and Dunn, A. K. (2016). Impact and influence of the natural Vibrio-squid Symbiosis in understanding bacterial-animal interactions. *Front. Microbiol.* 7, 1982. doi: 10.3389/fmicb.2016.01982

Mohammad Reza, S. (2018). Bacterial biofilm and its clinical implications. *Ann. Microbiol. Res.* 2, 45–50. doi: 10.36959/958/568

Morinaga, K., Yamamoto, T., Nomura, N., and Toyofuku, M. (2018). *Paracoccus denitrificans* can utilize various long-chain N-acyl homoserine lactones and sequester them in membrane vesicles. *Env. Microbiol. Rep.* 10, 651–654. doi: 10.1111/1758-2229.12674

Morinaga, K., Yoshida, K., Takahashi, K., Nomura, N., and Toyofuku, M. (2020). Peculiarities of biofilm formation by *Paracoccus denitrificans*. *Appl. Microbiol. Biotechnol.* 104, 2427–2433. doi: 10.1007/s00253-020-10400-w

Mukherjee, S., and Bassler, B. L. (2019). Bacterial quorum sensing in complex and dynamically changing environments. *Nat. Rev. Microbiol.* 17, 371–382. doi: 10.1038/s41579-019-0186-5

Orazi, G., and O'Toole, G. A. (2019). 'It takes a village': mechanisms underlying antimicrobial recalcitrance of polymicrobial biofilms. *J. Bacteriol.* 202, e00530–e00519. doi: 10.1128/JB.00530-19

Padmanabhan, A., Tong, Y., Wu, Q., Zhang, J., and Shah, N. P. (2018). Transcriptomic insights Into the growth phase-and sugar-associated changes in the exopolysaccharide production of a high EPS-producing *Streptococcus thermophilus* ASCC 1275. *Front. Microbiol.* 9:1919. doi: 10.3389/fmicb.2018.01919

Papenfort, K., and Bassler, B. (2016). Quorum sensing signal-response systems in gram-negative bacteria. *Nat. Rev. Microbiol.* 14, 576–588. doi: 10.1038/nrmicro.2016.89

Parsek, M. R., and Greenberg, E. P. (2005). Sociomicrobiology: the connections between quorum sensing and biofilms. *Trends Microbiol.* 13, 27–33. doi: 10.1016/j.tim.2004.11.007

Payne, D. E., and Boles, B. R. (2016). Emerging interactions between matrix components during biofilm development. *Curr. Genet.* 62, 137–141. doi: 10.1007/s00294-015-0527-5

Pisithkul, T., Schroeder, J. W., Trujillo, E. A., Yeesin, P., Stevenson, D. M., Chaiamarit, T., et al. (2019). Metabolic remodeling during biofilm development of *Bacillus subtilis*. *MBio* 10, e00623–e00619. doi: 10.1128/mBio.00623-19

Qin, Y., He, Y., She, Q., Larese-Casanova, P., Li, P., and Chai, Y. (2019). Heterogeneity in respiratory electron transfer and adaptive iron utilization in a bacterial biofilm. *Nat. Commun.* 10:3702. doi: 10.1038/s41467-019-11681-0

Rizzi, A., Roy, S., Bellenger, J.-P., and Beauregard, P. B. (2019). Iron homeostasis in *Bacillus subtilis* requires Siderophore production and biofilm formation. *Appl. Environ. Microbiol.* 85, e02439–e02418. doi: 10.1128/AEM

Sakuragi, Y., and Kolter, R. (2007). Quorum-sensing regulation of the biofilm matrix genes (pel) of *Pseudomonas aeruginosa*. *J. Bacteriol.* 189, 5383–5386. doi: 10.1128/JB.00137-07

Starosta, A. L., Lassak, J., Jung, K., and Wilson, D. N. (2014). The bacterial translation stress response. *FEMS Microbiol. Rev.* 38, 1172–1201. doi: 10.1111/1574-6976.12083

Steenackers, H. P., Parijs, I., Dubey, A., Foster, K. R., and Vanderleyden, J. (2016). Experimental evolution in biofilm populations. *FEMS Microbiol. Rev.* 40, 373–397. doi: 10.1093/femsre/fuw002

Stoodley, P., Sauer, K., Davies, D. G., and Costerton, J. W. (2002). Biofilms as complex differentiated communities. *Annu. Rev. Microbiol.* 56, 187–209. doi: 10.1146/annurev.micro.56.012302.160705

Sutherland, I. W. (2001). The biofilm matrix – an immobilized but dynamic microbial environment. *Trends Microbiol.* 9, 222–227. doi: 10.1016/S0966-842X(01)02012-1

Tait, G. H. (1975). The identification and biosynthesis of Siderochromes formed by Micrococcus denitrificans. *Biochem. J.* 146, 191–204. doi: 10.1042/bj1460191

Wang, N., Gao, J., Liu, Y., Wang, Q., Zhuang, X., and Zhuang, G. (2021). Realizing the role of N-acyl-homoserine lactone-mediated quorum sensing in nitrification and denitrification: a review. *Chemosphere* 274:129970. doi: 10.1016/j.chemosphere.2021.129970

Wang, N., Gao, J., Wang, Q., Xiao, S., and Zhuang, G. (2022). Antimicrobial peptide antibiotics inhibit aerobic denitrification via affecting electron transportation and remolding carbon metabolism. *J. Hazard. Mater.* 431:128616. doi: 10.1016/j.jhazmat.2022.128616

Wang, J., Jiao, H., Meng, J., Qiao, M., Du, H., He, M., et al. (2019). Baicalin inhibits biofilm formation and the quorum-sensing system by regulating the MsrA drug efflux pump in *Staphylococcus saprophyticus*. *Front. Microbiol.* 10:2800. doi: 10.3389/fmicb.2019.02800

Wang, L., Ling, Y., Jiang, H., Qiu, Y., Qiu, J., Chen, H., et al. (2013). AphA is required for biofilm formation, motility, and virulence in pandemic *Vibrio parahaemolyticus*. *Int. J. Food Microbiol.* 160, 245–251. doi: 10.1016/j.ijfoodmicro.2012.11.004

Yan, J., and Bassler, B. L. (2019). Surviving as a community: antibiotic tolerance and persistence in bacterial biofilms. *Cell Host Microbe* 26, 15–21. doi: 10.1016/j.chom.2019.06.002

Yoshida, K., Toyofuku, M., Obana, N., and Nomura, N. (2017). Biofilm formation by *Paracoccus denitrificans* requires a type I secretion system-dependent adhesin BapA. *FEMS Microbiol. Lett.* 364, 1–7. doi: 10.1093/femsle/fnx029

Yu, S., and Ma, L. (2017). Iron uptake and biofilm formation in *Pseudomonas aeruginosa*. *Sheng Wu Gong Cheng Xue Bao* 33, 1489–1512. doi: 10.13345/j.cjb.170140

Zhang, Y., Gao, J., Wang, L. S., Liu, S. J., Bai, Z. H., Zhuang, X. L., et al. (2018). Environmental adaptability and quorum sensing: Iron uptake regulation during biofilm formation by *Paracoccus denitrificans*. *Appl. Environ. Microbiol.* 84, e00865–e00818. doi: 10.1128/AEM.00865-18

frontiers | Frontiers in Microbiology

TYPE Review
PUBLISHED 12 August 2022
DOI 10.3389/fmicb.2022.955459

OPEN ACCESS

EDITED BY
Huancai Lin,
Sun Yat-sen University, China

REVIEWED BY
Zhejun Wang,
University of British Columbia, Canada
Anthonymuthu Selvaraj,
University of California,
Irvine, United States

*CORRESPONDENCE
Ling Zou
zouling@scu.edu.cn
Biao Ren
renbiao@scu.edu.cn

SPECIALTY SECTION
This article was submitted to Antimicrobials, Resistance and Chemotherapy, a section of the journal Frontiers in Microbiology

RECEIVED 28 May 2022
ACCEPTED 25 July 2022
PUBLISHED 12 August 2022

CITATION
Chi Y, Wang Y, Ji M, Li Y, Zhu H, Yan Y, Fu D, Zou L and Ren B (2022) Natural products from traditional medicine as promising agents targeting at different stages of oral biofilm development. *Front. Microbiol.* 13:955459. doi: 10.3389/fmicb.2022.955459

Natural products from traditional medicine as promising agents targeting at different stages of oral biofilm development

Yaqi Chi[1,2], Ye Wang[1,2], Mengzhen Ji[1,2], Yanyao Li[1,2], Hualing Zhu[1,2], Yujia Yan[1,2], Di Fu[1,2], Ling Zou[1,2]* and Biao Ren[1]*

[1]State Key Laboratory of Oral Diseases, National Clinical Research Center for Oral Diseases, West China Hospital of Stomatology, Sichuan University, Chengdu, China, [2]State Key Laboratory of Oral Diseases, National Clinical Research Center for Oral Diseases, Department of Endodontics, West China Hospital of Stomatology, Sichuan University, Chengdu, China

Oral cavity is an ideal habitat for more than 1,000 species of microorganisms. The diverse oral microbes form biofilms over the hard and soft tissues in the oral cavity, affecting the oral ecological balance and the development of oral diseases, such as caries, apical periodontitis, and periodontitis. Currently, antibiotics are the primary agents against infectious diseases; however, the emergence of drug resistance and the disruption of oral microecology have challenged their applications. The discovery of new antibiotic-independent agents is a promising strategy against biofilm-induced infections. Natural products from traditional medicine have shown potential antibiofilm activities in the oral cavity with high safety, cost-effectiveness, and minimal adverse drug reactions. Aiming to highlight the importance and functions of natural products from traditional medicine against oral biofilms, here we summarized and discussed the antibiofilm effects of natural products targeting at different stages of the biofilm formation process, including adhesion, proliferation, maturation, and dispersion, and their effects on multi-species biofilms. The perspective of antibiofilm agents for oral infectious diseases to restore the balance of oral microecology is also discussed.

KEYWORDS

natural products, antibiofilm effect, infection, microbiome balance, biofilm formation

Introduction

The oral cavity represents a favorable habitat for over 1,000 species of microorganisms, including viruses, bacteria, archaea, and fungi, due to its moist condition and suitable temperature (Marsh et al., 2011; Morse et al., 2018). Most oral microorganisms exist in the form of biofilms (Hu et al., 2019). Maintaining the ecological balance between the human host and intrinsic oral microorganisms is essential for oral health (Lof et al., 2017; Bacali et al., 2022). However, the dysbiosis of

oral microbiota may promote the growth of some pathogenic species to form the oral pathogenic biofilms, which cause many oral infectious diseases such as caries, apical periodontitis, and periodontitis (Lof et al., 2017). These diseases have highly increased economic pressure and seriously affected global public health (2020) (Olusanya et al., 2020).

In recent years, the overuse of antibiotics in infectious diseases has gradually challenged their clinical treatment due to the rapid increase in drug resistance (Tent et al., 2019). Moreover, the broad-spectrum antimicrobial effects of antibiotics have been proved to cause the microecological dysbiosis (Kuang et al., 2018). Therefore, many non-traditional treatments have been developed, such as the application of virulence disruptors, immunomodulators, phage therapies and so on (Tse et al., 2017). The natural products from traditional medicine have been proved to be one of the practical alterative for antibiotics in infectious diseases (Melander et al., 2020). The various functions, high safety and low cost of natural products also highlight their future broader application in clinical practice (Fan et al., 2021).

Oral infectious diseases are mainly caused by biofilms (Marsh and Zaura, 2017). To better understand the mechanisms and functions of natural products from traditional medicine against oral biofilms, we summarized and discussed the antibiofilm effects and mechanisms of natural products targeting at the different stages of oral biofilm formation. We also highlighted that restoring the balance of oral microecology without killing oral microorganisms broadly was a preferable way to develop new antimicrobial agents for oral infectious diseases.

Oral microbiome and its importance in oral cavity

According to the Human oral microbiome database (HOMD), there are nearly 150 genera and 700 prokaryote species in human oral cavity, and 96% of which are classified in six phyla (Gao et al., 2018). Over 250 species have been cultured and characterized; however, 20–60% of the species in the oral microbiome are unculturable currently. Some of the oral bacteria have been confirmed as the main pathogens of oral infectious diseases (Sedghi et al., 2021). For example, *Streptococcus mutans* and *Porphyromonas gingivalis* are considered as the key pathogens to cause caries and periodontitis, respectively. Beyond the bacterome, oral mycobiome is relatively rare (<0.1% in microbiome) and has not been well characterized (Baker et al., 2017). In recent years, large evidence proved the interaction between oral infectious diseases and oral microbiome, such as caries (Bowen et al., 2018), periodontitis (Lamont et al., 2018), and oral cancer (Irfan et al., 2020). Many systematic diseases, such as those from the gastrointestinal system and nervous system are also associated with oral microbial dysbiosis (Peng et al., 2022). The relationships between oral microbiome and oral or systematic health highlight the importance to maintain the balance of oral microbiome.

Mechanism of biofilm formation and its significance

Biofilms are composed of microbial cells living in a dynamic and structured manner as well as the three-dimensional (3D) extracellular matrix of polymeric substances such as exopolysaccharides, proteins, and nucleic acids (Klein et al., 2015). Oral biofilm development can be roughly divided into four steps: adhesion, proliferation, maturation, and dispersion (Figure 1). Initially, the planktonic cells reversibly adhere to the tooth surface or other niches in oral cavity. Then, they interact with polymeric substances to form an irreversible adhesion and build three-dimensional structures. Finally, the matured biofilm displays motility characteristics and disperses to other surfaces, starting the same cycle (Stoodley et al., 2002; Mann and Wozniak, 2012). Biofilms have higher virulence and reduced susceptibility to antimicrobial agents compared with planktonic microorganisms due to the following aspects: first, the abundance of extracellular polysaccharides in biofilms can surround the microbial cells, thus restricting the penetration of antibacterial agents (Ciofu et al., 2017); second, the gradient of the micronutrient composition of the biofilms allows opportunistic pathogens to survive in nutrient-limited areas where they may become dormant and resistant to antibiotics (Ciofu et al., 2017); third, reciprocal, symbiotic, and antagonistic relationships occur among different species in the biofilm community. Their interactions can be affected by the environment, nutrition, and other factors to promote the resistance of biofilms to antibacterial agents. Moreover, the quorum sensing (QS) systems activated in the biofilm also increase the virulence and survival rate of biofilm microorganisms (Marsh et al., 2011; Hu et al., 2019). Thus, biofilm infection is more difficult to control and it is necessary to find new approaches for the treatment and prevention of biofilm infection.

Advantages of antibiofilm therapy

Antibiofilm therapies are highly effective in controlling oral biofilm infections. For example, the usage of tetracycline, doxycycline, and minocycline in the clinical treatment of periodontitis resulted in a great effect on the primary outcome (probing pocket depth, PPD; Matesanz-Pérez et al., 2013). Except the antibiotics, many other therapies, including surgical therapy, bacteriophages and natural products, are also available to control oral biofilm infections with different specific advantages (Tse et al., 2017). Natural products, especially those from traditional medicine, are available from wide sources with various biological activities, which are well practical resources for oral biofilm control (Melander et al., 2020). Natural products have already been applicated in clinical practice for hundreds of years, thus, they are more cost-effective and safe in the controls of biofilm infections (Atanasov et al., 2021).

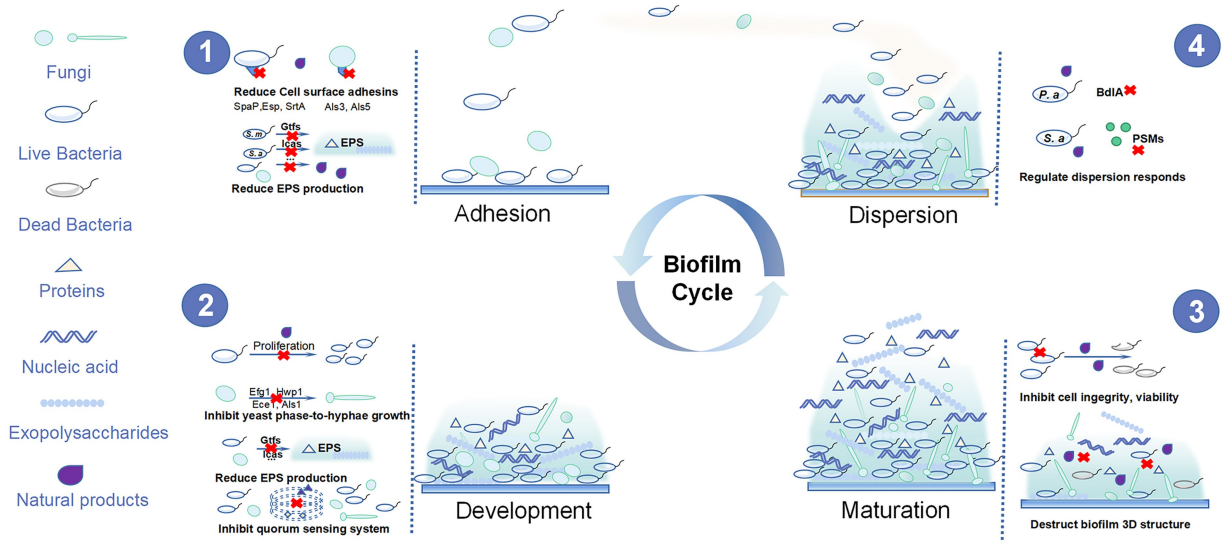

FIGURE 1
The four steps of oral biofilm formation and the anti-oral biofilm targets of natural products.

Antibiofilm effects and mechanisms of natural products targeting at the different stages of biofilm formation

Natural products have become a hot research topic in recent years due to their promising antibacterial effects and various mechanisms. Many natural products have shown effective potential in inhibiting oral biofilms and controlling biofilm-related diseases, such as caries and periodontitis (Zheng et al., 2011). However, the pharmacological mechanisms of most natural products are not fully elucidated, and their mechanisms of inhibiting biofilm formation may be quite different from those of inhibiting the planktonic microorganisms. Biofilm development can be roughly divided into four stages: adhesion, proliferation, maturation, and dispersion. Here, we summarized and discussed the natural products targeting at the different stages of oral biofilm development (Table 1).

Targeting at the cell colonization and adhesion

Adhesion is the initial step in biofilm formation and preventing the adhesion is the key strategy in controlling biofilm-related diseases. Oral microbial cells are reversibly attached to solid or non-solid surfaces and are further encapsulated by extracellular polymeric substances (EPS). The microcolonies formed by microorganisms and EPS are a hallmark feature of biofilms (Nadar et al., 2022). The interaction between microorganisms and substratum through specific protein receptors is essential during the adhesion process. Thus, the disruption of the interaction between microorganisms and substrate surfaces (such as cell surface-associated adhesins, EPS) can effectively prevent biofilm formation.

Effect of natural products on cell adhesion

Natural products have strong anti-adhesion effects on both bacteria and fungi. For some gram-positive oral bacteria, such as *Streptococcus* spp. and *Staphylococcus* spp., previous studies have shown that curcumin and tea extracts had excellent anti-adhesion effects. Curcumin, a natural product isolated from *Curcuma longa* (turmeric), decreased *Streptococcus mutans* adhesion to glass at a concentration of 8 μg/ml (Song et al., 2012) and inhibited 34–66% adhesion of *Staphylococcus aureus* to human keratinocytes (HaCaT) at 4.375 μmol/l (Sardi et al., 2017). Tea catechin epigallocatechin gallate (EGCG), a polyphenol extracted from tea, inhibited *S. mutans* adhesion in a dose-dependent manner at 7.8–31.25 μg/ml and reduced cell adhesion by 98.33% at 2 h (Xu et al., 2012). Similarly, the inhibition rate of emodin, an anthraquinone isolated from Chinese rhubarb, was 65% at the concentration of 4 μg/ml (Xiang et al., 2017). More importantly, natural products have also shown an excellent anti-adherent effect on antibiotic-resistant strains such as methicillin-resistant *Staphylococcus aureus* (MRSA). Curcumin showed an inhibitory effect at 8.65 μmol/l against MRSA (Sardi et al., 2017). For gram-negative oral species, EGCG showed a dose-dependent inhibition on *Porphyromonas gingivalis* adhesion at a concentration of 25–62.5 μg/ml (Fournier-Larente et al., 2016), whereas it inhibited *Fusobacterium nucleatum* adhesion at 125 μg/ml (Ben Lagha et al., 2017). Natural products can also inhibit the adhesion of oral fungi. Raspberry extracts (fruit of a shrub in Europe and northern Asia) exhibited a strong anti-adhesion effect on *Candida* spp. at

TABLE 1 Anti-oral biofilm natural products and their molecular mechanisms.

Plant extracts/ compounds	Mechanism	Target bacteria	Antibiofilm effect	Reference
Propolis	Inhibiting SpaP and glycosyltransferases enzymes (GtfB, GtfC, GtfD)	*S. mutans*	Decreased adhesion rate and EPS production.	Veloz et al. (2016)
Curcumin	Inhibition of SrtA, Gbps, Gtfs, Ftfs gene expression.	*S. mutans*	Decreased biofilm viability: 84.059%. Decreased biofilm thickness and EPS production.	Li et al. (2020b)
Curcumin	Inhibition of SpaP, Gtfs, SrtA, ComCD, and LuxS gene expression.	*S. mutans*	Decreased EPS production and biofilm formation.	Li et al. (2018)
Curcumin	Inhibition of key adhesins (Als1 and Als3) gene expression, promotion of genes related to aggregation (Als5 and Aaf1).	*C. albicans*	Decreased biofilm formation, initial adhesion, and promotion of *Candida albicans* aggregation.	Alalwan et al. (2017)
Theaflavins	Inhibition of Gbps and Gtfs	*S. mutans*	Decreased virulence factors (adherence, acid production, and EPS production) and biofilm formation.	Kong et al. (2021)
Sodium new houttuyfonate	Inhibition of Gtfs, quorum sensing	*S. mutans*	Decreased biofilm formation, EPS production, and quorum sensing. (100 μg/ml).	Shui et al. (2021)
Sodium houttuyfonate	Inhibition of BdlA (biofilm dispersion regulator) and FliC (gene related to flagella-mediated swimming motility) gene expression and pyocyanin production.	*P. aeruginosa*	Decreased biofilm formation, virulence factors, and inhibition of biofilm dispersion.	Shao et al. (2013); Wang et al. (2019)
Sodium New Houttuyfonate	Inhibition of Ras1-cAMP-Efg1 pathway related genes.	*C. albicans*	Decreased biofilm formation, adhesion, and change in the morphology of cells.	Wu et al. (2020)
EGCG	Inhibition of Gtfs, Ftfs gene expression.	*S. mutans*	Decreased biofilm viability:97% (4.4 mg/ml) and decreased EPS production.	Schneider-Rayman et al. (2021)
Green tea extract and EGCG	Inhibition of genes related to host colonization (FimA, HagA, HagB), tissue destruction (RgpA, Kgp), and heme acquisition (Hem).	*P. gingivalis*	Decreased biofilm initial adhesion and quorum sensing.	Fournier-Larente et al. (2016)
Tea extract/EGCG	Inhibition of H_2S production.	*F. nucleatum*	Decreased biofilm formation, adhesion; inhibition of the growth and hemolysis and hydrogen sulfide production	Ben Lagha et al. (2017)
Water extract of *Galla chinensis*	Inhibition of IcaABD, YycFG gene expression and carbohydrate metabolic processes.	MRSA	Decreased biofilm formation and EPS production.	Wu et al. (2019)
Aloe-emodin	Inhibition of extracellular proteins and PIA production.	*S. aureus*	Decreased adherence, extracellular matrix production and biofilm formation.	Xiang et al. (2017)
Emodin	Inhibition of biofilm-related genes (DltB, SarA, SrtA, AgrA, IcaA, CidA).	*S. aureus*	Decreased biofilm formation and eDNA (importance to initial adherence) level.	Yan et al. (2017)
Baicalin	Inhibition of genes related to acid production (Idh), quorum sensing (ComX), and biofilm formation (FtsZ, GtfC, GbpB VicR, LuxS and BrpA)	*S. mutans*	Decreased acid production and biofilm formation.	Elango et al. (2021)
Baicalin	Inhibition of virulence-related gene expression and suppression of T3SS *via* PqsR of the PQS System	*P. aeruginosa*	Decreased virulence factors, especially T3SS.	Zhang et al. (2021a)
Berberine	Inhibition of SrtA and esp. gene expression.	*E. faecalis*	Decreased biofilm formation and promotion of biofilm dispersion.	Chen et al. (2016)
Berberine	Inhibition of the aggregation of PSMs into amyloid fibrils.	MRSA	Decreased biofilm formation and extracellular amyloid fibrils production.	Chu et al. (2016)
Allicin	Inhibition of Hwp1 gene expression.	*C. albicans*	Decreased biofilm formation.	Khodavandi et al. (2011)

(Continued)

TABLE 1 Continued

Plant extracts/ compounds	Mechanism	Target bacteria	Antibiofilm effect	Reference
Farnesol	Inhibition of the Ras1-Cdc35-PKA-Efg1 pathway	*C. albicans*	Decreased hypha formation.	Davis-Hanna et al. (2008)
Luteolin	Inhibition of Agr quorum sensing system	*S. aureus*	Decreased biofilm formation and initial adhesion.	Yuan et al. (2022)
Quercetin	Inhibition of quorum sensing system related gene expression (LasI, LasR, RhlI and RhlR)	*P. aeruginosa*	Decreased biofilm formation and virulence factors (pyocyanin, protease and elastase).	Ouyang et al. (2016)
Coumarin compound DCH	Competitively bind to the arginine repressor ArgR.	MRSA	Decreased biofilm formation.	Qu et al. (2020)
Rhodiola rosea	Inhibition of Gtfs gene expression and quorum sensing system.	*S. mutans*	Decreased biofilm formation and EPS production.	Zhang et al. (2020a)
Paeoniflorin	Inhibition of LuxS/AI-2 system.	*S. suis*	Decreased biofilm formation and EPS production.	Li et al. (2021)
Macaranga tanarius	Inhibition of hypha/biofilm-related genes (Ece1 and Hwp1) and reduction in cell aggregation.	*C. albicans*	Decreased biofilm formation.	Lee et al. (2019)

100 μg/ml (Dutreix et al., 2018), and curcumin prevented *Candida albicans* adhesion at 50 μg/ml (Alalwan et al., 2017).

Anti-adhesion mechanisms of natural products

Reduction in cell surface adhesins

SpaP (also known as antigen I/II, Pac, P1, and antigen B) represents a series of proteins that contribute to cell-surface adhesion and can be encoded by the SpaP genes in oral bacteria (Brady et al., 2010). Propolis is a resinous substance collected by bees. SpaP gene expression in *S. mutans* was reduced by nearly 80% after being treated with 0.1 μg/ml polyphenol-rich extract from propolis (PEP), which was even better than chlorhexidine (CHX), a commonly used cation antimicrobial agent in oral cavity (Veloz et al., 2016). Similarly, the expression of SpaP gene in *S. mutans* was downregulated approximately one-fold after being treated with curcumin, which was similar with CHX (Li et al., 2018). Baicalin is a hydroxy-flavone extracted from the genus *Scutellaria*. SpaP gene expression of *S. mutans* was downregulated after baicalin treatment, indicating the ability of baicalin to reduce oral bacterial cell adhesion (Elango et al., 2021).

Glucan binding proteins (Gbps) can mediate bacterial aggregation. GbpB is crucial in the initial sucrose-dependent biofilm formation and cell shape maintenance in *S. mutans* (Duque et al., 2011). Gbps is also an essential protein involved in cell-surface adhesion (Zhu et al., 2009). Theaflavins (TFs), a bioactive component of black tea (Zhang et al., 2020c), inhibited GbpB and GbpC gene expression in *S. mutans* during its biofilm formation (Kong et al., 2021). Curcumin also decreased GbpB gene expression in *S. mutans* biofilm by approximately 0.5 times (Li et al., 2020b).

Sortase A (SrtA) is a membrane enzyme that facilitates the anchoring of surface proteins to the cell wall (Mazmanian et al., 2000). SrtA is a virulence factor in oral gram-positive species, including *Streptococcus* spp., *Staphylococcus* spp., and *Enterococcus* spp. (Cascioferro et al., 2014). SrtA in *S. mutans* is essential for sucrose-independent adhesion, which facilitates the antigen I/II and Gbps attachment to the cell wall (Scharnow et al., 2019), while the srtA gene expression in *S. mutans* was downregulated by approximately one-fold after curcumin treatment (Li et al., 2020b). SrtA in *Enterococcus* spp. has played a key role in bacterial survival and is the potential treatment target to combat *Enterococcus spp.* (Cascioferro et al., 2014). Berberine, one of the main alkaloids isolated from *Rhizoma coptidis*, inhibited SrtA gene expression by 50% compared with the control group at 80 μg/ml (Chen et al., 2016). SrtA in *Staphylococcus* spp. also acts as a catalyst for the adhesion of proteins (such as FnBPA and FnBPB) to the cell wall (Paterson and Mitchell, 2004). Kaempferol, a typical flavonol, inhibited both SrtA activity and cell adhesion at 64 μg/ml, suggesting that its inhibition of biofilm formation was achieved by inhibiting SrtA activity to weaken the adhesion of *S. aureus* (Ming et al., 2017).

Als family, a class of cell wall glycoproteins, regulates cell adhesion and biofilm formation in *C. albicans* (Xu et al., 2022). Als1 and Als3 proteins play a vital role in adhesion to host endothelial and epithelial cells. Als5 is related to the binding to host extracellular matrix proteins (Ponde et al., 2021). Curcumin treatment downregulated the Als1 and Als3 gene expression, while upregulated Als5, indicating that curcumin reduced cell adhesion but enhanced cell aggregation (Alalwan et al., 2017). Garlic, a member of the *Liliaceae* family, also exerted inhibitory effects on Als1 and Als3 from *C. albicans* (Fahim et al., 2022).

Esp is a key surface protein of *Enterococci* that regulates the initial adhesion of cells to the surface. Berberine treatment deceased its gene expression in *E. faecalis* at 80 μg/ml, indicating

the effectiveness of berberine in preventing *E. faecalis* cell adhesion (Chen et al., 2016).

Reduction in EPS generation

Extracellular polymeric substances is composed of proteins, polysaccharides, uronic acids, and nucleic acids, which significantly contribute to biofilm pathogenesis (Izadi et al., 2021). As a binding agent for initial bacterial adhesion, EPS also provides three-dimensional structure for oral biofilm. EPS can regulate the interactions among various bacterial species and protect the cells in the oral biofilm from antibiotics and environmental stresses (Lin et al., 2021). Thus, the inhibition of the EPS generation can be a promising target for the control of oral biofilm infection.

Extracellular polymeric substances of *S. mutans* is mainly produced by glucosyltransferases (Gtfs) and fucosyltransferases (Ftfs; Senadheera et al., 2005). Gtfs are a group of enzymes that split sucrose into glucose and fructose and then synthesize the EPS (Zhang et al., 2021b). Gtfs produce both insoluble and soluble glucans. GtfB produces insoluble glucans, GtfC can produce both insoluble and soluble glucans, while GtfD generates soluble glucans (Paes Leme et al., 2006; Wang et al., 2021). Insoluble glucans facilitate cell adhesion and provide a 3D structure in the biofilm, and soluble glucans act as an energy source and contribute to a low-pH microenvironment (Zhang et al., 2021b). Ftfs are encoded by the ftf gene, and they contribute to convert sucrose into extracellular fructose homopolymers (Burne and Penders, 1994).

Epigallocatechin gallate was able to inhibit EPS production as GtfBC gene expression of *S. mutans* were reduced by 77–90% at a sub-MIC concentration of 0.55 mg/ml (Schneider-Rayman et al., 2021). The Ftf gene expression of *S. mutans* was also downregulated by 70% after EGCG treatment for 24 h at this dosage (Schneider-Rayman et al., 2021). Sodium new houttuyfonate (SNH), a sodium bisulfite of houttuynia isolated from *Houttuynia cordata*, also showed an excellent ability to reduce EPS production. GtfBC of *S. mutans* was downregulated after the SNH treatment at 100 μg/ml (1/2 MIC), and GtfB expression was even downregulated by >50% (Shui et al., 2021). Curcumin treatment for 5 min was also downregulated the Ftf gene expression of *S. mutans* by 0.541-fold (Li et al., 2020b).

Staphylococcus spp. produce polysaccharide intercellular adhesin (PIA) to regulate their biofilm formation (Mack et al., 1994). PIA is encoded by a group of genes, including IcaADBC and the regulatory gene IcaR (Heilmann et al., 1996). Similar to EPS produced by *Streptococcus*, PIA is essential in the whole process of biofilm formation (Nguyen et al., 2020). In particular, PIA contributes to the hydrophobicity of *Staphylococcus epidermidis* and *S. aureus* cell surface and regulates the their initial adhesion during the biofilm formation (Nuryastuti and Krom, 2017). *Galla chinensis*, a natural product isolated from *Rhus chinensis*, suppressed IcaABCD gene expression in *S. aureus* at 7.81 μg/ml (Wu et al., 2019), while IcaABCD gene expressions in *S. epidermidis* was downregulated by 0.1–0.7-fold when treated with propolis (Ong et al., 2019), indicating their capabilities of anti-adhesion effects and furtherly inhibitory activities on the biofilm formation of *S. aureus* and *S. epidermidis*.

Targeting at the biofilm formation

After the initial adhesion, the biofilm accesses the proliferation phase. In this phase, cells adhering to the surface continue to grow and produce EPS to form a biofilm matrix (Blackman et al., 2021). This structure provides a stable condition for microorganisms in the biofilm. The QS system represents the intercellular signaling in bacteria community, which regulates gene expression and actions in response to local cell density during the formation of the biofilm (Parsek and Greenberg, 2005).

Antibiofilm effect of natural products on biofilm formation

Natural products exerted a strong antibiofilm effects and reduced the total biomass of biofilm formation. *Punica granatum*, the pomegranate fruit, inhibited *S. mutans* biofilm formation by 94.76% at 1.56 mg/ml (Gulube and Patel, 2016). Biofilm formation of *S. aureus* was reduced by 45% after berberine treatment at 256 μg/ml (Guo et al., 2015), and coumarin can inhibit MRSA biofilm formation in a dose-dependent manner (0.25–4 μg/ml; Qu et al., 2020). Theaflavins, the major ingredients of tea polyphenols, reduced *P. gingivalis* biofilm formation by 50% at 1,000 μg/ml (Kong et al., 2015), while *thymoquinone*, the major component of black cumin essential oil, significantly inhibited *F. nucleatum* biofilm formation (Tada et al., 2020). The biofilm formation of *C. albicans* was completely inhibited by the treatment of 150 μM magnoflorine (an aporphine alkaloid; Kim et al., 2018).

Mechanisms inhibiting oral bacterial biofilm formation

Inhibition of cell proliferation and killing bacterial cells

Many natural products have microbiocidal properties on planktonic cells through various ways, including cell wall decomposition (Zhang et al., 2020b), cell membrane disruption (Abram et al., 2013), leakage of cell contents (Kang et al., 2015), inhibition of the synthesis of proteins and DNA (Fathima and Rao, 2016), and blockage of cell metabolism (Belenky et al., 2015). The bacterial cells on the surface of the biofilm can also be eradicated by natural products, then inhibit bacterial cell proliferation and biofilm formation. *Rhodiola rosea,* a medicine plant, reduced the viability of *S. mutans* by >99% (Zhang et al., 2020a). EGCG reduced the cell viability of *P. gingivalis* by 40% at 5 mg/ml, and the ratio of live cells were also significantly decreased after the exposure to EGCG (Asahi et al., 2014), which was result of the reduction in biofilm biomass.

Reduction in EPS Production

Extracellular polymeric substances, the major component of the biofilm, is not only pivotal in the adhesion process of cells to

the surface but also important to the whole process of biofilm formation (Flemming and Wingender, 2010), thereby natural products which are capable to reduce the genes related to EPS generation (including Gtfs and Icas) can contribute to both inhibition of cell adhesion and biofilm formation. *Rhodiola rosea* reduced the total EPS *in S. mutans* biofilm at 0.25 μg/μL (Zhang et al., 2020a). *G. chinensis* inhibited EPS production of *S. aureus* biofilm by 44% at 7.81 μg/ml (Wu et al., 2019). The EPS inhibition of these natural products contributes to the total biofilm biomass reduction.

Inhibition of the QS system

The QS system regulates the bacterial behavior through small signaling molecules at the whole population levels, and this system is essential for biofilm formation in both gram-negative and gram-positive species (Abisado et al., 2018). The QS system can recognize the changes in the population density to regulate virulence factors (Holm and Vikström, 2014). The molecular mechanisms of the QS system are different in Gram-positive and Gram-negative species (Rutherford and Bassler, 2012; Papenfort and Bassler, 2016).

There are two main QS systems in the *S. mutans*: CSP-ComDE and ComRS systems (Kaur et al., 2015). The CSP-ComDE system is composed of a signal peptide (CSP, encoded by ComC; Leung et al., 2015) and the ComDE two-component system (Kaur et al., 2015; Figure 2). The ComRS system consists of the signaling peptide pheromone XIP (encoded by ComS) and a transcriptional regulator (ComR). The XIP interacts with and activates ComR to regulate the expression of ComX (Wenderska et al., 2017). *Rhodiola rosea* downregulated the ComDE gene expression at 0.25 mg/ml (Zhang et al., 2020a), while the gene expression of ComD was suppressed by >50% under SNH treatment at 100 μg/ml (Shui et al., 2021). Baicalin was able to inhibit ComX gene expression at 500 μg/ml (Elango et al., 2021).

The accessory gene regulator (Agr) system is a key QS pathway in *S. aureus*, which is also common in gram-positive bacteria and essential for their virulence (Le and Otto, 2015). The Agr system contains four elements: AgrA, AgrB, AgrC, and AgrD (Figure 3; Schilcher and Horswill, 2020). Emodin reduced the expression of AgrA gene by 2.2 folds at 4 μg/ml (Yan et al., 2017). Luteolin, a bioactive component in fruits and vegetables, decreased the pathogenesis of *S. aureus* through interference of the Agr system. The wild strain exhibited weaker virulence compared with △*AgrBCD*, including biofilm formation, initial adhesion, and virulence gene expression, suggesting that the Agr system is the target of luteolin against *S. aureus* (Yuan et al., 2022).

In gram-negative bacteria, such as *P. aeruginosa*, the autoinducer acyl-homoserine lactones (AHL) acted as QS molecule can bind to cytoplasmic receptors to regulate bacterial actions (Galloway et al., 2011). There are three key pathways in *the P. aeruginosa* QS system: two LuxI/LuxR-type QS pathways (Rutherford and Bassler, 2012) and the pseudomonas quinolone signal (PQS) system, named Las, Rhl, and Pqs (Guzzo et al., 2020; Figure 4). Quercetin (QCT), a flavonol extracted from vegetables and fruits, significantly suppressed the expression of LasI, LasR, RhlI, and RhlR, which were related to Las and Rhl pathways (Ouyang et al., 2016). Additionally, baicalin inhibited the Type III secretion system (a virulence factor for infection) through inhibiting the PQS system (Zhang et al., 2021a).

Mechanisms of inhibiting fungal biofilm formation

Candida albicans is a major opportunistic fungal pathogen in oral cavity and highly associated with several oral diseases, such as caries (especially root caries; Xiong et al., 2020; Du et al., 2021) and oral candidiasis (Zhou et al., 2021). Berberine induced a decrease in the viability of *C. albicans* biofilms with the actions on the integrity of plasma, mitochondrial membranes, and DNA (Da Silva et al., 2016). The viability rate of *C. albicans* after the treatment with berberine was reduced by 43.54% (Xie et al., 2020).

The hyphal form is an important phase of *C. albicans* biofilm formation and is the key virulence factor (Chen et al., 2020). Berberine inhibited the yeast to hyphae growth of *C. albicans* and significantly downregulated hypha growth-related gene expression (Efg1, Hwp1, Ece1, and Als1) at the sub-MIC concentration (8–128 μg/ml; Huang et al., 2020b). After SNH treatment, the transcriptome sequencing showed that the biofilm formation-related genes in the Ras1-cAMP-Efg1 pathway (Als1, Ala1, Als3, Eap1, Ras1, Efg1, Hwp1, and Tec1) were downregulated (Wu et al., 2020). The combination of garlic and bakuchiol significantly reduced Als3 and Sap5 gene expressions associated with hyphal growth (Fahim et al., 2022).

Farnesol and tyrosol are the major QS signaling molecules found in *C. albicans* (Davis-Hanna et al., 2008). Farnesol is an autoregulatory molecule that inhibits the yeast phase's transformation to the hypha phase (Xu et al., 2022). Farnesol is also widely distributed in propolis and fruits (Costa et al., 2021). Farnesol inhibited the hyphal growth by repressing Ras1-Cdc35-PKA-Efg1 pathway, indicating that farnesol is a promising molecule in inhibiting biofilm formation of *C. albicans* by interfering with the QS system (Davis-Hanna et al., 2008).

Eradication of mature biofilms

The EPS acts as a protective multifunctional scaffold in the mature biofilm (Flemming and Wingender, 2010). The cells in the biofilm are closely aggregated and facilitates interactions and food chains among proximal neighbors (Kuramitsu et al., 2007). In mature stage, biofilm shows an increased tolerance to antimicrobial agents (Cadena et al., 2019). For example, the minimum inhibitory concentration (MIC) of CHX to kill *Streptococcus sobrinus* in the established biofilm increased 300 times compared with planktonic cells (Shani et al., 2000). Therefore, many refractory infectious biofilm-related diseases caused by mature biofilms are difficult to remove (Noiri et al., 2002).

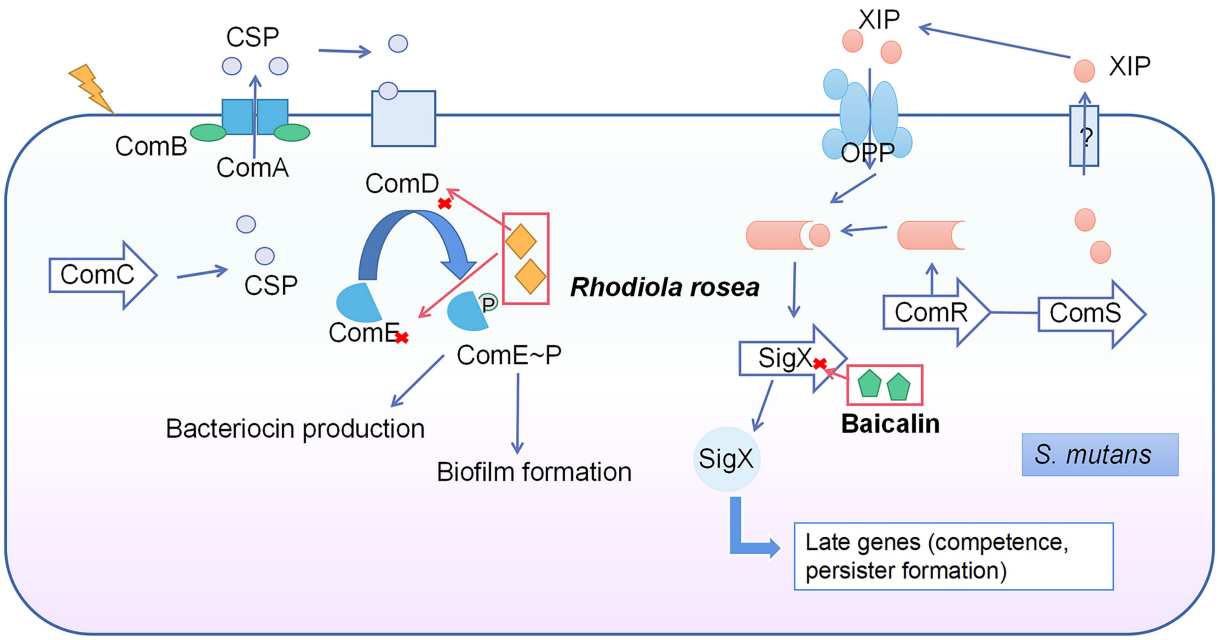

FIGURE 2
Quorum sensing system in *S. mutans* and the inhibitory effects of natural products on this system. The CSP-ComDE system is composed of a signal peptide (CSP, encoded by ComC) and the ComDE two-component system. During the cell density increase, the accumulated CSP interacts with ComD (membrane-bound histidine kinase receptor) directly to cause the phosphorylation and activation of ComE (the cytoplasmic response regulator). The activated ComE regulates the gene expression of bacteriocin production and biofilm formation. The ComRS system consists of signaling peptide pheromone (XIP, encoded by ComS) and a transcriptional regulator (ComR). The XIP interacts with and activates ComR to regulate the expression of ComX, and thus switches the genes related to competence and persister formation. *Rhodiola rosea* inhibited ComDE gene expression and baicalin inhibited ComX gene expression.

Natural products have the potential to remove mature microbial biofilms. Propolis was effective in eradicating *Candida.* spp. biofilms, which could eradicate 50% *Candida.* spp. biofilm with the concentration of 2.5% (Gucwa et al., 2018). Propolis also reduced the viability of *S. aureus* biofilm by 92.9% at a concentration of 125 μg/ml but did not decrease the total biomass. The results demonstrated that propolis penetrated the biofilm and killed the cells inside but did not decrease the total biomass of mature biofilms (De Oliveira Dembogurski et al., 2018). In another study, the treatment with propolis reduced *S. aureus* biofilm biomass by >50% at 200 μg/ml, and the thickness of biofilm decreased by 47–87% in different isolates (Bouchelaghem et al., 2022).

Inhibition of biofilm dispersion

When the nutrients are limited and waste products in the biofilm accumulate a lot, biofilm dispersion allows microorganisms to depart from biofilms and to colonize new niches (Solano et al., 2014). The biofilm dispersion made infection worse and hard to control, and even caused an acute infection, such as sepsis (Lister and Horswill, 2014). Sodium houttuyfonate was able to inhibit *P. aeruginosa* biofilm dispersion through the inhibition of chemotaxis transducer protein BdlA gene expression (a key gene that regulates the dispersion response of *P. aeruginosa*; Wang et al., 2019). Phenol-soluble modulins (PSMs) are biofilm-dispersion-associated factors related to *S. aureus* infection (Zheng et al., 2018). Berberine inhibited PSMs production as evidenced by the calculation of amyloid fibril formation (Chu et al., 2016). Reducing biofilm dispersion is of great significance in controlling infection spread in clinical practice (Rumbaugh and Sauer, 2020).

Combinational application of natural products and other strategies

Combination of natural products and nanoparticles

Nanoparticles have a significant potential in the delivery of drugs against oral biofilm due to their flexible properties (Benoit et al., 2019). Some natural products extracted by oil and ethanol, such as propolis and curcumin, have poor water solubility, which limits their clinical usage (Kubiliene et al., 2015). Nanoparticles can be designed to enhance drug solubility. Propolis-loaded poly (lactic-co-glycolic acid, PLGA) nanoparticles were synthesized to enhance the solubility of propolis, and this nanoparticles showed excellent antibiofilm effects on *C. albicans* (Iadnut et al., 2019). A combination of nanoparticles and natural products may result in synergistic antibiofilm effects due to the high surface area-to-volume ratios of nanoparticles (Shrestha and Kishen, 2016).

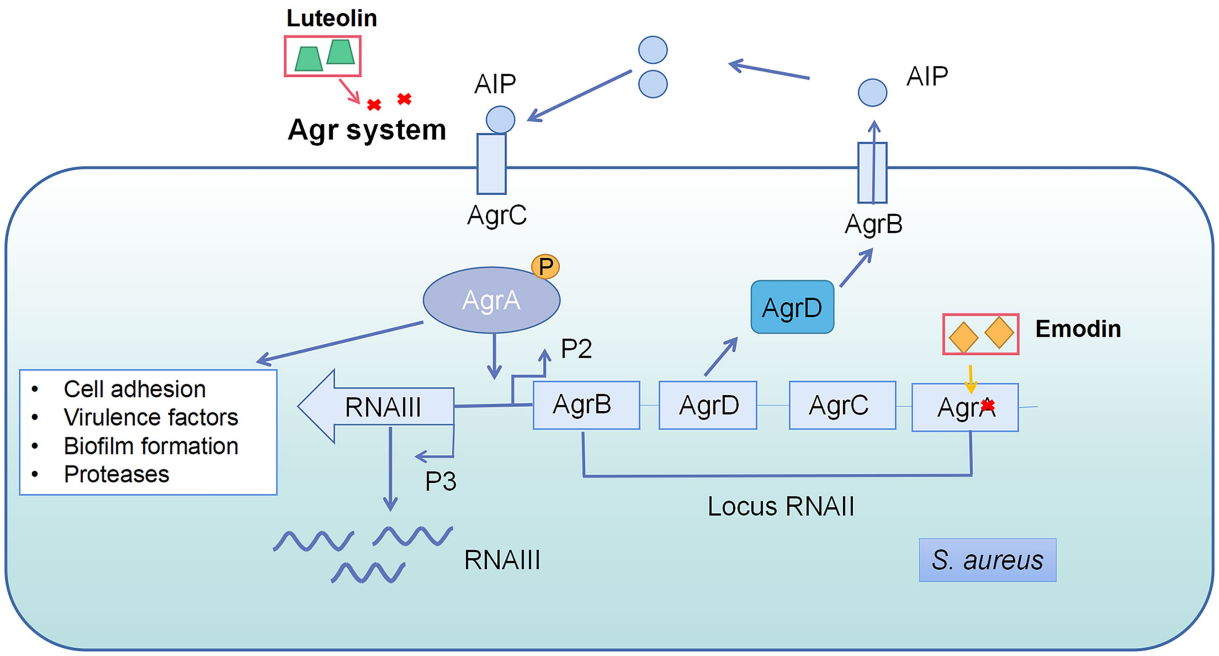

FIGURE 3
Quorum sensing system in *Staphylococcus aureus* and the interference of natural products on quorum sensing system. AgrD is the precursor of autoinducer peptides (AIP). AIP can be modified by AgrB and secreted into the matrix. AIP secreted by bacteria accumulates in the environment and binds to kinase receptors (AgrC) on the bacterial membrane to transmit signals, activating the related genes' expression, such as RNAII and RNAIII. RNAIII regulates most QS-related genes, while some genes are controlled by AgrA directly. Emodin inhibited AgrA gene expression and luteolin interfered Agr system.

Pterostilbene, a kind of *Vitis*-inducible phytoalexins, showed a much higher antibiofilm effect after being loaded in PLGA nanoparticles (Simonetti et al., 2019). Furthermore, the combination with nanoparticles extended the release time of natural products, which is important for long-term antibiofilm effects (Maghsoudi et al., 2017). For example, Berberine in nanoparticles exerted a better *S. aureus* biofilm removal ability than berberine alone, which might be attributed to the spontaneous adhesion property and continuous release characteristics of nanoparticles (Huang et al., 2020a). The integration of nanoparticles and natural products enhanced the efficacy of natural products for multifunction properties at the same time, providing a great potential in clinical applications (Yu et al., 2017, 2021).

Combination of natural products and antibiotics

The combination of products and antibiotics is a practical way to reduce the development of antibiotic resistance and also to reduce the toxicities or side effects of some antibiotics by decrease the antibiotic dosages against biofilms (Li et al., 2013; Zhu et al., 2021). Artemisinin, a famous antimalarial sesquiterpene lactone extracted from the traditional Chinese herb *Artemisia annua* L, was able to increase the cell membrane ergosterol levels of *C. albicans* to synergize with amphotericin B to inhibit *C. albicans* and oral candidiasis (Zhu et al., 2021). The combination of berberine and fluconazole showed synergic effects on *C. albicans* biofilms by enhancing the susceptibility of *C. albicans* to fluconazole. Interestingly, the antibiofilm effect was related to berberine in a concentration-dependent manner instead of fluconazole, indicating that berberine played a major role in the antifungal effect (Li et al., 2013). Similarly, natural products in combination can improve the antibiofilm properties in the elimination of mature biofilm. The combination of berberine and fusidic acid significantly inhibited cell viability in *S. aureus* mature biofilms, while the single drugs did not show any antibiofilm effects (Liang et al., 2014).

Combination of natural products and photodynamic therapy

Photodynamic therapy (PDT) is an effective method in cancer management (Li et al., 2020a), periodontitis (Manresa et al., 2018), and oral mucosal diseases (Cosgarea et al., 2020). In recent years, it has been demonstrated that PDT was able to enhance the activities of natural products, even on drug-resistant microorganisms. Many natural products have shown stronger antibiofilm effects in combination with PDT, such as emodin (Pourhajibagher et al., 2022), propolis (Afrasiabi et al., 2020), and curcumin (Santezi et al., 2018). The combination of curcumin and PDT is effective in infection control (Polat and Kang, 2021). Combination of curcumin and PDT reduced *P. aeruginosa* biofilm formation through interfering quorum sensing network, and

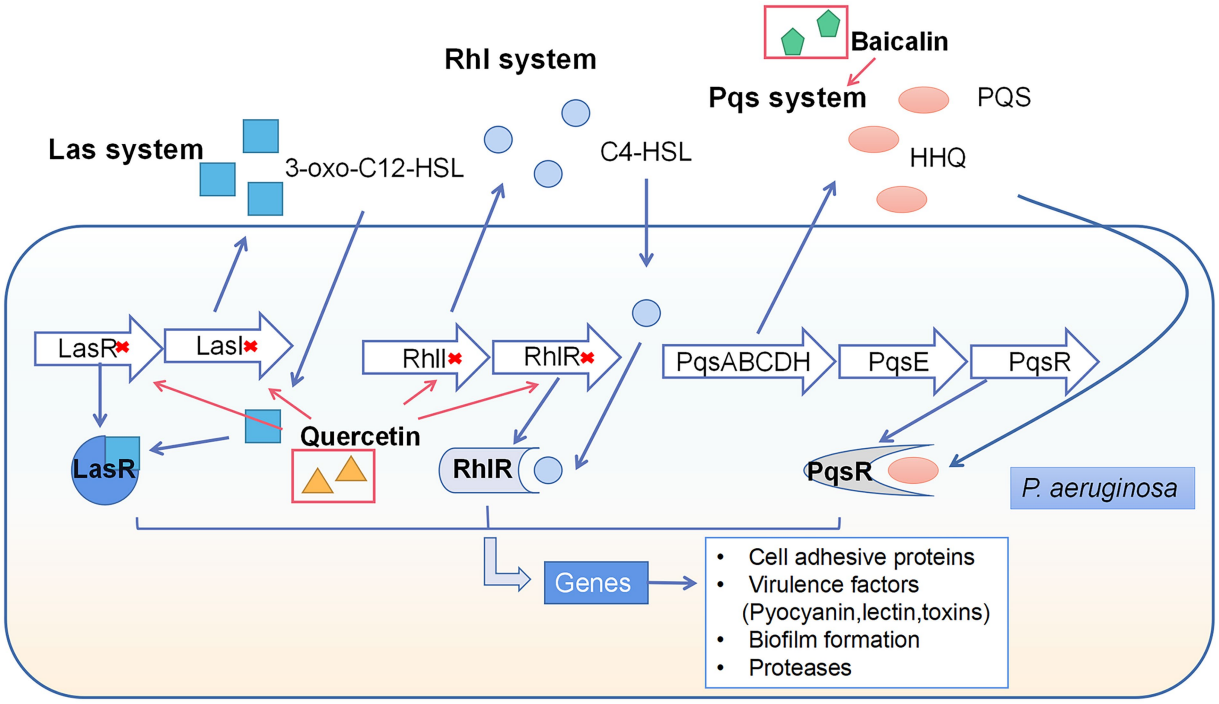

FIGURE 4
Quorum sensing system in *P. aeruginosa* and the interference of natural products on quorum sensing system. There are three key pathways in the *P. aeruginosa* QS system: two LuxI/LuxR-type QS pathways and the pseudomonas quinolone signal (PQS) system, named Las, rhl, and pqs. The synthesis of AI's 3-oxo-C12-HSL and C4-HSL is modulated by Las and Rhl, which serve as their autoinducers, respectively. In addition, alkyl-4-quinolones (AQs), including PQS and HHQ, are signal molecules in the PQS pathway. Interconnections between the three pathways regulate the activity of the QS system, resulting in changes in cell adhesive proteins, virulence factors, biofilm formation and proteases. Quercetin inhibited LasI, LasR, RhlI, RhlR gene expression and baicalin inhibited Pqs system.

importantly, the combination significantly enhanced antibiofilm effect compared with curcumin alone (Abdulrahman et al., 2020). The combination of natural products and PDT provides a new direction in managing biofilm-related oral infections.

Combination of two natural products

Propolis and carnosic acid (a compound extracted from rosemary) showed synergistic effects against *C. albicans*, while the 1:4 ratio of carnosic acid and propolis resulted in a best decrease in *C. albicans* survival rate and biofilm formation (Argüelles et al., 2020). Curcumin and berberine co-encapsulated in liposomes showed synergistic effects against MRSA by reducing their MICs by 87 and 96% compared with single drugs and the biofilm formation also significantly decreased (Bhatia et al., 2021). These results indicate that the combination of different natural products with different antimicrobial mechanisms can enhance their activities even on drug-resistant pathogens.

Effects of natural products on multi-species biofilms

Multi-species biofilms represent the most important lifestyle of oral microbes in oral cavity (Marsh et al., 2011; Yang et al., 2011). The interactions among microbes regulate the structure and function of biofilms and significantly influence the biofilm formation (Yang et al., 2011; Deng et al., 2019a,b). Microorganisms in the multi-species biofilm enhance the have metabolism efficient, tolerance to inhibitory agents and virulence (Marsh et al., 2011).

Natural products have shown effective activities in multi-species biofilms. Curcumin reduced the biomass and viability of *C. albicans* and *S. mutans* dual-species and mono-species biofilms. Interestingly, more eradication of *S. mutans* was found indicating that the effect of curcumin on *S. mutans* was enhanced in the *C. albicans* and *S. mutans* dual-species biofilm. Moreover, curcumin also blocked the EPS generation of *C. albicans* and *S. mutans* dual-species biofilm through the inhibitions on the QS system, EPS generation, and Als protein production (Li et al., 2019). Brazilian red propolis (BRP) showed an antibiofilm effect on multi-species biofilm composed of periodontopathogens (34 species). The metabolism of multi-species biofilms decreased to 45 and 55% after 800 μg/ml BRP and 0.12% CHX treatment, respectively. Biofilm cells were reduced to 10 and 5% after being treated with 1,600-μg/mL BRP and 0.12% CHX, respectively. In addition, BRP had a significant antibiofilm effect on species in the orange-complex group, while 0.12% CHX did not have such an effect (Miranda et al., 2019). BRP extract (400 μg/ml) also

exhibited an almost equal ability to that of amoxicillin (54 μg/ml) to remove red-complex of multi-species subgingival mature biofilms (De Figueiredo et al., 2020). These findings indicated its promising effects in periodontitis treatment.

In recent years, the microcosm biofilm model (consisting of natural oral microbiota) has been established to better simulate the *in vivo* oral cavity conditions (Garcia et al., 2021). *G. chinensis* extract inhibited biofilm formation in both nascent and mature microcosm biofilms, and the acid metabolism in biofilms was also inhibited (Cheng et al., 2011). *Coffea canephora* reduced mixed biofilms formed from the pooled human saliva by 15.2% at the concentration of 20% (Antonio et al., 2012). *Psidium cattleianum* leaf extract reduced *in situ* oral biofilms formation and EPS production at 167 mg/ml for 1 min per 12 h for 14 days treatment (Brighenti et al., 2012). Natural products contained in clinical products also showed antibiofilm effects on microcosm biofilms. *Myrcia bella* Cambess. and *Matricaria chamomilla* L. in the toothpastes reduced the bacterial number in the microcosm biofilms. The enamel demineralization assay revealed that *Vochysia tucanorum*, *Myrcia bella*, *Matricaria chamomilla*, and Myrrha & propolis toothpastes reduced mineral loss and lesion depth compared with the placebo group (Braga et al., 2022). Another study demonstrated that natural products (including Commiphora myrrha resin extract, propolis extract) in the commercial toothpastes reduced microcosm biofilm viability and increased mineral loss (Braga et al., 2019). These results indicated the clinical potential in the control of oral biofilms.

Natural products as an alternative treatment for oral infection

The strong antibiofilm effects of natural products on both mono-species biofilms and multi-species biofilms with various mechanisms highlight their clinical oral disease controls. Several *ex vivo* & *in vivo* studies and clinical trials have been implemented to evaluate the efficacity of natural products, especially in caries and periodontitis.

In dental caries, many natural products, such as propolis and sodium new houttuyfonate, were able to inhibit *S. mutans* biofilm virulence, EPS production and QS system (Veloz et al., 2016; Shui et al., 2021). Propolis inhibited *S. mutans* biofilm formation and dental caries development in a rat model (Duarte et al., 2006), while magnolol and honokiol extracted from magnolia bark reduced the biofilm formation by an *in vivo* Germ-kill model (Greenberg et al., 2007). Importantly, a randomized controlled trial also showed that magnolia bark have encouraging results in maintaining oral health by reducing *S. mutans* proliferation, plaque acidogenicity and bleeding on probing (Campus et al., 2011).

In periodontitis, the natural products EGCG showed a great antibiofilm effect on *P. gingivalis* (Fournier-Larente et al., 2016) and *F. nucleatum* (Ben Lagha et al., 2017). BRP extract (400 μg/ml) used in multi-species biofilms exhibited an almost equal ability to that of amoxicillin to eliminate the red-complex of multi-species subgingival mature biofilms which suggested its promising action in periodontitis treatment (De Figueiredo et al., 2020). The mouth rinses containing *Aloe vera* reduced the plaque and gingival inflammation and finally significantly reduced clinical scores indicating the potential application of *Aloe vera* in periodontitis (Laleman and Teughels, 2020).

Natural products have strong antibiofilm effects on key pathogens of other oral infectious diseases, and the diversity, efficiency and safety of natural products make them the alternative agents to antibiotics against biofilms even from the drug-resistant strains.

Prospects of maintaining oral microecology balance

The resident microflora in the oral cavity of healthy individuals has great significance in maintaining health, preventing foreign pathogens colonization and contributing to host physiology (Rosier et al., 2018). The oral microbiota in a healthy condition is more stable than other microbial communities (Zhou et al., 2013) and resists diseases (Rosier et al., 2018). However, many factors can disturb the balance, including systematic diseases, unhealthy diet, and poor oral hygiene, and the usage of broad spectrum antibiotics (Lamont et al., 2018). In caries, an unhealthy diet (fermentable carbohydrates in high amounts and frequency) often results in the accumulation of fermentation extract (organic acid; Lamont et al., 2018). When the acid caused the decrease in pH subsequently, the oral microbiota shifted toward the adaption of the low pH conditions and became the cariogenic microbiota (Pitts et al., 2017). It is important to restore the microecological balance instead of only killing the oral microbes indiscriminatingly (Baker et al., 2017).

BRP used in a periodontitis model showed an excellent antibiofilm effect on the red-complex and orange-complex species, but showed less effect on other species, indicating that this compound was less harmful to beneficial microorganisms (Miranda et al., 2019; De Figueiredo et al., 2020). Currently, the influence of natural products on the whole oral microflora and how does the microflora change after drug treatment remain unclear; however, natural products have shown potential to restore microecological balance compared with broad-spectrum antibiotics (Melander et al., 2020).

Discussion and future prospective

Biofilms represent the common form of microorganisms in the oral cavity and the dysbiosis of biofilms are highly related to many oral infectious diseases, such as caries and periodontitis (Marsh and Zaura, 2017). Natural products from traditional medicine are promising agents against oral biofilms due to their excellent antibiofilm effects, relatively low cost, and safety

(Atanasov et al., 2021). However, there are still many concerns on natural product applications in clinical practice. For example, many of them have low solubility, which greatly limits their usage. Meanwhile, the active ingredients of herbal medicines are complex, and currently, microbiocidal and antibiofilm mechanisms of most herbal medicines have not been fully elucidated. Although many studies performed clinical trials using many active ingredients such as tea, propolis, and *Aloe vera*, showing encouraging results (Laleman and Teughels, 2020), the toxicity to normal cells of natural products is another concern and need to be further explored. Previous study revealed the nephrotoxicity of traditional medicine (including anthraquinones and flavonoids; Yang et al., 2018), suggesting the necessity of a safety evaluation before the use of natural products in clinical practice.

Natural products have a broad prospective in oral clinical application. However, the effects of natural products on the local microbiota and their impact on the local microecological balance after drug treatment should be further explored. More clinical trials and safety test of natural products are also needed, while our review summarized and discussed the potential effects of natural products from traditional medicine against oral biofilms to highlight the importance of further investigations on natural products in treating oral infectious diseases.

Author contributions

YC wrote the original draft of the manuscript, compiled the tables, and made the figures. YW, MJ, YL, HZ, and YY collected the data. LZ and BR revised the manuscript. All authors contributed to the article and approved the submitted version.

Funding

This work was supported by grants from the National Natural Science Foundation of China (grant nos. 82071111, 81870778, 81991500, 81600858, and 81991501), the Project of the Science and Technology Department of Sichuan Province (grant nos. 2020YFSY0019 and 2021YFQ0064), and Applied Basic Research Programs of Sichuan Province (2020YJ0227).

Conflict of interest

The authors declare that the research was conducted in the absence of any commercial or financial relationships that could be construed as a potential conflict of interest.

Publisher's note

References

Abdulrahman, H., Misba, L., Ahmad, S., and Khan, A. U. (2020). Curcumin induced photodynamic therapy mediated suppression of quorum sensing pathway of *Pseudomonas aeruginosa*: An approach to inhibit biofilm in vitro. *Photodiagn. Photodyn. Ther.* 30:101645. doi: 10.1016/j.pdpdt.2019.101645

Abisado, R. G., Benomar, S., Klaus, J. R., Dandekar, A. A., and Chandler, J. R. (2018). Bacterial quorum sensing and microbial community. *Interactions* 9, e02331–e02317. doi: 10.1128/mBio.02331-17

Abram, V., Berlec, B., Ota, A., Šentjurc, M., Blatnik, P., and Ulrih, N. P. (2013). Effect of flavonoid structure on the fluidity of model lipid membranes. *Food Chem.* 139, 804–813. doi: 10.1016/j.foodchem.2013.01.100

Afrasiabi, S., Pourhajibagher, M., Chiniforush, N., and Bahador, A. (2020). Propolis nanoparticle enhances the potency of antimicrobial photodynamic therapy against *Streptococcus mutans* in a synergistic manner. *Sci. Rep.* 10, 15560. doi: 10.1038/s41598-020-72119-y

Alalwan, H., Rajendran, R., Lappin, D. F., Combet, E., Shahzad, M., Robertson, D., et al. (2017). The anti-adhesive effect of Curcumin on Candida albicans biofilms on denture materials. *Front. Microbiol.* 8:659. doi: 10.3389/fmicb.2017.00659

Antonio, A. G., Iorio, N. L. P., Farah, A., Netto dos Santos, K. R., and Maia, L. C. (2012). Effect of Coffea canephora aqueous extract on microbial counts in ex vivo oral biofilms: a case study. *Planta Med.* 78, 755–760. doi: 10.1055/s-0031-1298435

Argüelles, A., Sánchez-Fresneda, R., Guirao-Abad, J. P., Belda, C., Lozano, J. A., Solano, F., et al. (2020). Novel bi-factorial strategy against Candida albicans viability using Carnosic acid and Propolis: synergistic antifungal action. *Microorganisms* 8, 749. doi: 10.3390/microorganisms8050749

Asahi, Y., Noiri, Y., Miura, J., Maezono, H., Yamaguchi, M., Yamamoto, R., et al. (2014). Effects of the tea catechin epigallocatechin gallate on Porphyromonas gingivalis biofilms. *J. Appl. Microbiol.* 116, 1164–1171. doi: 10.1111/jam.12458

Atanasov, A. G., Zotchev, S. B., Dirsch, V. M., and Supuran, C. T. (2021). Natural products in drug discovery: advances and opportunities. *Nat. Rev. Drug Discov.* 20, 200–216. doi: 10.1038/s41573-020-00114-z

Bacali, C., Vulturar, R., Buduru, S., Cozma, A., Fodor, A., Chiș, A., et al. (2022). Oral microbiome: getting to know and befriend neighbors, a biological approach. *Biomedicine* 10:671. doi: 10.3390/biomedicines10030671

Baker, J. L., Bor, B., Agnello, M., Shi, W., and He, X. (2017). Ecology of the Oral microbiome: Beyond bacteria. *Trends Microbiol.* 25, 362–374. doi: 10.1016/j.tim.2016.12.012

Belenky, P., Ye, J. D., Porter, C. B. M., Cohen, N. R., Lobritz, M. A., Ferrante, T., et al. (2015). Bactericidal antibiotics induce toxic metabolic perturbations that Lead to cellular damage. *Cell Rep.* 13, 968–980. doi: 10.1016/j.celrep.2015.09.059

Ben Lagha, A., Haas, B., and Grenier, D. (2017). Tea polyphenols inhibit the growth and virulence properties of Fusobacterium nucleatum. *Sci. Rep.* 7:44815. doi: 10.1038/srep44815

Benoit, D. S. W., Sims, K. R., and Fraser, D. (2019). Nanoparticles for Oral biofilm treatments. *ACS Nano* 13, 4869–4875. doi: 10.1021/acsnano.9b02816

Bhatia, E., Sharma, S., Jadhav, K., and Banerjee, R. (2021). Combinatorial liposomes of berberine and curcumin inhibit biofilm formation and intracellular methicillin resistant infections and associated inflammation. *J. Mater. Chem. B* 9, 864–875. doi: 10.1039/d0tb02036b

Blackman, L. D., Qu, Y., Cass, P., and Locock, K. E. S. (2021). Approaches for the inhibition and elimination of microbial biofilms using macromolecular agents. *Chem. Soc. Rev.* 50, 1587–1616. doi: 10.1039/d0cs00986e

Bouchelaghem, S., Das, S., Naorem, R. S., Czuni, L., Papp, G., and Kocsis, M. (2022). Evaluation of Total phenolic and flavonoid contents, antibacterial and Antibiofilm activities of Hungarian Propolis Ethanolic extract against *Staphylococcus aureus*. *Molecules* 27, 574. doi: 10.3390/molecules27020574

Bowen, W. H., Burne, R. A., Wu, H., and Koo, H. (2018). Oral biofilms: pathogens, matrix, and Polymicrobial interactions in microenvironments. *Trends Microbiol.* 26, 229–242. doi: 10.1016/j.tim.2017.09.008

Brady, L. J., Maddocks, S. E., Larson, M. R., Forsgren, N., Persson, K., Deivanayagam, C. C., et al. (2010). The changing faces of streptococcus antigen I/II polypeptide family adhesins. *Mol. Microbiol.* 77, 276–286. doi: 10.1111/j.1365-2958.2010.07212.x

Braga, A. S., Abdelbary, M. M. H., Kim, R. R., Melo, F. P. D. S. R. D., Saldanha, L. L., Dokkedal, A. L., et al. (2022). The effect of toothpastes containing natural extracts on bacterial species of a microcosm biofilm and on enamel caries development. *Antibiotics* 11:414. doi: 10.3390/antibiotics11030414

Braga, A. S., Girotti, L. D., de Melo Simas, L. L., Pires, J. G., Pelá, V. T., Buzalaf, M. A. R., et al. (2019). Effect of commercial herbal toothpastes and mouth rinses on the prevention of enamel demineralization using a microcosm biofilm model. *Biofouling* 35, 796–804. doi: 10.1080/08927014.2019.1662897

Brighenti, F. L., Gaetti-Jardim, E., Danelon, M., Evangelista, G. V., and Delbem, A. C. B. (2012). Effect of Psidium cattleianum leaf extract on enamel demineralisation and dental biofilm composition in situ. *Arch. Oral Biol.* 57, 1034–1040. doi: 10.1016/j.archoralbio.2012.02.009

Burne, R. A., and Penders, J. E. (1994). Differential localization of the *Streptococcus mutans* GS-5 fructan hydrolase enzyme, FruA. *FEMS. Microbiol. Lett.* 121, 243–249. doi: 10.1111/j.1574-6968.1994.tb07105.x

Cadena, M., Kelman, T., Marco, M. L., and Pitesky, M. (2019). Understanding antimicrobial resistance (AMR) profiles of biofilm and planktonic bacteria challenged with disinfectants commonly used During poultry processing. *Foods* 8:275. doi: 10.3390/foods8070275

Campus, G., Cagetti, M. G., Cocco, F., Sale, S., Sacco, G., Strohmenger, L., et al. (2011). Effect of a sugar-free chewing gum containing magnolia bark extract on different variables related to caries and gingivitis: a randomized controlled intervention trial. *Caries Res.* 45, 393–399. doi: 10.1159/000330234

Cascioferro, S., Totsika, M., and Schillaci, D. (2014). Sortase A: an ideal target for anti-virulence drug development. *Microb. Pathog.* 77, 105–112. doi: 10.1016/j.micpath.2014.10.007

Chen, L., Bu, Q., Xu, H., Liu, Y., She, P., Tan, R., et al. (2016). The effect of berberine hydrochloride on enterococcus faecalis biofilm formation and dispersion in vitro. *Microbiol. Res.* 186, 44–51. doi: 10.1016/j.micres.2016.03.003

Chen, H., Zhou, X., Ren, B., and Cheng, L. (2020). The regulation of hyphae growth in Candida albicans. *Virulence* 11, 337–348. doi: 10.1080/21505594.2020.1748930

Cheng, L., Exterkate, R. A. M., Zhou, X., Li, J., and ten Cate, J. M. (2011). Effect of Galla chinensis on growth and metabolism of microcosm biofilms. *Caries Res.* 45, 87–92. doi: 10.1159/000324084

Chu, M., Zhang, M.-B., Liu, Y.-C., Kang, J.-R., Chu, Z.-Y., Yin, K.-L., et al. (2016). Role of Berberine in the treatment of methicillin-resistant *Staphylococcus aureus* infections. *Sci. Rep.* 6, 24748. doi: 10.1038/srep24748

Ciofu, O., Rojo-Molinero, E., Macià, M. D., and Oliver, A. (2017). Antibiotic treatment of biofilm infections. *APMIS* 125, 304–319. doi: 10.1111/apm.12673

Cosgarea, R., Pollmann, R., Sharif, J., Schmidt, T., Stein, R., Bodea, A., et al. (2020). Photodynamic therapy in oral lichen planus: A prospective case-controlled pilot study. *Sci. Rep.* 10, 1667. doi: 10.1038/s41598-020-58548-9

Costa, A. F., Silva, L., and Amaral, A. C. (2021). Farnesol: An approach on biofilms and nanotechnology. *Med. Mycol.* 59, 958–969. doi: 10.1093/mmy/myab020

Da Silva, A. R., de Andrade Neto, J. B., da Silva, C. R., Campos, R. D. S., Costa Silva, R. A., Freitas, D. D., et al. (2016). Berberine antifungal activity in fluconazole-resistant pathogenic yeasts: action mechanism evaluated by flow Cytometry and biofilm growth inhibition in Candida spp. *Antimicrob. Agents Chemother.* 60, 3551–3557. doi: 10.1128/AAC.01846-15

Davis-Hanna, A., Piispanen, A. E., Stateva, L. I., and Hogan, D. A. (2008). Farnesol and dodecanol effects on the Candida albicans Ras1-cAMP signalling pathway and the regulation of morphogenesis. *Mol. Microbiol.* 67, 47–62. doi: 10.1111/j.1365-2958.2007.06013.x

De Figueiredo, K. A., da Silva, H. D. P., Miranda, S. L. F., Gonçalves, F. J. D. S., de Sousa, A. P., de Figueiredo, L. C., et al. (2020). Brazilian red Propolis is as effective as amoxicillin in controlling red-complex of multispecies subgingival mature biofilm In vitro. *Antibiotics* 9:432. doi: 10.3390/antibiotics9080432

Deng, L., Li, W., He, Y., Wu, J., Ren, B., and Zou, L. (2019a). Cross-kingdom interaction of Candida albicans and Actinomyces viscosus elevated cariogenic virulence. *Arch. Oral Biol.* 100, 106–112. doi: 10.1016/j.archoralbio.2019.02.008

Deng, L., Zou, L., Wu, J., Liu, H., Luo, T., Zhou, X., et al. (2019b). Voriconazole inhibits cross-kingdom interactions between Candida albicans and Actinomyces viscosus through the ergosterol pathway. *Int. J. Antimicrob. Agents* 53, 805–813. doi: 10.1016/j.ijantimicag.2019.02.010

De Oliveira Dembogurski, D. S., Silva Trentin, D., Boaretto, A. G., Rigo, G. V., da Silva, R. C., Tasca, T., et al. (2018). Brown propolis-metabolomic innovative approach to determine compounds capable of killing *Staphylococcus aureus* biofilm and Trichomonas vaginalis. *Food Res. Int.* 111, 661–673. doi: 10.1016/j.foodres.2018.05.033

Du, Q., Ren, B., He, J., Peng, X., Guo, Q., Zheng, L., et al. (2021). Candida albicans promotes tooth decay by inducing oral microbial dysbiosis. *ISME J.* 15, 894–908. doi: 10.1038/s41396-020-00823-8

Duarte, S., Rosalen, P. L., Hayacibara, M. F., Cury, J. A., Bowen, W. H., Marquis, R. E., et al. (2006). The influence of a novel propolis on mutans streptococci biofilms and caries development in rats. *Arch. Oral Biol.* 51, 15–22. doi: 10.1016/j.archoralbio.2005.06.002

Duque, C., Stipp, R. N., Wang, B., Smith, D. J., Höfling, J. F., Kuramitsu, H. K., et al. (2011). Downregulation of GbpB, a component of the VicRK regulon, affects biofilm formation and cell surface characteristics of *Streptococcus mutans*. *Infect. Immun.* 79, 786–796. doi: 10.1128/IAI.00725-10

Dutreix, L., Bernard, C., Juin, C., Imbert, C., and Girardot, M. (2018). Do raspberry extracts and fractions have antifungal or anti-adherent potential against Candida spp.? *Int. J. Antimicrob. Agents* 52, 947–953. doi: 10.1016/j.ijantimicag.2018.08.020

Elango, A. V., Vasudevan, S., Shanmugam, K., Solomon, A. P., and Neelakantan, P. (2021). Exploring the anti-caries properties of baicalin against: an study. *Biofouling* 37, 267–275. doi: 10.1080/08927014.2021.1897789

Fahim, A., Himratul-Aznita, W. H., Abdul-Rahman, P. S., and Alam, M. K. (2022). Efficacy of bakuchiol-garlic combination against virulent genes of C. *PeerJ* 9:e12251. doi: 10.7717/peerj.12251

Fan, Y., Wang, Y., Yu, S., Chang, J., Yan, Y., Wang, Y., et al. (2021). Natural products provide a new perspective for anti-complement treatment of severe COVID-19: a review. *Chin. Med.* 16, 67. doi: 10.1186/s13020-021-00478-3

Fathima, A., and Rao, J. R. (2016). Selective toxicity of Catechin—a natural flavonoid towards bacteria. *Appl. Microbiol. Biotechnol.* 100, 6395–6402. doi: 10.1007/s00253-016-7492-x

Flemming, H.-C., and Wingender, J. (2010). The biofilm matrix. *Nat. Rev. Microbiol.* 8, 623–633. doi: 10.1038/nrmicro2415

Fournier-Larente, J., Morin, M.-P., and Grenier, D. (2016). Green tea catechins potentiate the effect of antibiotics and modulate adherence and gene expression in Porphyromonas gingivalis. *Arch. Oral Biol.* 65, 35–43. doi: 10.1016/j.archoralbio.2016.01.014

Galloway, W. R. J. D., Hodgkinson, J. T., Bowden, S. D., Welch, M., and Spring, D. R. (2011). Quorum sensing in gram-negative bacteria: small-molecule modulation of AHL and AI-2 quorum sensing pathways. *Chem. Rev.* 111, 28–67. doi: 10.1021/cr100109t

Gao, L., Xu, T., Huang, G., Jiang, S., Gu, Y., and Chen, F. (2018). Oral microbiomes: more and more importance in oral cavity and whole body. *Protein Cell* 9, 488–500. doi: 10.1007/s13238-018-0548-1

Garcia, M. T., Ward, R. A. D. C., Gonçalves, N. M. F., Pedroso, L. L. C., Neto, J. V. D. S., Strixino, J. F., et al. (2021). Susceptibility of dental caries microcosm biofilms to photodynamic therapy mediated by Fotoenticine. *Pharmaceutics* 13:1907. doi: 10.3390/pharmaceutics13111907

Greenberg, M., Urnezis, P., and Tian, M. (2007). Compressed mints and chewing gum containing magnolia bark extract are effective against bacteria responsible for oral malodor. *J. Agric. Food Chem.* 55, 9465–9469. doi: 10.1021/jf072122h

Gucwa, K., Kusznierewicz, B., Milewski, S., Van Dijck, P., and Szweda, P. (2018). Antifungal activity and synergism with azoles of polish Propolis. *Pathogens* 7, 56. doi: 10.3390/pathogens7020056

Gulube, Z., and Patel, M. (2016). Effect of Punica granatum on the virulence factors of cariogenic bacteria *Streptococcus mutans*. *Microb. Pathog.* 98, 45–49. doi: 10.1016/j.micpath.2016.06.027

Guo, N., Zhao, X., Li, W., Shi, C., Meng, R., Liu, Z., et al. (2015). The synergy of berberine chloride and totarol against *Staphylococcus aureus* grown in planktonic and biofilm cultures. *J. Med. Microbiol.* 64, 891–900. doi: 10.1099/jmm.0.000106

Guzzo, F., Scognamiglio, M., Fiorentino, A., Buommino, E., and D'Abrosca, B. (2020). Plant derived natural products against *Pseudomonas aeruginosa* and *Staphylococcus aureus*: Antibiofilm activity and molecular mechanisms. *Molecules* 25, 5024. doi: 10.3390/molecules25215024

Heilmann, C., Schweitzer, O., Gerke, C., Vanittanakom, N., Mack, D., and Götz, F. (1996). Molecular basis of intercellular adhesion in the biofilm-forming Staphylococcus epidermidis. *Mol. Microbiol.* 20, 1083–1091. doi: 10.1111/j.1365-2958.1996.tb02548.x

Holm, A., and Vikström, E. (2014). Quorum sensing communication between bacteria and human cells: signals, targets, and functions. *Front. Plant Sci.* 5:309. doi: 10.3389/fpls.2014.00309

Hu, C., Wang, L.-L., Lin, Y.-Q., Liang, H.-M., Zhou, S.-Y., Zheng, F., et al. (2019). Nanoparticles for the treatment of Oral biofilms: current state, mechanisms, influencing factors, and prospects. *Adv. Healthc. Mater.* 8:e1901301. doi: 10.1002/adhm.201901301

Huang, X., Wang, P., Li, T., Tian, X., Guo, W., Xu, B., et al. (2020a). Self-assemblies based on traditional medicine Berberine and Cinnamic acid for adhesion-induced

inhibition multidrug-resistant. *ACS Appl. Mater. Interfaces* 12, 227–237. doi: 10.1021/acsami.9b17722

Huang, X., Zheng, M., Yi, Y., Patel, A., Song, Z., and Li, Y. (2020b). Inhibition of berberine hydrochloride on Candida albicans biofilm formation. *Biotechnol. Lett.* 42, 2263–2269. doi: 10.1007/s10529-020-02938-6

Iadnut, A., Mamoon, K., Thammasit, P., Pawichai, S., Tima, S., Preechasuth, K., et al. (2019). In vitro antifungal and Antivirulence activities of biologically synthesized Ethanolic extract of Propolis-loaded PLGA nanoparticles against Candida albicans. *Evid. Based Complement. Alternat. Med.* 2019:3715481. doi: 10.1155/2019/3715481

Irfan, M., Delgado, R. Z. R., and Frias-Lopez, J. (2020). The Oral microbiome and cancer. *Front. Immunol.* 11:591088. doi: 10.3389/fimmu.2020.591088

Izadi, P., Izadi, P., and Eldyasti, A. (2021). Holistic insights into extracellular polymeric substance (EPS) in anammosx bacterial matrix and the potential sustainable biopolymer recovery: A review. *Chemosphere* 274:129703. doi: 10.1016/j.chemosphere.2021.129703

Kang, S., Li, Z., Yin, Z., Jia, R., Song, X., Li, L., et al. (2015). The antibacterial mechanism of berberine against Actinobacillus pleuropneumoniae. *Nat. Prod. Res.* 29, 2203–2206. doi: 10.1080/14786419.2014.1001388

Kaur, G., Rajesh, S., and Princy, S. A. (2015). Plausible drug targets in the *Streptococcus mutans* quorum sensing pathways to combat dental biofilms and associated risks. *Indian J. Microbiol.* 55, 349–356. doi: 10.1007/s12088-015-0534-8

Khodavandi, A., Harmal, N. S., Alizadeh, F., Scully, O. J., Sidik, S. M., Othman, F., et al. (2011). Comparison between allicin and fluconazole in Candida albicans biofilm inhibition and in suppression of HWP1 gene expression. *Phytomedicine* 19, 56–63. doi: 10.1016/j.phymed.2011.08.060

Kim, J., Ha Quang Bao, T., Shin, Y.-K., and Kim, K.-Y. (2018). Antifungal activity of magnoflorine against Candida strains. *World J. Microbiol. Biotechnol.* 34, 167. doi: 10.1007/s11274-018-2549-x

Klein, M. I., Hwang, G., Santos, P. H. S., Campanella, O. H., and Koo, H. (2015). *Streptococcus mutans*-derived extracellular matrix in cariogenic oral biofilms. *Front. Cell. Infect. Microbiol.* 5:10. doi: 10.3389/fcimb.2015.00010

Kong, L., Qi, X., Huang, S., Chen, S., Wu, Y., and Zhao, L. (2015). Theaflavins inhibit pathogenic properties of *P. gingivalis* and MMPs production in P. gingivalis-stimulated human gingival fibroblasts. *Arch. Oral Biol.* 60, 12–22. doi: 10.1016/j.archoralbio.2014.08.019

Kong, J., Xia, K., Su, X., Zheng, X., Diao, C., Yang, X., et al. (2021). Mechanistic insights into the inhibitory effect of theaflavins on virulence factors production in *Streptococcus mutans*. *AMB Express* 11:102. doi: 10.1186/s13568-021-01263-z

Kuang, X., Chen, V., and Xu, X. (2018). Novel approaches to the control of Oral microbial biofilms. *Biomed. Res. Int.* 2018, 6498932–6498913. doi: 10.1155/2018/6498932

Kubiliene, L., Laugaliene, V., Pavilonis, A., Maruska, A., Majiene, D., Barcauskaite, K., et al. (2015). Alternative preparation of propolis extracts: comparison of their composition and biological activities. *BMC Complement. Altern. Med.* 15, 156. doi: 10.1186/s12906-015-0677-5

Kuramitsu, H. K., He, X., Lux, R., Anderson, M. H., and Shi, W. (2007). Interspecies interactions within oral microbial communities. *Microbiol. Mol. Biol. Rev.* 71, 653–670. doi: 10.1128/MMBR.00024-07

Laleman, I., and Teughels, W. (2020). Novel natural product-based oral topical rinses and toothpastes to prevent periodontal diseases. *Periodontol.* 84, 102–123. doi: 10.1111/prd.12339

Lamont, R. J., Koo, H., and Hajishengallis, G. (2018). The oral microbiota: dynamic communities and host interactions. *Nat. Rev. Microbiol.* 16, 745–759. doi: 10.1038/s41579-018-0089-x

Le, K. Y., and Otto, M. (2015). Quorum-sensing regulation in staphylococci-an overview. *Front. Microbiol.* 6:1174. doi: 10.3389/fmicb.2015.01174

Lee, J.-H., Kim, Y.-G., Khadke, S. K., Yamano, A., Woo, J.-T., and Lee, J. (2019). Antimicrobial and antibiofilm activities of prenylated flavanones from Macaranga tanarius. *Phytomedicine* 63:153033. doi: 10.1016/j.phymed.2019.153033

Leung, V., Dufour, D., and Lévesque, C. M. (2015). Death and survival in *Streptococcus mutans*: differing outcomes of a quorum-sensing signaling peptide. *Front. Microbiol.* 6:1176. doi: 10.3389/fmicb.2015.01176

Li, J., Fan, Q., Jin, M., Mao, C., Zhang, H., Zhang, X., et al. (2021). Paeoniflorin reduce /AI-2 system-controlled biofilm formation and virulence in. *Virulence* 12, 3062–3073. doi: 10.1080/21505594.2021.2010398

Li, B., Li, X., Lin, H., and Zhou, Y. (2018). Curcumin as a promising antibacterial agent: effects on metabolism and biofilm formation in S. mutans. *Biomed. Res. Int.* 2018:4508709. doi: 10.1155/2018/4508709

Li, X., Lovell, J. F., Yoon, J., and Chen, X. (2020a). Clinical development and potential of photothermal and photodynamic therapies for cancer. *Nat. Rev. Clin. Oncol.* 17, 657–674. doi: 10.1038/s41571-020-0410-2

Li, B., Pan, T., Lin, H., and Zhou, Y. (2020b). The enhancing antibiofilm activity of curcumin on *Streptococcus mutans* strains from severe early childhood caries. *BMC Microbiol.* 20:286. doi: 10.1186/s12866-020-01975-5

Li, D.-D., Xu, Y., Zhang, D.-Z., Quan, H., Mylonakis, E., Hu, D.-D., et al. (2013). Fluconazole assists berberine to kill fluconazole-resistant Candida albicans. *Antimicrob. Agents Chemother.* 57, 6016–6027. doi: 10.1128/AAC.00499-13

Li, X., Yin, L., Ramage, G., Li, B., Tao, Y., Zhi, Q., et al. (2019). Assessing the impact of curcumin on dual-species biofilms formed by *Streptococcus mutans* and Candida albicans. *Microbiology* 8:e937. doi: 10.1002/mbo3.937

Liang, R.-M., Yong, X.-L., Duan, Y.-Q., Tan, Y.-H., Zeng, P., Zhou, Z.-Y., et al. (2014). Potent in vitro synergism of fusidic acid (FA) and berberine chloride (BBR) against clinical isolates of methicillin-resistant *Staphylococcus aureus* (MRSA). *World J. Microbiol. Biotechnol.* 30, 2861–2869. doi: 10.1007/s11274-014-1712-2

Lin, Y., Chen, J., Zhou, X., and Li, Y. (2021). Inhibition of biofilm formation by strategies targeting the metabolism of exopolysaccharides. *Crit. Rev. Microbiol.* 47, 667–677. doi: 10.1080/1040841X.2021.1915959

Lister, J. L., and Horswill, A. R. (2014). *Staphylococcus aureus* biofilms: recent developments in biofilm dispersal. *Front. Cell. Infect. Microbiol.* 4:178. doi: 10.3389/fcimb.2014.00178

Lof, M., Janus, M. M., and Krom, B. P. (2017). Metabolic interactions between bacteria and fungi in commensal Oral biofilms. *J. Fungi.* 3, 40. doi: 10.3390/jof3030040

Mack, D., Nedelmann, M., Krokotsch, A., Schwarzkopf, A., Heesemann, J., and Laufs, R. (1994). Characterization of transposon mutants of biofilm-producing *Staphylococcus epidermidis* impaired in the accumulative phase of biofilm production: genetic identification of a hexosamine-containing polysaccharide intercellular adhesin. *Infect. Immun.* 62, 3244–3253. doi: 10.1128/iai.62.8.3244-3253.1994

Maghsoudi, A., Yazdian, F., Shahmoradi, S., Ghaderi, L., Hemati, M., and Amoabediny, G. (2017). Curcumin-loaded polysaccharide nanoparticles: optimization and anticariogenic activity against *Streptococcus mutans*. *Mater. Sci. Eng. C Mater. Biol. Appl.* 75, 1259–1267. doi: 10.1016/j.msec.2017.03.032

Mann, E. E., and Wozniak, D. J. (2012). Pseudomonas biofilm matrix composition and niche biology. *FEMS Microbiol. Rev.* 36, 893–916. doi: 10.1111/j.1574-6976.2011.00322.x

Manresa, C., Sanz-Miralles, E. C., Twigg, J., and Bravo, M. (2018). Supportive periodontal therapy (SPT) for maintaining the dentition in adults treated for periodontitis. *Cochrane Database Syst. Rev.* 2018, CD009376. doi: 10.1002/14651858.CD009376.pub2

Marsh, P. D., Moter, A., and Devine, D. A. (2011). Dental plaque biofilms: communities, conflict and control. *Periodontol.* 55, 16–35. doi: 10.1111/j.1600-0757.2009.00339.x

Marsh, P. D., and Zaura, E. (2017). Dental biofilm: ecological interactions in health and disease. *J. Clin. Periodontol.* 44, S12–S22. doi: 10.1111/jcpe.12679

Matesanz-Pérez, P., García-Gargallo, M., Figuero, E., Bascones-Martínez, A., Sanz, M., and Herrera, D. (2013). A systematic review on the effects of local antimicrobials as adjuncts to subgingival debridement, compared with subgingival debridement alone, in the treatment of chronic periodontitis. *J. Clin. Periodontol.* 40, 227–241. doi: 10.1111/jcpe.12026

Mazmanian, S. K., Liu, G., Jensen, E. R., Lenoy, E., and Schneewind, O. (2000). *Staphylococcus aureus* sortase mutants defective in the display of surface proteins and in the pathogenesis of animal infections. *Proc. Natl. Acad. Sci. U. S. A.* 97, 5510–5515. doi: 10.1073/pnas.080520697

Melander, R. J., Basak, A. K., and Melander, C. (2020). Natural products as inspiration for the development of bacterial antibiofilm agents. *Nat. Prod. Rep.* 37, 1454–1477. doi: 10.1039/d0np00022a

Ming, D., Wang, D., Cao, F., Xiang, H., Mu, D., Cao, J., et al. (2017). Kaempferol inhibits the primary attachment phase of biofilm formation in *Staphylococcus aureus*. *Front. Microbiol.* 8:2263. doi: 10.3389/fmicb.2017.02263

Miranda, S. L. F., Damasceno, J. T., Faveri, M., Figueiredo, L., da Silva, H. D., Alencar, S. M. D. A., et al. (2019). Brazilian red propolis reduces orange-complex periodontopathogens growing in multispecies biofilms. *Biofouling* 35, 308–319. doi: 10.1080/08927014.2019.1598976

Morse, D. J., Wilson, M. J., Wei, X., Lewis, M. A. O., Bradshaw, D. J., Murdoch, C., et al. (2018). Denture-associated biofilm infection in three-dimensional oral mucosal tissue models. *J. Med. Microbiol.* 67, 364–375. doi: 10.1099/jmm.0.000677

Nadar, S., Khan, T., Patching, S. G., and Omri, A. (2022). Development of Antibiofilm therapeutics strategies to overcome antimicrobial drug resistance. *Microorganisms* 10, 303. doi: 10.3390/microorganisms10020303

Nguyen, H. T. T., Nguyen, T. H., and Otto, M. (2020). The staphylococcal exopolysaccharide PIA - biosynthesis and role in biofilm formation, colonization, and infection. *Comput. Struct. Biotechnol. J.* 18, 3324–3334. doi: 10.1016/j.csbj.2020.10.027

Noiri, Y., Ehara, A., Kawahara, T., Takemura, N., and Ebisu, S. (2002). Participation of bacterial biofilms in refractory and chronic periapical periodontitis. *J. Endod.* 28, 679–683. doi: 10.1097/00004770-200210000-00001

Nuryastuti, T., and Krom, B. P. (2017). Ica-status of clinical *Staphylococcus epidermidis* strains affects adhesion and aggregation: a thermodynamic analysis. *Antonie Van Leeuwenhoek* 110, 1467–1474. doi: 10.1007/s10482-017-0899-2

Olusanya, B. O., Ştefan, S., Kim, Y., Alcalde-Rabanal, J. E., Akinyemiju, T., and Koyanagi, A. (2020). Five insights from the Global Burden of Disease Study 2019. *Lancet* 396, 1135–1159. doi: 10.1016/S0140-6736(20)31404-5

Ong, T. H., Chitra, E., Ramamurthy, S., Ling, C. C. S., Ambu, S. P., and Davamani, F. (2019). Cationic chitosan-propolis nanoparticles alter the zeta potential of S. epidermidis, inhibit biofilm formation by modulating gene expression and exhibit synergism with antibiotics. *PLoS One* 14:e0213079. doi: 10.1371/journal.pone.0213079

Ouyang, J., Sun, F., Feng, W., Sun, Y., Qiu, X., Xiong, L., et al. (2016). Quercetin is an effective inhibitor of quorum sensing, biofilm formation and virulence factors in *Pseudomonas aeruginosa*. *J. Appl. Microbiol.* 120, 966–974. doi: 10.1111/jam.13073

Paes Leme, A. F., Koo, H., Bellato, C. M., Bedi, G., and Cury, J. A. (2006). The role of sucrose in cariogenic dental biofilm formation--new insight. *J. Dent. Res.* 85, 878–887. doi: 10.1177/154405910608501002

Papenfort, K., and Bassler, B. L. (2016). Quorum sensing signal-response systems in gram-negative bacteria. *Nat. Rev. Microbiol.* 14, 576–588. doi: 10.1038/nrmicro.2016.89

Parsek, M. R., and Greenberg, E. P. (2005). Sociomicrobiology: the connections between quorum sensing and biofilms. *Trends Microbiol.* 13, 27–33. doi: 10.1016/j.tim.2004.11.007

Paterson, G. K., and Mitchell, T. J. (2004). The biology of gram-positive sortase enzymes. *Trends Microbiol.* 12, 89–95. doi: 10.1016/j.tim.2003.12.007

Peng, X., Cheng, L., You, Y., Tang, C., Ren, B., Li, Y., et al. (2022). Oral microbiota in human systematic diseases. *Int. J. Oral Sci.* 14, 14. doi: 10.1038/s41368-022-00163-7

Pitts, N. B., Zero, D. T., Marsh, P. D., Ekstrand, K., Weintraub, J. A., Ramos-Gomez, F., et al. (2017). Dental caries. *Nat. Rev. Dis. Primers* 3, 17030. doi: 10.1038/nrdp.2017.30

Polat, E., and Kang, K. (2021). Natural photosensitizers in antimicrobial photodynamic therapy. *Biomedicine* 9:584. doi: 10.3390/biomedicines9060584

Ponde, N. O., Lortal, L., Ramage, G., Naglik, J. R., and Richardson, J. P. (2021). Candida albicans biofilms and polymicrobial interactions. *Crit. Rev. Microbiol.* 47, 91–111. doi: 10.1080/1040841X.2020.1843400

Pourhajibagher, M., Keshavarz Valian, N., and Bahador, A. (2022). Theranostic nanoplatforms of emodin-chitosan with blue laser light on enhancing the anti-biofilm activity of photodynamic therapy against *Streptococcus mutans* biofilms on the enamel surface. *BMC Microbiol.* 22, 68. doi: 10.1186/s12866-022-02481-6

Qu, D., Hou, Z., Li, J., Luo, L., Su, S., Ye, Z., et al. (2020). A new coumarin compound DCH combats methicillin-resistant *Staphylococcus aureus* biofilm by targeting arginine repressor. *Sci. Adv.* 6:eaay9597. doi: 10.1126/sciadv.aay9597

Rosier, B. T., Marsh, P. D., and Mira, A. (2018). Resilience of the Oral microbiota in health: mechanisms That prevent Dysbiosis. *J. Dent. Res.* 97, 371–380. doi: 10.1177/0022034517742139

Rumbaugh, K. P., and Sauer, K. (2020). Biofilm dispersion. *Nat. Rev. Microbiol.* 18, 571–586. doi: 10.1038/s41579-020-0385-0

Rutherford, S. T., and Bassler, B. L. (2012). Bacterial quorum sensing: its role in virulence and possibilities for its control. *Cold Spring Harb. Perspect. Med.* 2:427. doi: 10.1101/cshperspect.a012427

Santezi, C., Reina, B. D., and Dovigo, L. N. (2018). Curcumin-mediated photodynamic therapy for the treatment of oral infections-A review. *Photodiagn. Photodyn. Ther.* 21, 409–415. doi: 10.1016/j.pdpdt.2018.01.016

Sardi, J. D. C. O., Polaquini, C. R., Freires, I. A., Galvão, L. C. D. C., Lazarini, J. G., Torrezan, G. S., et al. (2017). Antibacterial activity of diacetylcurcumin against *Staphylococcus aureus* results in decreased biofilm and cellular adhesion. *J. Med. Microbiol.* 66, 816–824. doi: 10.1099/jmm.0.000494

Scharnow, A. M., Solinski, A. E., and Wuest, W. M. (2019). Targeting biofilms: a perspective on preventing dental caries. *Fortschr. Med.* 10, 1057–1067. doi: 10.1039/c9md00015a

Schilcher, K., and Horswill, A. R. (2020). Staphylococcal biofilm development: structure, regulation, and treatment strategies. *Microbiol. Mol. Biol. Rev.* 84, e00026–e00019. doi: 10.1128/MMBR.00026-19

Schneider-Rayman, M., Steinberg, D., Sionov, R. V., Friedman, M., and Shalish, M. (2021). Effect of epigallocatechin gallate on dental biofilm of *Streptococcus mutans*: An in vitro study. *BMC Oral Health* 21:447. doi: 10.1186/s12903-021-01798-4

Sedghi, L., DiMassa, V., Harrington, A., Lynch, S. V., and Kapila, Y. L. (2021). The oral microbiome: role of key organisms and complex networks in oral health and disease. *Periodontol.* 87, 107–131. doi: 10.1111/prd.12393

Senadheera, M. D., Guggenheim, B., Spatafora, G. A., Huang, Y.-C. C., Choi, J., Hung, D. C. I., et al. (2005). A VicRK signal transduction system in *Streptococcus mutans* affects gtfBCD, gbpB, and ftf expression, biofilm formation, and genetic competence development. *J. Bacteriol.* 187, 4064–4076. doi: 10.1128/JB.187.12.4064-4076.2005

Shani, S., Friedman, M., and Steinberg, D. (2000). The anticariogenic effect of amine fluorides on *Streptococcus sobrinus* and glucosyltransferase in biofilms. *Caries Res.* 34, 260–267. doi: 10.1159/000016600

Shao, J., Cheng, H., Wang, C., Wu, D., Zhu, X., Zhu, L., et al. (2013). Sodium houttuyfonate, a potential phytoanticipin derivative of antibacterial agent, inhibits bacterial attachment and pyocyanine secretion of *Pseudomonas aeruginosa* by attenuating flagella-mediated swimming motility. *World J. Microbiol. Biotechnol.* 29, 2373–2378. doi: 10.1007/s11274-013-1405-2

Shrestha, A., and Kishen, A. (2016). Antibacterial nanoparticles in Endodontics: A review. *J. Endod.* 42, 1417–1426. doi: 10.1016/j.joen.2016.05.021

Shui, Y., Jiang, Q., Lyu, X., Wang, L., Lin, Y., Ma, Q., et al. (2021). Inhibitory effects of sodium new houttuyfonate on growth and biofilm formation of *Streptococcus mutans*. *Microb. Pathog.* 157:104957. doi: 10.1016/j.micpath.2021.104957

Simonetti, G., Palocci, C., Valletta, A., Kolesova, O., Chronopoulou, L., Donati, L., et al. (2019). Anti-Candida biofilm activity of Pterostilbene or crude extract from non-fermented grape Pomace entrapped in biopolymeric nanoparticles. *Molecules* 24, 2070. doi: 10.3390/molecules24112070

Solano, C., Echeverz, M., and Lasa, I. (2014). Biofilm dispersion and quorum sensing. *Curr. Opin. Microbiol.* 18, 96–104. doi: 10.1016/j.mib.2014.02.008

Song, J., Choi, B., Jin, E. J., Yoon, Y., and Choi, K. H. (2012). Curcumin suppresses *Streptococcus mutans* adherence to human tooth surfaces and extracellular matrix proteins. *Eur. J. Clin. Microbiol. Infect. Dis.* 31, 1347–1352. doi: 10.1007/s10096-011-1448-y

Stoodley, P., Sauer, K., Davies, D. G., and Costerton, J. W. (2002). Biofilms as complex differentiated communities. *Annu. Rev. Microbiol.* 56, 187–209. doi: 10.1146/annurev.micro.56.012302.160705

Tada, A., Nakayama-Imaohji, H., Yamasaki, H., Elahi, M., Nagao, T., Yagi, H., et al. (2020). Effect of thymoquinone on Fusobacterium nucleatum-associated biofilm and inflammation. *Mol. Med. Rep.* 22, 643–650. doi: 10.3892/mmr.2020.11136

Tent, P. A., Juncar, R. I., Onisor, F., Bran, S., Harangus, A., and Juncar, M. (2019). The pathogenic microbial flora and its antibiotic susceptibility pattern in odontogenic infections. *Drug Metab. Rev.* 51, 340–355. doi: 10.1080/03602532.2019.1602630

Tse, B. N., Adalja, A. A., Houchens, C., Larsen, J., Inglesby, T. V., and Hatchett, R. (2017). Challenges and opportunities of nontraditional approaches to treating bacterial infections. *Clin. Infect. Dis.* 65, 495–500. doi: 10.1093/cid/cix320

Veloz, J. J., Saavedra, N., Alvear, M., Zambrano, T., Barrientos, L., and Salazar, L. A. (2016). Polyphenol-rich extract from Propolis reduces the expression and activity of *Streptococcus mutans* Glucosyltransferases at subinhibitory concentrations. *Biomed. Res. Int.* 2016:4302706. doi: 10.1155/2016/4302706

Wang, T., Huang, W., Duan, Q., Wang, J., Cheng, H., Shao, J., et al. (2019). Sodium houttuyfonate in vitro inhibits biofilm dispersion and expression of bdlA in *Pseudomonas aeruginosa*. *Mol. Biol. Rep.* 46, 471–477. doi: 10.1007/s11033-018-4497-9

Wang, Z., Zhou, Y., Han, Q., Ye, X., Chen, Y., Sun, Y., et al. (2021). Synonymous point mutation of gtfB gene caused by therapeutic X-rays exposure reduced the biofilm formation and cariogenic abilities of *Streptococcus mutans*. *Cell Biosci.* 11, 91. doi: 10.1186/s13578-021-00608-2

Wenderska, I. B., Latos, A., Pruitt, B., Palmer, S., Spatafora, G., Senadheera, D. B., et al. (2017). Transcriptional profiling of the Oral pathogen *Streptococcus mutans* in response to competence signaling peptide XIP. *Microbial Syst.* 2:16. doi: 10.1128/mSystems.00102-16

Wu, S., Liu, Y., Zhang, H., and Lei, L. (2019). The pathogenicity and Transcriptome analysis of methicillin-resistant *Staphylococcus aureus* in response to water extract of Galla chinensis. *Evid. Based Complement. Alternat. Med.* 2019:3276156. doi: 10.1155/2019/3276156

Wu, J., Wu, D., Zhao, Y., Si, Y., Mei, L., Shao, J., et al. (2020). Sodium new Houttuyfonate inhibits biofilm formation by inhibiting the Ras1-cAMP-Efg1 pathway revealed by RNA-seq. *Front. Microbiol.* 11:2075. doi: 10.3389/fmicb.2020.02075

Xiang, H., Cao, F., Ming, D., Zheng, Y., Dong, X., Zhong, X., et al. (2017). Aloe-emodin inhibits *Staphylococcus aureus* biofilms and extracellular protein production at the initial adhesion stage of biofilm development. *Appl. Microbiol. Biotechnol.* 101, 6671–6681. doi: 10.1007/s00253-017-8403-5

Xie, Y., Liu, X., and Zhou, P. (2020). In vitro antifungal effects of Berberine Against Candida spp. In planktonic and biofilm conditions. *Drug Des. Devel. Ther.* 14, 87–101. doi: 10.2147/DDDT.S230857

Xiong, K., Zhu, H., Li, Y., Ji, M., Yan, Y., Chen, X., et al. (2020). The arginine biosynthesis pathway of Candida albicans regulates its cross-kingdom interaction with Actinomyces viscosus to promote root caries. *Microbiol. Spectr.* 13, e00782–e00722. doi: 10.1128/spectrum.00782-22

Xu, Z., Huang, T., Min, D., Soteyome, T., Lan, H., Hong, W., et al. (2022). Regulatory network controls microbial biofilm development, with as a representative: from adhesion to dispersal. *Bioengineered* 13, 253–267. doi: 10.1080/21655979.2021.1996747

Xu, X., Zhou, X. D., and Wu, C. D. (2012). Tea catechin epigallocatechin gallate inhibits *Streptococcus mutans* biofilm formation by suppressing gtf genes. *Arch. Oral Biol.* 57, 678–683. doi: 10.1016/j.archoralbio.2011.10.021

Yan, X., Gu, S., Shi, Y., Cui, X., Wen, S., and Ge, J. (2017). The effect of emodin on *Staphylococcus aureus* strains in planktonic form and biofilm formation in vitro. *Arch. Microbiol.* 199, 1267–1275. doi: 10.1007/s00203-017-1396-8

Yang, L., Liu, Y., Wu, H., Hóiby, N., Molin, S., and Song, Z.-J. (2011). Current understanding of multi-species biofilms. *Int. J. Oral Sci.* 3, 74–81. doi: 10.4248/IJOS11027

Yang, B., Xie, Y., Guo, M., Rosner, M. H., Yang, H., and Ronco, C. (2018). Nephrotoxicity and Chinese herbal medicine. *Clin. J. Am. Soc. Nephrol.* 13, 1605–1611. doi: 10.2215/CJN.11571017

Yu, J., Yang, H., Li, K., Ren, H., Lei, J., and Huang, C. (2017). Development of Epigallocatechin-3-gallate-encapsulated Nanohydroxyapatite/Mesoporous silica for therapeutic Management of Dentin Surface. *ACS Appl. Mater. Interfaces* 9, 25796–25807. doi: 10.1021/acsami.7b06597

Yu, J., Zhang, Z., Guo, R., Peng, W., Yang, H., and Huang, C. (2021). Epigallocatechin-3-gallate/nanohydroxyapatite platform delivery approach to adhesive-dentin interface stability. *Mater. Sci. Eng. C Mater. Biol. Appl.* 122:111918. doi: 10.1016/j.msec.2021.111918

Yuan, Q., Feng, W., Wang, Y., Wang, Q., Mou, N., Xiong, L., et al. (2022). Luteolin attenuates the pathogenesis of *Staphylococcus aureus* by interfering with the agr system. *Microb. Pathog.* 165:105496. doi: 10.1016/j.micpath.2022.105496

Zhang, P., Guo, Q., Wei, Z., Yang, Q., Guo, Z., Shen, L., et al. (2021a). Baicalin represses type three secretion system of through PQS system. *Molecules* 26:1497. doi: 10.3390/molecules26061497

Zhang, Z., Liu, Y., Lu, M., Lyu, X., Gong, T., Tang, B., et al. (2020a). Rhodiola rosea extract inhibits the biofilm formation and the expression of virulence genes of cariogenic oral pathogen *Streptococcus mutans*. *Arch. Oral Biol.* 116:104762. doi: 10.1016/j.archoralbio.2020.104762

Zhang, Q., Ma, Q., Wang, Y., Wu, H., and Zou, J. (2021b). Molecular mechanisms of inhibiting glucosyltransferases for biofilm formation in *Streptococcus mutans*. *Int. J. Oral Sci.* 13, 30. doi: 10.1038/s41368-021-00137-1

Zhang, X., Sun, X., Wu, J., Wu, Y., Wang, Y., Hu, X., et al. (2020b). Berberine damages the cell surface of methicillin-resistant. *Front. Microbiol.* 11:621. doi: 10.3389/fmicb.2020.00621

Zhang, G., Yang, J., Cui, D., Zhao, D., Benedito, V. A., and Zhao, J. (2020c). Genome-wide analysis and metabolic profiling unveil the role of peroxidase CsGPX3 in theaflavin production in black tea processing. *Food Res. Int.* 137:109677. doi: 10.1016/j.foodres.2020.109677

Zheng, L. W., Hua, H., and Cheung, L. K. (2011). Traditional Chinese medicine and oral diseases: today and tomorrow. *Oral Dis.* 17, 7–12. doi: 10.1111/j.1601-0825.2010.01706.x

Zheng, Y., Joo, H.-S., Nair, V., Le, K. Y., and Otto, M. (2018). Do amyloid structures formed by *Staphylococcus aureus* phenol-soluble modulins have a biological function? *Int. J. Med. Microbiol.* 308, 675–682. doi: 10.1016/j.ijmm.2017.08.010

Zhou, Y., Cheng, L., Liao, B., Shi, Y., Niu, Y., Zhu, C., et al. (2021). Candida albicans CHK1 gene from two-component system is essential for its pathogenicity in oral candidiasis. *Appl. Microbiol. Biotechnol.* 105, 2485–2496. doi: 10.1007/s00253-021-11187-0

Zhou, Y., Gao, H., Mihindukulasuriya, K. A., La Rosa, P. S., Wylie, K. M., Vishnivetskaya, T., et al. (2013). Biogeography of the ecosystems of the healthy human body. *Genome Biol.* 14, R1. doi: 10.1186/gb-2013-14-1-r1

Zhu, M., Ajdić, D., Liu, Y., Lynch, D., Merritt, J., and Banas, J. A. (2009). Role of the *Streptococcus mutans* irvA gene in GbpC-independent, dextran-dependent aggregation and biofilm formation. *Appl. Environ. Microbiol.* 75, 7037–7043. doi: 10.1128/AEM.01015-09

Zhu, C., Liao, B., Ye, X., Zhou, Y., Chen, X., Liao, M., et al. (2021). Artemisinin elevates ergosterol levels of Candida albicans to synergise with amphotericin B against oral candidiasis. *Int. J. Antimicrob. Agents* 58:106394. doi: 10.1016/j.ijantimicag.2021.106394

frontiers | Frontiers in Microbiology

TYPE Mini Review
PUBLISHED 26 August 2022
DOI 10.3389/fmicb.2022.955286

OPEN ACCESS

EDITED BY
Dongmei Deng,
VU Amsterdam,
Netherlands

REVIEWED BY
Mariana Carmen Chifiriuc,
University of Bucharest,
Romania
Qiao Lin,
University of Pittsburgh,
United States
Wedad Abdelraheem,
Minia University,
Egypt

*CORRESPONDENCE
Jinshui Lin
linjinshui@yau.edu.cn

†These authors have contributed equally to this work

SPECIALTY SECTION
This article was submitted to Antimicrobials, Resistance and Chemotherapy, a section of the journal Frontiers in Microbiology

RECEIVED 28 May 2022
ACCEPTED 09 August 2022
PUBLISHED 26 August 2022

CITATION
Yin R, Cheng J, Wang J, Li P and Lin J (2022) Treatment of *Pseudomonas aeruginosa* infectious biofilms: Challenges and strategies.
Front. Microbiol. 13:955286.
doi: 10.3389/fmicb.2022.955286

Treatment of *Pseudomonas aeruginosa* infectious biofilms: Challenges and strategies

Rui Yin†, Juanli Cheng†, Jingyao Wang, Panxin Li and Jinshui Lin*

Shaanxi Key Laboratory of Chinese Jujube, College of Life Sciences, Yan'an University, Yan'an, Shaanxi Province, China

Pseudomonas aeruginosa, a Gram-negative bacterium, is one of the major pathogens implicated in human opportunistic infection and a common cause of clinically persistent infections such as cystic fibrosis, urinary tract infections, and burn infections. The main reason for the persistence of *P. aeruginosa* infections is due to the ability of *P. aeruginosa* to secrete extracellular polymeric substances such as exopolysaccharides, matrix proteins, and extracellular DNA during invasion. These substances adhere to and wrap around bacterial cells to form a biofilm. Biofilm formation leads to multiple antibiotic resistance in *P. aeruginosa*, posing a significant challenge to conventional single antibiotic therapeutic approaches. It has therefore become particularly important to develop anti-biofilm drugs. In recent years, a number of new alternative drugs have been developed to treat *P. aeruginosa* infectious biofilms, including antimicrobial peptides, quorum-sensing inhibitors, bacteriophage therapy, and antimicrobial photodynamic therapy. This article briefly introduces the process and regulation of *P. aeruginosa* biofilm formation and reviews several developed anti-biofilm treatment technologies to provide new directions for the treatment of *P. aeruginosa* biofilm infection.

KEYWORDS

***Pseudomonas aeruginosa*, antibiotic resistance, biofilm, anti-biofilm molecules, alternative therapeutics**

Introduction

Most microorganisms have different survival mechanisms when facing stress conditions, such as proteolytic systems and growth regulation (Kumar et al., 2017). Most bacteria live in biofilms, which provide a protective niche for the survival of microorganisms (Kumar et al., 2017; Flemming and Wuertz, 2019). Bacterial biofilms are defined as structured microbial communities encapsulated in a self-synthesizing extracellular polymeric substance (EPS) and attached to a tissue or surface (Costerton et al., 1999) that include exopolysaccharides, matrix proteins, and extracellular DNA (eDNA; Wang et al., 2020). Clinically, the long-term colonization of bacteria in humans causes chronic infections, mainly because the bacteria in biofilms are resistant to host immune responses and antibiotic therapy (Dufour et al., 2010). Research has shown that 65–80% of pathogenic

infections in hospitals are associated with biofilms (Kumar et al., 2017; Shrestha et al., 2022). Although numerous antimicrobial agents are available for clinical use, these agents only inhibit infection symptoms and are unable to eradicate bacteria embedded in biofilms (Li et al., 2020).

Pseudomonas aeruginosa is a Gram-negative opportunistic pathogenic bacterium that is widely found in nature. It has been established that *P. aeruginosa* is involved in a diverse array of infections, both community- and hospital-acquired, including pneumonia, cystic fibrosis, urinary tract infections, and burn infections (Al-Dahmoshi et al., 2021). Antimicrobial agents approved for clinical use may be ineffective in treating *P. aeruginosa* infections as this bacterium has the ability to form biofilms (Azam and Khan, 2019). The formation of biofilms enables *P. aeruginosa* to resist external adverse environments and enhance its colonization in the host. Biofilms can also act as diffusion barriers, restricting the entry of antibiotics into bacterial cells (Drenkard, 2003; Pang et al., 2019).

As *P. aeruginosa* is one of the major pathogens involved in opportunistic infections in humans, the clinical treatment and control of *P. aeruginosa* infections have become major challenges and have been the subject of extensive research (Azam and Khan, 2019; Das et al., 2020; Shao et al., 2020). The formation of biofilm effectively aids *P. aeruginosa* colonization, improving bacterial resistance to antimicrobial agents and countering the host immune system (Maurice et al., 2018; Elmanama et al., 2020; Tuon et al., 2022). Therefore, conventional single antibiotic therapy is limited in the treatment of biofilm infections, and an increasing number of studies have investigated the development of new antimicrobial drugs and anti-biofilm therapeutic programs to treat *P. aeruginosa* infection. This review will introduce the process of biofilm formation as well as biofilm regulation and anti-biofilm therapies in *P. aeruginosa*.

Composition, formation, and regulation of *Pseudomonas aeruginosa* biofilm

The biofilm matrix components that have been identified from *P. aeruginosa* mainly include exopolysaccharides, eDNA, and matrix proteins, which play an important role in the structural maintenance and drug resistance of biofilms (Ghafoor et al., 2011). *P. aeruginosa* can synthesize at least three types of exopolysaccharides: alginate, Pel polysaccharide, and Psl polysaccharide (Mann and Wozniak, 2012). Alginate is an anionic polysaccharide of α-L-guluronic acid and β-D-mannuronic acid linked by β-1-4 glycosidic bonds (Moradali and Rehm, 2019). The overproduction of alginate is responsible for the development of excessive slimy or mucoid biofilms, while mucoid biofilms are more resistant to host immune system attack and antibiotic treatment than non-mucoid biofilms, resulting in persistent infections in the body (Moradali et al., 2017; Moradali and Rehm, 2019). The Psl polysaccharide consists of 15 co-transcribed genes (*pslA* to *pslO*) that encode proteins to synthesize Psl, enhance cell-surface and cell-to-cell adhesion in *P. aeruginosa*, and play an important role in the initiation and maintenance of biofilm structure (Ma et al., 2006). Pel is a positively charged exopolysaccharide composed of partially acetylated 1→4 glycosidic linkages of N-acetylgalactosamine and N-acetylglucosamine (Jennings et al., 2015), which is important for biofilm formation in air–liquid interfaces (Byrd et al., 2009). Pel and Psl are the major structural polysaccharides in non-mucoid and mucoid *P. aeruginosa* biofilms (Colvin et al., 2012; Ma et al., 2012). Cell lysis releases DNA into the environment, and this eDNA can be used as a supporting component of biofilms to provide nutrients to bacteria in biofilms during periods of nutrient deficiency (Finkel and Kolter, 2001). Aside from exopolysaccharides and eDNA, extracellular proteins are also considered to be important components of biofilm matrices, including appendages (mainly flagella and type IV fimbriae), cytoadhesions, and lectins. Studies have found that these components mainly play an auxiliary role as adhesion factors and structural support in the process of *P. aeruginosa* biofilm formation (Qi and Christopher, 2019).

The formation of the biofilm structure of *P. aeruginosa* is a continuous process that includes four main stages (Figure 1; Kostakioti et al., 2013; Saxena et al., 2019). The first stage is the initial attachment. At this stage, adhesion is reversible, and bacteria can attach to the surface or revert back to planktonic cells (Olivares et al., 2019). Many early studies on the initial attachment of bacteria have suggested that bacterial cells initiate adhesion through acid–base, hydrophobic, and electrostatic interactions (Donlan, 2002). In addition, the production of polysaccharides also contributes to cell-to-cell adhesion in *P. aeruginosa* (Ma et al., 2006). In the second stage of biofilm development, attached bacteria gradually reproduce into a more independent structure, and bacterial cells undergo a transition from reversible to irreversible attachment (Thi et al., 2020). In this stage, bacteria grow and form microcolonies and begin to synthesize EPSs, which acts as a blockade between biofilm cells and surroundings to provide protection from various stress conditions such as antimicrobial exposure or immune cell attack (Mitchell et al., 2016; Roy et al., 2018). As the secretion of EPSs continues, the cells forming microcolonies gradually mature and undergo various physiological changes (Lee and Yoon, 2017; Roy et al., 2018), forming three-dimensional mushroom-like structures consisting of small channels that transport nutrients, water, and waste, and contribute to the distribution of nutrients and signaling molecules as well as intercellular communication (Jamal et al., 2018; Thi et al., 2020). As the biofilm matures, the bacteria produce stronger resistance to environmental stress or antibiotics (Koo et al., 2017). The final stage of biofilm development is detachment. Different detachment mechanisms have been reported, such as erosion, sloughing, and dispersal (Kim and Lee, 2016). The detachment of biofilm marks the transition of biofilm cells to the planktonic mode of growth (Rumbaugh and Sauer, 2020), which leads cells to attach to the surface of other biomolecules or start a new cycle of biofilm development (Kim and Lee, 2016).

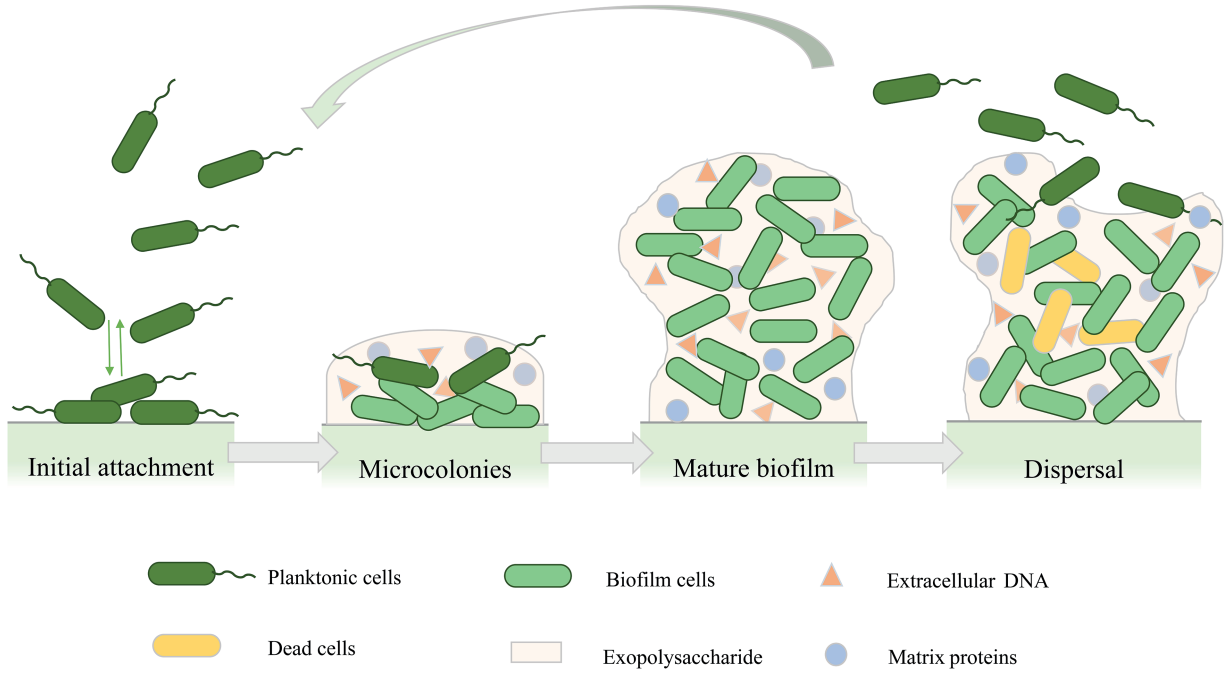

FIGURE 1
Cycle of *Pseudomonas aeruginosa* biofilm development. Biofilm formation includes four stages: initial attachment, microcolonies, mature biofilm, and biofilm dispersal.

Matrix components of *P. aeruginosa* biofilms play different regulatory roles in different formation stages (Wei and Ma, 2013; Ma et al., 2022). In the early stage of biofilm formation, Psl polysaccharides can form a fibrous matrix that is spirally anchored to the surface of bacterial cells and wraps around bacteria, thus increasing the contact between bacteria and promoting the interaction between bacterial cells, resulting in the assembly and early adhesion of biofilms (Ma et al., 2006, 2009). eDNA is also considered to be an important factor in promoting the formation of *P. aeruginosa* biofilm and is involved in the initial attachment of bacterial cells as well as cell–cell interconnection (Allesen-Holm et al., 2006). During the later maturation stages of biofilms, Pel can serve a structural and protective role in the biofilm matrix of *P. aeruginosa* and enhance resistance to aminoglycoside antibiotics (Colvin et al., 2011). The production of numerous EPSs can promote biofilm growth through providing structural scaffolds and maintaining their biofilm function (Ghafoor et al., 2011). Furthermore, quorum sensing (QS), as a cell-density-dependent bacteria-cell signaling mechanism, plays a key role in the regulation of *P. aeruginosa* biofilm formation (Bala et al., 2015). There are at least four QS systems in *P. aeruginosa*: *las*, *rhl*, *pqs*, and *iqs* (Lee and Zhang, 2015). As the two main QS systems of *P. aeruginosa*, both *las* and *rhl* systems use acyl homoserine lactone (AHL) as a signal molecule, which binds to the signal molecule receptor protein to play a regulatory role (Huang et al., 2019). The *las* system represses the *pel* locus, an operon encoding for the synthesis of extracellular matrix polysaccharides that induce biofilm formation and dispersion (Lin and Cheng, 2019), while the *rhl* system positively regulates the production of the biosurfactant rhamnolipid, which is important for late biofilm formation (Davey et al., 2003; Lequette and Greenberg, 2005; Chrzanowski et al., 2012). The *P. aeruginosa pqs* system uses 2-alkyl-4-quinolones (AQs) as signaling molecules. These AQs mainly include 2-heptyl-3-hydroxy-4-quinolone (PQS) and its precursor 2-heptyl-4-hydroxyquinoline (HHQ), both of which are recognized by the cognate receptor MvfR (Multiple virulence factor regulator, a *P. aeruginosa* quorum-sensing transcription factor, also known as PqsR; Lin et al., 2018a). Through interaction with this receptor, HHQ and PQS induce the expression of a variety of genes, including their own biosynthetic enzyme cascade and genes involved in biofilm formation (Schutz and Empting, 2018).

Anti-biofilm strategies: Current approaches and perspectives

Antibiotics have been widely used to treat biofilm infections, but clinical treatment still faces many challenges due to drug resistance issues, biofilm matrices that hinder drug penetration, and drug-microbe interactions (Kamaruzzaman et al., 2018). Therefore, many new anti-biofilm technologies have been developed (Hughes and Webber, 2017), such as combining antibiotics and using new strategies, for example, gallium, phage therapy, and antimicrobial photodynamic therapy (aPDT), to inhibit biofilm formation. Table 1 summarizes the strategies

TABLE 1 Different strategies to treat *Pseudomonas aeruginosa* infectious biofilms.

Strategy	Mechanism	Molecules associated	Reference
Antibiotics	Antibiotics are used in combination with antibiotics or other substances to destroy biofilms and prevent the development of antibiotic resistance	Gentamicin/ciprofloxacin, tobramycin/clarithromycin, linolenic acid-tobramycin, gentamicin-EDTA, glutamine-ampicillin	Chauhan et al., 2012; Chanda et al., 2017; Ghorbani et al., 2017; Wang et al., 2019; Zhao et al., 2021
AMPs[a]	Interact and penetrate with the bacterial cell membrane to cause the death of the bacteria	LL-37, P5, cationic peptide 1,037, MC1, WLBU2	Overhage et al., 2008; de la Fuente-Nunez et al., 2012; Lin et al., 2018b Martinez et al., 2019; Yu et al., 2019
QSIs[b]	Inhibit the QS system and interfere with signaling molecules and receptor proteins	Zingerone, trans-cinnamaldehyde and salicylic acid, chloroacetamide and maleimide analogs, halogenated furanone derivatives, M64, QSI4	Kumar et al., 2015; Ahmed et al., 2019; O'Brien et al., 2015; Maura and Rahme, 2017; Chang et al., 2019; Schutz et al., 2021
Enzymes or polysaccharides	Target extracellular polymeric substances (such as exopolysaccharides, matrix proteins, and eDNA) to disrupt biofilms	DNase I, glycoside hydrolases PelA and PslG, alginate lyase AlyP1400, A101, EPS273	Jiang et al., 2011; Hymes et al., 2013; Zhang et al., 2018; Daboor et al., 2021; Wu et al., 2021
Ga^{3+}	Acts as a "Trojan horse" to disrupt bacterial Fe metabolism and inhibit *P. aeruginosa* growth	Desferrioxamine-gallium, Ga-Cit, Ga $(NO_3)_3$	Banin et al., 2008; Rzhepishevska et al., 2011; Kang et al., 2021
NO	Creates nitrosative stress or oxidative stress in the biofilm and aids in biofilm dispersal	NO-sensing proteins	Hossain and Boon, 2017
Bacteriophages	Encode enzymes to destroy the extracellular matrix	IME180, quorum quenching lactamase	Pei and Lamas-Samanamud, 2014; Mi et al., 2019
aPDT[c]	PS binds to the biofilm matrix and generates ROS under light, initiating multi-target damage	Tetra-Py^+-Me, MB + GN, ICG-APTMS@SPION/laser	Beirao et al., 2014; Bilici et al., 2020; Perez-Laguna et al., 2020

[a]Antimicrobial peptides.
[b]Quorum-sensing inhibitors.
[c]Antimicrobial photodynamic therapy.

discovered in recent years for the treatment of *P. aeruginosa* biofilm infection and the different action mechanisms of related anti-biofilm molecules.

Antibiotics

It is well known that antibiotic therapy is the most important and effective measure to control bacterial infection. However, bacterial biofilms are highly resistant to antibiotic treatment and immune response (Shrivastava et al., 2018; Srinivasan et al., 2021). Due to the low outer membrane permeability of *P. aeruginosa* and its own adaptive mechanisms, it is less susceptible to most antibiotics and readily achieves clinical resistance. The use of single antibiotics to treat *P. aeruginosa* biofilm infections therefore presents significant challenges, and various strategies have been developed to treat biofilms and prevent the development of antibiotic resistance, including increasing antibiotic concentrations or the use of antibiotics in combination (Khan et al., 2020). Here, we divide the mechanism of action of combined antibiotics into two main categories: the synergistic effect between different antibiotics and the combined use of other substances and antibiotics.

The combined use of different antibiotics against *P. aeruginosa* biofilms has been described in detail in a previous review (Yadav et al., 2021). The antibiotic combinations that have been found to be effective against *P. aeruginosa* biofilm include gentamicin/ciprofloxacin (Wang et al., 2019) and tobramycin/clarithromycin (Ghorbani et al., 2017). These combinations all increase the therapeutic efficacy of antibiotics against *P. aeruginosa* biofilm. In addition to the synergistic effect between antibiotics, substances such as metal chelators, fatty acids, and amino acids combined with antibiotics will also help to prevent the formation of *P. aeruginosa* biofilms. Linolenic acid (LNA) is an essential fatty acid that has antibacterial effects on various microorganisms. Studies have found that LNA can not only interfere with intercellular communication and reduce the production of virulence factors, but can also enhance the potency of tobramycin and synergistically inhibits biofilm formation by affecting *P. aeruginosa* quorum-sensing systems (Chanda et al., 2017). The cation chelator EDTA acts as a therapeutic adjuvant to destabilize biofilm matrices (Lebeaux et al., 2015). Some studies have found that the combination of EDTA and antibiotics can quickly and persistently remove biofilms formed *in vivo* compared with the use of antibiotics alone (Chauhan et al., 2012; Lebeaux et al., 2015). Glutamine is an amino acid that is used as a nutritional source, and the exogenous addition of glutamine can stimulate the influx of ampicillin, resulting in the accumulation of intracellular antibiotic concentrations that exceed the amount tolerated by multidrug-resistant bacteria. Glutamine-enhanced ampicillin-mediated killing has been found to be effective against *P. aeruginosa* biofilms in a mouse model of urinary tract infection.

Moreover, glutamine also retards the development of ampicillin resistance, which may help in the future development of effective antibiotic drugs to prevent or manage difficult-to-treat bacterial biofilms (Zhao et al., 2021). In addition, the addition of extra O_2 *via* hyperbaric oxygen therapy (HBOT) can increase the susceptibility of pathogens to several antibiotics against metabolically active bacteria by activating aerobic respiration. When combined with tobramycin or ciprofloxacin, re-oxygenation with HBOT enhanced the killing of clinical *P. aeruginosa* and the eradication of biofilms (Lichtenberg et al., 2022).

In vitro and *in vivo* experiments showed that the minimum inhibitory concentration (MIC) and minimum bactericidal concentration of biofilm bacterial cells were usually much higher than those of planktonic cells (by about 10–1,000 times; Hoiby et al., 2010, 2011). Therefore, it is difficult to achieve the eradication of biofilms *in vivo* with the use of conventional single antibiotics (Wu et al., 2015; Sharma et al., 2019), while the combination of antibiotics with different antibiotics or other substances to increase their effect as a new strategy for the treatment of biofilm infections has broad prospects. In addition to antibiotics, a variety of compounds have been clinically used to treat *P. aeruginosa* biofilm infection (Soren et al., 2020; Pang and Zhu, 2021). These treatment methods can be roughly divided into two categories: preventing biofilm formation and destroying formed biofilms. For example, antimicrobial peptides (AMPs) and quorum-sensing inhibitors (QSIs) can prevent biofilm formation by regulating the biofilm formation process, while some exopolysaccharide hydrolases and DNases can target biofilm matrix components to destroy biofilms.

AMPs

The clinical application of AMPs is accelerating with increasing antibiotic resistance worldwide (Mahlapuu et al., 2016). AMPs are tiny macromolecules composed of amino acids that have the ability to stimulate innate immune responses and exhibit potent activity against a broad range of bacterial species, fungi, protozoa, and encapsulated viruses (Mahlapuu et al., 2016; Abdi et al., 2019; Seyfi et al., 2020). It is generally acknowledged that most AMPs can directly bind to the bacterial surface, such as the lipopolysaccharide (LPS) of Gram-negative bacteria, and then depolarize and permeate the membrane (Wen et al., 2013; Chou et al., 2019). LL-37, a classic human AMP, has been identified as capable of disrupting bacterial membranes, leading to cell death and inhibiting *P. aeruginosa* biofilm formation (Overhage et al., 2008), but subsequent study has shown that at sub-inhibitory concentrations it can promote *P. aeruginosa* DNA mutations and induce its resistance to antibiotics (Limoli et al., 2014). Despite this, as potential biofilm inhibitors, AMPs still hold great promise for the targeted elimination of biofilm proliferation in multi-drug resistant and extensively drug-resistant bacteria (Pontes et al., 2022). The target of these AMPs in the cell is typically the cell membrane. Through interacting with the bacterial cell membrane and penetrating the cell membrane, AMPs cause the death of the bacteria, thereby reducing the possibility of bacterial resistance (Annunziato and Costantino, 2020). As a promising class of compounds to overcome antimicrobial resistance, AMPs have been shown to have some advantages over traditional antibiotics.

Several studies have reported the mechanism of action of AMPs in detail (Annunziato and Costantino, 2020; Talapko and Skrlec, 2020). This review divides the anti-biofilm action mechanism of AMPs into two categories. AMPs in the first category exhibit anti-biofilm activity through their membrane dissolution mechanism, which directly affects the integrity of bacterial cell membranes and cell walls. The anti-biofilm peptide P5 has been found to have the ability to target the membrane permeability of *P. aeruginosa* and has synergistic and bactericidal effects with the carbapenem antibiotic meropenem (Martinez et al., 2019). An outer membrane permeability assay showed that P5 could easily permeate the cell membrane at concentrations below 0.5 × MIC, which occurred because meropenem entered the cytoplasmic space to interfere with the formation of peptidoglycans in the cell wall. In addition to meropenem, other antibiotics can also act on *P. aeruginosa* biofilms synergistically with AMPs, such as imipenem (Feng et al., 2015) and tobramycin (Beaudoin et al., 2018).

AMPs in the second category affect the growth pattern of biofilms by inhibiting bacterial adhesion and interfering with gene expression. While AMPs are generally considered to be membrane-active molecules that disrupt biofilms by perturbing the cell wall/membrane, AMPs also possess multifunctional activities such as protein synthesis and gene expression at multiple sites within the membrane or within the cell, enabling efficient killing (Le et al., 2017). A novel synthetic cationic peptide, 1,037, can significantly reduce *P. aeruginosa* biofilm formation and lead to cell death in biofilms at certain concentrations. Analysis of its effect on gene expression has revealed that 1,037 directly inhibits biofilms by reducing swimming and swarming motilities, stimulating twitching motility, and inhibiting the expression of various genes involved in biofilm formation, such as *PA2204* (de la Fuente-Nunez et al., 2012). Recent studies have found that the anti-biofilm peptide MC1 can inhibit biofilm formation by down-regulating the relative expression levels of *pelA*, *algD*, and *pslA* genes in *P. aeruginosa* and reducing the synthesis of exopolysaccharides (Yu et al., 2019). Another well-studied AMP, called WLBU2, and its D-amino acid enantiomer D8 have also shown gene modulating activity against *P. aeruginosa* in the biofilm mode of growth, as well as increased safety, stability, and antimicrobial efficacy when substituting the L-amino acids in WLBU2 with D-amino acids (Lashua et al., 2016; Lin et al., 2018b; Di et al., 2020).

As anti-biofilm peptides can inhibit the formation of biofilms or remove mature biofilms, they have been gradually recognized by an increasing number of researchers as a potential new drug for the prevention and treatment of bacterial biofilm infections. However, there are still many obstacles to clinical application. For example, anti-biofilm peptides tend to show a certain degree of

hemolysis or cytotoxicity to eukaryotic cells, and they are easily hydrolyzed by protease and cannot exist stably *in vivo* (Aoki and Ueda, 2013). In addition, the high production cost of anti-biofilm peptides and long drug development cycle also limit their potential clinical application.

QSIs

In recent years, an increasing number of studies have developed new antibacterial drugs by targeting specific virulence factors or their regulatory mechanisms to reduce the emergence of drug-resistant strains (Muhlen and Dersch, 2016; Kamal et al., 2017). One of these strategies is directed toward interference with QS-mediated signaling. The QS system of *P. aeruginosa* consists of four systems that interact to form a complex intercellular communication network that regulates the expression of its virulence-related genes and biofilm formation in a cell-density-dependent manner by generating QS signaling molecules (Rutherford and Bassler, 2012; Yong et al., 2018; Lin et al., 2018a).

QSIs can be either natural or synthetic, and both types of QSIs can inhibit the formation of biofilms by targeting different sites (Kalia, 2013). This review divides QSIs into two categories: QSIs that inhibit the expression of the QS system and QSIs that interfere with the combination between signaling molecules and receptor proteins. The first type of QSI interferes with and inhibits the expression of the QS system, altering the *P. aeruginosa* biofilm architecture and enabling antibiotics to better penetrate and more efficiently kill bacterial cells. In a previous study, the naturally isolated plant compounds trans-cinnamaldehyde and salicylic acid effectively down-regulated both the *las* and *rhl* QS systems, significantly inhibited the expression of QS regulatory and virulence genes in *P. aeruginosa* PAO1, and also reduced biofilm formation concomitantly with repressed rhamnolipid gene expression (Rajkumari et al., 2018; Ahmed et al., 2019). In addition, a host of synthetic biofilm inhibitors have also been developed. Chloroacetamide and maleimide analogs, as potent, drug-like small molecule inhibitors of QS in *P. aeruginosa*, are anticipated to be of significant medical interest. These inhibitors exhibit potent LasR antagonist activity and inhibit the expression of the *P. aeruginosa* virulence factor pyocyanin, as well as biofilm formation in PAO1 and PA14 (O'Brien et al., 2015). In addition, Chang et al. identified a new series of halogenated furanone derivatives and found that they effectively inhibited *lasB* expression in a dose-dependent manner and showed remarkable biofilm formation in *P. aeruginosa* (Chang et al., 2019).

The second category of QSI molecules functions by interfering with and inhibiting the combinations between signaling molecules and receptor proteins that are required for bacterial cell-to-cell communication, the production of virulence factors, and biofilm formation (Soukarieh et al., 2018). Ginger has been widely used as a medicinal herb with strong antimicrobial properties. Zingerone is one of the main components of dry ginger root, is found in many herbal spices, and can effectively regulate the biofilm structure of *P. aeruginosa* (Kumar et al., 2013). In *P. aeruginosa*, zingerone inhibits the *las*, *rhl*, and *pqs* systems by binding to their respective cognate receptors (LasR, RhlR, and MvfR), which silences the cell communication network and ultimately suppresses the virulence and biofilm formation of *P. aeruginosa* (Kumar et al., 2015). Furthermore, MvfR, as a crucial transcriptional regulator of the PQS system of *P. aeruginosa*, is considered to a potential target for inhibiting the PQS-MvfR QS system (Kitao et al., 2018). The benzamide-benzimidazole compound M64 can inhibit the *P. aeruginosa* QS regulator MvfR, resulting in reduced biofilm formation and the increased susceptibility of *P. aeruginosa* to antibiotics (Maura and Rahme, 2017). Recently, a study has reported a novel class of QSIs called QSI4, which possesses excellent activity in inhibiting pyocyanin production and the MvfR reporter-gene; when combined with antibiotics, QSI4 has a significant synergistic effect on the elimination of *P. aeruginosa* biofilm (Schutz et al., 2021).

As an important intercellular communication system in *P. aeruginosa*, the QS system plays a key role in the regulation of biofilm formation. QSIs inhibit biofilm formation through anti-virulence or a pathoblocker approach, which can synergize the efficacy of antibiotics but does not affect the viability of bacteria. Clinical application of QSIs will reduce the development of antibiotic resistance as well as some toxic side effects (Wagner et al., 2016). Therefore, QSIs are currently promising drug targets for the prevention and treatment of *P. aeruginosa* infection.

Targeting polysaccharides

As functionally rich and dynamically changing communities, biofilms can modify matrix components to adapt to changes in various environmental conditions and pressures. In *P. aeruginosa*, enzymes targeting biofilm EPSs may offer a general strategy to prevent clinical biofilm infections (Zhao et al., 2018). The bacteria themselves also synthesize polysaccharides or certain endogenous matrix-degrading enzymes to induce the dispersion of the biofilm, such as glycoside hydrolases (Srinivasan et al., 2021).

A key component of biofilm formation is the biosynthesis of the exopolysaccharides Pel, Psl, and alginate (Limoli et al., 2015). Enzymes targeting the extracellular matrix could serve as targets to disrupt biofilms. Alginate lyase can degrade alginate through the β-elimination of glycosidic bonds to disrupt the structure and integrity of biofilms and significantly increase biofilm diffusion (Kovach et al., 2020). Recently, a study has reported an alginate lyase (AlyP1400) purified from a marine bacterial *Pseudoalteromonas* species that can treat *P. aeruginosa* infections in cystic fibrosis lungs or other *P. aeruginosa* biofilm-related infections by combining the use of the alginate lyase with antibiotics (Daboor et al., 2021). The glycoside hydrolases alpha-amylase and cellulase can also break down complex polysaccharides, convert the bacteria into a planktonic state, effectively destroy *P. aeruginosa* biofilm, and increase antibiotic efficacy (Fleming et al., 2017; Redman et al., 2020). In addition, PelA and PslG, as naturally derived glycoside

hydrolases, can selectively target and degrade exopolysaccharides in the biofilm matrix, thus destroying the biofilm (Baker et al., 2016; Zhang et al., 2018). In a previous study, overexpressed or exogenously supplied PslG prevented biofilm formation by degrading Psl (Yu et al., 2015). As a hydrolase, PelA can scavenge polysaccharides in the periplasm, and its deacetylase activity is related to the formation of biofilms and the morphology of wrinkled colonies (Colvin et al., 2013; Marmont et al., 2017). Recently, our team has used *P. aeruginosa* as the starting strain to construct an engineered bacterium for the targeted transport and delivery of functional proteins that can use two polysaccharide hydrolases, PelA and PslG, to target biofilms (Figure 2). First, the engineered bacterium was constructed through synthetic biology so that it could initiate the lysis of its own cells, and then, the recombinant vectors were introduced to overexpress the two exopolysaccharide hydrolase genes *pelA* and *pslG*. Finally, the effect of engineered bacteria on *P. aeruginosa* biofilm was detected by biofilm formation experiments. It was found that overexpression of *pelA* and *pslG* could accumulate polysaccharide hydrolases in the intracellular matrix and release them to the extracellular matrix through the cell lysis site to disrupt the biofilm cytoskeletal components Psl and Pel, eventually destroying the biofilm and preventing further biofilm formation (Wang et al., 2021).

The extracellular biofilm matrix of *P. aeruginosa* is mainly composed of exopolysaccharides, which are involved in the formation and maintenance of the structural biofilm (Franklin et al., 2011). However, some bacterial exopolysaccharides can perform functions that inhibit or destabilize the biofilm (Rendueles et al., 2013). A former study showed that *P. aeruginosa* extracellular products, mainly polysaccharides, disrupted established biofilms (Qin et al., 2009). Recently, more exopolysaccharides have been found to show negative activity against biofilm formation in *P. aeruginosa*. A bacterial exopolysaccharide (A101) not only inhibits the biofilm formation of many bacteria but also disrupts established biofilms. In addition, A101 increased the ability of aminoglycoside antibiotics to eliminate *P. aeruginosa* biofilm, which may indicate that A101 has potential in the design of new therapeutic strategies for bacterial biofilm-associated infections and in limiting biofilm formation on medical indwelling devices (Jiang et al., 2011). A recent experiment has reported an exopolysaccharide, EPS273, that reduces biofilm formation in *P. aeruginosa* by reducing the expression levels of the two-component system *phoP–phoQ*, which then regulates the expression levels of the QS systems *lasI/lasR* and *rhlI/rhlR*. The QS system further regulates the genes involved in biofilm formation, such as the genes involved in the production of the extracellular

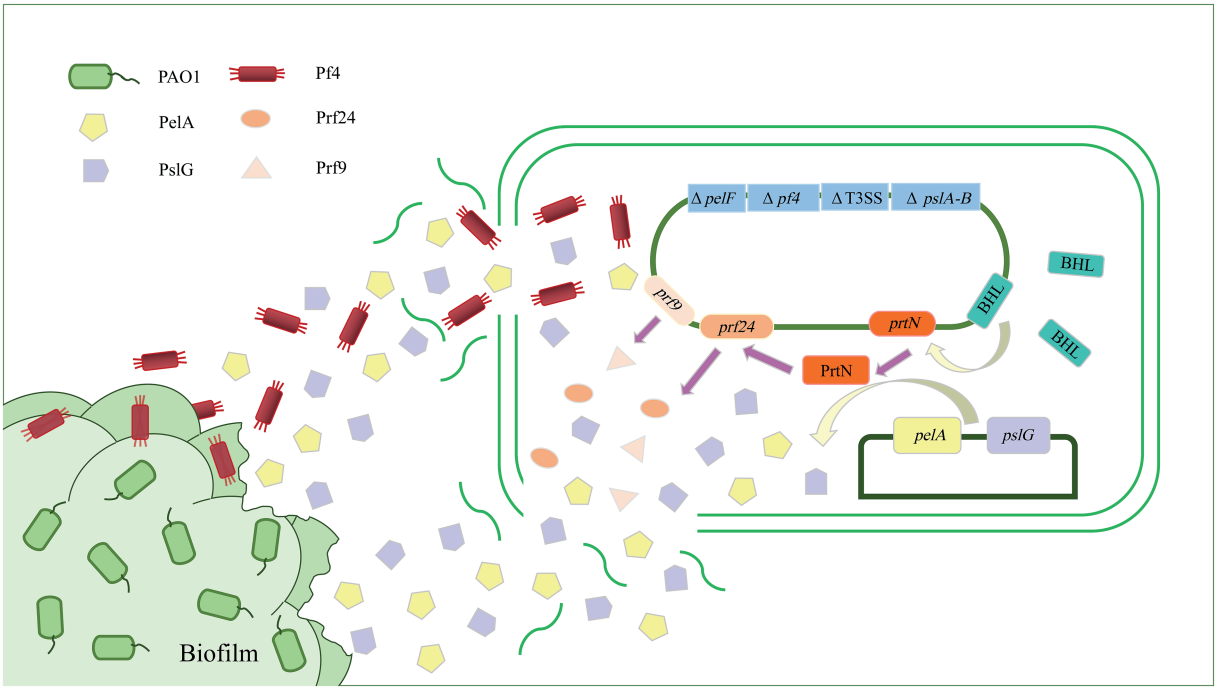

FIGURE 2
Schematic diagram of targeted delivery of extracellular glycoside hydrolase by engineered bacteria to destroy *Pseudomonas aeruginosa* biofilm. The biofilm formation and virulence-related genes *pelA-B*, *pelF*, and T3SS of *P. aeruginosa* were knocked out as parental strains, and exogenous recombinant vectors were introduced to overexpress the exopolysaccharide hydrolases PelA and PslG. PelA and PslG accumulated in cells and were then released into the extracellular matrix through cell lysis. There are two ways in which hydrolases are released into the extracellular matrix. The first is through regulating the *prtN* gene to activate the expression of cell lysis protein genes, thereby releasing PelA and PslG. The second is by deleting the Pf4 filamentous prophage-encoding gene cluster to sensitize it to the Pf4 phage in biofilms, thereby initiating the passive lysis mechanism of its own cells to release PelA and PslG. The PelA and PslG are released to the extracellular matrix to destroy the biofilm skeleton components Pel and Psl through enzymatic hydrolysis, thereby destroying the *P. aeruginosa* biofilm.

matrix and virulence factors, genes involved in flagella and cell motility, and genes involved in iron acquisition (Wu et al., 2021).

DNase

eDNA plays a structural role in the formation of biofilms (Allesen-Holm et al., 2006). eDNA can serve as a source of nutrients for bacteria under starvation and is involved in facilitating the twitching motility-mediated expansion of biofilms (Finkel and Kolter, 2001; Wei and Ma, 2013). In addition, eDNA interacts with Psl to form eDNA-Psl to provide structural support for biofilms (Wang et al., 2015). Based on these factors, drug pathways for targeting biofilm matrices *via* eDNA are emerging.

Deoxyribonuclease I (DNase I) is the only enzyme used clinically to disrupt the biofilm of *P. aeruginosa*. This therapeutic enzyme disrupts biofilms through the hydrolysis of DNA in the extracellular matrix (Hymes et al., 2013). DNase is involved in breaking the phosphodiester linkage in the eDNA molecular backbone in biofilms. As eDNA is essential for the initial attachment and aggregation of EPSs on the surface, this makes it difficult for bacteria to form an intact biofilm (Das et al., 2010; Srinivasan et al., 2021). Immature *P. aeruginosa* biofilms are therefore more sensitive to DNase treatment than mature biofilms (Hymes et al., 2013). Some studies have found that L-methionine (L-Met) can destroy *P. aeruginosa* biofilms through up-regulating DNase genes and inducing the expression of DNase, thereby targeting eDNA in biofilms (Gnanadhas et al., 2015). In addition, some DNase-like proteins have also been found to prevent and destroy bacterial biofilms. DNase1-like 2 (DNase1L2) expressed in human stratum corneum has enzymatic activity, can degrade eDNA, and can effectively inhibit *P. aeruginosa* biofilm formation (Eckhart et al., 2007). In addition, DNase I coatings are used as antimicrobial coatings for modern medical equipment. DNase I immobilization on surfaces has shown promise in reducing bacterial adhesion to surfaces, as this enzyme targets single biofilms and can effectively cleave eDNA on bacterial cell surfaces that are essential for bacterial adhesion (Swartjes et al., 2013; Sharma and Pagedar Singh, 2018). With the ongoing rise in antibiotic resistance, DNase I coating may provide a timely, potent new approach to prevent the formation of biofilms on biomaterial implants and devices.

When the biofilm matures to a certain extent, DNase treatment is no longer effective (Whitchurch et al., 2002). This resistance to DNase may be due to the replacement or supplementation of eDNA by other extracellular matrix components, or the binding of eDNA to another component that protects it from enzymatic degradation (Okshevsky et al., 2015). Therefore, enzymatic hydrolysis methods that destabilize biofilms by enzymatically degrading eDNA should also target polysaccharides or proteins bound to eDNA. For example, the interactions between eDNA with Psl and Type IV pili play important roles in biofilm formation (Barken et al., 2008), and disrupting these interactions could also be a potentially interesting target for biofilm treatment. In addition to DNase, the accumulation of eDNA itself in biofilms and infection sites can acidify the local environment (Wilton et al., 2016). The acidic environment stimulated increased *P. aeruginosa* biofilm formation, promoted faster bacterial evolution to improve antibiotic resistance, and increased the expression of multiple biofilm/virulence-related genes. Therefore, the use of simple pH-buffering agents alongside antibiotics may be a novel treatment strategy for combating chronic infection in the acidic, DNA-enriched lungs of clinic patients (Lin et al., 2021).

Gallium (Ga)

Recently, Ga ions have shown excellent anti-*Pseudomonal* activity and have been used as a novel biofilm treatment approach (Smith et al., 2017; Tummler, 2019; Tovar-Garcia et al., 2020). Previous research has used Ga as a "Trojan horse" to disrupt bacterial iron metabolism and exploit the Fe stress of *in vivo* environments because Ga has an ionic radius nearly identical to that of Fe, and many biological systems are unable to distinguish Ga^{3+} from Fe^{3+} (Kaneko et al., 2007). While Ga^{3+} chemically resembles Fe^{3+}, unlike iron, Ga cannot be reduced under physiological conditions, which also inhibits some of its basic functions (Minandri et al., 2014). Iron is not only a necessary element for growth but is also a cue in biofilm formation (Banin et al., 2005). Thus, interfering with bacterial iron homeostasis may serve as a potential therapeutic target that can block *P. aeruginosa* virulence in both the free-living and biofilm states.

Previous research found that low concentrations of Ga inhibited *P. aeruginosa* growth and prevented biofilm formation. This inhibition was mediated by the repression of the transcriptional regulator *pvdS*, as overriding *pvdS* repression partially protected bacteria from the growth-inhibitory action of Ga (Kaneko et al., 2007). Besides Ga alone, some complexes with Ga can also target *P. aeruginosa* iron metabolism to inhibit biofilm formation, such as desferrioxamine-Ga (DFO-Ga) and Ga citrate (Ga-Cit). Desferrioxamine (DFO) is a hydroxamate-based siderophore that induces proteins related to iron citrate and iron DFO uptake in iron-starved *P. aeruginosa* (Llamas et al., 2006; Marshall et al., 2009). The complex DFO-Ga, which can kill free-living bacteria and prevent biofilm formation, has been approved for clinical use (Banin et al., 2008). However, recent research indicates that Ga-Cit has an anti-biofilm effect and is more bactericidal than Ga-DFO (Rzhepishevska et al., 2011). Like other Ga complexes, Ga-Cit significantly inhibited biofilm production in *P. aeruginosa* at concentrations as low as 10 μM (Rzhepishevska et al., 2011). Moreover, several studies have explored the activity of Ga in combination with antibiotics in search of useful synergistic effects. Ga nitrate has been found to be an effective antimicrobial agent that inhibits *P. aeruginosa* growth. A recent study found that $Ga(NO_3)_3$ and tetracycline alone had a bactericidal effect, and the combined use of the two strongly inhibited the formation of *P. aeruginosa* biofilm (Kang et al., 2021).

Ga^{3+} is effective in destroying bacterial biofilms, and many drugs based on Ga have been approved for clinical treatment with remarkable results (Goss et al., 2018). For example, $Ga(NO_3)_3$, which is approved by the US Food and Drug Administration (FDA) for the treatment of infections, can be used to treat both acute and chronic pneumonia caused by *P. aeruginosa* infection (Bonchi et al., 2015). In addition to Ga and its compounds, combined use with antibiotics has achieved remarkable results in clinical treatment. Therefore, Ga, as a target for destroying biofilms, has potential in the development of more effective drugs for the treatment of biofilm infections.

Nitric oxide

Pseudomonas aeruginosa is a facultative anaerobe that can breathe under anaerobic conditions and denitrify in the presence of nitrate and nitrite. These abilities are associated with the virulence of bacteria (Cutruzzola and Frankenberg-Dinkel, 2016). NO is a radical diatomic gas molecule that plays important signaling roles in both eukaryotes and bacteria at low concentrations (Arora et al., 2015). NO has also been demonstrated to be an effective *P. aeruginosa* biofilm disruption agent that creates nitrosative or oxidative stress in the biofilm and induces the dispersal of *P. aeruginosa* and other bacterial biofilms by reducing c-di-GMP levels (Williams and Boon, 2019).

An early study of the effect of NO on biofilm formation showed that nanomolar NO caused biofilm dispersal in *P. aeruginosa* and enhanced the efficacy of antimicrobial compounds when combined with antibiotics (Barraud et al., 2006). This finding was confirmed in the clinical treatment of cystic fibrosis patients (Howlin et al., 2017). However, another study found that the exogenous addition of high concentrations of iron inhibited the diffusion of NO-induced biofilms and promoted the rapid attachment of plankton cells and resumed diffusion after the addition of iron chelator agents (Zhu et al., 2019). This is not due to the scavenging of NO by free iron but was related to an iron-induced cellular response that led to the increased production of the exopolysaccharide Psl and restored *P. aeruginosa* biofilm diffusion. Very recently, a novel family of heme-based NO binding proteins termed NO-sensing proteins (NosP) have been discovered in *P. aeruginosa* in the same operon as *PA1976* (NahK). NahK has been identified as a NosP-associated histidine kinase, and it has been previously associated with biofilm regulation (Hossain and Boon, 2017). Experiments have suggested that NosP binds to NO, which controls the phosphorylation of a histidine-containing phosphotransfer domain, thus resulting in biofilm dispersal. However, the specific players involved in the signaling pathway have yet to be identified.

Although NO has attracted particular interest due to its role in biofilm dispersal, this approach still presents many practical issues in clinical trials. For example, the current inhaled NO therapy method is extremely expensive, largely owing to the difficulty in handling the gas and its incompatibility with oxygen, which results in the formation of toxic nitrogen dioxide (NO_2; Yang et al., 2015). Therefore, while the bactericidal effect of antibacterial agents on biofilm-infected sites can be enhanced in a targeted manner, the NO-mediated toxicity should also be reduced so that it can be used in clinical anti-biofilm therapy (Barraud et al., 2012). In addition, the use of NO in combination with antibiotics can enhance the NO-mediated bactericidal effect and improve the specificity of NO delivery, so the use of NO is still very promising (Poh and Rice, 2022).

Bacteriophage therapy

Bacteriophages are natural bacterial viruses (Clokie et al., 2011). As they are unaffected by antibiotic resistance, bacteriophages have been used as therapeutic agents in early clinical practice (Kutter et al., 2010; Abedon et al., 2011). With the emergence of antibiotic-resistant strains, phage therapy has once again drawn attention, and a growing body of research has validated the use of bacteriophages in therapy and prophylaxis in the fight against drug-resistant bacteria (Kutateladze and Adamia, 2010). Phages can encode enzymes that degrade polymers and inhibit *P. aeruginosa* biofilm formation by disrupting the extracellular matrix and increasing the permeability, allowing antibiotics to reach the inner layer of biofilms (Harper et al., 2014). Therefore, an increasing number of studies have used bacteriophages to develop drugs to treat biofilm infections (Soothill, 2013).

The pathways by which phages destroy biofilms can be divided into two categories. First, phages can destroy biofilm structures by inducing the synthesis of enzymes such as polysaccharide depolymerases in *P. aeruginosa* (Pires et al., 2016; Chegini et al., 2020). Polysaccharide depolymerase is a polysaccharide hydrolase encoded by bacteriophages that can specifically degrade macromolecular carbohydrates on the host bacterial envelope (Yan et al., 2014). IME180, a *P. aeruginosa* phage isolated from a hospital, encodes an exopolysaccharide-degrading enzyme that is highly homologous to deglycans and can effectively degrade exopolysaccharides, inhibiting the formation of host bacterial biofilms and destroying established biofilms (Mi et al., 2019). In addition to polysaccharide hydrolases, bacteriophages can also produce endolysins, which inhibit bacterial cell wall synthesis by hydrolyzing peptidoglycan (Schmelcher et al., 2012). Another way in which bacteriophages inhibit biofilms is through the production of enzymes that inhibit biofilm production. A study has reported that phages can be genetically modified to induce the synthesis of quorum quenching lactamase, thereby inhibiting bacterial biofilm formation (Pei and Lamas-Samanamud, 2014). An engineered T7 phage incorporating the AHL lactonase *aiiA* gene can hydrolyze acyl AHL and inhibit QS activities in *P. aeruginosa*, ultimately inhibiting biofilm production (Whiteley et al., 2017). Unlike polysaccharide depolymerases, which can degrade one or several related polysaccharides, the T7*aiiA* phage can affect multiple bacteria in mixed-strain biofilms, rather than the host bacteria alone.

In addition to being directly used as a tool to destroy biofilms, phages can also indirectly aid in other strategies to destroy biofilms. In *P. aeruginosa* PAO1, Pf4 filamentous phages naturally parasitize by integrating into the genome and play critical roles in PAO1 virulence, biofilm development, and structural stability. Studies have shown that *P. aeruginosa* lacking the Pf4 filamentous phage-encoding gene cluster is highly susceptible to Pf4 filamentous phages. Therefore, we mutated the gene cluster encoding Pf4 filamentous phage when constructing the engineered bacteria, which made it very sensitive to Pf4 filamentous phage in biofilms. Upon contact, Pf4 filamentous phage could infect and lyse the engineered bacteria to release the intracellular accumulation of exopolysaccharide hydrolase PelA and PslG, thereby destroying the biofilm of *P. aeruginosa* (Figure 2; Wang et al., 2021).

As mentioned earlier, bacteriophages are considered to be potential drugs for the prevention and control of biofilms due to their infection diversity and specificity (Melo et al., 2019). However, the application of phages in biofilm control still has some limitations (Abedon et al., 2021). For example, a reduction in the metabolic activity of biofilm bacterial cells due to phage infection is dependent on host growth conditions (Chegini et al., 2020) and stimulates the rapid release of bacterial endotoxins, leading to an inflammatory response (Ferriol-Gonzalez and Domingo-Calap, 2020).

aPDT

aPDT is an emerging non-invasive treatment method that uses non-toxic photosensitizer (PS), specific wavelengths of visible or near-infrared light, and molecular oxygen around or inside pathogens to produce phototoxic reactions to kill pathogens (Rajesh et al., 2011). aPDT can also destroy microbial biofilms in a process that consists of two steps. The first step is the binding of PSs to the biofilm matrix. Although some types of PSs only bind to the cell surface, most types of PSs can pass through the cytoplasmic membrane and enter the cytoplasm. PSs bound to the biofilm matrix generate reactive oxygen species (ROS) under light, thereby initiating multi-target damage (Hu et al., 2018), which attacks various biofilm components, leading to disintegration, including the disintegration of lipids, proteins, DNA, and exopolysaccharides in the matrix (Dosselli et al., 2012; Martins Antunes de Melo et al., 2021). Studies have reported many examples of aPDT used in the treatment of biofilm infections, and some have been used in clinical trials (Tahmassebi et al., 2015; Liang et al., 2020).

Polysaccharides are the most abundant polymers in biofilm matrices In the presence of a certain concentration of Tetra-Py^{+}-Me, the polysaccharide concentration in the *P. aeruginosa* biofilm was significantly reduced after irradiation, and its biofilm substrate was attacked by photodynamic force and destroyed (Beirao et al., 2014). aPDT targeting related proteins also affect *P. aeruginosa* biofilm formation. The PS methylene blue (MB) combined with the antibiotic gentamicin (GN) has a synergistic antibacterial effect on plankton. Adding GN at a concentration where MB alone does not have a significant antibacterial effect can exert a positive bactericidal effect against *P. aeruginosa* biofilms. This synergistic killing mechanism may be caused by GN acting on the level of protein synthesis, changing the permeability of the bacterial wall and thereby promoting the accumulation of MB, but its potential mechanism needs further research (Perez-Laguna et al., 2020). Recently, antimicrobial photothermal therapy (aPTT) was demonstrated to be a promising method to eliminate planktonic cells and biofilms (Al-Bakri and Mahmoud, 2019; Li et al., 2019). The combined use of aPDT and aPTT has also become an effective local replacement therapy for the treatment of antibiotic-resistant bacterial infections and biofilms (Bilici et al., 2020). While 3-aminopropylsilane-coated superparamagnetic iron oxide nanoparticles have no significant inhibition on biofilms without laser treatment, the addition of laser treatment significantly reduces *P. aeruginosa* biofilms. Furthermore, after combining nanoparticles with PS, the biofilm can be reduced again. This combination of nanoparticles and PS may enhance the treatment of drug-resistant bacteria and their biofilms through the dual aPDT/aPTT mechanism (Bilici et al., 2020).

Due to its multi-targeted damage to microbial cells and its inability to induce drug resistance, aPDT has received increasing attention as an alternative treatment (Cieplik et al., 2018), and it is also effective in combination with antibiotics (Feng et al., 2021). However, the application of aPDT has certain limitations. The limitation of light transmission conditions makes it more effective in the clinical treatment of local infections. In addition, the characteristics of PS and the corresponding light source affect its application. PS with low molecular weight and high penetrating power should be selected, and the cost should also be controlled (Wainwright et al., 2017).

Conclusions and prospective applications

Pseudomonas aeruginosa biofilm includes three main parts: exopolysaccharides, eDNA, and matrix protein. Different components play different roles in its adhesion, maturation, and dispersal processes and are regulated by factors such as the QS system. The most commonly used treatment of *P. aeruginosa* biofilm infection is mainly a single antibiotic treatment, but this clinical treatment faces many challenges due to drug resistance. With the development of drug-resistant strains, many promising therapeutic strategies have been developed to address these issues, such as combining antibiotics, targeting biofilms through enzymes or quorum-sensing systems, or using new photodynamic therapies and other compounds to prevent or inhibit

P. aeruginosa biofilm formation by targeting the diffusion of biofilm formation. NO has also been shown to regulate biofilms through targeted diffusion (McDougald et al., 2011), exerting an inhibitory effect in the final stages of biofilm formation. However, when using dispersion as a therapeutic strategy, it is uncertain how efficient the dispersion reaction needs to be to become an effective therapeutic agent, and clinical treatments are mostly conducted on mixed biofilms (Lee and Yoon, 2017), which requires researchers to further explore diffusing agents and diffusion-inducing agents.

In addition to the above-mentioned therapeutic strategies, there are many other interesting methods that can be used to remove *P. aeruginosa* biofilms in clinical practice. *P. aeruginosa* itself can produce signal molecules that have inhibitory activity on its formed biofilm. For example, cis-2-decenoic acid, a short-chain fatty acid produced by *P. aeruginosa*, acts as a dispersal signal targeting the biofilm of some bacteria (Rahmani-Badi et al., 2014; Vuotto and Donelli, 2019; Jiang et al., 2020). In addition, some new materials such as nanoparticles, a class of emerging antibacterial agents, exhibit an antibacterial mechanism that includes the destruction of bacterial biofilms, and many innovative anti-biofilm nanomedicines and nanomaterials have been developed for clinical treatment (Xiu et al., 2021). A recent study developed a novel photocatalytic quantum dot-armed bacteriophage nanosystem that combined phage therapy and photodynamic therapy, not only specifically binding to host *P. aeruginosa*, but also targeting host bacteria through the inherent infectivity of phages, locally generating massive amounts of ROS under visible light irradiation, and thereby demonstrating potent anti-biofilm activity (Wang et al., 2022). However, microorganisms adhere to the surfaces of medical devices and are prone to forming biofilms, leading to inevitable and challenging issues with *P. aeruginosa* biofilm infection caused by the use of clinical medical devices (Wi and Patel, 2018). The surface modification of biomaterials has been the focus of extensive research to decrease microbial colonization and biofilm formation, and has been reviewed in detail (Yadav et al., 2021). An effective antimicrobial surface coating can prevent *P. aeruginosa* from adhering, achieving an anti-biofilm effect. One study achieved zero *P. aeruginosa* biofilm adhesion by adding lubricating fluids, consisting of perfluorinated liquids, to porous polytetrafluorethylene (PTFE) to fabricate liquid-infused surfaces (Epstein et al., 2012). In addition, the production of *P. aeruginosa* biofilms was reduced by four orders of magnitude after using a slippery omniphobic covalently attached liquid surface compared to polydimethylsiloxane (PDMS), a widely used medical implant material (Zhu et al., 2022). This biofilm-resistant liquid-like solid surface provides a novel strategy for the treatment of *P. aeruginosa* biofilms.

In addition to *P. aeruginosa*, there are multiple microorganisms that cause biofilm-related diseases, such as *Staphylococcus aureus*, *Candida albicans*, and *Mycobacterium tuberculosis*, which cause serious global health problems due to their resistance to antimicrobial agents. The rapid development of new antimicrobial agents to overcome resistance is urgent, and gaining insights into the specific mechanisms of biofilm occurrence and their interactions with the host is key to solving the problem. Although biofilms have been studied through genomics, proteomics, and RNA sequencing, the rapid evolution of microorganisms has exceeded the pace of therapeutic technology development. New technologies to monitor biofilm formation and the responses of biofilm to antibiotic therapy are required. Furthermore, direct eradication becomes difficult as pathogens evolve defenses against antimicrobial agents, and inhibiting bacterial virulence may be more effective than killing bacteria while also providing new possibilities for the treatment of biofilm infections.

Author contributions

JL conceptualized the article and critically revised the work. RY, JC, JW, and PL performed the literature search and wrote the manuscript. RY and JC prepared the figures and tables. All authors contributed to the article and approved the submitted version.

Funding

This work was supported by the National Natural Science Foundation of China (32070103, 31860012, and 31700031), the Natural Science Basic Research Plan in Shaanxi Province of China (2021JM-415), the Regional Development Talent Project of the "Special Support Plan" of Shaanxi Province, a grant from the Outstanding Young Talent Support Plan of the Higher Education Institutions of Shaanxi Province, the Youth Innovation Team of Shaanxi Universities (2022), and by the Startup Foundation for Doctors of Yan'an University (YDBK2016-01).

Conflict of interest

The authors declare that the research was conducted in the absence of any commercial or financial relationships that could be construed as a potential conflict of interest.

Publisher's note

References

Abdi, M., Mirkalantari, S., and Amirmozafari, N. (2019). Bacterial resistance to antimicrobial peptides. *J. Pept. Sci.* 25:e3210. doi: 10.1002/psc.3210

Abedon, S. T., Danis-Wlodarczyk, K. M., Wozniak, D. J., and Sullivan, M. B. (2021). Improving phage-biofilm in vitro experimentation. *Viruses* 13, 1175. doi: 10.3390/v13061175

Abedon, S. T., Kuhl, S. J., Blasdel, B. G., and Kutter, E. M. (2011). Phage treatment of human infections. *Bacteriophage* 1, 66–85. doi: 10.4161/bact.1.2.15845

Ahmed, S., Rudden, M., Smyth, T. J., Dooley, J. S. G., Marchant, R., and Banat, I. M. (2019). Natural quorum sensing inhibitors effectively downregulate gene expression of *Pseudomonas aeruginosa* virulence factors. *Appl. Microbiol. Biotechnol.* 103, 3521–3535. doi: 10.1007/s00253-019-09618-0

Al-Bakri, A. G., and Mahmoud, N. N. (2019). Photothermal-induced antibacterial activity of gold nanorods loaded into polymeric hydrogel against *Pseudomonas aeruginosa* biofilm. *Molecules* 24, 2661. doi: 10.3390/molecules24142661

Al-Dahmoshi, H., Al-Obaidi, R., and Al-Khafaji, N. (2021). "*Pseudomonas aeruginosa*: diseases, biofilm and antibiotic resistance." In: *Pseudomonas aeruginosa — Biofilm Formation, Infections and Treatments*. eds. T Das. (London: InTechOpen Limited).

Allesen-Holm, M., Barken, K. B., Yang, L., Klausen, M., Webb, J. S., Kjelleberg, S., et al. (2006). A characterization of DNA release in *Pseudomonas aeruginosa* cultures and biofilms. *Mol. Microbiol.* 59, 1114–1128. doi: 10.1111/j.1365-2958.2005.05008.x

Annunziato, G., and Costantino, G. (2020). Antimicrobial peptides (AMPs): A patent review (2015-2020). *Expert Opin. Ther. Pat.* 30, 931–947. doi: 10.1080/13543776.2020.1851679

Martins Antunes de Melo, W. C., Celiesiute-Germaniene, R., Simonis, P., and Stirke, A. (2021). Antimicrobial photodynamic therapy (aPDT) for biofilm treatments. Possible synergy between aPDT and pulsed electric fields. *Virulence* 12, 2247–2272. doi: 10.1080/21505594.2021.1960105

Aoki, W., and Ueda, M. (2013). Characterization of antimicrobial peptides toward the development of novel antibiotics. *Pharmaceuticals (Basel)* 6, 1055–1081. doi: 10.3390/ph6081055

Arora, D. P., Hossain, S., Xu, Y., and Boon, E. M. (2015). Nitric oxide regulation of bacterial biofilms. *Biochemistry* 54, 3717–3728. doi: 10.1021/bi501476n

Azam, M. W., and Khan, A. U. (2019). Updates on the pathogenicity status of *Pseudomonas aeruginosa*. *Drug Discov. Today* 24, 350–359. doi: 10.1016/j.drudis.2018.07.003

Baker, P., Hill, P. J., Snarr, B. D., Alnabelseya, N., Pestrak, M. J., Lee, M. J., et al. (2016). Exopolysaccharide biosynthetic glycoside hydrolases can be utilized to disrupt and prevent *Pseudomonas aeruginosa* biofilms. *Sci. Adv.* 2:e1501632. doi: 10.1126/sciadv.1501632

Bala, A., Kumar, L., Chhibber, S., and Harjai, K. (2015). Augmentation of virulence related traits of *pqs* mutants by *pseudomonas* quinolone signal through membrane vesicles. *J. Basic Microbiol.* 55, 566–578. doi: 10.1002/jobm.201400377

Banin, E., Lozinski, A., Brady, K. M., Berenshtein, E., Butterfield, P. W., Moshe, M., et al. (2008). The potential of desferrioxamine-gallium as an anti-*pseudomonas* therapeutic agent. *Proc. Natl. Acad. Sci. U. S. A.* 105, 16761–16766. doi: 10.1073/pnas.0808608105

Banin, E., Vasil, M. L., and Greenberg, E. P. (2005). Iron and *Pseudomonas aeruginosa* biofilm formation. *Proc. Natl. Acad. Sci. U. S. A.* 102, 11076–11081. doi: 10.1073/pnas.0504266102

Barken, K. B., Pamp, S. J., Yang, L., Gjermansen, M., Bertrand, J. J., Klausen, M., et al. (2008). Roles of type IV pili, flagellum-mediated motility and extracellular DNA in the formation of mature multicellular structures in *Pseudomonas aeruginosa* biofilms. *Environ. Microbiol.* 10, 2331–2343. doi: 10.1111/j.1462-2920.2008.01658.x

Barraud, N., Hassett, D. J., Hwang, S. H., Rice, S. A., Kjelleberg, S., and Webb, J. S. (2006). Involvement of nitric oxide in biofilm dispersal of *Pseudomonas aeruginosa*. *J. Bacteriol.* 188, 7344–7353. doi: 10.1128/JB.00779-06

Barraud, N., Kardak, B. G., Yepuri, N. R., Howlin, R. P., Webb, J. S., Faust, S. N., et al. (2012). Cephalosporin-3'-diazeniumdiolates: targeted NO-donor prodrugs for dispersing bacterial biofilms. *Angew. Chem. Int. Ed. Engl.* 51, 9057–9060. doi: 10.1002/anie.201202414

Beaudoin, T., Stone, T. A., Glibowicka, M., Adams, C., Yau, Y., Ahmadi, S., et al. (2018). Activity of a novel antimicrobial peptide against *Pseudomonas aeruginosa* biofilms. *Sci. Rep.* 8, 14728. doi: 10.1038/s41598-018-33016-7

Beirao, S., Fernandes, S., Coelho, J., Faustino, M. A., Tome, J. P., Neves, M. G., et al. (2014). Photodynamic inactivation of bacterial and yeast biofilms with a cationic porphyrin. *Photochem. Photobiol.* 90, 1387–1396. doi: 10.1111/php.12331

Bilici, K., Atac, N., Muti, A., Baylam, I., Dogan, O., Sennaroglu, A., et al. (2020). Broad spectrum antibacterial photodynamic and photothermal therapy achieved with indocyanine green loaded SPIONs under near infrared irradiation. *Biomater. Sci.* 8, 4616–4625. doi: 10.1039/d0bm00821d

Bonchi, C., Frangipani, E., Imperi, F., and Visca, P. (2015). Pyoverdine and proteases affect the response of *Pseudomonas aeruginosa* to gallium in human serum. *Antimicrob. Agents Chemother.* 59, 5641–5646. doi: 10.1128/AAC.01097-15

Byrd, M. S., Sadovskaya, I., Vinogradov, E., Lu, H., Sprinkle, A. B., Richardson, S. H., et al. (2009). Genetic and biochemical analyses of the *Pseudomonas aeruginosa* Psl exopolysaccharide reveal overlapping roles for polysaccharide synthesis enzymes in Psl and LPS production. *Mol. Microbiol.* 73, 622–638. doi: 10.1111/j.1365-2958.2009.06795.x

Chanda, W., Joseph, T. P., Padhiar, A. A., Guo, X., Min, L., Wang, W., et al. (2017). Combined effect of linolenic acid and tobramycin on *Pseudomonas aeruginosa* biofilm formation and quorum sensing. *Exp. Ther. Med.* 14, 4328–4338. doi: 10.3892/etm.2017.5110

Chang, Y., Wang, P. C., Ma, H. M., Chen, S. Y., Fu, Y. H., Liu, Y. Y., et al. (2019). Design, synthesis and evaluation of halogenated furanone derivatives as quorum sensing inhibitors in *Pseudomonas aeruginosa*. *Eur. J. Pharm. Sci.* 140:105058. doi: 10.1016/j.ejps.2019.105058

Chauhan, A., Lebeaux, D., Ghigo, J. M., and Beloin, C. (2012). Full and broad-spectrum in vivo eradication of catheter-associated biofilms using gentamicin-EDTA antibiotic lock therapy. *Antimicrob. Agents Chemother.* 56, 6310–6318. doi: 10.1128/AAC.01606-12

Chegini, Z., Khoshbayan, A., Taati Moghadam, M., Farahani, I., Jazireian, P., and Shariati, A. (2020). Bacteriophage therapy against *Pseudomonas aeruginosa* biofilms: A review. *Ann. Clin. Microbiol. Antimicrob.* 19, 45. doi: 10.1186/s12941-020-00389-5

Chou, S., Wang, J., Shang, L., Akhtar, M. U., Wang, Z., Shi, B., et al. (2019). Short, symmetric-helical peptides have narrow-spectrum activity with low resistance potential and high selectivity. *Biomater. Sci.* 7, 2394–2409. doi: 10.1039/c9bm00044e

Chrzanowski, L., Lawniczak, L., and Czaczyk, K. (2012). Why do microorganisms produce rhamnolipids? *World J. Microbiol. Biotechnol.* 28, 401–419. doi: 10.1007/s11274-011-0854-8

Cieplik, F., Deng, D., Crielaard, W., Buchalla, W., Hellwig, E., Al-Ahmad, A., et al. (2018). Antimicrobial photodynamic therapy – what we know and what we don't. *Crit. Rev. Microbiol.* 44, 571–589. doi: 10.1080/1040841X.2018.1467876

Clokie, M. R., Millard, A. D., Letarov, A. V., and Heaphy, S. (2011). Phages in nature. *Bacteriophage* 1, 31–45. doi: 10.4161/bact.1.1.14942

Colvin, K. M., Alnabelseya, N., Baker, P., Whitney, J. C., Howell, P. L., and Parsek, M. R. (2013). PelA deacetylase activity is required for Pel polysaccharide synthesis in *Pseudomonas aeruginosa*. *J. Bacteriol.* 195, 2329–2339. doi: 10.1128/JB.02150-12

Colvin, K. M., Gordon, V. D., Murakami, K., Borlee, B. R., Wozniak, D. J., Wong, G. C., et al. (2011). The pel polysaccharide can serve a structural and protective role in the biofilm matrix of *Pseudomonas aeruginosa*. *PLoS Pathog.* 7:e1001264. doi: 10.1371/journal.ppat.1001264

Colvin, K. M., Irie, Y., Tart, C. S., Urbano, R., Whitney, J. C., Ryder, C., et al. (2012). The Pel and Psl polysaccharides provide *Pseudomonas aeruginosa* structural redundancy within the biofilm matrix. *Environ. Microbiol.* 14, 1913–1928. doi: 10.1111/j.1462-2920.2011.02657.x

Costerton, J. W., Stewart, P. S., and Greenberg, E. P. (1999). Bacterial biofilms: A common cause of persistent infections. *Science* 284, 1318–1322. doi: 10.1126/science.284.5418.1318

Cutruzzola, F., and Frankenberg-Dinkel, N. (2016). Origin and impact of nitric oxide in *Pseudomonas aeruginosa* biofilms. *J. Bacteriol.* 198, 55–65. doi: 10.1128/JB.00371-15

Daboor, S. M., Rohde, J. R., and Cheng, Z. (2021). Disruption of the extracellular polymeric network of *Pseudomonas aeruginosa* biofilms by alginate lyase enhances pathogen eradication by antibiotics. *J. Cyst. Fibros.* 20, 264–270. doi: 10.1016/j.jcf.2020.04.006

Das, T., Manoharan, A., Whiteley, G., Glasbey, T., and Manos, J. (2020). "*Pseudomonas aeruginosa* biofilms and infections: roles of extracellular molecules," in *New and Future Developments in Microbial Biotechnology and Bioengineering: Microbial Biofilms*. eds. M. K. Yadav and B. P. Singh (Amsterdam: Elsevier), 29–46.

Das, T., Sharma, P. K., Busscher, H. J., van der Mei, H. C., and Krom, B. P. (2010). Role of extracellular DNA in initial bacterial adhesion and surface aggregation. *Appl. Environ. Microbiol.* 76, 3405–3408. doi: 10.1128/AEM.03119-09

Davey, M. E., Caiazza, N. C., and O'Toole, G. A. (2003). Rhamnolipid surfactant production affects biofilm architecture in *Pseudomonas aeruginosa* PAO1. *J. Bacteriol.* 185, 1027–1036. doi: 10.1128/JB.185.3.1027-1036.2003

de la Fuente-Nunez, C., Korolik, V., Bains, M., Nguyen, U., Breidenstein, E. B., Horsman, S., et al. (2012). Inhibition of bacterial biofilm formation and swarming motility by a small synthetic cationic peptide. *Antimicrob. Agents Chemother.* 56, 2696–2704. doi: 10.1128/AAC.00064-12

Di, Y. P., Lin, Q., Chen, C., Montelaro, R. C., Doi, Y., and Deslouches, B. (2020). Enhanced therapeutic index of an antimicrobial peptide in mice by increasing safety and activity against multidrug-resistant bacteria. *Sci. Adv.* 6, eaay6817. doi: 10.1126/sciadv.aay6817

Donlan, R. M. (2002). Biofilms: microbial life on surfaces. *Emerg. Infect. Dis.* 8, 881–890. doi: 10.3201/eid0809.020063

Dosselli, R., Millioni, R., Puricelli, L., Tessari, P., Arrigoni, G., Franchin, C., et al. (2012). Molecular targets of antimicrobial photodynamic therapy identified by a proteomic approach. *J. Proteome* 77, 329–343. doi: 10.1016/j.jprot.2012.09.007

Drenkard, E. (2003). Antimicrobial resistance of *Pseudomonas aeruginosa* biofilms. *Microbes Infect.* 5, 1213–1219. doi: 10.1016/j.micinf.2003.08.009

Dufour, D., Leung, V., and Lévesque, C. (2010). Bacterial biofilm: structure, function, and antimicrobial resistance. *Endod. Top.* 22, 2–16. doi: 10.1111/j.1601-1546.2012.00277.x

Eckhart, L., Fischer, H., Barken, K. B., Tolker-Nielsen, T., and Tschachler, E. (2007). DNase1L2 suppresses biofilm formation by *Pseudomonas aeruginosa* and *Staphylococcus aureus*. *Br. J. Dermatol.* 156, 1342–1345. doi: 10.1111/j.1365-2133.2007.07886.x

Elmanama, A. A., Al-Sheboul, S., and Abu-Dan, R. I. (2020). Antimicrobial resistance and biofilm formation of *Pseudomonas aeruginosa*. *Int. Arabic J. Antimicrob. Agents* 10, 3. doi: 10.3823/846

Epstein, A. K., Wong, T. S., Belisle, R. A., Boggs, E. M., and Aizenberg, J. (2012). Liquid-infused structured surfaces with exceptional anti-biofouling performance. *Proc. Natl. Acad. Sci. U. S. A.* 109, 13182–13187. doi: 10.1073/pnas.1201973109

Feng, Y., Coradi Tonon, C., Ashraf, S., and Hasan, T. (2021). Photodynamic and antibiotic therapy in combination against bacterial infections: efficacy, determinants, mechanisms, and future perspectives. *Adv. Drug Deliv. Rev.* 177:113941. doi: 10.1016/j.addr.2021.113941

Feng, Q., Huang, Y., Chen, M., Li, G., and Chen, Y. (2015). Functional synergy of alpha-helical antimicrobial peptides and traditional antibiotics against gram-negative and gram-positive bacteria in vitro and in vivo. *Eur. J. Clin. Microbiol. Infect. Dis.* 34, 197–204. doi: 10.1007/s10096-014-2219-3

Ferriol-Gonzalez, C., and Domingo-Calap, P. (2020). Phages for biofilm removal. *Antibiotics (Basel)* 9, 268. doi: 10.3390/antibiotics9050268

Finkel, S. E., and Kolter, R. (2001). DNA as a nutrient: novel role for bacterial competence gene homologs. *J. Bacteriol.* 183, 6288–6293. doi: 10.1128/JB.183.21.6288-6293.2001

Fleming, D., Chahin, L., and Rumbaugh, K. (2017). Glycoside hydrolases degrade polymicrobial bacterial biofilms in wounds. *Antimicrob. Agents Chemother.* 61, e01998-16. doi: 10.1128/AAC.01998-16

Flemming, H. C., and Wuertz, S. (2019). Bacteria and archaea on earth and their abundance in biofilms. *Nat. Rev. Microbiol.* 17, 247–260. doi: 10.1038/s41579-019-0158-9

Franklin, M. J., Nivens, D. E., Weadge, J. T., and Howell, P. L. (2011). Biosynthesis of the *Pseudomonas aeruginosa* extracellular polysaccharides, alginate, Pel, and Psl. *Front. Microbiol.* 2, 167. doi: 10.3389/fmicb.2011.00167

Ghafoor, A., Hay, I. D., and Rehm, B. H. (2011). Role of exopolysaccharides in *Pseudomonas aeruginosa* biofilm formation and architecture. *Appl. Environ. Microbiol.* 77, 5238–5246. doi: 10.1128/AEM.00637-11

Ghorbani, H., Memar, M. Y., Sefidan, F. Y., Yekani, M., and Ghotaslou, R. (2017). In vitro synergy of antibiotic combinations against planktonic and biofilm *Pseudomonas aeruginosa*. *GMS Hyg. Infect. Control.* 12, Doc17. doi: 10.3205/dgkh000302

Gnanadhas, D. P., Elango, M., Datey, A., and Chakravortty, D. (2015). Chronic lung infection by *Pseudomonas aeruginosa* biofilm is cured by L-methionine in combination with antibiotic therapy. *Sci. Rep.* 5, 16043. doi: 10.1038/srep16043

Goss, C. H., Kaneko, Y., Khuu, L., Anderson, G. D., Ravishankar, S., Aitken, M. L., et al. (2018). Gallium disrupts bacterial iron metabolism and has therapeutic effects in mice and humans with lung infections. *Sci. Transl. Med.* 10, eaat7520. doi: 10.1126/scitranslmed.aat7520

Harper, D., Parracho, H., Walker, J., Sharp, R., Hughes, G., Werthén, M., et al. (2014). Bacteriophages and Biofilms. *Antibiotics* 3, 270–284. doi: 10.3390/antibiotics3030270

Hoiby, N., Bjarnsholt, T., Givskov, M., Molin, S., and Ciofu, O. (2010). Antibiotic resistance of bacterial biofilms. *Int. J. Antimicrob. Agents* 35, 322–332. doi: 10.1016/j.ijantimicag.2009.12.011

Hoiby, N., Ciofu, O., Johansen, H. K., Song, Z. J., Moser, C., Jensen, P. O., et al. (2011). The clinical impact of bacterial biofilms. *Int. J. Oral Sci.* 3, 55–65. doi: 10.4248/IJOS11026

Hossain, S., and Boon, E. M. (2017). Discovery of a novel nitric oxide binding protein and nitric-oxide-responsive signaling pathway in *Pseudomonas aeruginosa*. *ACS Infect. Dis.* 3, 454–461. doi: 10.1021/acsinfecdis.7b00027

Howlin, R. P., Cathie, K., Hall-Stoodley, L., Cornelius, V., Duignan, C., Allan, R. N., et al. (2017). Low-dose nitric oxide as targeted anti-biofilm adjunctive therapy to treat chronic *Pseudomonas aeruginosa* infection in cystic fibrosis. *Mol. Ther.* 25, 2104–2116. doi: 10.1016/j.ymthe.2017.06.021

Hu, X., Huang, Y. Y., Wang, Y., Wang, X., and Hamblin, M. R. (2018). Antimicrobial photodynamic therapy to control clinically relevant biofilm infections. *Front. Microbiol.* 9, 1299. doi: 10.3389/fmicb.2018.01299

Huang, H., Shao, X., Xie, Y., Wang, T., Zhang, Y., Wang, X., et al. (2019). An integrated genomic regulatory network of virulence-related transcriptional factors in *Pseudomonas aeruginosa*. *Nat. Commun.* 10, 2931. doi: 10.1038/s41467-019-10778-w

Hughes, G., and Webber, M. A. (2017). Novel approaches to the treatment of bacterial biofilm infections. *Br. J. Pharmacol.* 174, 2237–2246. doi: 10.1111/bph.13706

Hymes, S. R., Randis, T. M., Sun, T. Y., and Ratner, A. J. (2013). DNase inhibits *Gardnerella vaginalis* biofilms in vitro and in vivo. *J. Infect. Dis.* 207, 1491–1497. doi: 10.1093/infdis/jit047

Jamal, M., Ahmad, W., Andleeb, S., Jalil, F., Imran, M., Nawaz, M. A., et al. (2018). Bacterial biofilm and associated infections. *J. Chin. Med. Assoc.* 81, 7–11. doi: 10.1016/j.jcma.2017.07.012

Jennings, L. K., Storek, K. M., Ledvina, H. E., Coulon, C., Marmont, L. S., Sadovskaya, I., et al. (2015). Pel is a cationic exopolysaccharide that cross-links extracellular DNA in the *Pseudomonas aeruginosa* biofilm matrix. *Proc. Natl. Acad. Sci. U. S. A.* 112, 11353–11358. doi: 10.1073/pnas.1503058112

Jiang, Y., Geng, M., and Bai, L. (2020). Targeting biofilms therapy: current research strategies and development hurdles. *Microorganisms* 8, 1222. doi: 10.3390/microorganisms8081222

Jiang, P., Li, J., Han, F., Duan, G., Lu, X., Gu, Y., et al. (2011). Antibiofilm activity of an exopolysaccharide from marine bacterium vibrio sp. QY101. *PLoS One* 6:e18514. doi: 10.1371/journal.pone.0018514

Kalia, V. C. (2013). Quorum sensing inhibitors: An overview. *Biotechnol. Adv.* 31, 224–245. doi: 10.1016/j.biotechadv.2012.10.004

Kamal, A. A. M., Maurer, C. K., Allegretta, G., Haupenthal, J., Empting, M., and Hartmann, R. W. (2017). "Quorum sensing inhibitors as pathoblockers for *Pseudomonas aeruginosa* infections: A new concept in anti-infective drug discovery," in *Antibacterials, Topics in Medicinal Chemistry*. eds. J. Fisher, S. Mobashery and M. Miller (Cham: Springer), 185–210.

Kamaruzzaman, N. F., Tan, L. P., Mat Yazid, K. A., Saeed, S. I., Hamdan, R. H., Choong, S. S., et al. (2018). Targeting the bacterial protective armour; challenges and novel strategies in the treatment of microbial biofilm. *Materials (Basel)* 11, 1705. doi: 10.3390/ma11091705

Kaneko, Y., Thoendel, M., Olakanmi, O., Britigan, B. E., and Singh, P. K. (2007). The transition metal gallium disrupts *Pseudomonas aeruginosa* iron metabolism and has antimicrobial and antibiofilm activity. *J. Clin. Invest.* 117, 877–888. doi: 10.1172/JCI30783

Kang, D., Revtovich, A. V., Deyanov, A. E., and Kirienko, N. V. (2021). Pyoverdine inhibitors and gallium nitrate synergistically affect *Pseudomonas aeruginosa*. *mSphere* 6:e0040121. doi: 10.1128/mSphere.00401-21

Khan, F., Pham, D. T. N., and Kim, Y. M. (2020). Alternative strategies for the application of aminoglycoside antibiotics against the biofilm-forming human pathogenic bacteria. *Appl. Microbiol. Biotechnol.* 104, 1955–1976. doi: 10.1007/s00253-020-10360-1

Kim, S. K., and Lee, J. H. (2016). Biofilm dispersion in *Pseudomonas aeruginosa*. *J. Microbiol.* 54, 71–85. doi: 10.1007/s12275-016-5528-7

Kitao, T., Lepine, F., Babloudi, S., Walte, F., Steinbacher, S., Maskos, K., et al. (2018). Molecular insights into function and competitive inhibition of *Pseudomonas aeruginosa* multiple virulence factor regulator. *mBio* 9, e02158-17. doi: 10.1128/mBio.02158-17

Koo, H., Allan, R. N., Howlin, R. P., Stoodley, P., and Hall-Stoodley, L. (2017). Targeting microbial biofilms: current and prospective therapeutic strategies. *Nat. Rev. Microbiol.* 15, 740–755. doi: 10.1038/nrmicro.2017.99

Kostakioti, M., Hadjifrangiskou, M., and Hultgren, S. J. (2013). Bacterial biofilms: development, dispersal, and therapeutic strategies in the dawn of the postantibiotic era. *Cold Spring Harb. Perspect. Med.* 3:a010306. doi: 10.1101/cshperspect.a010306

Kovach, K. N., Fleming, D., Wells, M. J., Rumbaugh, K. P., and Gordon, V. D. (2020). Specific disruption of established *Pseudomonas aeruginosa* biofilms using polymer-attacking enzymes. *Langmuir* 36, 1585–1595. doi: 10.1021/acs.langmuir.9b02188

Kumar, A., Alam, A., Rani, M., Ehtesham, N. Z., and Hasnain, S. E. (2017). Biofilms: survival and defense strategy for pathogens. *Int. J. Med. Microbiol.* 307, 481–489. doi: 10.1016/j.ijmm.2017.09.016

Kumar, L., Chhibber, S., and Harjai, K. (2013). Zingerone inhibit biofilm formation and improve antibiofilm efficacy of ciprofloxacin against *Pseudomonas aeruginosa* PAO1. *Fitoterapia* 90, 73–78. doi: 10.1016/j.fitote.2013.06.017

Kumar, L., Chhibber, S., Kumar, R., Kumar, M., and Harjai, K. (2015). Zingerone silences quorum sensing and attenuates virulence of *Pseudomonas aeruginosa*. *Fitoterapia* 102, 84–95. doi: 10.1016/j.fitote.2015.02.002

Kutateladze, M., and Adamia, R. (2010). Bacteriophages as potential new therapeutics to replace or supplement antibiotics. *Trends Biotechnol.* 28, 591–595. doi: 10.1016/j.tibtech.2010.08.001

Kutter, E., De Vos, D., Gvasalia, G., Alavidze, Z., Gogokhia, L., Kuhl, S., et al. (2010). Phage therapy in clinical practice: treatment of human infections. *Curr. Pharm. Biotechnol.* 11, 69–86. doi: 10.2174/138920110790725401

Lashua, L. P., Melvin, J. A., Deslouches, B., Pilewski, J. M., Montelaro, R. C., and Bomberger, J. M. (2016). Engineered cationic antimicrobial peptide (eCAP) prevents *Pseudomonas aeruginosa* biofilm growth on airway epithelial cells. *J. Antimicrob. Chemother.* 71, 2200–2207. doi: 10.1093/jac/dkw143

Le, C. F., Fang, C. M., and Sekaran, S. D. (2017). Intracellular targeting mechanisms by antimicrobial peptides. *Antimicrob. Agents Chemother.* 61, e02340-16. doi: 10.1128/AAC.02340-16

Lebeaux, D., Leflon-Guibout, V., Ghigo, J. M., and Beloin, C. (2015). In vitro activity of gentamicin, vancomycin or amikacin combined with EDTA or l-arginine as lock therapy against a wide spectrum of biofilm-forming clinical strains isolated from catheter-related infections. *J. Antimicrob. Chemother.* 70, 1704–1712. doi: 10.1093/jac/dkv044

Lee, K., and Yoon, S. S. (2017). *Pseudomonas aeruginosa* biofilm, a programmed bacterial life for fitness. *J. Microbiol. Biotechnol.* 27, 1053–1064. doi: 10.4014/jmb.1611.11056

Lee, J., and Zhang, L. (2015). The hierarchy quorum sensing network in *Pseudomonas aeruginosa*. *Protein Cell* 6, 26–41. doi: 10.1007/s13238-014-0100-x

Lequette, Y., and Greenberg, E. P. (2005). Timing and localization of rhamnolipid synthesis gene expression in *Pseudomonas aeruginosa* biofilms. *J. Bacteriol.* 187, 37–44. doi: 10.1128/JB.187.1.37-44.2005

Li, W., Geng, X., Liu, D., and Li, Z. (2019). Near-infrared light-enhanced protease-conjugated gold nanorods as a photothermal antimicrobial agent for elimination of exotoxin and biofilms. *Int. J. Nanomedicine* 14, 8047–8058. doi: 10.2147/IJN.S212750

Li, Y., Xiao, P., Wang, Y., and Hao, Y. (2020). Mechanisms and control measures of mature biofilm resistance to antimicrobial agents in the clinical context. *ACS Omega* 5, 22684–22690. doi: 10.1021/acsomega.0c02294

Liang, X., Zou, Z., Zou, Z., Li, C., Dong, X., Yin, H., et al. (2020). Effect of antibacterial photodynamic therapy on *Streptococcus mutans* plaque biofilm *in vitro*. *J. Innov. Opt. Health Sci.* 13, 2050022. doi: 10.1142/S1793545820500224

Lichtenberg, M., Jakobsen, T. H., Kuhl, M., Kolpen, M., Jensen, P. O., and Bjarnsholt, T. (2022). The structure-function relationship of *Pseudomonas aeruginosa* in infections and its influence on the microenvironment. *FEMS Microbiol. Rev.* doi: 10.1093/femsre/fuac018 [Epub ahead of print]

Limoli, D. H., Jones, C. J., and Wozniak, D. J. (2015). Bacterial extracellular polysaccharides in biofilm formation and function. *Microbiol. Spectr.* 3, MB-0011–2014. doi: 10.1128/microbiolspec.MB-0011-2014

Limoli, D. H., Rockel, A. B., Host, K. M., Jha, A., Kopp, B. T., Hollis, T., et al. (2014). Cationic antimicrobial peptides promote microbial mutagenesis and pathoadaptation in chronic infections. *PLoS Pathog.* 10:e1004083. doi: 10.1371/journal.ppat.1004083

Lin, J., and Cheng, J. (2019). "Quorum sensing in *Pseudomonas aeruginosa* and its relationship to biofilm development," in *Introduction to Biofilm Engineering*. eds. N. K. Rathinam and R. K. Sani (Washington, DC: ACS Publications), 1–16.

Lin, J., Cheng, J., Wang, Y., and Shen, X. (2018a). The *pseudomonas* quinolone signal (PQS): not just for quorum sensing anymore. *Front. Cell. Infect. Microbiol.* 8, 230. doi: 10.3389/fcimb.2018.00230

Lin, Q., Deslouches, B., Montelaro, R. C., and Di, Y. P. (2018b). Prevention of ESKAPE pathogen biofilm formation by antimicrobial peptides WLBU2 and LL37. *Int. J. Antimicrob. Agents* 52, 667–672. doi: 10.1016/j.ijantimicag.2018.04.019

Lin, Q., Pilewski, J. M., and Di, Y. P. (2021). Acidic microenvironment determines antibiotic susceptibility and biofilm formation of *Pseudomonas aeruginosa*. *Front. Microbiol.* 12:747834. doi: 10.3389/fmicb.2021.747834

Llamas, M. A., Sparrius, M., Kloet, R., Jimenez, C. R., Vandenbroucke-Grauls, C., and Bitter, W. (2006). The heterologous siderophores ferrioxamine B and ferrichrome activate signaling pathways in *Pseudomonas aeruginosa*. *J. Bacteriol.* 188, 1882–1891. doi: 10.1128/JB.188.5.1882-1891.2006

Ma, L., Conover, M., Lu, H., Parsek, M. R., Bayles, K., and Wozniak, D. J. (2009). Assembly and development of the *Pseudomonas aeruginosa* biofilm matrix. *PLoS Pathog.* 5:e1000354. doi: 10.1371/journal.ppat.1000354

Ma, L., Jackson, K. D., Landry, R. M., Parsek, M. R., and Wozniak, D. J. (2006). Analysis of *Pseudomonas aeruginosa* conditional Psl variants reveals roles for the Psl polysaccharide in adhesion and maintaining biofilm structure postattachment. *J. Bacteriol.* 188, 8213–8221. doi: 10.1128/JB.01202-06

Ma, L. Z., Wang, D., Liu, Y., Zhang, Z., and Wozniak, D. J. (2022). Regulation of biofilm exopolysaccharide biosynthesis and degradation in *Pseudomonas aeruginosa*. *Annu. Rev. Microbiol.* 76, 413–433. doi: 10.1146/annurev-micro-041320-111355

Ma, L., Wang, S., Wang, D., Parsek, M. R., and Wozniak, D. J. (2012). The roles of biofilm matrix polysaccharide Psl in mucoid *Pseudomonas aeruginosa* biofilms. *FEMS Immunol. Med. Microbiol.* 65, 377–380. doi: 10.1111/j.1574-695X.2012.00934.x

Mahlapuu, M., Hakansson, J., Ringstad, L., and Bjorn, C. (2016). Antimicrobial peptides: An emerging category of therapeutic agents. *Front. Cell. Infect. Microbiol.* 6, 194. doi: 10.3389/fcimb.2016.00194

Mann, E. E., and Wozniak, D. J. (2012). *Pseudomonas* biofilm matrix composition and niche biology. *FEMS Microbiol. Rev.* 36, 893–916. doi: 10.1111/j.1574-6976.2011.00322.x

Marmont, L. S., Whitfield, G. B., Rich, J. D., Yip, P., Giesbrecht, L. B., Stremick, C. A., et al. (2017). PelA and PelB proteins form a modification and secretion complex essential for Pel polysaccharide-dependent biofilm formation in *Pseudomonas aeruginosa*. *J. Biol. Chem.* 292, 19411–19422. doi: 10.1074/jbc.M117.812842

Marshall, B., Stintzi, A., Gilmour, C., Meyer, J. M., and Poole, K. (2009). Citrate-mediated iron uptake in *Pseudomonas aeruginosa*: involvement of the citrate-inducible FecA receptor and the FeoB ferrous iron transporter. *Microbiology (Reading)* 155, 305–315. doi: 10.1099/mic.0.023531-0

Martinez, M., Goncalves, S., Felicio, M. R., Maturana, P., Santos, N. C., Semorile, L., et al. (2019). Synergistic and antibiofilm activity of the antimicrobial peptide P5 against carbapenem-resistant *Pseudomonas aeruginosa*. *Biochim. Biophys. Acta Biomembr.* 1861, 1329–1337. doi: 10.1016/j.bbamem.2019.05.008

Maura, D., and Rahme, L. G. (2017). Pharmacological inhibition of the *Pseudomonas aeruginosa* MvfR quorum-sensing system interferes with biofilm formation and potentiates antibiotic-mediated biofilm disruption. *Antimicrob. Agents Chemother.* 61, e01362-17. doi: 10.1128/AAC.01362-17

Maurice, N. M., Bedi, B., and Sadikot, R. T. (2018). *Pseudomonas aeruginosa* biofilms: Host response and clinical implications in lung infections. *Am. J. Respir. Cell Mol. Biol.* 58, 428–439. doi: 10.1165/rcmb.2017-0321TR

McDougald, D., Rice, S. A., Barraud, N., Steinberg, P. D., and Kjelleberg, S. (2011). Should we stay or should we go: mechanisms and ecological consequences for biofilm dispersal. *Nat. Rev. Microbiol.* 10, 39–50. doi: 10.1038/nrmicro2695

Melo, L. D. R., Pires, D. P., Monteiro, R., and Azeredo, J. (2019). "Phage therapy of infectious biofilms: challenges and strategies," in *Phage Therapy: A Practical Approach*. eds. A. Górski, R. Międzybrodzki and J. Borysowski (Cham: Springer), 295–313.

Mi, L., Liu, Y., Wang, C., He, T., Gao, S., Xing, S., et al. (2019). Identification of a lytic *Pseudomonas aeruginosa* phage depolymerase and its anti-biofilm effect and bactericidal contribution to serum. *Virus Genes* 55, 394–405. doi: 10.1007/s11262-019-01660-4

Minandri, F., Bonchi, C., Frangipani, E., Imperi, F., and Visca, P. (2014). Promises and failures of gallium as an antibacterial agent. *Future Microbiol.* 9, 379–397. doi: 10.2217/fmb.14.3

Mitchell, K. F., Zarnowski, R., and Andes, D. R. (2016). Fungal super glue: the biofilm matrix and its composition, assembly, and functions. *PLoS Pathog.* 12:e1005828. doi: 10.1371/journal.ppat.1005828

Moradali, M. F., Ghods, S., and Rehm, B. H. (2017). *Pseudomonas aeruginosa* lifestyle: A paradigm for adaptation, survival, and persistence. *Front. Cell. Infect. Microbiol.* 7, 39. doi: 10.3389/fcimb.2017.00039

Moradali, M. F., and Rehm, B. H. (2019). "The role of alginate in bacterial biofilm formation," in *Extracellular Sugar-Based Biopolymers Matrices, Biologically-Inspired Systems*. eds. E. Cohen and H. Merzendorfer (Cham: Springer), 517–537.

Muhlen, S., and Dersch, P. (2016). Anti-virulence strategies to target bacterial infections. *Curr. Top. Microbiol. Immunol.* 398, 147–183. doi: 10.1007/82_2015_490

O'Brien, K. T., Noto, J. G., Nichols-O'Neill, L., and Perez, L. J. (2015). Potent irreversible inhibitors of LasR quorum sensing in *Pseudomonas aeruginosa*. *ACS Med. Chem. Lett.* 6, 162–167. doi: 10.1021/ml500459f

Okshevsky, M., Regina, V. R., and Meyer, R. L. (2015). Extracellular DNA as a target for biofilm control. *Curr. Opin. Biotechnol.* 33, 73–80. doi: 10.1016/j.copbio.2014.12.002

Olivares, E., Badel-Berchoux, S., Provot, C., Prevost, G., Bernardi, T., and Jehl, F. (2019). Clinical impact of antibiotics for the treatment of *Pseudomonas aeruginosa* biofilm infections. *Front. Microbiol.* 10, 2894. doi: 10.3389/fmicb.2019.02894

Overhage, J., Campisano, A., Bains, M., Torfs, E. C., Rehm, B. H., and Hancock, R. E. (2008). Human host defense peptide LL-37 prevents bacterial biofilm formation. *Infect. Immun.* 76, 4176–4182. doi: 10.1128/IAI.00318-08

Pang, Z., Raudonis, R., Glick, B. R., Lin, T. J., and Cheng, Z. (2019). Antibiotic resistance in *Pseudomonas aeruginosa*: mechanisms and alternative therapeutic strategies. *Biotechnol. Adv.* 37, 177–192. doi: 10.1016/j.biotechadv.2018.11.013

Pang, Z., and Zhu, Q. (2021). Traditional Chinese medicine is an alternative therapeutic option for treatment of *Pseudomonas aeruginosa* infections. *Front. Pharmacol.* 12:737252. doi: 10.3389/fphar.2021.737252

Pei, R., and Lamas-Samanamud, G. R. (2014). Inhibition of biofilm formation by T7 bacteriophages producing quorum-quenching enzymes. *Appl. Environ. Microbiol.* 80, 5340–5348. doi: 10.1128/AEM.01434-14

Perez-Laguna, V., Garcia-Luque, I., Ballesta, S., Perez-Artiaga, L., Lampaya-Perez, V., Rezusta, A., et al. (2020). Photodynamic therapy using methylene blue, combined or not with gentamicin, against *Staphylococcus aureus* and *Pseudomonas aeruginosa*. *Photodiagn. Photodyn. Ther.* 31:101810. doi: 10.1016/j.pdpdt.2020.101810

Pires, D. P., Oliveira, H., Melo, L. D., Sillankorva, S., and Azeredo, J. (2016). Bacteriophage-encoded depolymerases: their diversity and biotechnological applications. *Appl. Microbiol. Biotechnol.* 100, 2141–2151. doi: 10.1007/s00253-015-7247-0

Poh, W. H., and Rice, S. A. (2022). Recent developments in nitric oxide donors and delivery for antimicrobial and anti-biofilm applications. *Molecules* 27, 674. doi: 10.3390/molecules27030674

Pontes, J. T. C., Toledo Borges, A. B., Roque-Borda, C. A., and Pavan, F. R. (2022). Antimicrobial peptides as an alternative for the eradication of bacterial biofilms of multi-drug resistant bacteria. *Pharmaceutics* 14, 642. doi: 10.3390/pharmaceutics14030642

Qi, L., and Christopher, G. F. (2019). Role of flagella, type IV Pili, biosurfactants, and extracellular polymeric substance polysaccharides on the formation of pellicles by *Pseudomonas aeruginosa*. *Langmuir* 35, 5294–5304. doi: 10.1021/acs.langmuir.9b00271

Qin, Z., Yang, L., Qu, D., Molin, S., and Tolker-Nielsen, T. (2009). *Pseudomonas aeruginosa* extracellular products inhibit staphylococcal growth, and disrupt established biofilms produced by *Staphylococcus* epidermidis. *Microbiology (Reading)* 155, 2148–2156. doi: 10.1099/mic.0.028001-0

Rahmani-Badi, A., Sepehr, S., Mohammadi, P., Soudi, M. R., Babaie-Naiej, H., and Fallahi, H. (2014). A combination of cis-2-decenoic acid and antibiotics eradicates pre-established catheter-associated biofilms. *J. Med. Microbiol.* 63, 1509–1516. doi: 10.1099/jmm.0.075374-0

Rajesh, S., Koshi, E., Philip, K., and Mohan, A. (2011). Antimicrobial photodynamic therapy: An overview. *J. Indian Soc. Periodontol.* 15, 323–327. doi: 10.4103/0972-124X.92563

Rajkumari, J., Borkotoky, S., Murali, A., Suchiang, K., Mohanty, S. K., and Busi, S. (2018). Cinnamic acid attenuates quorum sensing associated virulence factors and biofilm formation in *Pseudomonas aeruginosa* PAO1. *Biotechnol. Lett.* 40, 1087–1100. doi: 10.1007/s10529-018-2557-9

Redman, W. K., Welch, G. S., and Rumbaugh, K. P. (2020). Differential efficacy of glycoside hydrolases to disperse biofilms. *Front. Cell. Infect. Microbiol.* 10, 379. doi: 10.3389/fcimb.2020.00379

Rendueles, O., Kaplan, J. B., and Ghigo, J. M. (2013). Antibiofilm polysaccharides. *Environ. Microbiol.* 15, 334–346. doi: 10.1111/j.1462-2920.2012.02810.x

Roy, R., Tiwari, M., Donelli, G., and Tiwari, V. (2018). Strategies for combating bacterial biofilms: A focus on anti-biofilm agents and their mechanisms of action. *Virulence* 9, 522–554. doi: 10.1080/21505594.2017.1313372

Rumbaugh, K. P., and Sauer, K. (2020). Biofilm dispersion. *Nat. Rev. Microbiol.* 18, 571–586. doi: 10.1038/s41579-020-0385-0

Rutherford, S. T., and Bassler, B. L. (2012). Bacterial quorum sensing: its role in virulence and possibilities for its control. *Cold Spring Harb. Perspect. Med.* 2:a012427. doi: 10.1101/cshperspect.a012427

Rzhepishevska, O., Ekstrand-Hammarstrom, B., Popp, M., Bjorn, E., Bucht, A., Sjostedt, A., et al. (2011). The antibacterial activity of Ga^{3+} is influenced by ligand complexation as well as the bacterial carbon source. *Antimicrob. Agents Chemother.* 55, 5568–5580. doi: 10.1128/AAC.00386-11

Saxena, P., Joshi, Y., Rawat, K., and Bisht, R. (2019). Biofilms: Architecture, resistance, quorum sensing and control mechanisms. *Indian J. Microbiol.* 59, 3–12. doi: 10.1007/s12088-018-0757-6

Schmelcher, M., Donovan, D. M., and Loessner, M. J. (2012). Bacteriophage endolysins as novel antimicrobials. *Future Microbiol.* 7, 1147–1171. doi: 10.2217/fmb.12.97

Schutz, C., and Empting, M. (2018). Targeting the *pseudomonas* quinolone signal quorum sensing system for the discovery of novel anti-infective pathoblockers. *Beilstein J. Org. Chem.* 14, 2627–2645. doi: 10.3762/bjoc.14.241

Schutz, C., Ho, D. K., Hamed, M. M., Abdelsamie, A. S., Rohrig, T., Herr, C., et al. (2021). A new PqsR inverse agonist potentiates tobramycin efficacy to eradicate *Pseudomonas aeruginosa* biofilms. *Adv. Sci. (Weinh)* 8:e2004369. doi: 10.1002/advs.202004369

Seyfi, R., Kahaki, F. A., Ebrahimi, T., Montazersaheb, S., Eyvazi, S., Babaeipour, V., et al. (2020). Antimicrobial peptides (AMPs): roles, functions and mechanism of action. *Int. J. Pept. Res. Ther.* 26, 1451–1463. doi: 10.1007/s10989-019-09946-9

Shao, X., Xie, Y., Zhang, Y., Liu, J., Ding, Y., Wu, M., et al. (2020). Novel therapeutic strategies for treating *Pseudomonas aeruginosa* infection. *Expert Opin. Drug Discov.* 15, 1403–1423. doi: 10.1080/17460441.2020.1803274

Sharma, D., Misba, L., and Khan, A. U. (2019). Antibiotics versus biofilm: An emerging battleground in microbial communities. *Antimicrob. Resist. Infect. Control* 8, 76. doi: 10.1186/s13756-019-0533-3

Sharma, K., and Pagedar Singh, A. (2018). Antibiofilm effect of DNase against single and mixed species biofilm. *Foods* 7, 42. doi: 10.3390/foods7030042

Shrestha, L., Fan, H. M., Tao, H. R., and Huang, J. D. (2022). Recent strategies to combat biofilms using antimicrobial agents and therapeutic approaches. *Pathogens* 11, 292. doi: 10.3390/pathogens11030292

Shrivastava, S., Shrivastava, P. S., and Ramasamy, J. (2018). World health organization releases global priority list of antibiotic-resistant bacteria to guide research, discovery, and development of new antibiotics. *J. Med. Soc.* 32, 76. doi: 10.4103/jms.jms_25_17

Smith, W. D., Bardin, E., Cameron, L., Edmondson, C. L., Farrant, K. V., Martin, I., et al. (2017). Current and future therapies for *Pseudomonas aeruginosa* infection in patients with cystic fibrosis. *FEMS Microbiol. Lett.* 364, fnx121. doi: 10.1093/femsle/fnx121

Soothill, J. (2013). Use of bacteriophages in the treatment of *Pseudomonas aeruginosa* infections. *Expert Rev. Anti Infect. Ther.* 11, 909–915. doi: 10.1586/14787210.2013.826990

Soren, O., Rineh, A., Silva, D. G., Cai, Y., Howlin, R. P., Allan, R. N., et al. (2020). Cephalosporin nitric oxide-donor prodrug DEA-C3D disperses biofilms formed by clinical cystic fibrosis isolates of *Pseudomonas aeruginosa*. *J. Antimicrob. Chemother.* 75, 117–125. doi: 10.1093/jac/dkz378

Soukarieh, F., Williams, P., Stocks, M. J., and Camara, M. (2018). *Pseudomonas aeruginosa* quorum sensing systems as drug discovery targets: current position and future perspectives. *J. Med. Chem.* 61, 10385–10402. doi: 10.1021/acs.jmedchem.8b00540

Srinivasan, R., Santhakumari, S., Poonguzhali, P., Geetha, M., Dyavaiah, M., and Xiangmin, L. (2021). Bacterial biofilm inhibition: A focused review on recent therapeutic strategies for combating the biofilm mediated infections. *Front. Microbiol.* 12:676458. doi: 10.3389/fmicb.2021.676458

Swartjes, J. J., Das, T., Sharifi, S., Subbiahdoss, G., Sharma, P. K., Krom, B. P., et al. (2013). A functional DNase I coating to prevent adhesion of bacteria and the formation of biofilm. *Adv. Funct. Mater.* 23, 2843–2849. doi: 10.1002/adfm.201202927

Tahmassebi, J. F., Drogkari, E., and Wood, S. R. (2015). A study of the control of oral plaque biofilms via antibacterial photodynamic therapy. *Eur. Arch. Paediatr. Dent.* 16, 433–440. doi: 10.1007/s40368-014-0165-5

Talapko, J., and Skrlec, I. (2020). The principles, mechanisms, and benefits of unconventional agents in the treatment of biofilm infection. *Pharmaceuticals (Basel)* 13, 299. doi: 10.3390/ph13100299

Thi, M. T. T., Wibowo, D., and Rehm, B. H. A. (2020). *Pseudomonas aeruginosa* biofilms. *Int. J. Mol. Sci.* 21, 8671. doi: 10.3390/ijms21228671

Tovar-Garcia, A., Angarita-Zapata, V., Cazares, A., Jasso-Chavez, R., Belmont-Diaz, J., Sanchez-Torres, V., et al. (2020). Characterization of gallium resistance induced in a *Pseudomonas aeruginosa* cystic fibrosis isolate. *Arch. Microbiol.* 202, 617–622. doi: 10.1007/s00203-019-01777-y

Tummler, B. (2019). Emerging therapies against infections with *Pseudomonas aeruginosa*. *F1000Res* 8:1371. doi: 10.12688/f1000research.19509.1

Tuon, F. F., Dantas, L. R., Suss, P. H., and Tasca Ribeiro, V. S. (2022). Pathogenesis of the *Pseudomonas aeruginosa* biofilm: A review. *Pathogens* 11, 300. doi: 10.3390/pathogens11030300

Vuotto, C., and Donelli, G. (2019). Novel treatment strategies for biofilm-based infections. *Drugs* 79, 1635–1655. doi: 10.1007/s40265-019-01184-z

Wagner, S., Sommer, R., Hinsberger, S., Lu, C., Hartmann, R. W., Empting, M., et al. (2016). Novel strategies for the treatment of *Pseudomonas aeruginosa* infections. *J. Med. Chem.* 59, 5929–5969. doi: 10.1021/acs.jmedchem.5b01698

Wainwright, M., Maisch, T., Nonell, S., Plaetzer, K., Almeida, A., Tegos, G. P., et al. (2017). Photoantimicrobials-are we afraid of the light? *Lancet Infect. Dis.* 17, e49–e55. doi: 10.1016/s1473-3099(16)30268-7

Wang, L., Di Luca, M., Tkhilaishvili, T., Trampuz, A., and Gonzalez Moreno, M. (2019). Synergistic activity of Fosfomycin, ciprofloxacin, and gentamicin Against *Escherichia coli* and *Pseudomonas aeruginosa* biofilms. *Front. Microbiol.* 10, 2522. doi: 10.3389/fmicb.2019.02522

Wang, L., Fan, X., Gonzalez Moreno, M., Tkhilaishvili, T., Du, W., Zhang, X., et al. (2022). Photocatalytic quantum dot-armed bacteriophage for combating drug-resistant bacterial infection. *Adv. Sci. (Weinh)* 9:e2105668. doi: 10.1002/advs.202105668

Wang, S., Gao, Q., Cheng, J., and Lin, J. (2020). Regulation of *Pseudomonas aeruginosa* biofilms by quorum sensing systems and c-di-GMP. *Acta Microbiol. Sin.* 61, 1106–1122. doi: 10.13343/j.cnki.wsxb.20200367

Wang, S., Liu, X., Liu, H., Zhang, L., Guo, Y., Yu, S., et al. (2015). The exopolysaccharide Psl-eDNA interaction enables the formation of a biofilm skeleton in *Pseudomonas aeruginosa*. *Environ. Microbiol. Rep.* 7, 330–340. doi: 10.1111/1758-2229.12252

Wang, S., Niu, Y., Zhang, H., Li, P., Zhang, N., Cheng, J., et al. (2021). An engineered bacterium for the targeted delivery of proteins to destroy *Pseudomonas aeruginosa* biofilms. *Acta Microbiol. Sin.* 61, 2726–2748. doi: 10.13343/j.cnki.wsxb.20200680

Wei, Q., and Ma, L. Z. (2013). Biofilm matrix and its regulation in *Pseudomonas aeruginosa*. *Int. J. Mol. Sci.* 14, 20983–21005. doi: 10.3390/ijms141020983

Wen, Y. L., Wu, B. J., Kao, P. H., Fu, Y. S., and Chang, L. S. (2013). Antibacterial and membrane-damaging activities of beta-bungarotoxin B chain. *J. Pept. Sci.* 19, 1–8. doi: 10.1002/psc.2463

Whitchurch, C. B., Tolker-Nielsen, T., Ragas, P. C., and Mattick, J. S. (2002). Extracellular DNA required for bacterial biofilm formation. *Science* 295, 1487. doi: 10.1126/science.295.5559.1487

Whiteley, M., Diggle, S. P., and Greenberg, E. P. (2017). Progress in and promise of bacterial quorum sensing research. *Nature* 551, 313–320. doi: 10.1038/nature24624

Wi, Y. M., and Patel, R. (2018). Understanding biofilms and novel approaches to the diagnosis, prevention, and treatment of medical device-associated infections. *Infect. Dis. Clin. N. Am.* 32, 915–929. doi: 10.1016/j.idc.2018.06.009

Williams, D. E., and Boon, E. M. (2019). Towards understanding the molecular basis of nitric oxide-regulated group behaviors in pathogenic bacteria. *J. Innate Immun.* 11, 205–215. doi: 10.1159/000494740

Wilton, M., Charron-Mazenod, L., Moore, R., and Lewenza, S. (2016). Extracellular DNA acidifies biofilms and induces aminoglycoside resistance in *Pseudomonas aeruginosa*. *Antimicrob. Agents Chemother.* 60, 544–553. doi: 10.1128/AAC.01650-15

Wu, H., Moser, C., Wang, H. Z., Hoiby, N., and Song, Z. J. (2015). Strategies for combating bacterial biofilm infections. *Int. J. Oral Sci.* 7, 1–7. doi: 10.1038/ijos.2014.65

Wu, Z., Zheng, R., Zhang, J., and Wu, S. (2021). Transcriptional profiling of *Pseudomonas aeruginosa* PAO1 in response to anti-biofilm and anti-infection agent exopolysaccharide EPS273. *J. Appl. Microbiol.* 130, 265–277. doi: 10.1111/jam.14764

Xiu, W., Shan, J., Yang, K., Xiao, H., Yu, W., Li, H., et al. (2021). Recent development of nanomedicine for the treatment of bacterial biofilm infections. *Viewpoints* 2, 20200065. doi: 10.1002/VIW.20200065

Yadav, J., Kumari, R. M., Verma, V., and Nimesh, S. (2021). Recent development in therapeutic strategies targeting *Pseudomonas aeruginosa* biofilms – a review. *Mater. Today Proc.* 46, 2359–2373. doi: 10.1016/j.matpr.2021.05.245

Yan, J., Mao, J., and Xie, J. (2014). Bacteriophage polysaccharide depolymerases and biomedical applications. *BioDrugs* 28, 265–274. doi: 10.1007/s40259-013-0081-y

Yang, Y., Qi, P. K., Yang, Z. L., and Huang, N. (2015). Nitric oxide based strategies for applications of biomedical devices. *Biosurf. Biotribol.* 1, 177–201. doi: 10.1016/j.bsbt.2015.08.003

Yong, V. F. L., Soh, M. M., Jaggi, T. K., Mac Aogain, M., and Chotirmall, S. H. (2018). The microbial endocrinology of *Pseudomonas aeruginosa*: inflammatory and immune perspectives. *Arch. Immunol. Ther. Exp.* 66, 329–339. doi: 10.1007/s00005-018-0510-1

Yu, Z., Kong, Y., Luo, Z., Liu, T., and Lin, J. (2019). Anti-bacterial activity of mutant chensinin-1 peptide against multidrug-resistant *Pseudomonas aeruginosa* and its effects on biofilm-associated gene expression. *Exp. Ther. Med.* 17, 2031–2038. doi: 10.3892/etm.2019.7182

Yu, S., Su, T., Wu, H., Liu, S., Wang, D., Zhao, T., et al. (2015). PslG, a self-produced glycosyl hydrolase, triggers biofilm disassembly by disrupting exopolysaccharide matrix. *Cell Res.* 25, 1352–1367. doi: 10.1038/cr.2015.129

Zhang, J., He, J., Zhai, C., Ma, L. Z., Gu, L., and Zhao, K. (2018). Effects of PslG on the surface movement of *Pseudomonas aeruginosa*. *Appl. Environ. Microbiol.* 84, e00219-18. doi: 10.1128/AEM.00219-18

Zhao, X. L., Chen, Z. G., Yang, T. C., Jiang, M., Wang, J., Cheng, Z. X., et al. (2021). Glutamine promotes antibiotic uptake to kill multidrug-resistant uropathogenic bacteria. *Sci. Transl. Med.* 13, eabj0716. doi: 10.1126/scitranslmed.abj0716

Zhao, T., Zhang, Y., Wu, H., Wang, D., Chen, Y., Zhu, M. J., et al. (2018). Extracellular aminopeptidase modulates biofilm development of *Pseudomonas aeruginosa* by affecting matrix exopolysaccharide and bacterial cell death. *Environ. Microbiol. Rep.* 10, 583–593. doi: 10.1111/1758-2229.12682

Zhu, Y., McHale, G., Dawson, J., Armstrong, S., Wells, G., Han, R., et al. (2022). Slippery liquid-Like solid surfaces with promising antibiofilm performance under both static and flow conditions. *ACS Appl. Mater. Interfaces* 14, 6307–6319. doi: 10.1021/acsami.1c14533

Zhu, X., Rice, S. A., and Barraud, N. (2019). Nitric oxide and iron signaling cues have opposing effects on biofilm development in *Pseudomonas aeruginosa*. *Appl. Environ. Microbiol.* 85, e02175-18. doi: 10.1128/AEM.02175-18

frontiers | Frontiers in Microbiology

TYPE Review
PUBLISHED 02 September 2022
DOI 10.3389/fmicb.2022.981203

OPEN ACCESS

EDITED BY
Huancai Lin,
Sun Yat-sen University, China

REVIEWED BY
Dongyeop Kim,
Jeonbuk National University, South Korea
Wei Hu,
Shandong University, China

*CORRESPONDENCE
Chang Liu
liuc0728@whu.edu.cn

SPECIALTY SECTION
This article was submitted to Antimicrobials, Resistance and Chemotherapy, a section of the journal Frontiers in Microbiology

RECEIVED 29 June 2022
ACCEPTED 11 August 2022
PUBLISHED 02 September 2022

CITATION
Chen R, Du M and Liu C (2022) Strategies for dispersion of cariogenic biofilms: Applications and mechanisms. *Front. Microbiol.* 13:981203. doi: 10.3389/fmicb.2022.981203

Strategies for dispersion of cariogenic biofilms: Applications and mechanisms

Rourong Chen, Minquan Du and Chang Liu*

The State Key Laboratory Breeding Base of Basic Science of Stomatology (Hubei-MOST), Key Laboratory of Oral Biomedicine Ministry of Education, School and Hospital of Stomatology, Wuhan University, Wuhan, China

Bacteria residing within biofilms are more resistant to drugs than planktonic bacteria. They can thus play a significant role in the onset of chronic infections. Dispersion of biofilms is a promising avenue for the treatment of biofilm-associated diseases, such as dental caries. In this review, we summarize strategies for dispersion of cariogenic biofilms, including biofilm environment, signaling pathways, biological therapies, and nanovehicle-based adjuvant strategies. The mechanisms behind these strategies have been discussed from the components of oral biofilm. In the future, these strategies may provide great opportunities for the clinical treatment of dental diseases.

KEYWORDS

dispersion, eradication, disruption, cariogenic biofilms, dental plaque, *Streptococcus mutans*

Introduction

Dental caries is a common oral disease that is mainly caused by cariogenic biofilm. Cariogenic biofilms constantly form in the oral cavity. Besides mechanical cleaning, auxiliary chemical methods are necessary to control their spread (Pratten et al., 1998).

For better physical settlement, microorganisms produce, and wrap themselves in a matrix that acts like a "protective scaffold" (Jamal et al., 2018). As an architectural colony, the microbial ecosystem of caries is an ordered and spatial community (Kim and Koo, 2020), which offers opportunities for close relationships and high mutation frequency to virulence genes. In addition, as active and complex organizations, cariogenic biofilms colonize competitive niches and are resistant to stressful environments. Cariogenic biofilms restrict and sequestrate the penetration of chemicals through the matrix (Sims et al., 2020). Therefore, it is not surprising that bacteria in the biofilm state are more tolerant to various antibiotics, and thus, are more difficult to control than bacteria in the planktonic state (Davies, 2003). With long-term applications, antibiofilm drugs may not only induce resistance of cariogenic bacteria but also disrupt healthy microbiota, resulting in the limitation of existing antimicrobial therapies (Perez-Diaz et al., 2015).

Several studies have focused on the inhibition of biofilms and most present agents can inhibit biofilm-forming bacteria without eradicating the mature biofilm. Due to the short effect time of inhibitors, they cannot control the biofilm well. Therefore, to some extent, dispersion and eradication of mature biofilms are very important for biofilm control.

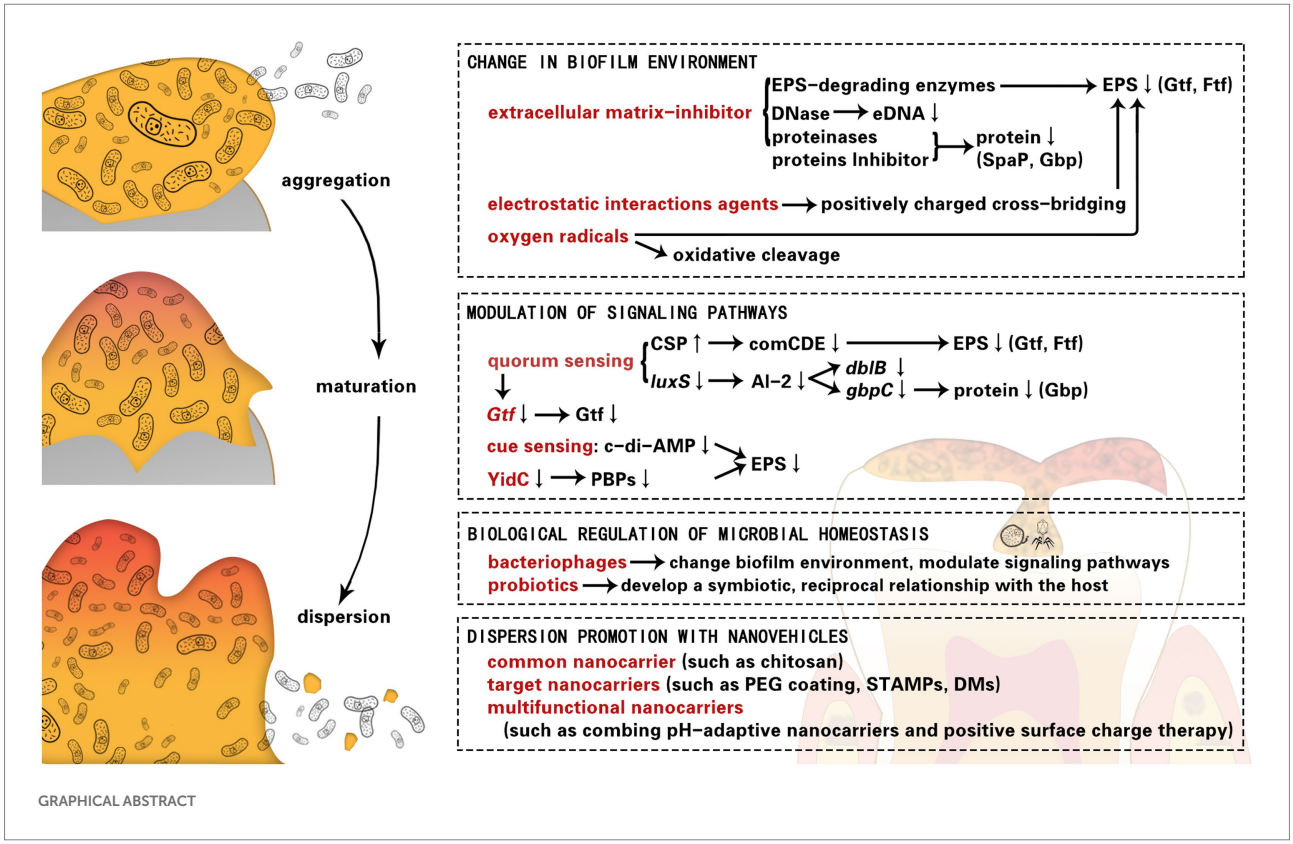

GRAPHICAL ABSTRACT

Most strategies for cariogenic biofilm dispersion are restricted to a particular approach; however, each approach has advantages and disadvantages. It is important to reinforce the concept of co-administration of different strategies. In this review, we summarize the applications and mechanisms of the strategies for dispersion of cariogenic biofilms, including changing the micro-environment, modulating signaling molecules, and so on. In addition, we explore a few novel biological and nanovehicle-based strategies, which have the potential to be combined with traditional approaches or strengthen the effects of cariogenic biofilm dispersion.

The biofilm lifestyle and dispersion

The life cycle of cariogenic biofilms has already been studied thoroughly. The development of biofilms is generally considered to be a different stage of a cyclic process. During the infection, biofilm formation is initiated by the aggregation of planktonic cells. In the biofilm, single bacterial cells are protected against the immune system and antimicrobial agents (Serra and Hengge, 2014). The concentration gradient of oxygen, nutrient resources and waste products become steepening. These stress factors of the different micro-environment may activate the starvation mechanisms and accumulation of molecules to induce dispersion (Nguyen et al., 2011). The life cycle of a biofilm is finalized with the cells escaping via dispersion to new sites for colonization. The biofilm releases the bacterial cells and allows them to recolonize at other sites (Koo et al., 2017). Evacuation of bacteria leave behind voids in the center of mature biofilm (Rumbaugh and Sauer, 2020). Although self-disassembly can result in infection and bacteremia (Fleming and Rumbaugh, 2018), the dispersed bacteria and biofilm with center voids become much more sensitive to antimicrobial agents.

Therefore, in the final stage of biofilm development, dispersion provides a great opportunity for us to remove biofilm unaffectedly (Lin et al., 2022). It is possible to create an environment that is experienced by bacteria in biofilms during the terminal stages (such as by mediating extracellular signaling molecules, nutrient resources, and oxygen) to induce biofilm degradation and diffusion. Taking advantage of the metabolites or enzymes of microorganisms would be a gentle and specific approach that would not affect the development of dysbiosis or the balance of the beneficial oral microbiome (Pleszczynska et al., 2015). Therefore, biofilm life cycles can be exploited in effective biofilm dispersion strategies.

Change in biofilm environment

Extracellular matrix-inhibitor

Degradation of the matrix is an effective strategy for the "physical collapse" of the biofilms (Rainey et al., 2019). As mentioned before, the extracellular matrix is a shield for the biofilm residents, which not only provides structural protection

to encase the community but also gain nutrients for metabolic utilization. Generally, these matrices comprise extracellular polymeric substances (EPS), extracellular DNA (eDNA), proteins, and lipids (Petersen et al., 2005; Jakubovics and Burgess, 2015).

Extracellular polymeric substance-degrading enzymes and inhibitor

Extracellular polymeric substances is one of the most important components in cariogenic biofilm matrices and includes glucans, and fructans. The polysaccharides in EPS promote bacterial aggregation and mediate biofilm adhesion (Lynch et al., 2007), which aids in avoiding a collapse of the biofilm architecture (Liljemark and Bloomquist, 1996). EPS are synthesized by extracellular enzymes of oral bacteria (Townsend-Lawman and Bleiweis, 1991; Vacca Smith and Bowen, 2000), such as glucosyltransferase (Gtf) and fructosyltransferase (Ftf). Gtf and Ftf transform glucose and fructose to glucan and fructans, respectively (Munro et al., 1991). Some antiplaque agents inhibit the activity of dental plaques by reducing the production of extracellular glucans (Koo et al., 2000) and fructans (Steinberg et al., 2002).

Glucans and fructans comprise primarily a mixture of different linkages, including α-(1→3), α-(1→6), and β-(1→6) glucans (Bowen and Koo, 2011), as well as β-(2→6)-linked fructan (Willcox and Drucker, 1987). As the key fractions of the matrix, EPS provides sites for the formation of metabolizable polysaccharides, cell aggregation microbial colonization (Koo et al., 2010; Xiao and Koo, 2010), and adhesion among different species (Gregoire et al., 2011). The α-(1→3)-linked glucan is presented in insoluble glucans with high concentrations and α-(1→6)-linked glucan is abundant in soluble glucans (Bowen and Koo, 2011). Glucanohydrolases contain mutanase for insoluble glucans and dextranase for soluble glucan (Hayacibara et al., 2004). Mutanases catalyze the hydrolysis of glucosidic linkages and effectively help fight against *Streptococcus mutans* (*S. mutans*) (Thallinger et al., 2013). These abilities of mutanases mainly manifest in the degree of saccharification and dissolution of water-insoluble EPS in *S. mutans*. Dextranase hydrolyzes dextran, which is an acceptor molecule to synthesize soluble glucans (Xiao et al., 2012). Similar effects have been observed for dispersin B, which hydrolyzes β-(1→6)-glucans (Kaplan et al., 2004). However, breaking one of the linkages in EPS monomers is not sufficient to degrade the biofilm completely. Ren et al. (2019) found that a combination of dextranase and mutanase can synergistically degrade different glycosyl linkages in a biofilm more efficiently.

Moreover, several phenols (including eugenol, catechins, quercetins, and sylvestris) showed similar functions as mutanase or dextranase. Eugenol inhibits both insoluble and soluble glucan activities of *Streptococcus sobrinus* (*S. sobrinus*) considerably (Li et al., 2012). Burt et al., reported that eugenol exhibits significant activity against the biofilm of *Candida albicans* (*C. albicans*) (Burt, 2004). *C. albicans* is one of the major etiological agents in early childhood caries (ECC), which may enhance the virulence of *S. sobrinus* and *S. mutans* as well (Wan et al., 2021). Meanwhile, eugenol presents low cytotoxicity and hemolytic activity. Catechins and quercetins interfere with both insoluble and soluble glucan activities (Zeng et al., 2019) by interacting with Gtf in *S. mutans* (Nakahara et al., 1993). This anti-Gtf action is also associated with sylvestris, which affects the quality of glucans formed by inhibiting GtfB activity. Ribeiro et al. (2019) reported that FLO/SC, PAC/CE, and PRE/SP extracts remove a significant amount of *S. mutans* biofilms, probably because of a decrease in the biomass of glucans produced by GtfB.

Although enzymes that degrade EPS can be used as moderate anti-biofilms agents (Otsuka et al., 2015), their applications alone have not been tested clinically due to their limited antimicrobial activity (Balakrishnan et al., 2000). Promising antibacterial activity in plant species has been noted. Piceatannol could be acted as an inhibitor of *gtfC*, which shares the same space as acarbose (Ito et al., 2011). Due to its specificity for the *S. mutans* Gtf, piceatannol interacted specifically with the adhesion of *S. mutans* biofilms and did not influence cell viability (Nijampatnam et al., 2018). Similarly, osteopontin exhibited an apparent selectivity toward *Streptococcus mitis* SK24 biofilms instead of the planktonic cells by changing the hydrophobicity of the biofilm surface (Schlafer et al., 2012).

Extracellular enzymes can successfully weaken the structure of the biofilms by targeting glucans, fructans, and their different linkages in EPS. Furthermore, a synergistic approach that combines antimicrobial agents with EPS matrix-degrading enzymes can potentially increase the effect of biofilm disruption and prevent dental caries.

Deoxyribonuclease

In recent years, environmental DNA (eDNA) has attracted much attention as a component of the matrix of cariogenic biofilms (Pedraza et al., 2017; Tawakoli et al., 2017). There are multiple functions of eDNA in biofilm formation, such as establishing the basis for initial bacterial adhesion and mediating subsequent attachment (Das et al., 2011). In addition, eDNA facilitates the transmission of genetic information among oral biofilms (Roberts and Kreth, 2014). It can also be a source of nutrients, including phosphate, carbon, and fixed nitrogen for oral bacteria (Liu et al., 2018b).

Zhang et al. (2020) designed a type of helical peptide, which could interact with eDNA to induce dispersion of the *S. mutans* biofilm. Several studies have used DNase to cleave eDNA. Endogenous DNase encoded by *deoC* can significantly decrease the biofilm biomass and regulate the dispersion of the *S. mutans* biofilm (Liu et al., 2017). Although DNase barely decreases the viability of planktonic *C. albicans* and *S. mutans*, the human recombinant DNase I can significantly enhance the eradication of dual-species biofilm during its initial stages (Guo et al., 2021). DNase can enhance the susceptibility of antimicrobial agents and their antibiofilm activities by cleaving eDNA.

Proteinases and proteins inhibitor

Besides EPS and eDNA, proteins also act as a scaffold to protect the community. Bacteria produce multiple proteins to enhance bacterial adhesion. Surface adhesion proteins, including glucan-binding proteins (GbpA, GbpB, GbpC, and GbpD) and streptococcal protein antigen P (SpaP), can facilitate sucrose-dependent attachment of matrix glucans, salivary agglutinin, and bacteria (Biswas and Biswas, 2005). For instance, Gbp in *S. mutans* can mediate the adhesion of *S. mutans* and promote the functions of the viscoelastic structure (Matsumoto-Nakano, 2018). Proteinase acting on the Gbp proteins exhibits an anti-Gtf effect, which leads to a reduction in the volume of EPS or even bacterial biomass. Proteinase K could affect the biofilm infrastructure of *S. mutans* and *Streptococcus oralis (S. oralis)* by removing most of the extracellular proteins (Karygianni et al., 2020). Flavonoids have a similar function as proteinase. They not only interact with extracellular and soluble proteins on the bacterial surface but also inhibit the activity of Gtfs (Koo et al., 2003).

In sum, endogenous and exogenous nucleases for eDNA and proteinase for surface adhesion proteins may effectively promote the dispersion of cariogenic biofilm.

Electrostatic interactions agents

The electrostatic interactions involved in the bonding of the biofilm matrix could be affected by hydrophilic agents (Venault et al., 2014), surfactants (Wang et al., 2021), and metal chelators (Roman et al., 2014). Such electrostatic interaction agents have been found to destabilize the biofilm matrix and facilitate biofilm separation (Xavier et al., 2005). However, there are a relatively small amount of studies about electrostatic interactions involved in the bonding of the cariogenic biofilm matrix.

Furthermore, electrostatic interactions exist among anionic metabolites and anionic components on the bacterial surface. Postollec et al. (2003) reported that static electricity affects bacterial adhesion and aggregation via isothermal reaction calorimetry. For instance, the static electricity of polypyrrole affects the positively charged cross-bridging. Most surfaces of the biofilm are negatively charged, and polypyrrole also binds to negatively charged amino acids. Enhancing electrostatic interactions may promote the physical removal of bacteria from the tooth surface by facilitating the biofilm to remain intact and by inhibiting cell separation from long chains. It has been shown that aspartic acid^{451} is a part of the active site that controls the catalytic activity in Gtfs in response to sucrose binding, i.e., the DSIRVDAVD (residues 446–454) (Mooser et al., 1991). High concentrations of polypyrrole can absorb Gtf-I and Gtf-SI and block the action of Gtfs (Kato et al., 1992). Through the electrostatic interactions with *S. mutans*, the polypyrrole structure physically inhibits the formation and colonization of the biofilm. It can also promote the physical removal of the biofilm from the tooth surface by enhancing electrostatic adsorption aggregation (Senpuku et al., 2019).

Either synchronous modification of antimicrobial polyethylene glycol (PEG) or pH-activated charge conversion with cationic peptides has recently emerged as effective approaches to target negatively charged sites (Tian et al., 2020). In this manner, the micelle structures enhanced penetration and self-regulation by anchoring to the targeted biofilm.

Such specific electrostatic interaction agents can facilitate cariogenic biofilm removal by promoting concentrations of effective constituent and affecting the Gtfs.

Oxygen radicals

During metabolism, endogenous H_2O_2 is produced by natural bacteria. The neighboring streptococci in oral micro-ecology, such as *Streptococcus gordonii* (*S. gordonii*), *Streptococcus sanguis*, and *Streptococcus oligofermentans,* can impact the pathogenesis of *S. mutans* via self-produced H_2O_2 (Kreth et al., 2009). H_2O_2 generates free radicals, which not only degrade EPS but also promote the physical removal of biofilms by oxidative cleavage (Noyori et al., 2003). Although *S. mutans* is sensitive to oxidative stress (Liu et al., 2018b), the inhibitory effect of *S. gordonii* through H_2O_2 is far from adequate (Tanzer et al., 2012).

Exogenous application of H_2O_2 is common in household and clinical disinfection. It has little toxicity even at concentrations as high as 10% of effective concentration. The high peroxidase-like catalytic activity of metals or metal oxides under acidic pH has led to an increased interest in their biomedical application. Silver (Metin-Gursoy et al., 2017) and zinc oxide nanoparticles (Hernandez-Sierra et al., 2008), as well as iron oxide nanozymes (Cormode et al., 2018), have been reported to have potent antibiofilm nature. For instance, iron oxide nanozymes in acidic environments have the similar activity as peroxidase. They disrupts the constituents of the biofilm matrix and kill *S. mutans* (Liu et al., 2018a). Dextran-coated iron oxide nanoparticles (Dex-NZM) can degrade EPS at an acidic pH (Naha et al., 2019). Furthermore, the combination of iron oxide nanozymes and H_2O_2-generating bacteria improves the overall cleansing effect (Wang et al., 2020). Gao et al. (2016) synthesized catalytic nanoparticles (CAT-NP) to degrade insoluble glucans by the generation of free radicals from H_2O_2 in pathogenic acidic biofilms.

Photosensitizer (PS) can also activate molecular oxygen radicals and produce reactive oxygen species (ROS) (Cieplik et al., 2018). Through an oxidative burst, the PS compounds cause bacterial death and biofilm dispersion (de Souza et al., 2020; Martins Antunes de Melo et al., 2021). This method provides a robust direct ablation without drug resistance (Zhao et al., 2019a). Methylene blue (MB) caused a significant reduction in *S. mutans* biofilms, allowing the prospect of eliminating bacterial infections in deep carious lesions (Legenova et al., 2020). Fotoenticine (FTC) is a new derivative of chlorin e-6, which showed significant photodynamic effects against cariogenic bacteria, including *S. mutans* that was isolated from patients with dental caries (Terra Garcia et al., 2018).

Due to the high carbohydrate content, the *S. mutans* biofilms exhibited greater absorption to PS than fungal cells, which might be the reason for the susceptibility of *S. mutans* (Sharma et al., 2011). Even in a complex polymicrobial biofilm, *S. mutans* are more susceptible to FTC-mediated photodynamic therapy (Garcia et al., 2021).

H_2O_2 and nanoparticles with the peroxidase-like activity present an ideal antibiofilm strategy by generating free radicals for the elimination of oral biofilms.

Modulation of signaling pathways

Instead of targeting the biofilm matrix, small molecules have been used to influence signaling systems by disaggregating bacteria (Ren et al., 2016; Fleming and Rumbaugh, 2017; Snarr et al., 2017). Due to its unique patterns of gene expression and protein production in each developmental stage of biofilms, bacterial signaling systems can minimize the impact on normal bacterial flora and prevent dental plaque infectious diseases (Lamont et al., 2018).

Quorum sensing

Quorum sensing (QS) is a microbial communication response in the entire cell population and has a significant impact on the biofilm life cycle (Li and Tian, 2012). QS is a typical microbial communication mode that enables bacteria to display cooperative group mechanistic behavior, which controls the expression of genes to virulence factors, biofilm dispersion, biofilm activity, and secondary metabolism (Li et al., 2001). Therefore, inhibition of the QS pathway would be a potential strategy for attenuating bacterial virulence.

The comCDE system

The comCDE system and the agglutinin-like sequence (Als) family are important in QS. The comCDE system responds to environmental signals, such as acid, and mediates pheromone competence stimulating peptide (CSP) activity (Lemos and Burne, 2008). High concentrations of CSP, which is a QS molecule in streptococci, may reduce biofilms and elongate the cells (Qi et al., 2005). Cvitkovitch et al., synthesized an analog of CSP (KBI-3221), which specifically targeted the QS pathway and decreased biofilms in various streptococcus biofilm dispersal (LoVetri and Madhyastha, 2010). Carolacton triggered the death of *S. mutans* by interfering with the comCDE system, and ComX in a growth-dependent way (Kunze et al., 2010).

Curcumin could downregulate the expression of the comCDE system (comC, comD, and comE) (Li et al., 2019) to inhibit QS (Li et al., 2018) and alter the EPS production (Falsetta et al., 2014). Hoyer et al., indicated that the expression of the Als family in *C. albicans*, which controls adhesion and aggregation, is suppressed by curcumin (Hoyer and Cota, 2016).

The *LuxS* system

In *S. oralis*, *S. gordonii*, and *S. mutans*, sulfated vizantin (Viz-S) reduces the expression of luxS and the downstream pathway of AI-2. With the deletion of the *luxS* gene, *gtfB* and *gtfC* genes are upregulated, which markedly reduces biofilm formation (Yoshida et al., 2005). Activation of the *luxS* gene downregulates the expression of *gtfG* in *S. gordoni* (Mcnab et al., 2003). AI-2 was also found in the inner cellular matrix of *S. mutans* and *S. sobrinus*. AI-2 inhibits the expression of *gbpC* and *dblB*, and induces the production of dextran-dependent aggregation (DDAG) (Lee et al., 2015).

Downregulation of the *luxS* gene alters biofilm structure in *S. oralis* and *S. gordonii* resulting in dispersion (Cuadra-Saenz et al., 2012).

Others

There has been increased interest in the QS system for the development of Chinese traditional medicine in recent years. Zingiber officinale reduces the expression of the entire set of *S. mutans* virulent genes and genes related to the biofilm life cycle, including *comDE* (for part of the QS cascade), relA (for oxidative stress and acid tolerance mechanisms) (Liu et al., 2011), *brpA* (for biofilm development and maturity), and *gtfC* (for the synthesis of glucans). The repression of these genes, especially their inhibition through the QS system, would attenuate their internal communication systems (Hasan et al., 2015). Cannabigerol also exerted an anti-bacterial effect against *S. mutans* (Karas et al., 2020; Aqawi et al., 2021). Cannabigerol suppressed the expressions of *gbpB* (for growth essential), *vicR* (for cell wall derivation and biofilm formation) (Lei et al., 2018), *brpA* (Wen et al., 2018), and *wapA* (for cell aggregation and biofilm architecture) (Zhu et al., 2006), with a concomitant increase in *spaA* (for binding *S. mutans* to tooth surfaces) expression and activity (Yang et al., 2019). Taken together, the above findings show that affecting the QS pathway can alter various gene expressions and attenuate the internal communication system, which may lead to biofilm disruption.

The *Gtf* gene family

All the QS pathways mentioned above involving the *Gtf* gene family. As we mentioned before, Gtfs maintain the integrity of the biofilm (Klein et al., 2015). The *Gtf* gene family, which encodes all Gtfs in *S. mutans*, directly responds to glucan matrix formation (Lei et al., 2015) and is regulated by the *rnc* gene. Increased expression of the *rnc* gene down-regulates *vicRKX* by posttranscriptional repression, followed by the promotion of the expression of *gtfB* and *gtfC* genes (Stipp et al., 2013; Mao et al., 2016). Therefore, the *rnc* gene could be responsible for decreasing the EPS (Mao et al., 2018).

Mao et al. (2021) reported that graphene oxide with Cu nanocomposites (GOCuNPs) can the antibacterial effects by decreasing the expression of the *rnc* gene. The regulatory role of graphene oxide with Ag nanocomposites has been reported to

be the same as GOCuNPs. They can alter the QS gene expressions of *S. mutans* and the biological process of adherence (Kulshrestha et al., 2017). GOCuNPs can also regulate the expression of the Cop family, including *CopA* (for P1-ATPase copper export), *CopY* (for negative DNA-binding repression), and *CopZ* (for copper chaperone) (Garcia et al., 2016). Cu is consistent with the effect of GOCuNPs in transcriptional repression of Gtfs by inhibiting the expression of the Cop family (Singh et al., 2015).

Besides being regulated by the QS system (Viszwapriya et al., 2017), WIG-synthesizing *Gtf* genes promoted caries in *Streptococcus* species (Xu et al., 2018). Therefore, *Gtf* genes family plays an important role in biofilm dispersion.

Cue sensing

In addition to QS, cue sensing also plays a key role in bacterial communication. Cue sensing and its signal transmission eventually lead to the downregulation of the cyclic di-guanosine monophosphate (c-di-GMP). c-di-GMP is an intracellular secondary messenger for signal transduction. c-di-GMP-based regulatory systems are involved in diverse aspects of each stage of biofilm development, including biofilm dispersion (Rumbaugh and Sauer, 2020).

Peng demonstrated that *S. mutans* modulates the production of EPS and biofilm formation by regulating c-di-AMP levels (Peng et al., 2016). The *gcp* gene in *S. mutans* encodes AAN59731, which is a conserved hypothetical protein, which acts as a diadenylate cyclase (Yan et al., 2010). It was reported that downregulation of cdaA decreases the production of diadenylate cyclase and the levels of c-di-AMP, resulting in reduced EPS content and increased sensitivity to H_2O_2 (Cheng et al., 2016). Due to a reduction in c-di-GMP levels, the expression of matrix-degrading enzymes increases, resulting in matrix dispersal (Romling et al., 2013; Srivastava et al., 2013). Therefore, a decrease in the levels of c-di-GMP induces biofilm dispersion to planktonic mode, while an increase in intracellular c-di-GMP levels fosters it to a sessile mode (Hengge, 2009).

YidC family

The deletion of *YidC* in *S. aureus* inhibited biofilm formation and attenuated virulence. In *Escherichia coli*, *YidC* mutations were lethal (Samuelson et al., 2000). Although with phenotypic differences, mutants of either *YidC1* or *YidC2* still reduce virulence in *S. mutans* (Palmer et al., 2012; Crowley and Brady, 2016). Particularly, *YidC2* has recently been identified to have the capability of folding plasminogen-binding protein (PBPs) and secreting enzymatic activities. Therefore, deletion of *YidC2* causes significant alterations not only in cell physiology properties and division, but also in the EPS matrix assembly and mechanical stability associated with dental caries (Palmer et al., 2019).

Biological regulation of microbial homeostasis

Bacteriophages

Bacteriophages are viruses that invade bacteria with high strain specificity and low toxicity (Chan and Abedon, 2015). When bacteriophages infect bacteria, they induce EPS depolymerization and lysis, which degrades the biofilm matrix and impairs cell wall integrity (Azeredo and Sutherland, 2008). After accessing the biofilm, bacteriophages disrupt key metabolic processes, such as the QS system, and even affect the regulation of the eDNA release, which induce bacterial lysis (Rehman et al., 2019). Bacteriophages are good candidates for genetic engineering. They can co-evolve with the bacterial host to resist the antibiotic (Khalifa et al., 2016). Dalmasso et al. (2015) isolated phage, ϕAPCM01, successfully. ϕAPCM01 is a *S. mutans* bacteriophage that inhibits the growth of *S. mutans* and efficiently destroys its biofilms. SMHBZ8 is also a *S. mutans* bacteriophage that is isolated from salivary samples and it has similar antimicrobial properties as ϕAPCM01 (Ben-Zaken et al., 2021). Overall, by invading bacteria, bacteriophages offer a broad prospect to be used as a novel biotherapy.

Probiotics

Probiotics treat oral infections by developing a symbiotic or reciprocal relationship with the host (Roberts and Darveau, 2015). They can prolong the therapeutic efficacy by niche occupation and prevent recolonization of the pathogenic bacteria. An ecological approach to caries treatment is to modulate and maintain the beneficial properties of the indigenous oral microflora.

There are already various commercial mouthwash and lozenges that are supplemented with probiotic bacteria, such as PerioBalance®, KForce Breath Guard®, and ProBiora3® (Yao and Fine, 2014). *Streptococcus salivarius* (*S. salivarius*) K12 and *Lactobacillus rhamnosus* GG are probiotic formulations for oral health (Caglar et al., 2005). Aggregation of *S. mutans* can cover up their surficial sites, rendering them unavailable for drug binding (di Cologna et al., 2021). Co-aggregation of *Lactobacillus paracasei* DSMZ16671 and *S. mutans* exposes these sites and removes *S. mutans* without disruption of other oral commensal species (Lang et al., 2010). Besides, *lactococcus* such as *Lactococcus lactis* produces nisin and disrupts oral pathogenic biofilms (Radaic et al., 2020). Therefore, by maintaining a healthy balance, probiotic bacteria and their metabolite can inhibit the process of biofilm development and preserve the beneficial properties of the oral microflora.

Dispersion promotion with nanovehicles

Due to the particularity of tooth anatomical structure, improper treatment for biofilm removal may expose pulp tissue

or adjacent soft tissue (Schwendicke et al., 2018). Potent antibiotics, such as CHX, are significantly cytotoxic with side effects, including discoloration or nerve damage due to pulp exposure (Nemezio et al., 2017). Furthermore, bacteria that may survive in the inner layer or the unintentional removal of tissues can weaken the tooth structure and even cause toothaches (Orhan et al., 2010). However, we can still take advantage of biofilm infiltration and intramembrane transport of drug delivery nanotechnology (Zhou et al., 2016). Polymer micelles (Zhao et al., 2019b), vesicles (Xi et al., 2019), and liposomes (Benoit et al., 2019) have been proven to have great potential for drug delivery. These nanocarriers are ideal materials with high surface area and specific catalytic and magnetic properties for use in nanomedicine (Ramos et al., 2017). Nanocarriers loaded with antimicrobials have displayed unique characteristics, including targeted bacterial enzyme decomposition of micellar carriers (Li et al., 2016) and enhanced infiltration or accumulation (Landis et al., 2017).

Common nanocarrier

Chitosan is a common nano-carrier, which can interact with both biofilm bacteria and enamel (Li et al., 2013). Chitosan, as a bio-adhesive polymer, can improve the adherence of its contents and interfere with the adhesion of biofilm bacteria (Aliasghari et al., 2016). Covarrubias et al. (2018) demonstrated that Cu coating inside chitosan (CuChNP) improves the adherence of Cu to *S. mutans* and the tooth surface. CuO-chitosan hybrid structure, silver nanoparticles containing lactose-modified chitosan (Chitlac-nAg) (Ionescu et al., 2015), poloxamer 407 formulations, capped lysozyme, and lactoferrin nanoparticles are known to reduce *S. mutans* biofilm burden (Tonguc-Altin et al., 2015). Nanocarriers, such as chitosan, can increase adherence or aggregation of the active ingredient to improve biofilm dispersion.

Target nanocarriers

One of the most important features of cariogenic biofilm microenvironments is their acidic nature. Once inside a biofilm, pH-responsive nanocarriers would expedite the release of antimicrobials through degradation of their biodegradable linkages. Zhao et al. (2019b) designed a pH-responsive detachable PEG shell that infiltrated the oral biofilms and embedded itself in the interlayer of the nanoplatforms through dynamic borate linkages. In the weakly acidic micro-ecological environments (pH 6.5), the linkages shed their PEG coating. The pH-responsive nanoparticles are capable of readily binding to EPS and reinforcing its penetration, which leads to enhanced drug anchorage followed by "on-site" drug release. Collectively, it can be a feasible strategy for the treatment of dental caries.

Specifically-targeted antimicrobial peptides (STAMPs) ensure targeted delivery to specific species in a mixed-species environment. Eckert et al. (2006) designed a STAMP molecule by combining a species-specific targeting peptide and a non-specific killing peptide. This STAMP bound specifically to *S. mutans* and eliminated it effectively while maintaining a healthy biofilm. It also showed considerable protective effects with the competitiveness of healthy normal flora against *S. mutans* colonization (Li et al., 2010).

Dextranomer (DMs) has a similar targeted delivery function as STAMPs with different principles. DMs exhibit a specific affinity for pathogenic oral streptococci, while causing limited disturbance to healthy biofilms. The affinity between DMs and oral streptococci may increase depending on the presence of sucrose. DMs with antimicrobial cargo not only protect healthy bacteria, but also improve bacterial aggregation of selectively adhered bacteria (Mashburn-Warren et al., 2017). Targeting a particular microbial species or a specific kind of pathogen can help maintain microbial homeostasis, and thus, and better eliminate pathogens significantly.

Multifunctional nanocarriers

Nanotechnology-based therapeutic modalities provide many versatile strategies to coordinate biofilm infiltration and bacterial anchoring functions.

To combine pH-adaptive nanocarriers and positive surface charge therapy, Benoit et al., developed p(DMAEMA)-b-p(DMAMEA-co-BMA-co-PAA) nanocarriers, which offer outstanding adhesion effect and can target negatively charged tooth matrix or biofilm components for drug accumulation in cariogenic biofilms (Horev et al., 2015). Furthermore, most of the cariogenic *S. mutans* are characterized by esterase activity, which degrades the ester-linkage of PAE (Hansel et al., 1998). Under acidic conditions, PAE is exposed, and can penetrate and accumulate in the biofilm. It also targets negatively charged bacterial cell surfaces with its positive charge (Liu et al., 2016). Combining the function of stealthy penetration with low pH and electrostatic attraction allows accumulation in biofilms. Therefore, PEG-PAE micelles significantly increase the efficacy of Triclosan (Wang et al., 2016). Such properties thwart dental caries by the enrichment of local drugs. The high drug bioavailability impacts overall biofilm dispersion, allowing bacterial retention at the infection site, which is a highly promising strategy for efficient bacteria killing.

Conclusion

In this review, we summarized the applications and mechanisms of the strategies for dispersion of cariogenic biofilms. Most of the studies that we have discussed focus on mono species. However, the real cariogenic biofilms comprise various acidogenic and aciduric microorganisms, including *S. mutans*, *S. sobrinus*, *Lactobacillus reuteri*, and even fungi (Pires et al., 2019). In addition,

the interaction between pathogenic species and salivary components can help bacterial species adapt to environmental stress, while aiding in the bacterial evolution of cariogenic biofilms. This phenomenon is referred to as horizontal gene transfer (HGT) (Kim et al., 2017). HGT is the main means for species to exchange metabolites and generate resistance (Lobo et al., 2019). Therefore, it is necessary to expand research on dual-species biofilms and biofilms with mixed pathogens.

Although much research has addressed bacterial biofilms, experimental conditions vary from one study to another. The oral hygiene of patients is also dependent on individual cleaning habits and orthodontic appliances used. There are novel research models that mimic the oral environment. To close the knowledge gap between ideal experimental conditions and the actual oral environment, more suitable experimental models and *in vivo,* mechanistic models are needed. Such research will play an important role in facilitating practical clinical applications. Furthermore, such therapeutic strategies can potentially be extended to other pathological conditions, such as periodontitis (Natan and Banin, 2017; Sun et al., 2021), and microbial communities. Useful strategies are by no means limited to one condition. Further research that aims to improve available strategies can shift their time, the proportion of medication applied, and dependence on auxiliary medical equipment, such as irradiation.

Many Chinese medicine ingredients comprise natural products that can contribute to overcoming the problem of chemical agents, including narrow specificity, slow action, expensive manufacturing, and drug purification for biomedical applications (Hannig et al., 2010). Focusing on strategies that can achieve biofilm dispersion to a certain degree can help preserve a balanced oral microbiome, and thus, can aid in preventing drug-resistant bacteria. It is worth noting that some of the strategies should be used together with antimicrobials to maximize biofilm dispersion. Based on the review of numerous relevant studies, we can improve therapeutic approaches by combining strategies instead of monotherapies (Xiao et al., 2018).

Author contributions

RC wrote the manuscript. CL designed this project and wrote the manuscript. MD designed this project. All authors contributed to the article and approved the submitted version.

Funding

This study was funded by grants from the National Natural Science Foundation of China (grant nos. 81201260 and 81771084).

Conflict of interest

The authors declare that the research was conducted in the absence of any commercial or financial relationships that could be construed as a potential conflict of interest.

Publisher's note

All claims expressed in this article are solely those of the authors and do not necessarily represent those of their affiliated organizations, or those of the publisher, the editors and the reviewers. Any product that may be evaluated in this article, or claim that may be made by its manufacturer, is not guaranteed or endorsed by the publisher.

References

Aliasghari, A., Rabbani Khorasgani, M., Vaezifar, S., Rahimi, F., Younesi, H., and Khoroushi, M. (2016). Evaluation of antibacterial efficiency of chitosan and chitosan nanoparticles on cariogenic streptococci: an *in vitro* study. *Iran J. Microbiol.* 8, 93–100. doi: none. PMID: 27307974

Aqawi, M., Sionov, R. V., Gallily, R., Friedman, M., and Steinberg, D. (2021). Anti-bacterial properties of cannabigerol toward *Streptococcus mutans*. *Front. Microbiol.* 12:656471. doi: 10.3389/fmicb.2021.656471

Azeredo, J., and Sutherland, I. W. (2008). The use of phages for the removal of infectious biofilms. *Curr. Pharm. Biotechnol.* 9, 261–266. doi: 10.2174/138920108785161604

Balakrishnan, M., Simmonds, R. S., and Tagg, J. R. (2000). Dental caries is a preventable infectious disease. *Aust. Dent. J.* 45, 235–245. doi: 10.1111/j.1834-7819.2000.tb00257.x

Benoit, D. S. W., Sims, K. R. Jr., and Fraser, D. (2019). Nanoparticles for oral biofilm treatments. *ACS Nano.* 13, 4869–4875. doi: 10.1021/acsnano.9b02816

Ben-Zaken, H., Kraitman, R., Coppenhagen-Glazer, S., Khalifa, L., Alkalay-Oren, S., Gelman, D., et al. (2021). Isolation and characterization of *Streptococcus mutans* phage as a possible treatment agent for caries. *Viruses* 13. doi: 10.3390/v13050825

Biswas, S., and Biswas, I. (2005). Role of Htra in surface protein expression and biofilm formation by *Streptococcus mutans*. *Infect. Immun.* 73, 6923–6934. doi: 10.1128/IAI.73.10.6923-6934.2005

Bowen, W. H., and Koo, H. (2011). Biology of *Streptococcus mutans*-derived glucosyltransferases: role in extracellular matrix formation of cariogenic biofilms. *Caries Res.* 45, 69–86. doi: 10.1159/000324598

Burt, S. (2004). Essential oils: their antibacterial properties and potential applications in foods-a review. *Int. J. Food Microbiol.* 94, 223–253. doi: 10.1016/j.ijfoodmicro.2004.03.022

Caglar, E., Kargul, B., and Tanboga, I. (2005). Bacteriotherapy and probiotics' role on oral Health. *Oral Dis.* 11, 131–137. doi: 10.1111/j.1601-0825.2005.01109.x

Chan, B. K., and Abedon, S. T. (2015). Bacteriophages and their enzymes in biofilm control. *Curr. Pharm. Des.* 21, 85–99. doi: 10.2174/1381612820666140905112311

Cheng, X., Zheng, X., Zhou, X., Zeng, J., Ren, Z., Xu, X., et al. (2016). Regulation of oxidative response and extracellular polysaccharide synthesis by a diadenylate cyclase in *Streptococcus mutans*. *Environ. Microbiol.* 18, 904–922. doi: 10.1111/1462-2920.13123

Cieplik, F., Deng, D., Crielaard, W., Buchalla, W., Hellwig, E., Al-Ahmad, A., et al. (2018). Antimicrobial photodynamic therapy-what we know and what we don't. *Crit. Rev. Microbiol.* 44, 571–589. doi: 10.1080/1040841X.2018.1467876

Cormode, D. P., Gao, L., and Koo, H. (2018). Emerging biomedical applications of enzyme-like catalytic nanomaterials. *Trends Biotechnol.* 36, 15–29. doi: 10.1016/j.tibtech.2017.09.006

Covarrubias, C., Trepiana, D., and Corral, C. (2018). Synthesis of hybrid copper-chitosan nanoparticles with antibacterial activity against cariogenic *Streptococcus mutans*. *Dent. Mater. J.* 37, 379–384. doi: 10.4012/dmj.2017-195

Crowley, P. J., and Brady, L. J. (2016). Evaluation of the effects of *Streptococcus mutans* chaperones and protein secretion machinery components on cell surface protein biogenesis, competence, and mutacin production. *Mol. Oral. Microbiol.* 31, 59–77. doi: 10.1111/omi.12130

Cuadra-Saenz, G., Rao, D. L., Underwood, A. J., Belapure, S. A., Campagna, S. R., Sun, Z., et al. (2012). Autoinducer-2 influences interactions amongst pioneer colonizing streptococci in oral biofilms. *Microbiology* 158, 1783–1795. doi: 10.1099/mic.0.057182-0

Dalmasso, M., De Haas, E., Neve, H., Strain, R., Cousin, F. J., Stockdale, S. R., et al. (2015). Isolation of a novel phage with activity against *Streptococcus mutans* biofilms. *PLoS One* 10:e0138651. doi: 10.1371/journal.pone.0138651

Das, T., Sharma, P. K., Krom, B. P., Van Der Mei, H. C., and Busscher, H. J. (2011). Role of eDNA on the adhesion forces between *Streptococcus mutans* and substratum surfaces: influence of ionic strength and substratum hydrophobicity. *Langmuir* 27, 10113–10118. doi: 10.1021/la202013m

Davies, D. (2003). Understanding biofilm resistance to antibacterial agents. *Nat. Rev. Drug Discov.* 2, 114–122. doi: 10.1038/nrd1008

De Souza, C. M., Garcia, M. T., De Barros, P. P., Pedroso, L. L. C., Ward, R., Strixino, J. F., et al. (2020). Chitosan enhances the antimicrobial photodynamic inactivation mediated by Photoditazine (R) against *Streptococcus mutans*. *Photodiagnosis Photodyn. Ther.* 32:102001. doi: 10.1016/j.pdpdt.2020.102001

Di Cologna, N. M., Samaddar, S., Valle, C. A., Vargas, J., Aviles-Reyes, A., Morales, J., et al. (2021). Amyloid aggregation of *Streptococcus mutans* Cnm influences its collagen-binding activity. *Appl. Environ. Microbiol.* 87:e0114921. doi: 10.1128/AEM.01149-21

Eckert, R., He, J., Yarbrough, D. K., Qi, F., Anderson, M. H., and Shi, W. (2006). Targeted Killing of *Streptococcus mutans* by a pheromone-guided "smart" antimicrobial peptide. *Antimicrob. Agents Chemother.* 50, 3651–3657. doi: 10.1128/AAC.00622-06

Falsetta, M. L., Klein, M. I., Colonne, P. M., Scott-Anne, K., Gregoire, S., Pai, C. H., et al. (2014). Symbiotic relationship between *Streptococcus mutans* and *Candida albicans* synergizes virulence of plaque biofilms *in vivo*. *Infect Immun.* 82, 1968–1981. doi: 10.1128/IAI.00087-14

Fleming, D., and Rumbaugh, K. (2018). The consequences of biofilm dispersal on the host. *Sci. Rep.* 8:10738. doi: 10.1038/s41598-018-29121-2

Fleming, D., and Rumbaugh, K. P. (2017). Approaches to dispersing medical biofilms. *Microorganisms* 5. doi: 10.3390/microorganisms5020015

Gao, L., Liu, Y., Kim, D., Li, Y., Hwang, G., Naha, P. C., et al. (2016). Nanocatalysts promote *Streptococcus mutans* biofilm matrix degradation and enhance bacterial killing to suppress dental caries *in vivo*. *Biomaterials* 101, 272–284. doi: 10.1016/j.biomaterials.2016.05.051

Garcia, M. T., Ward, R., Goncalves, N. M. F., Pedroso, L. L. C., Neto, J., Strixino, J. F., et al. (2021). Susceptibility of dental caries microcosm biofilms to photodynamic therapy mediated by fotoenticine. *Pharmaceutics* 13. doi: 10.3390/pharmaceutics13111907

Garcia, S. S., Du, Q., and Wu, H. (2016). *Streptococcus mutans* copper chaperone, Copz, is critical for biofilm formation and competitiveness. *Mol. Oral. Microbiol.* 31, 515–525. doi: 10.1111/omi.12150

Gregoire, S., Xiao, J., Silva, B. B., Gonzalez, I., Agidi, P. S., Klein, M. I., et al. (2011). Role of glucosyltransferase b in interactions of *Candida albicans* with *Streptococcus mutans* and with an experimental pellicle on hydroxyapatite surfaces. *Appl. Environ. Microbiol.* 77, 6357–6367. doi: 10.1128/AEM.05203-11

Guo, H., Chen, Y., Guo, W., and Chen, J. (2021). Effects of extracellular DNA on dual-species biofilm formed by *Streptococcus mutans* and *Candida albicans*. *Microb. Pathog.* 154:104838. doi: 10.1016/j.micpath.2021.104838

Hannig, C., Spies, B., Spitzmuller, B., and Hannig, M. (2010). Efficacy of enzymatic mouth rinses for immobilisation of protective enzymes in the *in situ* pellicle. *Arch. Oral. Biol.* 55, 1–6. doi: 10.1016/j.archoralbio.2009.10.004

Hansel, C., Leyhausen, G., Mai, U. E., and Geurtsen, W. (1998). Effects of various resin composite (co) monomers and extracts on two caries-associated micro-organisms *in vitro*. *J. Dent. Res.* 77, 60–67. doi: 10.1177/00220345980770010601

Hasan, S., Danishuddin, M., and Khan, A. U. (2015). Inhibitory effect of zingiber officinale towards *Streptococcus mutans* virulence and caries development: *in vitro* and *in vivo* studies. *BMC Microbiol.* 15:1. doi: 10.1186/s12866-014-0320-5

Hayacibara, M. F., Koo, H., Vacca-Smith, A. M., Kopec, L. K., Scott-Anne, K., Cury, J. A., et al. (2004). The influence of mutanase and dextranase on the production and structure of glucans synthesized by streptococcal glucosyltransferases. *Carbohydr. Res.* 339, 2127–2137. doi: 10.1016/j.carres.2004.05.031

Hengge, R. (2009). Principles of C-di-GMP signalling in bacteria. *Nat. Rev. Microbiol.* 7, 263–273. doi: 10.1038/nrmicro2109

Hernandez-Sierra, J. F., Ruiz, F., Pena, D. C., Martinez-Gutierrez, F., Martinez, A. E., Guillen Ade, J., et al. (2008). The antimicrobial sensitivity of *Streptococcus mutans* to nanoparticles of silver, zinc oxide, and gold. *Nanomedicine* 4, 237–240. doi: 10.1016/j.nano.2008.04.005

Horev, B., Klein, M. I., Hwang, G., Li, Y., Kim, D., Koo, H., et al. (2015). Ph-activated nanoparticles for controlled topical delivery of farnesol to disrupt oral biofilm virulence. *ACS Nano.* 9, 2390–2404. doi: 10.1021/nn507170s

Hoyer, L. L., and Cota, E. (2016). *Candida albicans* agglutinin-like sequence (Als) family vignettes: a review of Als protein structure and function. *Front. Microbiol.* 7:280. doi: 10.3389/fmicb.2016.00280

Ionescu, A. C., Brambilla, E., Travan, A., Marsich, E., Donati, I., Gobbi, P., et al. (2015). Silver-polysaccharide antimicrobial nanocomposite coating for methacrylic surfaces reduces streptococcus mutans biofilm formation *in vitro*. *J. Dent.* 43, 1483–1490. doi: 10.1016/j.jdent.2015.10.006

Ito, K., Ito, S., Shimamura, T., Weyand, S., Kawarasaki, Y., Misaka, T., et al. (2011). Crystal structure of glucansucrase from the dental caries pathogen *Streptococcus mutans*. *J. Mol. Biol.* 408, 177–186. doi: 10.1016/j.jmb.2011.02.028

Jakubovics, N. S., and Burgess, J. G. (2015). Extracellular DNA in oral microbial biofilms. *Microbes Infect.* 17, 531–537. doi: 10.1016/j.micinf.2015.03.015

Jamal, M., Ahmad, W., Andleeb, S., Jalil, F., Imran, M., Nawaz, M. A., et al. (2018). Bacterial biofilm and associated infections. *J. Chin. Med. Assoc.* 81, 7–11. doi: 10.1016/j.jcma.2017.07.012

Kaplan, J. B., Ragunath, C., Velliyagounder, K., Fine, D. H., and Ramasubbu, N. (2004). Enzymatic detachment of staphylococcus epidermidis biofilms. *Antimicrob. Agents Chemother.* 48, 2633–2636. doi: 10.1128/AAC.48.7.2633-2636.2004

Karas, J. A., Wong, L. J. M., Paulin, O. K. A., Mazeh, A. C., Hussein, M. H., Li, J., et al. (2020). The antimicrobial activity of cannabinoids. *Antibiotics (Basel)* 9. doi: 10.3390/antibiotics9070406

Karygianni, L., Attin, T., and Thurnheer, T. (2020). Combined DNase and proteinase treatment interferes with composition and structural integrity of multispecies oral biofilms. *J. Clin. Med.* 9. doi: 10.3390/jcm9040983

Kato, C., Nakano, Y., Lis, M., and Kuramitsu, H. K. (1992). Molecular genetic analysis of the catalytic site of *Streptococcus mutans* glucosyltransferases. *Biochem. Biophys. Res. Commun.* 189, 1184–1188. doi: 10.1016/0006-291x(92)92329-v

Khalifa, L., Shlezinger, M., Beyth, S., Houri-Haddad, Y., Coppenhagen-Glazer, S., Beyth, N., et al. (2016). Phage therapy against enterococcus faecalis in dental root canals. *J. Oral. Microbiol.* 8:32157. doi: 10.3402/jom.v8.32157

Kim, D., and Koo, H. (2020). Spatial design of polymicrobial oral biofilm in its native disease state. *J. Dent. Res.* 99, 597–603. doi: 10.1177/0022034520909313

Kim, D., Sengupta, A., Niepa, T. H., Lee, B. H., Weljie, A., Freitas-Blanco, V. S., et al. (2017). *Candida albicans* stimulates streptococcus mutans microcolony development via cross-kingdom biofilm-derived metabolites. *Sci. Rep.* 7:41332. doi: 10.1038/srep41332

Klein, M. I., Hwang, G., Santos, P. H., Campanella, O. H., and Koo, H. (2015). Streptococcus mutans-derived extracellular matrix in cariogenic oral biofilms. *Front. Cell. Infect. Microbiol.* 5:10. doi: 10.3389/fcimb.2015.00010

Koo, H., Allan, R. N., Howlin, R. P., Stoodley, P., and Hall-Stoodley, L. (2017). Targeting microbial biofilms: current and prospective therapeutic strategies. *Nat. Rev. Microbiol.* 15, 740–755. doi: 10.1038/nrmicro.2017.99

Koo, H., Hayacibara, M. F., Schobel, B. D., Cury, J. A., Rosalen, P. L., Park, Y. K., et al. (2003). Inhibition of *Streptococcus mutans* biofilm accumulation and polysaccharide production by apigenin and Tt-farnesol. *J. Antimicrob. Chemother.* 52, 782–789. doi: 10.1093/jac/dkg449

Koo, H., Vacca Smith, A. M., Bowen, W. H., Rosalen, P. L., Cury, J. A., and Park, Y. K. (2000). Effects of Apis mellifera propolis on the activities of streptococcal glucosyltransferases in solution and adsorbed onto saliva-coated hydroxyapatite. *Caries Res.* 34, 418–426. doi: 10.1159/000016617

Koo, H., Xiao, J., Klein, M. I., and Jeon, J. G. (2010). Exopolysaccharides produced by *Streptococcus mutans* glucosyltransferases modulate the establishment of microcolonies within multispecies biofilms. *J. Bacteriol.* 192, 3024–3032. doi: 10.1128/JB.01649-09

Kreth, J., Merritt, J., and Qi, F. (2009). Bacterial and host interactions of oral streptococci. *DNA Cell. Biol.* 28, 397–403. doi: 10.1089/dna.2009.0868

Kulshrestha, S., Qayyum, S., and Khan, A. U. (2017). Antibiofilm efficacy of green synthesized graphene oxide-silver nanocomposite using lagerstroemia speciosa floral Extract: a comparative study on inhibition of gram-positive and gram-negative biofilms. *Microb. Pathog.* 103, 167–177. doi: 10.1016/j.micpath.2016.12.022

Kunze, B., Reck, M., Dotsch, A., Lemme, A., Schummer, D., Irschik, H., et al. (2010). Damage of *Streptococcus mutans* biofilms by carolacton, a secondary metabolite from the *Myxobacterium sorangium* Cellulosum. *BMC Microbiol.* 10, 199. doi: 10.1186/1471-2180-10-199

Lamont, R. J., Koo, H., and Hajishengallis, G. (2018). The oral microbiota: dynamic communities and host interactions. *Nat. Rev. Microbiol.* 16, 745–759. doi: 10.1038/s41579-018-0089-x

Landis, R. F., Gupta, A., Lee, Y. W., Wang, L. S., Golba, B., Couillaud, B., et al. (2017). Cross-linked polymer-stabilized nanocomposites for the treatment of bacterial biofilms. *ACS Nano.* 11, 946–952. doi: 10.1021/acsnano.6b07537

Lang, C., Bottner, M., Holz, C., Veen, M., Ryser, M., Reindl, A., et al. (2010). Specific lactobacillus/mutans streptococcus co-aggregation. *J. Dent. Res.* 89, 175–179. doi: 10.1177/0022034509356246

Lee, H. J., Kim, S. C., Kim, J., Do, A., Han, S. Y., Lee, B. D., et al. (2015). Synergistic inhibition of streptococcal biofilm by ribose and xylitol. *Arch. Oral Biol.* 60, 304–312. doi: 10.1016/j.archoralbio.2014.11.004

Legenova, K., Kovalcikova, M., Cernakova, L., and Bujdakova, H. (2020). The contribution of photodynamic inactivation vs. corsodyl mouthwash to the control of streptococcus mutans biofilms. *Curr. Microbiol.* 77, 988–996. doi: 10.1007/s00284-020-01901-y

Lei, L., Stipp, R. N., Chen, T., Wu, S. Z., Hu, T., and Duncan, M. J. (2018). Activity of *Streptococcus mutans vicR* is modulated by antisense RNA. *J. Dent. Res.* 97, 1477–1484. doi: 10.1177/0022034518781765

Lei, L., Yang, Y., Mao, M., Li, H., Li, M., Yang, Y., et al. (2015). Modulation of biofilm exopolysaccharides by the *Streptococcus mutans* Vicx gene. *Front. Microbiol.* 6:1432. doi: 10.3389/fmicb.2015.01432

Lemos, J. A., and Burne, R. A. (2008). A model of efficiency: stress tolerance by *Streptococcus mutans*. *Microbiology* 154, 3247–3255. doi: 10.1099/mic.0.2008/023770-0

Li, B., Li, X., Lin, H., and Zhou, Y. (2018). Curcumin as a promising antibacterial agent: effects on metabolism and biofilm formation in S. Mutans. *Biomed Res. Int.* 2018, 4508709. doi: 10.1155/2018/4508709

Li, F., Weir, M. D., Chen, J., and Xu, H. H. (2013). Comparison of quaternary ammonium-containing with nano-silver-containing adhesive in antibacterial properties and cytotoxicity. *Dent. Mater.* 29, 450–461. doi: 10.1016/j.dental.2013.01.012

Li, L. N., Guo, L. H., Lux, R., Eckert, R., Yarbrough, D., He, J., et al. (2010). Targeted antimicrobial therapy against Streptococcus mutans establishes protective non-cariogenic oral biofilms and reduces subsequent infection. *Int. J. Oral. Sci.* 2, 66–73. doi: 10.4248/IJOS10024

Li, M. Y., Lai, G. Y., Wang, J., and Ye, D. X. (2012). The inhibition of eugenol on glucan is essential for the biofilm eradication effect on caries-related biofilm in an artificial mouth model. *Nat. Prod. Res.* 26, 1152–1155. doi: 10.1080/14786419.2011.561799

Li, X., Yin, L., Ramage, G., Li, B., Tao, Y., Zhi, Q., et al. (2019). Assessing the impact of curcumin on dual-species biofilms formed by *Streptococcus mutans* and *Candida albicans*. *Microbiologyopen* 8:e937. doi: 10.1002/mbo3.937

Li, Y., Liu, G., Wang, X., Hu, J., and Liu, S. (2016). Enzyme-responsive polymeric vesicles for bacterial-strain-selective delivery of antimicrobial agents. *Angew. Chem. Int. Ed. Engl.* 55, 1760–1764. doi: 10.1002/anie.201509401

Li, Y. H., Lau, P. C., Lee, J. H., Ellen, R. P., and Cvitkovitch, D. G. (2001). Natural genetic transformation of *Streptococcus mutans* growing in biofilms. *J. Bacteriol.* 183, 897–908. doi: 10.1128/JB.183.3.897-908.2001

Li, Y. H., and Tian, X. (2012). Quorum sensing and bacterial social interactions in biofilms. *Sensors* 12, 2519–2538. doi: 10.3390/s120302519

Liljemark, W. F., and Bloomquist, C. (1996). Human oral microbial ecology and dental caries and periodontal diseases. *Crit. Rev. Oral Biol. Med.* 7, 180–198. doi: 10.1177/10454411960070020601

Lin, Y., Zhou, X., and Li, Y. (2022). Strategies for *Streptococcus mutans* biofilm dispersal through extracellular polymeric substances disruption. *Mol. Oral Microbiol.* 37, 1–8. doi: 10.1111/omi.12355

Liu, C., Worthington, R. J., Melander, C., and Wu, H. (2011). A new small molecule specifically inhibits the cariogenic bacterium *Streptococcus mutans* in multispecies biofilms. *Antimicrob. Agents Chemother.* 55, 2679–2687. doi: 10.1128/AAC.01496-10

Liu, J., Sun, L., Liu, W., Guo, L., Liu, Z., Wei, X., et al. (2017). A nuclease from *Streptococcus mutans* facilitates biofilm dispersal and escape from killing by neutrophil extracellular traps. *Front. Cell. Infect. Microbiol.* 7:97. doi: 10.3389/fcimb.2017.00097

Liu, Y., Busscher, H. J., Zhao, B., Li, Y., Zhang, Z., Van Der Mei, H. C., et al. (2016). Surface-adaptive, antimicrobially loaded, micellar nanocarriers with enhanced penetration and killing efficiency in staphylococcal biofilms. *ACS Nano* 10, 4779–4789. doi: 10.1021/acsnano.6b01370

Liu, Y., Naha, P. C., Hwang, G., Kim, D., Huang, Y., Simon-Soro, A., et al. (2018a). Topical ferumoxytol nanoparticles disrupt biofilms and prevent tooth decay *in vivo* via intrinsic catalytic activity. *Nat. Commun.* 9:2920. doi: 10.1038/s41467-018-05342-x

Liu, Y., Palmer, S. R., Chang, H., Combs, A. N., Burne, R. A., and Koo, H. (2018b). Differential oxidative stress tolerance of *Streptococcus mutans* isolates affects competition in an ecological mixed-species biofilm model. *Environ. Microbiol. Rep.* 10, 12–22. doi: 10.1111/1758-2229.12600

Lobo, C. I. V., Rinaldi, T. B., Christiano, C. M. S., De Sales Leite, L., Barbugli, P. A., and Klein, M. I. (2019). Dual-species biofilms of *Streptococcus mutans* and *Candida albicans* exhibit more biomass and are mutually beneficial compared with single-species biofilms. *J. Oral Microbiol.* 11:1581520. doi: 10.1080/20002297.2019.1581520

Lovetri, K., and Madhyastha, S. (2010). Antimicrobial and antibiofilm activity of quorum sensing peptides and peptide analogues against oral biofilm bacteria. *Methods Mol. Biol.* 618, 383–392. doi: 10.1007/978-1-60761-594-1_24

Lynch, D. J., Fountain, T. L., Mazurkiewicz, J. E., and Banas, J. A. (2007). Glucan-binding proteins are essential for shaping *Streptococcus mutans* biofilm architecture. *FEMS Microbiol. Lett.* 268, 158–165. doi: 10.1111/j.1574-6968.2006.00576.x

Mao, M., Zhang, W., Huang, Z., Huang, J., Wang, J., Li, W., et al. (2021). Graphene oxide-copper nanocomposites suppress cariogenic *Streptococcus mutans* biofilm formation. *Int. J. Nanomed.* 16, 7727–7739. doi: 10.2147/IJN.S303521

Mao, M. Y., Li, M., Lei, L., Yin, J. X., Yang, Y. M., and Hu, T. (2018). The regulator gene rnc is closely involved in biofilm formation in *Streptococcus mutans*. *Caries Res.* 52, 347–358. doi: 10.1159/000486431

Mao, M. Y., Yang, Y. M., Li, K. Z., Lei, L., Li, M., Yang, Y., et al. (2016). The rnc gene promotes exopolysaccharide synthesis and represses the *vicR*kx gene expressions via microrna-size small rnas in *Streptococcus mutans*. *Front. Microbiol.* 7:687. doi: 10.3389/fmicb.2016.00687

Martins Antunes de Melo, W. C., Celiesiute-Germaniene, R., Simonis, P., and Stirke, A. (2021). Antimicrobial photodynamic therapy (Apdt) for biofilm treatments. Possible synergy between Apdt and pulsed electric fields. *Virulence* 12, 2247–2272. doi: 10.1080/21505594.2021.1960105

Mashburn-Warren, L., Downey, J. S., and Goodman, S. D. (2017). Novel method for the depletion of cariogenic bacteria using dextranomer microspheres. *Mol. Oral Microbiol.* 32, 475–489. doi: 10.1111/omi.12186

Matsumoto-Nakano, M. (2018). Role of *Streptococcus mutans* surface proteins for biofilm formation. *Jpn. Dent. Sci. Rev.* 54, 22–29. doi: 10.1016/j.jdsr.2017.08.002

Mcnab, R., Ford, S. K., El-Sabaeny, A., Barbieri, B., Cook, G. S., and Lamont, R. J. (2003). Luxs-based signaling in *Streptococcus gordonii*: autoinducer 2 controls carbohydrate metabolism and biofilm formation with *Porphyromonas gingivalis*. *J. Bacteriol.* 185, 274–284. doi: 10.1128/JB.185.1.274-284.2003

Metin-Gursoy, G., Taner, L., and Akca, G. (2017). Nanosilver coated orthodontic brackets: *in vivo* antibacterial properties and ion release. *Eur. J. Orthod.* 39, 9–16. doi: 10.1093/ejo/cjv097

Mooser, G., Hefta, S. A., Paxton, R. J., Shively, J. E., and Lee, T. D. (1991). Isolation and sequence of an active-site peptide containing a catalytic aspartic acid from two *Streptococcus sobrinus* alpha-glucosyltransferases. *J. Biol. Chem.* 266, 8916–8922. doi: 10.1016/S0021-9258(18)31531-X

Munro, C., Michalek, S. M., and Macrina, F. L. (1991). Cariogenicity of *Streptococcus mutans* V403 glucosyltransferase and fructosyltransferase mutants constructed by allelic exchange. *Infect. Immun.* 59, 2316–2323. doi: 10.1128/iai.59.7.2316-2323.1991

Naha, P. C., Liu, Y., Hwang, G., Huang, Y., Gubara, S., Jonnakuti, V., et al. (2019). Dextran-coated iron oxide nanoparticles as biomimetic catalysts for localized and Ph-activated biofilm disruption. *ACS Nano* 13, 4960–4971. doi: 10.1021/acsnano.8b08702

Nakahara, K., Kawabata, S., Ono, H., Ogura, K., Tanaka, T., Ooshima, T., et al. (1993). Inhibitory effect of oolong tea polyphenols on glycosyltransferases of mutans streptococci. *Appl. Environ. Microbiol.* 59, 968–973. doi: 10.1128/aem.59.4.968-973.1993

Natan, M., and Banin, E. (2017). From nano to micro: using nanotechnology to combat microorganisms and their multidrug resistance. *FEMS Microbiol. Rev.* 41, 302–322. doi: 10.1093/femsre/fux003

Nemezio, M. A., De Souza Farias, S. S., Borsatto, M. C., Aires, C. P., and Corona, S. A. M. (2017). Effect of methylene blue-induced photodynamic therapy on a *Streptococcus mutans* biofilm model. *Photodiagnosis Photodyn. Ther.* 20, 234–237. doi: 10.1016/j.pdpdt.2017.10.025

Nguyen, D., Joshi-Datar, A., Lepine, F., Bauerle, E., Olakanmi, O., Beer, K., et al. (2011). Active starvation responses mediate antibiotic tolerance in biofilms and nutrient-limited bacteria. *Science* 334, 982–986. doi: 10.1126/science.1211037

Nijampatnam, B., Zhang, H., Cai, X., Michalek, S. M., Wu, H., and Velu, S. E. (2018). Inhibition of *Streptococcus mutans* biofilms by the natural stilbene piceatannol through the inhibition of glucosyltransferases. *ACS Omega* 3, 8378–8385. doi: 10.1021/acsomega.8b00367

Noyori, R., Aoki, M., and Sato, K. (2003). Green oxidation with aqueous hydrogen peroxide. *Chem. Commun.* 1977-86:1977. doi: 10.1039/b303160h

Orhan, A. I., Oz, F. T., and Orhan, K. (2010). Pulp exposure occurrence and outcomes after 1- or 2-visit indirect pulp therapy vs. complete caries removal in primary and permanent molars. *Pediatr. Dent.* 32, 347–355. doi: none. PMID: 20836956

Otsuka, R., Imai, S., Murata, T., Nomura, Y., Okamoto, M., Tsumori, H., et al. (2015). Application of chimeric glucanase comprising mutanase and dextranase for

prevention of dental biofilm formation. *Microbiol. Immunol.* 59, 28–36. doi: 10.1111/1348-0421.12214

Palmer, S. R., Crowley, P. J., Oli, M. W., Ruelf, M. A., Michalek, S. M., and Brady, L. J. (2012). *Yidc* 1 and *Yidc* 2 are functionally distinct proteins involved in protein secretion, biofilm formation and cariogenicity of *Streptococcus mutans*. *Microbiology* 158, 1702–1712. doi: 10.1099/mic.0.059139-0

Palmer, S. R., Ren, Z., Hwang, G., Liu, Y., Combs, A., Soderstrom, B., et al. (2019). *Streptococcus mutans Yidc* 1 and *Yidc* 2 impact cell envelope biogenesis, the biofilm matrix, and biofilm biophysical properties. *J. Bacteriol.* 201. doi: 10.1128/JB.00396-18

Pedraza, M. C. C., Novais, T. F., Faustoferri, R. C., Quivey, R. G., Terekhov, A., Hamaker, B. R., et al. (2017). Extracellular DNA and lipoteichoic acids interact with exopolysaccharides in the extracellular matrix of *Streptococcus mutans* biofilms. *Biofouling* 33, 722–740. doi: 10.1080/08927014.2017.1361412

Peng, X., Zhang, Y., Bai, G., Zhou, X., and Wu, H. (2016). Cyclic di-amp mediates biofilm formation. *Mol. Microbiol.* 99, 945–959. doi: 10.1111/mmi.13277

Perez-Diaz, M. A., Boegli, L., James, G., Velasquillo, C., Sanchez-Sanchez, R., Martinez-Martinez, R. E., et al. (2015). Silver nanoparticles with antimicrobial activities against *Streptococcus mutans* and their cytotoxic effect. *Mater. Sci. Eng. C Mater. Biol. Appl.* 55, 360–366. doi: 10.1016/j.msec.2015.05.036

Petersen, F. C., Tao, L., and Scheie, A. A. (2005). DNA binding-uptake system: a link between cell-to-cell communication and biofilm formation. *J. Bacteriol.* 187, 4392–4400. doi: 10.1128/JB.187.13.4392-4400.2005

Pires, J. G., Braga, A. S., Andrade, F. B., Saldanha, L. L., Dokkedal, A. L., Oliveira, R. C., et al. (2019). Effect of hydroalcoholic extract of *Myracrodruon urundeuva* all and *Qualea grandiflora* mart leaves on the viability and activity of microcosm biofilm and on enamel demineralization. *J. Appl. Oral Sci.* 27:e20180514. doi: 10.1590/1678-7757-2018-0514

Pleszczynska, M., Wiater, A., Janczarek, M., and Szczodrak, J. (2015). (1-->3)-alpha-D-glucan hydrolases in dental biofilm prevention and control: a review. *Int. J. Biol. Macromol.* 79, 761–778. doi: 10.1016/j.ijbiomac.2015.05.052

Postollec, F., Norde, W., Van Der Mei, H. C., and Busscher, H. J. (2003). Enthalpy of interaction between coaggregating and non-coaggregating oral bacterial pairs--A microcalorimetric study. *J. Microbiol. Methods* 55, 241–247. doi: 10.1016/s0167-7012(03)00145-3

Pratten, J., Wills, K., Barnett, P., and Wilson, M. (1998). *In vitro* studies of the effect of antiseptic-containing mouthwashes on the formation and viability of Streptococcus sanguis biofilms. *J. Appl. Microbiol.* 84, 1149–1155. doi: 10.1046/j.1365-2672.1998.00462.x

Qi, F., Kreth, J., Levesque, C. M., Kay, O., Mair, R. W., Shi, W., et al. (2005). Peptide pheromone induced cell death of *Streptococcus mutans*. *FEMS Microbiol. Lett.* 251, 321–326. doi: 10.1016/j.femsle.2005.08.018

Radaic, A., Ye, C., Parks, B., Gao, L., Kuraji, R., Malone, E., et al. (2020). Modulation of pathogenic oral biofilms towards health with nisin probiotic. *J. Oral Microbiol.* 12:1809302. doi: 10.1080/20002297.2020.1809302

Rainey, K., Michalek, S. M., Wen, Z. T., and Wu, H. (2019). Glycosyltransferase-mediated biofilm matrix dynamics and virulence of *Streptococcus mutans*. *Appl. Environ. Microbiol.* 85. doi: 10.1128/AEM.02247-18

Ramos, A. P., Cruz, M. A. E., Tovani, C. B., and Ciancaglini, P. (2017). Biomedical applications of nanotechnology. *Biophys. Rev.* 9, 79–89. doi: 10.1007/s12551-016-0246-2

Rehman, S., Ali, Z., Khan, M., Bostan, N., and Naseem, S. (2019). The dawn of phage therapy. *Rev. Med. Virol.* 29:e2041. doi: 10.1002/rmv.2041

Ren, Z., Cui, T., Zeng, J., Chen, L., Zhang, W., Xu, X., et al. (2016). Molecule targeting glucosyltransferase inhibits *Streptococcus mutans* biofilm formation and virulence. *Antimicrob. Agents Chemother.* 60, 126–135. doi: 10.1128/AAC.00919-15

Ren, Z., Kim, D., Paula, A. J., Hwang, G., Liu, Y., Li, J., et al. (2019). Dual-targeting approach degrades biofilm matrix and enhances bacterial killing. *J. Dent. Res.* 98, 322–330. doi: 10.1177/0022034518818480

Ribeiro, S. M., Fratucelli, E. D. O., Bueno, P. C. P., De Castro, M. K. V., Francisco, A. A., Cavalheiro, A. J., et al. (2019). Antimicrobial and antibiofilm activities of *Casearia sylvestris* extracts from distinct Brazilian biomes against *Streptococcus mutans* and *Candida albicans*. *BMC Complement Altern. Med.* 19:308. doi: 10.1186/s12906-019-2717-z

Roberts, A. P., and Kreth, J. (2014). The Impact of horizontal gene transfer on the adaptive ability of the human oral microbiome. *Front. Cell. Infect. Microbiol.* 4:124. doi: 10.3389/fcimb.2014.00124

Roberts, F. A., and Darveau, R. P. (2015). Microbial protection and virulence in periodontal tissue as a function of polymicrobial communities: symbiosis and dysbiosis. *Periodontol* 69, 18–27. doi: 10.1111/prd.12087

Roman, M. J., Decker, E. A., and Goddard, J. M. (2014). Metal-chelating active packaging film enhances lysozyme inhibition of listeria monocytogenes. *J. Food. Prot.* 77, 1153–1160. doi: 10.4315/0362-028X.JFP-13-545

Romling, U., Galperin, M. Y., and Gomelsky, M. (2013). Cyclic di-GMP: the first 25 years of a universal bacterial second messenger. *Microbiol. Mol. Biol. R.* 77, 1–52. doi: 10.1128/MMBR.00043-12

Rumbaugh, K. P., and Sauer, K. (2020). Biofilm dispersion. *Nat. Rev. Microbiol.* 18, 571–586. doi: 10.1038/s41579-020-0385-0

Samuelson, J. C., Chen, M., Jiang, F., Moller, I., Wiedmann, M., Kuhn, A., et al. (2000). *Yidc* mediates membrane protein insertion in bacteria. *Nature* 406, 637–641. doi: 10.1038/35020586

Schlafer, S., Meyer, R. L., Sutherland, D. S., and Stadler, B. (2012). Effect of osteopontin on the initial adhesion of dental bacteria. *J. Nat. Prod.* 75, 2108–2112. doi: 10.1021/np300514z

Schwendicke, F., Leal, S., Schlattmann, P., Paris, S., Dias Ribeiro, A. P., Gomes Marques, M., et al. (2018). Selective carious tissue removal using subjective criteria or polymer bur: study protocol for a randomised controlled trial (select). *BMJ Open* 8:e022952. doi: 10.1136/bmjopen-2018-022952

Senpuku, H., Tuna, E. B., Nagasawa, R., Nakao, R., and Ohnishi, M. (2019). The inhibitory effects of polypyrrole on the biofilm formation of *Streptococcus mutans*. *PLoS One* 14:e0225584. doi: 10.1371/journal.pone.0225584

Serra, D. O., and Hengge, R. (2014). Stress responses go three dimensional - the spatial order of physiological differentiation in bacterial macrocolony biofilms. *Environ. Microbiol.* 16, 1455–1471. doi: 10.1111/1462-2920.12483

Sharma, S. K., Dai, T., Kharkwal, G. B., Huang, Y. Y., Huang, L., De Arce, V. J., et al. (2011). Drug discovery of antimicrobial photosensitizers using animal models. *Curr. Pharm. Des.* 17, 1303–1319. doi: 10.2174/138161211795703735

Sims, K. R. Jr., Maceren, J. P., Liu, Y., Rocha, G. R., Koo, H., and Benoit, D. S. W. (2020). Dual antibacterial drug-loaded nanoparticles synergistically improve treatment of streptococcus mutans biofilms. *Acta Biomater.* 115, 418–431. doi: 10.1016/j.actbio.2020.08.032

Singh, K., Senadheera, D. B., Levesque, C. M., and Cvitkovitch, D. G. (2015). The copYAZ operon functions in copper efflux, biofilm formation, genetic transformation, and stress tolerance in *Streptococcus mutans*. *J. Bacteriol.* 197, 2545–2557. doi: 10.1128/JB.02433-14

Snarr, B. D., Baker, P., Bamford, N. C., Sato, Y., Liu, H., Lehoux, M., et al. (2017). Microbial glycoside hydrolases as antibiofilm agents with cross-kingdom activity. *Proc. Natl. Acad. Sci. U.S.A.* 114, 7124–7129. doi: 10.1073/pnas.1702798114

Srivastava, D., Hsieh, M. L., Khataokar, A., Neiditch, M. B., and Waters, C. M. (2013). Cyclic di-GMP Inhibits vibrio cholerae motility by repressing induction of transcription and inducing extracellular polysaccharide production. *Mol. Microbiol.* 90, 1262–1276. doi: 10.1111/mmi.12432

Steinberg, D., Bachrach, G., Gedalia, I., Abu-Ata, S., and Rozen, R. (2002). Effects of various antiplaque agents on fructosyltransferase activity in solution and immobilized onto hydroxyapatite. *Eur. J. Oral Sci.* 110, 374–379. doi: 10.1034/j.1600-0722.2002.21303.x

Stipp, R. N., Boisvert, H., Smith, D. J., Hofling, J. F., Duncan, M. J., and Mattos-Graner, R. O. (2013). Covr and *vicR*k regulate cell surface biogenesis genes required for biofilm formation in *Streptococcus mutans*. *PLoS One* 8:e58271. doi: 10.1371/journal.pone.0058271

Sun, Y., Sun, X., Li, X., Li, W., Li, C., Zhou, Y., et al. (2021). A versatile nanocomposite based on nanoceria for antibacterial enhancement and protection from aPDT-aggravated inflammation via modulation of macrophage polarization. *Biomaterials* 268:120614. doi: 10.1016/j.biomaterials.2020.120614

Tanzer, J. M., Thompson, A., Sharma, K., Vickerman, M. M., Haase, E. M., and Scannapieco, F. A. (2012). *Streptococcus mutans* out-competes *Streptococcus gordonii in vivo*. *J. Dent. Res.* 91, 513–519. doi: 10.1177/0022034512442894

Tawakoli, P. N., Neu, T. R., Busck, M. M., Kuhlicke, U., Schramm, A., Attin, T., et al. (2017). Visualizing the dental biofilm matrix by means of fluorescence lectin-binding analysis. *J. Oral Microbiol.* 9. doi: 10.1080/20002297.2017.1345581

Terra Garcia, M., Correia Pereira, A. H., Figueiredo-Godoi, L. M. A., Jorge, A. O. C., Strixino, J. F., and Junqueira, J. C. (2018). Photodynamic therapy mediated by chlorin-type photosensitizers against *Streptococcus mutans* biofilms. *Photodiagnosis Photodyn. Ther.* 24, 256–261. doi: 10.1016/j.pdpdt.2018.08.012

Thallinger, B., Prasetyo, E. N., Nyanhongo, G. S., and Guebitz, G. M. (2013). Antimicrobial enzymes: an emerging strategy to fight microbes and microbial biofilms. *Biotechnol. J.* 8, 97–109. doi: 10.1002/biot.201200313

Tian, S., Su, L., Liu, Y., Cao, J., Yang, G., Ren, Y., et al. (2020). Self-targeting, zwitterionic micellar dispersants enhance antibiotic killing of infectious biofilms—an intravital imaging study in mice. *Sci. Adv.* 6:eabb1112. doi: 10.1126/sciadv.abb1112

Tonguc-Altin, K., Sandalli, N., Duman, G., Selvi-Kuvvetli, S., Topcuoglu, N., and Kulekci, G. (2015). Development of novel formulations containing lysozyme and lactoferrin and evaluation of antibacterial effects on mutans streptococci and lactobacilli. *Arch. Oral Biol.* 60, 706–714. doi: 10.1016/j.archoralbio.2015.02.004

Townsend-Lawman, P., and Bleiweis, A. S. (1991). Multilevel control of extracellular sucrose metabolism in *Streptococcus salivarius* by sucrose. *J. Gen. Microbiol.* 137, 5–13. doi: 10.1099/00221287-137-1-5

Vacca Smith, A. M., and Bowen, W. H. (2000). *In situ* studies of pellicle formation on Hydroxyapatite discs. *Arch. Oral Biol.* 45, 277–291. doi: 10.1016/s0003-9969(99)00141-7

Venault, A., Yang, H. S., Chiang, Y. C., Lee, B. S., Ruaan, R. C., and Chang, Y. (2014). Bacterial resistance control on mineral surfaces of hydroxyapatite and human teeth via surface charge-driven antifouling coatings. *ACS Appl. Mater. Interfaces* 6, 3201–3210. doi: 10.1021/am404780w

Viszwapriya, D., Subramenium, G. A., Radhika, S., and Pandian, S. K. (2017). Betulin inhibits cariogenic properties of *Streptococcus mutans* by targeting *vicR*k and Gtf genes. *Antonie Van Leeuwenhoek* 110, 153–165. doi: 10.1007/s10482-016-0785-3

Wan, S. X., Tian, J., Liu, Y., Dhall, A., Koo, H., and Hwang, G. (2021). Cross-kingdom cell-to-cell interactions in cariogenic biofilm initiation. *J. Dent. Res.* 100, 74–81. doi: 10.1177/0022034520950286

Wang, B., Liu, T., Chen, H., Yin, B., Zhang, Z., Russell, T. P., et al. (2021). Molecular brush surfactants: versatile emulsifiers for stabilizing and structuring liquids. *Angew. Chem. Int. Ed. Engl.* 60, 19626–19630. doi: 10.1002/anie.202104653

Wang, L. S., Gupta, A., and Rotello, V. M. (2016). Nanomaterials for the treatment of bacterial biofilms. *ACS Infect. Dis.* 2, 3–4. doi: 10.1021/acsinfecdis.5b00116

Wang, Y., Shen, X., Ma, S., Guo, Q., Zhang, W., Cheng, L., et al. (2020). Oral biofilm elimination by combining iron-based nanozymes and hydrogen peroxide-producing bacteria. *Biomater. Sci.* 8, 2447–2458. doi: 10.1039/c9bm01889a

Wen, Z. Z. T., Scott-Anne, K., Liao, S. M., De, A. P., Luo, M., Kovacs, C., et al. (2018). Deficiency of *brpA* in *Streptococcus mutans* reduces virulence in rat caries model. *Mol. Oral Microbiol.* 33, 353–363. doi: 10.1111/omi.12230

Willcox, D. P., and Drucker, D. B. (1987). A simple method for determining extracellular polysaccharide-producing ability of oral streptococci. *Microbios* 51, 175–181. doi: none. PMID: 3316938

Xavier, J. B., Picioreanu, C., Rani, S. A., Van Loosdrecht, M. C. M., and Stewart, P. S. (2005). Biofilm-control strategies based on enzymic disruption of the extracellular polymeric substance matrix--a modelling study. *Microbiology* 151, 3817–3832. doi: 10.1099/mic.0.28165-0

Xi, Y., Wang, Y., Gao, J., Xiao, Y., and Du, J. (2019). Dual corona vesicles with intrinsic antibacterial and enhanced antibiotic delivery capabilities for effective treatment of biofilm-induced periodontitis. *ACS Nano* 13, 13645–13657. doi: 10.1021/acsnano.9b03237

Xiao, J., Grier, A., Faustoferri, R. C., Alzoubi, S., Gill, A. L., Feng, C., et al. (2018). Association between oral candida and bacteriome in children with severe ECC. *J. Dent. Res.* 97, 1468–1476. doi: 10.1177/0022034518790941

Xiao, J., Klein, M. I., Falsetta, M. L., Lu, B. W., Delahunty, C. M., Yates, J. R., et al. (2012). The exopolysaccharide matrix modulates the interaction between 3D architecture and virulence of a mixed-species oral biofilm. *Plos Pathogens* 8:e1002623. doi: 10.1371/journal.ppat.1002623

Xiao, J., and Koo, H. (2010). Structural organization and dynamics of exopolysaccharide matrix and microcolonies formation by *Streptococcus mutans* in biofilms. *J. Appl. Microbiol.* 108, 2103–2113. doi: 10.1111/j.1365-2672.2009.04616.x

Xu, R. R., Yang, W. D., Niu, K. X., Wang, B., and Wang, W. M. (2018). An update on the evolution of glucosyltransferase (Gtf) genes in streptococcus. *Front. Microbiol.* 9:2979. doi: 10.3389/fmicb.2018.02979

Yan, W., Qu, T., Zhao, H., Su, L., Yu, Q., Gao, J., et al. (2010). The effect of C-di-GMP (3'-5'-cyclic diguanylic Acid) on the biofilm formation and adherence of *Streptococcus mutans*. *Microbiol. Res.* 165, 87–96. doi: 10.1016/j.micres.2008.10.001

Yang, J. M., Deng, D. M., Brandt, B. W., Nazmi, K. R., Wu, Y. F., Crielaard, W., et al. (2019). Diversity of SpaP in genetic and salivary agglutinin mediated adherence among *Streptococcus mutans* strains. *Sci. Rep.* 9:19943. doi: 10.1038/s41598-019-56486-9

Yao, S. G., and Fine, J. B. (2014). Probiotics for bacterial disease treatment in the oral environment. *Compend. Contin. Educ. Dent.* 35, 658–663 : quiz 664. doi: none

Yoshida, A., Ansai, T., Takehara, T., and Kuramitsu, H. K. (2005). Luxs-based signaling affects *Streptococcus mutans* biofilm formation. *Appl. Environ. Microbiol.* 71, 2372–2380. doi: 10.1128/AEM.71.5.2372-2380.2005

Zeng, Y., Nikitkova, A., Abdelsalam, H., Li, J., and Xiao, J. (2019). Activity of quercetin and kaemferol against *Streptococcus mutans* biofilm. *Arch. Oral Biol.* 98, 9–16. doi: 10.1016/j.archoralbio.2018.11.005

Zhang, J., Chen, C., Chen, J., Zhou, S., Zhao, Y., Xu, M., et al. (2020). Dual mode of anti-biofilm action of G3 against *Streptococcus mutans*. *ACS Appl. Mater. Interfaces* 12, 27866–27875. doi: 10.1021/acsami.0c00771

Zhao, Y., Guo, Q., Dai, X., Wei, X., Yu, Y., Chen, X., et al. (2019a). A biomimetic non-antibiotic approach to eradicate drug-resistant infections. *Adv. Mater.* 31:e1806024. doi: 10.1002/adma.201806024

Zhao, Z., Ding, C., Wang, Y., Tan, H., and Li, J. (2019b). Ph-responsive polymeric nanocarriers for efficient killing of cariogenic bacteria in biofilms. *Biomater. Sci.* 7, 1643–1651. doi: 10.1039/c8bm01640b

Zhou, J., Horev, B., Hwang, G., Klein, M. I., Koo, H., and Benoit, D. S. (2016). Characterization and optimization of PH-responsive polymer nanoparticles for drug delivery to oral biofilms. *J. Mater. Chem. B.* 4, 3075–3085. doi: 10.1039/C5TB02054A

Zhu, L., Kreth, J., Cross, S. E., Gimzewski, J. K., Shi, W. Y., and Qi, F. X. (2006). Functional characterization of cell-wall-associated protein *WapA* in Streptococcus mutans. *Microbiology* 152, 2395–2404. doi: 10.1099/mic.0.28883-0

frontiers | Frontiers in Microbiology

TYPE Original Research
PUBLISHED 23 September 2022
DOI 10.3389/fmicb.2022.958132

OPEN ACCESS

EDITED BY
Huancai Lin,
Sun Yat-sen University, China

REVIEWED BY
Biao Ren,
Sichuan University,
China
Runhui Liu,
East China University of Science and Technology, China

*CORRESPONDENCE
Chun Liu
liuch393@mail.sysu.edu.cn
Xuenong Zou
zouxuen@mail.sysu.edu.cn

†These authors have contributed equally to this work and share first authorship

SPECIALTY SECTION
This article was submitted to Antimicrobials, Resistance and Chemotherapy, a section of the journal Frontiers in Microbiology

RECEIVED 31 May 2022
ACCEPTED 24 August 2022
PUBLISHED 23 September 2022

CITATION
Chen Y, Hu H, Huang F, Ling Z, Chen B, Tan B, Wang T, Liu X, Liu C and Zou X (2022) Cocktail of isobavachalcone and curcumin enhance eradication of *Staphylococcus aureus* biofilm from orthopedic implants by gentamicin and alleviate inflammatory osteolysis. *Front. Microbiol.* 13:958132. doi: 10.3389/fmicb.2022.958132

Cocktail of isobavachalcone and curcumin enhance eradication of *Staphylococcus aureus* biofilm from orthopedic implants by gentamicin and alleviate inflammatory osteolysis

Yan Chen[1,2†], Hao Hu[1,2†], Fangli Huang[1,2], Zemin Ling[1,2], Bolin Chen[1,2], Bizhi Tan[1,2], Tingxuan Wang[1,2], Xiao Liu[1,2], Chun Liu[2,3*] and Xuenong Zou[1,2*]

[1]Department of Spine Surgery, The First Affiliated Hospital, Sun Yat-sen University, Guangzhou, China, [2]Guangdong Provincial Key Laboratory of Orthopaedics and Traumatology, The First Affiliated Hospital, Sun Yat-sen University, Guangzhou, China, [3]Precision Medicine Institute, The First Affiliated Hospital, Sun Yat-sen University, Guangzhou, China

Orthopedic device-related infection (ODRI) caused by *Staphylococcus aureus*, especially methicillin-resistant *S. aureus* (MRSA) biofilm may lead to persist infection and severe inflammatory osteolysis. Previous studies have demonstrated that both isobavachalcone and curcumin possess antimicrobial activity, recent studies also reveal their antiosteoporosis, anti-inflammation, and immunoregulatory effect. Thus, this study aims to investigate whether the combination of isobavachalcone and curcumin can enhance the anti-*S. aureus* biofilm activity of gentamicin and alleviate inflammatory osteolysis *in vivo*. EUCAST and a standardized MBEC assay were used to verify the synergy between isobavachalcone and curcumin with gentamicin against planktonic *S. aureus* and its biofilm *in vitro*, then the antimicrobial and immunoregulatory effect of cocktail therapy was demonstrated in a femoral ODRI mouse model *in vivo* by μCT analysis, histopathology, quantification of bacteria in bone and myeloid-derived suppressor cell (MDSC) in bone marrow. We tested on standard MSSA ATCC25923 and MRSA USA300, 5 clinical isolated MSSA, and 2 clinical isolated MRSA strains and found that gentamicin with curcumin (62.5–250μg/ml) and gentamicin with isobavachalcone (1.56μg/ml) are synergistic against planktonic MSSA, while gentamicin (128μg/ml) with curcumin (31.25–62.5, 250–500μg/ml) and gentamicin (64–128μg/ml) with isobavachalcone (1.56–12.5μg/ml) exhibit synergistic effect against MSSA biofilm. Results of further study revealed that cocktail of 128μg/ml gentamicin together with 125μg/ml curcumin +6.25μg/ml isobavachalcone showed promising biofilm eradication effect with synergy against USA300 biofilm *in vitro*. Daily intraperitoneal administration of 20mg/kg/day isobavachalcone, 20mg/kg/day curcumin, and 20mg/kg/day gentamicin, can reduce inflammatory osteolysis and maintain microarchitecture of trabecular bone during orthopedic device-related MRSA infection in mice. Cocktail therapy also enhanced reduction of MDSC M1 polarization in peri-implant tissue, suppression of MDSC amplification in bone

marrow, and Eradication of USA300 biofilm *in vivo*. Together, these results suggest that the combination of isobavachalcone and curcumin as adjuvants administrated together with gentamicin significantly enhances its antimicrobial effect against *S. aureus* biofilm, and can also modify topical inflammation in ODRI and protect bone microstructure *in vivo*, which may serve as a potential treatment strategy, especially for *S. aureus* induced ODRI.

KEYWORDS

biofilm, *Staphylococcus aureus*, synergy, isobavachalcone, curcumin, orthopedic device-related infection, inflammatory osteolysis, myeloid-derived suppressor cells

Introduction

Device-related Infection (DRI; Costerton et al., 1999) is a serious complication of orthopedic surgery, which may lead to severe bacterial osteomyelitis (OM) and inflammatory osteolysis and the destruction of surrounding soft tissues (Molin and Tolker-Nielsen, 2003; Arciola et al., 2008). Despite the improvement of aseptic surgery techniques and the standardized use of antimicrobial drugs over a considerable period of time, orthopedic device-related infections still have an incidence of ~2.3%–20% (depending on the patient's systemic status and surgical area conditions, as well as the type of surgery and implant; Ribeiro et al., 2012; Oikonomidis et al., 2020). The infection incidence ranges from 1% to 2% in first total joint replacement and 2% to 6% in revision joints (Rao et al., 2011; Fagotti et al., 2018), while the incidence of infection after spinal internal fixation fusion ranges from 0.7% to 11.9% (Schimmel et al., 2010). With the increased use of orthopedic implants, including various types of joint prostheses, plates, and screws, the number of implant-related infections will likely continue to increase. DRI and the resulting osteomyelitis are usually caused by *Staphylococcus aureus* (*S. aureus*), which, as a Gram-positive (G+) bacterium (Montanaro et al., 2011), is also the main pathogen causing community-associated hospital-acquired infections (Jones et al., 2014). However, with the overuse of antibiotics, methicillin-resistant *S. aureus* (MRSA) has gradually increased in the proportion of clinically isolated *S. aureus* (Hiramatsu et al., 2002), showing a > 50% prevalence of nosocomial infections in several Asian countries (Drago et al., 2007).

Bacterial biofilm (BF) is an important mechanism mediating the antibiotic resistance of MRSA, which is a multilayered three-dimensional complex structure formed by bacteria as well as hydrated extracellular polymers (EPS) composed of polysaccharides, proteins, lipids and extracellular nucleic acids (Flemming et al., 2007). The formation of biofilm on the surface of implants creates a physical barrier that makes it difficult for antibiotics to enter, while the microenvironment within the biofilm, such as pH and ion concentration, is significantly altered, thus reducing the effectiveness of antibiotics. Strategies to cope with biofilm-induced resistance include developing novel antibiotics, increasing antibiotics dosing, and the combination of multiple antibiotics or small molecules. However, the speed of new antibiotic development is limited, and high concentrations of antibiotics or multiple antibiotic combinations may lead to liver and kidney damage(Lebeaux et al., 2014; Huang et al., 2020); therefore, screening small molecules to be used in combination with existing antibiotics to enhance their efficacy is a very economical and practical strategy.

Previous studies have shown that many molecules from widely used herbal medicines have antibacterial effect. Curcumin (CRM), a natural polyphenolic substance, was first isolated and identified in the rhizome of the turmeric, and also as one of the components in the patent Chinese traditional medicine compound Xian-ling-gu-bao (XLGB), which was approved by China's CFDA in the treatment of osteoporosis, aseptic osteolysis, fracture, and osteoarthritis. Several studies have shown that CRM has potential antioxidant, anti-inflammatory, antibacterial and antitumor effects (Daniel et al., 2004; Moghadamtousi et al., 2014; Bimonte et al., 2016; Kunnumakkara et al., 2017). In terms of antibacterial activity, curcumin increases the bidirectional permeability of the cell membrane of *S. aureus* (Tyagi et al., 2015) and its antimicrobial activity may act by disrupting cell membrane (Mun et al., 2014; Teow et al., 2016), while other studies have shown enhanced membrane penetration and membrane depolarization by its improved molecules (Prince et al., 2019). Isobavachalcone (ISB) is a pentenyl chalcone isolated from plants of the Fabaceae, Umbelliferae, Moraceae, Schisandrae, and Bee families, which is also a component of XLGB. ISB is active against Gram-positive bacteria, mainly methicillin-sensitive *Staphylococcus aureus* (MSSA) and methicillin-resistant *Staphylococcus aureus* (MRSA). It's reported that ISB inhibited more than 50% of MSSA and MRSA biofilm formation at 0.78 μg/ml, while cytotoxicity assays showed that it did not influence cell viability (Wang X. et al., 2021). Curcumin was widely used for decade and served as a FDA-approved compounded drug additives for oral administration, and for injection in some circumstances, and they both have antimicrobial effects alone. Thus, whether they have synergistic effects in combination with conventional antibiotics that increase their antimicrobial effects is worthy of in-depth study.

In addition, it has been reported that following orthopedic device-related infection, *S. aureus* biofilm could induce polarization of macrophages in the surrounding bone marrow lumen toward pro-inflammation M1 macrophages. M1-type macrophages are associated with an excessive and sustained activation of the inflammatory response, which may lead to inflammatory-related bone resorption and consequent implant loosening. Interestingly, it has been shown that curcumin could inhibit M1-type macrophage polarization to prevent osteocyte apoptosis in a glucocorticoid-related femoral head necrosis mouse model (Jin et al., 2020). Another study showed that curcumin could maintain the M0-like phenotype of macrophage under the influence of PE particles and inhibit macrophage-involved osteolysis and inflammation *via* promoting cholesterol efflux(Liu et al., 2019). Besides, Isobavachalcone could prevent osteoporosis by inhibiting M1 polarization of macrophages (Wang X. et al., 2021). Therefore, curcumin and Isobavachalcone may prevent inflammatory bone resorption associated with *S. aureus* infection by modulating the macrophage phenotype.

In summary, curcumin and Isobavachalcone have both anti-bacterial and anti-inflammatory effects; however, it remains unclear whether they have synergistic effects with conventional antibiotics and whether their combination exerts stronger effects on preventing inflammatory bone resorption in orthopedic device-related infection. In order to address the above questions, this study would first verify the synergistic effects of curcumin and Isobavachalcone separately or simultaneously with conventional antibiotics through *in vitro Staphylococcus aureus* biofilm model, and then confirm the anti-infective and anti-inflammatory effect *in vivo* through an MRSA-induced mouse femoral implant infection model.

Materials and methods

Microbiology

Bacterial strains and reagents

Methicillin-susceptible *S. aureus* (MSSA) ATCC 25923 and Methicillin-resistant *S. aureus* (MRSA) ATCC 700699 (USA300) were purchased from China General Microbiological Culture Collection Center (CGMCC), China. Clinical isolated strain *S. aureus* JAR was provided by AO Research Institute Davos, Switzerland. Clinical isolated strains *S. aureus* MSSA 2222, MSSA 2557, MSSA 2039, MSSA 2031, MRSA 2435, and MRSA 2027 from various patients with ODRI were provided by The First Affiliated Hospital of Jinan University, China. Gentamicin sulfate (HY-A0276), Daptomycin (HY-B0108), Rifampicin (HY-B0272), and Levofloxacin (HY-B0330) were purchased from MedChemExpress, China. Curcumin (HY-N0005) and isobavachalcone (HY-13065) were purchased from MedChemExpress, China. All reagents were prepared as stock solutions according to manufacturer's instructions and stored at −20°C.

Bacteria suspensions and biofilm cultural conditions

Isolated colonies of *S. aureus* strains on TSA agar plate were picked to inoculate a flask containing 40 ml of Tryptone Soya Broth (TSB, 1268857, OXOID) and incubated on a shaker at 100 rpm at 36 ± 1°C overnight to obtain bacteria suspension. The overnight culture was used for the inoculum on MBEC™ Biofilm Inoculator (16120015, Innovotech, Canada) according to manufacturer instructions to generate biofilm. Bacteria suspensions were centrifuged and washed with PBS twice, then resuspended in PBS, and sonicated for 3 min. The bacterial suspension was adjusted to an OD_{600nm} range between 1.1 and 1.2 (~4–5 × 10^8 per ml). Vortexed again, diluted 22 µl of the bacteria solution with 22 ml TSB (with 1% human plasma, P9523, Sigma, China) in the trough base to reach a 1,000× dilution (~4–5 × 10^8 per ml). Then, the peg lid was placed on the trough base. The inoculator was placed on a rocking table set to 5 rocks/min at 36 ± 1°C for 24 h. The plates' orientation was changed for 90° every 12 h. Medium for each plate was refreshed every day. For biofilms used for laser scanning confocal microscopy imaging, 24-well cell slides were used instead of MBEC inoculators, and the rest of the culture conditions remain the same.

MIC and MBC against *Staphylococcus aureus*

The minimum inhibitory concentration (MIC) and minimum bactericidal concentration (MBC) of isobavachalcone, curcumin, and antibiotics and their combinations were determined by EUCAST guidelines with modifications for a broth microdilution checkerboard procedure (Kahlmeter et al., 2006; Cusack et al., 2019). The combinations of XLGB molecules and antibiotics on a two-dimensional checkerboard with two-fold dilutions. Checkerboard challenge plates were established using 96-well microtiter plates. The final concentrations of ISB (0.20–12.50 µg/ml) and CRM (0.24–2,000 µg/ml) were chosen according to literature (Yin et al., 2004; Tajbakhsh et al., 2008; Dzoyem et al., 2013; Mun et al., 2013; Sasidharan et al., 2014; Cui et al., 2015; Teow and Ali, 2015; Gunes et al., 2016; Sandikci et al., 2016; Wang et al., 2016; Faegheh et al., 2018), and the antibiotics tested were chosen according to EUCAST database.

Bacteria inoculum adjusted to OD between 1.1 and 1.2 (4–5 × 10^8/ml) were prepared as aforementioned. Adjust the density of the bacteria suspension to 1–1.25 × 10^7/ml. 5 µl of 1–1.25 × 10^7/ml bacteria suspension was inoculated to each well containing 200 µl TSB to reach an approximate density of 5 × 10^5/ml except for sterile control. OD_{600nm} before incubation were measured, all microtiter plates are incubated at 36.5 ± 1°C for 24 h in an incubator with constant humidity, then microtiter plates were measured at OD_{600nm} again, ratio of OD_{600nm} readings after incubation, and the ones before incubation need to be calculated. In this study, not all solutions were clear and transparent, therefore MIC was defined by MIC_{90} (inhibits 90% of growth). The MIC of antibiotics, ISB, and CRM alone are determined as $MIC_{antibiotic}$, MIC_{ISB}, and MIC_{CRM}, respectively. The MICs of antibiotics, ISB, and CRM in each combination are also determined as

$MIC_{antibiotic}$-combination, MIC_{ISB}-combination, and MIC_{CRM}-combination, respectively. After MIC was determined, 20 µl of liquid in each well was transferred from microtiter plates to single-well MHA plates by using a 96 solid Pin MULTI-BLOT™ Replicator (V.P. Scientific Inc., United States, VP 405). Colonies on single-well MHA plates were photographed and checked after incubated at 36.5 ± 1°C for 24 h. MBC was defined as the lowest concentration of eradicating bacteria, leading to no colony formation. The MBCs of ISB, CRM, and antibiotics alone are determined as MBC_{ISO}, MBC_{CRM}, and $MBC_{antibiotic}$, respectively. The MBCs of ISB, CRM, and antibiotics in each combination are also determined as MBC_{ISB}-combination, MBC_{CRM}-combination, and $MBC_{antibiotic}$-combination, respectively. All modified EUCASTs were repeated at least three times.

MBEC assay against *Staphylococcus aureus* biofilm

The minimum biofilm eradication concentration (MBEC) is determined by MBEC™ Assay as per the manufacturer's instruction with optimized protocol. Checkerboard technique similar to the EUCAST was used to prepare antibiotic challenge plates for MBEC, including a two-fold concentrations gradient both with antibiotics ISB, and CRM according to the results of EUCAST. Inoculum preparation biofilm cultural conditions were described aforementioned. Transfer the MBEC Assay inoculator lid with homogeneous 24 h biofilm to the challenge plate and incubate at 36.5 ± 1°C for 24 h. Rinse biofilms with 96-well plates with 250 µl/well for ~10 s. Detached pegs with sterilized pliers into individual sterile glass vials with 10 ml of D/E broth, vortex for 10 s and sonicate for 15 min to remove the biofilm from the pegs. Vortex the D/E broth again for 3 s before pipetting 200 µl per well into a new 96-well microtiter plate according to the challenge plate layout. All vials with D/E broth will be stored at 4°C in case for further culture. Use a sterile 96 solid Pin Replicator to transfer 20 µl D/E broth in each well onto a single well TSA plate. Check the colony formation on TSA plates after being incubated at 36.5 ± 1°C for 24 h, the desired group of D/E broth with biofilm will be further conducted bacterial cell counts by using a serial dilution plating method. MBEC is defined as the minimum concentration of antimicrobial that eradicates the biofilm. All biofilm experiments were repeated at least three times.

Interpretation of EUCAST and MBEC assay results

For the calculation of the Fractional inhibition concentration index (FICI) and Fractional bactericidal concentration index (FBCI), The FICI and FBCI were calculated as follows: FICI = MIC_A-combined/MIC_A + MIC_B-combined/MIC_B; FBCI = MBC_A-combined/ MBC_A + MBC_B-combined/MBC_B, A and B stand for different antibacterial molecules. The FICI and FBCI data were interpreted the following way: FICI ≤ 0.5 = synergy, FICI > 0.5–4 = no interaction, and FICI > 4.0 = antagonism (Odds, 2003).

After the residual biofilm was quantified, the synergistic effect could not be further calculated based on its MBEC if multiple drug combinations failed to completely remove the biofilm. The commonly used Coefficient of drug interaction (CDI) was introduced to evaluate synergy according to previous studies (Tallarida, 2011; Song et al., 2020), and the calculation is as follows: CDI = AB/(A × B). Based on the residual CFU per peg of each group, AB is the ratio of the combination group to the control group. A or B is the ratio of the stand-alone antibiotics or ISB/CRM group to the control group. Thus, CDI < 1, =1, or >1 indicate drug synergy, superposition or antagonism, respectively, where CDI < 0.7 indicates significant synergy.

Fluorescence and confocal imaging of biofilms

MRSA USA300 biofilms were cultured and challenge as cultural conditions detailed previously on sterile cell slides. For live and dead staining, an aliquot (2 ml) of MHB diluted overnight culture was used to incubate the biofilm on cell slides in 12-well plates for 24 h. The 24 h culture biofilm was removed and washed with PBS. Controls were treated with 128 µg/ml of GEN (MBEC90) only, and 128 µg/ml of GEN combined with 125 µm/ml CRM, 6.25 µm/ml ISB, and 125 µm/ml CRM + 6.25 µm/ml ISB, respectively, for 24 h. Then biofilms were washed with PBS with cautions three times and stained with LIVE/DEAD™ BacLight™ Bacterial Viability Kit (L7012, Invitrogen, United States) according to the manufacturer's instructions in constant with previous literature (Tawakoli et al., 2013), and the biofilm samples were then imaged by confocal laser scanning microscopy system (CLSM TCS XP8, Leica, Germany).

Scanning electron microscopy of biofilm

The 24-h MRSA USA300 biofilm challenged with antimicrobial combination on the cell slides for 24 h was rinsed 3 times with PBS. Then fixed with 3% glutaraldehyde for 5 h at 4°C, and then gently rinsed with saline 3 times for 15 min each. The 12-well cell slides were dehydrated twice for 5 min with each gradient of 30%, 50%, 70%, 90%, 95%, and 100% ethanol, respectively. Ethanol was replaced with isoamyl acetate 2 times for 5 min each. The samples were dried using a critical point drier (HCP-2, Hitachi, Japan). The samples were plated on a copper table with an automatic gold plating apparatus, and the bacterial morphology was observed by an SEM (Regulus 8100, Hitachi, Japan).

In vivo study of antimicrobial and anti-inflammatory effect

Animal model and cocktail treatment

Animal experiments were carried out in accordance with the principles and guidelines of the Animal Ethics Committee of the Guangzhou Huateng Education Incorporation and was acknowledged by the First Affiliated Hospital of Sun Yet-sen University. 48 eight-week-old male C57BL/6 J mice (wild type) used in this experiment were purchased from the Experimental Animal Center of the First Hospital of Sun Yat-sen University

(Guangzhou, China) and weighed ~22.05 ± 1.87 g. All animals were housed in individual ventilated cages under controlled conditions (temperature 22°C–24°C, relative humidity 40%–70%), with free access to food and water and 12-h circadian rhythm.

Animals were randomized and divided into 4 equal groups according to post-surgery treatments, including a control group (MRSA-infected + 20 mg/kg/day Gentamicin) and 3 different treatment groups ($n = 12$ per group), including: (A) MRSA-infected + 20 mg/kg/day Gentamicin (GEN) + 20 mg/kg/day Curcumin (CRM); (B) MRSA-infected + 20 mg/kg/day GEN + 20 mg/kg/day Isobavachalcone (ISB); (D) MRSA-infected + 20 mg/kg/day GEN + 20 mg/kg/day CRM + 20 mg/kg/day ISB (Figure 1A). According to *in vitro* results, USA300 was used as pathogen in mouse model, which is one of the most clinically-related MRSA strains in biofilm research, especially in ODRI (Lauderdale et al., 2010). As the pharmacokinetics of ISB and CRM in bone and bone marrow tissue is not clear, no previous report reveals the local drug concentrations in bone tissue and bone marrow after subcutaneous administration. The dosage of ISB (Wang X. et al., 2021) and CRM (Wang et al., 2016; Liu et al., 2019) in mouse model were chosen according to previous literature in order to achieve either anti-bacterial, anti-inflammatory, or anti-osteoporosis, respectively. The Dosage of gentamicin in the animal experiment was chosen according to previous *in vivo* study (Espersen et al., 1994), and is much lower than that can induce acute kidney injury (Huang et al., 2020).

The distal femoral implant was inserted using a trans-knee approach established in intramedullary nailing mice model (as in Figure 1B) and widely used in the ODRI mouse model (Bernthal et al., 2010; Lovati et al., 2013). Animals were fasted with free access to water for 8 h prior to surgery. Animals were anesthetized under pentobarbital sodium (80 mg/kg, i.p.). After disinfection with 75% alcohol and povidone iodine, a medial parapatellar arthrotomy was used to approach the intercondylar notch, and a 25 gauge syringe needle (Ø 0.5 mm) was used as drill to breakthrough subchondral bone, a 27 gauge insulin syringe needle was carefully inserted into for 3–4 mm without expansion to open a retrograde corridor into the femoral medullary canal. When there is no continuous bleeding, switch to a Hamilton microinjector with a 30G needle (25 µl) to slowly inject 5 µl of MRSA USA300 suspension ($1–2 \times 10^6$ CFU/ml, prepared as aforementioned) into the medullary canal to achieve a total bacterial inoculum of $0.5–1 \times 10^4$ CFU per animal. A customized Ø 0.6 mm, 7–8 mm long Kirschner needle was then implanted retrogradely into the femoral medullary canal through the corridor with 1 mm protruded into the joint space. The patella was then repositioned and incision was closed layer by layer with 4–0 synthetic sutures.

Animals were housed in original environment after awakening from anesthesia. One day after surgery and MRSA USA300 inoculation, antibiotics and ISB, CRM, or their combination were intraperitoneally administrated for 4 weeks according to the study design, followed by a daily subcutaneous administration of Meloxicam for 5 days post-surgery. All animals were monitored daily for general status and welfare, and checked weekly to record data on body weight, signs of wound healing, swelling, infection, pain, and suffering. After 4 weeks, the mice were euthanized to perform further investigations.

MDSCs in blood analysis

To determine the MDSCs population in the peripheral blood of mice, 1 ml of peripheral blood samples were collected using cardiac puncture from 6 animals per group at the end of animal experiment for flow cytometry analysis. After lysis of erythrocytes using erythrocyte lysis solution, the remaining leukocytes were resuspended in PBS containing 2% FBS and then incubated for 30 min at 4°C with rat anti-mouse CD11b-FITC (ab24874, Abcam, United States) and rat anti-mouse Gr-1-PE (12-9668-82, Thermo Fisher, United States) at the manufacturer's recommended concentration. MDSCs in mouse peripheral blood was analyzed by co-staining with rat anti-mouse CD11b-FITC (ab24874, Abcam, United States), Gr-1-PE (12-9668-82, Thermo Fisher, United States). BD FACSCantoII flow cytometry data were further analyzed using FACSDiva software (BD Biosciences). The number of cells analyzed per sample was ~10,000. Analysis was performed using FlowJo software (Tree Star, United States).

µCT analysis

Distal femur specimens were collected and fixed in 4% paraformaldehyde. The bone microarchitectures surrounding implant of the distal femurs were analyzed by a desktop µCT SkyScan1276 (Bruker Micro CT, Belgium). In the present study, µCT scanner was operated at 85 kV and 200 µA, with a scaled image pixel size of 10.0 µm, 1 mm Al filter was used for optimal image contrast, and spiral scanning was used to reduce metal artifacts. Images were reconstructed and processed with Software Nrecon (Bruker micro-CT, Belgium). Software CTAn (Bruker micro-CT, Belgium) was used to perform bone morphometry analysis. Trabecular bone was separated from cortical bone by free-drawing region of interest (ROI), and metallic implant in the distal femur was ruled out by setting bony binary selection threshold as 75–150. Volume of interest (VOI, 2 mm proximal to the distal metaphyseal line) was chosen within 200 continuous slices. We performed bone morphologic measurements in CTAn and obtained corresponding parameters, including trabecular bone volume fraction (BV/TV; %), trabecular thickness (Tb.Th; mm), trabecular number (Tb.N; mm^{-1}), bone surface density (BS/TV; mm^{-1}), trabecular separation (Tb.Sp; mm), and bone mineral density (BMD; mg/cm^3). Then, the 3D models of VOI were reconstructed with CTAn and then visualized in CTVol (Bruker micro-CT, Belgium). The operators conducting the µCT analysis were blinded to the treatments associated with samples.

Histological assessment and immunofluorescence staining

After µCT scanning, 6 femur specimens per group were fixed in 4% paraformaldehyde for at least 48 h, and washed three times with PBS buffer. Samples were decalcified in 10% EDTA (E1171,

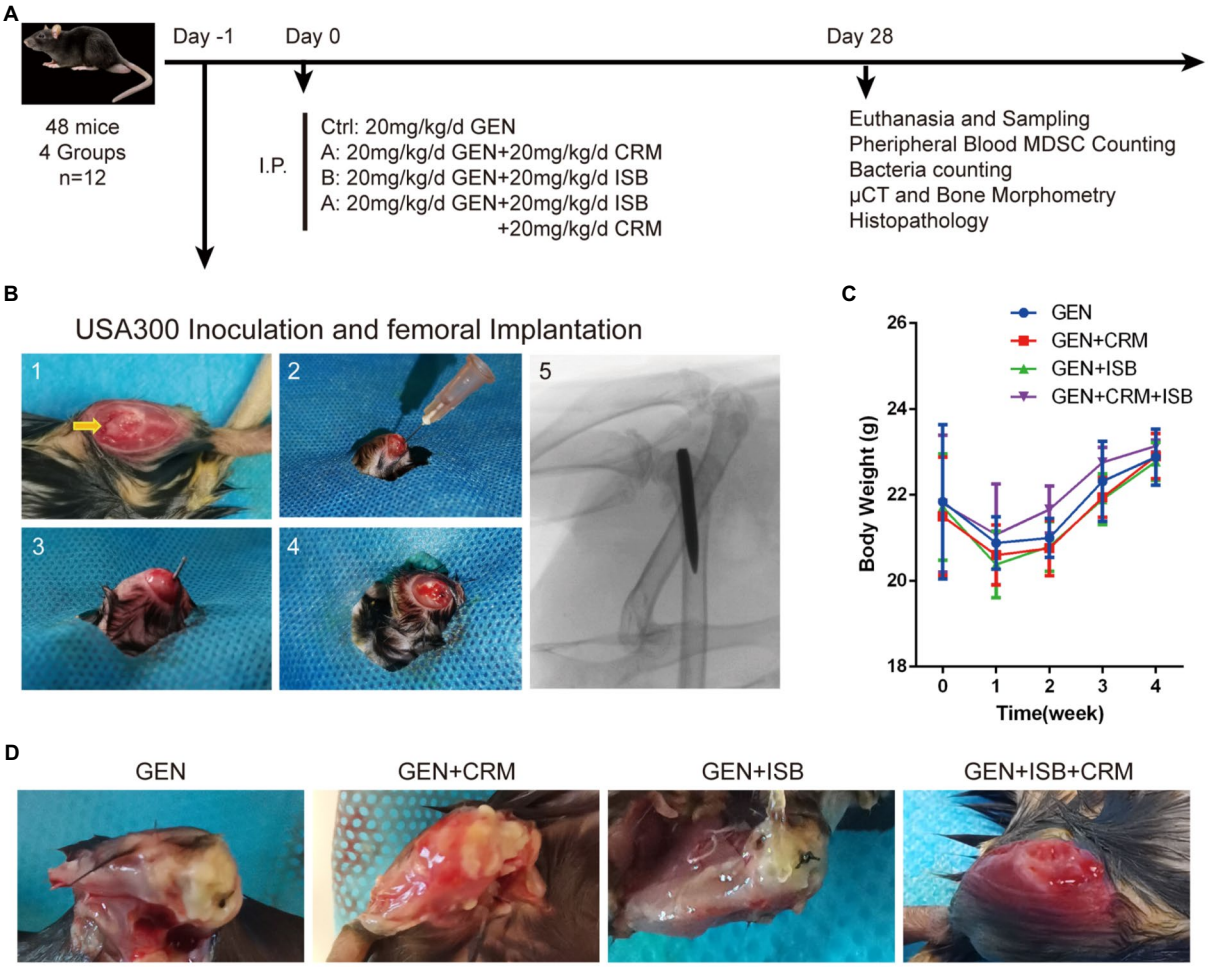

FIGURE 1
Orthopedic implant-related infection animal model of cocktail of isobavachalcone and curcumin with gentamycin against MRSA. **(A)** *In vivo* study design. **(B)** Surgical procedures of distal femoral implant-related infection mouse model. 1–5 refer to: (1) Distal femoral implant using a trans-knee approach, after incise internally alongside patella and externally dislocating patella to expose the distal femoral articular surface, and the entry point, intercondylar notch, was shown by the yellow arrow. (2) 25-gauge needle was used to open a corridor into the femoral medullary canal. (3) The customized 0.6mm diameter needle was implanted after the inoculation of 5μl MRSA USA300 inoculum suspension. (4) The caudal end of the implant was left about 1mm outside the femur after implantation. (5) The representative X-ray image of implant well positioned in the medullary canal and distal femur. **(C)** Body weight of animals throughout *in vivo* experiment. **(D)** Representative appearance of distal femurs of mice 28days after intraperitoneal administration of different groups of antimicrobials combinations, gentamicin served as control. I.P., intraperitoneal injection; GEN, Gentamycin; ISB, Isobavachalcone; CRM, Curcumin.

Solarbio, China) on a shaker at 4°C, the solution was changed every 3 days for 21 days. The specimens were then washed 3 times with PBS buffer and subjected to dehydrated, paraffin-embedded, and sectioned 4 μm slides. HE staining was performed in order to analyze the inflammation and general changes of bone microstructure at histological and cytological levels.

Immunofluorescence staining was applied to analyze MDSCs polarization to M1 according to standard protocols. The sections were incubated at 4°C overnight with primary antibodies rabbit anti-mouse CD11b (ab184308, 1:500, Abcam, United States) and rabbit anti-mouse CXCL10 (10H11L3, 1:500, Thermo Fisher, United States) for multiplex, respectively; the corresponding secondary antibodies were added onto the sections for 1 h. For immunofluorescence, slides were counterstained with DAPI. The slide images were observed and captured by Eclipse Ti-SR microscope (Nikon, Japan). ImageJ was used for the quantitative analysis if necessary.

Quantification of bacteria in bone

Surgical dissection of femur for bacteria counting was performed under sterile conditions at 4°C. Femur specimens were weighed and cut into small pieces under aseptic conditions using small Petri dishes, then pulverized using a tissue grinder (DHS TL2010S, China). Tissue samples were resuspended with D/E neutralizing broth and then sonicated for 15 min along with the implanted Kirschner pins to detach residual bacterial biofilm from both bone tissue and implant. The sonicated suspension was immediately inoculated onto TSA agar plates by gradient dilution

and incubated at 37°C for 24 h. Colony counting was performed to quantify the amount of bacteria per unit mass of femur (CFU/mg).

Statistical analysis

Statistical analysis was performed by using the GraphPad Prism 6 (GraphPad Software, CA, United States). All data were presented as mean ± SD. All error bars in figures represent SD Group comparison was made by using unpaired, two-tailed Student's *t*-test. For all statistical analyses, $^{*}p < 0.05$ was considered to be significant.

Results

Synergy of ISB or CRM with antibiotics against planktonic *Staphylococcus aureus*

Prior to biofilm challenge assays, it is critical to verify the interactions between ISB or CRM and antimicrobials against planktonic *S. aureus*. Daptomycin (DAP), rifampicin (RIF), gentamicin (GEN), and levofloxacin (LEV) were chosen as antimicrobials according to our preliminary biofilm challenge data on the *in vitro* 24 h model, and experimental concentrations were chosen according to their MICs and MBCs (Supplementary data). The fractional inhibition concentration index (FICI), as described in the methodology, reflects the combined inhibitory effect of the two antimicrobial substances. The FICIs of Isobavachalcone (ISB) or Curcumin (CRM) with four antibiotics were calculated (Figure 2A), and the results implied that in all combinations with four antibiotics the MICs were acquired within the experimental concentration range. There is synergy (FICI ≤ 0.5) in combinations of GEN with ISB (0.39, 1.56 μg/ml), GEN with CRM (15.6–500 μg/ml) against six MSSAs. For MRSAs, all combinations with antibiotics also had the MIC cut-off values, and synergy existed only in the combinations of DAP with ISB (0.2–1.56 μg/ml) and DAP with CRM (3.9, 7.8 μg/ml); ISB and CRM were synergistic only in the combination of GEN with CRM (15.6–62.5 μg/ml). In the case of a well-investigated clinical isolated MSSA strain *S. aureus* JAR (Campoccia et al., 2008; Figure 2C), the combinations with synergy are GEN with CRM (15.6, 32–128 μg/ml), GEN and ISB (1.56 μg/ml).

The fractional bactericidal concentration index (FBCI) reflects the combined bactericidal effect of the two antimicrobial substances. The FBCIs of ISB or CRM with antibiotics were also calculated (Figure 2B), which showed that the combinations with all four antibiotics, except RIF could acquire MBCs for all MSSAs tested within the experimental concentration range. The combination of GEN with CRM (0.98–3.9, 7.98–500 μg/ml) are synergistic (FBCI ≤ 0.5). The absence of bactericidal effect of RIF-containing combinations against all MSSA and MRSA may be due to the low concentration range (0.001–0.5 μg/ml) of RIF, which is concentration-dependent (Hirai et al., 2016) and required a higher concentration (>0.5 μg/ml for MSSA and >128 μg/ml for MRSA). For MRSAs, all combinations with DAP acquire MBC cut-off values and there is synergy in the combinations of DAP with ISB (0.39–1.56 μg/ml) and DAP with CRM (3.9, 7.8 μg/ml). GEN-containing combinations with ISB and CRM against MRSAs reach the MBC cut-off values, and the combination of GEN with CRM (62.5–250 μg/ml) is synergistic. The low concentration of GEN (0.16–8 μg/ml) tested may be the reason for the absence of bactericidal effect on three MRSA strains (Atashbeyk et al., 2014). Neither the combination of RIF nor LEV eradicate three MRSA strains, in addition to the low concentration of RIF as previously explained, concentrations of LEV in this study (0.079–4 μg/ml) is lower than MBC (8–20 μg/ml) against MRSA (Drago et al., 2001; John et al., 2009). In the case of *S. aureus* JAR strain (Figure 2D), the only combination with significant synergy is GEN with CRM (7.8–500 μg/ml). In summary, FICIs and FBCIs indicate the combination of GEN with ISB or CRM is worthy of further investigation.

Synergy of ISB or CRM with antibiotics against MSSA biofilm

To further analyze the synergistic efficacy of ISB/CRM and antibiotics against *S. aureus* biofilms, the MBEC™ Assay was performed to quantify the surviving bacteria on MSSA JAR biofilms challenged by the combinations of GEN with CRM or ISB. Viable bacteria in biofilms were quantified after challenge (Figure 3A), and it shows that for all tested concentrations of ISB and CRM, the number of bacteria on biofilm decreased with increasing antibiotics concentration, where the MBEC for gentamicin (GEN) is >1,024 μg/ml, which is consistent with previous study (Kaneko et al., 2020). ISB and CRM alone cannot eradicate biofilm without GEN. As the concentration of CRM and ISB increased, the number of viable bacteria of MSSA JAR biofilm show a decreasing trend (Figure 3A) at identical GEN concentration. Although the mean value of CFU/per failed to decrease to zero, higher ISB/CRM concentration significantly enhance anti-biofilm efficacy of GEN and a lower MBEC of GEN than normal (>1,024 μg/ml) can be observed on some samples, where biofilm was entirely eliminated. Thus GEN + CRM and GEN + ISB may have a synergistic eradication against MSSA JAR biofilm.

In present study, all combinations have no MBEC cut-off value, in order to further analyze the synergistic effect of those combinations aforementioned, the combinations with synergy on *S. aureus* biofilm were identified by Coefficient of Drug Interaction (CDI), commonly used in other pharmacodynamic fields, was introduced as a parameter as described in methods. The results revealed that GEN with CRM or ISB were synergistic (Figure 3B), and with significant synergy

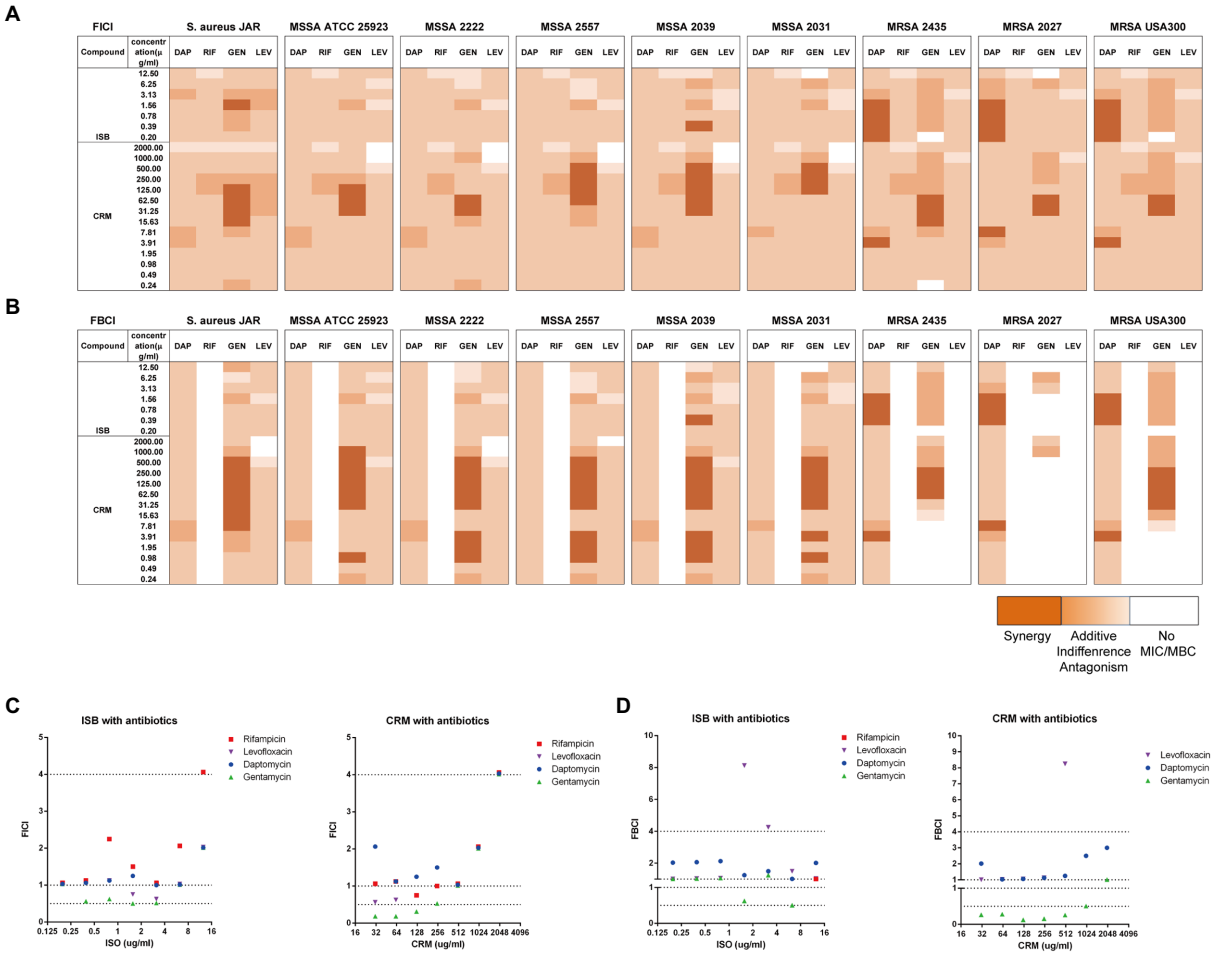

FIGURE 2
Interaction of Isobavachalcone and Curcumin with Antibiotics on MSSA and MRSA strains. **(A,B)** Heatmaps of fractional inhibitory concentration index (FICI) and fractional bactericidal concentration index (FBCI) of combination of gentamycin with isobavachalcone or curcumin, darker orange color indicates interaction is superimposed or synergistic. **(C,D)** FICI and FBCI of Isobavachalcone and Curcumin with antibiotics against *Staphylococcus aureus* JAR strain, respectively. FICI≤0.5 represents synergy, FICI>0.5–4 represents no synergistic interaction, and FICI>4.0 represents antagonism. FICI: fractional inhibition concentration index; FBCI: fractional bactericidal concentration index; DAP: Daptomycin with 50μg/ml Ca2+; RIF: Rifampicin; GEN: Gentamycin; LEV: Levofloxacin; ISB: Isobavachalcone; CRM: Curcumin; MSSA: Methicillin-susceptible *Staphylococcus aureus*; MRSA: Methicillin-resistant *Staphylococcus aureus*.

(CDI < 0.7) at specific concentrations, namely GEN (128 μg/ml) + CRM (31.25, 62.5, 250, 500 μg/ml), GEN (64,128 μg/ml) + ISB (1.56, 3.13, 6.25, 12.5 μg/ml; Figure 3B). Further analysis of synergistic combinations suggests that in the combination of GEN + ISB, with GEN at 64 and 128 μg/ml, when ISB rises above 6.25 μg/ml, the number of bacteria on biofilm reduced significantly by log-2 to log-3 compared to control (Figure 3C). In the combination of GEN + CRM, the reduction of bacteria in biofilm by CRM alone was also not statistically significant. Whereas to GEN at 128 and 1,024 μg/ml, with CRM concentration increased (≥250 μg/ml with 128 μg/ml of GEN, ≥500 μg/ml with 1,024 μg/ml of GEN), bacteria on biofilm could be significantly reduced up to log-2–log-4 compared to control. There is also a significant reduction in colony counts between GEN at 0, 128, and 1,024 μg/ml with high concentrations of CRM (Figure 3C). Overall, MBEC assays indicate the combination of ISB or CRM is efficient in enhancing the susceptibility of MSSA to Gentamicin.

Synergy of cocktail of ISB, CRM with gentamicin against MRSA biofilm

In order to first analyze the synergistic efficacy of ISB with CRM against planktonic *S. aureus*, the EUCAST checkerboard assay was conducted with presence of Gentamicin range from sub-MIC against MSSA (0.25 μg/ml) to sub-MIC against MRSA (8 μg/ml) for FICI analysis, and from sub-MBC against MSSA (0.5 μg/ml) to sub-MBC against MRSA (16 μg/ml) for FBCI analysis. The FICI analysis shows that synergistic inhibitory effect exists between combinations of 6.25 μg/ml ISB with 31.25–500 μg/ml CRM against various MSSA strains, and with 31.25–62.5 μg/

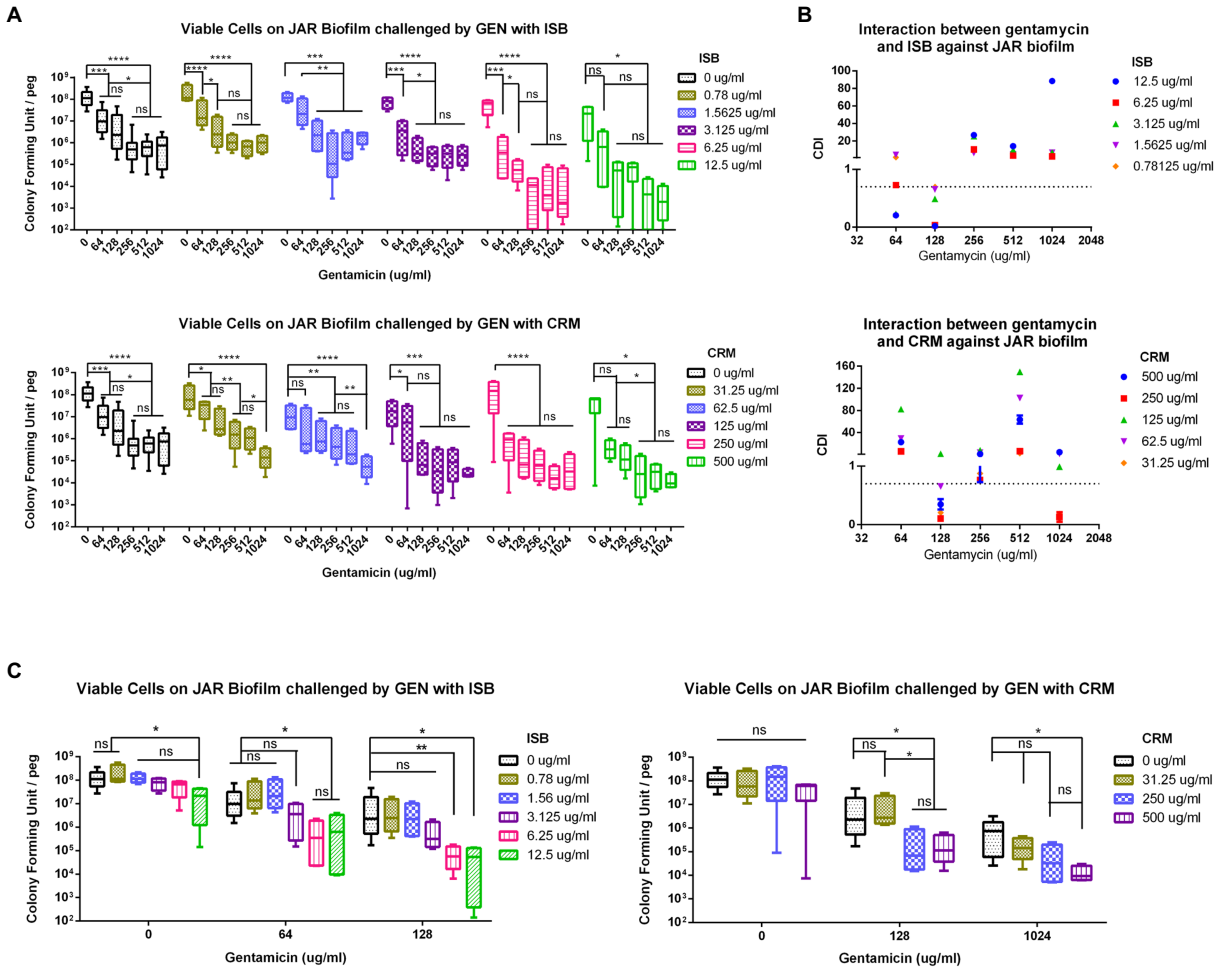

FIGURE 3
Interaction of isobavachalcone and curcumin with Gentamycin against *Staphylococcus aureus* JAR biofilm. **(A)** Residual *S. aureus* JAR on Biofilm challenged by combination of Gentamycin with Isobavachalcone or Curcumin. **(B)** Coefficient of Drug Interaction (CDI) of the combination of Gentamycin with isobavachalcone or curcumin. **(C)** Synergistic Combination of isobavachalcone with Gentamycin, and Curcumin with Gentamycin. CDI<1, =1 or >1 indicate synergy, superposition or antagonism, respectively, CDI<0.7 indicates significant synergism. Data were presented as mean±SD. * represents $p<0.05$, ** represents $p<0.01$, *** represents $p<0.001$, **** represents $p<0.001$, when compared to ISB/CRM with the same Gentamycin concentration, ns represents no significance. GEN, Gentamycin; ISB, Isobavachalcone; CRM, Curcumin; CDI, Coefficient of Drug Interaction.

ml CRM against MRSA strains with 64 or 128 μg/ml Gentamicin presence (Figure 4A). The FBICs also show similar synergy pattern as FICI, and synergy exists between combinations of 6.25 μg/ml ISB with 31.25–125 μg/ml CRM against various MSSA strains, and with 62.5–250 μg/ml CRM against MRSA strains (Figure 4B). Not all synergistic combinations are with the same concentration range of CRM, which is bacteria strain-dependent against MSSAs; however, the synergistic concentration range for CRM is relatively more consistent for different MRSAs. As the typical clinical isolated prolific biofilm former MSSA JAR strain (Campoccia et al., 2008), synergistic combinations are 6.25 μg/ml ISB with 31.5–125 μg/ml CRM with presence of Gentamicin. Another standard prolific biofilm former MRSA USA300 (Vanhommerig et al., 2014), 6.25 μg/ml ISB with 31.5–62.5 μg/ml CRM exhibits synergistic inhibition with gentamicin, while bactericidal synergy requires 6.25 μg/ml ISB with 62.5–250 μg/ml CRM with presence of Gentamicin (Figures 4C,D). Notably, In the present study, combinations of ISB and CRM with other concentrations of Gentamicin did not show synergy both in inhibition and bactericidal effect (data not showed), which may be related to the insufficient antibacterial potency of lower concentrations (<sub-MIC/sub-MBC) of gentamicin (data not showed), while in this study higher concentrations of gentamicin (≥MIC/MBC) had independent antibacterial effects against planktonic *S. aureus*, and the synergistic effects of ISB and CRM were difficult to manifest, therefore, combinations with gentamicin higher than MIC and MBC were not investigated. Given the synergy between ISB with 64, 128 μg/ml GEN, and CRM with 128, 1,024 μg/ml GEN against MSSA biofilm (Figure 3B), and the significant reduction of bacteria on biofilm treated with combination of ISB/CRM with 128 μg/ml GEN revealed in previous experiments (Figure 3C), thus we tested the combination

of ISB + CRM with a 128 μg/ml GEN concentration in biofilm experiment.

To investigate whether there is synergy of ISB, CRM, and Gentamicin against *S. aureus* JAR and MRSA USA300 biofilm, the MBEC™ assays of their combinations were performed with presence of Gentamicin at 128 μg/ml, which is proven to be synergistic with ISB/CRM against MSSA biofilm as aforementioned, respectively. Quantification of viable cells both on 24 h *S. aureus* JAR or USA300 biofilm challenged by the cocktails reveals a significant decreased MRSA with increasing CRM concentration with both 6.25 and 12.5 μg/ml ISB, and with Gentamicin at 128 μg/ml, whereas although ISB exhibit significant enhancement of susceptibility of USA300 biofilm to 128 μg/ml Gentamicin and CRM (62.5–250 μg/ml), this enhanced eradication effect was not in a ISB concentration-dependent manner (Figures 5A,C). Further analysis of Coefficient of Drug Interaction (CDI) showed that cocktails of 6.25–12.5 μg/ml ISB and 62.5–250 μg/ml CRM with 128 μg/ml Gentamicin are all synergistic against both 24 h *S. aureus* JAR and MRSA USA300 biofilm (Figures 5B,D). Overall, *S. aureus* JAR biofilm treated with the same formulae contains less viable bacteria than USA300 biofilm, especially with 6.25 μg/ml ISB and 125–250 μg/ml CRM (Figures 5A,C); however, their CDIs were very similar. The synergistic eradication of 24 h MRSA USA300 biofilm was also confirmed through SEM and live/dead cell staining (Figure 5E), where cocktail of 128 μg/ml Gentamicin together with 125 μg/ml CRM + 6.25 μg/ml ISB showed promising biofilm eradication effect. We also tested the ISB + CRM combination with 64 and 1,024 μg/ml GEN, which was proven to be synergistic with ISB or CRM against MSSA biofilm. However, there is neither significant reduction of bacteria on biofilm (probably due to lower 64 μg/ml GEN) nor synergy between the three antimicrobials (1,024 μg/ml GEN; data not showed). The results also indicates the biofilm eradication effect of Gentamicin with ISB is more potent than Gentamicin w/o CRM, which is consistent with previous MSSA biofilm experiments.

Cocktail therapy of ISB and CRM reduce Osteolysis during device-related infection

After surgery, all the animals had normal feeding during the *in vivo* experiment; however, as femoral intramedullary implant infection progressed, mice in Gentamicin and Gentamicin + CRM groups gradually exhibited restricted knee joint mobility of the affected hind limb and line to reduce movement with affected limb. All mice except for those in Gentamicin + ISB + CRM group showed various degrees of swelling and pain in the knee joint of the limb with implant. We monitored the body weight of mice in each group before operation and 1–4 week postoperation (Figure 1C). There was no significant difference in the initial body weight of the mice between all four groups of experimental animals. Generally, the body weight of mice in all groups decreased significantly ($p < 0.05$) 1 week post-surgery due to surgical trauma, and then with rehabilitation, the body weight of mice gradually increased until they were euthanized. Although body weight of mice in Gentamicin group was expected to be gradually lower than other three groups as MRSA infection progressed, there was no significant difference in body weight among each groups at each time point, suggesting that the dosage of gentamicin used in the present study may be sufficient to stop the progression of topical infection to the systemic level in an animal model with a relatively strong resistance to infection, like murines. After 28 days of antimicrobials administration, when femur with implant was sampled after sacrifice, significant soft tissue abscess penetration into the subcutaneous tissue was observed in the Gentamicin and Gentamicin+CRM groups, accompanied by significant soft tissue congestion and edema around the knee joint, while no significant local soft tissue abscess formation was observed in the GEN + ISB group, but with mild soft tissue thickening and edema. Soft tissues around knee joint of mice in Gentamicin+ISB + CRM group were only mildly congested and clearly hierarchical without edema in appearance (Figure 1D). No obvious hepatorenal toxicity of cocktail therapy compared to gentamicin alone was observed (serum biochemical analysis data not showed).

μCT imaging and bone morphometry of distal femur suggests the protection of cocktail therapy against osteolysis in orthopedic device-related infections due to MRSA (Figure 6). X-ray imaging showed mild to moderate bone absorption both in Gentamicin + CRM and Gentamicin + ISB group, and moderate to severe absorption in Gentamicin group accompanied with commonly seen periosteal reaction and in some cases with fracture (Figure 6A). 3D reconstructed micro-architecture of distal femoral bone around implant indicates osteolysis and microstructural destruction in the femur of infected mice (Figure 6B), which was also confirmed by quantitative bone morphometry. BV/TV, BMD, Tb.N, and Tb.Th were significantly lower ($p < 0.05$) in the Gentamicin-alone treated mice, while BS/TV and Tb.Sp were higher (Figure 6C). Treatment with Gentamicin with CRM/ISB significantly increased morphometry parameters indicating trabecular bone microstructure, while cocktail therapy with Gentamicin+ISB + CRM can further enhance such protection significantly.

Cocktail therapy enhance reduction of MDSC M1 polarization and eradication of MRSA biofilm *in vivo*

HE and immunofluorescent staining was used to further verify the alleviation of local tissue inflammation and bacteria in distal femur were quantified to reveal the eradication of

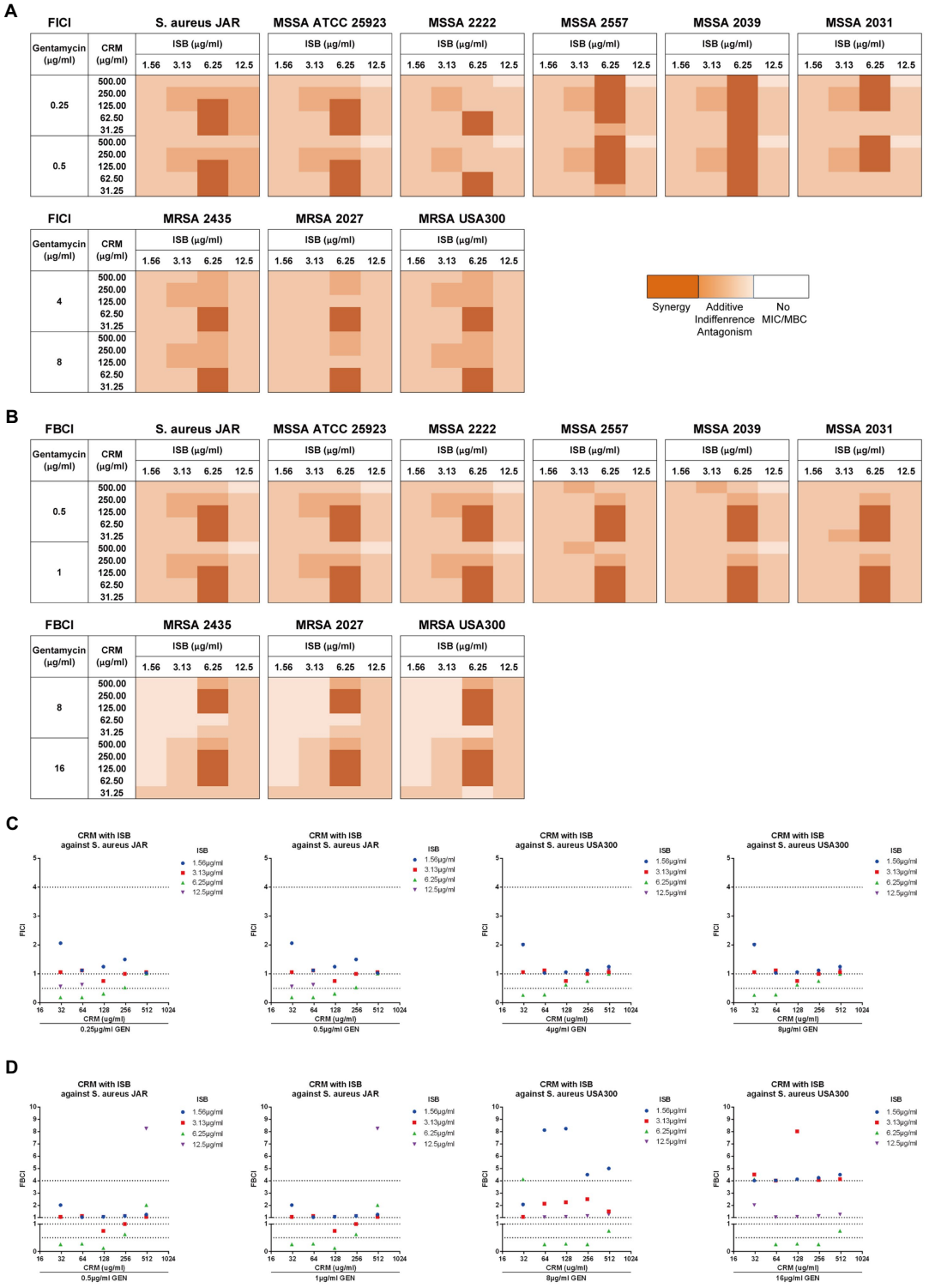

FIGURE 4
EUCAST checkerboard assay showed isobavachalcone and curcumin interact synergistically with presence of gentamycin against planktonic *Staphylococcus aureus*. **(A,B)** Heatmaps of fractional inhibitory concentration index (FICI) and fractional bactericidal concentration index (FBCI) of combination of isobavachalcone and curcumin, darker orange color indicates interaction is superimposed or synergistic. **(C)** FICI of isobavachalcone with curcumin against *S. aureus* JAR and USA300 strain. **(D)** FBCI of isobavachalcone with curcumin against *S. aureus* JAR and USA300 strain. FICI≤0.5 represents synergy, FICI>0.5–4 represents no synergistic interaction, and FICI>4.0 represents antagonism. CDI<1, =1 or >1 indicate synergy, superposition or antagonism, respectively, CDI<0.7 indicates significant synergism. Data were presented as mean±SD. FICI, fractional inhibition concentration index; FBCI, fractional bactericidal concentration index; GEN, Gentamycin; ISB, Isobavachalcone; CRM, Curcumin; CDI, Coefficient of Drug Interaction; MSSA, Methicillin-susceptible *Staphylococcus aureus*; MRSA, Methicillin-resistant *Staphylococcus aureus*.

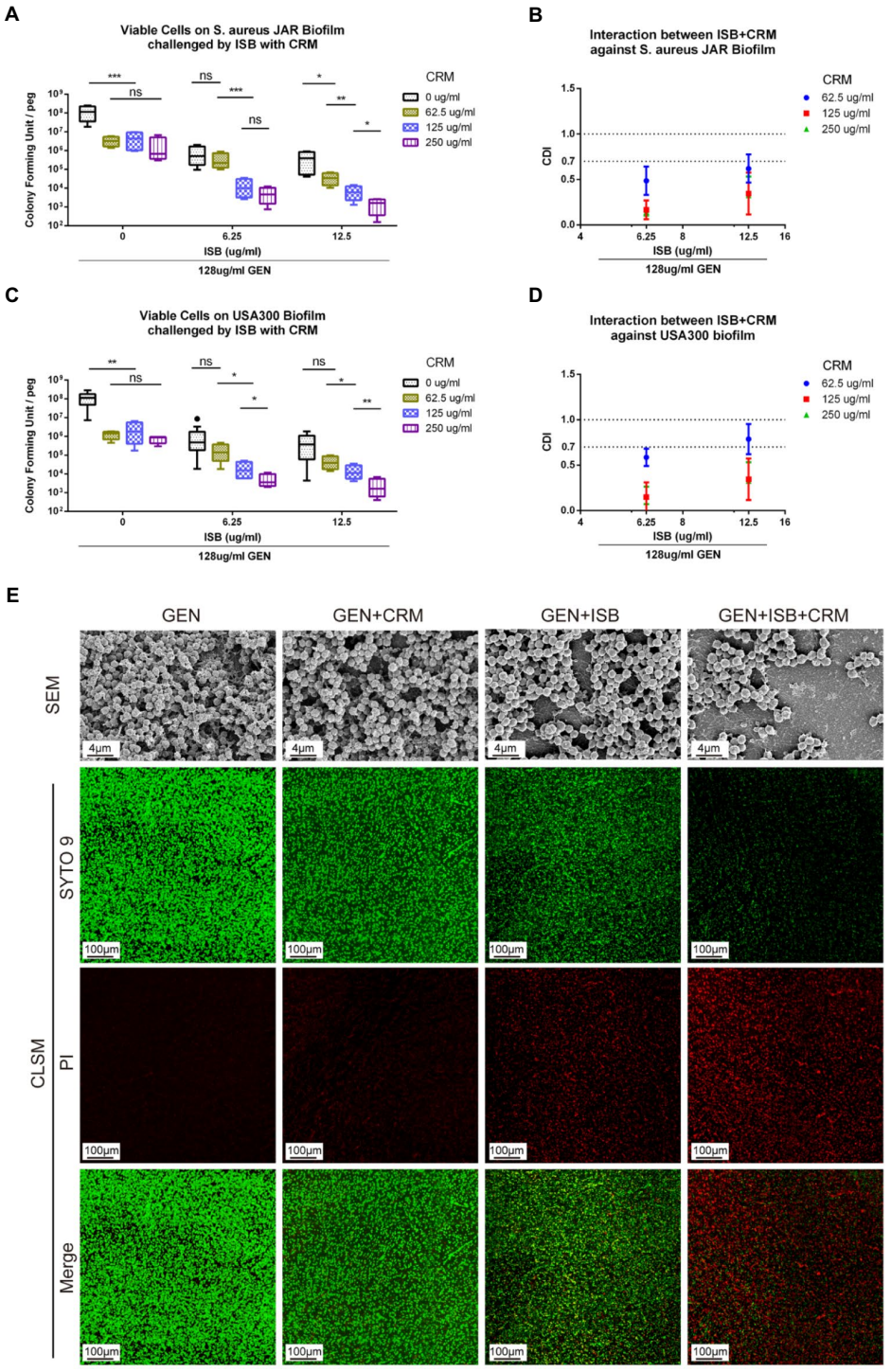

FIGURE 5
In vitro Eradication of *Staphylococcus aureus* biofilms by the GEN-ISB-CRM combination. **(A,C)** Quantification of residual viable cells on *S. aureus* JAR biofilm and USA300 biofilm, respectively. **(B,D)** Coefficient of Drug Interaction (CDI) shows synergy between Isobavachalcone and Curcumin with 128μg/ml Gentamycin against *S. aureus* JAR biofilm and USA300 biofilm, respectively. **(E)** Representative characteristics of MRSA USA300 biofilm after 24h challenge. SEM: biofilms cultured at 37°C for 24h were treated with 128μg/ml GEN (control), 128μg/ml GEN+125μg/ml CRM, 128μg/ml GEN+6.25μg/ml ISB, 128μg/ml GEN+125μg/ml CRM+6.25μg/ml ISB for 24h, respectively. All SEM images were captured at EHT=10kV, Mag=5KX. CLSM: representative confocal laser scanning microscopy (100× oil immersion) images of LIVE/DEAD® BacLight staining showing the synergistic effect of different drug combinations on USA300 biofilm challenged for 24h, green: live cells; red: dead cells. Data were presented as mean±SD. * represents $p<0.05$, ** represents $p<0.01$, *** represents $p<0.01$ when compared to 0μg/ml CRM with the same ISB concentration group, ns represents no significance. GEN, Gentamycin; ISB, Isobavachalcone; CRM, Curcumin; CDI, Coefficient of Drug Interaction; SEM, Scanning Electron Microscopy; CLSM, Confocal Laser Scanning Microscopy.

MRSA biofilm *in vivo*. H and E staining of distal femur revealed that, except for the Gentamicin+ISB + CRM group, bones around implants infected by MRSA exhibited severe resorption, destruction of the epiphyseal plate, with a large quantity of mononuclear cells filling the medullary canal and bone marrow cavity in between trabecular bones and marked thickening of the soft tissue with leukocyte infiltration (Figure 7A). Osteolysis was significantly reduced after combined treatment with CRM/ISB and gentamicin, compared to the group treated with gentamicin alone, which were consistent with μCT analysis and X-ray findings. In addition, bacterial quantification suggested that the viable MRSA USA300 on the peri-implant bone tissue and implant biofilm decreased significantly after treatment with Gentamicin+ISB compared to Gentamicin alone ($p < 0.05$), and that the cocktail therapy significantly enhance the eradication of MRSA *in vivo* (Figure 7B). In addition, to confirm whether cocktail therapy could inhibit MDSC amplification in peripheral blood in an *in vivo* model of MRSA device-related infection, we quantified the MDSCs in peripheral blood of mice. MDSC level was higher after Gentamicin treatment of MRSA infection, and MDSC amplification in peripheral blood was slightly suppressed after Gentamicin + CRM treatment, but the difference was not statistically significant. The combination of gentamicin and ISB significantly affected MDSC amplification in peripheral blood compared with treatment with gentamicin alone, whereas the cocktail of gentamicin + ISB + CRM significantly reduced the number of MDSC in peripheral blood in mice with MRSA infections (Figures 7C,D). Together, these results suggest that ISB + CRM significantly inhibits MRSA-induced MDSC amplification in orthopedic device-related infections *in vivo*, the combination of ISB + CRM may act as an adjuvant with gentamicin, which administrated alone is ineffective against MRSA biofilms at conventional concentrations, to significantly enhance its antimicrobial effect.

Discussion

Despite the discovery of penicillin in 1928 and the development of antibiotics, antimicrobial therapy has brought more satisfactory results for patients, but in the last decades we have had to face the emergence of drug-resistant pathogens and the current conventional antibiotic therapy is becoming ineffective for patients (Li and Knetsch, 2018; Xu et al., 2018). *Staphylococcus aureus* is a major cause of orthopedic device-related infections (ODRI) that lead to implant failure, loosening, and reoperation of implants after surgery. In particular, antimicrobial-resistant *S. aureus* (such as Methicillin-resistant *Staphylococcus aureus*, MRSA) is the most difficult to resolve in the clinic (Biedenbach et al., 2004), which are becoming a global public health challenge. Although more advanced antibiotics could be applied in patients, they still have disadvantages such as insusceptibility to resistant strains, increased toxicity at high doses, and long duration (Lebeaux et al., 2014). Therefore, there is an urgent need for research into new therapeutic approaches for drug-resistant pathogens and associated infectious diseases (Microbiology by Numbers, 2011). Bacterial biofilms on the surface of orthopedic implants are considered to be a major cause of antimicrobial resistance because antibodies and bactericidal agents have difficulty penetrating biofilm due to EPS, resulting in a persistent chronic inflammatory response (Flemming et al., 2007; Bjarnsholt et al., 2018), then followed by tissue structural destruction and impaired function. Therefore, there is an urgent need for the development of new drugs, new drug combinations, and alternative therapeutic approaches.

In this study, a standard "biofilm inoculator" (MBEC™ biofilm inoculator) was used *in vitro* to mimic the formation of biofilm by bacteria in a fluid environment on the surface of metal, in this case, bacterial biofilms were generated on the plastic peg on the cover. Previous *in vitro* studies reported no significant differences in the adhesion of *S. aureus*, *S. epidermidis*, and *P. aeruginosa* to the different surfaces of cobalt-chromium meta, ceramic, highly cross-linked polyethylene, and titanium porous-coated acetabular components of commonly used orthopedic prostheses or implants (Slullitel et al., 2018). In our study, four clinically used representative antibiotics with different antimicrobial mechanisms had been initially tested for interaction with isobavachalcone (ISB) and curcumin (CRM), and we found both ISB and CRM exhibit synergy or addition with gentamicin. We further investigate their interaction on six MSSA and three MRSA strains including clinical isolates, and gentamicin was found to be synergistic against planktonic MSSA with curcumin, and is additive against MSSA with isobavachalcone at specific concentrations. Although the daptomycin (DAP) is a much more potent antibiotics against MRSA than gentamicin, and is seemed to be synergistic with isobavachalcone (ISB) against planktonic MSSA, we did not observe any synergy between DAP with ISB against MSSA or MRSA biofilm (data not showed) as for reducing CFU in the biofilm. Gentamicin with curcumin together with isobavachalcone also exhibits synergistic effect in this 24 h formation and 24 h antimicrobials challenge MSSA biofilm model. Therefore, we chose gentamicin for further combinational investigation on the MRSA strains and found that cocktail of 128 μg/ml gentamicin together with 125 μg/ml curcumin + 6.25 μg/ml isobavachalcone showed potent eradication effect with synergy of curcumin and isobavachalcone against USA300 biofilm.

In this "cocktail" of antimicrobials, gentamicin is one of aminoglycosides that has been widely used in ODRI because of its antimicrobial efficacy against non-resistant Staphylococcus, relatively low prevalence of toxicity, and thermal stability. However, if gentamicin is used at higher dosages for bacterial biofilm removal, its ototoxicity and nephrotoxicity cannot be ignored. The antimicrobial mechanism of gentamicin is to mainly interact with bacterial

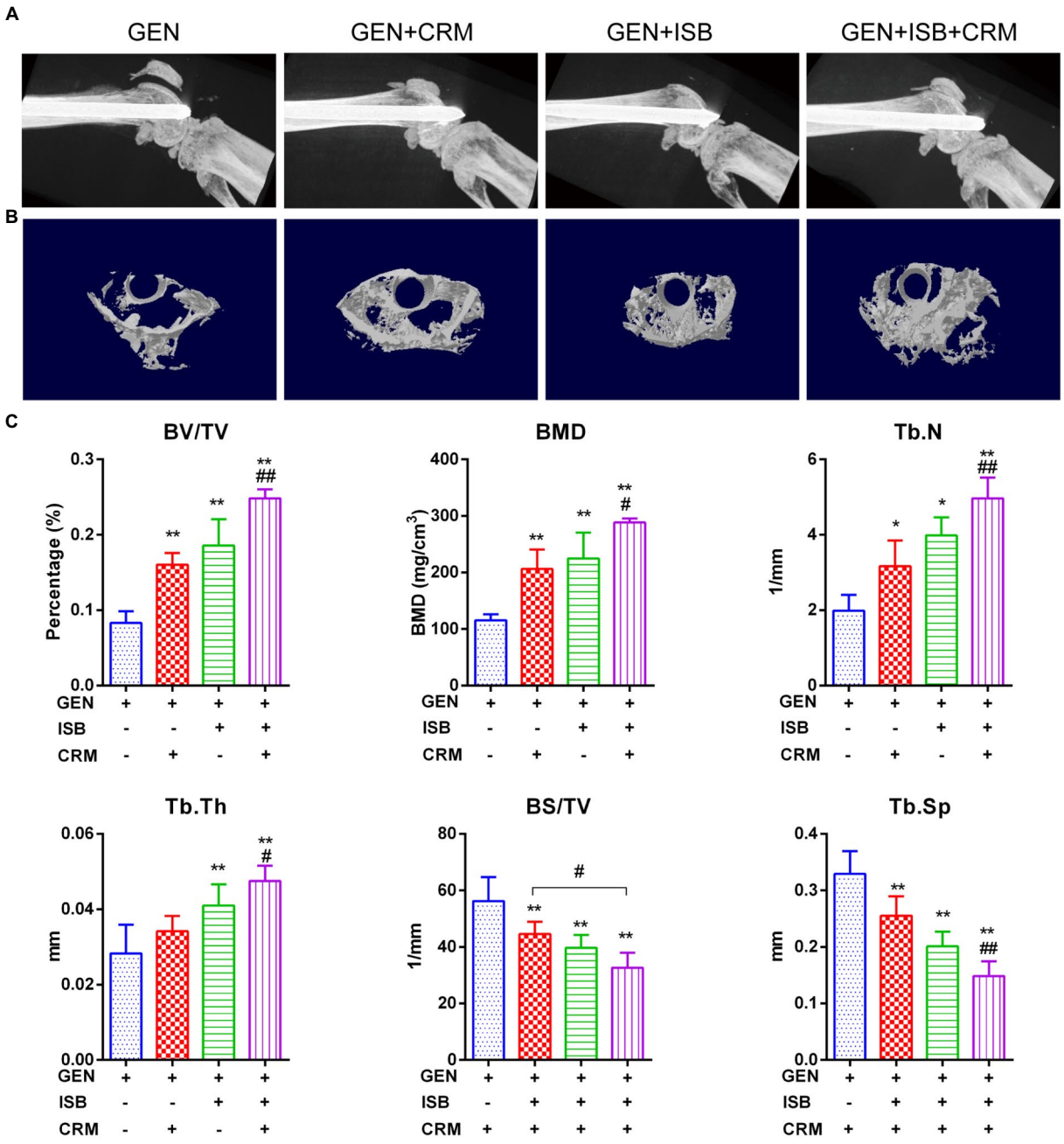

FIGURE 6
Micro Computed tomography (μCT) imaging suggests protection of cocktail therapy against osteolysis in orthopedic implant-related infections due to MRSA. **(A)** Representative X-ray images of distal femur of mouse with intramedullary implant. **(B)** Representative images of trans axial 3D reconstructed micro-architecture of distal femur around implant. **(C)** Bone morphometry in distal femur shows protection of combination of Isobavachalcone and Curcumin against osteolysis during orthopedic implant-related infection, related parameters including percent bone volume (BV/TV), trabecular thickness (Tb.Th), trabecular number (Tb.N), and trabecular separation (Tb.Sp), bone mineral density (BMD) and bone surface density (BS/TV) were measured, data were presented as mean±SD, * represents $p<0.05$ and ** represents $p<0.01$ when compared to Gentamicin group; # represents $p<0.05$ and ## represents $p<0.01$ when GEN+ISB+CRM group compared to GEN+ISB/CRM group; GEN, 20mg/kg/day Gentamycin; ISB, 20mg/kg/day Isobavachalcone; CRM, 20mg/kg/day Curcumin.

ribosomes, inhibit bacterial protein synthesis, and disrupt the integrity of bacterial cell membranes (Appel and Neu, 1978). Curcumin is one of the most well-known antibacterial molecules from herbal medicine (Teow et al., 2016), and the synergistic anti-*S. aureus* effect with gentamicin is concentration-dependent, which is consistent with previous study (Teow and Ali, 2015). The major mechanism of CRM interact with *S. aureus* is to inhibit cytoplasmic division and

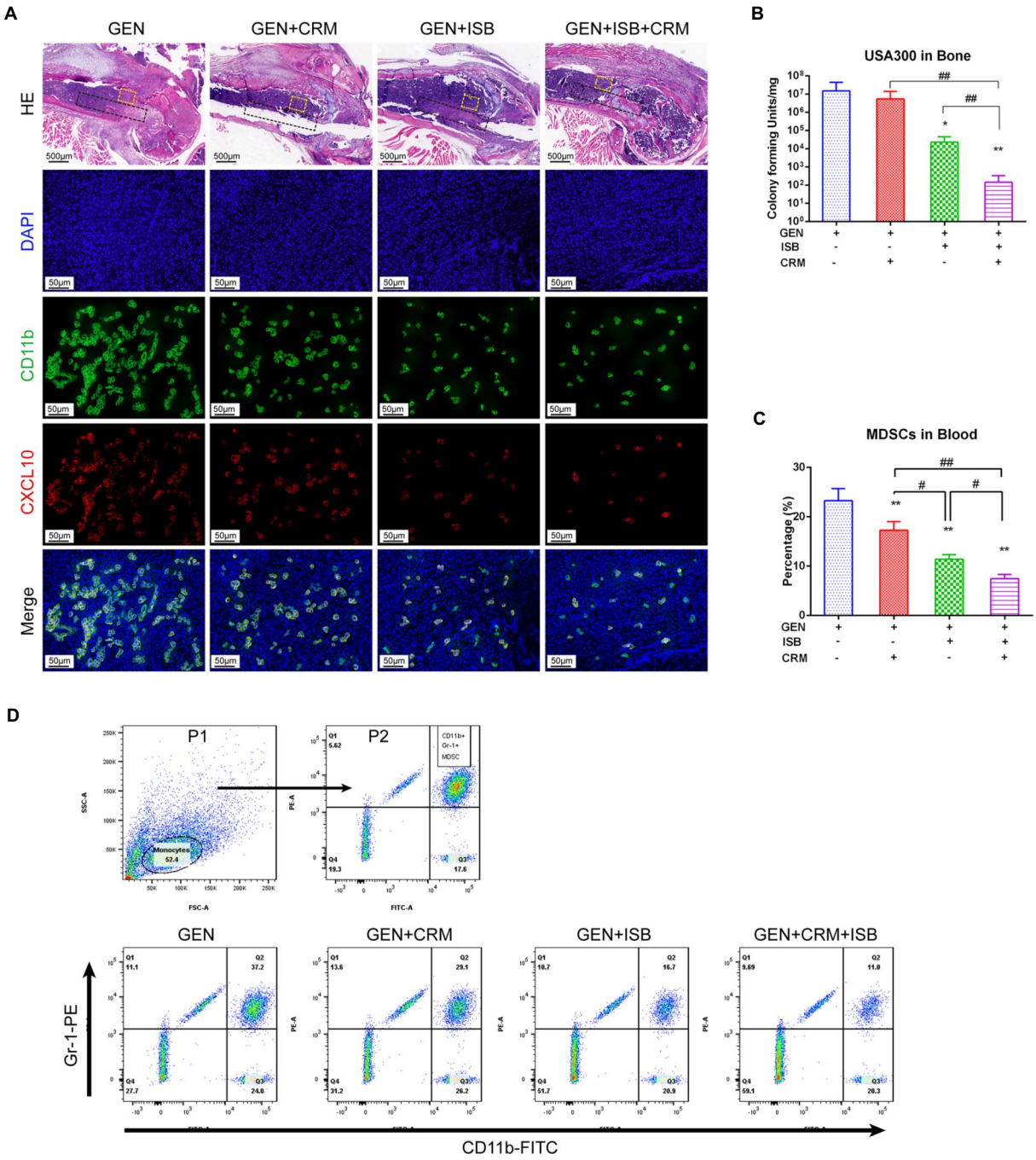

FIGURE 7
Cocktail therapy of Gentamicin with Isobavachalcone and Curcumin alleviate local tissue inflammation, enhance reduction of MDSC M1 Polarization and Eradication of MRSA biofilm *in vivo*. **(A)** HE and immunofluorescent staining of distal femur suggest reduction of tissue inflammation and M1 polarization of MDSC, green represents CD11b, a key marker to identify MDSC, while red represents CXCL10, a key marker of activated M1, he black dashed box indicates the approximate location of the implant, and the yellow dashed box range is the area where M1-polarized MDSC in the adjacent implant tissue is observed. **(B)** Quantification of remaining MRSA in bone with implant. **(C)** Flow cytometry analysis showed reduction of MDSC in peripheral blood by Gentamicin with ISB or CRM and cocktail therapy. **(D)** Gating strategy for flow cytometry analysis and representative analysis of frequency of MDSC in peripheral blood. All data were presented as mean±SD, * represents $p<0.05$ and ** represents $p<0.01$ when compared to Gentamicin group; # represents $p<0.05$ and ## represents $p<0.01$ when GEN+ISB+CRM group compared to GEN+ISB/CRM group; GEN, 20mg/kg/day Gentamycin; ISB, 20mg/kg/day Isobavachalcone; CRM, 20mg/kg/day Curcumin.

bacterial proliferation *via* suppressing Z-loop formation (Rai et al., 2008), inhibit transcription of the mecA in MRSA to reverse resistance to β-lactam antibiotics (Mun et al., 2014), or bind to peptidoglycan in the cell wall to trigger cell wall damage and increase the membrane bidirectional permeability (Mun et al., 2014; Teow et al., 2016). Moreover, other studies

also reported that *S. aureus* strain-dependence and no antagonistic effect were observed in its interaction with other antibiotics (Mun et al., 2013; Teow and Ali, 2015; Betts et al., 2016), which would probably also be related to the different biofilm formation condition, we adopted 1% human plasma, which has been demonstrated that fibronectin and its binding proteins are critical for MSSA and MRSA biofilms formation (Vergara-Irigaray et al., 2009; McCourt et al., 2014). Although the antimicrobial activity of isobavachalcone as a herbal extract has been investigated for the past decade (Wang M. et al., 2021), its anti-Staphylococcus activity has not been fully understood, a few studies reported its anti-*S. aureus* effect (Yin et al., 2004; Dzoyem et al., 2013; Cui et al., 2015; Faegheh et al., 2018). A recent study reported that the antibacterial activity of ISB against Gram-positive bacteria, specifically the *S. aureus* including MSSA and MRSA (with a MIC of 1.56 and 3.12 μg/ml, respectively) is associated with membrane disruption (Assis et al., 2022), hence ISB displayed no antibacterial effect on EPS in biofilm or Gram-negative species. Although the specific mechanism of antibacterial activity of this combination against *S. aureus* has not been fully investigated in this study, putting all the recent advances together, this process may be a synergistic multi-target action against *S. aureus* involving its cell wall integrity, membrane permeability, drug-resistant gene transcription, and protein biosynthesis, and cell wall and cell membrane could be their collaborative target.

To evaluate whether cocktail of Gentamicin + ISB + CRM can be used as a treatment for orthopedic implant-associated infections due to MRSA, a well-established femoral implant infection mouse model for simulating *in vivo* implant biofilm infection. Daily intraperitoneal administration of 20 mg/kg/day isobavachalcone, 20 mg/kg/day curcumin and 20 mg/kg/day gentamicin, can suppress progress of local infection. As we show *in vitro* and *in vivo* experiments, using gentamicin alone was difficult to suppress MRSA proliferation and local infection progression, but once added both ISB and CRM, the inhibitory and bactericidal effect of gentamicin against MRSA enhanced significantly. Although the antimicrobial effect of ISB or CRM has been investigated for the past decade (Wang M. et al., 2021), its anti-Staphylococcus activity has not been fully understood. Recent studies reported that the antibacterial effect of ISB and CRM are also associated with membrane disruption (Mun et al., 2014; Teow et al., 2016; Assis et al., 2022), specifically for the *S. aureus* including MSSA and MRSA (Assis et al., 2022) as aforementioned. So, the enhanced antimicrobial effect of gentamicin combined with ISB and CRM may result from their similar function of membrane disruption.

Cocktail treatment reduces inflammatory osteolysis and maintains microarchitecture of trabecular bone during orthopedic device-related MRSA infection in mice as well. Many studies have shown that *S. aureus* cell wall or biofilm components are the main causes of *S. aureus*-induced local inflammatory responses in the physiopathology of chronic osteomyelitis in ODRI, which is considered to be the classical animal model for studying the damage of bacterial products on bone structures in chronic osteomyelitis (Rochford et al., 2016). Therefore, we chose this animal model to study the pharmacological effects of isobavachalcone and curcumin on the tissue destruction induced by *S. aureus* biofilm. Microarchitecture of trabecular bone was found to be drastically deteriorated by μCT scanning and histopathology due to MRSA infection. However, treatment with isobavachalcone and curcumin significantly alleviated this process. The presence of local pathogenic microorganisms, such as *S. aureus*, can directly invade osteoblasts to form an intracellular infection (Tuchscherr et al., 2011; Jauregui et al., 2013; Hamza and Li, 2014), altering the autoimmune phenotype while decreasing osteoblast viability and osteogenic activity (Takayanagi, 2015). Previous studies have confirmed that RANKL/OPG signaling, TNF and TNF receptor superfamily, and the NF-kB signaling pathway play important roles in osteomyelitis in *S. aureus* infection (Lio et al., 2012; Krauss et al., 2019), and other studies also demonstrated that curcumin can inhibit NF-κB signaling pathway (Mohankumar et al., 2015; Kao et al., 2016). Isobavachalcone was reported capable of preventing osteoporosis by suppressing activation of ERK and NF-kappaB pathways of macrophages (Wang X. et al., 2021). It is probably that ISB combined with CRM treatment can protect bone microarchitecture under inflammatory microenvironment of device-related MRSA infection, attenuate osteolysis and avoid pathological fractures. These results validate the protection of cocktail of CRM + ISB, when administrated with Gentamicin, can attenuate inflammatory osteolysis induced by MRSA biofilm in ODRI.

Cocktail therapy also enhanced the reduction of MDSC M1 polarization in peri-implant tissue, suppression of MDSC amplification in peripheral blood *in vivo*. More interesting is that the bone density around the implant is increased in gentamicin combined with ISB or CRM group comparing to others according to μCT and histopathology. The number of MDSCs was significantly decreased, which suggested ISB and CRM may inhibit the expansion of MDSCs in *S. aureus* biofilm-induced myeloid cells and bidirectionally regulated the conversion of MSDC to polarized. Isobavachalcone was reported can prevent osteoporosis by suppressing M1 polarization of macrophages (Wang X. et al., 2021). A moderate M1-mediated inflammation is beneficial for tissue repair (Saqib et al., 2018), However, whether M1 phenotype plays a critical role in this osteogenesis process is still unclear. The persistence of bacteria stimuli in inflammatory osteogenesis may play another key factor in the tissue regeneration, because cell wall component lipoteichoic acid (LTA) has been reported to be beneficial for activation of osteoblast differentiation and Inhibition osteoclast activation in both *vivo* and *vitro* (Hu et al., 2020).

Notably, the fact that tissue destruction and regeneration in an inflammatory microenvironment during ODRI has always

been a dilemma for surgeons. Without effective control of infection, there is no possibility of tissue regeneration. This study focus on investigating synergy of two small molecules both with anti-osteoporosis, anti-inflammation, and anti-bacteria characteristics. However, there are still several questions that need to be further addressed. First of all, although zero mortality was observed in this ODRI mouse model and no obvious hepatorenal toxicity of cocktail therapy compared to gentamicin alone for 1 month, their long-term toxicity and their pharmacokinetics *in vivo* remain unknown. Secondly, the major mechanism of enhancing gentamicin efficacy against *S. aureus* is not fully understood, especially whether new compounds would form in the interaction of the two molecules. And how will the promising cocktail work on a more mature and thicker 5-day biofilm? Thirdly, the mechanism of balance of bone resorption and promoting bone formation is unknown, and the mechanism of M1 reduction still needs further verification, for example, whether the suppression of *S. aureus* infection or M1 reduction plays an initial or fundamental role in this process. Last but not least, although most studies suggest that antimicrobial drugs maintain bone mass in osteomyelitis mainly by their direct and effective antimicrobial activity, and not indirectly by modulating immune cells to affect bone mass, whether cocktail therapy exhibits identical effect on immune cells with gold standard, for example, vancomycin, still needs to be studied.

In summary, these results suggest that the combination of isobavachalcone and curcumin can enhance the susceptibility of MRSA to gentamicin, thus promoting the eradication of MRSA biofilm. When administrated as cocktail *in vivo*, they can significantly modify local inflammation in orthopedic device-related infection and maintain trabecular bone microstructure while substantially eradication MRSA in ODRI. Although our current study did not reveal specific mechanism about the synergy of this cocktail of gentamicin, isobavachalcone and curcumin against *S. aureus*, their bone microarchitecture maintenance characteristic did provide us the insight and evidence for future potential topical application by incorporating the mixture of these two small molecules with conventional antibiotics, like gentamicin bone cement chain beads and antimicrobial biomaterials, etc. The combination of isobavachalcone and curcumin as adjuvants administrated together with gentamicin to significantly enhance its antimicrobial effect, which may serve as a new potential treatment strategy especially for MRSA-induced ODRI, to rationalize the use of high-level antibiotics and reduce the emergence of drug-resistant strains of bacteria.

Data availability statement

The original contributions presented in the study are included in the article/Supplementary material, further inquiries can be directed to the corresponding authors.

Ethics statement

The animal study was reviewed and approved by Animal Ethics Committee of the Guangzhou Huateng Education Incorporation and was acknowledged by the First Affiliated Hospital of Sun Yet-sen University.

Author contributions

YC and XZ: conceptualization. YC, HH, FH, ZL, and XZ: design of research. YC and XZ: methodology. YC, HH, FH, BC, and XL: investigation. BC, BT, and TW: formal check and data analysis. CL and XZ: resources and funding acquisition. YC, HH, and ZL: writing the original manuscript. YC, HH, ZL, and XZ: major review and editing. All authors contributed to the article and approved the submitted version.

Funding

This work was supported in part by National Natural Science Foundation of China (32071341, 32101062); Guangdong Basic and Applied Basic Research Foundation (2019A1515110005, 2020A1515110620, and 2022A1515012607); Chinese Postdoctoral Science Foundation (2021M693628); Science and Technology Program of Guangzhou (201804020011); the National Natural Science Foundation of Guangdong Province-Major Fundamental Research Fostering Program, China (2017A030308004); and the Fundamental Research Funds for the Central Universities, Sun Yat-sen University.

Acknowledgments

Clinical isolated *S. aureus* JAR strains were kindly provided by AO Research Institute, Davos, Switzerland. Clinical isolated *S. aureus* strains MSSA 2222, MSSA 2557, MSSA 2039, MSSA 2031, MRSA 2435, and MRSA 2027 were kindly provided by the First Affiliated Hospital of Jinan University, Guangzhou, China.

Conflict of interest

The authors declare that the research was conducted in the absence of any commercial or financial relationships that could be construed as a potential conflict of interest.

The handling editor declared a shared parent affiliation with the authors at the time of review.

Publisher's note

All claims expressed in this article are solely those of the authors and do not necessarily represent those of

their affiliated organizations, or those of the publisher, the editors and the reviewers. Any product that may be evaluated in this article, or claim that may be made by its manufacturer, is not guaranteed or endorsed by the publisher.

Supplementary material

The Supplementary material for this article can be found online at: https://www.frontiersin.org/articless/10.3389/fmicb.2022.958132/full#supplementary-material

References

Appel, G. B., and Neu, H. C. (1978). Gentamicin in 1978. *Ann. Intern. Med.* 89, 528–538. doi: 10.7326/0003-4819-89-4-528

Arciola, C. R., Baldassarri, L., Campoccia, D., Creti, R., Pirini, V., Huebner, J., et al. (2008). Strong biofilm production, antibiotic multi-resistance and high gelE expression in epidemic clones of enterococcus faecalis from orthopaedic implant infections. *Biomaterials* 29, 580–586. doi: 10.1016/j.biomaterials.2007.10.008

Assis, L. R., Theodoro, R. D. S., Costa, M. B. S., Nascentes, J. A. S., Rocha, M. D. D., Bessa, M. A. S., et al. (2022). Antibacterial activity of Isobavachalcone (IBC) is associated with membrane disruption. *Membranes (Basel)* 12:269. doi: 10.3390/membranes12030269

Atashbeyk, D. G., Khameneh, B., Tafaghodi, M., and Fazly Bazzaz, B. S. (2014). Eradication of methicillin-resistant *Staphylococcus aureus* infection by nanoliposomes loaded with gentamicin and oleic acid. *Pharm. Biol.* 52, 1423–1428. doi: 10.3109/13880209.2014.895018

Bernthal, N. M., Stavrakis, A. I., Billi, F., Cho, J. S., Kremen, T. J., Simon, S. I., et al. (2010). A mouse model of post-arthroplasty *Staphylococcus aureus* joint infection to evaluate in vivo the efficacy of antimicrobial implant coatings. *PLoS One* 5:e12580. doi: 10.1371/journal.pone.0012580

Betts, J. W., Sharili, A. S., La Ragione, R. M., and Wareham, D. W. (2016). In vitro antibacterial activity of Curcumin-Polymyxin B combinations against multidrug-resistant bacteria associated with traumatic wound infections. *J. Nat. Prod.* 79, 1702–1706. doi: 10.1021/acs.jnatprod.6b00286

Biedenbach, D. J., Moet, G. J., and Jones, R. N. (2004). Occurrence and antimicrobial resistance pattern comparisons among bloodstream infection isolates from the SENTRY antimicrobial surveillance program (1997-2002). *Diagn. Microbiol. Infect. Dis.* 50, 59–69. doi: 10.1016/j.diagmicrobio.2004.05.003

Bimonte, S., Barbieri, A., Leongito, M., Piccirillo, M., Giudice, A., Pivonello, C., et al. (2016). Curcumin AntiCancer studies in pancreatic cancer. *Nutrients* 8:433. doi: 10.3390/nu8070433

Bjarnsholt, T., Buhlin, K., Dufrene, Y. F., Gomelsky, M., Moroni, A., Ramstedt, M., et al. (2018). Biofilm formation – what we can learn from recent developments. *J. Intern. Med.* 284, 332–345. doi: 10.1111/joim.12782

Campoccia, D., Montanaro, L., Moriarty, T. F., Richards, R. G., Ravaioli, S., and Arciola, C. R. (2008). The selection of appropriate bacterial strains in preclinical evaluation of infection-resistant biomaterials. *Int. J. Artif. Organs* 31, 841–847. doi: 10.1177/039139880803100913

Costerton, J. W., Stewart, P. S., and Greenberg, E. P. (1999). Bacterial biofilms: a common cause of persistent infections. *Science* 284, 1318–1322. doi: 10.1126/science.284.5418.1318

Cui, Y., Taniguchi, S., Kuroda, T., and Hatano, T. (2015). Constituents of Psoralea corylifolia fruits and their effects on methicillin-resistant *Staphylococcus aureus*. *Molecules* 20, 12500–12511. doi: 10.3390/molecules200712500

Cusack, T. P., Ashley, E. A., Ling, C. L., Roberts, T., Turner, P., Wangrangsimakul, T., et al. (2019). Time to switch from CLSI to EUCAST? A southeast Asian perspective. *Clin. Microbiol. Infect.* 25, 782–785. doi: 10.1016/j.cmi.2019.03.016

Daniel, S., Limson, J. L., Dairam, A., Watkins, G. M., and Daya, S. (2004). Through metal binding, curcumin protects against lead- and cadmium-induced lipid peroxidation in rat brain homogenates and against lead-induced tissue damage in rat brain. *J. Inorg. Biochem.* 98, 266–275. doi: 10.1016/j.jinorgbio.2003.10.014

Drago, L., De Vecchi, E., Mombelli, B., Nicola, L., Valli, M., and Gismondo, M. R. (2001). Activity of levofloxacin and ciprofloxacin against urinary pathogens. *J. Antimicrob. Chemother.* 48, 37–45. doi: 10.1093/jac/48.1.37

Drago, L., De Vecchi, E., Nicola, L., and Gismondo, M. R. (2007). In vitro evaluation of antibiotics' combinations for empirical therapy of suspected methicillin resistant *Staphylococcus aureus* severe respiratory infections. *BMC Infect. Dis.* 7:111. doi: 10.1186/1471-2334-7-111

Dzoyem, J. P., Hamamoto, H., Ngameni, B., Ngadjui, B. T., and Sekimizu, K. (2013). Antimicrobial action mechanism of flavonoids from Dorstenia species. *Drug Discov. Ther.* 7, 66–72. doi: 10.5582/ddt.2013.v7.2.66

Espersen, F., Frimodt-Moller, N., Corneliussen, L., Riber, U., Rosdahl, V. T., and Skinhoj, P. (1994). Effect of treatment with methicillin and gentamicin in a new experimental mouse model of foreign body infection. *Antimicrob. Agents Chemother.* 38, 2047–2053. doi: 10.1128/AAC.38.9.2047

Faegheh, F., B, K., Mehrdad, I., and Milad, I. (2018). Antibacterial activity of flavonoids and their structure–activity relationship: an update review. *Phytother. Res.* 33, 13–40. doi: 10.1002/ptr.6208

Fagotti, L., Tatka, J., Salles, M. J. C., and Queiroz, M. C. (2018). Risk factors and treatment options for failure of a two-stage exchange. *Curr. Rev. Musculoskelet. Med.* 11, 420–427. doi: 10.1007/s12178-018-9504-1

Flemming, H. C., Neu, T. R., and Wozniak, D. J. (2007). The EPS matrix: the "house of biofilm cells". *J. Bacteriol.* 189, 7945–7947. doi: 10.1128/JB.00858-07

Gunes, H., Gulen, D., Mutlu, R., Gumus, A., Tas, T., and Topkaya, A. E. (2016). Antibacterial effects of curcumin: an in vitro minimum inhibitory concentration study. *Toxicol. Ind. Health* 32, 246–250. doi: 10.1177/0748233713498458

Hamza, T., and Li, B. (2014). Differential responses of osteoblasts and macrophages upon *Staphylococcus aureus* infection. *BMC Microbiol.* 14:207. doi: 10.1186/s12866-014-0207-5

Hirai, J., Hagihara, M., Kato, H., Sakanashi, D., Nishiyama, N., Koizumi, Y., et al. (2016). Investigation on rifampicin administration from the standpoint of pharmacokinetics/pharmacodynamics in a neutropenic murine thigh infection model. *J. Infect. Chemother.* 22, 387–394. doi: 10.1016/j.jiac.2016.02.011

Hiramatsu, K., Katayama, Y., Yuzawa, H., and Ito, T. (2002). Molecular genetics of methicillin-resistant *Staphylococcus aureus*. *Int. J. Med. Microbiol.* 292, 67–74. doi: 10.1078/1438-4221-00192

Hu, C. C., Chang, C. H., Hsiao, Y. M., Chang, Y., Wu, Y. Y., Ueng, S. W. N., et al. (2020). Lipoteichoic acid accelerates bone healing by enhancing osteoblast differentiation and inhibiting osteoclast activation in a mouse model of femoral defects. *Int. J. Mol. Sci.* 21:5550. doi: 10.3390/ijms21155550

Huang, H., Jin, W. W., Huang, M., Ji, H., Capen, D. E., Xia, Y., et al. (2020). Gentamicin-induced acute kidney injury in an animal model involves programmed necrosis of the collecting duct. *J. Am. Soc. Nephrol.* 31, 2097–2115. doi: 10.1681/ASN.2019020204

Jauregui, C. E., Mansell, J. P., Jepson, M. A., and Jenkinson, H. F. (2013). Differential interactions of Streptococcus gordonii and *Staphylococcus aureus* with cultured osteoblasts. *Mol Oral Microbiol* 28, 250–266. doi: 10.1111/omi.12022

Jin, S., Meng, C., He, Y., Wang, X., Zhang, Q., Wang, Z., et al. (2020). Curcumin prevents osteocyte apoptosis by inhibiting M1-type macrophage polarization in mice model of glucocorticoid-associated osteonecrosis of the femoral head. *J. Orthop. Res.* 38, 2020–2030. doi: 10.1002/jor.24619

John, A. K., Baldoni, D., Haschke, M., Rentsch, K., Schaerli, P., Zimmerli, W., et al. (2009). Efficacy of daptomycin in implant-associated infection due to methicillin-resistant *Staphylococcus aureus*: importance of combination with rifampin. *Antimicrob. Agents Chemother.* 53, 2719–2724. doi: 10.1128/AAC.00047-09

Jones, M., Ying, J., Huttner, B., Evans, M., Maw, M., Nielson, C., et al. (2014). Relationships between the importation, transmission, and nosocomial infections of methicillin-resistant *Staphylococcus aureus*: an observational study of 112 veterans affairs medical centers. *Clin. Infect. Dis.* 58, 32–39. doi: 10.1093/cid/cit668

Kahlmeter, G., Brown, D. F., Goldstein, F. W., MacGowan, A. P., Mouton, J. W., Odenholt, I., et al. (2006). European committee on antimicrobial susceptibility testing (EUCAST) technical notes on antimicrobial susceptibility testing. *Clin. Microbiol. Infect.* 12, 501–503. doi: 10.1111/j.1469-0691.2006.01454.x

Kaneko, H., Nakaminami, H., Ozawa, K., Wajima, T., and Noguchi, N. (2020). In vitro anti-biofilm effect of anti-methicillin-resistant *Staphylococcus aureus* (anti-MRSA) agents against the USA300 clone. *J. Glob. Antimicrob. Resist.* 24, 63–71. doi: 10.1016/j.jgar.2020.11.026

Kao, N. J., Hu, J. Y., Wu, C. S., and Kong, Z. L. (2016). Curcumin represses the activity of inhibitor-kappaB kinase in dextran sulfate sodium-induced colitis by S-nitrosylation. *Int. Immunopharmacol.* 38, 1–7. doi: 10.1016/j.intimp.2016.05.015

Krauss, J. L., Roper, P. M., Ballard, A., Shih, C. C., Fitzpatrick, J. A. J., Cassat, J. E., et al. (2019). *Staphylococcus aureus* infects osteoclasts and replicates Intracellularly. *mBio* 10:e02447-19. doi: 10.1128/mBio.02447-19

Kunnumakkara, A. B., Bordoloi, D., Padmavathi, G., Monisha, J., Roy, N. K., Prasad, S., et al. (2017). Curcumin, the golden nutraceutical: multitargeting for multiple chronic diseases. *Br. J. Pharmacol.* 174, 1325–1348. doi: 10.1111/bph.13621

Lauderdale, K. J., Malone, C. L., Boles, B. R., Morcuende, J., and Horswill, A. R. (2010). Biofilm dispersal of community-associated methicillin-resistant *Staphylococcus aureus* on orthopedic implant material. *J. Orthop. Res.* 28, 55–61. doi: 10.1002/jor.20943

Lebeaux, D., Ghigo, J. M., and Beloin, C. (2014). Biofilm-related infections: bridging the gap between clinical management and fundamental aspects of recalcitrance toward antibiotics. *Microbiol. Mol. Biol. Rev.* 78, 510–543. doi: 10.1128/MMBR.00013-14

Li, Z., and Knetsch, M. (2018). Antibacterial strategies for wound dressing: preventing infection and stimulating healing. *Curr. Pharm. Des.* 24, 936–951. doi: 10.2174/1381612824666180213141109

Lio, P., Paoletti, N., Moni, M. A., Atwell, K., Merelli, E., and Viceconti, M. (2012). Modelling osteomyelitis. *BMC Bioinformatics* 13:S12. doi: 10.1186/1471-2105-13-S14-S12

Liu, Y. W., An, S. B., Yang, T., Xiao, Y. J., Wang, L., and Hu, Y. H. (2019). Protection effect of Curcumin for macrophage-involved polyethylene Wear particle-induced inflammatory Osteolysis by increasing the cholesterol efflux. *Med. Sci. Monit.* 25, 10–20. doi: 10.12659/MSM.914197

Lovati, A. B., Drago, L., Monti, L., De Vecchi, E., Previdi, S., Banfi, G., et al. (2013). Diabetic mouse model of orthopaedic implant-related *Staphylococcus aureus* infection. *PLoS One* 8:e67628. doi: 10.1371/journal.pone.0067628

McCourt, J., O'Halloran, D. P., McCarthy, H., O'Gara, J. P., and Geoghegan, J. A. (2014). Fibronectin-binding proteins are required for biofilm formation by community-associated methicillin-resistant *Staphylococcus aureus* strain LAC. *FEMS Microbiol. Lett.* 353, 157–164. doi: 10.1111/1574-6968.12424

Moghadamtousi, S. Z., Kadir, H. A., Hassandarvish, P., Tajik, H., Abubakar, S., and Zandi, K. (2014). A review on antibacterial, antiviral, and antifungal activity of curcumin. *Biomed. Res. Int.* 2014:186864. doi: 10.1155/2014/186864

Mohankumar, K., Sridharan, S., Pajaniradje, S., Singh, V. K., Ronsard, L., Banerjea, A. C., et al. (2015). BDMC-A, an analog of curcumin, inhibits markers of invasion, angiogenesis, and metastasis in breast cancer cells via NF-kappaB pathway–a comparative study with curcumin. *Biomed. Pharmacother.* 74, 178–186. doi: 10.1016/j.biopha.2015.07.024

Molin, S., and Tolker-Nielsen, T. (2003). Gene transfer occurs with enhanced efficiency in biofilms and induces enhanced stabilisation of the biofilm structure. *Curr. Opin. Biotechnol.* 14, 255–261. doi: 10.1016/s0958-1669(03)00036-3

Montanaro, L., Speziale, P., Campoccia, D., Ravaioli, S., Cangini, I., Pietrocola, G., et al. (2011). Scenery of staphylococcus implant infections in orthopedics. *Future Microbiol.* 6, 1329–1349. doi: 10.2217/fmb.11.117

Mun, S. H., Joung, D. K., Kim, Y. S., Kang, O. H., Kim, S. B., Seo, Y. S., et al. (2013). Synergistic antibacterial effect of curcumin against methicillin-resistant *Staphylococcus aureus*. *Phytomedicine* 20, 714–718. doi: 10.1016/j.phymed.2013.02.006

Mun, S. H., Kim, S. B., Kong, R., Choi, J. G., Kim, Y. C., Shin, D. W., et al. (2014). Curcumin reverse methicillin resistance in *Staphylococcus aureus*. *Molecules* 19, 18283–18295. doi: 10.3390/molecules191118283

Microbiology by Numbers. (2011). Microbiology by numbers. *Nat. Rev. Microbiol.* 9:628. doi: 10.1038/nrmicro2644

Odds, F. C. (2003). Synergy, antagonism, and what the chequerboard puts between them. *J. Antimicrob. Chemother.* 52:1. doi: 10.1093/jac/dkg301

Oikonomidis, S., Altenrath, L., Westermann, L., Bredow, J., Eysel, P., and Scheyerer, M. J. (2020). Implant-associated infection of long-segment spinal instrumentation: a retrospective analysis of 46 consecutive patients. *Asian Spine J.* 15, 234–243. doi: 10.31616/asj.2019.0391

Prince, K., Kandi, S. K., Sunny, M., Kasturi, M., and Diwan, S. R. (2019). Monocarbonyl Curcuminoids with improved stability as antibacterial agents against *Staphylococcus aureus* and their mechanistic studies. *ACS Omega* 4, 675–687. doi: 10.1021/acsomega.8b02625

Rai, D., Singh, J. K., Roy, N., and Panda, D. (2008). Curcumin inhibits FtsZ assembly: an attractive mechanism for its antibacterial activity. *Biochem. J.* 410, 147–155. doi: 10.1042/BJ20070891

Rao, N., Ziran, B. H., and Lipsky, B. A. (2011). Treating osteomyelitis: antibiotics and surgery. *Plast. Reconstr. Surg.* 127, 177S–187S. doi: 10.1097/PRS.0b013e3182001f0f

Ribeiro, M., Monteiro, F. J., and Ferraz, M. P. (2012). Infection of orthopedic implants with emphasis on bacterial adhesion process and techniques used in studying bacterial-material interactions. *Biomatter* 2, 176–194. doi: 10.4161/biom.22905

Rochford, E. T. J., Sabate Bresco, M., Zeiter, S., Kluge, K., Poulsson, A., Ziegler, M., et al. (2016). Monitoring immune responses in a mouse model of fracture fixation with and without *Staphylococcus aureus* osteomyelitis. *Bone* 83, 82–92. doi: 10.1016/j.bone.2015.10.014

Sandikci, A. S., Y, A. F., Issa, G., Basaran, K. B., Dulger, A. D., and Buyukunal, S. (2016). Antimicrobial effects of curcumin against *L. monocytogenes*, *S. aureus*, *S. Typhimurium* and *E. coli* O157: H7 pathogens in minced meat. *Vet. Med.* 61, 256–262. doi: 10.17221/8880-vetmed

Saqib, U., Sarkar, S., Suk, K., Mohammad, O., Baig, M. S., and Savai, R. (2018). Phytochemicals as modulators of M1-M2 macrophages in inflammation. *Oncotarget* 9, 17937–17950. doi: 10.18632/oncotarget.24788

Sasidharan, N. K., Sreekala, S. R., Jacob, J., and Nambisan, B. (2014). In vitro synergistic effect of curcumin in combination with third generation cephalosporins against bacteria associated with infectious diarrhea. *Biomed. Res. Int.* 2014:561456. doi: 10.1155/2014/561456

Schimmel, J. J., Horsting, P. P., de Kleuver, M., Wonders, G., and van Limbeek, J. (2010). Risk factors for deep surgical site infections after spinal fusion. *Eur. Spine J.* 19, 1711–1719. doi: 10.1007/s00586-010-1421-y

Slullitel, P. A., Buttaro, M. A., Greco, G., Onativia, J. I., Sanchez, M. L., Mc Loughlin, S., et al. (2018). No lower bacterial adhesion for ceramics compared to other biomaterials: an in vitro analysis. *Orthop. Traumatol. Surg. Res.* 104, 439–443. doi: 10.1016/j.otsr.2018.03.003

Song, F., Liu, J., Zhao, W., Huang, H., Hu, D., Chen, H., et al. (2020). Synergistic effect of Eugenol and probiotic lactobacillus Plantarum Zs2058 against salmonella infection in C57bl/6 mice. *Nutrients* 12:1611. doi: 10.3390/nu12061611

Tajbakhsh, S., Mohammadi, K., Deilami, I., Zandi, K., Fouladvand, M., Ramedani, E., et al. (2008). Antibacterial activity of indium curcumin and indium diacetylcurcumin. *Afr. J. Biotechnol.* 7, 3832–3835. doi: 10.5897/AJB08.790

Takayanagi, H. (2015). Osteoimmunology in 2014: two-faced immunology-from osteogenesis to bone resorption. *Nat. Rev. Rheumatol.* 11, 74–76. doi: 10.1038/nrrheum.2014.219

Tallarida, R. J. (2011). Quantitative methods for assessing drug synergism. *Genes Cancer* 2, 1003–1008. doi: 10.1177/1947601912440575

Tawakoli, P. N., Al-Ahmad, A., Hoth-Hannig, W., Hannig, M., and Hannig, C. (2013). Comparison of different live/dead stainings for detection and quantification of adherent microorganisms in the initial oral biofilm. *Clin. Oral Investig.* 17, 841–850. doi: 10.1007/s00784-012-0792-3

Teow, S. Y., and Ali, S. A. (2015). Synergistic antibacterial activity of Curcumin with antibiotics against *Staphylococcus aureus*. *Pak. J. Pharm. Sci.* 28, 2109–2114.

Teow, S. Y., Liew, K., Ali, S. A., Khoo, A. S., and Peh, S. C. (2016). Antibacterial action of Curcumin against *Staphylococcus aureus*: a brief review. *J. Trop. Med.* 2016:2853045. doi: 10.1155/2016/2853045

Tuchscherr, L., Medina, E., Hussain, M., Volker, W., Heitmann, V., Niemann, S., et al. (2011). *Staphylococcus aureus* phenotype switching: an effective bacterial strategy to escape host immune response and establish a chronic infection. *EMBO Mol. Med.* 3, 129–141. doi: 10.1002/emmm.201000115

Tyagi, P., Singh, M., Kumari, H., Kumari, A., and Mukhopadhyay, K. (2015). Bactericidal activity of curcumin I is associated with damaging of bacterial membrane. *PLoS One* 10:e0121313. doi: 10.1371/journal.pone.0121313

Vanhommerig, E., Moons, P., Pirici, D., Lammens, C., Hernalsteens, J. P., De Greve, H., et al. (2014). Comparison of biofilm formation between major clonal lineages of methicillin resistant *Staphylococcus aureus*. *PLoS One* 9:e104561. doi: 10.1371/journal.pone.0104561

Vergara-Irigaray, M., Valle, J., Merino, N., Latasa, C., Garcia, B., de Los, R., et al. (2009). Relevant role of fibronectin-binding proteins in *Staphylococcus aureus* biofilm-associated foreign-body infections. *Infect. Immun.* 77, 3978–3991. doi: 10.1128/IAI.00616-09

Wang, X., Ji, Q., Hu, W., Zhang, Z., Hu, F., Cao, S., et al. (2021). Isobavachalcone prevents osteoporosis by suppressing activation of ERK and NF-kappaB pathways and M1 polarization of macrophages. *Int. Immunopharmacol.* 94:107370. doi: 10.1016/j.intimp.2021.107370

Wang, M., Lin, L., Lu, J. J., and Chen, X. (2021). Pharmacological review of isobavachalcone, a naturally occurring chalcone. *Pharmacol. Res.* 165:105483. doi: 10.1016/j.phrs.2021.105483

Wang, J., Zhou, X., Li, W., Deng, X., Deng, Y., and Niu, X. (2016). Curcumin protects mice from *Staphylococcus aureus* pneumonia by interfering with the self-assembly process of alpha-hemolysin. *Sci. Rep.* 6:28254. doi: 10.1038/srep28254

Xu, W., Dong, S., Han, Y., Li, S., and Liu, Y. (2018). Hydrogels as antibacterial biomaterials. *Curr. Pharm. Des.* 24, 843–854. doi: 10.2174/1381612824666180213122953

Yin, S., Fan, C. Q., Wang, Y., Dong, L., and Yue, J. M. (2004). Antibacterial prenylflavone derivatives from *Psoralea corylifolia*, and their structure-activity relationship study. *Bioorg. Med. Chem.* 12, 4387–4392. doi: 10.1016/j.bmc.2004.06.014

frontiers | Frontiers in Microbiology

TYPE Original Research
PUBLISHED 30 September 2022
DOI 10.3389/fmicb.2022.957879

OPEN ACCESS

EDITED BY
Fang Yang,
Qingdao Municipal Hospital, China

REVIEWED BY
Dhirendra Kumar Singh,
University of North Carolina at Chapel Hill, United States
Megan L. Falsetta,
University of Rochester, United States

*CORRESPONDENCE
Yingming Yang
ymyang@scu.edu.cn
Tao Hu
hutao@scu.edu.cn

†These authors have contributed equally to this work

SPECIALTY SECTION
This article was submitted to Antimicrobials, Resistance and Chemotherapy, a section of the journal Frontiers in Microbiology

RECEIVED 31 May 2022
ACCEPTED 18 August 2022
PUBLISHED 30 September 2022

CITATION
Lu Y, Lei L, Deng Y, Zhang H, Xia M, Wei X, Yang Y and Hu T (2022) RNase III coding genes modulate the cross-kingdom biofilm of *Streptococcus mutans* and *Candida albicans*. *Front. Microbiol.* 13:957879. doi: 10.3389/fmicb.2022.957879

RNase III coding genes modulate the cross-kingdom biofilm of *Streptococcus mutans* and *Candida albicans*

Yangyu Lu[1,2†], Lei Lei[1†], Yalan Deng[1†], Hongyu Zhang[1], Mengying Xia[1], Xi Wei[2], Yingming Yang[1*] and Tao Hu[1*]

[1]State Key Laboratory of Oral Diseases, Department of Preventive Dentistry, National Clinical Research Center for Oral Diseases, West China Hospital of Stomatology, Sichuan University, Chengdu, China, [2]Guangdong Provincial Key Laboratory of Stomatology, Department of Operative Dentistry and Endodontics, Hospital of Stomatology, Guanghua School of Stomatology, Sun Yat-sen University, Guangzhou, China

Streptococcus mutans constantly coexists with *Candida albicans* in plaque biofilms of early childhood caries (ECC). The progression of ECC can be influenced by the interactions between *S. mutans* and *C. albicans* through exopolysaccharides (EPS). Our previous studies have shown that *rnc*, the gene encoding ribonuclease III (RNase III), is implicated in the cariogenicity of *S. mutans* by regulating EPS metabolism. The *DCR1* gene in *C. albicans* encodes the sole functional RNase III and is capable of producing non-coding RNAs. However, whether *rnc* or *DCR1* can regulate the structure or cariogenic virulence of the cross-kingdom biofilm of *S. mutans* and *C. albicans* is not yet well understood. By using gene disruption or overexpression assays, this study aims to investigate the roles of *rnc* and *DCR1* in modulating the biological characteristics of dual-species biofilms of *S. mutans* and *C. albicans* and to reveal the molecular mechanism of regulation. The morphology, biomass, EPS content, and lactic acid production of the dual-species biofilm were assessed. Quantitative real-time polymerase chain reaction (qRT-PCR) and transcriptomic profiling were performed to unravel the alteration of *C. albicans* virulence. We found that both *rnc* and *DCR1* could regulate the biological traits of cross-kingdom biofilms. The *rnc* gene prominently contributed to the formation of dual-species biofilms by positively modulating the extracellular polysaccharide synthesis, leading to increased biomass, biofilm roughness, and acid production. Changes in the microecological system probably impacted the virulence as well as polysaccharide or pyruvate metabolism pathways of *C. albicans*, which facilitated the assembly of a cariogenic cross-kingdom biofilm and the generation of an augmented acidic milieu. These results may provide an avenue for exploring new targets for the effective prevention and treatment of ECC.

KEYWORDS

***Streptococcus mutans*, *rnc* gene, *Candida albicans*, *DCR1* gene, cross-kingdom biofilm**

Introduction

Early childhood caries (ECC) is an aggressive form of tooth decay in children younger than 6 years, with a high prevalence of 70% in disadvantaged groups worldwide (James et al., 2018; Peres et al., 2019; Duan et al., 2021). *Streptococcus mutans* (*S. mutans*) is a critical pathogen of dental caries due to its acidogenicity, aciduricity, and capacity to develop cariogenic biofilms by synthesizing exopolysaccharides (EPS) (Lemos et al., 2019). As the main virulence factor of *S. mutans*, EPS are conducive to the energy storage, adhesion, and three-dimensional (3D) architecture of dental plaque biofilms (Koo et al., 2017; Yang et al., 2019). Another microbe frequently detected with *S. mutans* in plaque biofilms of ECC is *Candida albicans* (*C. albicans*), an opportunistic fungal pathogen usually isolated from the human oral cavity (Ponde et al., 2021; Ramadugu et al., 2021). *C. albicans* is closely correlated with the occurrence and development of ECC or persistent apical periodontitis in which the pathogens are difficult to eradicate especially in molars with complicated root canal morphology (Zhang et al., 2011a,b; Mustafa et al., 2022). Children with oral *C. albicans* have a more than 5 times higher possibility of developing ECC than those without *C. albicans* (Xiao et al., 2018b). *C. albicans* can strengthen the ability of microflora to produce or tolerate acid, elevate the abundance of *S. mutans*, and enhance the activity of glucosyltransferases (Gtfs) secreted by *S. mutans* in plaque biofilms of severe early childhood caries (S-ECC) (Xiao et al., 2018a). These findings suggest that the coexistence of *S. mutans* and *C. albicans* is closely related to the progression of ECC. In the co-culture biofilm, the presence of *C. albicans* improves the carbohydrate metabolism of *S. mutans* and affects its environmental fitness and biofilm formation (He et al., 2017). Mannans located in the cell wall of *C. albicans* binds to *S. mutans*-derived GtfB to regulate EPS formation, mechanical stability, and colonization of dual-species biofilms (Hwang et al., 2017; Khoury et al., 2020). *S. mutans*-secreted GtfB, in turn, can not only break sucrose down into monosaccharides that are efficiently utilized by *C. albicans* to enhance its acid production but also improve fungal colonization onto the tooth surface and antifungal resistance to fluconazole (Kim et al., 2018; Ellepola et al., 2019). Transcriptomics and proteomics studies have implied that genes and proteins of *C. albicans* associated with polysaccharide metabolism and cell morphogenesis are significantly upregulated in dual-species biofilms of *S. mutans* and *C. albicans* (Ellepola et al., 2019). Therefore, EPS play important roles in the cross-kingdom interaction between *S. mutans* and *C. albicans*.

Ribonuclease III (RNase III) is the endonuclease in bacteria and eukaryotes that participates in RNA biogenesis to control gene expression (Svensson and Sharma, 2021). Our previous studies have illuminated that the gene encoding *S. mutans* RNase III, *rnc*, enhances the EPS synthesis and cariogenicity of bacterial biofilms through non-coding RNAs that target *vicR*, the gene encoding a response regulator of EPS metabolism (Lei et al., 2018, 2020). On the one hand, *rnc* impairs *vicR* expression by affecting the generation of microRNA-size small RNA 1657 (msRNA 1657), which can bind to the 5′-UTR regions of the *vicR* mRNA (Lei et al., 2019). On the other hand, *rnc* increases the expression of *vicR* antisense (AS*vicR*) RNA, thus influencing the transcriptional level of the *vicR* gene (Lei et al., 2020). *C. albicans* also has *DCR1* as the sole functional RNase III, which is instrumental in small interfering RNA (siRNA), ribosomal RNA (rRNA), and small nuclear RNA (snRNA) generation (Drinnenberg et al., 2009; Bernstein et al., 2012). Notably, although deletions of one copy of the *DCR1* gene in diploids do not restrict *C. albicans* growth, mutants deficient in both copies of the *DCR1* allele cannot be recovered, indicating that *DCR1* is essential for *C. albicans* survival (Bernstein et al., 2012). In summary, as RNase III-coding genes in bacteria and eukaryotes, *rnc* regulates extracellular matrix synthesis and cariogenic characteristics of *S. mutans* biofilms at the post-transcriptional level, while *DCR1* catalyzes the production of non-coding RNAs in *C. albicans*. However, whether *rnc* and *DCR1* affect the EPS and cariogenicity of cross-kingdom biofilms of *S. mutans* and *C. albicans* has not yet been elucidated.

In this study, *C. albicans DCR1* low-expressing and overexpressing strains were constructed and co-cultured with *S. mutans* wild-type or *rnc*-mutant strains to explore the roles of *rnc* and *DCR1* in the modulation of dual-species biofilms of *S. mutans* and *C. albicans*. We demonstrated that *DCR1* regulated the fungal yeast-to-hyphae transition, spatial structure, acid production, and glucan/microorganism ratio of biofilms, while *rnc* prominently contributed to cross-kingdom biofilm formation by boosting extracellular polysaccharide synthesis. Alterations of the microecosystem caused by *rnc* might affect the virulence of *C. albicans* that facilitated the assembly of a cariogenic cross-kingdom biofilm and the formation of an intensive acidic milieu. According to these results, *rnc* and *DCR1* may be new potential targets for ECC prevention and treatment.

Materials and methods

Microorganisms and construction of mutant strains

The strains and plasmids used in this study are summarized in **Table 1**. *C. albicans* SC5314 and CAI4, and *S. mutans* UA159 were kindly provided by the State Key Laboratory of Oral Diseases (Sichuan University, Chengdu, China). *S. mutans* strains were cultured on brain heart infusion (BHI; BD, Franklin Lakes, United States) medium with erythromycin or spectinomycin when necessary at 37°C anaerobically (10% CO_2, 80% N_2, 10% H_2). *C. albicans* SC5314 and CAI4 were

grown in the YPD medium (1% yeast extract, 2% peptone, and 2% dextrose) at 30°C with shaking (150 rpm) under aerobic conditions. A *C. albicans DCR1* low-expressing strain (*DCR1/dcr1*Δ) was constructed by deleting one copy of the *DCR1* gene using plasmid p5921 according to the URA-Blaster method (Janik et al., 2019). Upstream and downstream fragments of *DCR1* from the chromosome were inserted into both ends of the *hisG-URA3-hisG* cassette of p5921 to obtain the recombinant plasmid pUC-*DCR1-URA3* to replace one of the *DCR1* alleles in *C. albicans*. The open reading frame (ORF) of the *DCR1* gene was cloned into the pCaEXP plasmid to establish the recombinant vector pCaEXP-*DCR1*, which could integrate into the *RP10* locus of the *C. albicans* genome to create a *DCR1* overexpressing strain ($DCR1^{OE}$) (Jia et al., 2011; Basso et al., 2017; Znaidi et al., 2018). All recombinant plasmids were transformed into *C. albicans* CAI4 utilizing the Yeast Transformation Kit (Sigma-Aldrich, St Louis, United States). The mutagenic strains were selected on a synthetic dropout (SD) medium without uridine, methionine, and cysteine and then verified by PCR, DNA sequencing, and quantitative real-time polymerase chain reaction (qRT-PCR) with the primers listed in **Supplementary Table 1**. The *rnc*-deficient strain (Smurnc) was constructed by an erythromycin cassette based on homologous recombination. Meanwhile, the recombinant plasmid pDL278 containing the *rnc* ORF and promoter region was transformed into *S. mutans* UA159 to generate an *rnc* overexpressing strain ($Smurnc^{+}$), as previously described (Lau et al., 2002; Lei et al., 2020).

Biofilm formation

Streptococcus mutans and *C. albicans* were grown to mid-exponential phase and co-cultured in YNBB medium (0.67% YNB, 75 mM Na_2HPO_4-NaH_2PO_4, 0.5% sucrose, and essential amino acids) at the concentrations of 2×10^6 colony forming units (CFU)/ml (*S. mutans*) and 2×10^4 CFU/ml (*C. albicans*). Cross-kingdom biofilms were formed in microtiter plates at 37°C with 5% CO_2 for 24 h (Sztajer et al., 2014; Liu et al., 2017).

Biofilm observation and assessment

The structure of cross-kingdom biofilms was analyzed by scanning electron microscopy (SEM; FEI, Hillsboro, United States). Briefly, after being cultivated on sterile polystyrene slides, the biofilms were washed two times with sterile phosphate-buffered saline (PBS) and fixed with 2.5% glutaraldehyde at 4°C for 4 h in the dark, followed by serial dehydration with ethanol solutions (30, 50, 75, 85, 95, and 99%) and coating with gold for image collection. The biomass of the biofilms was quantified by the crystal violet (CV) microtiter assay. After incubation in 24-well polystyrene plates, the biofilms were stained with 0.1% (w/v) CV for 10 min at room temperature when the planktonic cells and supernatant were gently removed. The specimens were rinsed carefully with water, and then 33% acetic acid was added to dissolve the dye under gentle shaking at 37°C for 5 min. Finally, biofilm formation was detected by the absorbance of acetic acid at 575 nm.

Lactic acid generation evaluation

The mature biofilms were cultured in buffered peptone water (BPW; Hopebio, Qingdao, China) supplemented with 0.2% (w/v) sucrose at 37°C with 5% CO_2 for 3 h after rinsing with PBS (Chen et al., 2020). The concentrations of lactic acid produced by the biofilms were calculated based on the standard curve according to the instructions of the Lactic Acid Assay Kit (Nanjing Jiancheng, China).

Exopolysaccharide distribution in biofilms

Glucan in the biofilms that grew in polystyrene cell culture dishes with modified bottoms was stained with Alexa Fluor 647 (Invitrogen, Waltham, United States) at a final concentration of 1 μl/ml during incubation. Microorganisms were labeled with 2.5 μM SYTO 9 green fluorescent dye (Invitrogen), while *C. albicans* was stained with calcofluor white dye (Sigma-Aldrich) (Punjabi et al., 2020). The distribution of microbes or glucan was detected by confocal laser scanning microscopy (CLSM; Olympus, Tokyo, Japan). Biofilms were reconstructed, and imaging biomass quantification was analyzed using Imaris version 7.2.3 (Bitplane, Zurich, Switzerland) (Lei et al., 2020).

Exopolysaccharide production measurement

The biofilms were cultivated in 6-well polystyrene plates before the EPS content was determined by the anthrone method. Water-insoluble EPS extraction from dual-species biofilms was performed according to previous protocols with modifications (Lei et al., 2020). Biofilms were gently washed with PBS, collected by scraping, and centrifuged at 4°C (2,422 × *g*) for 15 min. The precipitates were solubilized in 1 M NaOH (Sigma, United States) by incubation at 37°C for 2 h at 120 rpm. After centrifugation (2,422 × *g*) at 4°C for 15 min, the supernatant containing water-insoluble EPS was collected and diluted with an anthrone-sulfuric acid reagent to a final concentration of 25% (v/v). The mixed samples were blended and incubated at 95°C for 6 min, and the absorbance was measured at an optical density of 625 nm.

TABLE 1 Microbial strains and plasmid used in this study.

Strains, plasmid	Relevant characteristics	Source or reference
***S. mutans* strains**		
UA159	Parent strain	ATCC 700610
Smurnc	UA159 *rnc: ermAM*; Erm^r	Lei et al., 2020
Smurnc$^+$	UA159 derived; pDL278-*rnc*; Spec^r	Lei et al., 2020
***C. albicans* strains**		
SC5314	Parent strain	ATCC MYA-2876
CAI4	*ura3*Δ:*imm434*/*ura3*Δ:*imm434*	Fonzi and Irwin, 1993
*DCR1/dcr1*Δ	*dcr1*Δ: *hisG-URA3-hisG*/*DCR1*	This study
DCR1^{OE}	*rp10*Δ:pCaEXP-*DCR1-URA3*/*RP10*	This study
Plasmid		
pDL278	*Escherichia coli-Streptococcus* shuttle vector; Spec^r	Wen et al., 2011
pDL278-*rnc*	Recombinant and expression of *rnc*; Spec^r	Lei et al., 2020
p5921	Containing *hisG-URA3-hisG*; Amp^r	Mao et al., 1999
pUC-*DCR1-URA3*	p5921 derived; containing *DCR1* upstream and downstream sequence	This study
pCaEXP	Containing *RP10* sequence; Amp^r	Care et al., 1999
pCaEXP-*DCR1*	pCaEXP derived; recombinant and expression of *DCR1*	This study

Erm, erythromycin; Spec, spectinomycin; Amp, ampicillin.

Characteristics of the biofilm surface

The surface morphology and roughness of the biofilm were visualized and examined by atomic force microscopy (AFM). In brief, the biofilms cultured on polystyrene slides were mildly washed with PBS and dried in the air, followed by the measurement of surface roughness, which is represented by the arithmetic mean deviation of the profile (Ra) counted by an STM9700 system (Shimadzu, Tokyo, Japan) using a cantilever probe (HYDRA-ALL-G-20, AppNANO, Syracuse, United States) in contact mode (Deng et al., 2021). The scanning range was 10 × 10 μm.

RNA isolation and quantitative real-time polymerase chain reaction assays

Biofilm cells were collected by scraping into PBS and harvested by centrifugation (4,500 × *g*) at 4°C for 10 min. Total RNA was extracted by a MasterPure^{TM} complete DNA and RNA purification kit (Lucigen, Middleton, United States). Purification and reverse transcription of the isolated RNAs were performed by using the RevertAid First Strand cDNA Synthesis Kit (Thermo Scientific, Waltham, United States) with gDNA Eraser (Takara, Dalian, China). qRT-PCR was conducted using TB Green® *Premix Ex Taq*^{TM} (Takara) in a LightCycler 480 System (Roche, Vaud, Switzerland). All primer sequences are listed in **Supplementary Table 1**. The relative gene expression level of virulence factors of *C. albicans* was normalized to the gene expression level of the reference gene *ACT1*, and the data were interpreted as fold changes based on the control group according to the $2^{-\Delta\Delta Ct}$ method.

Transcriptome sequencing and data analysis

Total RNA was quantified and qualified using a NanoDrop 2000 instrument (Thermo Scientific) and the 2100 Bioanalyzer (Agilent, Santa Clara, United States), respectively. The mRNA was isolated by the polyA selection method using oligo(dT) magnetic beads, followed by chemical fragmentation, and then double-stranded cDNA was prepared using a SuperScript double-stranded cDNA synthesis kit (Invitrogen) with random hexamer primers (Illumina, San Diego, United States). Libraries were size-selected for end-repaired cDNA target fragments of 300 bp on 2% low-range ultra agarose, followed by PCR amplification. Subsequently, RNA-Seq was conducted with the Illumina HiSeq xten/NovaSeq 6000 sequencer (2 × 150 bp read length). The differential expression genes (DEGs) were classified by Clusters of Orthologous Groups (COG). Furthermore, we performed Gene Ontology (GO) functional enrichment and Kyoto Encyclopedia of Genes and Genomes (KEGG) pathway analysis to identify which DEGs were significantly enriched in GO terms and metabolic pathways using Fisher's exact tests.

Statistical analysis

Statistical analysis was performed using SPSS 16.0 (SPSS Inc., Chicago, United States), and differences in data were considered significant if $P < 0.05$. Data normality and the homogeneity of variance were tested by the Shapiro–Wilk method and Bartlett method, respectively. If the data obeyed the homogeneity of variance, one-way analysis of variance (ANOVA) with Fisher's least significant difference (LSD) multiple-comparison test was used to examine the statistical significance; otherwise, Dunnett's T3 multiple-comparison test was used.

Results

The *DCR1* gene modulated the fungal yeast-to-hyphae transition, spatial structure, acid production, and glucan/microorganism volume ratio of the cross-kingdom biofilm

We successfully constructed a *DCR1* low-expressing mutant *DCR1/dcr1*Δ and a *DCR1* overexpressing mutant $DCR1^{OE}$ (**Supplementary Figure 1**). The biofilm of UA159 + Ca formed a pronounced 3D structure, and *C. albicans* was present mainly in the hyphal form (**Figure 1A**). Nevertheless, the cross-kingdom biofilms containing *DCR1/dcr1*Δ or $DCR1^{OE}$ seemed to lack skeletal architecture, and there were mostly *C. albicans* yeast cells (**Figure 1A**), which was in line with the CLSM results (**Figure 1D**). The glucan/microorganism ratio was used to reflect the capacity of microbial strains to produce glucan. The biofilm of UA159 + *DCR1/dcr1*Δ exhibited a conspicuously decreased glucan/microorganism volume ratio (**Figure 1E**), while UA159 + $DCR1^{OE}$ displayed increased lactic acid production compared to UA159 + Ca (**Figure 1C**). We also used the Ra (nm) value as an indication of the biofilm surface roughness. There was no significant difference in biomass (**Figure 1B**), biofilm roughness (**Figures 1G,H**), or total content of water-insoluble EPS (**Figure 1F**) among the three groups.

The *rnc* gene promoted the exopolysaccharide synthesis and cariogenic characteristics of cross-kingdom biofilms

Microorganisms appeared to gather into condensed clusters surrounded by abundant extracellular polymeric substances to form the 3D structure in biofilms of the UA159 + Ca or $Smurnc^{+}$ + Ca group (**Figures 2A,D,G**). Conversely, the biofilm of Smurnc + Ca had scattered microcolonies with barren extracellular matrix (**Figures 2A,D,G**); this was in line with the results of quantitative calculation which affirmed that the glucan/microorganisms ratio and total content of water-insoluble EPS became diminished in Smurnc + Ca biofilm when compared to UA159 + Ca or $Smurnc^{+}$ + Ca (**Figures 2E,F** and **Supplementary Figure 3**). The fungi among Smurnc + Ca biofilms were predominantly yeast cells, whereas *C. albicans* was present mainly in the hyphal form in the UA159 + Ca or $Smurnc^{+}$ + Ca group (**Figures 2A,D**). Moreover, the biomass of Smurnc + Ca dual-species biofilms was attenuated significantly, which was accompanied by the conspicuous reduction of biofilm roughness and acid production (**Figures 2B,C,H**). To further explore the combined effect of *rnc* and *DCR1* on the cariogenic characteristics of cross-kingdom biofilms, *S. mutans rnc* mutant strains were co-cultured with *C. albicans DCR1* mutant strains. There were principally *C. albicans* yeast cells in the biofilms containing Smurnc, *DCR1/dcr1*Δ, or $DCR1^{OE}$ (**Figures 3**, **5A**). Notably, when *S. mutans* was defective in *rnc*, the dual-species biofilms were devoid of scaffold structure and had the least and loosest matrix compared to other groups (**Figure 3**), resulting in planar architecture with exposed microbial cells, reduced biomass, and low surface roughness (**Figure 4**). AFM detection also revealed that the cells were densely immersed in the flourishing extracellular matrix in the biofilms of $Smurnc^{+}$ + Ca, $Smurnc^{+}$ + *DCR1/dcr1*Δ, and $Smurnc^{+}$ + $DCR1^{OE}$, which was similar to the UA159 + Ca group (**Figure 4A**). Bacteria were sparsely distributed in biofilms composed of Smurnc and *C. albicans* wild-type strain or mutant strains (**Figure 5A**). Quantitative analysis showed that the Smurnc + Ca biofilm exhibited a markedly lower glucan/microorganism volume ratio, restrained synthesis of water-insoluble EPS, and impaired lactic acid production (**Figures 5B–D**). Taken together, the *rnc* gene in *S. mutans* has more pronounced regulatory effects on the cariogenic properties of cross-kingdom biofilms than *DCR1*. Consequently, we chose biofilms consisting of UA159 + Ca and Smurnc + *Ca* and $Smurnc^{+}$ + Ca for the following research.

The *rnc* gene affected virulence factor expression and the pathways of polysaccharide metabolism in *Candida albicans*

To further investigate the effects of *rnc* on the biological properties of *C. albicans* in the cross-kingdom biofilm, the virulence gene transcription level and pathway alterations were revealed by qRT-PCR, RNA-seq, and bioinformatics. The COG results showed that 12 fungal genes were observably downregulated and 5 fungal genes were upregulated in Smurnc + Ca biofilms compared to UA159 + Ca biofilms (**Figure 6A**). These genes are related mainly to carbohydrate bioprocess, cell wall biogenesis, signal transduction, and transcription (**Figure 6A**). GO demonstrated that the majority of downregulated genes were involved in yeast-hyphae

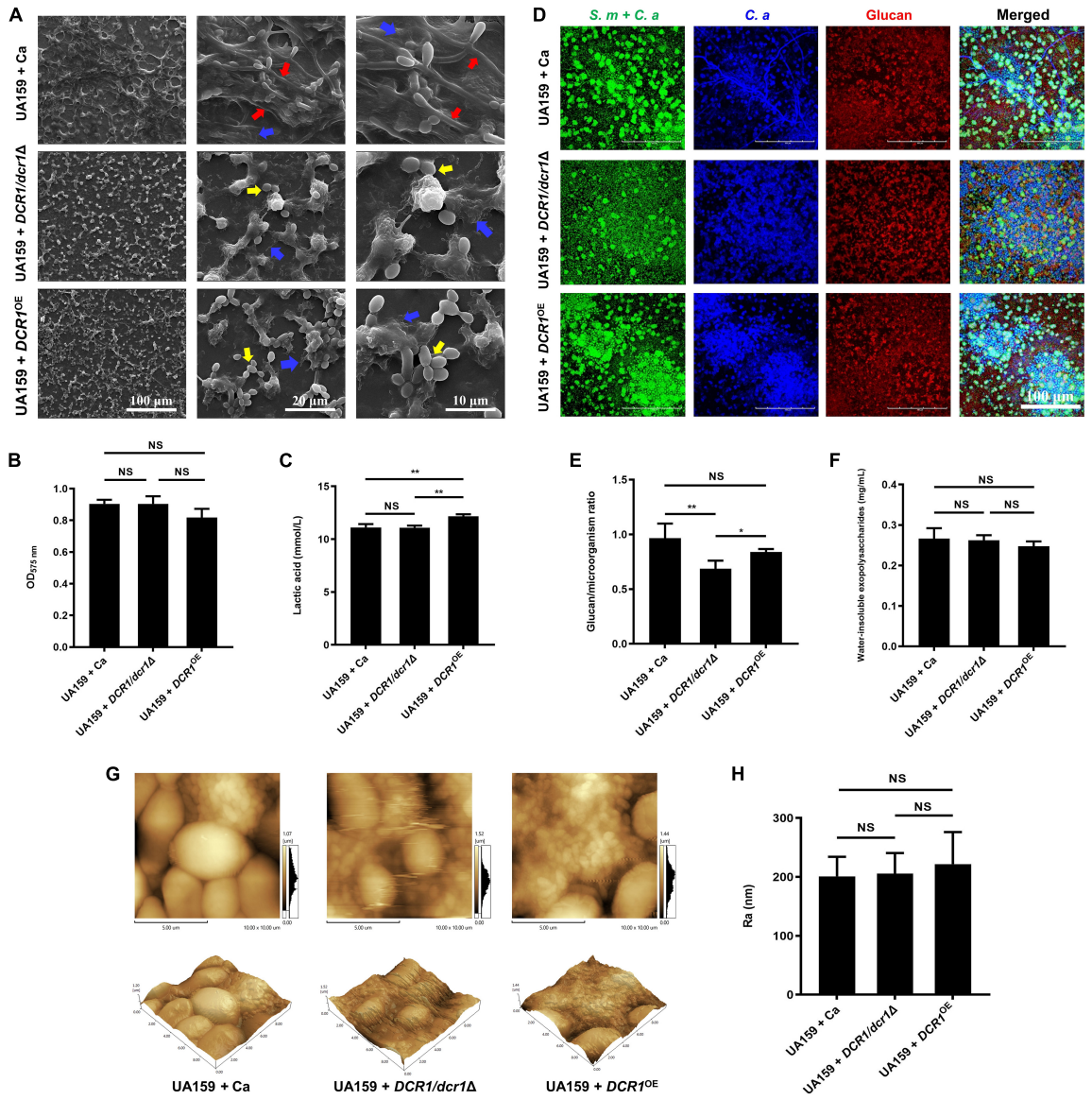

FIGURE 1
The effects of *DCR1* gene on formation and exopolysaccharide synthesis of cross-kingdom biofilm. **(A)** Biofilms architecture was observed by scanning electron microscopy (SEM). Blue arrows, *S. mutans*; red arrows, *C. albicans* hyphae; yellow arrows, *C. albicans* yeast cells. Images were taken at 1,000 × (scale bar, 100 μm), 5,000 × (scale bar, 20 μm), and 10,000 × (scale bar, 10 μm) magnifications, respectively. **(B)** Biofilms volume was quantified by CV microtiter assay. **(C)** Lactic acid generation was assessed by the Lactic Acid Assay Kit. **(D,E)** Exopolysaccharide production and distribution in biofilms were visualized by confocal laser scanning microscopy (CLSM), and the ratio of glucan to microbes was calculated using Imaris version 7.2.3. Green, total microbes (SYTO 9); blue, *C. albicans* (calcofluor white); red, glucan (Alexa Fluor 647). **(F)** Water-insoluble exopolysaccharides from samples were measured by the anthrone method. **(G,H)** Biofilm morphology was detected by AFM and the surface roughness average (Ra) of biofilms was evaluated. Experiments were performed in biological triplicate. $^{*}P < 0.05$, $^{**}P < 0.01$.

transformation, monosaccharide metabolic processes, and pyruvate metabolism (Figure 6B). Through the KEGG pathway analysis, *C. albicans* showed decreased glycolysis/gluconeogenesis, galactose metabolism, and fructose and mannose metabolism (Figure 6C), suggesting that the *C. albicans* pathways associated with carbohydrate metabolism and pyruvate metabolism were suppressed in biofilms of Smurnc + Ca compared to the UA159 + Ca group (Figures 6B,C). Transcriptome data were further confirmed by qRT-PCR which illustrated that the *rnc* mutant strains significantly downregulated the expression of *C. albicans* genes relevant to biofilm formation (*BRG1*, *NDT80*, and *EFG1*) compared with UA159 (Figure 6D). The transcriptional level of the *C. albicans* glucan synthesis gene *GSC1* in Smurnc + *C.a* biofilm was depressed compared to that in UA159 + Ca or Smurnc^{+} + Ca biofilms (Figure 6D).

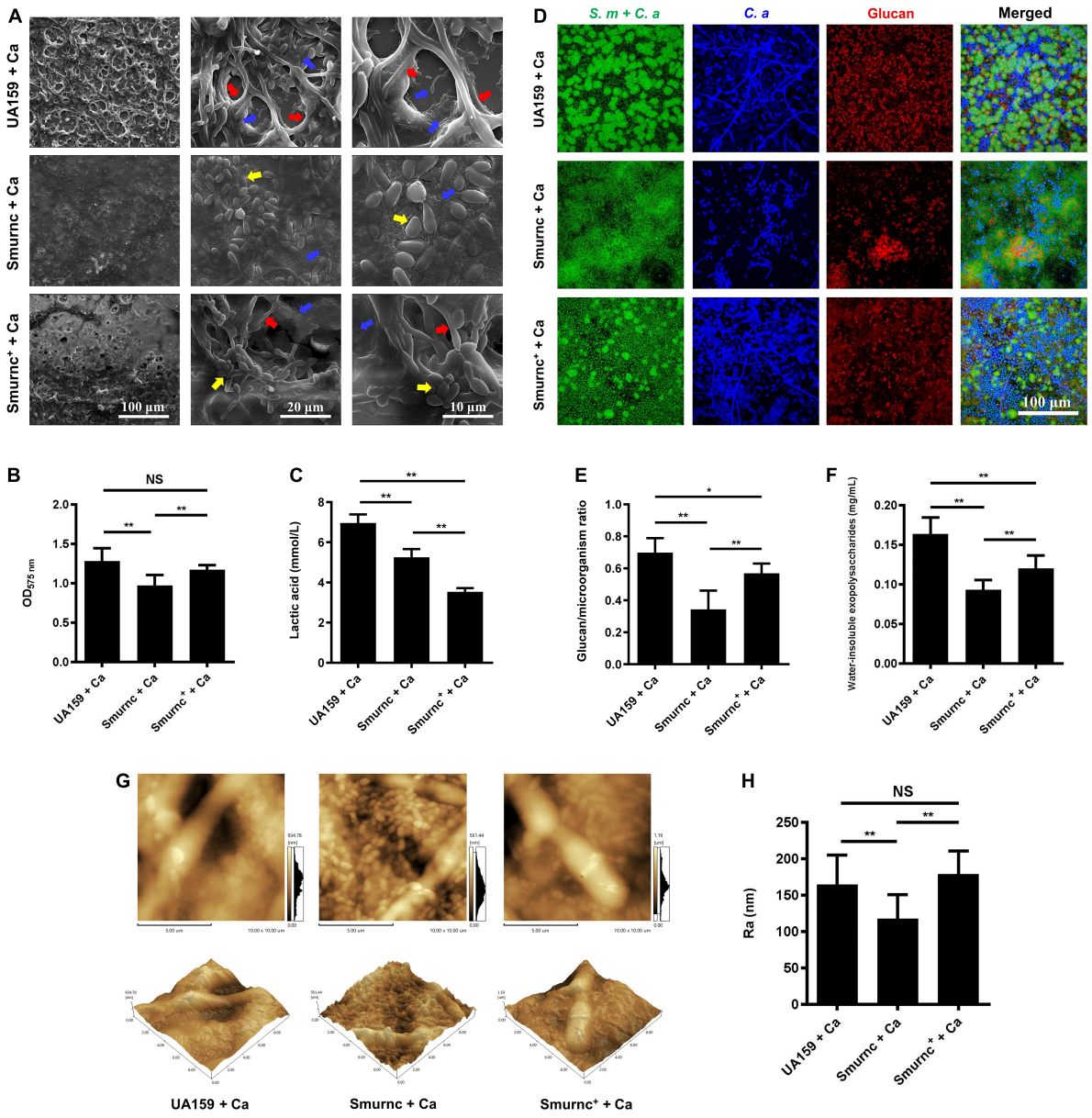

FIGURE 2
The regulation of *rnc* gene in cariogenic characteristics of cross-kingdom biofilm. **(A)** SEM observation of biofilm architecture. Blue arrows, *S. mutans*; red arrows, *C. albicans* hyphae; yellow arrows, *C. albicans* yeast cells. Images were taken at 1,000 × (scale bar, 100 μm), 5,000 × (scale bar, 20 μm), and 10,000 × (scale bar, 10 μm) magnifications, respectively. **(B)** CV microtiter assay was used to quantify the biofilm biomass. **(C)** Lactic acid generation was assessed by the Lactic Acid Assay Kit. **(D,E)** Exopolysaccharide production and distribution in biofilms were visualized by CLSM. Green, total microbes; blue, *C. albicans*; red, glucan. The glucan to microbes ratio was calculated using Imaris version 7.2.3. **(F)** Water-insoluble exopolysaccharides from biofilms were measured by the anthrone method. **(G,H)** Biofilm morphology was detected by AFM, and the surface roughness indicated by Ra (nm) was evaluated. Experiments were performed in biological triplicate. $^{*}P < 0.05$, $^{**}P < 0.01$.

Discussion

Biofilms are dynamic and organized communities in which microbial cells are packed with and embraced by EPS to form a 3D structure to resist environmental interference (Lobo et al., 2019; Zhang et al., 2022). Microorganisms carry out complex life activities in biofilms; therefore, expounding the interactions between microorganisms in dual-species biofilms is paramount to developing management strategies for dental caries (Flemming et al., 2016). Among the dental plaque of ECC, *S. mutans* was always detected with *C. albicans* that can also produce acids and survive in an acidic environment, implying the important role of *C. albicans* in biofilm-induced caries (Yang et al., 2012). In previous studies, we found that the *rnc*

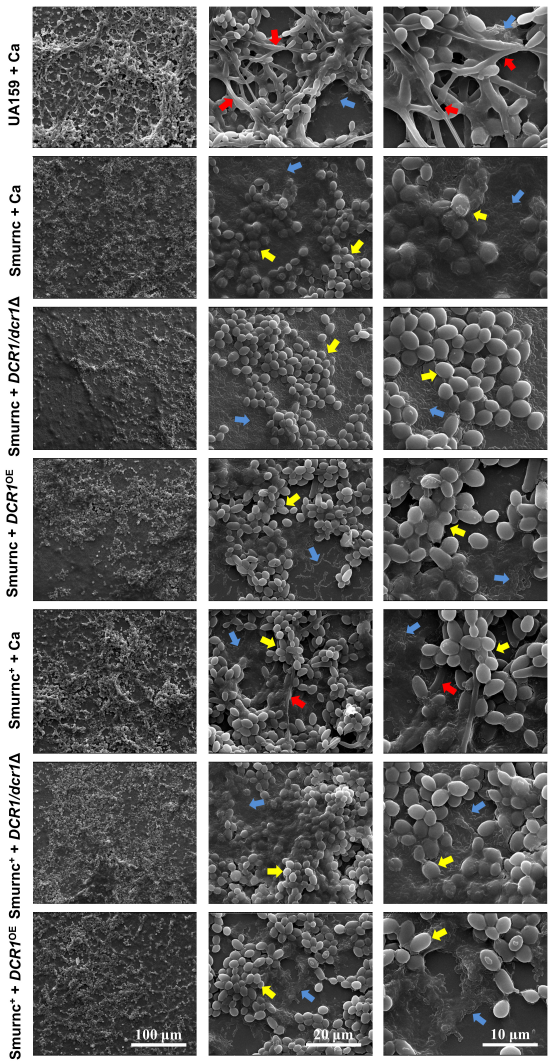

FIGURE 3
The effects of genes coding RNase III on the architecture of cross-kingdom biofilms were observed by SEM. Blue arrows, *S. mutans*; red arrows, *C. albicans* hyphae; yellow arrows, *C. albicans* yeast cells. All images were taken at 1,000 × (scale bar, 100 μm), 5,000 × (scale bar, 20 μm), and 10,000 × (scale bar, 10 μm) magnifications, respectively.

gene was able to promote the synthesis and configuration of EPS, thus amplifying the cariogenicity of *S. mutans* (Lei et al., 2019, 2020; Lu et al., 2021). Here, our study provided new insights that the *rnc* gene of *S. mutans* and the *DCR1* gene of *C. albicans* modulated extracellular polysaccharide synthesis, thus contributing to the cross-kingdom biofilm formation of *S. mutans* and *C. albicans*.

For the first time, we investigated the effects of the essential gene *DCR1* on the biological characteristics of cross-kingdom biofilms. When the *DCR1* expression level was changed, the arrangement of cell clusters in the biofilm was loose, and the 3D structure formed by the cells and matrix was not obvious (**Figures 1A,D**). The transformation of cells from yeast to hyphal type is an important virulence factor of *C. albicans* (Carlisle et al., 2009; Sapaar et al., 2014). *C. albicans* hyphae can express a variety of specific virulence factors such as adhesins and antioxidant defense proteins, which participate in the establishment of biofilm structure and immune escape (Greig et al., 2015; Noble et al., 2017). *C. albicans* was present mostly in the yeast form in biofilms containing *DCR1/dcr1*Δ or $DCR1^{OE}$ (**Figures 1A,D**), congruent with the downregulation of mycelium-related virulence factor genes in *DCR1*-mutant strains (**Supplementary Figure 2**). These results suggest that abnormalities in *DCR1* could change the spatial structure of cross-kingdom biofilms. The roughness of the biofilm surface is conducive to providing a larger area for microbial adhesion and producing surfaces with low shear stress, which can protect the biofilm from elimination (Shen et al., 2015). Nevertheless, we found that the regulatory effect of *DCR1* on biofilm roughness was limited (**Figures 1G,H**).

Extracellular polysaccharides are the main component as well as the vital cariogenic virulence factor of dental plaque biofilms (Koo et al., 2013). *DCR1* regulated the ability of glucan metabolism of microbes but could not affect the biomass and water-insoluble EPS content of biofilms (**Figures 1B,E,F**). In dental plaque, the microbiome can ferment carbohydrates to produce lactic acid, reduce the pH of the biofilm microenvironment, and finally cause demineralization of tooth hard tissue (Valm, 2019; Gabe et al., 2020). From this point of view, *DCR1* overexpression presumably facilitates ECC formation by enhancing acid production (**Figures 1C, 5D**). We conjectured that the gene expression associated with lactic acid production of the $DCR1^{OE}$ mutant may be regulated by siRNAs at the post-transcriptional level (Bernstein et al., 2012). Further studies are still needed to investigate the regulatory effects and underlying mechanisms of *DCR1* on acid production of the cross-kingdom biofilm.

Although low- or over-expression of *DCR1* could downregulate virulence genes related to biofilm formation of *C. albicans*, the water-insoluble EPS content and biomass of cross-kingdom biofilms of *S. mutans* and *C. albicans* did not change when *DCR1* was expressed abnormally, implying that there are likely complex interactions between these two strains to seek advantages and avoid disadvantages, thus forming a micro-ecological environment that is more beneficial to resist external adverse factors (Arnold, 2022). In contrast, *S. mutans* was supposed to play a more pivotal role in regulating the formation of dual-species biofilms.

We further explored the role of *rnc* in the cariogenic characteristics of cross-kingdom biofilms. Biofilms with Smurnc lacked an obvious scaffold structure and had less matrix wrapped around the microbes, revealing that *rnc* assisted in the formation of the extracellular matrix of dual-species biofilms and led to changes in their morphological structure. The EPS layer in biofilms was a manifestation of the defective biofilm,

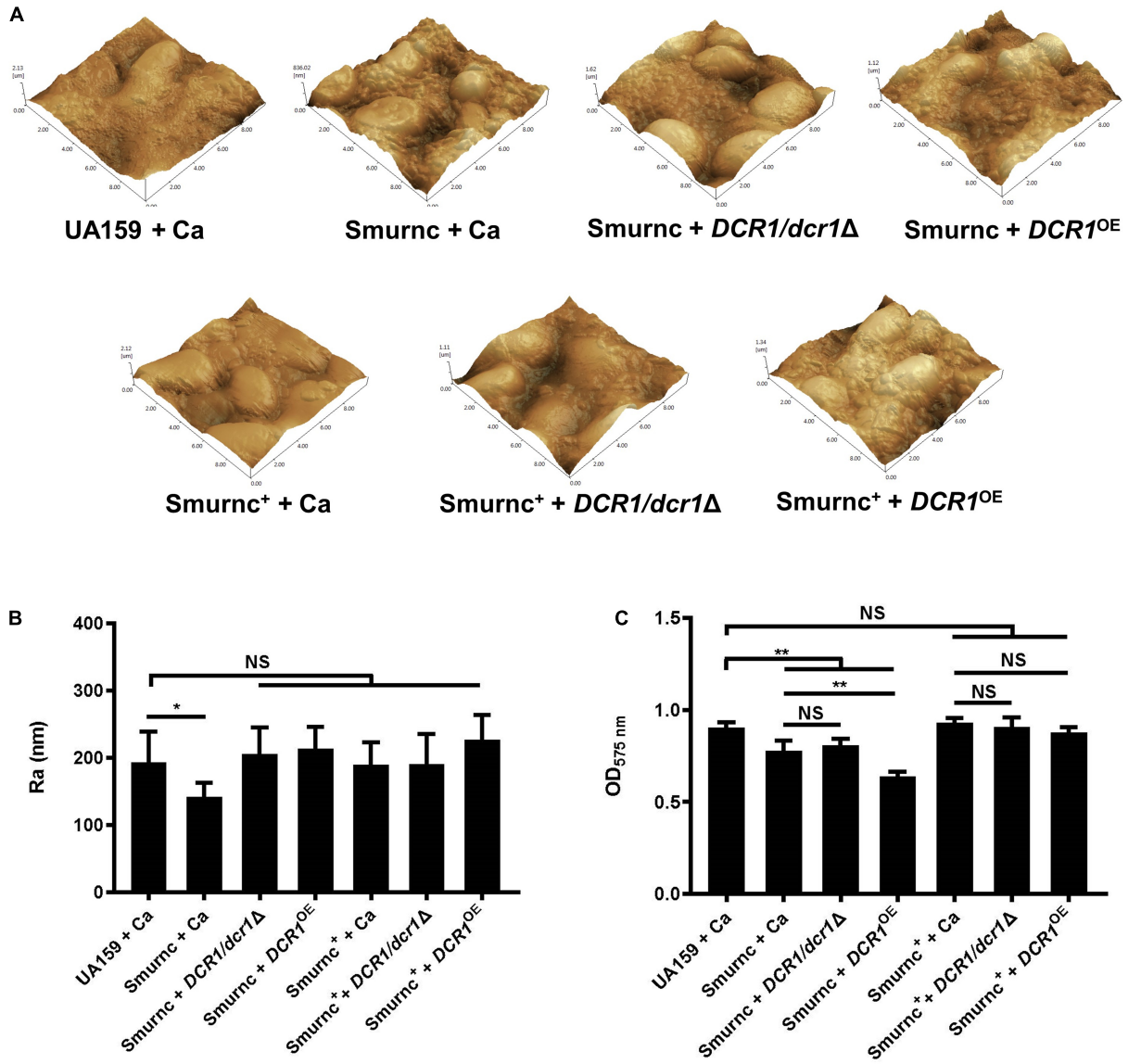

FIGURE 4
The genes coding RNase III modulated the formation and surface characteristics of cross-kingdom biofilms. **(A,B)** Biofilm morphology and surface roughness (Ra) were tested by AFM. **(C)** Biofilm volume was examined by the CV microtiter assay. Experiments were performed in biological triplicate. *$P < 0.05$, **$P < 0.01$.

which was devoid of stereoscopic architecture. Deletion of the *rnc* gene inhibited the EPS metabolism instead of completely eliminating EPS synthesis in *S. mutans*, consistent with the quantitative data detected by the anthrone assay and the visualized images obtained by CLSM. Therefore, *rnc*-deficient *S. mutans* has defective biofilms but still with an EPS layer compared to the UA159 + Ca group (**Figure 3**). When compared to the *DCR1* gene, deficiency of *rnc* could conspicuously restrain extracellular polysaccharide synthesis, decrease surface roughness, and cause attenuated acid production, which diminished the construction of cariogenic dual-species biofilms. Meanwhile, changes induced by the lack of *rnc* possibly impacted *C. albicans* virulence by affecting its biological behavior, such as biofilm formation, which may ultimately repress the cross-kingdom biofilm.

Ndt80, *EFG1*, and *BRG1* are important transcription factors involved in the formation of *C. albicans* biofilms. After the knockout of these genes, *C. albicans* cannot display normal biofilms *in vivo* or *in vitro* (Nobile et al., 2012). β-1,3 glucan is one of the three major components of the *C. albicans* extracellular matrix, and its synthesis pathway involves mainly the *GSC1* gene (glucan synthase catalytic subunit 1), which amplifies biofilm formation and drug resistance by increasing the extracellular matrix (Mitchell et al., 2015). Based on the

10.3389/fmicb.2022.957879

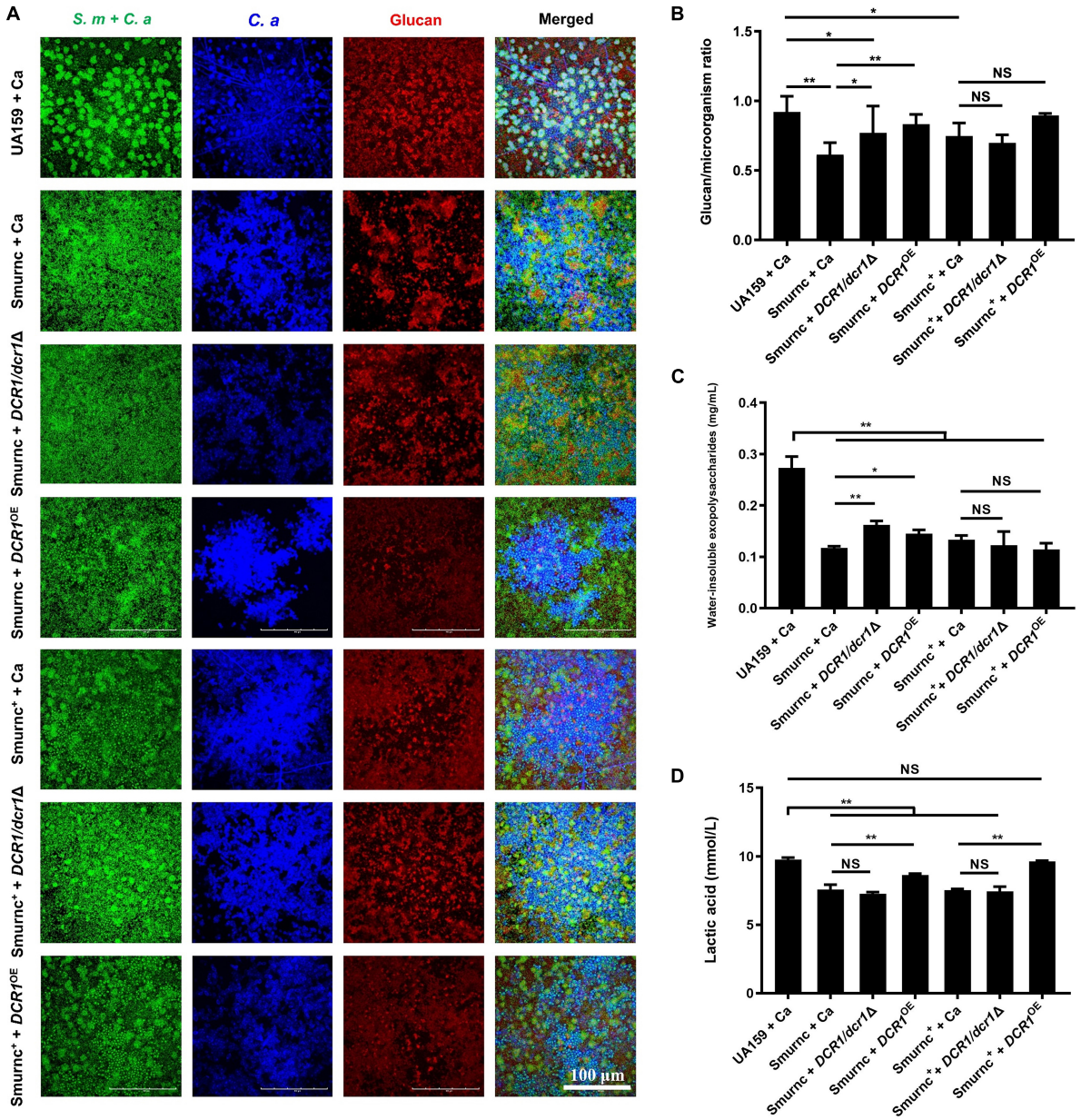

FIGURE 5
The genes coding RNase III regulated the exopolysaccharides synthesis and lactic acid production of cross-kingdom biofilms. **(A,B)** Exopolysaccharide production and distribution in biofilms were visualized by CLSM. Green, total microbes; blue, *C. albicans*; red, glucan and the ratio of exopolysaccharides to microbes was calculated. **(C)** Water-insoluble exopolysaccharides of biofilms were quantified by the anthrone method. **(D)** Lactic acid production was detected by the Lactic Acid Assay Kit. Experiments were performed in biological triplicate. $^{*}P < 0.05$, $^{**}P < 0.01$.

phenotype and gene expression results, we speculated that *rnc* expedited the formation of cross-kingdom biofilms through EPS anabolism and catabolism, also propitious to the growth and the upregulated expression of the virulence genes of *C. albicans*. Related biological activities of *C. albicans*, such as hyphal transformation, glucan synthesis, and biofilm development, could further improve the structure of cross-kingdom biofilms and give full play to biofilm cariogenic properties such as acid production. In this study, we elucidated that *S. mutans* may play a more prominent role in regulating the formation of dual-species biofilms. Therefore, although the virulence- or biofilm-associated genes such as *BRG1*and *EFG1* of *C. albicans* were significantly lower in Smurnc^{+} + Ca than in Smurnc + Ca, Smurnc + Ca might have defective biofilms because of the impaired EPS synthesis and biofilm establishment induced by the absence of *rnc* (Figure 6D). Moreover, the cross-kingdom

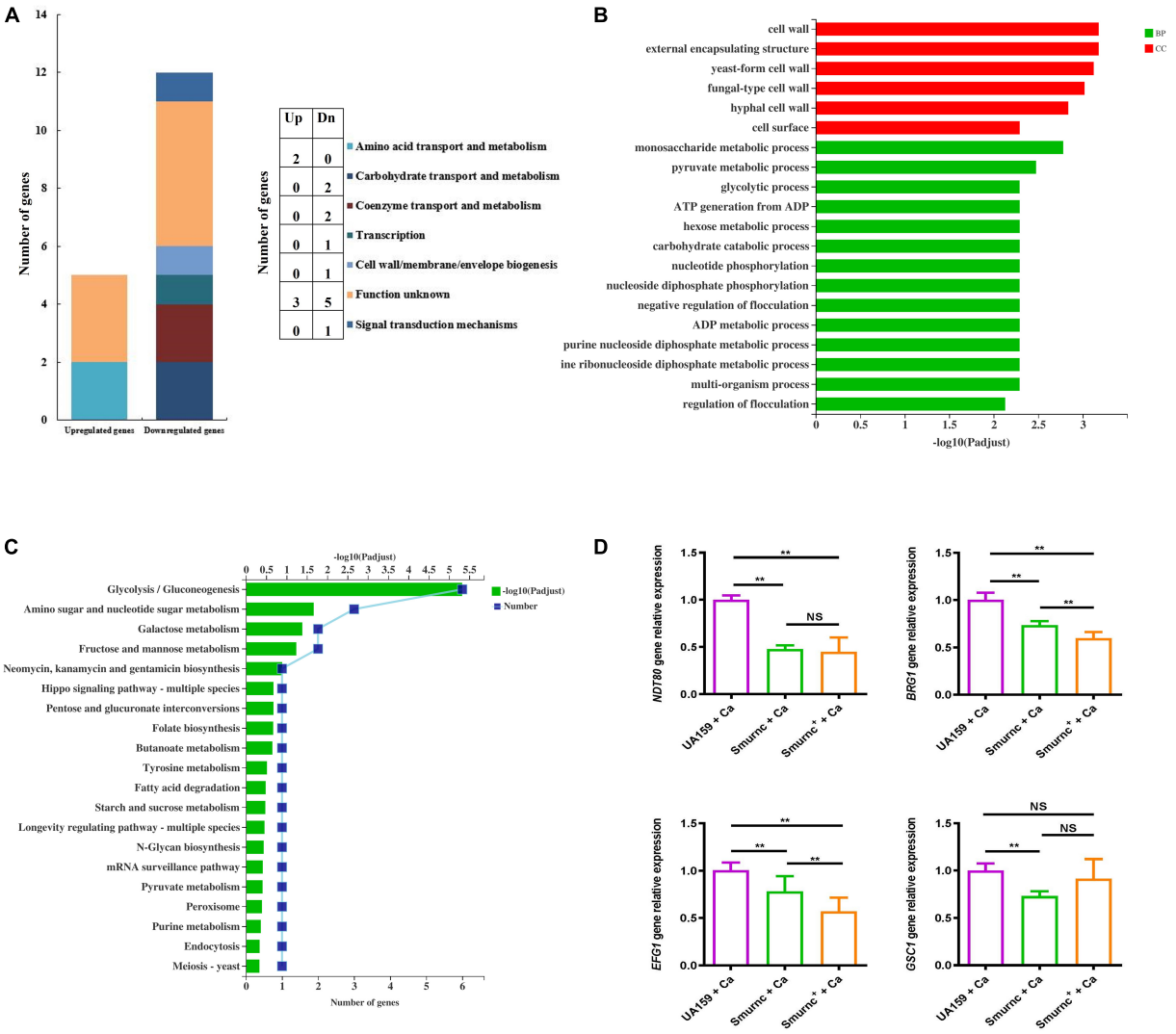

FIGURE 6
rnc gene was associated with the gene expression of virulence factors of *C. albicans*. Transcriptomic analysis of the Smurnc + Ca group compared to the UA159 + Ca group. **(A)** The differently expressed genes were classified by gene annotation based on COG. **(B)** Functional categories and enrichment analysis of differently down-expressed genes based on GO. **(C)** Functional categories and enrichment analysis of differently down-expressed genes based on KEGG. **(D)** The gene transcripts of *C. albicans* in the cross-kingdom biofilms were relatively quantified by RT-qPCR using *ACT1* as a reference gene and interpreted as fold changes based on the UA159 + Ca group. Experiments were performed in biological triplicate. $^{**}P < 0.01$.

biofilm of *S. mutans* and *C. albicans* may be modulated by *C. albicans* virulence genes in addition to *BRG1* and *EFG1*, which need to be further explored.

Transcriptomics helped us clarify the specific molecular mechanism and main pathway by which the *rnc* gene affects *C. albicans* (Motaung et al., 2017). It is possible that the phenotype of different morphological transformations of *C. albicans* in the Smurnc + Ca group was attributed to the downregulation of cell wall-related genes (Figure 6B). The downregulated genes in glycometabolism pathways suggested that the deletion of *rnc* in *S. mutans* possibly impacted the polysaccharide synthesis of *C. albicans* in the cross-kingdom biofilms, leading to the disruption of biofilm formation. Pyruvate metabolism is an important way to generate lactic acid. In the Smurnc + Ca group, the significantly decreased lactic acid production might be associated with the weak acid production capacity of *C. albicans* caused by the downregulation of genes relevant to the pyruvate metabolism pathway.

In conclusion, both RNase III coding genes of *S. mutans* and *C. albicans* can regulate the biological characteristics of the cross-kingdom biofilm. The *rnc* gene of *S. mutans* was able to crucially promote the formation of cross-kingdom biofilms with cariogenic characteristics by affecting the synthesis and metabolism of EPS. At the same time,

changes in the dual-species environment were conducive to hyphal transformation, biofilm formation, polysaccharide metabolism, and pyruvate metabolism in *C. albicans*. The *DCR1* gene of *C. albicans* mainly played a role in improving the biofilm structure and affecting the development of the acidic microecological environment. This research may provide an avenue for exploring new targets for the effective prevention and treatment of ECC.

Data availability statement

The data presented in the study are deposited in the NCBI repository under BioProject accession number PRJNA854798 (https://www.ncbi.nlm.nih.gov/sra/PRJNA854798).

Author contributions

TH, YY, and XW designed the experiments and revised and finalized the manuscript. YL, LL, and YD performed the experiments, analyzed the data, and wrote and finalized the manuscript. HZ and MX contributed to data collection and analysis. All authors contributed to the article and approved the submitted version.

Funding

This study was supported by the National Natural Science Foundation of China (Grant Nos. 31971196 and 82170948) and the Chengdu Key Industry R&D Support Plan Grant (Grant No. 2019-YF05-01090-SN). The funding sources had no role in the study design, data acquisition and analysis, or preparation of the manuscript.

Conflict of interest

The authors declare that the research was conducted in the absence of any commercial or financial relationships that could be construed as a potential conflict of interest.

Publisher's note

All claims expressed in this article are solely those of the authors and do not necessarily represent those of their affiliated organizations, or those of the publisher, the editors and the reviewers. Any product that may be evaluated in this article, or claim that may be made by its manufacturer, is not guaranteed or endorsed by the publisher.

Supplementary material

The Supplementary Material for this article can be found online at: https://www.frontiersin.org/articles/10.3389/fmicb.2022.957879/full#supplementary-material

References

Arnold, A. E. (2022). Bacterial-fungal interactions: Bacteria take up residence in the house that Fungi built. *Curr. Biol.* 32, R327–R328. doi: 10.1016/j.cub.2022.02.024

Basso, V., Znaidi, S., Lagage, V., Cabral, V., Schoenherr, F., LeibundGut-Landmann, S., et al. (2017). The two-component response regulator Skn7 belongs to a network of transcription factors regulating morphogenesis in Candida albicans and independently limits morphogenesis-induced ROS accumulation. *Mol. Microbiol.* 106, 157–182. doi: 10.1111/mmi.13758

Bernstein, D. A., Vyas, V. K., Weinberg, D. E., Drinnenberg, I. A., Bartel, D. P., and Fink, G. R. (2012). Candida albicans Dicer (CaDcr1) is required for efficient ribosomal and spliceosomal RNA maturation. *Proc. Natl. Acad. Sci. U.S.A.* 109, 523–528. doi: 10.1073/pnas.1118859109

Care, R. S., Trevethick, J., Binley, K. M., and Sudbery, P. E. (1999). The MET3 promoter: A new tool for Candida albicans molecular genetics. *Mol. Microbiol.* 34, 792–798. doi: 10.1046/j.1365-2958.1999.01641.x

Carlisle, P. L., Banerjee, M., Lazzell, A., Monteagudo, C., Lopez-Ribot, J. L., and Kadosh, D. (2009). Expression levels of a filament-specific transcriptional regulator are sufficient to determine Candida albicans morphology and virulence. *Proc. Natl. Acad. Sci. U.S.A.* 106, 599–604. doi: 10.1073/pnas.0804061106

Chen, H., Zhang, B., Weir, M. D., Homayounfar, N., Fay, G. G., Martinho, F., et al. (2020). S. mutans gene-modification and antibacterial resin composite as dual strategy to suppress biofilm acid production and inhibit caries. *J. Dent.* 93:103278. doi: 10.1016/j.jdent.2020.103278

Deng, Y., Yang, Y., Zhang, B., Chen, H., Lu, Y., Ren, S., et al. (2021). The vicK gene of Streptococcus mutans mediates its cariogenicity via exopolysaccharides metabolism. *Int. J. Oral. Sci.* 13:45. doi: 10.1038/s41368-021-00149-x

Drinnenberg, I. A., Weinberg, D. E., Xie, K. T., Mower, J. P., Wolfe, K. H., Fink, G. R., et al. (2009). RNAi in budding yeast. *Science* 326, 544–550. doi: 10.1126/science.1176945

Duan, S., Li, M., Zhao, J., Yang, H., He, J., Lei, L., et al. (2021). A predictive nomogram: A cross-sectional study on a simple-to-use model for screening 12-year-old children for severe caries in middle schools. *BMC Oral. Health* 21:457. doi: 10.1186/s12903-021-01819-2

Ellepola, K., Truong, T., Liu, Y., Lin, Q., Lim, T. K., Lee, Y. M., et al. (2019). Multi-omics Analyses Reveal Synergistic Carbohydrate Metabolism in Streptococcus mutans-Candida albicans Mixed-Species Biofilms. *Infect. Immun.* 87:e00339–19. doi: 10.1128/IAI.00339-19

Flemming, H. C., Wingender, J., Szewzyk, U., Steinberg, P., Rice, S. A., and Kjelleberg, S. (2016). Biofilms: An emergent form of bacterial life. *Nat. Rev. Microbiol.* 14, 563–575. doi: 10.1038/nrmicro.2016.94

Fonzi, W. A., and Irwin, M. Y. (1993). Isogenic strain construction and gene mapping in Candida albicans. *Genetics* 134, 717–728. doi: 10.1093/genetics/134.3.717

Gabe, V., Zeidan, M., Kacergius, T., Bratchikov, M., Falah, M., and Rayan, A. (2020). Lauryl Gallate Activity and Streptococcus mutans: Its Effects on Biofilm

Formation, Acidogenicity and Gene Expression. *Molecules* 25:3685. doi: 10.3390/molecules25163685

Greig, J. A., Sudbery, I. M., Richardson, J. P., Naglik, J. R., Wang, Y., and Sudbery, P. E. (2015). Cell cycle-independent phospho-regulation of Fkh2 during hyphal growth regulates Candida albicans pathogenesis. *PLoS Pathog.* 11:e1004630. doi: 10.1371/journal.ppat.1004630

He, J., Kim, D., Zhou, X., Ahn, S. J., Burne, R. A., Richards, V. P., et al. (2017). RNA-Seq Reveals Enhanced Sugar Metabolism in Streptococcus mutans Co-cultured with Candida albicans within Mixed-Species Biofilms. *Front. Microbiol.* 8:1036. doi: 10.3389/fmicb.2017.01036

Hwang, G., Liu, Y., Kim, D., Li, Y., Krysan, D. J., and Koo, H. (2017). Candida albicans mannans mediate Streptococcus mutans exoenzyme GtfB binding to modulate cross-kingdom biofilm development in vivo. *PLoS Pathog.* 13:e1006407. doi: 10.1371/journal.ppat.1006407

James, S. L., Abate, D., Abate, K. H., Abay, S. M., Abbafati, C., Abbasi, N., et al. (2018). Global, regional, and national incidence, prevalence, and years lived with disability for 354 diseases and injuries for 195 countries and territories, 1990–2017: A systematic analysis for the Global Burden of Disease Study 2017. *Lancet* 392, 1789–1858. doi: 10.1016/s0140-6736(18)32279-7

Janik, A., Niewiadomska, M., Perlinska-Lenart, U., Lenart, J., Kolakowski, D., Skorupinska-Tudek, K., et al. (2019). Inhibition of Dephosphorylation of Dolichyl Diphosphate Alters the Synthesis of Dolichol and Hinders Protein N-Glycosylation and Morphological Transitions in Candida albicans. *Int. J. Mol. Sci.* 20:5067. doi: 10.3390/ijms20205067

Jia, X. M., Wang, Y., Zhang, J. D., Tan, H. Y., Jiang, Y. Y., and Gu, J. (2011). CaIPF14030 negatively modulates intracellular ATP levels during the development of azole resistance in Candida albicans. *Acta Pharmacol. Sin.* 32, 512–518. doi: 10.1038/aps.2010.232

Khoury, Z. H., Vila, T., Puthran, T. R., Sultan, A. S., Montelongo-Jauregui, D., Melo, M. A. S., et al. (2020). The Role of Candida albicans Secreted Polysaccharides in Augmenting Streptococcus mutans Adherence and Mixed Biofilm Formation: In vitro and in vivo Studies. *Front. Microbiol.* 11:307. doi: 10.3389/fmicb.2020.00307

Kim, D., Liu, Y., Benhamou, R. I., Sanchez, H., Simon-Soro, A., Li, Y., et al. (2018). Bacterial-derived exopolysaccharides enhance antifungal drug tolerance in a cross-kingdom oral biofilm. *ISME J.* 12, 1427–1442. doi: 10.1038/s41396-018-0113-1

Koo, H., Allan, R. N., Howlin, R. P., Stoodley, P., and Hall-Stoodley, L. (2017). Targeting microbial biofilms: Current and prospective therapeutic strategies. *Nat. Rev. Microbiol.* 15, 740–755. doi: 10.1038/nrmicro.2017.99

Koo, H., Falsetta, M. L., and Klein, M. I. (2013). The exopolysaccharide matrix: A virulence determinant of cariogenic biofilm. *J. Dent. Res.* 92, 1065–1073. doi: 10.1177/0022034513504218

Lau, P. C., Sung, C. K., Lee, J. H., Morrison, D. A., and Cvitkovitch, D. G. (2002). PCR ligation mutagenesis in transformable streptococci: Application and efficiency. *J. Microbiol. Methods* 49, 193–205. doi: 10.1016/s0167-7012(01)00369-4

Lei, L., Stipp, R. N., Chen, T., Wu, S. Z., Hu, T., and Duncan, M. J. (2018). Activity of Streptococcus mutans VicR Is Modulated by Antisense RNA. *J. Dent. Res.* 97, 1477–1484. doi: 10.1177/0022034518781765

Lei, L., Yang, Y., Yang, Y., Wu, S., Ma, X., Mao, M., et al. (2019). Mechanisms by Which Small RNAs Affect Bacterial Activity. *J. Dent. Res.* 98, 1315–1323. doi: 10.1177/0022034519876898

Lei, L., Zhang, B., Mao, M., Chen, H., Wu, S., Deng, Y., et al. (2020). Carbohydrate Metabolism Regulated by Antisense vicR RNA in Cariogenicity. *J. Dent. Res.* 99, 204–213. doi: 10.1177/0022034519890570

Lemos, J. A., Palmer, S. R., Zeng, L., Wen, Z. T., Kajfasz, J. K., Freires, I. A., et al. (2019). The Biology of Streptococcus mutans. *Microbiol. Spectr.* 7:10.1128/microbiolspec.GPP3-0051-2018. doi: 10.1128/microbiolspec.GPP3-0051-2018

Liu, S., Qiu, W., Zhang, K., Zhou, X., Ren, B., He, J., et al. (2017). Nicotine Enhances Interspecies Relationship between Streptococcus mutans and Candida albicans. *Biomed. Res. Int.* 2017:7953920. doi: 10.1155/2017/7953920

Lobo, C. I. V., Rinaldi, T. B., Christiano, C. M. S., De Sales Leite, L., Barbugli, P. A., and Klein, M. I. (2019). Dual-species biofilms of Streptococcus mutans and Candida albicans exhibit more biomass and are mutually beneficial compared with single-species biofilms. *J. Oral. Microbiol.* 11:1581520. doi: 10.1080/20002297.2019.1581520

Lu, Y., Zhang, H., Li, M., Mao, M., Song, J., Deng, Y., et al. (2021). The rnc Gene Regulates the Microstructure of Exopolysaccharide in the Biofilm of Streptococcus mutans through the beta-Monosaccharides. *Caries Res.* 55, 534–545. doi: 10.1159/000518462

Mao, Y., Kalb, V. F., and Wong, B. (1999). Overexpression of a dominant-negative allele of SEC4 inhibits growth and protein secretion in Candida albicans. *J. Bacteriol.* 181, 7235–7242. doi: 10.1128/JB.181.23.7235-7242.1999

Mitchell, K. F., Zarnowski, R., Sanchez, H., Edward, J. A., Reinicke, E. L., Nett, J. E., et al. (2015). Community participation in biofilm matrix assembly and function. *Proc. Natl. Acad. Sci. U.S.A.* 112, 4092–4097. doi: 10.1073/pnas.1421437112

Motaung, T. E., Ells, R., Pohl, C. H., Albertyn, J., and Tsilo, T. J. (2017). Genome-wide functional analysis in Candida albicans. *Virulence* 8, 1563–1579. doi: 10.1080/21505594.2017.1292198

Mustafa, M., Alamri, H. M., Almokhatieb, A. A., Alqahtani, A. R., Alayad, A. S., and Divakar, D. D. (2022). Effectiveness of antimicrobial photodynamic therapy as an adjunct to mechanical instrumentation in reducing counts of Enterococcus faecalis and Candida albicans from C-shaped root canals. *Photodermatol. Photoimmunol. Photomed.* 38, 328–333. doi: 10.1111/phpp.12751

Nobile, C. J., Fox, E. P., Nett, J. E., Sorrells, T. R., Mitrovich, Q. M., Hernday, A. D., et al. (2012). A recently evolved transcriptional network controls biofilm development in Candida albicans. *Cell* 148, 126–138. doi: 10.1016/j.cell.2011.10.048

Noble, S. M., Gianetti, B. A., and Witchley, J. N. (2017). Candida albicans cell-type switching and functional plasticity in the mammalian host. *Nat. Rev. Microbiol.* 15, 96–108. doi: 10.1038/nrmicro.2016.157

Peres, M. A., Macpherson, L. M. D., Weyant, R. J., Daly, B., Venturelli, R., Mathur, M. R., et al. (2019). Oral diseases: A global public health challenge. *Lancet* 394, 249–260. doi: 10.1016/s0140-6736(19)31146-8

Ponde, N. O., Lortal, L., Ramage, G., Naglik, J. R., and Richardson, J. P. (2021). Candida albicans biofilms and polymicrobial interactions. *Crit. Rev. Microbiol.* 47, 91–111. doi: 10.1080/1040841X.2020.1843400

Punjabi, V., Patel, S., Pathak, J., and Swain, N. (2020). Comparative evaluation of staining efficacy of calcofluor white and acridine orange for detection of Candida species using fluorescence microscopy - A prospective microbiological study. *J. Oral. Maxillofac. Pathol.* 24, 81–86. doi: 10.4103/jomfp.JOMFP_315_18

Ramadugu, K., Bhaumik, D., Luo, T., Gicquelais, R. E., Lee, K. H., Stafford, E. B., et al. (2021). Maternal Oral Health Influences Infant Salivary Microbiome. *J. Dent. Res.* 100, 58–65. doi: 10.1177/0022034520947665

Sapaar, B., Nur, A., Hirota, K., Yumoto, H., Murakami, K., Amoh, T., et al. (2014). Effects of extracellular DNA from Candida albicans and pneumonia-related pathogens on Candida biofilm formation and hyphal transformation. *J. Appl. Microbiol.* 116, 1531–1542. doi: 10.1111/jam.12483

Shen, Y., Monroy, G. L., Derlon, N., Janjaroen, D., Huang, C., Morgenroth, E., et al. (2015). Role of biofilm roughness and hydrodynamic conditions in *Legionella pneumophila* adhesion to and detachment from simulated drinking water biofilms. *Environ. Sci. Technol.* 49, 4274–4282. doi: 10.1021/es505842v

Svensson, S. L., and Sharma, C. M. (2021). RNase III-mediated processing of a trans-acting bacterial sRNA and its cis-encoded antagonist. *elife* 10:e69064. doi: 10.7554/eLife.69064

Sztajer, H., Szafranski, S. P., Tomasch, J., Reck, M., Nimtz, M., Rohde, M., et al. (2014). Cross-feeding and interkingdom communication in dual-species biofilms of Streptococcus mutans and Candida albicans. *ISME J.* 8, 2256–2271. doi: 10.1038/ismej.2014.73

Valm, A. M. (2019). The Structure of Dental Plaque Microbial Communities in the Transition from Health to Dental Caries and Periodontal Disease. *J. Mol. Biol.* 431, 2957–2969. doi: 10.1016/j.jmb.2019.05.016

Wen, Z. T., Nguyen, A. H., Bitoun, J. P., Abranches, J., Baker, H. V., and Burne, R. A. (2011). Transcriptome analysis of LuxS-deficient Streptococcus mutans grown in biofilms. *Mol. Oral. Microbiol.* 26, 2–18. doi: 10.1111/j.2041-1014.2010.00581.x

Xiao, J., Grier, A., Faustoferri, R. C., Alzoubi, S., Gill, A. L., Feng, C., et al. (2018a). Association between Oral Candida and Bacteriome in Children with Severe ECC. *J. Dent. Res.* 97, 1468–1476. doi: 10.1177/0022034518790941

Xiao, J., Huang, X., Alkhers, N., Alzamil, H., Alzoubi, S., Wu, T. T., et al. (2018b). Candida albicans and Early Childhood Caries: A Systematic Review and Meta-Analysis. *Caries Res.* 52, 102–112. doi: 10.1159/000481833

Yang, X. Q., Zhang, Q., Lu, L. Y., Yang, R., Liu, Y., and Zou, J. (2012). Genotypic distribution of Candida albicans in dental biofilm of Chinese children associated with severe early childhood caries. *Arch. Oral. Biol.* 57, 1048–1053. doi: 10.1016/j.archoralbio.2012.05.012

Yang, Y., Mao, M., Lei, L., Li, M., Yin, J., Ma, X., et al. (2019). Regulation of water-soluble glucan synthesis by the Streptococcus mutans dexA gene effects biofilm aggregation and cariogenic pathogenicity. *Mol. Oral. Microbiol.* 34, 51–63. doi: 10.1111/omi.12253

Zhang, H., Xia, M., Zhang, B., Zhang, Y., Chen, H., Deng, Y., et al. (2022). Sucrose selectively regulates Streptococcus mutans polysaccharide by GcrR. *Environ. Microbiol.* 24, 1395–1410. doi: 10.1111/1462-2920.15887

Zhang, R., Wang, H., Tian, Y. Y., Yu, X., Hu, T., and Dummer, P. M. (2011a). Use of cone-beam computed tomography to evaluate root and canal morphology of mandibular molars in Chinese individuals. *Int. Endod. J.* 44, 990–999. doi: 10.1111/j.1365-2591.2011.01904.x

Zhang, R., Yang, H., Yu, X., Wang, H., Hu, T., and Dummer, P. M. (2011b). Use of CBCT to identify the morphology of maxillary permanent molar teeth in a Chinese subpopulation. *Int. Endod. J.* 44, 162–169. doi: 10.1111/j.1365-2591.2010.01826.x

Znaidi, S., van Wijlick, L., Hernandez-Cervantes, A., Sertour, N., Desseyn, J. L., Vincent, F., et al. (2018). Systematic gene overexpression in Candida albicans identifies a regulator of early adaptation to the mammalian gut. *Cell. Microbiol.* 20:e12890. doi: 10.1111/cmi.12890

frontiers | Frontiers in Microbiology

TYPE Original Research
PUBLISHED 01 November 2022
DOI 10.3389/fmicb.2022.1003692

OPEN ACCESS

EDITED BY
Huancai Lin,
Sun Yat-sen University, China

REVIEWED BY
Adline Princy Solomon,
SASTRA University,
India
Khristina Judan Cruz,
Central Luzon State University, Philippines
Krassimira Hristova,
Marquette University,
United States

*CORRESPONDENCE
Ji-Yu Zhang
infzjy@sina.com

SPECIALTY SECTION
This article was submitted to Antimicrobials, Resistance and Chemotherapy, a section of the journal Frontiers in Microbiology

RECEIVED 26 July 2022
ACCEPTED 14 October 2022
PUBLISHED 01 November 2022

CITATION
Bai Y-B, Shi M-Y, Wang W-W, Wu L-Y, Bai Y-T, Li B, Zhou X-Z and Zhang J-Y (2022) Novel quorum sensing inhibitor Echinatin as an antibacterial synergist against *Escherichia coli*. *Front. Microbiol.* 13:1003692. doi: 10.3389/fmicb.2022.1003692

Novel quorum sensing inhibitor Echinatin as an antibacterial synergist against *Escherichia coli*

Yu-Bin Bai[1,2,3], Meng-Yan Shi[1,2,3], Wei-Wei Wang[1,2,3], Ling-Yu Wu[1,2,3], Yu-Ting Bai[1,2,3], Bing Li[1,2,3], Xu-Zheng Zhou[1,2,3] and Ji-Yu Zhang[1,2,3]*

[1]Key Laboratory of New Animal Drug Project of Gansu Province, Lanzhou, China, [2]Key Laboratory of Veterinary Pharmaceutical Development, Ministry of Agriculture, Lanzhou, China, [3]Lanzhou Institute of Husbandry and Pharmaceutical Sciences, Chinese Academy of Agricultural Sciences, Lanzhou, China

A new antibacterial strategy based on inhibiting bacterial quorum sensing (QS) has emerged as a promising method of attenuating bacterial pathogenicity and preventing bacterial resistance to antibiotics. In this study, we screened Echinatin (Ech) with high-efficiency anti-QS from 13 flavonoids through the AI-2 bioluminescence assay. Additionally, crystal violet (CV) staining combined with confocal laser scanning microscopy (CLSM) was used to evaluate the effect of anti-biofilm against *Escherichia coli (E. coli)*. Further, the antibacterial synergistic effect of Ech and marketed antibiotics were measured by broth dilution and Alamar Blue Assay. It was found that Ech interfered with the phenotype of QS, including biofilm formation, exopolysaccharide (*EPS*) production, and motility, without affecting bacterial growth and metabolic activity. Moreover, qRT-PCR exhibited that Ech significantly reduced the expression of QS-regulated genes (*luxS*, *pfs*, *lsrB*, *lsrK*, *lsrR*, *flhC*, *flhD*, *fliC*, *csgD*, and *stx2*). More important, Ech with currently marketed colistin antibiotics (including colistin B and colistin E) showed significantly synergistically increased antibacterial activity in overcoming antibiotic resistance of *E. coli*. In summary, these results suggested the potent anti-QS and novel antibacterial synergist candidate of Ech for treating *E. coli* infections.

KEYWORDS

***Escherichia coli*, quorum sensing, inhibitor, Echinatin, biofilm, *EPS*, motility, antibacterial synergist**

Introduction

As one of the pathogenically versatile bacterial organisms, *E. coli* can cause various infections, including diarrhea, urinary tract infections, sepsis, and hemolytic-uremic syndrome (Riley, 2020). Pathogenic *E. coli* causes great economic losses to animal and poultry industries, as well as a serious threat to human health. For example, millions of dollars are lost each year due to Avian pathogenic *E. coli* (APEC) infections (Lutful Kabir, 2010). In the United States, *E. coli* O157:H7 is estimated to cause 95,000 illnesses a year

(Scallan et al., 2011; Beshearse et al., 2021), and Shiga-producing *E. coli* (STEC) causes 5,960 infections annually (Hale et al., 2012). Antimicrobial resistance has become a worldwide concern and an increasing threat to human and animal health (Hawkey, 2008). Currently, most antibacterial compounds target the basic physiological processes of bacteria, which increases the likelihood of bacteria developing resistance to multiple drugs (Munguia and Nizet, 2017). Thus, new therapeutic strategies are urgently needed for treating multidrug-resistant pathogen infections.

At present, alternative approaches to antimicrobial therapy have focused on inhibiting the virulence factors of bacterial pathogens (Dickey et al., 2017; Buroni and Chiarelli, 2020; Loubet et al., 2020; Piewngam et al., 2020; Silva et al., 2020). QS is a cellular mechanism mediated by autoinducers, which allows bacteria to organize behavior depending on their density (Ng and Bassler, 2009). Interference with QS systems does not exert selection pressure on bacteria compared with antibiotics thus reducing the emergence and spread of resistant mutants (Sully et al., 2014; Quave et al., 2015; Ning et al., 2021). QS is a process that involves bacteria communicating with signaling molecules called autoinducers (AIs). There are several types of AI molecules, including diffusible signaling factors (DSFs), autoinducer-2 (AI-2), indole, and Acyl-homoserine lactones (AHLs, AI-1), etc. (Guo et al., 2013; Whiteley et al., 2017, 2018). QS systems function based on cell density, which increases the concentration of AI as cell density increases. Upon reaching a certain level of concentration of AI, signaling is activated that modulates the expression of genes related to bacterial physiology, biofilm formation, motility, and virulence (Papenfort and Bassler, 2016). Antibacterial strategies based on inhibiting bacterial QS have emerged as a new promising method of preventing bacterial resistance to antibiotics, as well as inhibiting the expression of virulence factors (Manner and Fallarero, 2018; Wang et al., 2019; Minich et al., 2022).

AI-2 has been considered to be a "universal" signaling molecule involved in bacterial communication at the inter-and intra-species level, which is widely found in Gram-negative and Gram-positive bacteria. For most bacteria, the regulatory function of the AI-2 QS system is mainly reflected in four aspects, including bacterial virulence, biofilm, motility, and other functions (Bassler, 2002; Sturme et al., 2002; Reading and Sperandio, 2006; Choudhary and Schmidt-Dannert, 2010). For example, AI-2 could influence the production of virulence factors and the formation of biofilm in *E. coli*, *Salmonella*, and *S. suis* (Kendall et al., 2007; Ju et al., 2018; Sun et al., 2020; Li et al., 2021). The inhibition of AI-2 can effectively reduce bacterial virulence, biofilm formation, and bacterial resistance, which can be used to replace antibiotics. In this context, it's reported that plant-derived compounds with diverse structures have been widely investigated as AI-2 QS inhibitors (Karnjana et al., 2020; Li et al., 2021; Meng et al., 2022). Ech, a flavonoid isolated from glycyrrhiza, had antioxidant, antitumor, anti-virus, and other biological activities (Ji et al., 2016; Zhu et al., 2018; Kwak et al., 2019; Hu et al., 2021; Ran et al., 2021). Despite many pharmacologic investigations, there have been no reports on the anti-QS activity of Ech.

AI-2 bioluminescence assay (*Vibrio harveyi* (*V. harveyi*) BB170 bioluminescence assay) is the most commonly used method to detect AI-2 signal molecules. The bioluminescence reporter strain *V. harveyi* BB170 (luxN:: Tn5) is a mutant strain, whose fluorescence is only regulated by AI-2 signal molecule (Bassler et al., 1994, 1997; Surette et al., 1999). Therefore, the inhibitory effect of the inhibitors on *E. coli* AI-2 production can be judged by the intensity of *V. harveyi* bioluminescence. Here, based on *V. harveyi* BB170 bioluminescence assay, 13 natural product compounds that inhibit AI-2 production were screened and evaluated. Notably, we found that one of the compounds, Ech, effectively blocks *E. coli* QS. Furthermore, the study examined the antibiofilm and antivirulence properties of Ech against *E. coli* and evaluated the synergistic effects of combining Ech with antibiotics.

Materials and methods

Natural product compounds

Echinatin, Aloeemodin, Loureirin B, Cardamonin, Cynaroside, Artemetin, Neosperidin dihydrochalcone, Hesperetin, and Vitexin used in the study were obtained from Shanghai Yuanye Bio-Technology Co., Ltd. (Shanghai, China). Phloretin was purchased from Macklin Inc. (Shanghai, China). Scutellarin and Acacetin were obtained from MCE (Shanghai, China). Gentisin was obtained from ChemFaces (Wuhan, China). Dimethylsulfoxide (DMSO, Sigma) was used to dissolve all compounds to the concentration of 40 mM.

Bacterial strains and cells

Escherichia coli O157:H7 (ATCC 43895) was purchased from Beina Chuanglian Biotechnology Research Institute (Beijing, China). Clinical strains *E. coli* O101、*E. coli* C83654、*E. coli* O149、*E. coli* XJ24、*E. coli* KD-13-1 were isolated and maintained in our laboratory. Luria-Bertani (LB, HuanKai Microbial, Guangdong, China) and Luria-Bertani agar (LA, HuanKai Microbial, Guangdong, China) medium were used to cultivate all *E. coli* strains. *V. harveyi* BB170 and *V. harveyi* BB152 were kindly provided by Researcher Han Xiangan (Shanghai Veterinary Research Institute, Chinese Academy of Agricultural Sciences). AB medium supplemented with 1 mM L-arginine, 1% glycerol, and 10 mM Phosphate buffer (pH = 7.2) for culturing *V. harveyi*.

Caco-2 cell lines were obtained from ATCC and cultured under standard conditions containing MEM medium (Gibco, Grand Island, NY, United States) supplemented with 20% FBS (Gibco, Grand Island, NY, USA), 1% non-essential amino acids (Gibco, Grand Island, NY, USA), 10 mM HEPES (Solarbio, Beijing, China), 1 mM L-glutamine (Gibco, Grand Island, NY,

USA), and 1 mM sodium pyruvate (Gibco, Grand Island, NY, United States).

Anti-QS inhibitor screening

AI-2 bioluminescence assay was used to screen QS inhibitors as described previously (Bassler et al., 1994; Taga and Xavier, 2011) with minor modifications. Briefly, *E. coli* O157:H7 was cultured for 16 h with 50 μM of natural product compounds and centrifuged at 12000 × g for 5 min. Cell-free supernatant was collected in a 0.22 μm filter. The bioluminescence reporter strain *V. harveyi* BB170 grew in AB medium to 1.0 ~ 1.1 of OD_{600nm} at 30°C under shaking and then diluted at 1:2500 with fresh AB medium. Twenty micro liter of cell-free supernatant mixed with 180 μl of *V. harveyi* BB170 culture in black 96-well plates (Jingan, Shanghai, China) and incubated for 3.5 h at 30°C in the dark. A multipurpose microplate reader (Enspire; PerkinElmer, USA) was used to measure bioluminescence. Cell-free supernatants of *V. harveyi* BB152 overnight cultures were used as control. Further study was conducted on the compound with the highest AI-2 inhibition. We also determined the IC50 for AI-2 inhibition with the selected compound with the same procedure described above.

Cytotoxicity

Ech's toxicity was evaluated in Caco-2 cells using the CCK-8 assay. Caco-2 cells (10^5 cells/mL) were plated in a 96-well plate with 5% CO_2 for 24 h at 37°C. The culture medium was then replaced by different concentrations of Ech (6.25, 12.5, 25, 50, 100, 200, 400 μM) for 24 h. After incubation, the plate was incubated at 37°C for an additional hour with 10 μl of CCK-8 (MCE, China). The absorbance was measured at 450 nm using Multiskan Go Reader (Thermo Fisher Scientific, United States).

Growth and metabolic activity

As described previously, the growth ability of *E. coli* was studied by the broth dilution method (CLSI, 2018; Swetha et al., 2019). In brief, *E. coli* O157:H7 bacterial suspension (OD_{600} = 0.01) with various concentration of Ech (6.25, 12.5, 25, 50, 100, 200 μM) was seeded into 96-well plate and incubated for 24 h at 37°C. The Multiskan Go Reader (Thermo Fisher Scientific, United States) was used to measure the absorbance at 600 nm.

Metabolic activity was measured with an Alamar Blue assay (Swetha et al., 2019). *E. coli* O157:H7 bacterial suspension (OD_{600} = 0.01) with various concentrations of Ech (6.25, 12.5, 25, 50, 100, 200 μM) was seeded into 12-well plate and incubated for 24 h at 37°C. Cells from each well were harvested at 10000 × g for 5 min and then washed twice using PBS (pH = 7.2). Metabolic activity was measured using Alamar Blue assay according to the manufacturer's prescribed protocol (Invitrogen™, Thermo Fisher Scientific, USA). PBS containing only AB dye was considered a blank. The metabolic activity was calculated based on the absorbance at 570 nm and 600 nm using the following formula (Swetha et al., 2019):

$$\textbf{Metabolic activity}(\%) = \frac{\left(\begin{array}{l}\left(E_{oxi(OD570)} \times T_{OD570}\right)\\ -\left(E_{oxi(OD600)} \times T_{OD600}\right)\end{array}\right)}{\left(\begin{array}{l}\left(E_{red(OD570)} \times B_{OD570}\right)\\ -\left(E_{red(OD600)} \times B_{OD600}\right)\end{array}\right)} \times 100\%$$

Eoxi (OD570) – extinction coefficient in oxidized form of AB at 570 nm = 80,586;

Ered (OD570) – extinction coefficient in reduced form of AB at 570 nm = 155,677;

Eoxi (OD600) – extinction coefficient in oxidized form of AB at 600 nm = 117,216;

Ered (OD600) – extinction coefficient in reduced form of AB at 570 nm = 14,652;

B-blank; T-samples.

Biofilm assay

CV staining

The formation of biofilms was assessed using CV staining based on previous study (O'Toole, 2011) with slight modification. In brief, *E. coli* O157:H7 bacterial suspension (OD_{600} = 0.01) was cultured in LB medium at the various concentrations of Ech (6.25, 12.5, 25, 50, 100, 200 μM) in a 96-well plate (Corning Costar® 3,599, Corning, NY, United States) for 24 h at 37°C. The plate was washed three times with PBS (pH = 7.2) and then fixed for 1 h at 60°C. Methanol was used to fix the cells and 0.1% CV was used to stain them for 30 min. Next, the CV was rinsed with distilled water and dried under heat. Finally, the CV attached to wells was dissolved in 95% ethanol and then measured the absorbance at 570 nm using Multiskan Go Reader (Thermo Fisher Scientific, United States).

Confocal laser scanning microscopy

Biofilm formation of *E. coli* was determined using CLSM according to previous study (Zhang et al., 2020) with slight modification. In brief, *E. coli* O157:H7 bacterial suspension (OD_{600} = 0.01) supplemented with different concentrations of Ech (12.5, 25, 50 μM) was seeded into a 6-well plate with coverslips and incubated for 24 h at 37°C. The suspensions were removed, and the wells were washed with PBS (pH = 7.2). The biofilm was stained using BacLight Live/Dead viability kit (L7012, Invitrogen™, Thermo Fisher Scientific, United States) according to the procedure and observed by CLSM (Zeiss LSM800, Zeiss, Tokyo, Japan).

EPS production

According to the previous method, Ruthenium Red staining assessed *EPS* production (Adnan et al., 2020). Cell suspensions (10^6 CFU/ml) of *E. coli* O157:H7 and different concentrations of Ech were cultured in a 96-well plate for 24 h at 37°C. The plate was washed with PBS (pH = 7.2), stained with 0.01% ruthenium red (Yuanye, Shanghai, China), and then incubated at 37°C for 1 h. 0.01% ruthenium red was used to fill the wells without biofilm was used as blank. 0.01% ruthenium red was used to fill the wells with biofilm and without Ech was used as a positive control. The absorbance was performed at 450 nm using Multiskan Go Reader after the liquid carrying the residual stain was transferred to new 96-well plates (Thermo Fisher Scientific, USA). *EPS* inhibition was calculated as follows formula (Adnan et al., 2020):

$$\textbf{\textit{EPS inhibition}}(\%) = \frac{\mathbf{AS - AP}}{\mathbf{AB - AP}} \times \mathbf{100}$$

Whereas:
AB = absorbance of the blank.
AS = absorbance of the sample.
AP = absorbance of the positive control.

Motility assay

According to the previous description, the motility of *E.coli* was performed (Vikram et al., 2013). Briefly, overnight *E. coli* O157:H7 was diluted to $OD_{600} = 0.01$, and then a semisolid agar media (0.3% LB agar) containing 12.5, 25, and 50 μM of Gin was used for the motility assay. One micro liter of the diluted bacterial solution was inserted into the middle of the plate. DMSO alone was used as the control. Halo zone diameters were measured after incubation for 16–18 h at 37°C to assess motility.

qRT-PCR

qRT-PCR was used to measure Ech's effect on QS-regulated, biofilm formation, motility, and virulence factor-related genes of *E. coli*. *Escherichia coli* O157:H7 was incubated in the 12-wells plate with and without Ech at 37°C for 24 h. Bacterial RNA Kit(Omega, USA) was used to extract total RNA. RNA concentration was determined by NanoDrop OneC spectrophotometer (Thermo Scientific, USA). PrimeScript™ RT reagent Kit with gDNA Eraser (TAKARA Corporation, Japan) was used to reverse transcribe RNA into cDNA. qRT -PCR was analyzed using TB Green® Premix Ex TaqTM II (Tli RNaseH Plus) (TAKARA Corporation, Japan). Based on the $2^{-\Delta\Delta Ct}$ method, the relative changes in gene expression levels were analyzed. The *gapA* gene was used as an internal control (Hu et al., 2013). This study used the primers listed in Supplementary Table 1.

Antibacterial activity

Antibacterial activity was evaluated based on the previous method (Swetha et al., 2019; Liu et al., 2021) with some modifications. Briefly, *E. coli* O157:H7 and five clinical strains (*E. coli* O101, *E. coli* C83654, *E. coli* O149, *E. coli* XJ24, *E. coli* KD-13-1) bacterial suspensions ($OD_{600} = 0.01$) were mixed with antibiotics (1/2 MIC, 1/4 MIC, 1/8 MIC) with or without Ech (50 μM) at 37°C for 16–18 h. Antibacterial effects were assessed by metabolic activity with Alamar Blue assay. Tests were conducted in triplicate.

Statistical analysis

The experiment was repeated three times with three replicates for each treatment, and data represent the mean ± SD. The significance of differences was evaluated with multiple t-tests for two groups or non-parametric one-way ANOVA for multiple groups using GraphPad Prism (GraphPad Prism 8; GraphPad). Where $^*p < 0.05$; $^{**}p < 0.01$; $^{***}p < 0.001$; $^{****}p < 0.0001$.

Results

Screening of QS inhibitors against *Escherichia coli*

To identify new QS inhibitors, 13 flavonoid compounds from nature compounds were screened by the *V. harveyi* BB170 bioluminescence assay (Supplementary Table 2). The results showed that the QS inhibition rates of two compounds Ech and aloeemodin were greater than 70% at 50 μM. The QS inhibition rates of six compounds loureirin B, phloretin, cardamonin, neosperidin dihydrochalcone, cynaroside, and acacetin were between 60 and 70%, and five compounds scutellarin, artemetin, hesperetin, vitexin, and gentiin were less than 50%. In particular, Ech was the better anti-QS activity with an IC50 of 21.67 μM (Figure 1). Therefore, it was focused on during our study.

Cytotoxicity of Ech On Caco-2

Ech's cytotoxicity was assessed in the study to develop it as a safer alternative to antibiotics. The viability of Caco-2 cells was evaluated using CCK-8 assay after treatment with Ech at various concentrations (6.25, 12.5, 25, 50, 100, 200 μM). Compared with the control, Ech is non-toxic to Caco-2 cells at concentrations below 100 μM (Figure 2).

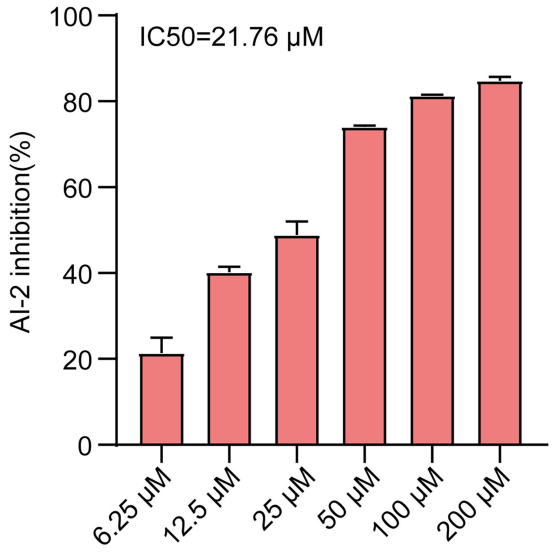

FIGURE 1
AI-2 inhibition of *E. coli* was treated with various concentrations of Ech (6.25, 12.5, 25, 50, 100, 200μM) by AI-2 Bioluminescence assay and IC50=21.76μM. All experiments were carried out in triplicate, and data represent the mean±SD.

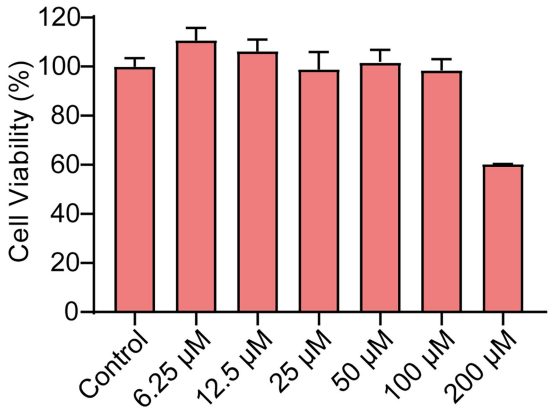

FIGURE 2
The Cytotoxicity of Ech in Caco-2 cells. The cells were treated with Ech at different concentrations (0, 6.25, 12.5, 25, 50, 100, and 200μM) for 24h. Data represent means ± SD of three experiments conducted in triplicate.

Effects of Ech on growth and metabolic activity of *Escherichia coli*

The effects of Ech on growth and metabolic activity were revealed by the microbroth dilution and Alamar Blue (AB) assay (Figure 3). Results showed that control and Ech treated cells showed no significant differences in the fluorescent intensity of AB dye. In addition, *E. coli* growth was not significantly different between the Ech treated sample and the control culture. These results showed the non-antibacterial effect of Ech.

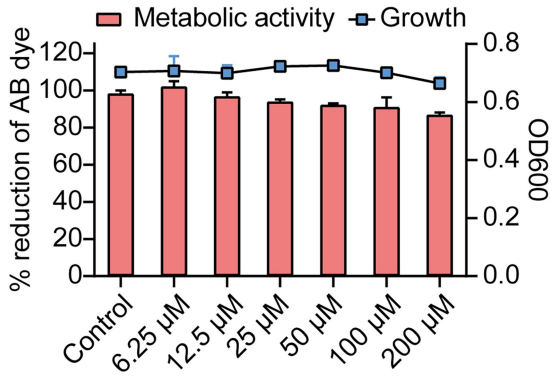

FIGURE 3
Growth and metabolic activity of *E. coli* in the presence of Ech. The line graph shows the growth of *E. coli* with Ech measured using a microbroth dilution assay. The bar graph shows the metabolic activity of *E. coli* based on the AB assay. Data represent means± SD of three experiments conducted in triplicate.

Effects of Ech on biofilm formation of *Escherichia coli*

Next, we assessed the effects of QS inhibitor on the formation of biofilm against *E. coli* by CV staining and CLSM. CV staining showed that Ech significantly inhibited the biofilm formation of *E. coli* in a dose-dependent manner (Figure 4A). More specifically, inhibition reached 40% at 6.25 μM of inhibitor concentration, while 71.54% inhibition was achieved at 200 μM. In addition, the antibiofilm of Ech was further verified by CLSM. As shown in Figure 4B, green fluorescence (living cells) and red fluorescence (death cells) showed significant decreases with increasing concentration, which proved that Ech could effectively inhibit the adhesion of *E. coli* and reduce biofilm formation.

Effects of Ech on EPS production of *Escherichia coli*

In a biofilm matrix, *EPS* is among the most critical components (Branda et al., 2005). As was shown in Figure 5, Ech inhibited *EPS* production dose-dependently. The *EPS* inhibition reached 50% at the concentration of 100 μM. It was consistent with the results of CV staining. This result further confirms the inhibition of Ech on the formation of biofilm.

Effects of Ech on the motility of *Escherichia coli*

Quorum-sensing controls the motility of *E.coli*. Figure 6A showed that QS inhibitor Ech reduced the motility in a dose-dependent. Further, we assessed the halo zone quantitatively (Figure 6B). Results showed that Ech significantly inhibited the motility of *E. coli* in comparison with the control group ($p < 0.0001$).

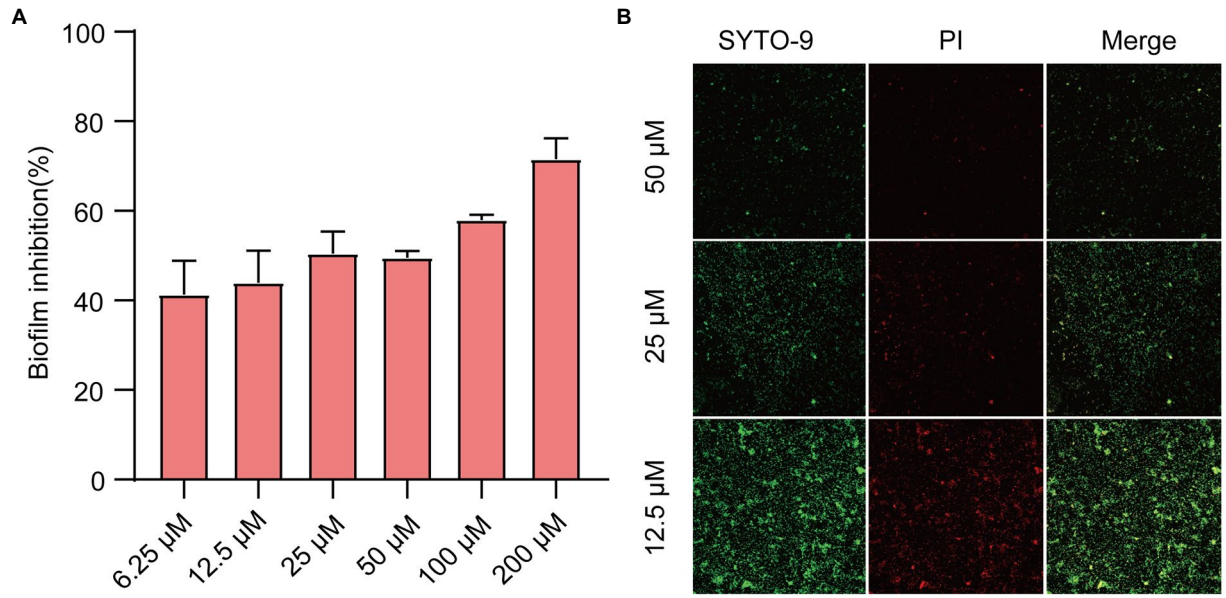

FIGURE 4
Effects of Ech on *E. coli* biofilm formation. **(A)** Biofilm formation inhibition at various concentrations of Ech (6.25, 12.5, 25, 50, 100, and 200μM) for 24h by CV staining. **(B)** Three-dimensional (3D) image of *E. coli* biofilm with Ech (12.5, 25, and 50μM) for 24h by CLSM. Error bars are mean±SD.

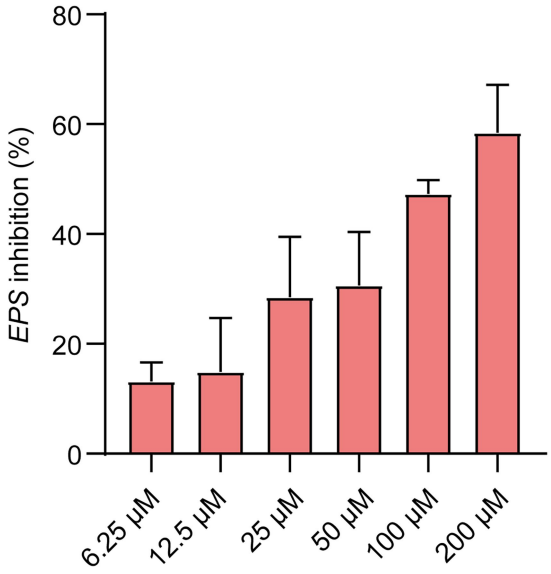

FIGURE 5
EPS inhibition (%) showed at the various concentrations of Ech (6.25, 12.5, 25, 50, 100, and 200μM) for 24h. Data represent means ± SD of three experiments conducted in triplicate.

Effect of Ech on the expression of QS-regulated genes of *Escherichia coli*

To further evaluate the potential molecular basis responsible for QS inhibition by Ech, we measured the expression of QS, motility, and biofilm genes by qRT - PCR. Ech reduced the expression of QS-regulated genes like *luxS*, *pfs*, *lsrB*, *lsrK*, and *lsrR* (43, 48, 52, 90, and 61% respectively), motility-regulated genes *flhC*, *flhD*, and *fliC* (61, 35, and 53%, respectively), biofilm-regulated genes *csgD* (52%), and virulence factor-regulated gene *stx2* (69%; Figure 7). The result demonstrated that Ech inhibited QS, biofilm formation, motility, and virulence factor production.

Synergistic effects of Ech with antibiotics against *Escherichia coli*

It was reported that antibiotic resistance was closed related to QS. So, we evaluated the synergistic antimicrobial effect of QS inhibitor Ech with conventional antibiotics against *E. coli* O157:H7 and five clinical isolates of strains (*E. coli* C83654, *E. coli* XJ24, *E. coli* O101, *E. coli* O149, *E. coli* KD-13-1). First, we evaluated the synergistic antibacterial effect of Ech and six different antibiotics against *E. coli* O157:H7. According to Figure 8, QS inhibitor Ech only has synergistic antibacterial activity with colistin antibiotics (1/2 MIC, 1/4 MIC, 1/8 MIC). In addition, the synergistic antibacterial effect of Ech with polymyxin B and polymyxin E on five clinical isolates of *E. coli* was further verified (Figures 9, 10). These results suggested that QS inhibitor Ech in conjunction with conventional antibiotics could be an efficient therapeutic strategy for inhibiting pathogens like *E. coli*.

Discussion

Microbial infections continue to pose a serious problem because of antibiotic resistance, making alternative therapies

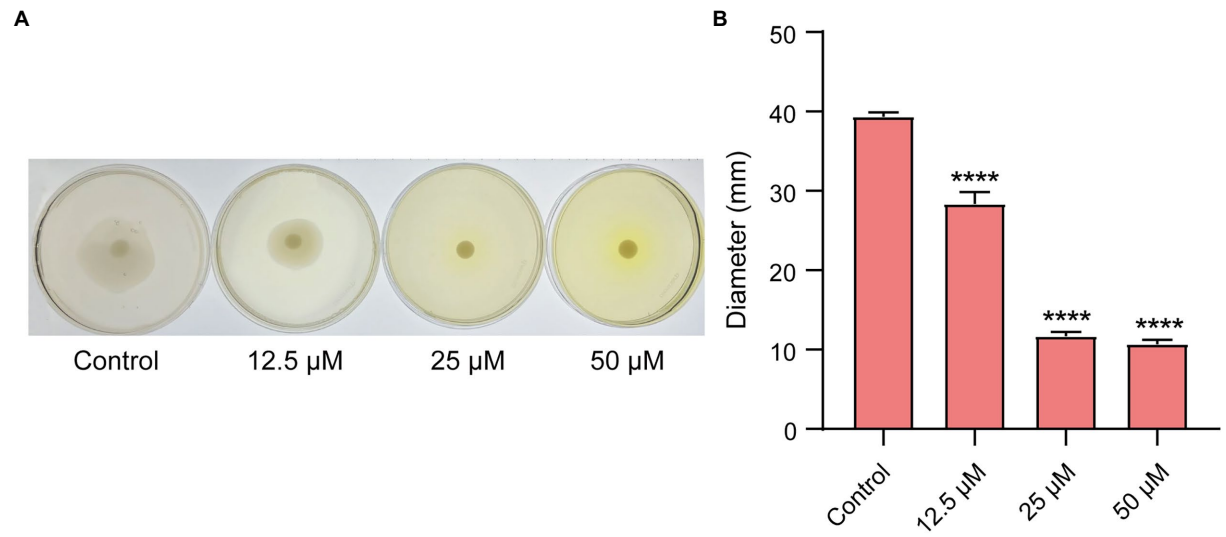

FIGURE 6
Motility inhibition of *E. coli* with Ech. **(A)** Images of motility following incubation with *E. coli* at the various concentration of Ech (0, 12.5, 25, and 50μM). **(B)** Quantitative estimation of motility based on the halo zone's diameter. ****=p<0.0001.

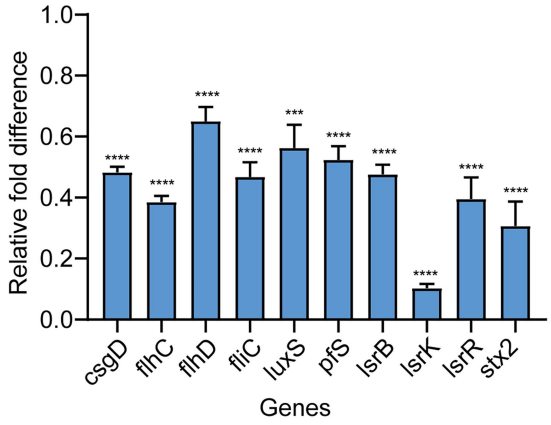

FIGURE 7
Effects of Ech on expression QS-regulated genes of *E. coli*. The qRT-PCR results showed significantly different nine genes (*csgD*, *flhC*, *flhD*, *fliC*, *luxS*, *pfs*, *lsrB*, *lsrK*, *lsrR*, and *stx2*) compared with the control. Data represent means ± SD of three experiments conducted in triplicate.

imperative. QS not only regulates different pathogenic processes like virulence production (Defoirdt, 2018), biofilm formation (Rickard et al., 2006; Irie and Parsek, 2008), and antibiotic sensitivity (Stenvang et al., 2016; Liu et al., 2021) but also does not result in the development of resistance (Sully et al., 2014; Quave et al., 2015; Ning et al., 2021). It has emerged as the potential target for fighting antibiotic resistance (Suga and Smith, 2003; Geske et al., 2005; Rasmussen and Givskov, 2006). In the present study, we identified that Ech, a novel QS inhibitor selected from 13 different flavonoids, did not inhibit *E. coli* growth and metabolic activity but affected QS-regulated processes like biofilm formation, *EPS* production, motility, and virulence factor production. Furthermore, we demonstrated the synergistic effect of Ech combination with colistin B and colistin E against *E. coli* O157:H7 and five clinical isolates of strains. In short, we concluded that Ech presents excellent anti-QS and synergistic antibacterial effects against *E. coli*.

At present, the detection methods of signal molecule AI-2 mainly include *V. harveyi* BB170 bioluminescence assay, LuxP-based fluorescence resonance energy transfer (LuxP-FRET) reporting system assay, QS engineering protein detection assay, Gas Chromatography-Mass Spectrometer (GC–MS) assay, high-performance liquid chromatography with tandem mass spectrometric (HPLC-MS/MS) assay, and high-performance liquid chromatography with fluorescence detection (HPLC-FLD) assay (Yan et al., 2016). Among them, *V harveyi* BB170 bioluminescence assay is the most commonly used method at present. In this study, we screened Ech with high-efficiency anti-QS from 13 different flavonoids through the AI-2 bioluminescence assay. In addition, we proved that Ech had no cell toxicity in Caco-2 in the effective dose and adverse effects on bacterial growth and metabolic activity. Further, Ech also significantly decreased the expression of QS-regulated genes, including *luxS*, *pfs*, *lsrB*, *lsrK*, and *lsrR*. Several studies have shown that AI-2 regulates the formation of biofilm, the production of virulence factors, motility, and resistance of bacteria. So, pathogen virulence could be reduced by inhibiting AI-2 production (Ma et al., 2017; Sedlmayer et al., 2021; Jiang et al., 2022). *LuxS* and *pfs* are responsible for the synthesis of AI-2 with S-adenosylhomocysteine (SAH) as substrate (Figure 11; Zhao et al., 2018; Wu et al., 2019). Similarly, it has been reported that *luxS* and *pfs* deletion mutants of *E. coli* inhibit AI-2 production, biofilm formation, and motility (Yang et al., 2014;

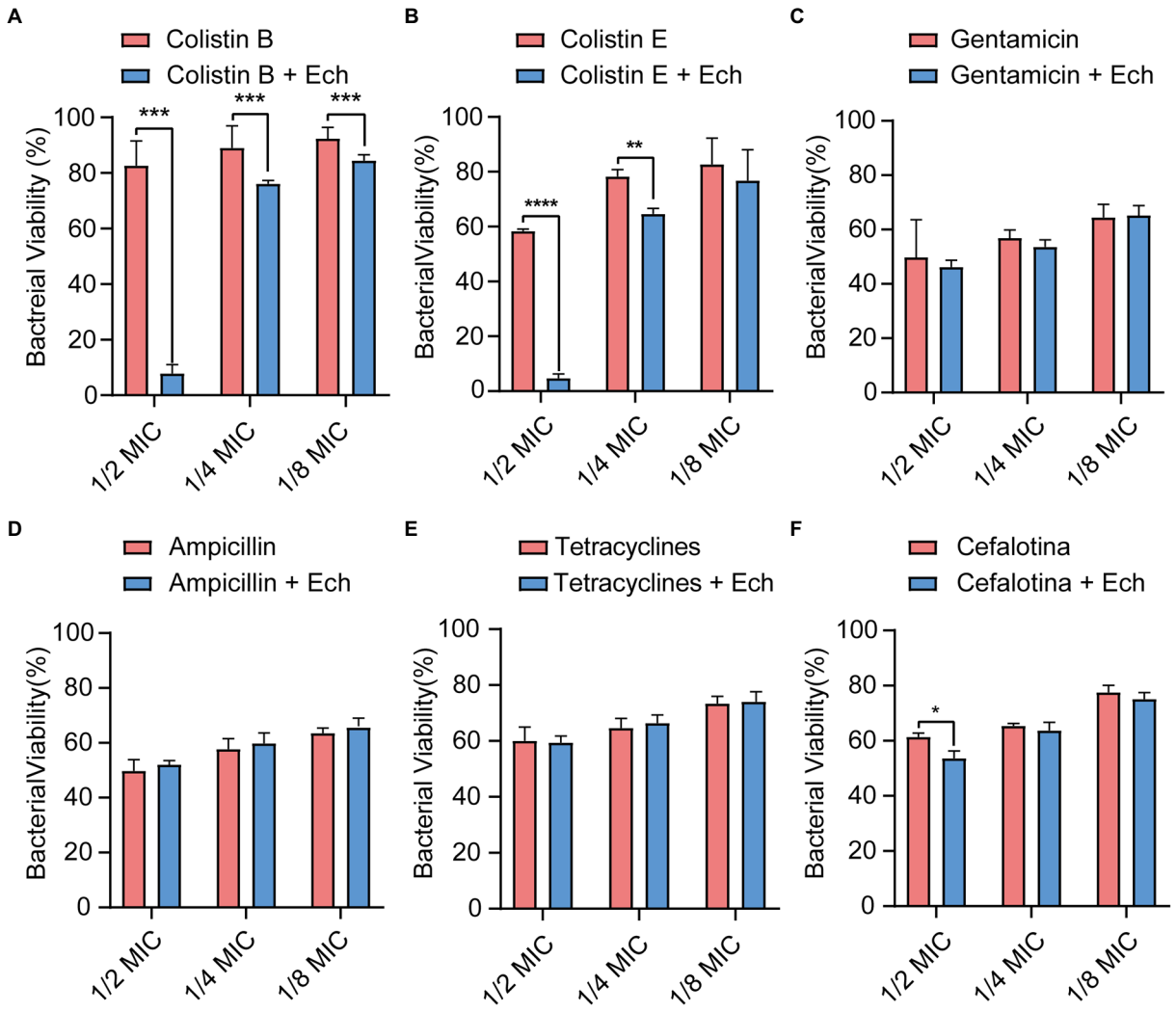

FIGURE 8
Synergistic effects of Ech (50μM) with six different antibiotics in *E. coli* O157:H7 on bacterial viability. Data represent means ± SD of three experiments conducted in triplicate. *=p<0.05; **=p<0.01; ***=p<0.001;****=p<0.0001.

Wang et al., 2016; Zuberi et al., 2017). Therefore, the *luxS* and *pfs* have been considered important therapeutic drug targets, and many inhibitors against *luxS* and *pfs* have been investigated (Shivaprasad et al., 2021; Sharifi and Nayeri Fasaei, 2022). The *lsr* system is liable for AI-2 detection, uptake, and signal transduction in *E. coli* (Pereira et al., 2013). *LsrR* is an inhibitor of the *lsr* system. There is very little extracellular AI-2 during the early stages of bacterial growth. *LsrR* is active and inhibits the transcription of the *lsr* system. *LsrK* phosphorylates uptake of AI-2 as it accumulates in the extracellular space. The binding of phospho-AI-2 to *lsrR* results in the initiation of transport by the *lsr* system. *LsrB* is an AI-2 receptor responsible for the internalization of AI-2 in *E. coli* (Figure 11). Similarly, *lsrR*, *lsrK*, and *lsrB* deletion mutant has been reported to interfere with signal transduction and inhibit biofilm, motility, and pathogenicity (Li et al., 2007; Jani et al., 2017; Laganenka and Sourjik, 2018; Zuo et al., 2019). So, the *lsrR*, *lsrK*, and *lsrB* have been considered important therapeutic drug targets. Many inhibitors against *lsrR, lsrK, and lsrB* have been investigated (Peng et al., 2018; Gatta et al., 2019; Stotani et al., 2019; Gatta et al., 2020). Our results suggested that Ech could interfere with the AI-2 synthesis, secretion, or transport through their effects on *luxS*, *pfs*, *lsrK*, or *lsrB*.

The biofilm is an aggregate of microorganisms where microorganisms are adhered to the substrate (e.g., stainless, glass, meats, and vegetables) and encapsulated within a self-produced matrix of *EPS*, proteins, and extracellular DNA (eDNA) (Hobley et al., 2015; Flemming et al., 2016; Karygianni et al., 2020). *EPS* can separate colonies and form a pathway for transporting metabolites and nutrients. In addition, *EPS* can maintain the biofilm's structure and contribute to bacteria colonization on the non-biological surface (Fan et al., 2022). Curli fimbriae and cellulose, whose products are regulated by *csgD*, are common *EPS* components found in bacterial biofilms (Dieltjens et al., 2020).

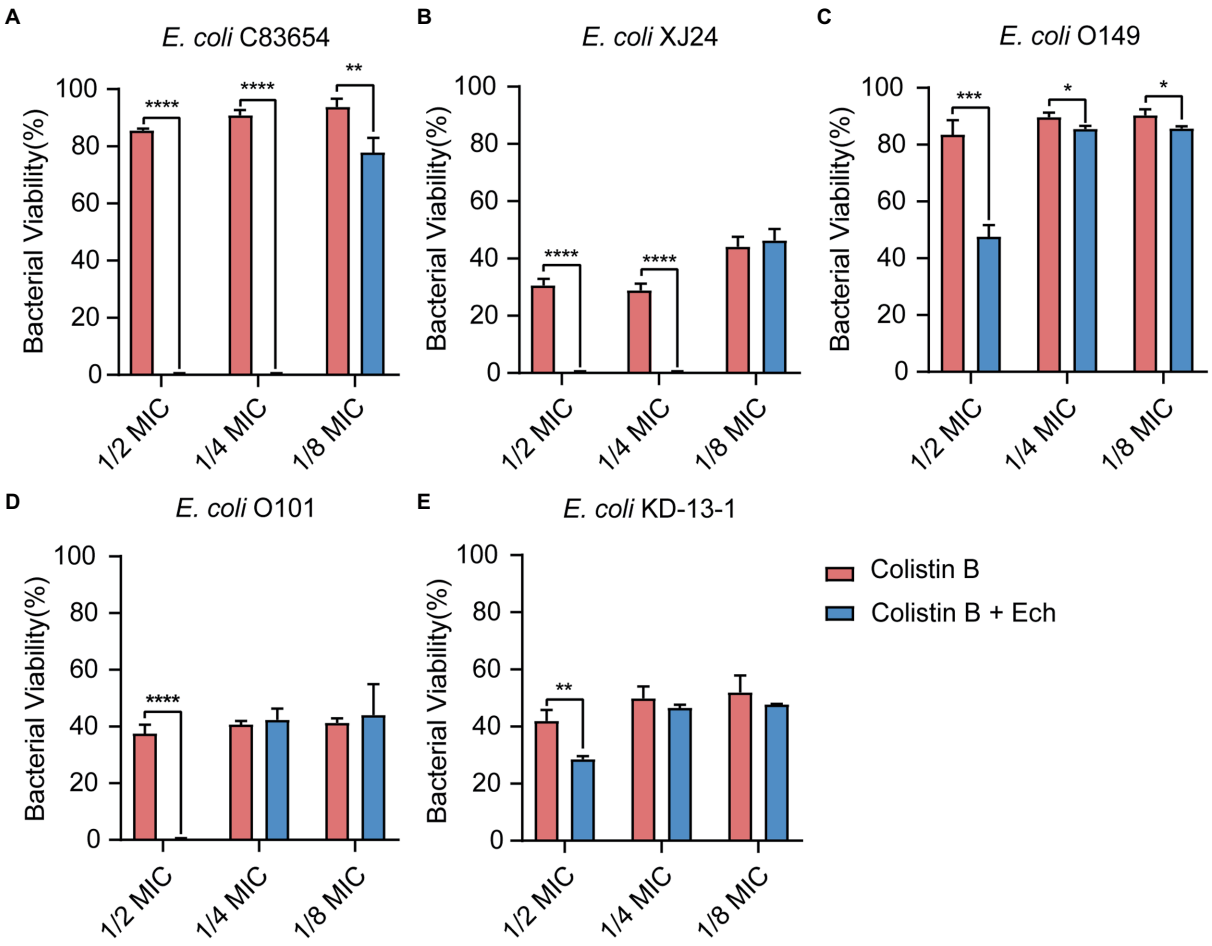

FIGURE 9
Synergistic effects of Ech (50μM) with Colistin B in five different *E. coli* on bacterial viability. *E. coli* **(A)** C83654, **(B)** XJ24, **(C)** O149, **(D)** O101, **(E)** KD-13-1. Data represent means ± SD of three experiments conducted in triplicate. *=p<0.05; **=p<0.01; ***=p<0.001; ****=p<0.0001.

CsgD stimulates the formation of *E. coli* biofilms by simultaneously activating the expression of the curli- encoding genes *csg* operon and inhibiting negative affect factors such as *yagS* and *pepD* (Brombacher et al., 2003). Otherwise, *csgD* directly inhibits flagellum formation of *fliE* and *fliEFGH* operon, thereby regulating biofilm formation and cell motility by inhibiting flagellum formation and rotation. This study showed that Ech inhibited *EPS* production in a dose-dependent manner by Ruthenium Red stain. Further, Ech also significantly decreased *csgD* expression (Figure 7). The results demonstrated that Ech reduced *EPS* production by inhibiting QS.

We performed motility experiments in a semi-solid agar medium to determine whether Ech affects bacterial motility. The results showed that Ech inhibited bacterial motility in a dose-dependent manner. Additionally, flagellum-regulated genes such as *flhC*, *flhD*, and *fliC* were also significantly down-regulated by Ech. *FlhDC* is an activator of the flagellum regulatory cascade, which regulates flagellum synthesis and motility (Guttenplan and Kearns, 2013). *FliC*, as a flagellum filament structural protein, is involved in the pathogenesis of infection, the production of biofilm, and motility (Chaban et al., 2015). The results demonstrated that Ech reduced flagellum motility by inhibiting QS.

Substances that constitute bacterial virulence are called virulence factors including invasiveness and virulence. Among the six major pathotypes of *E. coli*, Shiga toxin-producing *E. coli* is the most prevalent (Moreau et al., 2021). Shiga toxin is one of the major virulence factors of Shiga toxin-producing *E. coli* O157: H7. It can induce the formation of A/E lesions, and cause HUS if it enters the circulatory system (Kordbacheh et al., 2019). In humans, the stx2 gene codes for the Stx2 which is associated with more severe diseases caused by Shiga toxins, which play an essential role in the pathogenesis of *E. coli* O157:H7 (Sheng et al., 2016). In the present student, we found that the virulence factor regulatory gene stx2 was downregulated by 69%. The results demonstrated that Ech reduced virulence factor production by inhibiting QS.

Multiple antibiotic resistance mechanisms have evolved due to the extensive use of antibiotics during clinical treatment. The primary resistance mechanisms are to passivate antibiotics by eliminating antibiotics by efflux pump system, chemical

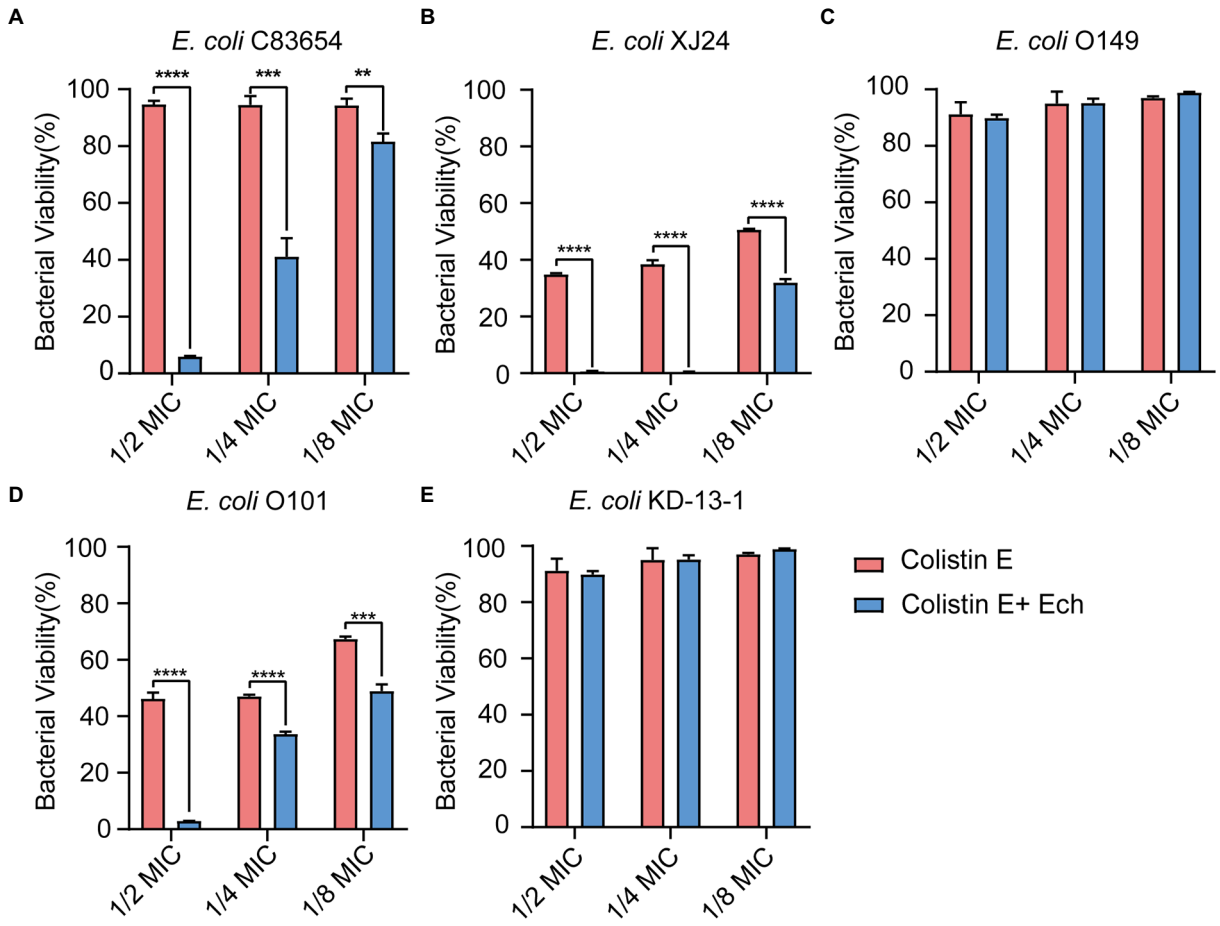

FIGURE 10
Synergistic effects of Ech (50μM) with Colistin E in five different *E. coli* on bacterial viability. *E. coli* **(A)** C83654, **(B)** XJ24, **(C)** O149, **(D)** O101, **(E)** KD-13-1. Data represent means ± SD of three experiments conducted in triplicate. **=p<0.01; ***=p<0.001; ****=p<0.0001.

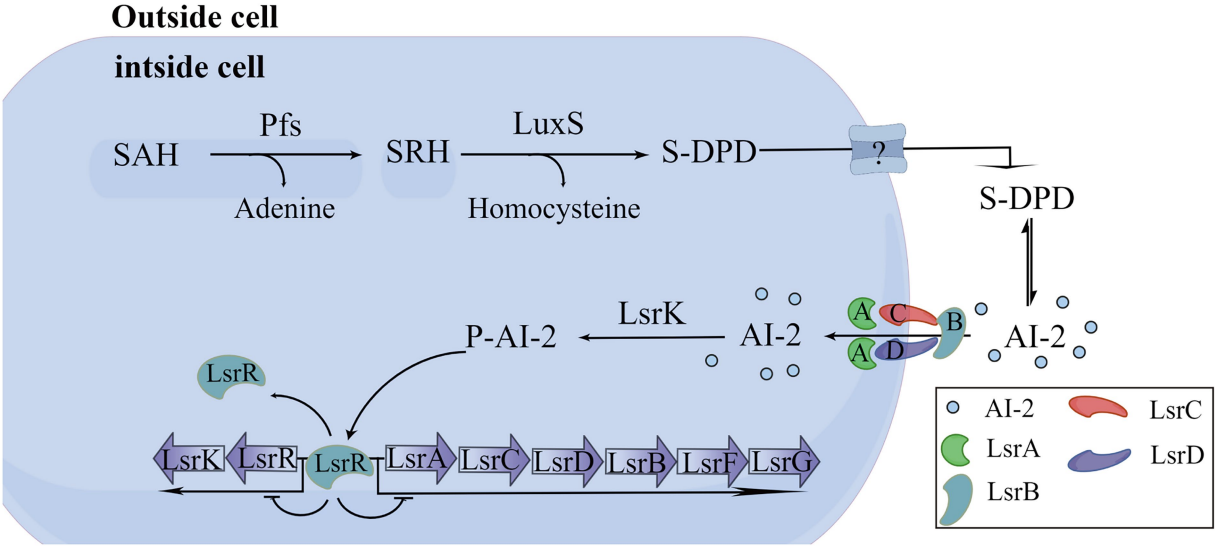

FIGURE 11
Biosynthesis, and transport of AI-2 in *E. coli*.

modifications, and target gene modification (Zhao et al., 2020). Meanwhile, the biofilms formed by many pathogens result in strong resistance (Rajput et al., 2018). QS system can reduce antibiotic resistance by regulating biofilm formation (Zhao et al., 2020). In this study, we found that combined QS inhibitor Ech and colistin antibiotics could play a synergistic antibacterial effect. The results suggested that combining antibiotics with anti-QS compounds appears to be an effective therapeutic strategy for treating pathogen infections.

Data availability statement

The original contributions presented in the study are included in the article/Supplementary material, further inquiries can be directed to the corresponding author.

Author contributions

Y-BB wrote the manuscript and participated in some experiments. M-YS, L-YW, and Y-TB performed part of the experiments. W-WW, X-ZZ, and BL revised the manuscript. J-YZ and W-WW directed the project and reviewed the manuscript. All authors contributed to the article and approved the submitted version.

Funding

This research was funded by the research on the National Natural Science Foundation of China, grant number 32102727–the earmarked fund for CARS, grant number CARS-37–Innovation Project of Chinese Academy of Agricultural Sciences, grant number 25-LZIHPS-05.

Acknowledgments

We thank Researcher Xiangan Han for providing the strain *Vibrio harveyi* BB170 and *Vibrio harveyi* BB152. Additionally, we are grateful for the suggestions made by reviewers.

Conflict of interest

The authors declare that the research was conducted in the absence of any commercial or financial relationships that could be construed as a potential conflict of interest.

Publisher's note

All claims expressed in this article are solely those of the authors and do not necessarily represent those of their affiliated organizations, or those of the publisher, the editors and the reviewers. Any product that may be evaluated in this article, or claim that may be made by its manufacturer, is not guaranteed or endorsed by the publisher.

Supplementary material

The Supplementary material for this article can be found online at: https://www.frontiersin.org/articles/10.3389/fmicb.2022.1003692/full#supplementary-material

References

Adnan, M., Patel, M., Deshpande, S., Alreshidi, M., Siddiqui, A. J., Reddy, M. N., et al. (2020). Effect of adiantum philippense extract on biofilm formation, adhesion with its antibacterial activities against foodborne pathogens, and characterization of bioactive metabolites: an in vitro-in silico approach. *Front. Microbiol.* 11:823. doi: 10.3389/fmicb.2020.00823

Bassler, B. L. (2002). Small talk. Cell-to-cell communication in bacteria. *Cells* 109, 421–424. doi: 10.1016/s0092-8674(02)00749-3

Bassler, B. L., Greenberg, E. P., and Stevens, A. M. (1997). Cross-species induction of luminescence in the quorum-sensing bacterium *Vibrio harveyi*. *J. Bacteriol.* 179, 4043–4045. doi: 10.1128/jb.179.12.4043-4045.1997

Bassler, B. L., Wright, M., and Silverman, M. R. (1994). Multiple signalling systems controlling expression of luminescence in *Vibrio harveyi*: sequence and function of genes encoding a second sensory pathway. *Mol. Microbiol.* 13, 273–286. doi: 10.1111/j.1365-2958.1994.tb00422.x

Beshearse, E., Bruce, B. B., Nane, G. F., Cooke, R. M., Aspinall, W., Hald, T., et al. (2021). Attribution of illnesses transmitted by food and water to comprehensive transmission pathways using structured expert judgment. *United States Emerg. Infect. Dis.* 27, 182–195. doi: 10.3201/eid2701.200316

Branda, S. S., Vik, S., Friedman, L., and Kolter, R. (2005). Biofilms: the matrix revisited. *Trends Microbiol.* 13, 20–26. doi: 10.1016/j.tim.2004.11.006

Brombacher, E., Dorel, C., Zehnder, A. J. B., and Landini, P. (2003). The curli biosynthesis regulator *csgD* co-ordinates the expression of both positive and negative determinants for biofilm formation in *Escherichia coli*. *Microbiology* 149, 2847–2857. doi: 10.1099/mic.0.26306-0

Buroni, S., and Chiarelli, L. R. (2020). Antivirulence compounds: a future direction to overcome antibiotic resistance? *Future Microbiol.* 15, 299–301. doi: 10.2217/fmb-2019-0294

Chaban, B., Hughes, H. V., and Beeby, M. (2015). The flagellum in bacterial pathogens: for motility and a whole lot more. *Semin. Cell Dev. Biol.* 46, 91–103. doi: 10.1016/j.semcdb.2015.10.032

Choudhary, S., and Schmidt-Dannert, C. (2010). Applications of quorum sensing in biotechnology. *Appl. Microbiol. Biotechnol.* 86, 1267–1279. doi: 10.1007/s00253-010-2521-7

CLSI (2018). *Methods for Dilution Antimicrobial Susceptibility Tests for Bacteria that Grow Aerobically 11th ed.* (Wayne, PA: Clinical and Laboratory Standards Institute).

Defoirdt, T. (2018). Quorum-sensing systems as targets for antivirulence therapy. *Trends Microbiol.* 26, 313–328. doi: 10.1016/j.tim.2017.10.005

Dickey, S. W., Cheung, G. Y. C., and Otto, M. (2017). Different drugs for bad bugs: antivirulence strategies in the age of antibiotic resistance. *Nat. Rev. Drug Discov.* 16, 457–471. doi: 10.1038/nrd.2017.23

Dieltjens, L., Appermans, K., Lissens, M., Lories, B., Kim, W., Van der Eycken, E. V., et al. (2020). Inhibiting bacterial cooperation is an evolutionarily robust anti-biofilm strategy. *Nat. Commun.* 11:107. doi: 10.1038/s41467-019-13660-x

Fan, Q., Zuo, J., Wang, H., Grenier, D., Yi, L., and Wang, Y. (2022). Contribution of quorum sensing to virulence and antibiotic resistance in zoonotic bacteria. *Biotechnol. Adv.* 59:107965. doi: 10.1016/j.biotechadv.2022.107965

Flemming, H. C., Wingender, J., Szewzyk, U., Steinberg, P., Rice, S. A., and Kjelleberg, S. (2016). Biofilms: an emergent form of bacterial life. *Nat. Rev. Microbiol.* 14, 563–575. doi: 10.1038/nrmicro.2016.94

Gatta, V., Ilina, P., Porter, A., McElroy, S., and Tammela, P. (2019). Targeting quorum sensing: high-throughput screening to identify novel *lsrK* inhibitors. *Int. J. Mol. Sci.* 20:3112. doi: 10.3390/ijms20123112

Gatta, V., Tomašič, T., Ilaš, J., Zidar, N., Peterlin Mašič, L., Barančoková, M., et al. (2020). A new cell-based AI-2-mediated quorum sensing interference assay in screening of *lsrK*-targeted inhibitors. *Chembiochem* 21, 1918–1922. doi: 10.1002/cbic.201900773

Geske, G. D., Wezeman, R. J., Siegel, A. P., and Blackwell, H. E. (2005). Small molecule inhibitors of bacterial quorum sensing and biofilm formation. *J. Am. Chem. Soc.* 127, 12762–12763. doi: 10.1021/ja0530321

Guo, M., Gamby, S., Zheng, Y., and Sintim, H. O. (2013). Small molecule inhibitors of AI-2 signaling in bacteria: state-of-the-art and future perspectives for anti-quorum sensing agents. *Int. J. Mol. Sci.* 14, 17694–17728. doi: 10.3390/ijms140917694

Guttenplan, S. B., and Kearns, D. B. (2013). Regulation of flagellar motility during biofilm formation. *FEMS Microbiol. Rev.* 37, 849–871. doi: 10.1111/1574-6976.12018

Hale, C. R., Scallan, E., Cronquist, A. B., Dunn, J., Smith, K., Robinson, T., et al. (2012). Estimates of enteric illness attributable to contact with animals and their environments in the United States. *Clin. Infect. Dis.* 54, S472–S479. doi: 10.1093/cid/cis051

Hawkey, P. M. (2008). The growing burden of antimicrobial resistance. *J. Antimicrob. Chemother.* 62, i1–i9. doi: 10.1093/jac/dkn241

Hobley, L., Harkins, C., MacPhee, C. E., and Stanley-Wall, N. R. (2015). Giving structure to the biofilm matrix: an overview of individual strategies and emerging common themes. *FEMS Microbiol. Rev.* 39, 649–669. doi: 10.1093/femsre/fuv015

Hu, Y., Liu, M., Qin, H., Lin, H., An, X., Shi, Z., et al. (2021). Artemether, Artesunate, Arteannuin B, Echinatin, Licochalcone B and Andrographolide effectively inhibit SARS-CoV-2 and related viruses *in vitro*. *Front. Cell. Infect. Microbiol.* 11:680127. doi: 10.3389/fcimb.2021.680127

Hu, J., Wang, B., Fang, X., Means, W. J., McCormick, R. J., Gomelsky, M., et al. (2013). C-di-GMP signaling regulates *E. coli* O157:H7 adhesion to colonic epithelium. *Vet. Microbiol.* 164, 344–351. doi: 10.1016/j.vetmic.2013.02.023

Irie, Y., and Parsek, M. R. (2008). Quorum sensing and microbial biofilms. *Curr. Top. Microbiol. Immunol.* 322, 67–84. doi: 10.1007/978-3-540-75418-3_4

Jani, S., Seely, A. L., Peabody, V. G., Jayaraman, A., and Manson, M. D. (2017). Chemotaxis to self-generated AI-2 promotes biofilm formation in *Escherichia coli*. *Microbiology* 163, 1778–1790. doi: 10.1099/mic.0.000567

Ji, S., Li, Z., Song, W., Wang, Y., Liang, W., Li, K., et al. (2016). Bioactive constituents of glycyrrhiza uralensis (licorice): discovery of the effective components of a traditional herbal medicine. *J. Nat. Prod.* 79, 281–292. doi: 10.1021/acs.jnatprod.5b00877

Jiang, K., Xu, Y., Yuan, B., Yue, Y., Zhao, M., Luo, R., et al. (2022). Effect of autoinducer-2 quorum sensing inhibitor on interspecies quorum sensing. *Front. Microbiol.* 13:791802. doi: 10.3389/fmicb.2022.791802

Ju, X. Y., Li, J. J., Zhu, M. J., Lu, Z. X., Lv, F. X., Zhu, X. Y., et al. (2018). Effect of the *luxS* gene on biofilm formation and antibiotic resistance by *salmonella serovar Dublin*. *Food Res. Int.* 107, 385–393. doi: 10.1016/j.foodres.2018.02.039

Karnjana, K., Nobsathian, S., Soowannayan, C., Zhao, W., Tang, Y. J., and Wongprasert, K. (2020). Purification and evaluation of N-benzyl cinnamamide from red seaweed gracilaria fisheri as an inhibitor of *Vibrio harveyi* AI-2 quorum sensing. *Mar. Drugs* 18:80. doi: 10.3390/md18020080

Karygianni, L., Ren, Z., Koo, H., and Thurnheer, T. (2020). Biofilm matrixome: extracellular components in structured microbial communities. *Trends Microbiol.* 28, 668–681. doi: 10.1016/j.tim.2020.03.016

Kendall, M. M., Rasko, D. A., and Sperandio, V. (2007). Global effects of the cell-to-cell signaling molecules autoinducer-2, autoinducer-3, and epinephrine in a *luxS* mutant of enterohemorrhagic *Escherichia coli*. *Infect. Immun.* 75, 4875–4884. doi: 10.1128/iai.00550-07

Kordbacheh, E., Nazarian, S., Hajizadeh, A., Fasihi-Ramandi, M., and Fathi, J. (2019). Recombinant HcpA-EspA-Tir-Stx2B chimeric protein induces immunity against attachment and toxicity of *Escherichia coli* O157:H7. *Microb. Pathog.* 129, 176–182. doi: 10.1016/j.micpath.2019.02.004

Kwak, A. W., Choi, J. S., Lee, M. H., Oh, H. N., Cho, S. S., Yoon, G., et al. (2019). Retrochalcone Echinatin triggers apoptosis of esophageal squamous cell carcinoma via ROS- and ER stress-mediated signaling pathways. *Molecules* 24:4055. doi: 10.3390/molecules24224055

Laganenka, L., and Sourjik, V. (2018). Autoinducer 2-dependent *Escherichia coli* biofilm formation is enhanced in a dual-species coculture. *Appl. Environ. Microbiol.* 84, e02638–02617. doi: 10.1128/aem.02638-17

Li, J., Attila, C., Wang, L., Wood, T. K., Valdes, J. J., and Bentley, W. E. (2007). Quorum sensing in *Escherichia coli* is signaled by AI-2/*lsrR*: effects on small RNA and biofilm architecture. *J. Bacteriol.* 189, 6011–6020. doi: 10.1128/JB.00014-07

Li, J. P., Fan, Q. Y., Jin, M. Y., Mao, C. L., Zhang, H., Zhang, X. L., et al. (2021). Paeoniflorin reduce *luxS*/AI-2 system-controlled biofilm formation and virulence in *Streptococcus suis*. *Virulence* 12, 3062–3073. doi: 10.1080/21505594.2021.2010398

Liu, J., Hou, J. S., Chang, Y. Q., Peng, L. J., Zhang, X. Y., Miao, Z. Y., et al. (2021). New *pqs* quorum sensing system inhibitor as an antibacterial synergist against multidrug-resistant *Pseudomonas aeruginosa*. *J. Med. Chem.* 65, 688–709. doi: 10.1021/acs.jmedchem.1c01781

Loubet, P., Ranfaing, J., Dinh, A., Dunyach-Remy, C., Bernard, L., Bruyère, F., et al. (2020). Alternative therapeutic options to antibiotics for the treatment of urinary tract infections. *Front. Microbiol.* 11:1509. doi: 10.3389/fmicb.2020.01509

Lutful Kabir, S. M. (2010). Avian *Colibacillosis* and *salmonellosis*: a closer look at epidemiology, pathogenesis, diagnosis, control and public health concerns. *Int. J. Environ. Res. Public Health* 7, 89–114. doi: 10.3390/ijerph7010089

Ma, Y. P., Hao, L., Ke, H., Liang, Z. L., Ma, J. Y., Liu, Z. X., et al. (2017). *LuxS*/AI-2 in *Streptococcus agalactiae* reveals a key role in acid tolerance and virulence. *Res. Vet. Sci.* 115, 501–507. doi: 10.1016/j.rvsc.2017.07.032

Manner, S., and Fallarero, A. (2018). Screening of natural product derivatives identifies two structurally related flavonoids as potent quorum sensing inhibitors against gram-negative bacteria. *Int. J. Mol. Sci.* 19:1346. doi: 10.3390/ijms19051346

Meng, F., Zhang, F., Chen, Q., Yang, M., Yang, Y., Li, X., et al. (2022). Virtual screening and *in vitro* experimental verification of LuxS inhibitors from natural products for *lactobacillus reuteri*. *Biomed. Pharmacother.* 147:112521. doi: 10.1016/j.biopha.2021.112521

Minich, A., Levarski, Z., Mikulášová, M., Straka, M., Liptáková, A., and Stuchlík, S. (2022). Complex analysis of vanillin and syringic acid as natural antimicrobial agents against *Staphylococcus epidermidis* biofilms. *Int. J. Mol. Sci.* 23:1816. doi: 10.3390/ijms23031816

Moreau, M. R., Kudva, I. T., Katani, R., Cote, R., Li, L., Arthur, T. M., et al. (2021). Nonfimbrial adhesin mutants reveal divergent *Escherichia coli* O157:H7 adherence mechanisms on human and cattle epithelial cells. *Int. J. Microbiol.* 2021:8868151. doi: 10.1155/2021/8868151

Munguia, J., and Nizet, V. (2017). Pharmacological targeting of the host-pathogen interaction: alternatives to classical antibiotics to combat drug-resistant superbugs. *Trends Pharmacol. Sci.* 38, 473–488. doi: 10.1016/j.tips.2017.02.003

Ng, W. L., and Bassler, B. L. (2009). Bacterial quorum-sensing network architectures. *Annu. Rev. Genet.* 43, 197–222. doi: 10.1146/annurev-genet-102108-134304

Ning, Q., Wang, D., and You, J. (2021). Joint effects of antibiotics and quorum sensing inhibitors on resistance development in bacteria. *Environ Sci Process Impacts* 23, 995–1005. doi: 10.1039/d1em00047k

O'Toole, G. A. (2011). Microtiter dish biofilm formation assay. *J. Vis. Exp.* 47:2437. doi: 10.3791/2437

Papenfort, K., and Bassler, B. L. (2016). Quorum sensing signal-response systems in gram-negative bacteria. *Nat. Rev. Microbiol.* 14, 576–588. doi: 10.1038/nrmicro.2016.89

Peng, L. Y., Yuan, M., Cui, Z. Q., Wu, Z. M., Yu, Z. J., Song, K., et al. (2018). Rutin inhibits quorum sensing, biofilm formation and virulence genes in avian pathogenic *Escherichia coli*. *Microb. Pathog.* 119, 54–59. doi: 10.1016/j.micpath.2018.04.007

Pereira, C. S., Thompson, J. A., and Xavier, K. B. (2013). AI-2-mediated signalling in bacteria. *FEMS Microbiol. Rev.* 37, 156–181. doi: 10.1111/j.1574-6976.2012.00345.x

Piewngam, P., Chiou, J., Chatterjee, P., and Otto, M. (2020). Alternative approaches to treat bacterial infections: targeting quorum-sensing. *Expert Rev. Anti-Infect. Ther.* 18, 499–510. doi: 10.1080/14787210.2020.1750951

Quave, C. L., Lyles, J. T., Kavanaugh, J. S., Nelson, K., Parlet, C. P., Crosby, H. A., et al. (2015). *Castanea sativa* (European chestnut) leaf extracts rich in ursene and oleanane derivatives block *Staphylococcus aureus* virulence and pathogenesis without detectable resistance. *PLoS One* 10:e0136486. doi: 10.1371/journal.pone.0136486

Rajput, A., Thakur, A., Sharma, S., and Kumar, M. (2018). ABiofilm: a resource of anti-biofilm agents and their potential implications in targeting antibiotic drug resistance. *Nucleic Acids Res.* 46, D894–d900. doi: 10.1093/nar/gkx1157

Ran, H., Liu, H., and Wu, P. (2021). Echinatin mitigates H_2O_2-induced oxidative damage and apoptosis in lens epithelial cells via the Nrf2/HO-1 pathway. *Adv. Clin. Exp. Med.* 30, 1195–1203. doi: 10.17219/acem/139130

Rasmussen, T. B., and Givskov, M. (2006). Quorum-sensing inhibitors as anti-pathogenic drugs. *Int. J. Med. Microbiol.* 296, 149–161. doi: 10.1016/j.ijmm.2006.02.005

Reading, N. C., and Sperandio, V. (2006). Quorum sensing: the many languages of bacteria. *FEMS Microbiol. Lett.* 254, 1–11. doi: 10.1111/j.1574-6968.2005.00001.x

Rickard, A. H., Palmer, R. J., Blehert, D. S., Campagna, S. R., Semmelhack, M. F., Egland, P. G., et al. (2006). Autoinducer 2: a concentration-dependent signal for mutualistic bacterial biofilm growth. *Mol. Microbiol.* 60, 1446–1456. doi: 10.1111/j.1365-2958.2006.05202.x

Riley, L. W. (2020). Distinguishing pathovars from nonpathovars: *Escherichia coli*. *Microbiol. Spectr.* 8, 1–23. doi: 10.1128/microbiolspec.AME-0014-2020

Scallan, E., Hoekstra, R. M., Angulo, F. J., Tauxe, R. V., Widdowson, M. A., Roy, S. L., et al. (2011). Foodborne illness acquired in the United States--major pathogens. *Emerg. Infect. Dis.* 17, 7–15. doi: 10.3201/eid1701.p11101

Sedlmayer, F., Woischnig, A. K., Unterreiner, V., Fuchs, F., Baeschlin, D., Khanna, N., et al. (2021). 5-fluorouracil blocks quorum-sensing of biofilm-embedded methicillin-resistant *Staphylococcus aureus* in mice. *Nucleic Acids Res.* 49:e73. doi: 10.1093/nar/gkab251

Sharifi, A., and Nayeri Fasaei, B. (2022). Selected plant essential oils inhibit biofilm formation and *luxS*- and *pfs*-mediated quorum sensing by *Escherichia coli* O157:H7. *Lett. Appl. Microbiol.* 74, 916–923. doi: 10.1111/lam.13673

Sheng, L., Rasco, B., and Zhu, M. J. (2016). Cinnamon oil inhibits Shiga toxin type 2 phage induction and Shiga toxin type 2 production in *Escherichia coli* O157:H7. *Appl. Environ. Microbiol.* 82, 6531–6540. doi: 10.1128/aem.01702-16

Shivaprasad, D. P., Taneja, N. K., Lakra, A., and Sachdev, D. (2021). *In vitro* and *in situ* abrogation of biofilm formation in *E. coli* by vitamin C through ROS generation, disruption of quorum sensing and exopolysaccharide production. *Food Chem.* 341:128171. doi: 10.1016/j.foodchem.2020.128171

Silva, D. R., Sardi, J. D. C. O., Pitangui, N. D. S., Roque, S. M., Silva, A. C. B. D., and Rosalen, P. L. (2020). Probiotics as an alternative antimicrobial therapy: current reality and future directions. *J. Funct. Foods* 73:104080. doi: 10.1016/j.jff.2020.104080

Stenvang, M., Dueholm, M. S., Vad, B. S., Seviour, T., Zeng, G., Geifman-Shochat, S., et al. (2016). Epigallocatechin gallate remodels overexpressed functional amyloids in *Pseudomonas aeruginosa* and increases biofilm susceptibility to antibiotic treatment. *J. Biol. Chem.* 291, 26540–26553. doi: 10.1074/jbc.M116.739953

Stotani, S., Gatta, V., Medarametla, P., Padmanaban, M., Karawajczyk, A., Giordanetto, F., et al. (2019). DPD-inspired discovery of novel *lsrK* kinase inhibitors: an opportunity to fight antimicrobial resistance. *J. Med. Chem.* 62, 2720–2737. doi: 10.1021/acs.jmedchem.9b00025

Sturme, M. H., Kleerebezem, M., Nakayama, J., Akkermans, A. D., Vaugha, E. E., and de Vos, W. M. (2002). Cell to cell communication by autoinducing peptides in gram-positive bacteria. *Antonie Van Leeuwenhoek* 81, 233–243. doi: 10.1023/a:1020522919555

Suga, H., and Smith, K. M. (2003). Molecular mechanisms of bacterial quorum sensing as a new drug target. *Curr. Opin. Chem. Biol.* 7, 586–591. doi: 10.1016/j.cbpa.2003.08.001

Sully, E. K., Malachowa, N., Elmore, B. O., Alexander, S. M., Femling, J. K., Gray, B. M., et al. (2014). Selective chemical inhibition of agr quorum sensing in Staphylococcus aureus promotes host defense with minimal impact on resistance. *PLoS Pathog.* 10:e1004174. doi: 10.1371/journal.ppat.1004174

Sun, Y., Li, Y., Luo, Q., Huang, J., Chen, J., Zhang, R., et al. (2020). *LuxS*/AI-2 quorum sensing system in *Edwardsiella piscicida* promotes its biofilm formation and pathogenicity. *Infect. Immun.* 88, e00907–00919. doi: 10.1128/iai.00907-19

Surette, M. G., Miller, M. B., and Bassler, B. L. (1999). Quorum sensing in *Escherichia coli*, *salmonella typhimurium*, and *Vibrio harveyi*: a new family of genes responsible for autoinducer production. *Proc. Natl. Acad. Sci. U. S. A.* 96, 1639–1644. doi: 10.1073/pnas.96.4.1639

Swetha, T. K., Pooranachithra, M., Subramenium, G. A., Divya, V., Balamurugan, K., and Pandian, S. K. (2019). Umbelliferone impedes biofilm formation and virulence of methicillin-resistant *Staphylococcus epidermidis* via impairment of initial attachment and intercellular adhesion. *Front. Cell. Infect. Microbiol.* 9:357. doi: 10.3389/fcimb.2019.00357

Taga, M. E., and Xavier, K. B. (2011). Methods for analysis of bacterial autoinducer-2 production. *Curr. Protoc. Microbiol. Chapter* 1:Unit1C.1. doi: 10.1002/9780471729259.mc01c01s23

Vikram, A., Jayaprakasha, G. K., Uckoo, R. M., and Patil, B. S. (2013). Inhibition of *Escherichia coli* O157:H7 motility and biofilm by β-sitosterol glucoside. *Biochim. Biophys. Acta* 1830, 5219–5228. doi: 10.1016/j.bbagen.2013.07.022

Wang, W., Huang, X., Yang, H., Niu, X., Li, D., Yang, C., et al. (2019). Antibacterial activity and anti-quorum sensing mediated phenotype in response to essential oil from melaleuca bracteata leaves. *Int. J. Mol. Sci.* 20:5696. doi: 10.3390/ijms20225696

Wang, X., Li, S., Lu, X., Hu, P., Chen, H., Li, Z., et al. (2016). Rapid method of *luxS* and *pfs* gene inactivation in enterotoxigenic *Escherichia coli* and the effect on biofilm formation. *Mol. Med. Rep.* 13, 257–264. doi: 10.3892/mmr.2015.4532

Whiteley, M., Diggle, S. P., and Greenberg, E. P. (2017). Progress in and promise of bacterial quorum sensing research. *Nature* 551, 313–320. doi: 10.1038/nature24624

Whiteley, M., Diggle, S. P., and Greenberg, E. P. (2018). Corrigendum: Progress in and promise of bacterial quorum sensing research. *Nature* 555:126. doi: 10.1038/nature25977

Wu, S., Liu, J., Liu, C., Yang, A., and Qiao, J. (2019). Quorum sensing for population-level control of bacteria and potential therapeutic applications. *Cell. Mol. Life Sci.* 77, 1319–1343. doi: 10.1007/s00018-019-03326-8

Yan, C., Li, B., Gu, Y., Jia, Y., Liu, Y., and He, Y. (2016). Methods for the determination of autoinducer-2—a review. *J. Microbiol. China* 43, 1333–1338. doi: 10.13344/j.microbiol.china.150514

Yang, Y., Zhou, M., Hou, H., Zhu, J., Yao, F., Zhang, X., et al. (2014). Quorum-sensing gene luxS regulates flagella expression and Shiga-like toxin production in F18ab *Escherichia coli*. *Can. J. Microbiol.* 60, 355–361. doi: 10.1139/cjm-2014-0178

Zhang, P., Xu, C., Zhou, X., Qi, R., Liu, L., Lv, F., et al. (2020). Cationic conjugated polymers for enhancing beneficial bacteria adhesion and biofilm formation in gut microbiota. *Colloids Surf. B Biointerfaces* 188:110815. doi: 10.1016/j.colsurfb.2020.110815

Zhao, J., Quan, C., Jin, L., and Chen, M. (2018). Production, detection and application perspectives of quorum sensing autoinducer-2 in bacteria. *J. Biotechnol.* 268, 53–60. doi: 10.1016/j.jbiotec.2018.01.009

Zhao, X., Yu, Z., and Ding, T. (2020). Quorum-sensing regulation of antimicrobial resistance in bacteria. *Microorganisms* 8:425. doi: 10.3390/microorganisms8030425

Zhu, G., Ma, S., Li, X., Zhang, P., Tang, L., Cao, L., et al. (2018). The effect of ethanol extract of Glycyrrhiza uralensis on the voltage-gated sodium channel subtype 1.4. *J. Pharmacol. Sci.* 136, 57–65. doi: 10.1016/j.jphs.2017.11.008

Zuberi, A., Misba, L., and Khan, A. U. (2017). CRISPR interference (CRISPRi) inhibition of *luxS* gene expression in *E. coli*: an approach to inhibit biofilm. *Front. Cell. Infect. Microbiol.* 7:214. doi: 10.3389/fcimb.2017.00214

Zuo, J., Yin, H., Hu, J., Miao, J., Chen, Z., Qi, K., et al. (2019). *Lsr* operon is associated with AI-2 transfer and pathogenicity in avian pathogenic *Escherichia coli*. *Vet. Res.* 50:109. doi: 10.1186/s13567-019-0725-0

frontiers | Frontiers in Microbiology

TYPE Original Research
PUBLISHED 06 January 2023
DOI 10.3389/fmicb.2022.987164

OPEN ACCESS

EDITED BY
Huancai Lin,
Sun Yat-sen University, China

REVIEWED BY
Jintae Lee,
Yeungnam University,
South Korea
Jules-Roger Kuiate,
University of Dschang, Cameroon

*CORRESPONDENCE
Hans P. Steenackers
hans.steenackers@kuleuven.be

SPECIALTY SECTION
This article was submitted to Antimicrobials, Resistance and Chemotherapy, a section of the journal Frontiers in Microbiology

RECEIVED 05 July 2022
ACCEPTED 18 November 2022
PUBLISHED 06 January 2023

CITATION
Villanueva X, Zhen L, Ares JN, Vackier T, Lange H, Crestini C and Steenackers HP (2023) Effect of chemical modifications of tannins on their antimicrobial and antibiofilm effect against Gram-negative and Gram-positive bacteria. *Front. Microbiol.* 13:987164. doi: 10.3389/fmicb.2022.987164

Effect of chemical modifications of tannins on their antimicrobial and antibiofilm effect against Gram-negative and Gram-positive bacteria

Xabier Villanueva[1], Lili Zhen[2,3], José Nunez Ares[4], Thijs Vackier[1], Heiko Lange[3,5], Claudia Crestini[3,6] and Hans P. Steenackers[1]*

[1]Faculty of Bioscience Engineering, Centre of Microbial and Plant Genetics (CMPG), KU Leuven, Heverlee, Belgium, [2]Department of Chemical Science and Technologies, University of Rome 'Tor Vergata', Rome, Italy, [3]CSGI – Center for Colloid and Surface Science, Sesto Fiorentino, Italy, [4]Division of Mechatronics, Biostatistics and Sensors (MeBioS), Department of Biosystems (BIOSYST), KU Leuven, Heverlee, Belgium, [5]Department of Earth and Environmental Sciences, University of Milano-Bicocca, Milan, Italy, [6]Department of Molecular Science and Nanosystems, Ca' Foscari University of Venice, Venice, Italy

Background: Tannins have demonstrated antibacterial and antibiofilm activity, but there are still unknown aspects on how the chemical properties of tannins affect their biological properties. We are interested in understanding how to modulate the antibiofilm activity of tannins and in delineating the relationship between chemical determinants and antibiofilm activity.

Materials and methods: The effect of five different naturally acquired tannins and their chemical derivatives on biofilm formation and planktonic growth of *Salmonella* Typhimurium, *Pseudomonas aeruginosa*, *Escherichia coli* and *Staphylococcus aureus* was determined in the Calgary biofilm device.

Results: Most of the unmodified tannins exhibited specific antibiofilm activity against the assayed bacteria. The chemical modifications were found to alter the antibiofilm activity level and spectrum of the tannins. A positive charge introduced by derivatization with higher amounts of ammonium groups shifted the anti-biofilm spectrum toward Gram-negative bacteria, and derivatization with lower amounts of ammonium groups and acidifying derivatization shifted the spectrum toward Gram-positive bacteria. Furthermore, the quantity of phenolic OH-groups per molecule was found to have a weak impact on the anti-biofilm activity of the tannins.

Conclusion: We were able to modulate the antibiofilm activity of several tannins by specific chemical modifications, providing a first approach for fine tuning of their activity and antibacterial spectrum.

KEYWORDS

tannins, antibiofilm activity, structure–activity relationships, *Salmonella* Typhimurium, *Escherichia coli*, *Pseudomonas aeruginosa*, *Staphylococcus aureus*

Introduction

Plant-derived tannins have been used from ancient times in leather industry because of their ability of making leather last over time, and the name "tannin" comes from the use of these chemicals for "tanning" leather (Falcão and Araújo, 2011; Pizzi, 2019). Accordingly, it was hypothesized that the resistance of leather to microbial decomposition could be explained by this use of tannin-rich compounds in leather curation and several studies have pointed to multiple additional pharmacological properties of tannins, including anti-inflammatory and anti-cancer effects, which are contributing to a renewed interest in these products as a source of new bio-based pharmaceuticals (Widsten et al., 2014; Vu et al., 2017; Pizzi, 2019; Farha et al., 2020). Tannins have been shown to inhibit bacterial growth of different Gram-positive and Gram-negative bacteria (Taguri et al., 2004; Ekambaram et al., 2016; Slobodníková et al., 2016; Chandra et al., 2017; Vu et al., 2017), and are shown to be able to disperse biofilms (Trentin et al., 2013). On some occasions this antibiofilm activity is specific and independent from the ability to inhibit bacterial growth (Ulrey et al., 2014). Common examples of tannins with antibacterial activity are tannic acid (Chung et al., 1998), ellagic acid (De et al., 2018) and epigallocatechin gallate (Akiyama, 2001).

From a molecular point of view, tannins can be divided in two main groups: condensed and hydrolysable tannins. Hydrolysable tannins are esters of gallic acid with a core sugar, often glucose or quinic acid. Tannic acid is the most prominent representative of the family of hydrolysable tannins comprising a glucose center (Koleckar et al., 2008; Ekambaram et al., 2016). Condensed tannins are oligomeric and polymeric proanthocyanidins, consisting of flavan-3-ol units, linked by carbon–carbon bonds not susceptible to hydrolytic cleavage (Koleckar et al., 2008; Versari et al., 2013). The scaffold of the subclass of tannins called complex tannins is very similar to those found in condensed and hydrolysable tannins, where a flavan-3-ol unit is linked to gallic acid in a monomeric or polymeric system (Falcão and Araújo, 2011). However, there is no reference in literature that this kind of differentiation has any effect on the level and kind of antimicrobial activity of the tannins.

To date, there is no clear understanding on the factors that explain the antimicrobial activity of tannins. It has been suggested that the observable activity could be explained by the presence of free phenolic hydroxyl groups which can affect, for example, enzymatic activity *via* covalent or non-covalent linking (Scalbert, 1991). In this respect, it has been seen that phenolic compounds can have antimicrobial effects against *Pseudomonas aeruginosa* and *Staphylococcus aureus* (Jagani et al., 2009; Lahiri et al., 2019). This ultimately means that the typical phenolic character of the tannins could play an important role for the antimicrobial activity (Mori et al., 1987; Baba and Malik, 2015). Other mechanisms of action for the antimicrobial activity of tannins have also been described, in particular for tannic acid, like disruption of peptidoglycan formation (Dong et al., 2018), iron chelation (Chung et al., 1998), membrane disruption (Kim et al., 2010), efflux pump inhibition (Tintino et al., 2016) and fatty acid synthesis (Wu et al., 2010).

It has also been shown in previous literature that tannins have the ability to reduce biofilm formation (Jagani et al., 2009; Klug et al., 2017; Dettweiler et al., 2019; Lahiri et al., 2019). Biofilms are conglomerates of bacteria, usually at an interphase (solid-air, solid–liquid, liquid-air), that are surrounded by a protective mesh of extracellular polymeric substances (EPS). This enhances the ability of the bacteria to survive dehydration, disinfectants and antibiotics (Rabin et al., 2015; Roy et al., 2018). The mechanisms of protection include reduced penetration of antimicrobial compounds, reduced bacterial metabolism, induction of efflux pumps and more frequent horizontal gene transfer (Rabin et al., 2015).

Regarding the antibiofilm activity of tannins, it has been described that some of them have a biofilm-specific mechanism of action, such as inhibition of quorum sensing (QS) in *P. aeruginosa* by the tannin-rich fractions of *Terminalia catappa* (Taganna et al., 2011) and *T. chebulata* (Sarabhai et al., 2013), and induction of transglucosylase activity in *S. aureus* by tannic acid (Payne et al., 2013). This type of biofilm-specific behavior is actually desired, because the lack of direct growth inhibition decreases the selective pressure toward resistance phenotypes (Allen et al., 2010; Imperi et al., 2019; Dieltjens et al., 2020).

Because of this reduced potential of resistance development, in the current study we evaluated selected chemical variants of tannins for their ability to inhibit biofilm formation without inhibiting planktonic growth. A diverse range of five commercially obtained tannins, three condensed tannins and two hydrolysable tannins, were included. The tannins were selected because they have been structurally thoroughly characterized in prior works and they are representative of the known molecular diversity of tannins. Also, we investigated how different chemical modifications change the activity level and spectrum of the tannins. Understanding the effect of structural features on activity allows to enhance or finetune activity. The functional groups chosen for derivatization were selected for known capacity (i) to interfere with membranes, i.e., ammonium groups; and (ii) to alter modes of interactions with surfaces, i.e., carboxylic acids and poly(ethylene glycol). The objective was to study the consequences of such chemical derivatizations at the molecular level and at the level of intermolecular interaction possibilities and obtain hints regarding matches and mismatches between tannin-type and tannin functionalization with respect to tuning anti-biofilm activities. The scarcity of structure–activity relationship (SAR) research in the field of tannins and bioactive phenolic compounds from plant sources as antimicrobial compounds highlights the value of this work (Fang et al., 2016; Bouarab-Chibane et al., 2019).

Materials and methods

Tannin assays and modifications

Assayed tannins

Five commercially available tannin extracts, comprising three condensed and two hydrolysable tannins were used. The three

condensed tannins were Omnivin 20R (monomeric (epi) catechin, ***Vv-20***), Omnivin WG (procyanidins (62%)/profisetidins (34%), ***Vv***) and Mimosa ATO ME (prorobinetidins (33%)/profisetidins (67%), ***Am***), and the two hydrolysable tannins were Tanal 01 (tannic acid, **Ta-01**) and Tanal 04 (galloylquinic acid, **Ta-04**). The chemical structures of these tannins were elucidated in detail as reported elsewhere (Zhen et al., 2021a). Figure 1A gives an overview of the structural features.

Modification of tannins

The five selected tannins were chemically modified by derivatizing them *via* their phenolic functionalities, as reported in detail elsewhere (Zhen et al., 2021b), with different levels of specific functional motifs: (i) hydroxy-*N*,*N*,*N*-trimethylpropanyl-3-aminium chloride (C_3NMe_3Cl-eq), (ii) hydroxypropyl-1-carboxylic acid (C_3COOH-eq), and (iii) oligomeric ethylene glycol polyether (PEG_{500}-eq), whereby "eq." in the compounds listed in Figure 1B indicates the equivalents of the functional motif that were used for the chemical modification (Zhen et al., 2021b). These chemical functionalizations gave several properties to the tannins: (i) C_3NMe_3Cl-eq added positive charges to the tannin molecule, (ii) C_3COOH-eq, as a weak acid, potentially added negative charges to the molecule, and (iii) PEG_{500}-eq polymerized the tannin molecules. During the various functionalizations, control tannins were re-isolated from blank reactions. Tannins labeled as "Blank-W" are tannins isolated from blank reactions performed in water and tannins labeled as "Blank-D" are tannins isolated from blank reaction preformed in dimethylformamide.

Because of the low solubility of the tannins in aqueous media, the dry compounds were first suspended in dimethyl sulfoxide (DMSO) at a stock concentration of 60 g/L and from there diluted to the desired concentration in the following experiments. A 1% v/v concentration of DMSO was never exceeded in order to prevent potential effects of DMSO on bacterial growth or biofilm formation.

All the tests were done in aerobic conditions in growth media with a pH of ~7.4 and a salinity range of 0.025–0.5% w/v.

Study of antibiofilm activities of tannins

The antibiofilm activities of the tannins were determined using 96-well plates with a cover lid with pegs for growing the bacterial biofilms in presence of several concentration of the assayed tannins. These assays, divided in a 1st exploratory screening (Section "Antibiofilm screening") and a 2nd validation experiment (Section "Validation anti-biofilm screening: Experimental design and statistical analysis"), are explained in detail in the following section.

Generation of biofilms of each microorganism

Biofilms of *Salmonella enterica* var. Typhimurium ATCC14028, *Pseudomonas aeruginosa* PA14, *Escherichia coli* TG1 and *Staphylococcus aureus* SH1000 were grown in the Calgary biofilm device *via* a protocol that was previously described (Janssens et al., 2008; Steenackers et al., 2011). The bacteria were grown overnight (ON) in LB broth at 37°C. These ON cultures were then diluted 1/100 in diluted (1/20) Tryptic Soy Broth (TSB, Thermo Fisher Scientific) for Gram-negative bacteria and in undiluted TSB for *S. aureus*. 100 µl of growth medium or a solution of the tannins in growth medium was added to the wells of a 96-well Calgary device (Nunc nos. 269789 and 445497, Thermo Fisher Scientific). The diluted ON cultures were then added to the wells to obtain a starting inoculum of 10^6 cfu/ml in a final volume of 200 µl of growth medium per well. Also, both for the exploratory screening test and validation of anti-biofilm activity, one row of the plate was filled with inoculum with growth media without tannin and another row was filled with media without bacteria. To account for potential effects of the compounds themselves, the same tannin-concentration was added to separate control 96-well Calgary biofilm plates without the inoculation of the bacteria. Afterwards, all plates were incubated in a wet chamber for the appropriate time and temperature: 48 h at 37°C for *S. aureus*, 24 h at 25°C for the Gram-negatives.

Biofilm formation and planktonic growth were determined by crystal violet staining of the pegs and OD_{600} measurements of the base plate of the device, respectively. Specifically, after incubation the covers of the plates (which contain the pegs) were removed and washed once with PBS. The pegs were then stained with 200 µl per well of 0.1% v/v of crystal violet (CV, VWR International) for 30 min. After staining, the excess of CV was washed once with 200 µl per well of distilled water and let dry for 30 min. Finally, the CV was recovered in a new 96-well plate with 200 µl per well of 30% v/v glacial acetic and the optical density at 570 nm (OD_{570}) measured in a plate reader. The optical density at 600 nm (OD_{600}) of the bacteria in the base plates was measured to determine the growth of the planktonic cells.

Antibiofilm screening

In a preliminary experiment, the tannins were tested in two-fold dilution series ranging from 600 to 9.38 mg/L in 3 independent replicates. The obtained raw OD_{570} (for the biofilm formation) and OD_{600} (for the planktonic growth) were corrected by the OD of the tannins incubated in absence of bacterial inoculum and then normalized using the average OD of the bacterial inoculum incubated in absence of tannin, thus being converted to percentage of biofilm formation (OD_{570}) and percentage of bacterial growth (OD_{600}).

The BIC_{50} and IC_{50} (the compound concentration required to inhibit the biofilm formation and the bacterial growth by 50%, respectively) were calculated by applying a log [tannin] vs. percentage of biofilm formation or percentage of planktonic growth non-linear regression (four-parameters) using the statistical package GraphPad 8.0.

Validation anti-biofilm screening: Experimental design and statistical analysis

Based on the information from the preliminary experiment, a definitive antibiofilm experiment in the Calgary biofilm device

10.3389/fmicb.2022.987164

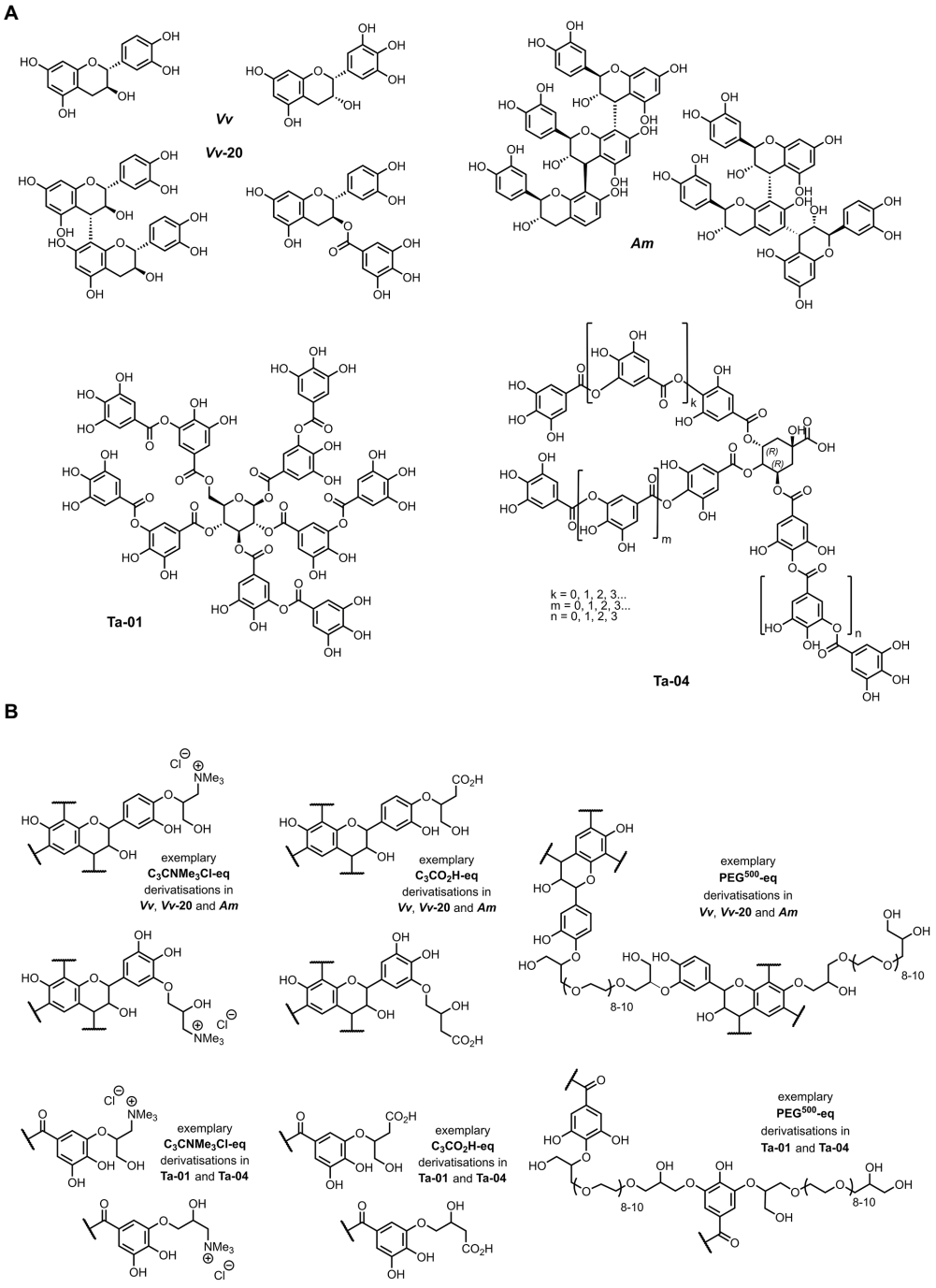

FIGURE 1
(A) Chemical structure of commercially available condensed and hydrolysable tannins used in this study (40) and **(B)** their chemically derivatized structures as described elsewhere (41). Exemplary structural aspects are shown; synthetic route leads to generation of both primary and secondary aliphatic alcohols within the total C_3 linker moiety connecting the functional to the tannin (41). (i) C_3NMe_3Cl-eq – hydroxy-*N*,*N*,*N*-trimethylpropanyl-3-aminium chloride; (ii) C_3COOH-eq – hydroxypropyl-1-carboxylic acid; and (iii) PEG_{500}-eq – oligomeric ethylene glycol polyether (PEG_{500}-eq).

was set up with eight independent repeats. We first defined the factors under study, i.e., the parameters that potentially have an influence on the formation of biofilm. The considered parameters are: (i) original unmodified tannin: ***Vv-20***, ***Vv***, ***Am,*** **Ta-01**, **Ta-04**; (ii) concentration of tannin (mg/L): 9.38, 79.69, 150; (iii) chemical modifier: C_3COOH, PEG, C_3NMe_3Cl, Blank-D (blank reaction with dimethylformamide), Blank-W (blank reaction with water), unmodified; and (iv) concentration of applied chemical modifier: low and high (low: 0.05 and 0.1 eq of chemical substitution; high: 0.25 and 0.5 eq of chemical substitution). In order to minimize

effects of plate-to-plate variation, we applied an optimal randomized experimental design with the statistical package JMP 15.0 to reduce experimental noise and confounding factors. Different to the preliminary experiment, only three concentrations were assayed, which were chosen to best capture the antibiofilm activity of the tannins: 9.38, 79.69, and 150 mg/L. The remaining part of the protocol of this experiment is identical to that of the preliminary experiment described above.

To determine the effect of the chemical derivatizations on the antibiofilm and antibacterial effect of the unmodified tannins on each of the assayed bacteria, an ANOVA test with Tukey post-hoc test comparing the unmodified tannins with their respective derivatized tannins was done based on the obtained biofilm formation and planktonic growth levels.

Relationship between the phenolic hydroxyl content and antibiofilm effect

To determine the effect of phenolic hydroxyl (OH) content on the antimicrobial and antibiofilm effect of the different tannins, a simple linear regression between the phenolic OH content of the tannins and the level of biofilm formation (or planktonic growth) was performed. To better calculate this correlation, we used the different tannin assayed concentrations and the obtained mmol of phenolic OH per gram of material to calculate the mmol of phenolic OH present in the system for each tannin at each assayed concentration, and we correlated this value with the respective percentage of biofilm inhibition and planktonic growth inhibition. The phenolic OH content of the tannins was determined *via* ^{31}PNMR as described elsewhere (Zhen et al., 2021a).

Results and discussion

Exploratory screening to determine the concentration test range

A diverse range of five commercially obtained tannins, and five types of derivatives, were selected and screened for anti-biofilm activity. The condensed tannins were previously identified as mixtures of (epi) catechins and fisetinidols (Zhen et al., 2021a) and consisted of (i) the essentially monomeric ***Vv-20***, (ii) the low oligomeric ***Vv*** and (iii) the higher oligomeric ***Am***. The hydrolysable tannins consisted of two large tannins: (i) the "typical" tannic acid **Ta-01** and (ii) the galloquinic acid derivative **Ta-04**. All tannins were previously functionalized with a positive charge introducing ammonium salt hydroxy-*N*,*N*,*N*-trimethylpropanyl-3-aminium chloride (C_3NMe3Cl-0.1 and C_3NMe3Cl-0.5), an acidifying hydroxypropyl-1-carboxylic acid (C_3COOH-0.1 and C_3COOH-0.1-0.5) motive and a polymerizing oligomeric ethylene glycol polyether (PEG_{500}-0.05; Figure 1). The preventive activity of both the natural and derivatized tannins against the biofilm formation and planktonic growth of the Gram-negative species *S.* Typhimurium, *P. aeruginosa*, *E. coli* and the Gram-positive species *S. aureus* was evaluated by means of the Calgary biofilm device. In a first set of exploratory experiments, two-fold serial dilutions (from 600 till 4.96 mg/L) of the tannins were evaluated in order to obtain a first glance on activity spectrum and active concentration range. Activities against all four bacterial species were observed, with BIC_{50} values ranging from 4.69 to 545.8 mg/L and IC_{50} values ranging from 37.5 to 459.2 mg/L (Supplementary Table S1). As such this experiment allowed to determine the test concentrations for future validation experiments: 9.38 mg/L was the lowest assayed concentration in the preliminary screening and the most active tannins exhibited BIC_{50} equal to or below that value; 150 mg/L was the concentration at which almost all tannins with antibiofilm effect were active; and 79.69 mg/L is the average of those two concentrations. Such validation experiments were required because the exploratory experiments only had three independent repeats and this did not provide sufficient statistical power to distinguish the levels of activity of the different tannins and delineate the relationship between the chemistry and the antibiofilm level of the tannins. Furthermore, there was a statistically significant plate-to-plate variation between the controls of each plate (see Supplementary Figures S1, S2).

Extensive randomized validation screening at limited number of concentrations

To allow a multivariate analysis considering tannin scaffold, derivatization and concentration as well as bacterial target species, the previous antibiofilm and antimicrobial experiments were repeated in one experiment with eight repeats per condition, but only focusing on the three tannin concentrations that could capture best the antibiofilm effect of the tannins: 9.38, 79.69, and 150 mg/L. In order to minimize previously observed effects of plate-to-plate variation, these experiments were designed in a randomized way, i.e., all the tannins were distributed through all the plates in a random fashion. This allowed to decrease the random error and the possibility of confounding factors, a necessary step for doing a complex statistical analysis that allows to link the different chemical characteristics. In what follows we will first focus on the unmodified tannins, after which we will elaborate on the effect of chemical derivatization.

To determine the percentual inhibition of biofilm formation and planktonic growth of the assayed tannins against the selected bacteria, the bacterial growth and biofilm development in absence of tannin was taken as reference. As can be seen in Supplementary Figure S3, the assayed bacteria exhibited differences in their biofilm formation and bacterial growth, *Staphylococcus aureus* being the bacterium that reached the highest planktonic population density and formed most biofilm. On the contrary, the assayed Gram-negative bacteria showed less biofilm and less planktonic growth in comparison with *S. aureus*.

Effect of unmodified tannin scaffold on the antibiofilm activity level and spectrum

In Figure 2 it can be seen that the commercially available natural tannins showed different antibiofilm activities against the four assayed bacterial species. All unmodified tannins can be considered to have "broad spectrum activity," since all of them exhibited statistically significant antibiofilm activity against Gram-positive and Gram-negative bacteria at least at the concentration of 150 mg/L, according to an ANOVA test with Tukey post-hoc analysis. Also, most of the assayed tannins exhibited a concentration-dependent activity, depending on the assayed tannin and the tested bacteria.

However, there were clear differences in the degree of antibiofilm activity of each tannin. Starting from the condensed tannins, the monomeric ***Vv-20*** exhibited significant antibiofilm activity against all the assayed bacteria at all the assayed concentrations in a clear dose-dependent way, a dose of 79.69 mg/L being sufficient for inhibiting biofilm formation more than 50% against the four assayed bacteria. Also, ***Vv-20*** was the most effective tannin against *S.* Typhimurium, with more than 75% of biofilm inhibition at 79.69 and 150 mg/L, and against *E. coli*, with more than 80% biofilm inhibition at 79.69 mg/L. Regarding the low oligomeric ***Vv***, the antibiofilm activity was preferential against *P. aeruginosa* and *S. aureus*, for which it exhibited potent dose-dependent antibiofilm activity. This compound was able to inhibit more than 50% of biofilm formation by *S. aureus* both at 79.69 and 150 mg/L, and is the unmodified tannin with highest effect against *P. aeruginosa*, displaying antibiofilm activity of more than 90% at 79.69 mg/L and more than 95% at 150 mg/L. On the contrary, ***Vv*** was less effective against *S.* Typhimurium and *E. coli* and was able to inhibit <30% of biofilm formation of both bacterial species, regardless of the assayed concentration. Contrary to the previous two unmodified condensed tannins, the high oligomeric *Am* had preferential antibiofilm activity against *S.* Typhimurium and *S. aureus*, but also had significant antibiofilm activity against *P. aeruginosa*. Moreover, *Am* is the unmodified tannin with the highest antibiofilm activity against *S. aureus*, with more than 85% of antibiofilm activity at 79.69 and 150 mg/L, also inhibiting more than 50% of biofilm formation of *S.* Typhimurium both at 79.69 and 150 mg/L, and inhibiting *P. aeruginosa* biofilm formation in more than 30% at 79.69 mg/L and more than 50% at 150 mg/L. On the contrary, *Am* had unnoticeable inhibitory activity against *E. coli* biofilms at any of the assayed concentrations.

With respect to the hydrolysable tannins, tannic acid, **Ta-01** exhibited preferential activity against *P. aeruginosa* and *S.* Typhimurium. The biofilm inhibitory activity of **Ta-01** ranged from 40% at 9.38 mg/L to 60% at 150 mg/L against *S.* Typhimurium, and from 15% at 9.38 mg/L to more than 90% at 150 mg/L against *P. aeruginosa*. On the contrary, the galloquinic acid derivative, **Ta-04** exhibited preferential activity against *S. aureus*. While the antibiofilm activity of **Ta-04** against *S.* Typhimurium and *E. coli* was dose dependent (reaching a maximum of 50% biofilm inhibition against both bacteria at a concentration of 150 mg/L), the antibiofilm activity of **Ta-04** against *S. aureus* was not dose dependent, with more than 70% biofilm inhibition at the three assayed concentrations.

Importantly, the unmodified tannins were in general not found to have antibacterial activity against the planktonic bacteria, except for the low oligomeric condensed ***Vv*** against *S.* Typhimurium and the hydrolysable tannic acid **Ta-01** against *E. coli* at the highest concentration of compound (Figure 2). In previous reports, it was found that hydrolysable tannins similar to galloylquinic acid, hence similar to **Ta-04**, exhibit broad spectrum antibiofilm activity (Widsten et al., 2014; Ekambaram et al., 2016; Puljula et al., 2020). Those same reports, however, also suggest that hydrolysable tannins have antibacterial effects against planktonic Gram positive and Gram bacteria, which was not observed in our experiment. On the other hand, tannic acid (Lee et al., 2013) and 1,2,3,4,6-penta-*O*-galloyl-β-D-glucopyranose (Lin et al., 2011), both hydrolysable tannins, have been reported to inhibit biofilm formation of *S. aureus* without inhibiting planktonic growth, which is consistent with the results observed for tannic acid **Ta-01**. In our assay, also galloylquinic acid **Ta-04** showed such activity. This selective activity against biofilms offers opportunities for potential applications, such as the titanium-tannin composite coating for implants developed by Shukla and Bhathena (2015), that allows sustained release of the tannin.

Effect of chemical substitutions on the antibiofilm and antibacterial activity of the tannins

The aim of the modifications was to partially functionalize *via* ether linkages the phenolic OH-groups of each tannin molecule and to add tannin-alien functionalities at various levels to test the possibility to modulate the native activity of tannins toward biofilms and planktonic bacteria.

Figure 3 shows the effect of derivatization on the antibiofilm activity. The differences in antibiofilm activity between the different modifications were assessed *via* the Tukey test for multiple comparisons, by comparing if there were differences in the maximum activity (i.e., the antibiofilm activity at the highest assayed concentration). If there were no differences in the maximum activity, the activity at lower concentrations was also evaluated, thus allowing to determine if a derivatization was able to obtain the same effect as the unmodified tannin, but at a lower concentration.

As a general conclusion, it could be established that most of the chemical derivatizations, but especially positive charge introducing **C_3NMe_3Cl-0.1** reduce the antibiofilm activity of the tannins, while some of them can shift the activity spectrum toward preferential activity against Gram-positive or Gram-negative bacteria. More importantly, it must be noted that, in general, the chemical derivatizations increased the activity against

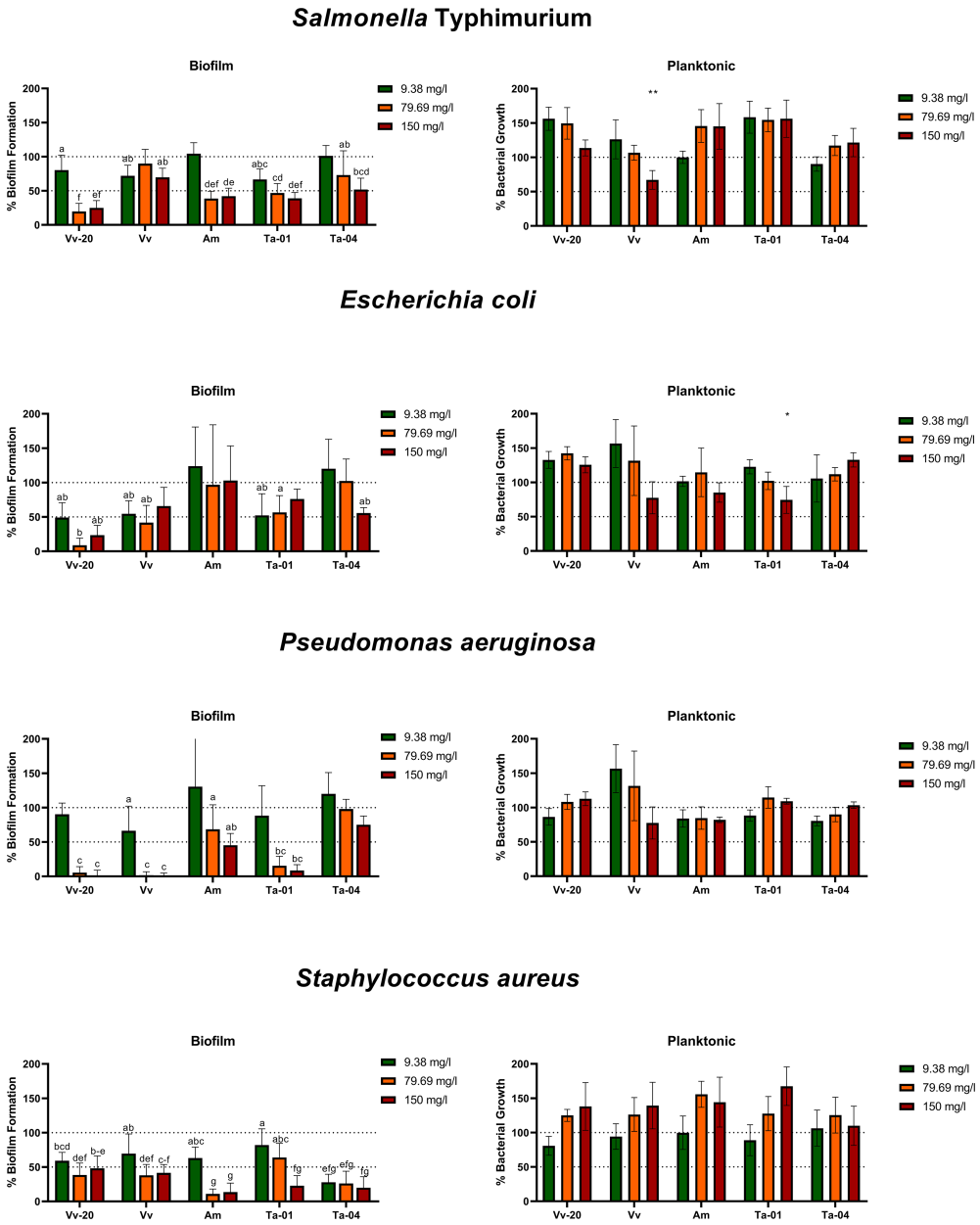

FIGURE 2
Biofilm formation and planktonic growth of the assayed bacteria (expressed as percentage in comparison to control) in the presence of 9.38, 79.69, and 150mg/L of unmodified tannins. The letters in the biofilm formation graphs indicate groups of tannin-concentration combinations whose effects are significantly different from the control but not significantly different to each other; the bars with no letter are those tannin-concentration combinations which are not significantly different from the control. Asterixis in the planktonic growth graphs indicate a significant difference from control, *=p<0.05; **=p<0.01. The statistical differences were determined *via* ANOVA test with Tukey post-hoc analysis, with a p-value of 0.05.

planktonic bacteria and decreased the activity against bacterial biofilms of the unmodified tannins, thus decreasing the biofilm specificity of the assayed tannins (see Supplementary Figures S4–S7 for a direct comparison between growth inhibitory effect and biofilm inhibitory capability of the assayed tannins against each bacterial species). This effect will be discussed in more detail in Section "Biofilm selectivity of the antibiofilm effect of the assayed tannins."

Two derivatizations generally shifted the antibiofilm spectrum toward the Gram-negative group of bacteria: polymerizing **PEG_{500}-0.05** and positive charge-introducing **C_3NMe_3Cl-0.5**. Contrarily, derivatization with acidifying **C_3COOH-0.1** and **C_3COOH-0.5** in general decreased the antibiofilm activity against Gram-negative bacteria, while it retained activity against *S. aureus* for larger tannins ***Am***, **Ta-01** and **Ta-04**, and increased activity against *S. aureus* for monomeric and low oligomeric ***Vv-20*** and

Vv. The other derivatizations in general decreased the activity against *S. aureus*. However, this effect of derivatizations on the spectrum and potency was highly dependent on the specific tannin submitted to the derivatization.

In more detail, it can be seen that the blank reaction (both in water -Blank-W- and in dimethylformamide -Blank-D-) already modified the antibiofilm effect of the assayed tannins, a phenomenon that could be attributed to removal of impurities that affect the antibiofilm effect of the tannins. It can be seen that Blank-W conditions increased the maximum antibiofilm effect of ***Vv*** against *Salmonella* Typhimurium, but decreased the maximum antibiofilm effect of ***Vv-20*** and ***Vv*** against *P. aeruginosa* and decreases the antibiofilm effect of ***Vv-20*** against *E. coli* at 79.69 mg/L without affecting its maximum antibiofilm effect. It can also be seen that Blank-D conditions only affected the antibiofilm activity of **Ta-04**, by reducing its antibiofilm effect against Gram-negative bacteria.

Regarding actual substitutions, it can be seen that the effect of a derivatization with positive charge introducing ammonium groups, i.e., C_3NMe_3Cl, was different depending on the equivalents of chemical substitution.

On the one hand, C_3NMe_3Cl-0.5, the high equivalent derivatization, decreased the maximum antibiofilm effect of condensed tannins against *S. aureus* but did not affect the anti-staphylococcal effect of hydrolysable tannins. However, C_3NMe_3Cl-0.5 derivatization had a tannin-dependent effect against Gram-negative bacteria. It did not affect the antibiofilm effect of monomeric ***Vv-20*** against any Gram-negative bacteria but increased the maximum antibiofilm effect of low oligomeric ***Vv*** against *Salmonella* Typhimurium while decreasing the

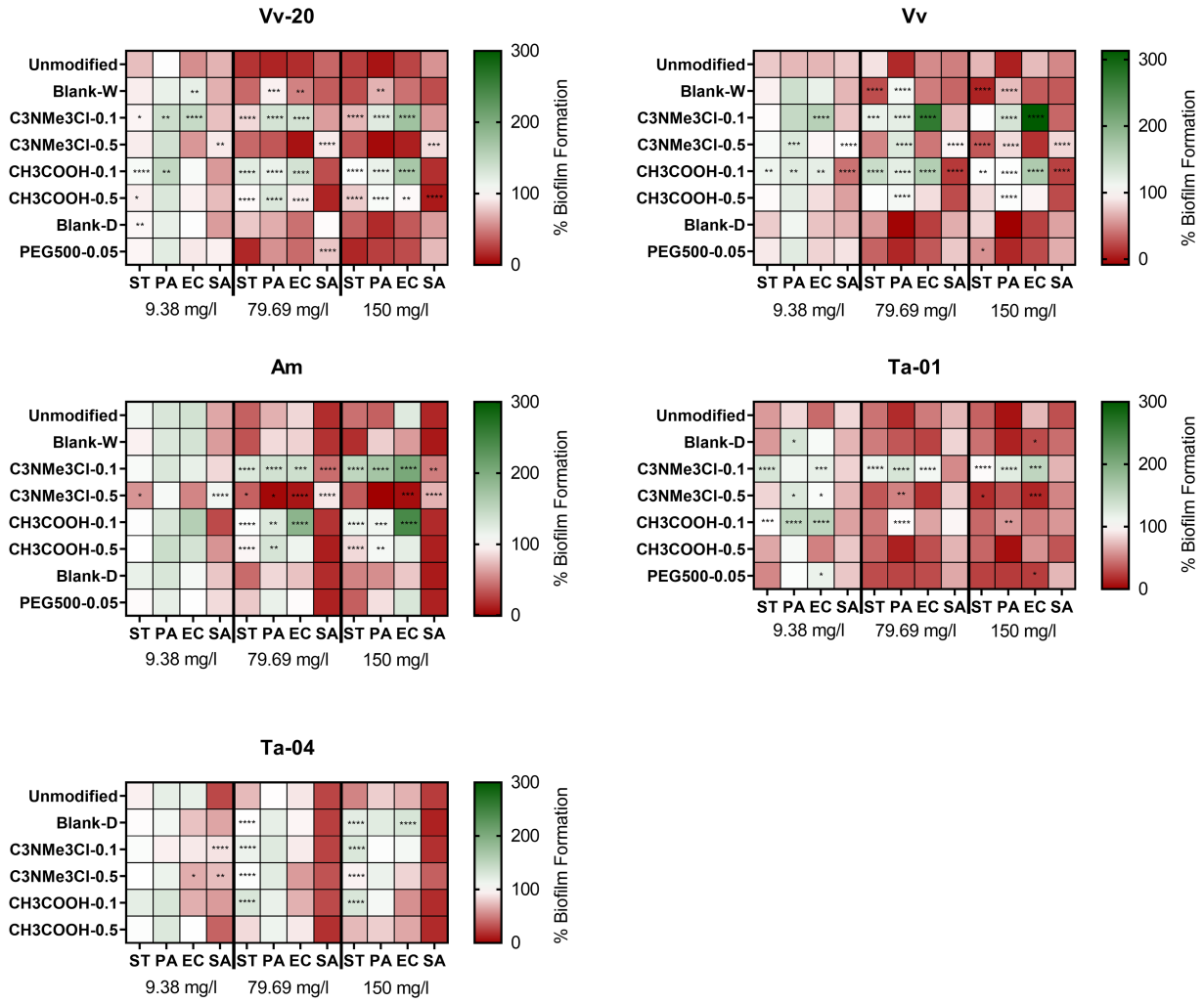

FIGURE 3
Effect of natural and chemically modified tannins on biofilm formation (expressed as percentage compared with positive control) on several bacterial species at 9.38, 79.69, and 150mg/L of tannin. The colors indicate the percentage of biofilm formation in presence of several concentrations of the assayed tannins compared to the untreated control. The asterisks indicate significant differences with the unmodified tannin, following ANOVA test with Tukey post-hoc analysis. *: $p \leq 0.05$; **: $p \leq 0.01$; ***: $p \leq 0.001$; ****: $p \leq 0.0001$.

maximum antibiofilm effect of ***Vv*** against *P. aeruginosa*. It increased the effect of high oligomeric *Am* against all the Gram-negative bacteria at 79.69 mg/L without significantly changing the maximum effect compared to the unmodified tannin. It increased the maximum effect of tannic acid **Ta-01** against *E. coli* and *Salmonella* Typhimurium but decreased the effect against *P. aeruginosa* at 79.69 mg/L and it significantly decreased the maximum antibiofilm effect of galloquinic acid derivative **Ta-04** against *Salmonella* Typhimurium. On the other hand, C_3NMe_3Cl-0.1, the low equivalent derivatization, reduced the maximum effect of all tannins (with the exception of the galloquinic acid derivative **Ta-04**, which was not affected) against Gram-negative bacteria without affecting the antibiofilm effect against *S. aureus*.

Contrary to C_3NMe_3Cl, there were no big differences between different levels of derivatizations with acidifying motif CH_3COOH, i.e., CH_3COOH-0.1 and CH_3COOH-0.5, in terms of their impact on the activities compared to the unmodified tannins. For *S. aureus*, neither derivatization level affected the antibiofilm effect exerted by larger tannins ***Am***, **Ta-01**, and **Ta-04**, comparable to the C_3NMe_3Cl-0.1 derivatization, while CH_3COOH-0.1 increased the maximum effect of low oligomeric ***Vv***. CH_3COOH-0.5 had a similar effect on essentially monomeric ***Vv-20***. For the Gram-negative bacteria, both derivatizations equally decreased the maximum antibiofilm effect of condensed tannins ***Vv-20*** and ***Am***, as well as for hydrolysable tannin **Ta-04** against *S.* Typhimurium, but only CH_3COOH-0.1 significantly decreased the maximum antibiofilm effect against *S.* Typhimurium of ***Vv***. While both derivatization levels drastically decreased the maximum antibiofilm effect of condensed tannins against *P. aeruginosa*, only CH_3COOH-0.1 decreased the maximum antibiofilm effect of tannic acid **Ta-01**. Neither derivatization level significantly affected the antibiofilm effect of hydrolysable **Ta-04**. This effect was similar regarding *E. coli* because neither derivatization level affected the maximum antibiofilm effect of hydrolysable tannins, while CH_3COOH-0.1 decreased the maximum antibiofilm effect of all condensed tannins. CH_3COOH-0.5 only significantly decreased the maximum antibiofilm effect of ***Vv-20*** against *E. coli*.

Regarding derivatization with polymerizing PEG_{500}, it can be seen that PEG_{500}-0.05 in general did not affect the antibiofilm effect of the assayed tannins. The only exceptions are the increase in the maximum antibiofilm effect of low oligomeric ***Vv*** against *Salmonella* Typhimurium and the decrease in the antibiofilm effect of monomeric ***Vv-20*** against *S. aureus* at 79.69 mg/L without changing the maximum antibiofilm effect. It has to be taken in account that, due to technical issues, it was not possible to analyze the effect of polymerizing PEG_{500}-0.05 derivatization on **Ta-04**. Polymerizing PEG_{500}-0.05 derivatization proofed difficult to analyze in terms of loading for **Ta-04** (Zhen et al., 2021b).

No literature data are yet available that would describe the effects of chemical modifications of tannins on their antibiofilm, or more generally antibacterial activity. With the aim of elucidating a hypothesis about the reason behind the effect of the derivatizations on our assayed tannins in comparison to the parent tannins and the blanks, we decided to look into other non-tannin organic compounds.

One of these examples targets the effect of the high equivalent derivatization C_3NMe_3Cl-0.5 in shifting the antibiofilm spectrum toward Gram-negative bacteria, which may be associated with addition of positive charges in the form of ammonium groups to the tannin molecules. This allows for comparison of our results with data obtained by Dalcin et al. (2017), who discovered that nanoencapsulation of dihydromyricetin within the polycationic polymer Eudragit RS 100® not only increased its antibiofilm activity against *P. aeruginosa*, but that the polymer itself had antibiofilm activity. This finding goes in accordance with a previous publication of Campanac et al. (2002) which states that cationic quaternary ammonium compounds were more effective against *P. aeruginosa* than *S. aureus* biofilm. Also, Gao et al. (2019) showed a decreased biofilm formation in *E. coli* and *S. aureus* using positively charged nanoaggregates based on zwitterionic pillar-[5] arene, requiring a 10 times lower concentration of nanoaggregate to decrease biofilm formation in *E. coli* compared to *S. aureus*. These results suggest that equipping the tannins with positive charge-introducing ammonium groups may give preferential action against Gram-negative bacteria. However, tannins should be derivatized with enough positive charge-introducing ammonium groups to obtain this shift toward inhibition of Gram-negative bacteria since the low equivalent derivatization C_3NMe_3Cl-0.1 appeared to lower the activity against Gram-negative bacteria.

Regarding the effect of acidifying CH_3COOH derivatizations, there is a precedent of the effect of several substitutions on the antibiofilm effect of anthraquinones against methicillin-resistant *S. aureus* (MRSA; Song et al., 2021). This study shows that a carboxyl group at position 2 of the anthraquinone molecule increases both the antibiofilm and the antimicrobial activity, which is partially in agreement with our data that shows that CH_3COOH derivatizations increase the antibiofilm activity of low oligomeric ***Vv-20*** and essentially monomeric ***Vv*** without affecting the bacterial growth. Relatedly, Warraich et al. (2020) found that the acidic D-amino acids D-aspartic acid and D-glutamic acid were effective in dispersing and inhibiting biofilm formation in *S. aureus*, and they attributed this effect to the negative charges introduced by carboxyl groups of the molecules under growth conditions.

Finally, regarding polymerizing PEG derivatizations, there are several studies about the potential of PEG cross-linked hydrogels for wound healing because of their antimicrobial, pro-angiogenesis and pro-epithelization capabilities (Chen et al., 2019), but there is no indication regarding the effect of an introduction of a PEG-motif on the antibiofilm capability of an organic compound.

Biofilm selectivity of the antibiofilm effect of the assayed tannins

In the last years, there has been increasing research on non-lethal antimicrobial targets against several bacterial species, from virulence factors to biofilm formation, including inhibition of regulatory mechanisms such as quorum sensing and production of public goods (Defoirdt et al., 2013; Defoirdt, 2016; Maura et al., 2016; Totsika, 2016). The rationale behind this research is the assumption that if bacterial viability is not affected, the selective pressure will be lower and thus the risk for emergence of antimicrobial resistance will be lower too (Kalia et al., 2014; Dieltjens et al., 2020; Hemmati et al., 2020). However, there is still discussion about the effectiveness of this "resistant-proof" approach (García-Contreras et al., 2016).

The heatmap of Figure 4 shows the anti-planktonic activity of the tannins at the assayed concentrations. We defined that the antibiofilm activity of a particular tannin was biofilm specific in case the tannin did not exhibit significant anti-planktonic effect at that concentration (Dos Santos Goncalves et al., 2014; Vijayakumar and Thirunanasambandham, 2021). Most of the tannins with antibiofilm activity did not exhibit anti-planktonic effects, indicating that they are biofilm specific. This is particularly true for unmodified tannins, of which only ***Vv*** and **Ta-01** exhibited anti-planktonic activity against *Salmonella* Typhimurium and *E. coli*, respectively. Also, unmodified tannins re-isolated from blank reactions, i.e., Blank-W or Blank-D, with the exception of Blank-D against *Salmonella* Typhimurium, did not reduce the planktonic growth of the assayed bacteria.

Regarding the effect of derivatizations on the biofilm specificity of the tannins, this was both derivatization and species dependent. Derivatization with positive charge introducing C_3NMe_3Cl-0.1 not only generally decreased the antibiofilm activity of the assayed tannins, but also increased the anti-planktonic activity specifically against Gram-negative bacteria. Antibiofilm specificity of tannins derivatized with C_3NMe_3Cl-0.5 was highly dependent on both the assayed bacteria and the derivatized tannin: the antibiofilm effect was non-specific when the derivatization was applied to ***Vv-20***, but it was biofilm-specific for ***Vv***, ***Am*** and **Ta-01**. Also, tannins derivatized with C_3NMe_3Cl-0.5 most strongly affected the growth of *P. aeruginosa* except for ***Am***-C_3NMe_3Cl-0.5, which did not affect the growth of *P. aeruginosa* at any concentration. Only a derivatization of **Ta-04**, and here especially with C_3NMe_3Cl-0.5, led to a dose-dependent anti-planktonic effect, thus exhibiting non-specific antibiofilm activity at higher concentrations. With respect to a functionalization with the acidifying element CH_3COOH at various concentrations, it can be stated that these in this study did not significantly change the anti-planktonic behavior of the derivatized ***Vv***, ***Am*** and **Ta-01** against the assayed bacteria, but increased the antibacterial effect of ***Vv-20*** and **Ta-04** against planktonic bacteria. However, one notable exception are the tannins that were modified with crosslinking PEG_{500}-0.05, whose antibiofilm activity against Gram negative bacteria was highly correlated with the ability to inhibit the planktonic growth (Figure 4).

As a general summary, tannin derivatization did not affect biofilm specificity against *S. aureus* but affected the biofilm specificity against Gram-negative bacteria in a tannin-specific and derivatization specific manner. More importantly, there was no correlation in the assayed tannins between the degree of inhibition of planktonic growth and the degree of antibiofilm effect, a situation that goes in accordance with some previous reports (Janecki and Kolodziej, 2010; Payne et al., 2013; Hricovíniová et al., 2021).

Relation between antibiofilm effect and phenolic hydroxyl group content of the tannins

One of the potential consequences of the chemical derivatization of the tannins are changes in the content of free phenolic hydroxyl groups present in the chemical structure of the tannins, since functionalization occurs at these hydroxyl groups. This is potentially important, because in previous literature it has been described that the biological activity of polyphenols could be mediated by their phenolic hydroxyl groups (Ultee et al., 2002; Ito et al., 2005; Ben Arfa et al., 2006; Veldhuizen et al., 2006; Alves et al., 2013; d'Avila Farias et al., 2014; Salar et al., 2017). Particularly regarding hydrolysable tannins, Taguri linked the degree of antibacterial activity to the presence of galloyl groups (Taguri et al., 2004). Because of this, we aimed to determine if there was a significant impact of the derivatizations on the phenolic hydroxyl (OH) content of the tannins, and if the phenolic OH content affected the antibiofilm.

In a first approach, we studied the impact of derivatizations on the phenolic OH content of the tannins. As can be seen in Table 1, derivatizations with C_3NMe_3Cl-0.1 decreased the phenolic OH content of the unmodified tannin. This is important, since derivatization with C_3NMe_3Cl-0.1 significantly decreased the antibiofilm effect of tannins, mostly against Gram negative bacteria. In a similar trend, derivatizations with CH_3COOH tended to decrease the phenolic content of condensed tannins: derivatization with CH_3COOH decreased the antibiofilm effect against Gram negative bacteria of condensed tannins, but, interestingly, not of still larger hydrolysable tannins.

In a second approach, we hence studied potential correlations between the phenolic OH content and the antibiofilm activity and we observed a weak correlation between the phenolic OH content and the antibiofilm activity against Gram negative bacteria and, to a lesser extent, against *S. aureus* (see Supplementary Figure S8). These data, combined with the previously mentioned effect of the different derivatizations on the phenolic OH content of the tannins,

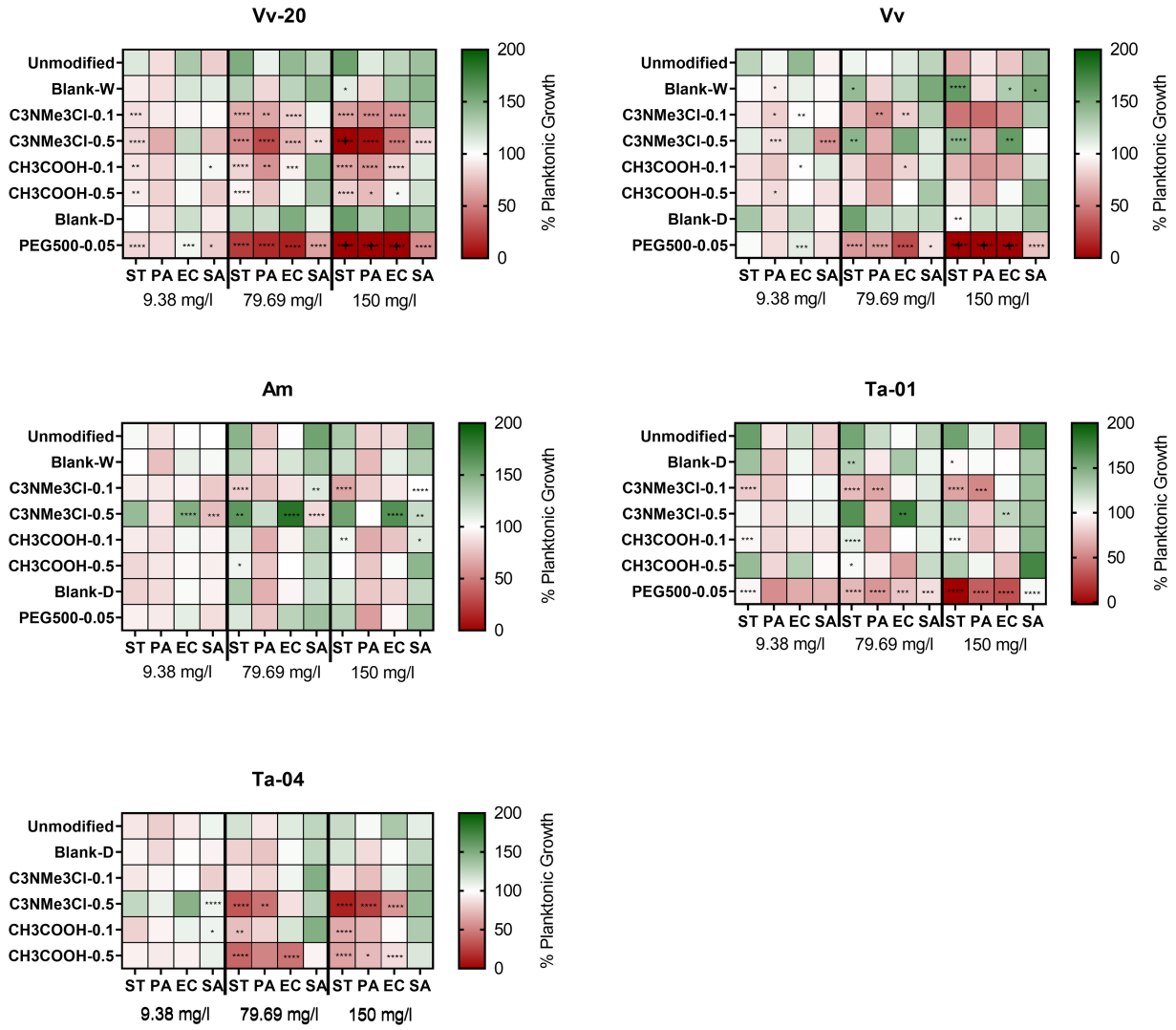

FIGURE 4
Effect of natural and chemically modified tannins on planktonic growth (expressed as percentage compared with control) on several bacterial species at 9.38, 79.69, and 150mg/L of tannin. The crosses (+) for PEG_{500}-0.05 derivatization on ***Vv-20*** and ***Vv*** indicate values below zero, which is an effect of potential overcorrection of the raw values by the negative control. The colors indicate the percentage of planktonic growth in presence of several concentrations of the assayed tannins compared to the untreated control. The asterisks indicate significant differences with the unmodified tannin, following ANOVA test with Tukey post-hoc analysis. *: $p \leq 0.05$, **: $p \leq 0.01$; ***: $p \leq 0.001$; ****: $p \leq 0.0001$.

suggest that the phenolic OH content of the tannins is more important for the antibiofilm effect against Gram negative bacteria than against *S. aureus*. However, we did not observe a correlation between the antibacterial activity against planktonic bacteria and the phenolic OH content of the assayed tannins (see Supplementary Figure S9), which is in accordance with the study Kim et al. (2020), who did not find a significant correlation between the total phenolic content of several plant extracts from Chinese traditional medicine and the antimicrobial activity against *S. aureus*. However, this contradicts a previous study from Vattem et al. (2004), who found a linear correlation between the phenolic content of cranberry pomace and the antimicrobial activity against *Listeria monocytogenes*, *Vibrio parahaemolyticus* and *E. coli*.

It is important to note that the previous studies are focused on the antibacterial effect against planktonic bacteria, since there are no previous studies pointing to the effect of the hydroxyl or phenolic content on the capability of tannins to inhibit biofilms. However, research on other classes of polyphenolic compounds showed that the quantity and the position of the hydroxyl groups affects the capabilities of polyphenolic compounds to disperse biofilm, which could explain the results obtained in this research with the assayed tannins. In more detail, the research of Cho et al. on the capability of flavonoids to disperse *S. aureus* biofilms

TABLE 1 Phenolic OH content (in mmol phenolic OH/g materials) of unmodified and derivatized tannins.

Tannin	Unmodified	Blank-W	Blank-D	C_3NMe_3Cl-0.1	C_3NMe_3Cl-0.5	CH_3COOH-0.1	CH_3COOH-0.5	PEG_{500}-0.05
Vv-20	10.37	7.85	8.79	4.35	N.d.[a]	6.19	6.15	7.03
Vv	5.38	6.83	11.7	3.26	5.21	1.51	5.09	7.11
Am	8.35	7.64	10.27	0.45	N.d.[a]	5.76	3.76	8.03
Ta-01	12.56	■[b]	10.99	1.55	7.22	10.05	11.61	8.87
Ta-04	10.49	■[b]	6.89	6	N.d.[a]	9.89	9	6.77

The values were obtained using ^{31P}NMR. [a]N.d.: Not possible to calculate phenolic OH content due to solubility issues.
[b]■ Blank-W reaction was not performed with **Ta-01** and **Ta-04** (hydrolysable tannins).

showed that there is a direct correlation between the quantity of hydroxyl substitutions of the flavonoid molecules and their antibiofilm capability (Cho et al., 2015), and the research of Kim et al. with phorbaketals against *S. aureus* biofilms indicated that the position and quantity of hydroxyls substitutions in the molecule affects their antibiofilm capacity (Kim et al., 2021), which is also consistent with the results of Arshia et al. (2017).

Conclusion

Our work provides a clear understanding on which chemical modifications can be made to enhance the activity level or change the activity spectrum of natural tannins, and which chemical modifications are inconvenient for increasing their antibiofilm activity. This is one of the few studies that uses a systematic and statistical analysis to correlate specific chemical characteristics of modified tannins with their antibiofilm activity (Ge et al., 2003; Peeters et al., 2016; Kemegne et al., 2017; Bouarab-Chibane et al., 2019; De Paiva et al., 2019; Jia et al., 2019).

From our work, it can be concluded that tannins not only have good activity against biofilms of different bacterial species, but that this antibiofilm activity is in most cases also biofilm specific. More important, we could identify that modifying the tannins with C_3NMe_3Cl-0.5 and PEG_{500}-0.05 can increase the antibiofilm activity against Gram-negative bacteria, although this often coincides with a decrease in activity against Gram-positive bacteria. Modifying the tannins with C_3NMe_3Cl-0.1, CH_3COOH-0.1 and CH_3COOH-0.5 generally decreases the effect against Gram-negatives, without affecting the activity against *S. aureus*. We can thus modulate the spectrum and the antibiofilm potency of tannins by the applied chemical modifications.

We could identify a weak correlation between the antibiofilm effect and the content of phenolic hydroxyl groups for Gram-negative bacteria and, to a lesser extent, for *S. aureus*. However, exploring the mode of action against other bacteria is a necessary and interesting avenue to explore further based on the initial insights generated in this work, pointing to a more complex interplay between functionalization, type of tannin in the sense of exposed galloyl units, and tannin size. A continued exploration of the possible mechanisms of actions of these compounds and the possible modifications that can be made to enhance their effect is necessary to better optimize the antibiofilm potential of the tannins.

Data availability statement

The original contributions presented in the study are included in the article/Supplementary material, further inquiries can be directed to the corresponding author.

Author contributions

XV performed the experimental biological work, data analysis, and article writing. LZ performed the chemical manipulations and provided the chemical analysis of the assayed tannins. JA developed the experimental design and contributed to the statistical analysis. TV contributed to the article writing and data analysis. HL was part of the coordination of the research project, and contributed to the results analysis and the writing of the text. CC contributed to the research project funding and coordination. HS contributed to project funding, project coordination, article writing, and data analysis. All authors contributed to the article and approved the submitted version.

Funding

This work was supported by H2020-MSCA-ITN-2016-BIOCLEAN project (grant agreement no. 722871). HL would like to additionally thank the MIUR for the Grant "Dipartimento di Eccellenza 2018-2022" to the Department of Earth and Environmental Sciences of the University of Milano-Bicocca. CC acknowledges the Ca'Foscari FPI 2019 funding.

Acknowledgments

We would like to thank A.S. Ajinomoto OmniChem N.V. in Belgium for generously providing samples of commercialized tannins. We especially like to thank David De Coster for his technical support during the experimental work.

Conflict of interest

The authors declare that the research was conducted in the absence of any commercial or financial relationships that could be construed as a potential conflict of interest.

Publisher's note

All claims expressed in this article are solely those of the authors and do not necessarily represent those of their affiliated organizations, or those of the publisher, the editors and the reviewers. Any product that may be evaluated in this article, or claim that may be made by its manufacturer, is not guaranteed or endorsed by the publisher.

Supplementary material

The Supplementary material for this article can be found online at: https://www.frontiersin.org/articles/10.3389/fmicb.2022.987164/full#supplementary-material

References

Akiyama, H. (2001). Antibacterial action of several tannins against *Staphylococcus aureus*. *J. Antimicrob. Chemother.* 48, 487–491. doi: 10.1093/jac/48.4.487

Allen, H. K., Donato, J., Wang, H. H., Cloud-Hansen, K. A., Davies, J., and Handelsman, J. (2010). Call of the wild: antibiotic resistance genes in natural environments. *Nat. Rev. Microbiol.* 8, 251–259. doi: 10.1038/nrmicro2312

Alves, M. J., Ferreira, I. C. F. R., Froufe, H. J. C., Abreu, R. M. V., Martins, A., and Pintado, M. (2013). Antimicrobial activity of phenolic compounds identified in wild mushrooms, SAR analysis and docking studies. *J. Appl. Microbiol.* 115, 346–357. doi: 10.1111/jam.12196

Arshia, K. A. K., Khan, K. M., Ahmed, A., Taha, M., and Perveen, S. (2017). Antibiofilm potential of synthetic 2-amino-5-chlorobenzophenone Schiff bases and its confirmation through fluorescence microscopy. *Microb. Pathog.* 110, 497–506. doi: 10.1016/j.micpath.2017.07.040

Baba, S. A., and Malik, S. A. (2015). Determination of total phenolic and flavonoid content, antimicrobial and antioxidant activity of a root extract of Arisaema jacquemontii Blume. *J. Taibah Univ. Sci.* 9, 449–454. doi: 10.1016/j.jtusci.2014.11.001

Ben Arfa, A., Combes, S., Preziosi-Belloy, L., Gontard, N., and Chalier, P. (2006). Antimicrobial activity of carvacrol related to its chemical structure. *Lett. Appl. Microbiol.* 43, 149–154. doi: 10.1111/j.1472-765X.2006.01938.x

Bouarab-Chibane, L., Forquet, V., Lantéri, P., Clément, Y., Léonard-Akkari, L., Oulahal, N., et al. (2019). Antibacterial properties of polyphenols: characterization and QSAR (quantitative structure–activity relationship) models. *Front. Microbiol.* 10:829. doi: 10.3389/fmicb.2019.00829

Campanac, C., Pineau, L., Payard, A., Baziard-Mouysset, G., and Roques, C. (2002). Interactions between biocide cationic agents and bacterial biofilms. *Antimicrob. Agents Chemother.* 46, 1469–1474. doi: 10.1128/AAC.46.5.1469-1474.2002

Chandra, H., Bishnoi, P., Yadav, A., Patni, B., Mishra, A., and Nautiyal, A. (2017). Antimicrobial resistance and the alternative resources with special emphasis on plant-based antimicrobials—a review. *Plan. Theory* 6:16. doi: 10.3390/plants6020016

Chen, H., Cheng, R., Zhao, X., Zhang, Y., Tam, A., Yan, Y., et al (2019). An injectable self-healing coordinative hydrogel with antibacterial and angiogenic properties for diabetic skin wound repair. *NPG Asia Mater* 11, 3. doi: 10.1038/s41427-018-0103-9

Cho, H. S., Lee, J.-H., Cho, M. H., and Lee, J. (2015). Red wines and flavonoids diminish *Staphylococcus aureus* virulence with anti-biofilm and anti-hemolytic activities. *Biofouling* 31, 1–11. doi: 10.1080/08927014.2014.991319

Chung, K.-T., Lu, Z., and Chou, M. (1998). Mechanism of inhibition of tannic acid and related compounds on the growth of intestinal bacteria. *Food Chem. Toxicol.* 36, 1053–1060. doi: 10.1016/S0278-6915(98)00086-6

d'Avila Farias, M., Oliveira, P. S., Dutra, F. S. P., Fernandes, T. J., De Pereira, C. M. P., De Oliveira, S. Q., et al. (2014). Eugenol derivatives as potential anti-oxidants: is phenolic hydroxyl necessary to obtain an effect? *J. Pharm. Pharmacol.* 66, 733–746. doi: 10.1111/jphp.12197

Dalcin, A. J. F., Santos, C. G., Gündel, S. S., Roggia, I., Raffin, R. P., Ourique, A. F., et al. (2017). Anti biofilm effect of dihydromyricetin-loaded nanocapsules on urinary catheter infected by Pseudomonas aeruginosa. *Colloids Surf. B Biointerfaces* 156, 282–291. doi: 10.1016/j.colsurfb.2017.05.029

De Paiva, R. K. C., Da Silva, J. F., Moreira, H. A., Pinto, O. G., Camargo, L. T. F. M., Naves, P. L. F., et al. (2019). Synthesis, antimicrobial activity and structure-activity relationship of some 5-Arylidene-thiazolidine-2, 4-dione derivatives. *J. Braz. Chem. Soc.* 30, 164–172. doi: 10.21577/0103-5053.20180167

De, R., Sarkar, A., Ghosh, P., Ganguly, M., Karmakar, B. C., Saha, D. R., et al. (2018). Antimicrobial activity of ellagic acid against helicobacter pylori isolates from India and during infections in mice. *J. Antimicrob. Chemother.* 73, 1595–1603. doi: 10.1093/jac/dky079

Defoirdt, T. (2016). Specific Antivirulence activity, a new concept for reliable screening of virulence inhibitors. *Trends Biotechnol.* 34, 527–529. doi: 10.1016/j.tibtech.2016.01.009

Defoirdt, T., Brackman, G., and Coenye, T. (2013). Quorum sensing inhibitors: how strong is the evidence? *Trends Microbiol.* 21, 619–624. doi: 10.1016/j.tim.2013.09.006

Dettweiler, M., Lyles, J. T., Nelson, K., Dale, B., Reddinger, R. M., Zurawski, D. V., et al. (2019). American civil war plant medicines inhibit growth, biofilm formation, and quorum sensing by multidrug-resistant bacteria. *Sci. Rep.* 9:7692. doi: 10.1038/s41598-019-44242-y

Dieltjens, L., Appermans, K., Lissens, M., Lories, B., Kim, W., Van der Eycken, E. V., et al. (2020). Inhibiting bacterial cooperation is an evolutionarily robust anti-biofilm strategy. *Nat. Commun.* 11:107. doi: 10.1038/s41467-019-13660-x

Dong, G., Liu, H., Yu, X., Zhang, X., Lu, H., Zhou, T., et al. (2018). Antimicrobial and anti-biofilm activity of tannic acid against *Staphylococcus aureus*. *Nat. Prod. Res.* 32, 2225–2228. doi: 10.1080/14786419.2017.1366485

Dos Santos Goncalves, M., Delattre, C., Balestrino, D., Charbonnel, N., Elboutachfaiti, R., Wadouachi, A., et al. (2014). Anti-biofilm activity: a function of Klebsiella pneumoniae capsular polysaccharide. *PLoS One* 9:e99995. doi: 10.1371/journal.pone.0099995

Ekambaram, S. P., Perumal, S. S., and Balakrishnan, A. (2016). Scope of hydrolysable tannins as possible antimicrobial agent. *Phyther. Res.* 30, 1035–1045. doi: 10.1002/ptr.5616

Falcão, L., and Araújo, M. E. M. (2011). Tannins characterisation in new and historic vegetable tanned leathers fibres by spot tests. *J. Cult. Herit.* 12, 149–156. doi: 10.1016/j.culher.2010.10.005

Fang, Y., Lu, Y., Zang, X., Wu, T., Qi, X., Pan, S., et al. (2016). 3D-QSAR and docking studies of flavonoids as potent *Escherichia coli* inhibitors. *Sci. Rep.* 6:23634. doi: 10.1038/srep23634

Farha, A. K., Yang, Q.-Q., Kim, G., Li, H.-B., Zhu, F., Liu, H.-Y., et al. (2020). Tannins as an alternative to antibiotics. *Food Biosci.* 38:100751. doi: 10.1016/j.fbio.2020.100751

Gao, L., Li, M., Ehrmann, S., Tu, Z., and Haag, R. (2019). Positively charged nanoaggregates based on Zwitterionic pillar[5]arene that combat planktonic bacteria and disrupt biofilms. *Angew. Chemie – Int. Ed.* 58, 3645–3649. doi: 10.1002/anie.201810314

García-Contreras, R., Maeda, T., and Wood, T. K. (2016). Can resistance against quorum-sensing interference be selected? *ISME J.* 10, 4–10. doi: 10.1038/ismej.2015.84

Ge, J., Shi, X., Cai, M., Wu, R., and Wang, M. (2003). A novel biodegradable antimicrobial PU foam from wattle tannin. *J. Appl. Polym. Sci.* 90, 2756–2763. doi: 10.1002/app.12928

Hemmati, F., Salehi, R., Ghotaslou, R., Samadi Kafil, H., Hasani, A., Gholizadeh, P., et al. (2020). Quorum quenching: a potential target for antipseudomonal therapy. *Infect. Drug Resist.* 13, 2989–3005. doi: 10.2147/IDR.S263196

Hricovíniová, Z., Mascaretti, Š., Hricovíniová, J., Čížek, A., and Jampílek, J. (2021). New unnatural Gallotannins: a way toward green antioxidants, antimicrobials and antibiofilm agents. *Antioxidants* 10:1288. doi: 10.3390/antiox10081288

Imperi, F., Fiscarelli, E. V., Visaggio, D., Leoni, L., and Visca, P. (2019). Activity and impact on resistance development of two antivirulence fluoropyrimidine drugs in *Pseudomonas aeruginosa*. *Front. Cell. Infect. Microbiol.* 9, 1–11. doi: 10.3389/fcimb.2019.00049

Ito, M., Murakami, K., and Yoshino, M. (2005). Antioxidant action of eugenol compounds: role of metal ion in the inhibition of lipid peroxidation. *Food Chem. Toxicol.* 43, 461–466. doi: 10.1016/j.fct.2004.11.019

Jagani, S., Chelikani, R., and Kim, D. S. (2009). Effects of phenol and natural phenolic compounds on biofilm formation by *Pseudomonas aeruginosa*. *Biofouling* 25, 321–324. doi: 10.1080/08927010802660854

Janecki, A., and Kolodziej, H. (2010). Anti-adhesive activities of Flavan-3-ols and Proanthocyanidins in the interaction of group A-streptococci and human epithelial cells. *Molecules* 15, 7139–7152. doi: 10.3390/molecules15107139

Janssens, J. C. A., Steenackers, H., Robijns, S., Gellens, E., Levin, J., Zhao, H., et al. (2008). Brominated furanones inhibit biofilm formation by salmonella enterica serovar typhimurium. *Appl. Environ. Microbiol.* 74, 6639–6648. doi: 10.1128/AEM.01262-08

Jia, B., Ma, Y. M., Liu, B., Chen, P., Hu, Y., and Zhang, R. (2019). Synthesis, antimicrobial activity, structure-activity relationship, and molecular docking studies of indole Diketopiperazine alkaloids. *Front. Chem.* 7, 1–13. doi: 10.3389/fchem.2019.00837

Kalia, V. C., Wood, T. K., and Kumar, P. (2014). Evolution of resistance to quorum-sensing inhibitors. *Microb. Ecol.* 68, 13–23. doi: 10.1007/s00248-013-0316-y

Kemegne, G. A., Mkounga, P., Essia Ngang, J. J., Sado Kamdem, S. L., and Nkengfack, A. E. (2017). Antimicrobial structure activity relationship of five anthraquinones of emodine type isolated from Vismia laurentii. *BMC Microbiol.* 17, 41–48. doi: 10.1186/s12866-017-0954-1

Kim, G., Gan, R.-Y., Zhang, D., Farha, A. K., Habimana, O., Mavumengwana, V., et al. (2020). Large-scale screening of 239 traditional Chinese medicinal plant extracts for their antibacterial activities against multidrug-resistant *Staphylococcus aureus* and cytotoxic activities. *Pathogens* 9:185. doi: 10.3390/pathogens9030185

Kim, J.-K., Kim, N., and Lim, Y.-H. (2010). Evaluation of the antibacterial activity of Rhapontigenin produced from Rhapontin by biotransformation against Propionibacterium acnes. *J. Microbiol. Biotechnol.* 20, 82–87. doi: 10.4014/jmb.0907.07022

Kim, Y.-G., Lee, J.-H., Lee, S., Lee, Y.-K., Hwang, B. S., and Lee, J. (2021). Antibiofilm activity of Phorbaketals from the marine sponge *Phorbas* sp. against *Staphylococcus aureus*. *Mar. Drugs* 19:301. doi: 10.3390/md19060301

Klug, T. V., Novello, J., Laranja, D. C., Aguirre, T. A. S., de Oliveira Rios, A., Tondo, E. C., et al. (2017). Effect of tannin extracts on biofilms and attachment of *Escherichia coli* on lettuce leaves. *Food Bioprocess Technol.* 10, 275–283. doi: 10.1007/s11947-016-1812-0

Koleckar, V., Kubikova, K., Rehakova, Z., Kuca, K., Jun, D., Jahodar, L., et al. (2008). Condensed and hydrolysable tannins as antioxidants influencing the health. *Mini-Reviews Med. Chem.* 8, 436–447. doi: 10.2174/138955708784223486

Lahiri, D., Dash, S., Dutta, R., and Nag, M. (2019). Elucidating the effect of anti-biofilm activity of bioactive compounds extracted from plants. *J. Biosci.* 44:52. doi: 10.1007/s12038-019-9868-4

Lee, J.-H., Park, J.-H., Cho, H. S., Joo, S. W., Cho, M. H., and Lee, J. (2013). Anti-biofilm activities of quercetin and tannic acid against *Staphylococcus aureus*. *Biofouling* 29, 491–499. doi: 10.1080/08927014.2013.788692

Lin, M. H., Chang, F. R., Hua, M. Y., Wu, Y. C., and Liu, S. T. (2011). Inhibitory effects of 1,2,3,4,6-penta-O-galloyl-β-D-glucopyranose on biofilm formation by *Staphylococcus aureus*. *Antimicrob. Agents Chemother.* 55, 1021–1027. doi: 10.1128/AAC.00843-10

Maura, D., Ballok, A. E., and Rahme, L. G. (2016). Considerations and caveats in anti-virulence drug development. *Curr. Opin. Microbiol.* 33, 41–46. doi: 10.1016/j.mib.2016.06.001

Mori, A., Nishino, C., Enoki, N., and Tawata, S. (1987). Antibacterial activity and mode of action of plant flavonoids against Proteus vulgaris and *Staphylococcus aureus*. *Phytochemistry* 26, 2231–2234. doi: 10.1016/S0031-9422(00)84689-0

Payne, D. E., Martin, N. R., Parzych, K. R., Rickard, A. H., Underwood, A., and Boles, B. R. (2013). Tannic acid inhibits *Staphylococcus aureus* surface colonization in an IsaA-dependent manner. *Infect. Immun.* 81, 496–504. doi: 10.1128/IAI.00877-12

Peeters, E., Hooyberghs, G., Robijns, S., Waldrant, K., De Weerdt, A., Delattin, N., et al. (2016). Modulation of the substitution pattern of 5-Aryl-2-Aminoimidazoles allows fine-tuning of their Antibiofilm activity Spectrum and toxicity. *Antimicrob. Agents Chemother.* 60, 6483–6497. doi: 10.1128/AAC.00035-16

Pizzi, A. (2019). Tannins: prospectives and actual industrial applications. *Biomol. Ther.* 9:344. doi: 10.3390/biom9080344

Puljula, E., Walton, G., Woodward, M. J., and Karonen, M. (2020). Antimicrobial activities of Ellagitannins against *Clostridiales perfringens*, *Escherichia coli*, *Lactobacillus plantarum* and *Staphylococcus aureus*. *Molecules* 25:3714. doi: 10.3390/molecules25163714

Rabin, N., Zheng, Y., Opoku-Temeng, C., Du, Y., Bonsu, E., and Sintim, H. O. (2015). Biofilm formation mechanisms and targets for developing antibiofilm agents. *Future Med. Chem.* 7, 493–512. doi: 10.4155/fmc.15.6

Roy, R., Tiwari, M., Donelli, G., and Tiwari, V. (2018). Strategies for combating bacterial biofilms: a focus on anti-biofilm agents and their mechanisms of action. *Virulence* 9, 522–554. doi: 10.1080/21505594.2017.1313372

Salar, R. K., Purewal, S. S., and Sandhu, K. S. (2017). Relationships between DNA damage protection activity, total phenolic content, condensed tannin content and antioxidant potential among Indian barley cultivars. *Biocatal. Agric. Biotechnol.* 11, 201–206. doi: 10.1016/j.bcab.2017.07.006

Sarabhai, S., Sharma, P., and Capalash, N. (2013). Ellagic acid derivatives from Terminalia chebula Retz. Downregulate the expression of quorum sensing genes to attenuate Pseudomonas aeruginosa PAO1 virulence. *PLoS One* 8:e53441. doi: 10.1371/journal.pone.0053441

Scalbert, A. (1991). Antimicrobial properties of tannins. *Phytochemistry* 30, 3875–3883. doi: 10.1016/0031-9422(91)83426-L

Shukla, V., and Bhathena, Z. (2015). Sustained release of a purified tannin component of Terminalia chebula from a titanium implant surface prevents biofilm formation by *Staphylococcus aureus*. *Appl. Biochem. Biotechnol.* 175, 3542–3556. doi: 10.1007/s12010-015-1525-2

Slobodníková, L., Fialová, S., Rendeková, K., Kováč, J., and Mučaji, P. (2016). Antibiofilm activity of plant polyphenols. *Molecules* 21:1717. doi: 10.3390/molecules21121717

Song, Z.-M., Zhang, J.-L., Zhou, K., Yue, L.-M., Zhang, Y., Wang, C.-Y., et al. (2021). Anthraquinones as potential Antibiofilm agents against methicillin-resistant *Staphylococcus aureus*. *Front. Microbiol.* 12, 1–16. doi: 10.3389/fmicb.2021.709826

Steenackers, H. P. L., Ermolatev, D. S., Savaliya, B., Weerdt, A. D., Coster, D. D., Shah, A., et al. (2011). Structure–activity relationship of 2-hydroxy-2-aryl-2,3-dihydro-imidazo[1,2-a]pyrimidinium salts and 2N-substituted 4(5)-aryl-2-amino-1H-imidazoles as inhibitors of biofilm formation by *Salmonella typhimurium* and *Pseudomonas aeruginosa*. *Bioorg. Med. Chem.* 19, 3462–3473. doi: 10.1016/j.bmc.2011.04.026

Taganna, J. C., Quanico, J. P., Perono, R. M. G., Amor, E. C., and Rivera, W. L. (2011). Tannin-rich fraction from Terminalia catappa inhibits quorum sensing (QS) in *Chromobacterium violaceum* and the QS-controlled biofilm maturation and LasA staphylolytic activity in *Pseudomonas aeruginosa*. *J. Ethnopharmacol.* 134, 865–871. doi: 10.1016/j.jep.2011.01.028

Taguri, T., Tanaka, T., and Kouno, I. (2004). Antimicrobial activity of 10 different plant polyphenols against bacteria causing food-borne disease. *Biol. Pharm. Bull.* 27, 1965–1969. doi: 10.1248/bpb.27.1965

Tintino, S. R., Oliveira-Tintino, C. D. M., Campina, F. F., Silva, R. L. P., Costa, M. D. S., Menezes, I. R. A., et al. (2016). Evaluation of the tannic acid inhibitory effect against the NorA efflux pump of *Staphylococcus aureus*. *Microb. Pathog.* 97, 9–13. doi: 10.1016/j.micpath.2016.04.003

Totsika, M. (2016). Benefits and challenges of Antivirulence antimicrobials at the Dawn of the post-antibiotic era. *Drug Deliv. Lett.* 6, 30–37. doi: 10.2174/2210303106666160506120057

Trentin, D. S., Silva, D. B., Amaral, M. W., Zimmer, K. R., Silva, M. V., Lopes, N. P., et al. (2013). Tannins possessing bacteriostatic effect impair *Pseudomonas aeruginosa* adhesion and biofilm formation. *PLoS One* 8:e66257. doi: 10.1371/journal.pone.0066257

Ulrey, R. K., Barksdale, S. M., Zhou, W., and van Hoek, M. L. (2014). Cranberry proanthocyanidins have anti-biofilm properties against *Pseudomonas aeruginosa*. *BMC Complement. Altern. Med.* 14:499. doi: 10.1186/1472-6882-14-499

Ultee, A., Bennik, M. H. J., and Moezelaar, R. (2002). The phenolic hydroxyl Group of Carvacrol is Essential for action against the food-borne pathogen *Bacillus cereus*. *Appl. Environ. Microbiol.* 68, 1561–1568. doi: 10.1128/AEM.68.4.1561-1568.2002

Vattem, D. A., Lin, Y.-T., Labbe, R. G., and Shetty, K. (2004). Antimicrobial activity against select food-borne pathogens by phenolic antioxidants enriched in cranberry pomace by solid-state bioprocessing using the food grade fungus *Rhizopus oligosporus*. *Process Biochem.* 39, 1939–1946. doi: 10.1016/j.procbio.2003.09.032

Veldhuizen, E. J. A., Tjeerdsma-van Bokhoven, J. L. M., Zweijtzer, C., Burt, S. A., and Haagsman, H. P. (2006). Structural requirements for the antimicrobial activity of Carvacrol. *J. Agric. Food Chem.* 54, 1874–1879. doi: 10.1021/jf052564y

Versari, A., du Toit, W., and Parpinello, G. P. (2013). Oenological tannins: a review. *Aust. J. Grape Wine Res.* 19, 1–10. doi: 10.1111/ajgw.12002

Vijayakumar, K., and Thirunanasambandham, R. (2021). 5-Hydroxymethylfurfural inhibits *Acinetobacter baumannii* biofilms: an in vitro study. *Arch. Microbiol.* 203, 673–682. doi: 10.1007/s00203-020-02061-0

Vu, T. T., Kim, H., Tran, V. K., Vu, H. D., Hoang, T. X., Han, J. W., et al. (2017). Antibacterial activity of tannins isolated from *Sapium baccatum* extract and use for control of tomato bacterial wilt. *PLoS One* 12:e0181499. doi: 10.1371/journal.pone.0181499

Warraich, A. A., Mohammed, A. R., Perrie, Y., Hussain, M., Gibson, H., and Rahman, A. (2020). Evaluation of anti-biofilm activity of acidic amino acids and synergy with ciprofloxacin on *Staphylococcus aureus* biofilms. *Sci. Rep.* 10:9021. doi: 10.1038/s41598-020-66082-x

Widsten, P., Cruz, C. D., Fletcher, G. C., Pajak, M. A., and McGhie, T. K. (2014). Tannins and extracts of fruit byproducts: antibacterial activity against foodborne bacteria and antioxidant capacity. *J. Agric. Food Chem.* 62, 11146–11156. doi: 10.1021/jf503819t

Wu, D., Wu, X.-D., You, X.-F., Ma, X.-F., and Tian, W.-X. (2010). Inhibitory effects on bacterial growth and b-ketoacyl-ACP reductase by different species of maple leaf extracts and tannic acid. *Phyther. Res.* 24, S35–S41. doi: 10.1002/ptr.2873

Zhen, L., Lange, H., and Crestini, C. (2021a). An analytical toolbox for fast and straightforward structural characterisation of commercially available tannins. *Molecules* 26:2532. doi: 10.3390/molecules26092532

Zhen, L., Lange, H., Zongo, L., and Crestini, C. (2021b). Chemical derivatization of commercially available condensed and Hydrolyzable tannins. *ACS Sustain. Chem. Eng.* 9, 10154–10166. doi: 10.1021/acssuschemeng.1c02114

frontiers | Frontiers in Microbiology

TYPE Original Research
PUBLISHED 20 February 2023
DOI 10.3389/fmicb.2023.1030401

OPEN ACCESS

EDITED BY
Fang Yang,
Qingdao Municipal Hospital,
China

REVIEWED BY
Renátó Kovács,
University of Debrecen,
Hungary
Priya Arumugam,
North Carolina State University,
United States

*CORRESPONDENCE
Reza Ranjbar
✉ ranjbar@bmsu.ac.ir

SPECIALTY SECTION
This article was submitted to Antimicrobials, Resistance and Chemotherapy, a section of the journal Frontiers in Microbiology

RECEIVED 28 August 2022
ACCEPTED 01 February 2023
PUBLISHED 20 February 2023

CITATION
Mirzaei R, Esmaeili Gouvarchin Ghaleh H and Ranjbar R (2023) Antibiofilm effect of melittin alone and in combination with conventional antibiotics toward strong biofilm of MDR-MRSA and -*Pseudomonas aeruginosa*. *Front. Microbiol.* 14:1030401. doi: 10.3389/fmicb.2023.1030401

Antibiofilm effect of melittin alone and in combination with conventional antibiotics toward strong biofilm of MDR-MRSA and -*Pseudomonas aeruginosa*

Rasoul Mirzaei[1], Hadi Esmaeili Gouvarchin Ghaleh[2] and Reza Ranjbar[3]*

[1]Department of Microbiology, School of Medicine, Hamadan University of Medical Sciences, Hamadan, Iran, [2]Applied Virology Research Center, Baqiyatallah University of Medical Sciences, Tehran, Iran, [3]Molecular Biology Research Center, Systems Biology and Poisonings Institute, Baqiyatallah University of Medical Sciences, Tehran, Iran

Introduction: Multidrug-resistant (MDR) pathogens are being recognized as a critical threat to human health if they can form biofilm and, in this sense, biofilm-forming MDR-methicillin resistant *Staphylococcus aureus* (MRSA) and -*Pseudomonas aeruginosa* strains are a worse concern. Hence, a growing body of documents has introduced antimicrobial peptides (AMPs) as a substitute candidate for conventional antimicrobial agents against drug-resistant and biofilm-associated infections. We evaluated melittin's antibacterial and antibiofilm activity alone and/or in combination with gentamicin, ciprofloxacin, rifampin, and vancomycin on biofilm-forming MDR-*P. aeruginosa* and MDR-MRSA strains.

Methods: Antibacterial tests [antibiogram, minimum inhibitory concentration (MIC), and minimum bactericidal concentration (MBC)], anti-biofilm tests [minimum biofilm inhibition concentration (MBIC), and minimum biofilm eradication concentration (MBEC)], as well as synergistic antibiofilm activity of melittin and antibiotics, were performed. Besides, the influence of melittin alone on the biofilm encoding genes and the cytotoxicity and hemolytic effects of melittin were examined.

Results: MIC, MBC, MBIC, and MBEC indices for melittin were in the range of 0.625–5, 1.25–10, 2.5–20, and 10–40 μg/ml, respectively. The findings found that the combination of melittin AMP with antibiotics was synergistic and fractional biofilm inhibitory concentration index (FBICi) for most tested concentrations was <0.5, resulting in a significant reduction in melittin, gentamicin, ciprofloxacin, vancomycin, and rifampin concentrations by 2–256.4, 2–128, 2–16, 4–64 and 4–8 folds, respectively. This phenomenon reduced the toxicity of melittin, whereby its synergist concentration required for biofilm inhibition did not show cytotoxicity and hemolytic activity. Our findings found that melittin decreased the expression of *icaA* in *S. aureus* and *LasR* in *P. aeruginosa* genes from 0.1 to 4.11 fold for *icaA*, and 0.11 to 3.7 fold for *LasR*, respectively.

Conclusion: Overall, the results obtained from our study show that melittin alone is effective against the strong biofilm of MDR pathogens and also offers sound synergistic effects with antibiotics without toxicity. Hence, combining melittin and antibiotics can be a potential candidate for further evaluation of *in vivo* infections by MDR pathogens.

KEYWORDS

MDR, MRSA, *Pseudomonas aeruginosa*, biofilm, antibiofilm peptide, melittin, synergism

1. Introduction

Multidrug-resistant (MDR) pathogens are widely noted as one of the most significant public health issues nowadays (van Duin and Paterson, 2020). MDR pathogens are typically related to nosocomial bacterial infections, and also MDR pathogens have become a common cause of bacterial community-acquired illnesses (van Duin and Paterson, 2020). Accordingly, a broader range of antibiotics and combination agents is advised for the empirical treatment of MDR infections when the occurrence of a given resistance pattern in bacterial infections surpasses a certain threshold, which can have negative outputs (van Duin and Paterson, 2016; Lertwattanachai et al., 2020; Bassetti and Garau, 2021). In this regard, antibiotic resistance among *Pseudomonas aeruginosa* strains is a growing concern, and some Extensively Drug-Resistant (XDR) *P. aeruginosa* have recently become issues of public health concern (Horcajada and Montero, 2019; Pang et al., 2019). On the other hand, *Staphylococcus aureus* infections are also deadly and difficult to treat over the current decades due to the rising frequency of antibiotic resistance (Foster, 2017). In this sense, MDR methicillin-resistant *S. aureus* (MRSA) is of great concern (Lee et al., 2018).

Of note, MDR pathogens can pose a substantial threat to patients due to biofilm formation (Sobisch et al., 2019). Aside from its resistance determinants, bacterial biofilm development is also a significant factor contributing to unsuccessful treatment attempts (Mahdiun et al., 2017; Mirzaei et al., 2020a). Biofilms are bacterial populations encased in an extracellular matrix that enhance bacterial adherence to various surfaces like the host cells (Mirzaei et al., 2020b, 2022b). This mode of growth is a crucial virulence factor in the development of some bacterial infections like wounds, device-associated infections, dental caries, and other chronic infections because of its resistance to antibiotics and protective barriers toward harsh environmental stressors and the immune system (Mirzaei and Ranjbar, 2022). In this aspect, antibiotic resistance in biofilm often happens during monotherapy; therefore, these antibiotics should usually be used as combination therapy with other antimicrobial agents (Howden et al., 2010; Bardbari et al., 2018). Antibiotic monotherapy is frequently ineffective in treating MDR infections; moreover, antibiotic-induced toxicity at higher concentrations in monotherapy necessitates careful monitoring of the patients (Mirzaei et al., 2022a). As a result, researchers discovered that combining antimicrobial peptides (AMPs) and antibiofilm peptides (ABPs) with antibiotics can be a viable therapy for treating MDR pathogens infections. Notably, AMPs, as part of the innate immunity of organisms, are a promising class of compounds that are currently receiving special attention as an emerging alternative to conventional antibacterial drugs against biofilm-producing MDR pathogens (Mahlapuu et al., 2016). In this way, melittin as a cationic AMP is well demonstrated against a wide range of bacterial pathogens alone, and this powerful AMP exhibit synergistic activity in combination with some antibiotics against different MDR species pathogens (Khozani et al., 2019; Zarghami et al., 2021b; Mirzaei et al., 2022a,b). As the main component of bee venom, melittin is one of the studied AMPs with strong antimicrobial activity, and its potential effects against viruses and cancer cells have also been found (Choi et al., 2015b; Askari et al., 2021). Hence, the current work was done to survey the effect of melittin AMP alone and/or in combination with gentamicin, ciprofloxacin, rifampin, and vancomycin on biofilm-forming MDR-MRSA and MDR-*P. aeruginosa*.

Abbreviations: MDR, Multidrug-resistant; MRSA, methicillin-resistant *S. aureus*; AMPs, antimicrobial peptides; ABPs, antibiofilm peptides; MSA, Mannitol Salt Agar; MHA, Mueller Hinton Agar; MHB, Mueller Hinton broth; TSB, Trypticase soy broth; FBS, Fetal bovine serum; DMEM, Dulbecco's Modified Eagle's Medium; FCS, Fetal-Calf Serum; MTT, 3-(4, 5-dimethyl-2-thiazolyl)-2, 5-diphenyl-2 H-tetrazoliumbromide; DMSO, dimethyl sulfoxide; PCR, polymerase chain reaction; OD, optical density; CFUs, colony-forming units; MIC, minimum inhibitory concentration; MBC, minimum bactericidal concentration; MBIC, minimum biofilm inhibitory concentration; MBEC, minimal biofilm eradication concentration; FBICi, fractional biofilm inhibitory concentration index; MRSE, methicillin-resistant *Staphylococcus epidermidis*.

2. Methods

2.1. Antibiotics, media, and reagents

The present study provided the disks and powdered antibiotics from the MAST (Mast Diagnostics, United Kingdom) and Sigma-Aldrich (Taufkirchen, Germany). The following items were acquired from Merck (Merck, United States): Blood Agar, Mannitol Salt Agar (MSA), MacConkey agar, Cetrimide agar, Mueller Hinton Agar (MHA), DNA Agar, Mueller Hinton Broth (MHB), Trypticase Soy Broth (TSB), NaCl, glucose, and MgCl2. Fetal bovine serum (FBS), Dulbecco's Modified Eagle's Medium (DMEM), Fetal-Calf Serum (FCS), 3-(4, 5-dimethyl-2-thiazolyl)-2, 5-diphenyl-2 H-tetrazoliumbromide (MTT), Triton X-100, dimethyl sulfoxide (DMSO), agarose, ethanol, methanol, and crystal violet were provided from Sigma-Aldrich (Saint Louis, MO, United States). 96-well microplates, including flat-and round-bottom, were supplied by Jet Biofil (Guangzhou, China) and NEST Biotechnology (Wuxi, China), respectively.

2.2. Melittin synthesis order

The complete sequence of melittin peptide (GIGAVLKVLTT GLPALISWIKRKRQQ) blasted in NCBI with a purity of >96% was synthesized *via* the Solid-Phase method by DGpeptides (Hubei, China). In this regard, the corporation applied reversed-phase high-performance liquid chromatography to evaluate the purity of synthesized peptides. The company used liquid chromatography-mass spectrometry to verify accurate synthesis for mass spectrometry. Finally, the bicinchoninic acid test and reversed-phase high-performance liquid chromatography were used to confirm the peptide content and purity (Eisapoor et al., 2016).

2.3. Collection and confirmation of clinical isolates and standard strains

The Centers for Disease Control followed inclusion guidelines in this study (Horan et al., 2008). The isolates were obtained from individuals of varying ages and genders and were not duplicated; just one sample per patient was collected. In this regard, 30 *S. aureus* isolates were obtained from the wound ($n = 8$), blood ($n = 11$), urine

($n = 6$), as well as sputum ($n = 5$) and further characterized and confirmed using biochemical tests like colony morphology, gram-positive, clustered-shaped cocci, catalase, mannitol, DNase, and coagulase (Murray et al., 1995). In addition, 20 clinical *P. aeruginosa* were collected from respiratory tracts retrieved from sputum ($n = 6$), bronchoalveolar lavage (8), and endotracheal aspirates ($n = 6$) patients hospitalized in the intensive care unit (ICU) wards and then confirmed on selective media *via* conventional phenotypical tests such as colony morphology, oxidase, catalase, motility, citrate, indole synthesis, methyl red, and voges-proskauer. Finally, molecular confirmation of *S. aureus* and *P. aeruginosa* isolates was done by the polymerase chain reaction (PCR) *via* previously described primers (Atshan et al., 2012; Abdelraheem et al., 2020). Besides, *S. aureus* ATCC 25923, *S. aureus* ATCC 29213, and *P. aeruginosa* PAO1 were provided by the Pasteur Institute of Iran.

2.4. Screening for MRSA isolates

According to the Clinical and Laboratory Standards Institute (CLSI) 2020 recommendations, *S. aureus* isolates were phenotypically evaluated for resistance to methicillin using the cefoxitin (FOX; 30 μg) by Kirby-Bauer method (Wayne, 2010). In this regard, briefly, *S. aureus* colonies were cultivated in the MHB overnight at 37°C with 180 rpm shaking, and then the optical density (OD) of bacteria was set on 0.5 McFarland, followed by the suspension was swabbed onto the MHA plates, and then the FOX disk was placed and 24 h incubated at 37°C. Then, the diameter of the inhibition zone developed around the FOX disk was assessed. Then, MRSA isolates were genotypically confirmed using PCR *via* the *mecA* gene by the previously designed primer (Kelley et al., 2013). In brief, genomic DNA from colonies of isolates was extracted using the Purification kit (Roche, Germany) based on the manufacturer's instruction, and PCR reactions were done in a 20 μl volume containing 1.5 μl MgCl2, 2.5 μl of PCR buffer (10X), 0.5 μl dNTP (10 mmol/l), 0.5 μl of each reverse and forward primers, 1 μl of Taq DNA polymerase (5 U; Ampliqon, Denmark), 2 μl of bacterial DNA, and 10.5 μl sterile distilled water. Then, the mixtures were incubated with the following conditions in a thermal gradient cycler (Eppendorf, Germany): denaturation at 95°C for 5 min, 35 cycles with denaturation at 95°C for 2 min, annealing at 60°C for 45 s, extension at 70°C for 45 s and final extension at 72°C for 10 min. Finally, PCR products were run with 1% agarose gel in Tris/Borate/EDTA for 40 min and the gel documentation system was used for visualizing them on the gel.

2.5. Screening of biofilm formation in isolates

Most importantly, the biofilm formation ability among confirmed *S. aureus* and *P. aeruginosa* isolates was tested using the microtiter plate method as described before with some modifications (Mirzaei et al., 2022b). In the first step, fresh colonies were grown in 5 ml TSB containing 1% glucose with 180 rpm shaking at 37°C overnight, and then the OD of bacteria was set on 0.5 McFarland and then 100 μl diluted suspension containing 10^7 colony-forming units (CFUs) was added to 900 μl of TSB containing 1% glucose, and finally, 200 μl of this suspension containing 2×10^6 CFUs was added to the wells of 96 U-shape microplate and afterward overnight incubated at 37°C with shaking at 60 rpm. Afterward, the contents of the wells were outed, and wells were washed with normal saline and air-dried. Finally, 200 μl of 100% methanol was injected into wells and aspirated after 15 min, and then air-dried at room temperature again and, in the next step, were stained with 0.05% crystal violet at a volume of 200 μl for 5 min, and after which the stain was outed. The wells were washed with normal saline and air-dried again. Eventually, 200 μl of 100% ethanol was entered into wells and mixed for 30 min at 37°C while shaking, and then absorbance of wells at 595 nm after transferring their contents to the new wells in the new microplate was recorded *via* a microplate reader (BioTek, United States). TSB with 1% glucose devoid of bacteria served as the negative control, while *S. aureus* ATCC 29213 and *P. aeruginosa* PAO1 served as the positive controls. Briefly, a cut-off OD (ODc) was defined as three standard deviations (SD) above the mean OD of the negative control (uninoculated medium): ODc = average OD of negative control + (3 × SD of negative control). The biofilm production capability of the tested isolates was categorized as follows: OD ≤ OD cut-off (ODc), non-biofilm forming; ODc < OD ≤ 2 × ODc, weak biofilm-forming; 2 × ODc < OD ≤ 4 × ODc, moderate biofilm-forming; and 4 × ODc < OD, strong biofilm-forming (Mirzaei et al., 2022c). Finally, in this study, 20 biofilm-producer strains of MRSA and *P. aeruginosa* were selected including clinical isolates, PAO1, and ATCC for further evaluation.

2.6. Antibiotic susceptibility pattern and MDR isolates

Finally, for the determination of antibiotic susceptibility and MDR patterns of MRSA isolates, the Kirby-Bauer procedure was done according to CLSI recommendations as above mentioned for the following antibiotics: clindamycin (CD; 2 μg), trimethoprim-sulfamethoxazole (TS; 1.25 μg), gentamicin (GM; 10 μg), erythromycin (E; 15 μg), and linezolid (LZD; 30 μg) for *S. aureus*, as well as nalidixic acid (NA; 30 μg), colistin (CT; 10 μg), ampicillin (AMP; 10 μg), piperacillin (PRL; 100 μg), imipenem (IMP; 10 μg), cefepime (CPE; 30 μg), and chloramphenicol (C; 30 μg) for *P. aeruginosa* (Wayne, 2010). *S. aureus* ATCC 25923 was applied as the quality control. Finally, by observing at least one or more antibiotic resistances for three or more classes of antibiotics, MDR in selected MRSA and *P. aeruginosa* isolates was characterized (Mirzaei et al., 2022a).

2.7. Minimum inhibitory concentration (MIC), minimum bactericidal concentration (MBC), and MBC/MIC

The MIC values for melittin, gentamicin, vancomycin, ciprofloxacin, and rifampin were determined *via* microdilution assay with some changes according to CLSI guidelines for selective isolates (Wayne, 2010; Mirzaei et al., 2022a). In the first step, the fresh bacterial colonies were cultured overnight in MHB with 180 rpm shaking at 37°C, and then, the OD of bacteria was set to 0.5 McFarland as above-mentioned and quickly reached 10^6 CFUs in MHB. In addition, 100 μl of antimicrobial agent serial dilutions were simultaneously made on MHB in 96-well F-bottom microplates. The concentrations of melittin, gentamicin, ciprofloxacin, vancomycin, and rifampin were between

0.156–10, 0.25–512, 0.125–128, 0.5–64, and 0.007–64 μg/ml, respectively. Eventually, 100 μl of the provided suspension equal to 10^5 CFUs was added to wells of the serially diluted antimicrobial agents, and the microplate was overnight incubated at 37°C and then, the lowest concentration of the tested antimicrobial agents caused full inhibition of observable growth was considered as MIC.

The MBC values of melittin, gentamicin, ciprofloxacin, rifampin, and vancomycin were determined using broth microdilution assay with some modifications per CLSI guidelines (Wayne, 2010; Mirzaei et al., 2022a). In brief, the bacterial colonies were cultured overnight in the MHB at 37°C with 180 rpm shaking, and then, the number of bacteria was set to the 0.5 McFarland as above-mentioned and then reached 10^6 CFUs in MHB. In addition, as mentioned above, 100 μl of serial dilutions of antimicrobial agents were simultaneously made on MHB in 96-well F-bottom microplates. Eventually, 100 μl of the suspension equal to 10^5 CFUs was added to wells of the serially diluted antimicrobial agents, and the microplates were overnight incubated at 37°C, and then, 10 μl was cultured on the MHA overnight and grew colonies were determined. Finally, the MBC for melittin, gentamicin, vancomycin, ciprofloxacin, and rifampin was defined as the minimum concentration necessary to kill 100% of cultured bacteria (Wayne, 2010; Mirzaei et al., 2022a). For MIC and MBC of antibiotics, we tested gentamicin and ciprofloxacin for *P. aeruginosa* and vancomycin and rifampin for *S. aureus*, respectively. Additionally, the MBC/MIC values were determined to identify the presence or absence of antibiotic tolerance in isolates (Traczewski et al., 2009).

2.8. Minimum biofilm inhibitory concentration (MBIC), and minimal biofilm eradication concentration (MBEC) against biofilm

The MBIC of melittin, gentamicin, ciprofloxacin, vancomycin, and rifampin on the 24 h preformed biofilm was investigated. Regarding this, fresh bacterial colonies were grown overnight in 5 ml of TSB with 1% glucose at 37°C with 180 rpm shaking. Afterward, the OD of cells was set to 0.5 McFarland, as stated previously. Then an inoculation of 2×10^6 CFUs provided as described above in TSB with 1% glucose was entered into wells of U-shape microplate and incubated at 37°C overnight with 60 rpm shaking. On the next day, the content of the wells of the U-shape microplate was carefully disposed of and rinsed with normal saline. Simultaneously, melittin at a range of 20 to 0.625 μg/ml and antibiotics at a range of 256 to 1 μg/ml were serially diluted in normal saline at the volume of 100 μl and applied to a microplate and then incubated overnight at 37°C and the amount of biofilm was then quantified as above-mentioned. The MBIC was defined as the minimum concentration of tested agents that inhibited biofilm formation by 90%. The percentage of inhibition of biofilm was computed as follows (Bardbari et al., 2018): MBIC = [1-(OD test/OD control)] × 100.

The MBEC experiment was conducted using the same 96 U-shape microplate as MBIC, to evaluate the biofilm degradative, as well as the killing potential of embedded bacterial in biofilm for melittin, gentamicin, ciprofloxacin, vancomycin, as well as rifampin (Mirzaei et al., 2022b). Briefly, the biofilm of isolates was allowed to produce, as mentioned above, in TSB with 1% glucose. The wells' contents were then disposed of and rinsed with normal saline. Simultaneously, 100 μl of serially diluted melittin in a range of 20 to 1.25 μg/ml and antibiotics at a range of 1,024 to 2 μg/ml in 100 μl of normal saline were added to the wells. The microplates were incubated overnight at 37°C. On the next day, the contents of the wells were outed, the wells were washed with normal saline, and 100 μl of fresh normal saline was added to the wells and mixed. Then 10 μl of this content was cultured on MHA at 37°C for 48 h, and finally, the number of grown bacterial colonies was determined. The MBEC was considered as the minimum quantity of tested agents to 100% killing of the biofilm-embedded bacteria. It should be noted that we tested gentamicin, and ciprofloxacin for *P. aeruginosa* and also vancomycin and rifampin for *S. aureus*, respectively.

2.9. Synergistic effects of melittin and antibiotics toward biofilm

The anti-biofilm effect of melittin, gentamicin, ciprofloxacin, vancomycin, and rifampin in combination was surveyed *via* the microdilution method with some modifications (Mirzaei et al., 2022b). In this regard, fractional antibiofilm indices for MBIC named fractional biofilm inhibitory concentration index (FBICi) of antibiofilm agents against selected biofilm-forming MDR-MRSA and MDR-*P. aeruginosa* isolates were calculated. In brief, at first, 24 h preformed biofilm was generated in 96 U-shape microplates as mentioned above, and then serial dilutions of melittin at a range of 20 to 0.625 μg/ml and antibiotics at a range of 256 to 1 μg/ml at a volume of 100 μl were added to each well and microplate was incubated overnight at 37°C. Finally, the FBICi for combined agents were determined as follows: (MBIC agent 1 in combination/ MBIC agent 1 alone) + (MBIC agent 2 in combination/MBIC agent 2 alone). FBICi refers to the interaction based on the theses findings: Synergy if the conclusion was ≤0.5; Partial synergy if the discovery was 0.5 < to <1; Additive if the result was equal to1; Indifferent if the finding was 1 < to <4; Antagonistic if the finding was 4 ≤ (Mirzaei et al., 2022b). It should be noted that gentamicin, ciprofloxacin for *P. aeruginosa*, vancomycin, and rifampin for *S. aureus* were tested, respectively.

2.10. Effect of melittin on the biofilm encoding genes

Selected biofilm-forming strains similar to synergism testing were chosen further for real-time PCR analysis to survey the expression of biofilm-encoding genes *icaA* in *S. aureus* and *LasR* in *P. aeruginosa*. Selected strains were exposed to sub-MIC concentrations of melittin in the range of 5 to 0.039 μg overnight, and on the next day, total RNA was extracted by the extraction kit based on the manufacturer's recommendations (Gene All, South Korea). The concentration, purity, and integrity of the extracted RNAs were assessed. Then, 1 μg of RNA was then utilized for cDNA synthesis *via* RT-PCR kit according to the manufacturer's instructions. In the next step, using the 2X Q-PCR Master Mix with 2 μl of cDNA and 1 μl of each *icaA*, *LasR*, and *16S rRNA* primers in a volume of 20 μl on the real-time-PCR equipment (LightCycler® 96 Instrument, Roche, United States), gene expression was measured. The *icaA*, *LasR*, and *16S rRNA* primers were obtained from previous works (Atshan et al., 2012; Koohsari et al., 2016;

Abdelraheem et al., 2020; Bai et al., 2020). Initial denaturation took place at 95°C for 10 min, and then 40 cycles of 95°C for 15 s, annealing at 60°C for 45 s, and extension at 72°C for 30 s. To control the amplification efficiency, the standard curve was designed using the serial dilution of mRNA of untreated ATCC 29213 for the *icaA*, and untreated *P. aeruginosa* PAO1 for the *LasR*. Finally, gene expression was calculated *via* Ct assay, and *16S rRNA* genes were used as the internal controls for each bacterium (Rao et al., 2013).

2.11. Toxicity assays

The host cell cytotoxicity of melittin was evaluated by the MTT test, as described before (Akbari et al., 2019). Briefly, the HEK-293 cell line was grown in DMEM (containing 10% FCS and antibiotics (100 U/ml penicillin and 100 U/ml streptomycin)). In the next step, the cells were incubated with 5% CO2 and relative humidity equal to 95% at 37°C, and they reached 4×10^4 per well and cultured overnight. After 24 h, the serial dilutions of melittin in the range of 5 to 0.039 μg were applied to the wells of a 96-well microplate and incubated for 24 h at 37°C, and afterward, 20 ml of MTT reagent with the concentration of 5 mg/ml was applied to each well, followed by a 4 h incubation. Finally, the supernatant was outed, and 100 ml of DMSO was added to the wells. Absorbance was ultimately determined at 570 nm *via* the spectrophotometer reader (BioTek, United States). The proportion of surviving cells was computed as follows: Percent of survival = (OD test/OD control) × 100 (Akbari et al., 2019).

Besides, to survey the hemolytic effect, several melittin concentrations were utilized per the previously reported approach (Zarrinnahad et al., 2018). A healthy volunteer's heparinized blood was collected, then centrifuged at 3500 rpm for 10 min, and washed three times with PBS; the supernatant was outed, and 100 μl of 2% human red blood cells (RBCs) stock 2% provided in PBS was then entered into each well of a microplate and treated with melittin (from 5 to 0.039 to 5 μg) and incubated at 37°C for 2 h and then centrifuged at 3000 rpm for 10 min, and the OD of released hemoglobin was read at 540 nm using the microplate spectrophotometer reader (BioTek, United States). Besides, for positive control, 200 μl containing 100 μl 2% RBC and 100 μl of 1% Triton X-100, and for the negative control, 200 μl containing 100 μl 2% RBC and 100 μl PBS were used, respectively. Finally, the percentage of RBC hemolysis was determined as follows: [(OD test − OD negative control)/(OD positive control − OD negative control)] × 100 (Zarrinnahad et al., 2018).

2.12. Statistical analysis

In all assays, the GraphPad Prism 9 software (GraphPad Software, Inc., La Jolla, CA, United States) was applied for the various statistical techniques. In this sense, a t-test was applied to evaluate the significance of the findings from concentrations of the anti-biofilm effect of melittin and antibiotics in combination. In addition, the ANOVA test was used to compare the survival rate of the HEK-293 cell line exposed to concentrations of melittin and the control, as well as in gene expression between the treated isolated and the control, and also between the FBIC values. It should be noted that findings were reported as the mean ± standard deviation except for the cases stated otherwise and assays were accomplished with a confidence level of 95%, and a value of $p < 0.05$ was considered significant. To describe the correlation between the examined concentrations and the percent of activities, the non-linear regression test was performed. All experiments were done three times.

3. Results

3.1. Isolates, MRSA, and biofilm production assay

The result of antibacterial susceptibility testing and molecular test of isolates toward FOX disc and *mecA* gene showed that 66.6% ($n = 20$) of *S. aureus* isolates were demonstrated as MRSA. Notably, 75% ($n = 6$), 72% ($n = 8$), 75% ($n = 3$), and 50% ($n = 3$), of the wound, blood, sputum, and urine were methicillin-resistant, respectively. In this regard, there was no correlation between the source and MRSA isolates ($p = 0.66$). Finally, most *S. aureus* and *P. aeruginosa* isolates could produce varying rates of biofilm. In this regard, the minimum and maximum OD for all isolates were 0.1 and 2.9, respectively. Besides, according to these findings, the biofilm production ability of the isolates was categorized as strong, intermediated, and weak producers, as depicted in Table 1. Finally, after entry and exit criteria for determining pathogenic isolates and biofilm formation ability, 9 clinical MRSA and 9 clinical *P. aeruginosa* isolates were chosen and used for further analysis along *S. aureus* ATCC 29213 and *P. aeruginosa* PAO1.

3.2. Antibacterial susceptibility testing and MDR isolates

According to the disk diffusion data for selected clinical isolates, the antibiotic resistance rate of *S. aureus* toward E, TS, CD, GM, and LZD was 60, 30, 50, 50, and 0%, respectively. Additionally, based on disk diffusion data for selected clinical *P. aeruginosa* isolates, the antibiotic resistance rate toward NA, CT, PRL, AMP, IMP, CPE, and C was 70, 10, 70, 80, 0, 50, and 0%, respectively. In total, 60% of MRSA isolates and 70% of *P. aeruginosa* isolates were MDR. In this regard, there was no correlation between the source and MDR isolates ($p = 0.23$). Further detail on antimicrobial susceptibility testing of antibiotics against isolates is depicted in Table 1.

3.3. MIC, MBC, and MBC/MIC values

The results showed that melittin suppressed the growth of MRSA and *P. aeruginosa* isolates, with MIC ranging from 0.625 to 2.5 μg/ml for MRSA, and 1.25 to 10 μg/ml for *P. aeruginosa*. The findings also demonstrated melittin's bactericidal effect on tested isolates, with MBC ranging from 1.25 to 5 μg/ml for MRSA and 1.25 to 10 μg/ml for *P. aeruginosa*, respectively. The value of the geometric mean of MIC for melittin, gentamicin, ciprofloxacin, vancomycin, and rifampin was 2.1, 8.5, 6.4, 3.03, and 0.46 μg/ml, respectively. Besides, the value of the geometric mean of MBC for melittin, gentamicin, ciprofloxacin, vancomycin, and rifampin was 3.18, 103.96, 12.99, 6.06, and 6.4 μg/ml, respectively. Finally, the geometric mean value for the MBC/MIC for melittin, gentamicin, ciprofloxacin, vancomycin, and rifampin was

10.3389/fmicb.2023.1030401

TABLE 1 Findings of antimicrobial susceptibility testing and biofilm of *Staphylococcus aureus* and *Pseudomonas aeruginosa*.

Strain	FOX	E	TS	CD	GM	LZD	NA	CT	PRL	AMP	IPM	CPE	C	MDR/ NonMDR	Biofilm producer
ATCC 29213	S	S	S	S	S	S	–	–	–	–	–	–	–	NonMDR	Intermediate
MRSA 1	R	R	S	R	S	S	–	–	–	–	–	–	–	MDR	Intermediate
MRSA 2	R	S	R	S	R	S	–	–	–	–	–	–	–	NonMDR	Strong
MRSA 3	R	R	S	R	R	S	–	–	–	–	–	–	–	MDR	Weak
MESA 4	R	S	S	S	S	S	–	–	–	–	–	–	–	NonMDR	Intermediate
MRSA 5	R	R	R	R	S	S	–	–	–	–	–	–	–	MDR	Strong
MRSA 6	R	R	S	R	R	S	–	–	–	–	–	–	–	MDR	Intermediate
MRSA 7	R	R	R	S	R	S	–	–	–	–	–	–	–	MDR	Weak
MRSA 8	R	S	S	S	S	S	–	–	–	–	–	–	–	NonMDR	Intermediate
MRSA 9	R	R	S	R	R	S	–	–	–	–	–	–	–	MDR	Strong
PAO1	–	–	–	–	–	–	S	S	R	R	S	S	S	NonMDR	Strong
P. aeruginosa 1	–	–	–	–	–	–	R	S	R	R	S	R	S	MDR	Intermediate
P. aeruginosa 2	–	–	–	–	–	–	S	S	S	S	S	S	S	NonMDR	Weak
P. aeruginosa 3	–	–	–	–	–	–	R	S	R	R	S	R	R	MDR	Intermediate
P. aeruginosa 4	–	–	–	–	–	–	R	R	R	R	S	S	R	MDR	Strong
P. aeruginosa 5	–	–	–	–	–	–	R	S	R	R	S	R	S	MDR	Weak
P. aeruginosa 6	–	–	–	–	–	–	R	S	S	S	S	R	R	MDR	Intermediate
P. aeruginosa 7	–	–	–	–	–	–	S	S	S	R	S	S	S	Non MDR	Strong
P. aeruginosa 8	–	–	–	–	–	–	R	S	R	R	S	R	R	MDR	Intermediate
P. aeruginosa 9	–	–	–	–	–	–	R	S	R	R	S	S	R	MDR	Intermediate

Abbreviations: ATCC, American Type Culture Collection; MRSA, methicillin-resistant *S. aureus*; *P. aeruginosa*, *Pseudomonas aeruginosa*; R, resistant; I, intermediate; S, sensitive; FOX, cefoxitin; E, Erythromycin; TS, Trimethoprim-Sulfamethoxazole; CD, Clindamycin; GM, Gentamicin; LZD, Linezolid; NA, nalidixic acid; CT, Colistin; PRL, Piperacillin; AMP, Ampicillin; IPM, Imipenem; CPE, Cefepime; C, Chloramphenicol; MDR, multidrug-resistant.

1.51, 12.12, 2, 2, and 13.92, respectively. Details on MIC and MBC findings are depicted in Table 2.

3.4. MBIC and MBEC

Most importantly, the findings also demonstrated that melittin suppressed the preformed biofilm of tested isolates, with MBIC values from 10 to 2.5 μg/ml for MRSA and 20 to 5 μg/ml for *P. aeruginosa,* respectively. Besides, the MBIC results for gentamicin, ciprofloxacin, vancomycin, and rifampin ranged from 4 to 128, 2 to 128, 16 to 128, and 8 to 128 μg/ml, respectively. The value of the geometric mean of MBIC for melittin, gentamicin, ciprofloxacin, vancomycin, and rifampin was 7.07, 34.29, 27.85, 39.39, and 25.99 μg/ml, respectively. Besides, the findings also found that melittin eradicated the biofilm-embedded bacteria, with MBEC values ranging from 10 to 40 μg/ml for MRSA and *P. aeruginosa*. Besides, the MBEC ranges for gentamicin, ciprofloxacin, vancomycin, and rifampin were 64 to 512, 8 to 1,024, 64 to 512, and 32 to 1,024/mL, respectively. The value of the geometric mean of the MBEC value for melittin, gentamicin, ciprofloxacin, vancomycin, and rifampin was 20, 207.93, 181.01, 194.01, and 256 μg/ml, respectively. Further details on MBIC and MBEC are shown in Table 3.

3.5. Synergistic activity of antimicrobial agents on biofilm

In the current study, the value of the geometric mean for best synergistic melittin–vancomycin concentrations based on FBICi against MRSA 5, MRSA 6, and ATCC 29213 was 0.09, 0.09, and 0.25, respectively. Besides, the value of the geometric mean for best synergistic melittin–rifampin concentrations based on FBICi against MRSA 2, MRSA 9, and ATCC 29213 was 0.35, 0.35, and 0.62, respectively. Besides, the geometric means for best synergistic melittin–gentamicin concentrations based on FBICi against *P. aeruginosa* PAO1, *P. aeruginosa* 4, and *P. aeruginosa* 8 were 0.18, 0.08, and 0.06, respectively. Besides, for best synergistic melittin–ciprofloxacin concentrations based on FBICi against *P. aeruginosa,* PAO1, *P. aeruginosa* 7, and *P. aeruginosa* 8 were 0.37, 0.24, and 0.5, respectively. Further details on antibiofilm synergistic effects of melittin and antibiotics are shown in Tables 4, 5.

3.6. Activity of melittin on biofilm encoding genes

The activity of sub-lethal melittin concentrations from 5 to 0.039 μg on the expression of the *icaA* and *LasR* was tested for the selected isolates after 24 h. In this regard, log 2-fold change demonstrated that expression of the *icaA* in *S. aureus* and *LasR* in *P. aeruginosa* exposed to sub-MIC melittin were downregulated at a range from 4.11 to 0.1 fold for *icaA*, and 3.7 to 0.11 fold for *LasR*, respectively (Figure 1).

In particular, for *icaA* of *S. aureus* ATCC 29213, at 0.078 to 0.625 μg, the downregulation range was from 0.34 to 3.63. The downregulation range for MRSA 2 at 0.039 to 0.625 μg was from 0.11 to 4.11. The downregulation range for MRSA 5 at 0.039 to 1.25 μg was from 0.4 to 4.4. Besides, the downregulation range for MRSA 6 at 0.039 to 0.625 μg was from 0.1 to 3.6. Finally, the downregulation range for MRSA 9 at 0.039 to 0.625 μg was from 0.35 to 3.2. On the other side, for *LasR* of *P. aeruginosa* PAO1, at 0.156 to 5 μg, the downregulation range was from 0.1 to 3.4. The downregulation range for *P. aeruginosa* 4 at 0.156 to 5 μg was from 0.1 to 2.93. The downregulation range for *P. aeruginosa* 7 at 0.039 to 1.25 μg was from 0.22 to 3.7. Finally, the downregulation range for *P. aeruginosa* 8 at 0.078 to 2.5 μg was from 0.11 to 3.54. In this sense, a linearity

TABLE 2 MIC, MBC, and MBC/MIC values for melittin, vancomycin, rifampin, gentamicin, and ciprofloxacin against *S. aureus* and *P. aeruginosa*.

Strain	MEL-MIC	MEL-MBC	VAN-MIC	VAN-MBC	RIF-MIC	RIF-MBC	GEN-MIC	GEN-MBC	CIP-MIC	CIP-MBC	VAN-MBC/MIC ratio	RIF-MBC/MIC ratio	GEN-MBC/MIC ratio	CIP-MBC/MIC ratio	MEL-MBC/MIC ratio
ATCC 29213	1.25	5	1	2	0.015	0.5	–	–	–	–	2	32	–	–	4
MRSA 1	2.5	5	4	8	0.5	8	–	–	–	–	2	16	–	–	2
MRSA 2	1.25	2.5	8	16	1	16	–	–	–	–	2	16	–	–	2
MRSA 3	1.25	1.25	2	4	1	8	–	–	–	–	2	8	–	–	1
MESA 4	0.625	1.25	4	8	0.5	4	–	–	–	–	2	8	–	–	2
MRSA 5	2.5	5	8	16	2	16	–	–	–	–	2	8	–	–	2
MRSA 6	1.25	2.5	4	8	1	8	–	–	–	–	2	8	–	–	2
MRSA 7	0.625	1.25	2	4	0.25	4	–	–	–	–	2	16	–	–	2
MRSA 8	2.5	5	4	8	0.25	8	–	–	–	–	2	32	–	–	2
MRSA 9	1.25	2.5	1	2	1	16	–	–	–	–	2	16	–	–	2
PAO1	5	10	–	–	–	–	0.5	8	0.25	1	–	–	16	4	2
P. aeruginosa 1	2.5	5	–	–	–	–	8	128	8	16	–	–	16	2	2
P. aeruginosa 2	5	5	–	–	–	–	4	64	2	8	–	–	16	4	1
P. aeruginosa 3	2.5	5	–	–	–	–	32	256	16	32	–	–	8	2	2
P. aeruginosa 4	10	10	–	–	–	–	64	512	32	32	–	–	8	1	1
P. aeruginosa 5	2.5	2.5	–	–	–	–	32	512	1	2	–	–	8	2	1
P. aeruginosa 6	1.25	2.5	–	–	–	–	16	128	2	4	–	–	8	2	2
P. aeruginosa 7	2.5	5	–	–	–	–	4	64	32	64	–	–	16	2	2
P. aeruginosa 8	5	10	–	–	–	–	16	128	16	32	–	–	16	2	2
P. aeruginosa 9	1.25	1.25	–	–	–	–	2	32	64	64	–	–	16	1	1

Abbreviations: ATCC, American Type Culture Collection; VAN, vancomycin; GEN, gentamicin; CIP, ciprofloxacin; MIC, minimum inhibitory concentration; MBC, minimum bactericidal concentrations; RIF, rifampin, Mel; melittin; MRSA, methicillin-resistant Staphylococcus aureus.

10.3389/fmicb.2023.1030401

TABLE 3 MBIC and MBEC values of melittin, vancomycin, rifampin, gentamicin, and ciprofloxacin against *S. aureus* and *P. aeruginosa*.

Isolate (*n* =20)	MEL-MBIC (μg/ml)	MEL-MBEC (μg/ml)	Van-MBIC (μg/ml)	Van-MBEC (μg/ml)	Rif-MBIC (μg/ml)	Rif-MBEC (μg/ml)	GEN-MBIC (μg/ml)	GEN-MBEC (μg/ml)	CIP-MBIC (μg/ml)	CIP-MBEC (μg/ml)
S. aureus ATCC 29213	10	40	32	128	8	128	–	–	–	–
MRSA 1	5	10	64	256	8	128	–	–	–	–
MRSA 2	10	20	16	64	32	128	–	–	–	–
MRSA 3	5	10	32	128	8	32	–	–	–	–
MESA 4	5	20	16	128	64	512	–	–	–	–
MRSA 5	10	20	64	256	16	512	–	–	–	–
MRSA 6	5	20	128	512	32	256	–	–	–	–
MRSA 7	2.5	20	32	256	64	512	–	–	–	–
MRSA 8	5	20	64	512	32	512	–	–	–	–
MRSA 9	10	40	32	128	128	1,024	–	–	–	–
P. aeruginosa PAO1	20	40	–	–	–	–	4	64	2	8
P. aeruginosa 1	10	20	–	–	–	–	32	128	8	64
P. aeruginosa 2	5	20	–	–	–	–	16	128	32	128
P. aeruginosa 3	5	10	–	–	–	–	64	256	16	64
P. aeruginosa 4	10	20	–	–	–	–	128	512	64	256
P. aeruginosa 5	5	10	–	–	–	–	64	256	64	512
P. aeruginosa 6	10	20	–	–	–	–	64	512	16	128
P. aeruginosa 7	10	40	–	–	–	–	32	128	128	1,024
P. aeruginosa 8	10	40	–	–	–	–	64	256	64	1,024
P. aeruginosa 9	5	10	–	–	–	–	16	256	64	512

Abbreviations: MBIC, Minimum biofilm inhibition concentration; MBEC, Minimum biofilm eradication concentration; MRSA, methicillin-resistant *S. aureus*.

relationship was found at evaluated concentrations of melittin, and it also indicated that the downregulation of biofilm-associated genes was generally dose-dependent ($R^2 = 0.89$). Besides, ANOVA showed a statistical difference in biofilm-associated genes between the treated and untreated samples ($p < 0.05$).

3.7. Cytotoxicity and hemolytic activity of melittin

The cytotoxicity findings ranged from 5, 2.5, 1.25, 0.625, 0.312, and 0.156 μg of melittin 85.9, 69.4, 45.3, 25.2, 10, and 3.5% cytotoxicity on HEK-293 was seen, respectively. Notably, at the best synergistic concentrations of melittin with antibiotics, i.e., 0.078 and 0.039 μg, this peptide did not show any toxicity toward the HEK-293 (Table 6). Of note, a t-test demonstrated no difference between the survival rate of 0.078 and 0.039 μg of melittin and the control sample ($p = 0.085$). Finally, the hemolytic effect of melittin against RBCs ranging from 5, 2.5, 1.25, 0.625, 0.312, and 0.156 μg was 91.6, 80.5, 74.2, 59.5, 25, and 6%, respectively, whilst melittin with 0.078 and 0.039 concentrations showed 0% hemolysis on RBCs (Table 6).

4. Discussion

MDR pathogens are difficult to treat with antibiotics, especially when they generate biofilm, and these pathogens are a leading source of death in some cases, such as burn and *CF* patients, as well as infection in diabetes patients with chronic non-healing wounds (Emerson et al., 2002; Hiramatsu et al., 2014; Akbari et al., 2019). There is a critical need for novel antimicrobial agents that more effectively target biofilm and its embedded bacteria because nearly all antimicrobials currently used in clinics are active against planktonic growing bacteria. Regarding this, among the limited number of novel agents under investigation, AMPs have shown to be promising to ensure their advancement as active agents toward MDR bacterial infections, as well as potential targets for novel antibiofilm therapeutics (Hale and Hancock, 2007).

Our findings showed that melittin suppressed the growth of isolates, with MIC from 0.625 to 2.5 μg/ml for MRSA and 1.25 to 10 μg/ml for *P. aeruginosa.* The findings also demonstrated the bactericidal effect of melittin on tested isolates, with MBC from 1.25 to 5 μg/ml for MRSA and 1.25 to 10 μg/ml for *P. aeruginosa*, respectively. A comparison of the antibacterial effects of melittin on MRSA and MDR methicillin-resistant *Staphylococcus epidermidis* (MRSE), MDR *P aeruginosa,* and MDR *Acinetobacter baumannii* by others (Choi et al., 2015a; Akbari et al., 2019; Mirzaei et al., 2022a) shows the same result as our findings. Besides, the value of the geometric mean of MBC of the gentamicin, ciprofloxacin, vancomycin, and rifampin isolates was 8.5, 6.4, 3.03, and 0.46 μg/ml, respectively. The geometric mean value of MBC for gentamicin, ciprofloxacin, vancomycin, and rifampin for all isolates was 103.96, 12.99, 6.06, and 6.4 μg/ml, respectively. It has been found that melittin binds to bacterial membranes and creates pores, resulting in osmotic bacterial lysis (Bevalian et al., 2021).

Most importantly, our investigation of MBIC and MBEC demonstrated the potent anti-biofilm action of melittin toward all tested isolates with MBIC from 2.5 to 10 μg/ml for MRSA and 5 to 20 μg/ml for *P. aeruginosa*, as well as MBEC from 10 to 40 μg/ml for MRSA and *P. aeruginosa,* respectively. These findings are per our previous study on the strong biofilm of MDR MRSE (Mirzaei et al., 2022b) as well as by others on strong biofilm-forming MDR *A. baumannii* strains (Bardbari et al., 2018), biofilm-forming solid MDR *P. aeruginosa* (Khozani et al., 2019), and biofilm of MRSA (Lima et al., 2021). Besides, the MBIC results for gentamicin, ciprofloxacin, vancomycin, and rifampin were in the range 4 to 128, 2 to 128, 16 to

TABLE 4 The best synergistic concentrations of vancomycin-melittin and rifampin-melittin against biofilm of selected *S. aureus* isolates.

ATCC 29213		MRSA 5		MRSA 6		ATCC 29213		MRSA 2		MRSA 9	
VAN+MEL (μg/ml)	FBIC indices	VAN+MEL (μg/ml)	FBIC indices	VAN+MEL (μg/ml)	FBIC indices	RIF+MEL (μg/ml)	FBIC indices	RIF+MEL (μg/ml)	FBIC indices	RIF+MEL (μg/ml)	FBIC indices
32 + 10	2	64 + 2.5	1.25	64 + 1.25	1.12	8 + 2.5	1.25	32 + 10	2	128 + 10	2
16 + 5	1.5	32 + 1.25	0.62	32 + 0.625	0.56	4 + 1.25	0.62	16 + 5	1	64 + 5	1
8 + 2.5	0.75	16 + 0.625	0.31	16 + 0.312	0.25	–	–	8 + 2.5	0.5	32 + 2.5	0.5
4 + 1.25	0.37	8 + 0.312	0.15	8 + 0.156	0.14	–	–	4 + 1.25	0.25	16 + 1.25	0.25
2 + 0.625	0.18	4 + 0.156	0.07	4 + 0.078	0.07	–	–	–	–	–	–
–	–	2 + 0.078	0.03	2 + 0.039	0.03	–	–	–	–	–	–

Abbreviations: ATCC, American type culture collection; VAN, vancomycin; MEL; melittin; RIF, Rifampin; MRSA, methicillin-resistant *S. aureus*; FBIC, fractional biofilm inhibitory concentration.

TABLE 5 The best synergistic concentrations of gentamicin-melittin and ciprofloxacin-melittin against biofilm of selected *P. aeruginosa* isolates.

P. aeruginosa PAO1		*P. aeruginosa* 4		*P. aeruginosa* 8		*P. aeruginosa* PAO1		*P. aeruginosa* 7		*P. aeruginosa* 8	
GEN+MEL (μg/ml)	FBIC indices	GEN+MEL (μg/ml)	FBIC indices	GEN+MEL (μg/ml)	FIC indices	CIP+MEL (μg/ml)	FBIC indices	CIP+MEL (μg/ml)	FBIC indices	CIP+MEL (μg/ml)	FBIC indices
4 + 10	1.5	64 + 5	1	32 + 2.5	0.75	2 + 10	1.5	128 + 10	2	64 + 10	2
2 + 5	0.75	32 + 2.5	0.5	16 + 1.25	0.37	1 + 5	0.75	64 + 5	1	32 + 5	1
1 + 2.5	0.37	16 + 1.25	0.25	8 + 0.625	0.18	0.5 + 2.5	0.37	32 + 2.5	0.5	16 + 2.5	0.5
0.5 + 1.25	0.18	8 + 0.625	0.12	4 + 0.312	0.09	–	–	16 + 1.25	0.25	–	–
0.25 + 0.625	0.09	4 + 0.312	0.06	2 + 0.156	0.04	–	–	8 + 0.625	0.12	–	–
–	–	2 + 0.156	0.03	1 + 0.078	0.02	–	–	–	–	–	–
–	–	1 + 0.078	0.01	0.5 + 0.039	0.01	–	–	–	–	–	–

Abbreviation: *P. aeruginosa*, *Pseudomonas aeruginosa*; GEN, Gentamicin; MEL, melittin; CIP, Ciprofloxacin; FBIC, fractional biofilm inhibitory concentration.

10.3389/fmicb.2023.1030401

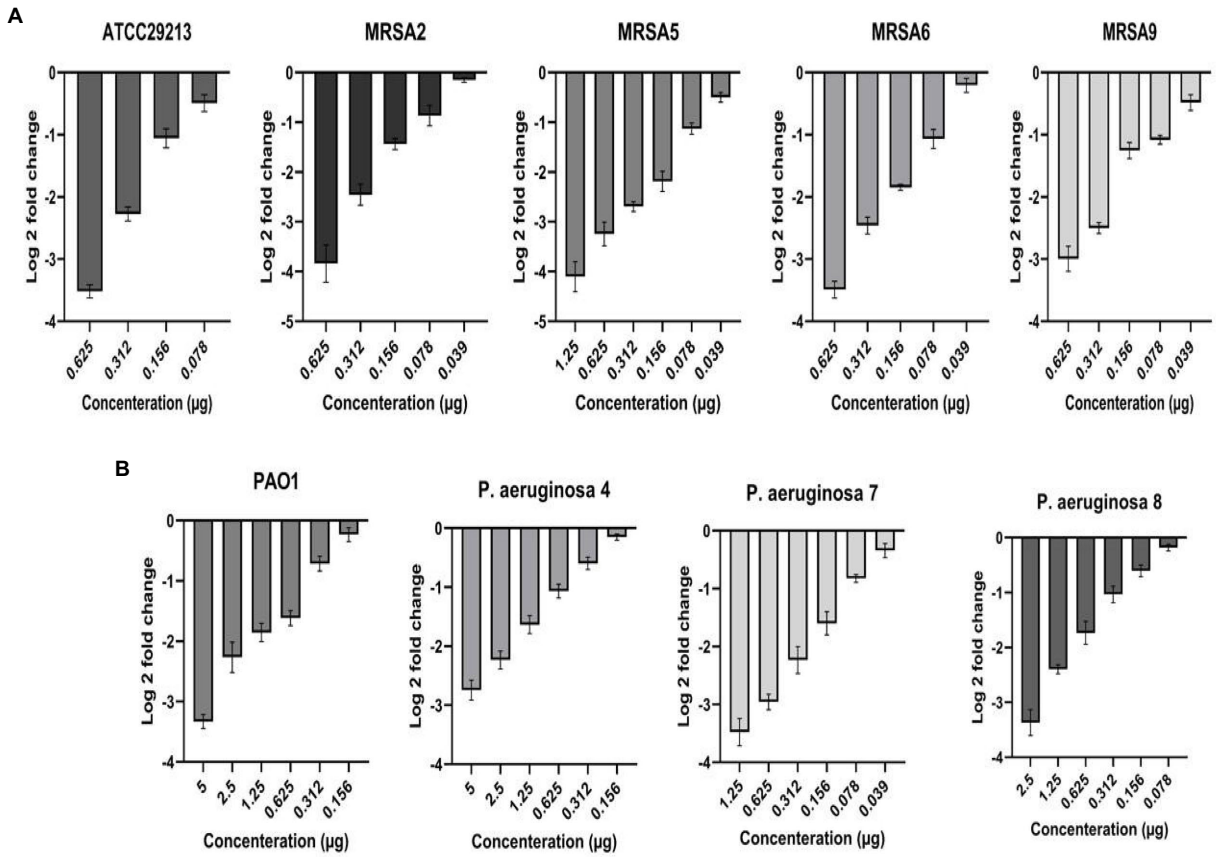

FIGURE 1
Downregulation of biofilm-associated genes *icaA* **(A)** and *Las* R **(B)** in *Staphylococcus aureus* and *Pseudomonas aeruginosa* at sub-inhibitory concentrations of melittin, respectively.

TABLE 6 Overview of toxicity and hemolysis of melittin at the best synergistic concentrations.

Melittin (µg/ml)	Cell death (%)	RBC hemolysis (%)
5	85.9 ± 3.4	91.6 ± 2.4
2.5	69.4 ± 3.2	80.5 ± 2
1.25	45.3 ± 3.5	74.2 ± 1.8
0.625	25.2 ± 3.1	59.5 ± 2.1
0.312	10 ± 2.1	25 ± 1.7
0.156	3.5 ± 2.2	6 ± 2
0.078	0	0
0.039	0	0

128, and 8 to 128 µg/ml, respectively, and MBEC results for gentamicin, ciprofloxacin, vancomycin, and rifampin were 64 to 512, 8 to 1,024, 64 to 512, and 32 to 1,024 µg/ml, respectively. Our findings are higher than those reported by others such as Douthit and colleagues who noted that MBIC values for vancomycin and rifampin were 1 µg/ml and 80 ng/ml, respectively, and also, MBEC of vancomycin and rifampin was 6 µg/mL and 80 ng/ml, respectively, against biofilm of *S. aureus* (Douthit et al., 2020). Besides, the determined MBEC gentamicin was >1,490 µg against *P. aeruginosa* by Das et al. (2016) is higher than our study.

Our results also found a synergistic effect of melittin in combination with antibiotics toward biofilm-forming MDR-MRSA and MDR-*P. aeruginosa*. The geometric mean values for best synergistic melittin–vancomycin and melittin–rifampin concentrations based on FBICi against *S. aureus* were 0.12 and 0.42, respectively. Besides, the geometric mean values for best synergistic melittin–gentamicin and melittin–ciprofloxacin concentrations based on FBICi against *P. aeruginosa* were 0.09 and 0.3, respectively. Some reports noted melittin for its synergistic effect on biofilm when used with antibiotics. Mohammadi et al. (Bardbari et al., 2018) found that melittin has a highly synergistic impact with imipenem and colistin toward the biofilm of MDR *A. baumannii*. Maiden et al. (2019) found that melittin acted alone and/or in combination with tobramycin to kill biofilm-embedded *P. aeruginosa*. Besides, our previous results found the synergistic action of melittin with rifampin and vancomycin toward potent biofilm of MDR-MRSE (Mirzaei et al., 2022b). These findings are in agreement with our results.

The synergy caused by melittin with antibiotics is most likely related to the site of their action on the bacterial membrane, cell wall, RNA polymerase, DNA gyrase, and protein synthesis inhibition (Zarghami et al., 2021b, 2022; Mirzaei et al., 2022a). Melittin disrupts the integrity of the cell membrane and creates pores that probably facilitate the penetration of antibiotics into the bacteria, and in the

next step, the antibiotics inhibit the growth of the bacteria and also kill the bacteria through the mentioned targets (Lee et al., 2013; Światły-Błaszkiewicz and Mrówczyńska, 2020; Zarghami et al., 2021a, 2022; Akbari et al., 2022). Most importantly, melittin has been found to have some convergent anti-biofilm mechanisms, including membrane degradation of biofilm-embedded bacteria, degradation of biofilm matrix, and downregulation of genes responsible for biofilm formation (Bardbari et al., 2018; Khozani et al., 2019; Shams et al., 2020; Zarghami et al., 2021b). For further determination of the anti-biofilm effect of melittin and its underlying mechanism of biofilm attenuation, real-time PCR for biofilm encoding genes was done. Hence, it found that biofilm-associated genes *icaA* in *S. aureus* and *LasR* in *P. aeruginosa were downregulated in all tested isolates at a range from 4.11 to 0.1 fold for icaA* and from 3.7 to 0.11 fold for *LasR*, respectively. These results are in agreement with our previous work (Mirzaei et al., 2022b), that sub-MIC of melittin significantly downregulated *icaA* expression in MDR MRSE, and also Mohammadi et al. (Bardbari et al., 2018), found that sub-MIC of melittin significantly decreased the biofilm-associated *bap* gene expression in MDR *A. baumannii*.

Along with arresting the emergence of antibiotic-resistant bacterial mutants, a further goal of multidrug therapy is to decrease the risk of single-drug toxicity to improve the quality of life for patients. In this regard, it has been found that melittin could disrupt the phospholipids packaging in the lipid bilayer, causing pore formation, resulting in the lysis of human RBC (Światły-Błaszkiewicz and Mrówczyńska, 2020). Our findings found synergistic melittin concentrations to destroy biofilm did not have cytotoxicity or hemolytic activities. However, the hemolytic effect of melittin alone (0.625 and 1.25 μg) on erythrocytes was toxic (25–45% cell death); therefore, we recommend that this AMP be used in combination and also in future studies, the ability to modify the melittin sequence to reduce cytotoxicity and improve bactericidal effects can be investigated. This peptide has shown various antimicrobial effects in preclinical *in vitro* and *in vivo*, and despite convincing efficacy data, its applicability to humans may be met with challenges due to issues including its non-specific cytotoxicity, degradation, and hemolytic activity. Hence, some optimization approaches, including the utilization of melittin-derived peptides, nanoparticle-based delivery of melittin, and combination therapy, can circumvent the issues. More importantly, reducing the concentration of antibiotics in synergism with melittin AMP can decrease drug side effects, especially in patients with kidney failure. Our results are consistent with the cytotoxic and hemolytic effects of melittin performed by others (Akbari et al., 2019; Mirzaei et al., 2022a).

5. Conclusion

As the occurrence of MDR pathogens is rising, the need for novel antimicrobials and ways to potentiate conventional antibiotics is crucial. Besides, as most conventional antibiotics are only active against proliferating planktonic bacteria, hence, eradicating persisters embedded in biofilm is difficult, and also, the biofilm matrix acts as a pharmacokinetic barrier, restricting the diffusion of antimicrobial agents and other noxious substances into the biofilm matrix. Accordingly, the use of newer and combination approaches to control and eradicate biofilm-mediated infection is one of the crucial requirements. In this regard, we found that melittin has a good effect against MDR MRSA and MDR *P. aeruginosa* as well as mature biofilms of both pathogens alone and in combination with conventional antibiotics. We also demonstrated the synergistic effects of melittin and antibiotics at low concentrations, suggesting that decreasing the concentration of antimicrobial drugs required for therapy can decrease their cytotoxic effects. Hence, these findings show that melittin can be a promising candidate for further evaluation *in vivo* and clinical biofilm-associated infection by MDR pathogens alone or in combination with antibiotics.

Data availability statement

The original contributions presented in the study are included in the article/Supplementary materials, further inquiries can be directed to the corresponding author.

Author contributions

RM performed all experiments and analyses, and also wrote the manuscript. HEGG served as advisor. RR contributed as a supervisor and also in the revision of the manuscript. All authors contributed to the article and approved the submitted version.

Acknowledgments

The authors would like to thank the Clinical Research Development Unit of Baqiyatallah Hospital, Tehran, Iran, for guidance and advice.

Conflict of interest

The authors declare that the research was conducted in the absence of any commercial or financial relationships that could be construed as a potential conflict of interest.

Publisher's note

References

Abdelraheem, W. M., Abdelkader, A. E., Mohamed, E. S., and Mohammed, M. S. (2020). Detection of biofilm formation and assessment of biofilm genes expression in different Pseudomonas aeruginosa clinical isolates. *Meta Gene* 23:100646. doi: 10.1016/j.mgene.2020.100646

Akbari, R., Hakemi Vala, M., Sabatier, J.-M., and Pooshang Bagheri, K. (2022). Fast killing kinetics, significant therapeutic index, and high stability of melittin-derived antimicrobial peptide. *Amino Acids* 54, 1275–1285. doi: 10.1007/s00726-022-03180-2

Akbari, R., Hakemi-Vala, M., Pashaie, F., Bevalian, P., Hashemi, A., and Pooshang Bagheri, K. (2019). Highly synergistic effects of melittin with conventional antibiotics against multidrug-resistant isolates of acinetobacter baumannii and pseudomonas aeruginosa. *Microb. Drug Resist.* 25, 193–202. doi: 10.1089/mdr.2018.0016

Askari, P., Namaei, M. H., Ghazvini, K., and Hosseini, M. (2021). In vitro and in vivo toxicity and antibacterial efficacy of melittin against clinical extensively drug-resistant bacteria. *BMC Pharmacol. Toxicol.* 22:42. doi: 10.1186/s40360-021-00503-z

Atshan, S. S., Nor Shamsudin, M., Sekawi, Z., Lung, L. T., Hamat, R. A., Karunanidhi, A., et al. (2012). Prevalence of adhesion and regulation of biofilm-related genes in different clones of Staphylococcus aureus. *J. Biomed. Biotechnol.* 2012:976972, 1–10. doi: 10.1155/2012/976972

Bai, B., Ren, J., Bai, F., and Hao, L. (2020). Selection and validation of reference genes for gene expression studies in pseudomonas brassicacearum GS20 using real-time quantitative reverse transcription PCR. *PLoS One* 15:e0227927. doi: 10.1371/journal.pone.0227927

Bardbari, A. M., Arabestani, M. R., Karami, M., Keramat, F., Aghazadeh, H., Alikhani, M. Y., et al. (2018). Highly synergistic activity of melittin with imipenem and colistin in biofilm inhibition against multidrug-resistant strong biofilm producer strains of Acinetobacter baumannii. *Eur. J. Clin. Microbiol. Infect. Dis.* 37, 443–454. doi: 10.1007/s10096-018-3189-7

Bassetti, M., and Garau, J. (2021). Current and future perspectives in the treatment of multidrug-resistant gram-negative infections. *J. Antimicrob. Chemother.* 76, iv23–iv37. doi: 10.1093/jac/dkab352

Bevalian, P., Pashaei, F., Akbari, R., and Pooshang Bagheri, K. (2021). Eradication of vancomycin-resistant Staphylococcus aureus on a mouse model of third-degree burn infection by melittin: an antimicrobial peptide from bee venom. *Toxicon* 199, 49–59. doi: 10.1016/j.toxicon.2021.05.015

Choi, J. H., Jang, A. Y., Lin, S., Lim, S., Kim, D., Park, K., et al. (2015). Melittin, a honeybee venom-derived antimicrobial peptide, may target methicillin-resistant Staphylococcus aureus. *Mol. Med. Rep.* 12, 6483–6490. doi: 10.3892/mmr.2015.4275

Das, M. C., Sandhu, P., Gupta, P., Rudrapaul, P., De, U. C., Tribedi, P., et al. (2016). Attenuation of Pseudomonas aeruginosa biofilm formation by Vitexin: a combinatorial study with azithromycin and gentamicin. *Sci. Rep.* 6, 1–13. doi: 10.1038/srep23347

Douthit, C., Gudenkauf, B., Hamood, A., Mudaliar, N., Caroom, C., and Jenkins, M. (2020). Effects of powdered rifampin and vancomycin solutions on biofilm production of staphylococcus aureus on orthopedic implants. *J. clinical orthopaedics and trauma* 11, S113–S117. doi: 10.1016/j.jcot.2019.10.002

Eisapoor, S. S., Jamili, S., Shahbazzadeh, D., Ghavam Mostafavi, P., and Pooshang Bagheri, K. (2016). A new, high yield, rapid, and cost-effective protocol to deprotection of cysteine-rich conopeptide, omega-conotoxin MVIIA. *Chem. Biol. Drug Des.* 87, 687–693. doi: 10.1111/cbdd.12702

Emerson, J., Rosenfeld, M., Mcnamara, S., Ramsey, B., and Gibson, R. L. (2002). Pseudomonas aeruginosa and other predictors of mortality and morbidity in young children with cystic fibrosis. *Pediatr. Pulmonol.* 34, 91–100. doi: 10.1002/ppul.10127

Foster, T. J. (2017). Antibiotic resistance in Staphylococcus aureus. Current status and future prospects. *FEMS Microbiol. Rev.* 41, 430–449. doi: 10.1093/femsre/fux007

Hale, J. D., and Hancock, R. E. (2007). Alternative mechanisms of action of cationic antimicrobial peptides on bacteria. *Expert Rev. Anti-Infect. Ther.* 5, 951–959. doi: 10.1586/14787210.5.6.951

Hiramatsu, K., Katayama, Y., Matsuo, M., Sasaki, T., Morimoto, Y., Sekiguchi, A., et al. (2014). Multi-drug-resistant Staphylococcus aureus and future chemotherapy. *J. Infect. Chemother.* 20, 593–601. doi: 10.1016/j.jiac.2014.08.001

Horan, T. C., Andrus, M., and Dudeck, M. A. (2008). CDC/NHSN surveillance definition of health care–associated infection and criteria for specific types of infections in the acute care setting. *Am. J. Infect. Control* 36, 309–332. doi: 10.1016/j.ajic.2008.03.002

Horcajada, J. P., and Montero, M. (2019). Epidemiology and treatment of multidrug-resistant and extensively drug-resistant Pseudomonas aeruginosa infections. *Clin. Microbiol. Rev.* 32:00031-19. doi: 10.1128/CMR.00031-19

Howden, B. P., Davies, J. K., Johnson, P. D., Stinear, T. P., and Grayson, M. L. (2010). Reduced vancomycin susceptibility in Staphylococcus aureus, including vancomycin-intermediate and heterogeneous vancomycin-intermediate strains: resistance mechanisms, laboratory detection, and clinical implications. *Clin. Microbiol. Rev.* 23, 99–139. doi: 10.1128/CMR.00042-09

Kelley, K., Cosman, A., Belgrader, P., Chapman, B., and Sullivan, D. C. (2013). Detection of methicillin-resistant Staphylococcus aureus by a duplex droplet digital PCR assay. *J. Clin. Microbiol.* 51, 2033–2039. doi: 10.1128/JCM.00196-13

Khozani, R. S., Shahbazzadeh, D., Harzandi, N., Feizabadi, M. M., and Bagheri, K. P. (2019). Kinetics study of antimicrobial peptide, melittin, in simultaneous biofilm degradation and eradication of potent biofilm producing MDR Pseudomonas aeruginosa isolates. *Int. J. Pept. Res. Ther.* 25, 329–338. doi: 10.1007/s10989-018-9675-z

Koohsari, H., Ghaemi, E. A., Mozaffari, N. A., and Moradi, A. (2016). Association of agr gene expression with Staphylococcus aureus virulence genes in BHI broth. *Medical Lab. J.* 10, 1–6. doi: 10.18869/acadpub.mlj.10.1.1

Lee, A. S., De Lencastre, H., Garau, J., Kluytmans, J., Malhotra-Kumar, S., Peschel, A., et al. (2018). Methicillin-resistant Staphylococcus aureus. *Nat. Rev. Dis. Primers.* 4:18033. doi: 10.1038/nrdp.2018.33

Lee, M. T., Sun, T. L., Hung, W. C., and Huang, H. W. (2013). Process of inducing pores in membranes by melittin. *Proc. Natl. Acad. Sci. U. S. A.* 110, 14243–14248. doi: 10.1073/pnas.1307010110

Lertwattanachai, T., Montakantikul, P., Tangsujaritvijit, V., Sanguanwit, P., Sueajai, J., Auparakkitanon, S., et al. (2020). Clinical outcomes of empirical high-dose meropenem in critically ill patients with sepsis and septic shock: a randomized controlled trial. *J. Intensive Care* 8:26. doi: 10.1186/s40560-020-00442-7

Lima, W. G., De Brito, J. C. M., Cardoso, V. N., and Fernandes, S. O. A. (2021). In-depth characterization of antibacterial activity of melittin against Staphylococcus aureus and use in a model of non-surgical MRSA-infected skin wounds. *Eur. J. Pharm. Sci.* 156:105592. doi: 10.1016/j.ejps.2020.105592

Mahdiun, F., Mansouri, S., Khazaeli, P., and Mirzaei, R. (2017). The effect of tobramycin incorporated with bismuth-ethanedithiol loaded on niosomes on the quorum sensing and biofilm formation of Pseudomonas aeruginosa. *Microb. Pathog.* 107, 129–135. doi: 10.1016/j.micpath.2017.03.014

Mahlapuu, M., Håkansson, J., Ringstad, L., and Björn, C. (2016). Antimicrobial peptides: an emerging category of therapeutic agents. *Front. Cell. Infect. Microbiol.* 6:194. doi: 10.3389/fcimb.2016.00194

Maiden, M. M., Zachos, M. P., and Waters, C. M. (2019). Hydrogels embedded with Melittin and tobramycin are effective against Pseudomonas aeruginosa biofilms in an animal wound model. *Front. Microbiol.* 10:1348. doi: 10.3389/fmicb.2019.01348

Mirzaei, R., Alikhani, M. Y., Arciola, C. R., Sedighi, I., Irajian, G., Jamasbi, E., et al. (2022a). Highly synergistic effects of Melittin with vancomycin and rifampin against vancomycin and rifampin resistant Staphylococcus epidermidis. *Front. Microbiol.* 13:869650. doi: 10.3389/fmicb.2022.869650

Mirzaei, R., Alikhani, M. Y., Arciola, C. R., Sedighi, I., Yousefimashouf, R., and Bagheri, K. P. (2022b). Prevention, inhibition, and degradation effects of melittin alone and in combination with vancomycin and rifampin against strong biofilm producer strains of methicillin-resistant Staphylococcus epidermidis. *Biomed. Pharmacother.* 147:112670. doi: 10.1016/j.biopha.2022.112670

Mirzaei, R., Mohammadzadeh, R., Alikhani, M. Y., Shokri Moghadam, M., Karampoor, S., Kazemi, S., et al. (2020a). The biofilm-associated bacterial infections unrelated to indwelling devices. *IUBMB Life* 72, 1271–1285. doi: 10.1002/iub.2266

Mirzaei, R., Mohammadzadeh, R., Sholeh, M., Karampoor, S., Abdi, M., Dogan, E., et al. (2020b). The importance of intracellular bacterial biofilm in infectious diseases. *Microb. Pathog.* 147:104393. doi: 10.1016/j.micpath.2020.104393

Mirzaei, R., and Ranjbar, R. (2022). Hijacking host components for bacterial biofilm formation: an advanced mechanism. *Int. Immunopharmacol.* 103:108471. doi: 10.1016/j.intimp.2021.108471

Mirzaei, R., Yousefimashouf, R., Arabestani, M. R., Sedighi, I., and Alikhani, M. Y. (2022c). The issue beyond resistance: methicillin-resistant Staphylococcus epidermidis biofilm formation is induced by subinhibitory concentrations of cloxacillin, cefazolin, and clindamycin. *PLoS One* 17:e0277287. doi: 10.1371/journal.pone.0277287

Murray, P.R., Baron, E.J., Pfaller, M.A., Tenover, F.C., Yolken, R.H., and Morgan, D.R. (1995). Manual of clinical microbiology (6th). *Trends Microbiol.* 3,:449.

Pang, Z., Raudonis, R., Glick, B. R., Lin, T. J., and Cheng, Z. (2019). Antibiotic resistance in Pseudomonas aeruginosa: mechanisms and alternative therapeutic strategies. *Biotechnol. Adv.* 37, 177–192. doi: 10.1016/j.biotechadv.2018.11.013

Rao, X., Huang, X., Zhou, Z., and Lin, X. (2013). An improvement of the 2ˆ (−delta delta CT) method for quantitative real-time polymerase chain reaction data analysis. *Biostat., bioinfo. biomathemat.* 3, 71–85. PMID: 25558171

Shams, K. R., Shahbazzadeh, D., Feizabadi, M. M., Harzandi, N., and Pooshang, B. K. (2020). *Anti-biofilm effect of Melittin peptide on clinical isolates of pseudomonas aeruginosa isolated from hospital burn infections*.

Sobisch, L.-Y., Rogowski, K. M., Fuchs, J., Schmieder, W., Vaishampayan, A., Oles, P., et al. (2019). Biofilm forming antibiotic resistant gram-positive pathogens isolated from surfaces on the international space station. *Front. Microbiol.* 10:543. doi: 10.3389/fmicb.2019.00543

Świątły-Błaszkiewicz, A., and Mrówczyńska, L. (2020). The effect of bee venom peptides Melittin, Tertiapin, and Apamin on the human erythrocytes ghosts: a preliminary study. *Meta* 10. doi: 10.3390/metabo10050191

Traczewski, M. M., Katz, B. D., Steenbergen, J. N., and Brown, S. D. (2009). Inhibitory and bactericidal activities of daptomycin, vancomycin, and teicoplanin against methicillin-resistant Staphylococcus aureus isolates collected from 1985 to 2007. *Antimicrob. Agents Chemother.* 53, 1735–1738. doi: 10.1128/AAC.01022-08

Van Duin, D., and Paterson, D. L. (2016). Multidrug-resistant bacteria in the community: trends and lessons learned. *Infect. Dis. Clin. N. Am.* 30, 377–390. doi: 10.1016/j.idc.2016.02.004

Van Duin, D., and Paterson, D. L. (2020). Multidrug-resistant bacteria in the community: an update. *Infect. Dis. Clin. N. Am.* 34, 709–722. doi: 10.1016/j.idc.2020.08.002

Wayne, P. (2010). Clinical and laboratory standards institute: performance standards for antimicrobial susceptibility testing: 20th informational supplement. *CLSI document*, M100–S20.

Zarghami, V., Ghorbani, M., Bagheri, K. P., and Shokrgozar, M. A. (2021a). Melittin antimicrobial peptide thin layer on bone implant chitosan-antibiotic coatings and their bactericidal properties. *Mater. Chem. Phys.* 263:124432. doi: 10.1016/j.matchemphys.2021.124432

Zarghami, V., Ghorbani, M., Bagheri, K. P., and Shokrgozar, M. A. (2021b). Prevention the formation of biofilm on orthopedic implants by melittin thin layer on chitosan/bioactive glass/vancomycin coatings. *J. Mater. Sci. Mater. Med.* 32, 1–9. doi: 10.1007/s10856-021-06551-5

Zarghami, V., Ghorbani, M., Bagheri, K. P., and Shokrgozar, M. A. (2022). Improving bactericidal performance of implant composite coatings by synergism between Melittin and tetracycline. *J. Mater. Sci. Mater. Med.* 33, 1–12. doi: 10.1007/s10856-022-06666-3

Zarrinnahad, H., Mahmoodzadeh, A., Hamidi, M. P., Mahdavi, M., Moradi, A., Bagheri, K. P., et al. (2018). Apoptotic effect of melittin purified from Iranian honey bee venom on human cervical cancer HeLa cell line. *Int. J. Pept. Res. Ther.* 24, 563–570. doi: 10.1007/s10989-017-9641-1

Frontiers in Microbiology

Explores the habitable world and the potential of microbial life

The largest and most cited microbiology journal which advances our understanding of the role microbes play in addressing global challenges such as healthcare, food security, and climate change.

Discover the latest Research Topics

See more →

Frontiers

Avenue du Tribunal-Fédéral 34
1005 Lausanne, Switzerland
frontiersin.org

Contact us

+41 (0)21 510 17 00
frontiersin.org/about/contact